EPRI
Electric Power
Research Institute

Keywords:
Deuterium
Palladium
Cold fusion
Electrolysis
Heat
Heavy water

EPRI TR-104188-V1
Project 3170
Proceedings
July 1994

Proceedings: Fourth International Conference on Cold Fusion Volume 1: Plenary Session Papers

Prepared by
Electric Power Research Institute
Palo Alto, California

Proceedings: Fourth International Conference on Cold Fusion

Volume 1: Plenary Session Papers

TR-104188-V1

Proceedings, July 1994

December 6-9, 1993
Lahaina, Maui, Hawaii

Conference Co-chairmen

T.O. Passell
Electric Power Research Institute

M.C.H. McKubre
SRI International

Prepared by
ELECTRIC POWER RESEARCH INSTITUTE
3412 Hillview Avenue
Palo Alto, California 94304

Sponsored by
Electric Power Research Institute
Palo Alto, California

T.O. Passell
Nuclear Power Group

and

Office of Naval Research
Arlington, Virginia

R. Nowak

DISCLAIMER OF WARRANTIES AND LIMITATION OF LIABILITIES

ORGANIZATION(S) THAT PREPARED THIS REPORT:
ELECTRIC POWER RESEARCH INSTITUTE
PALO ALTO, CALIFORNIA

ORDERING INFORMATION

Requests for copies of this report should be directed to the EPRI Distribution Center, 207 Coggins Drive, P.O. Box 23205, Pleasant Hill, CA 94523, (510) 934-4212. There is no charge for reports requested by EPRI member utilities.

FOREWORD

These four volumes include the full text or, in five cases, just the visual materials of papers presented at the Fourth International Conference on Cold Fusion. This meeting was the latest in a series of conferences devoted to a new area of scientific endeavor, variously called, "Deuterated Metals Research", "Anomalous Nuclear Phenomena in Solids", and "Research on New Hydrogen Energy". The first three conferences were held in Salt Lake City, Utah, (U.S.A)., Como, (Italy), and Nagoya, (Japan), in March, 1990, June, 1991, and October 1992, respectively. The authors and participants in this fourth conference should be thanked for four days of stimulating presentations and discussions. A conscious effort was made to maintain a high standard of scientific content and avoid exaggerated claims propagated by various public media. It is gratifying that this effort was largely successful without the need for extraordinary measures.

A number of new experimental approaches were evident compared with the Nagoya meeting. Use of ceramic proton conductors at high temperature was one such. Another was the use of ultrasonic cavitation in heavy water to load palladium and titanium foils with deuterium. Many theoretical papers were given, with some progress evident toward explaining some of these puzzling experimental observations. However, the wide range of theoretical models and speculations shows that the field remains in an exploratory phase, at least for the majority of theorists.

The use of concurrent sessions for the first time caused some attendees to miss hearing significant papers. It is hoped that this compendium of papers will serve to redress that shortcoming. Proceedings, including only those papers passing a rigorous peer review, will appear later as a publication of the American Nuclear Society's Fusion Technology Journal, thanks to the initiative of Editor George Miley.

242 persons from 12 countries registered and attended the conference. The hotel facility and the weather were such as to allow concentration on the technical meetings without serious distraction. Attendees included 124 from the United States, 62 from Japan, 19 from Italy, 11 from Russia, 10 from France, 5 from Canada, 4 from China, 2 from Switzerland, 2 from Germany, and 1 each from Spain, India, and England. A large number of interested persons from the former Soviet Union and eastern Europe were unable to attend but sent several papers that are included in these volumes.

Some 156 abstracts were originally submitted of which 125 papers appear in these proceedings. Since some of the enclosed material is in an unfinished state, the authors would appreciate being contacted by those who desire to reference the work reported here. The papers are divided so that Volume 1 contains all the papers received from authors who participated in the four plenary sessions, Volume 2 includes contributed papers on calorimetry and materials, Volume 3 has contributions on nuclear particle detection and measurement, and Volume 4 contains the papers contributed on theory and special topics. The papers are ordered in the same order of abstracts in the two volumes distributed at the meeting, with a few minor exceptions.

Thanks are due to the International Advisory and the Organizing Committees for their supportive efforts in arranging a successful meeting on such a controversial, yet potentially significant and hence absorbing, topic. Persons particularly active in arranging the agenda were M.C.H. McKubre, S. Crouch-Baker, D. Rolison, T. Claytor, H. Ikegami, and P. Hagelstein. I also wish to thank the following persons who ably served as session chairmen or co-chairmen during the meeting: M. Srinivasan, S. Smedley, P. Hagelstein, F. Tanzella, A. Miller, D. Rolison, S. Crouch-Baker, M. McKubre, K. Kunimatsu, E. Storms, F. Will, T. Claytor, F. Scaramuzzi, H. Ikegami, J. Bockris, G. Miley, B. Liaw, A. Takahashi, J. Cobble and M. Rabinowitz.

Supporting the logistical and physical arrangements were EPRI and the Office of Naval Research (ONR), represented by L. Nelson and R. Nowak respectively. Cosponsoring the meeting in addition to EPRI and ONR, was Comitato Nationale per la Ricerca e per lo Sviluppo dell'Energia Nucleare e delle Energie Alternative (ENEA), represented by Franco Scaramuzzi. My sincere gratitude goes out to these persons and organizations. Many other organizations implicitly supported the meeting by funding the travel of a number of attendees. Notable among these were ENECO with 21, NEDO with 26, and IMRA with 10 attendees respectively.

The search for a definitive signature of some nuclear reaction correlated with the production of excess heat in the palladium-deuterium system was advanced by the presentations of D. Gozzi, G. Gigli, and M. Miles and their respective coworkers who reported measuring He^4 in the vapor phase of both closed and open electrochemical cells. However, the concentrations observed were at levels well below the atmospheric concentration of He^4 (5.2 ppmv) and hence are not robustly above criticism as possible atmospheric air contamination. On the other hand, the tritium results of F. Will and coworkers appear robust, with great care taken to establish reliable backgrounds and checking for contamination. I also found the tritium results of T. Claytor and coworkers convincing.

M. Fleischmann, S. Pons, and coworkers provided two papers elaborating the excess heat phenemena: one of the more intriguing results was the excess heat observed well after complete cessation of current flow due to evaporative loss of electrolyte in "boil-off" experiments of the kind first described at the Nagoya meeting.

Several papers using gas loading of palladium claimed evidence of nuclear reaction products. Y. Iwamura and coworkers appear to have replicated the experiment reported by E. Yamaguchi and his NTT coworkers at Nagoya, but emphasizing neutrons and a mass 5 peak in the mass spectrum tentatively assigned to the TD molecule.

The paper chosen by M. Fleischmann in the final panel session as the most outstanding of the conference was by D. Cravens, who on a very modest budget, had discovered many of the better methods for loading palladium with deuterium to high levels and getting the excess heat phenomenon.

Insight into the loading of hydrogen and deuterium into metals was provided by four excellent papers by R. Huggins, R. Oriani, K. Kunimatsu and coworkers, and F. Cellani and coworkers, respectively.

Particularly insightful papers on the theoretical side were presented by R. Bush, S. Chubb, P. Hagelstein, G. Hale, S. Ichimaru, Y. Kim, X. Li, G. Preparata, M. Rabinowitz, A. Takahashi, and J. Vigier .

A thoughtful paper by J. Schwinger was read by E. Mallove at a special evening session. Also, E. Storms gave an excellent summation of the meeting in the final panel session.

I apologize in advance for failing to mention here results from many other equally excellent and significant papers given at the conference.

I agree with and echo H. Ikegami's remarks in the preface of the Nagoya meeting proceedings, "It is my belief that cold fusion will become one of the most important subjects in science, one for which we have been working so patiently, with dedication and with courage, for future generations, for those who will live in the twenty-first century. In order to achieve our goal, our ultimate goal, we must continue and extend our interdisciplinary and international collaboration".

The International Advisory and Organizing Committees met late in the sessions to set the location of the next two meetings. For the next meeting (April 9-13, 1995) Monaco (near Nice, France) was chosen, and in 1996, Beijing, China.

Besides Linda Nelson of EPRI who ably handled the logistics before and at the Conference, S. Creamer of SRI International and E. Lanum of EPRI deserve our thanks for dealing with on-site issues that arise at every large gathering such as this.

I acknowledge with thanks the support of my colleagues at EPRI in planning and organizing this meeting, namely N. Ferris, L. Fielder, K. Werfelman, S. Ennis, B. Klein, R. Claeys, T. Schneider, F. Will, J. Byron, A. Rubio, R. Shaw, R. Jones, J. Taylor, K. Yeager, and R. Balzhiser.

Thomas O. Passell, Editor
Electric Power Research Institute
June 1994

International Advisory Committee

J.O'M. Bockris (USA)
H. Ikegami (Japan)
X.Z. Li (China)
G. Preparata (Italy)
F. Scaramuzzi (Italy)
A. Takahashi (Japan)
M. Fleischmann (U.K.)
K. Kunimatsu (Japan)
S. Pons (France)
C. Sanchez (Spain)
M. Srinivasan (India)
D. Thompson (U.K.)

VOLUME 1

PAPERS FROM FOUR PLENARY SESSIONS

TABLE OF CONTENTS

VOLUME 2

CALORIMETRY AND MATERIALS PAPERS

TABLE OF CONTENTS

VOLUME 3

NUCLEAR MEASUREMENT PAPER

TABLE OF CONTENTS

VOLUME 4

THEORETICAL PAPERS AND SPECIAL TOPICS

TABLE OF CONTENTS

CALORIMETRY OF THE PD-D_20 SYSTEM: THE SEARCH FOR SIMPLICITY AND ACCURACY

M. Fleischmann
S. Pons
Monique Le Roux
Jeanne Roulette
IMRA Europe, S.A.
Science Centre
220, Rue Albert Caquot
Sophia Antipolis, 06560
FRANCE

Abstract

Our search for high levels of the rates of excess enthalpy generation in the Pd–D_2O and Pd–alloy–D_2O systems has been based *inter alia* on the following preconditions and suppositions:

(i) that it is necessary to use materials which will withstand the high stresses induced by the experiments;

(ii) given that (i) is assured, that it is necessary to adopt particular experimental protocols to achieve excess enthalpy generation at elevated temperatures;

(iii) that the protocols (ii) should ensure a high D/Pd ratio under all conditions;

(iv) that the protocols (ii) and (iii) should allow one to take advantage of "positive feedback" in the systems;

(v) that the systems are sensitive to "hidden state variables;"

(vi) that the state variables need to be further generalised to take account of cross–terms and of gradients with position.

The influence of factors (i)–(v) on the experiment design will be outlined (the factor (vi) will be touched on in a further communication at this Meeting).

The exploration of even a small part of the parameter space requires the execution of large numbers of experiments while (v) requires that the systems should not be subjected to constraints. Furthermore, the experiment durations are long (typically 10-90 days). It follows that the routine evaluation of these experiments should be based on simple on–line procedures so as to cope with the large volume of data generated. At the same time, it is necessary to raise the precision and accuracy of the data treatments so as to ensure a high level of the statistical significance of the derived information.

In this paper we will illustrate the ways in which we have sought to achieve the twin objectives of simplicity and accuracy while at the same time ensuring that the data treatments assess the validity of the modelling of the calorimeters.

Introduction

Four and a half years after our initial disclosure[1] that excess enthalpy is generated in Pd cathodes during the prolonged electrolysis of 0.1M LiOD in D_2O one might well ask:

"are there any general questions and topics which need to be addressed concerning the calorimetry of this strange system (and of related strange systems)?"

We recall the context of our initial disclosure: the excess enthalpy released was by orders of magnitude larger than that of any conceivable chemical or physical process. As against this the release of excess enthalpy was not accompanied by commensurate rates of production of the expected nuclear products for the known fusion reactions of deuterium[2] viz tritium and neutrons.*

In the intervening time there have been extensive efforts to detect other signatures of the putative nuclear processes in the lattices such as the generation of X–rays and γ–rays (other than those due to the (n,γ) reaction on ^1H), the emission of charged particles and the search for activation products and isotope shifts. However, it remains true to say that the generation of excess enthalpy is the major signature and that, so far, there are no quantitative correlations between the excess enthalpy and the expected (or unexpected!) "nuclear ashes." We observe that the general question which we have posed here has never been answered and we therefore now pose this in the specific form:

"what are the general principles which should guide the calorimetric investigations?"

In the following sections we outline the considerations which have guided our own approach to this topic.

Outline of the considerations which have governed our choice of calorimetric method

The system which we have used in the bulk of our investigations is illustrated in Fig 1. Cathodic discharge of D_2O at the surface of a Pd or Pd-alloy electrode leads to the formation of adsorbed atoms; these atoms may remain on the surface or be removed either via a further discharge step to form D_2 gas or be incorporated in the lattice as deuterons and electrons†;(see further below). If the rates of the desorption steps are sufficiently retarded, then, by applying a quasi-thermodynamic argument to the first step, we can readily see that the activity of D^+ in the lattice will be raised by changing the difference in Galvani potential between the metal and the solution. Such an argument leads us directly to the view that the state vectors of the system can be described as in equation (1).

---

*At this late stage we recall some further aspects of our observations prior to March 1989. The tritium production was sporadic; explanation of the accumulation of tritium in terms of conventional isotopic separation would have required D/T separation factors as high as 13.7. We considered such high values to be beyond the realms of possibility. There was some evidence for the detritiation of the solutions, again beyond the level of the known D/T separation factors for D and T dissolved in palladium. We noted that neutron production occured in bursts (i.e. did not obey Poisson statistics) and we had some early indications of the formation of ^4He.

†An alternative desorption step is via the recombination of two adsorbed atoms. The description which we have given here is based on present day formulations of the kinetics of the surface reactions. It should be noted, however, that the kinetics of incorporation of D^+ into the host lattice (and, more especially, of its removal from the lattice) have not been established. This topic will be discussed elsewhere.[3]

State Vectors
The Simple View

$$Q_f = f_0\Big[\underset{\substack{\text{processing variables}\\ \text{alloy composition}}}{\text{electrode materials, solution composition}}\Big] f_1\Big[E_{cell}(t),\ \theta(t)\Big] \qquad (1)$$

In writing down this equation we have taken due note of the fact that the development of satisfactory electrode materials is a necessary precondition for such investigations. This need automatically brings in its train the need to investigate the metallurgical variables of the system, the function f_0. We shall assume here that the issue of developing satisfactory materials – or, at least reproducible materials – has been adequately resolved so that we can omit f_0 from the further discussion‡.

It is generally believed that the implementation of the experiment illustrated by Fig 1 was the starting point of our investigation but this view is incorrect. Our actual starting point was our understanding of the significance of the early work of Coehn on the electrodiffusion of protons in palladium[4]. We will discuss this topic in a further paper presented at this meeting[5]. We note here that the application of a Galvani potential difference along a wire or sheet, Fig 2, can lead to the development of changes in the chemical potential of D^+ in the lattice far in excess of those which can be achieved in the simple electrolytic system, Fig 1§. It was the observation of specific rates of excess enthalpy generation in the range 1–10 W cm^{-3} which focussed our attention on the electrolytic rather than the solid state systems as it appeared unlikely at that time that the latter could be developed into energy efficient thermal generators.

However, in considering the state vectors of the system, we do need to take into account the fact that we may wish to impose changes in the Galvani potential on the lattice (see equation (2) below). This automatically introduces the spatial dependencies of the phenomena although these have not been indicated in equation (2). Spatial dependencies are also introduced by the possible application of hydrostatic forces¶ which we have separated from the possible compression of the ambient D_2 atmosphere‖. We also include

‡It goes without saying that this is a pious hope. The development of satisfactory electrode materials remains one of the central problems of the whole subject area.

§There is virtually no limit to the change in the chemical potential which can be achieved using pulsed potentials while at the same time maintaining the structural integrity of the systems[3] (except those set by the need to restrict voltage differences in laboratory apparatus). Changes in the Potential Energy of the order 10 keV should be achievable which may be compared to the target figure of 10 keV in the Kinetic Energy for Hot Fusion. The starting point of our investigation therefore had a close parallel to the topic of Hot Fusion; we will discuss elsewhere the implications of raising the Potential rather than the Kinetic Energy[3].

¶The effects of these (the Gorsky factors) will normally be small[6] except under extreme conditions such as those used in the programme on Structure Breaking Energy Release, SBER, (a topic which has its origins in the pioneering work of Bridgeman[7]) which was developed in the former Soviet Union. We believe that the Soviet work on fractofusion was carried out under the umbrella of the SBER programme.

‖We note here that changes in the fugacity of the D_2 atmosphere cannot necessarily be related in any simple way to changes of the Galvani potential differences between the metal and the solution or

the charging ratio (X = D/Pd) as a description of the composition of the system; however, we note that it is probably necessary to include several such compositional variables to denote the ratio of deuterium species to the number of lattice sites of different types (octahedral sites, tetrahedral sites, defect sites). Finally, we include the possible effects of phase changes and arrive at the more detailed description of the actual situation embodied in equation (2):

The Actual Situation

$$Q_f = f_2\Big[E_{cell}(t),\ \theta(t),\ \phi(t),\ \text{phase changes},\ X(t),\ P_{D_2}(t),\ \underset{\substack{\text{shear}\\ \text{compression}}}{P_{hydrostatic}(t)\ \ldots\ ?}\Big] \qquad (2)$$

The variables expressed in equation (2) are not necessarily independent of each other. Thus if the first step in the reaction sequence, Fig 1, is in quasi-thermodynamic equilibrium, the cell potential, Galvani potential in the lattice and deuterium concentration can be combined in a single variable, the electrochemical potential (eg see[8]).

$$\underset{\substack{\text{electrochemical}\\ \text{potential}}}{\overline{\mu}(t)} = \underset{\substack{\text{chemical}\\ \text{potential}}}{\mu} + \underset{\substack{\text{Galvani potential}\\ \text{work term}}}{\phi F}$$

$$= \underset{\substack{\text{chemical}\\ \text{potential}}}{\mu} + \underset{\substack{\text{Volta potential}\\ \text{work term}}}{\psi F} + \underset{\substack{\text{surface potential}\\ \text{work term}}}{\chi F} \qquad (3)$$

We observe that the composition of the solution (which has been somewhat arbitrarily incorporated in the function f_0) may also affect the chemical potential (eg via the activity of D_3O^+ if discharge is carried out from acid solutions).** For the situation described above (the discharge step in quasi-equilibrium and slow desorption of adsorbed deuterons), the fugacity of deuterium gas will not affect the system and we arrive at the description

$$Q_f = f_2\Big[\overline{\mu},\ \theta,\ P_{hydrostatic}\Big] \qquad (4)$$

(the state variables θ and P cannot be incorporated into $\overline{\mu}$).

As will be seen, the description (4) only applies to the thermodynamic limit $t \rightarrow \infty$ (as is indicated by the omission of the functional dependence of $\overline{\mu}$, θ and $P_{hydrostatic}$ on time). While it is certainly possible to carry out experiments which approximate to these conditions (measurements at constant electrode potential and temperature, see futher below) we note that we are dealing with a system which is under kinetic rather than

---

between different positions within the metal.

**The second line of equation (3) contains an important alternative decomposition of the electrochemical potential. The surface potential may have a special rôle in confining deuterons within the lattice[5] and changes in the composition may in turn induce marked changes in χ[9] ie the charging ratio may affect both μ and χ.

thermodynamic control[††]. It is therefore necessary to use a description which retains the temporal dependence of the state variables; furthermore, it is desirable to use the temporal dependencies to gain an insight into the phenomena and, if possible to enhance the rates of excess enthalpy generation. A possible starting point is the description embodied in the simplification, equation (5):

Simplification

$$Q_f = f_3 \left[E_{cell}(t),\ \theta(t),\ \phi(t),\ X(t),\ \text{phase changes} \right] \tag{5}$$

Here, we have assumed that the system will be free from hydrostatic perturbations (see further below), that changes in the composition, temperature and cell potential as well as phase transformations will take place on different time-scales and that the Galvani potential within the electrode can be changed independently of changes in the electrode potential.

An underlying difficulty in the investigation of the phenomena is that there are only two variables which can easily be changed independently ($E_{cell}(t)$ and $\theta(t)$); the independent change of $\phi(t)$ requires more complicated instrumentation. At the same time, the system is controlled by numerous variables which remain "hidden". For example, it has become apparent that excess enthalpy generation behaves as though there is some form of "threshold phenomenon"[10,11] as is revealed by the marked dependence on the charging ratio[12,13]: thus the achievement of a sufficiently high value of X is a necessary precondition. However, it has not been possible so far to make X(t) a control variable of the system: the values of X(t) must be derived by independent measurements[12,13].

In order to extend the investigation, it is therefore useful to be guided by a standard approach of control theory: the influence of the "hidden variables" can be revealed by making the time dependencies of the state variables part of the state vectors (the Lyapunov criteria). For the present case we obtain[‡‡]:

Hidden Variables: the Conventional View

$$\begin{aligned} Q_f = f_4 \Big[& E_{cell}(t),\ \frac{dE_{cell}(t)}{dt},\ \ldots;\ \theta(t),\ \frac{d\theta(t)}{dt} \ldots; \\ & \phi(t),\ \frac{d\phi(t)}{dt},\ldots;\ X(t),\ \frac{dX(t)}{dt},\ldots; \\ & \text{phase changes},\ \frac{d\,[\text{ phase changes }]}{dt}\ (\text{chaos?}).\ \ldots \Big] \end{aligned} \tag{6}$$

The usefulness of casting the problem in such general terms is rapidly revealed by the experimental investigations. As an example we can note that the act of writing $d[\text{phase changes}]/dt$ reveals that we should look for oscillations in the cell potentials and

[††]Measurements at the thermodynamic limit would be feasible (and sensible) for gas phase systems at extremely high pressures.

[‡‡]Physical Chemists will recognise the similarity between this approach and the investigation of Chemical Kinetics.

rates of enthalpy generation (not necessarily the rates of excess enthalpy generation) and, in the limit, for chaotic behaviour. That this is indeed observed is shown by Figs 3A and B (palladium-rhodium alloys are especially prone to show this behaviour).

It follows that we need to establish whether (and under what conditions) the system is subject to one or more strange attractors as well as the cause(s) of the marked non-linearities. It also follows that this type of behaviour is undesirable[†] and the establishment of the root cause(s) can guide the choice of protocols to minimise such effects. A possible cause is the marked variation of the partial molar enthalpy with the charging ratio, Fig 4[14]. Under the usual conditions for the investigation of the Pd/H and Pd/D systems, the absorption is exothermic but it is apparent that it becomes endothermic in the region of the "threshold value" of X required for excess enthalpy generation[12,13]. It may well be that this reversal in the molar heat of absorption is due to the formation of a third phase, the proposed γ-phase[9] but, in any event, the fluctuations in entropy will become unbounded when $\overline{\Delta H} = 0$ and these would explain the chaotic behaviour of the system.

It is convenient to consider at this point the way in which this type of behaviour, Figs 3 and 4, has guided our search for the conditions required for high rates of excess enthalpy generation at intermediate temperatures[15,16], say 100°C. The usual prediction would be that it would be impossible to achieve this objective because the charging ratio falls with temperature: the negative partial molar heat of absorption, Fig 4, is an equivalent statement of this effect. However, as we have noted above, the partial molar enthalpy of absorption becomes positive at the charging ratios required for excess enthalpy generation, Fig 4 ie the absorption becomes endothermic. Provided the electrodes are driven into this regime by prolonged charging at low temperatures, a subsequent increase of temperature will lead to further increases in the charging ratio and, consequently, to high rates of excess enthalpy generation at these higher temperatures. A corollary of these effects is that the charging ratio must become limited at low temperatures. Consideration of Fig 4 in combination with results of the type shown in Fig 3 reveals that the rates of excess enthalpy generation which can be achieved at the intermediate temperatures are dependent on the exact experimental protocol adopted[‡]. Furthermore, it is necessary to allow the temperatures of the calorimeters to rise sufficiently rapidly so as to avoid the compositional changes which are at the root of the behaviour seen in Fig 4. In particular, the protocols required would not be achievable when using isothermal calorimetry (the benefits of which have been much expounded[17]).

An alternative way of describing the influence of the changes in the partial molar heat of absorption with the charging ratio is that the system is subject to positive feedback under particular conditions[15,16] ie an increase of temperature leads to further increases of temperature[§]. We became aware of the effects of such feedback at an early stage of our investigations and reiterate our warnings: such systems need to be handled with due care. The way in which the need for care has influenced our experimental procedures is described below.

[†]In the limit, it destroys the excess enthalpy generation.

[‡]In particular, the time of polarisation at low temperatures has been a variable of our investigations.[15,16]

[§]We do not know whether the changes induced by the reversal of the partial molar heat of absorption with the charging ratio are the only reason for such positive feedback: we suspect that there are further factors which enhance this effect.

We note finally that the approach to the "hidden variables" embodied in conventional control theory is itself unduly restrictive. Comprehensive investigations require us to include the spatial dependencies, equation (7):

Hidden Variables: the Actual Situation
(Spatial Dependence Included)

$$
\begin{aligned}
Q_f = f_5\Big\{ & E_{cell}(t,z),\ \frac{\partial E_{cell}(t,z)}{\partial t},\ \ldots \frac{\partial E_{cell}(t,z)}{\partial z},\ \ldots; \\
& \theta(t,z),\ \frac{\partial \theta(t,z)}{\partial t},\ \ldots \frac{\partial \theta(t,z)}{\partial z},\ \ldots; \\
& X(t,z),\ \frac{\partial X(t,z)}{\partial t},\ \ldots \frac{\partial X(t,z)}{\partial z},\ \ldots \frac{\partial^2 X(t,z)}{\partial z^2}\ \ldots; \\
& \phi,(t,z),\ \frac{\partial \phi(t,z)}{\partial t},\ \ldots \frac{\partial \phi(t,z)}{\partial z},\ \ldots; \\
& \text{phase changes},(t,z),\ \frac{\partial[\text{ phase changes (t,z)}]}{\partial \text{t}},\ \ldots; \\
& \frac{\partial[\text{ phase changes (t,z)}]}{\partial \text{z}},\ \ldots; \quad \Big\}
\end{aligned}
\tag{7}
$$

(for simplicity, only one coordinate has been taken into account). While some of these spatial dependencies would normally be expected to be small,[¶] other dependencies will certainly be important. Thus the inclusion of $\partial E(t,z)/\partial z$ focusses our attention on the effects of poor cell design leading to non-uniform distributions of the cathode potential which prevent the achievement of uniform high charging ratios. At a more elaborate level, this term illustrates the importance of the secondary and tertiary current distribution. The slope impedance of the electrode reaction counteracts the non-uniformities introduced by the primary current distribution. The deposition of blocking layers is a particularly important factor in achieving uniform charging at the macroscopic level. At the same time, the process becomes non-uniform at the microscopic level because of the effects of the tertiary current distribution. This is a topic beyond the scope of the present report[3].

Equation (7) also points to the fact that the effects of steady-state and non-steady-state diffusion need to be expored by using suitable cell and electrode designs as well as suitable experimental protocols (the terms $\partial X(t,z)/\partial z$ and $\partial^2 X(t,z)/\partial z^2$). There is fragmentary evidence for the importance of these terms (for the observation of the nuclear signatures as well as the generation of excess enthalpy). We also note that there are yet further terms which need to be incorporated into the state vectors eg the term $X(t,z)\partial\phi(t,z)/\partial z$ for systems in which migration in the lattice is important. The complexity of the required investigation should be contrasted with the naivety embodied in Isothermal Calorimetry, equation (8).

[¶]Thus for normal cell designs $\partial\theta(t,z)/\partial z$ might be expected to be negligible. However, note that chemical flow reactors are frequently optimised by controlling the variation of temperature with distance. Equivalent concepts could well apply to larger scale devices generating excess enthalpy.

$$Q_f = f_6\left\{E_{cell}(t)\right\} \tag{8}$$

Implementation of the Calorimetric Measurements: The Search for Simplicity and Accuracy

Instrumentation

It will be apparent from the previous section that the search for the "hidden variables" and the implementation of the protocols required to achieve high rates of excess enthalpy generation at intermediate temperatures requires that the systems should not be subjected to constraints. The choice of Isoperibolic Calorimetry fulfills this requirement.

Further considerations are that the exploration of even a small part of the parameter space requires the execution of large numbers of experiments and that the durations of these experiments are long (typically 10-90 days). It follows therefore that one needs to search for low unit costs in the instrumentation and simple on-line evaluation procedures to cope with the large volume of data generated. At the same time, it is necessary to aim for precision and accuracy in the data treatments so as to reach a high level of statistical significance of the derived information.

Our solutions for achieving these multiple objectives are known in part. The "main stream" of the instrumentation consists of up to 64 calorimeters (typically two five factor experiments) of the type illustrated in Fig 5 (the design of these is discussed briefly below) housed in 16 water thermostats ie up to 4 calorimeters per thermostat. These thermostats consist of 1cm thick Perspex sheeting insulated by 2cm thick sheets of polystyrene foam housed in an aluminium casing; windows are cut in the casing and foam insulation so as to allow viewing of the cell contents and video recording of the experiments where necessary. The ensemble of thermostats is housed in a single thermostatted room whose temperature is controlled to $\pm$ 0.5°C using two independent temperature controllers. The thermostats are cooled using Techne cooler units and their temperature is controlled using Techne TE8A Tempette temperature-stirrer control units. The temperature of the thermostats is set to be equal to the room temperature. We have found that in this way it is possible to control the thermostat temperature locally to within $\pm$0.003°C and to within $\pm$0.01°C throughout the bath.

The calorimetric electrochemical cells consist of single compartment Dewars silvered in their top portion. This silvering ensures that heat transfer is confined to radiation across the lower, unsilvered portion. The heat transfer coefficents are then virtually independent both of the level of water in the thermostats and of the electrolyte in the cells provided both levels are maintained in the silvered regions of the Dewars (the heat transfer coefficients are given to a close approximation by the product of the Stefan-Bolzmann coefficient and the radiant surface areas). Nevertheless, the level of water in the thermostat is controlled to within 0.3 cm and the Dewar cells are refilled on a controlled schedule, the level being inspected using a dentist's mirror (the level falls typically by 0.8 cm between the refilling of the cells because the cells are "open" ie the deuterium and oxygen produced in the electrolysis vent to the atmosphere). A schedule of additions is kept to monitor the Faradaic efficiency of the systems and, at higher temperatuares, the combined effects of electrolysis and of evaporation (see further below).

The Pd, Pd-alloy or Pt cathodes used in these investigations are spot-welded to Pt lead wires and surrounded either by a helical Pt wire anode wound on a glass frame or else by a Pt wire mesh cylinder. The lead wires are covered by glass to avoid recombination of deuterium and oxygen produced in the electrolysis. Temperatures of the cells (and of the thermostats) are read every 300s using specially stabilised thermistors, (Thermometrics Ultrastable Thermistors, $\sim$ 10kΩ $\pm$ 0.02% stability per year) calibrated against NIST calibrated thermometers. These thermistors are connected to Dumet leads and are housed in special drawn thin walled glass tubing. The measuring circuits are maintained open for 290s, then closed for 10s, readings being taken 9s after closure. The atmospheric pressure is also monitored continuously to within 0.1 millibars.

The cells are calibrated using constant currents supplied by galvanostats (Hi-Tek DT 2101 potentiostats connected as galvanostats) to resistor chains. These resistor chains are made up of high stability metal film resistors maintained in glass tubes filled with heat transfer oil. In the normal mode of operation the constant currents are supplied for 12 hours exactly 12 hours after the refilling of the cells, the temperature decay then being followed for a further 24 hours. We note that the thermal relaxation time of the Dewar cells, $\tau = C_{P,D_2O,\ell}M^\circ/4k'_R$ (see below), is $\sim$1 hour so that all process are followed for a minimum of $\sim$12 thermal relaxation times.

Polarisations are usually carried out galvanostatically again using Hi-Tek DT2101 potentiostats connected as galvanostats. Special steps are taken to guard against oscillations[10]; the ripple content of the current is 0.04% of the D.C. current and these D.C. currents are normally set with an accuracy of 0.02-0.1%. For experiments at temperatures up to 60°C, up to 4 calorimetric cells are connected in series; for experiments up to the boiling point, cells are supplied by individual galvanostats.

Data acquisition from the ensemble of cells is carried out by Keithley 199 System DMM/Scanner Units operated in conjunction with Keithley 705 Scanners, these Scanners being controlled by a single data acquisition computer.

We draw attention also to some further important design features of the calorimetric cells as well as their mode of operation. As has been noted above, heat transfer from the cells is controlled by radiation through the lower unsilvered part. Conduction through the top of the cell is reduced as far as possible by making all connections through a deep Kel-F plug which is further sealed to the cell by using Parafilm. The base of the inner tube is flat and the electrode assemble is supported on this base by using a 0.5 cm thick Kel-F plug. In this way we ensure that there are no stagnant zones of electrolyte in the cell. Gas evolution at the electrodes ensures rapid radial mixing (time scale $\sim$3s); axial mixing is somewhat slower (time scale $\sim$20s); but this time scale is still so short compared to the thermal relaxation time of the system ($\sim$3,600s) that the cells behave as "well-stirred tanks".

The level of electrolyte in the cells is set to be 1 cm below the base of the Kel-F plugs following refilling of the cells. This level falls a further $\sim$0.8 cm in the intervals between the refilling in the normal mode of operation (see above). The minimisation of the gas volume is important both to assure the safe operation of the cells and to minimise the thermal capacity of the head space in comparison to the heavy water equivalents of the Dewars and their contents (this is dominated by the thermal capacity of the electrolyte). For operation at temperatures close to the boiling point, individual cells are driven towards boiling and are then allowed to boil dry before disconnecting the cells from the galvanostats. There are three major reasons for choosing this procedure. In the first place, the fall of electrolyte in the cells ensures the effective disengagement of gas and vapour from the electrolyte

(without producing spray). Secondly, we note that the rates of excess enthalpy production can reach such high values that the rates of thermal output per unit area of the electrodes are close to the transition from nucleate to film boiling for normal operation (ie in the absence of gas evolution). It is important therefore to remove the electrolyte before interrupting the polarisations. Thirdly, it becomes possible to study the cooling curves in the empty cells following polarisations under such extreme conditions[18].

Fourthly, we note that the dimensions of the cells are usually chosen to give a rate of change of the cell temperature with enthalpy input of about 10 K W^{-1}; this rather high value allows us to achieve high precision and accuracy in carrying out the thermal balances for a wide range of operating conditions (electrode dimensions and current densities). However, the high value is also important for the achievement of "boiling conditions" at relatively low cell currents (typically 0.5 A) and, in turn, low rates of gas evolution. Low rates of gas evolution are important to prevent spray formation during the operation of cells close to the boiling point.

Modelling of the Cells and Data Processing

The behaviour of the cells illustrated in Fig 5 can be expressed by the "Black Box Model", Fig 6. By taking the temperature of the thermostat as the reference value for all the enthalpy flows,we can describe this model by the differential equation[15,16,19]

Model of the Calorimeter

$$\underset{\substack{\text{rate of}\\ \text{change in the enthalpy}\\ \text{content of the}\\ \text{calorimeter}}}{C_{P,D_2O,\ell}M^{\circ}\left(\frac{d\Delta\theta}{dt}\right)} = \underset{\substack{\text{rate of}\\ \text{enthalpy input due}\\ \text{to electrolysis}}}{[E_{cell}(t) - E_{thermoneutral,bath}]I} + \underset{\substack{\text{rate of}\\ \text{excess}\\ \text{enthalpy}\\ \text{generation}}}{Q_f(t)}$$

$$+\underbrace{\Delta QH(t-t_1) - \Delta QH(t-t_2)}_{\text{calibration pulse}} - \underbrace{\frac{3I}{4F}\left[\frac{P(t)}{P^{*} - P(t)}\right]\left[(C_{P,D_2O,g} - C_{P,D_2O,\ell})\Delta\theta(t) + L_{D_2O}\right]}_{\text{rate of enthalpy removal in the gas stream}}$$

$$\underbrace{-k'_R[(\theta_{bath} + \Delta\theta(t))^4 - \theta_{bath}^4]}_{\substack{\text{rate of}\\ \text{radiative heat transfer to the water bath}}} \qquad (9)$$

In common with our earlier analyses (eg see[10]) we have expressed the heat transfer from the cell by a purely radiative term: any small conductive contribution, $k_c\ \Delta\theta$, is lumped into this term by increasing the true radiative heat transfer coefficient, k_R, to k'_R. As we have shown elsewhere[10] this leads to a small underestimate of the heat output and, therefore, to a small underestimate of Q_f.

It is evident that it is necessary to calibrate the system (however see below for the application of the lower bound heat transfer coefficient) and we have normally done this by using the square pulse enthalpy input $\Delta QH(t-t_1) - \Delta QH(t-t_2)$ (other methods will be discussed elsewhere[3]). The result of applying such a calibration pulse is illustrated in the schematic diagram, Fig 7. Heat transfer coefficients can then be evaluated in a number of ways which include:

(i) applications of the steady state approximation, $\left(C_{P,D_2O,\ell}M^\circ\frac{d\Delta\theta}{dt} = 0\right)$

(ii) making a thermal balance at a single point while lifting the steady-state approximation;

(iii) applying linear regression procedures;

(iv) applying multi-linear regression procedures;

(v) applying non-linear regression procedures.

In our investigations carried out up to October 1989 (and which formed the basis of our first full paper on this topic*) we used two procedures based on (ii) coupled to detailed analyses of selected data sets by means of (v). We consider first of all the first of the procedures based on (ii). In this we assume that there is no generation of excess enthalpy in the system and we rearrange equation (9) to give the "lower bound heat transfer coefficient"

$$(k'_R)_{11} = \Big\{ [E_{cell}(t) - E_{thermoneutral,\ bath}]I + \Delta QH(t-t_1) - \Delta QH(t-t_2) - \frac{3I}{4F}\left[\frac{P}{P^* - P}\right]\left[(C_{P,D_2O,g} - C_{P,D_2O,\ell})\Delta\theta(t) + L_{D_2O}\right] - C_{P,D_2O,\ell}\,M^\circ\left(\frac{d\Delta\theta}{dt}\right)_t \Big\} \Big/ [(\theta_{bath} + \Delta\theta(t))^4 - \theta^4_{bath}] \quad (10)$$

The reason why $(k'_R)_{11}$ is a "lower bound" is because the inclusion of any excess enthalpy term inevitably raises the derived heat transfer coefficient. For appropriate blank experiments, (Pt in H_2O or D_2O), $(k'_R)_{11}$ rapidly approaches a constant value and for cells of the type in current use the standard deviation of the measurements is 0.1 - 0.2% of the mean. The cells used in the first part of our work (up to October 1989) were not silvered in the top portion. In consequence the heat transfer coefficients fell progressively with time. Nevertheless the standard deviations of $(k'_R)_{11}$ were comparable to those measured with cells of the type shown in Fig 5 provided measurements were made at fixed times following the refilling of the cells.

We regarded this standard deviation as a measure of the precision of the experiments (and we still hold to that view). The reason why it cannot be regarded as a measure of the

*The contents of this paper were presented at the NSF-EPRI Conference held in Washington in October 1989. The Proceedings of that Conference have not been published

accuracy (even for blank experiments) is because the possible reduction of electrogenerated oxygen would contribute an extra rate of enthalpy generation (electrogenerated hydrogen of deuterium cannot be reoxidised at the oxide coated Pt anodes). It is important therefore to calibrate the system so as to compare the precision of $(k'_R)_{11}$ with the accuracy of k'_R[†]. The most immediate way of achieving such calibrations is to make a thermal balance at a single point in time just before the termination of the calibration pulse, $t = t_2$, Fig 7. We have designated the heat transfer coefficient derived in this way as $(k'_R)_2$. Equation (9) leads to the value

$$
\begin{aligned}
(k'_R)_2 \;=\; \Big\{ & [E_{cell}(\Delta\theta_1, t_2) - E_{cell}(\Delta\theta_2, t_2)]I \;+\; \Delta Q \\
& - \frac{3I}{4F}\left[\frac{P(t)}{P^* - P(t)}\right]\Big[(C_{P,D_2O,g} - C_{P,D_2O,\ell})\Delta\theta_2(t_2) + L_{D_2O}\Big] \\
& + \frac{3I}{4F}\left[\frac{P(0)}{P^* - P(0)}\right]\Big[(C_{P,D_2O,g} - C_{P,D_2O,\ell})\Delta\theta_1(t_2) + L_{D_2O}\Big] \\
& \frac{-C_{P,D_2O,\ell}\, M^\circ\left(\frac{d\Delta\theta}{dt}\right)_{\Delta\theta_2,t_2} + C_{P,D_2O,\ell}\, M^\circ\left(\frac{d\Delta\theta}{dt}\right)_{\Delta\theta_1,t_2}\Big\}}{[(\theta_{bath} + \Delta\theta(t))^4 - (\theta_{bath} + \Delta\theta(0))^4]}
\end{aligned}
\tag{11}
$$

for cells of the type illustrated in Fig 5. The major consequence of the fall of the heat transfer coefficient with time for the cells used in the first part of our work was that the differential equation governing the behaviour was inhomogeneous (as well as non-linear). To a close approximation:

$$
\begin{aligned}
[C_{P,D_2O,\ell}M^0\big[1 - \frac{It}{2FM^0}\big]\frac{d\Delta\theta}{dt} = & \\
& \Big[E_{cell}(t) - E_{thermoneutral,bath}\Big]I + Q_f(t) + \Delta QH[t - t_1] - \Delta QH[t - t_2] \\
& -\frac{3I}{4F}\left[\frac{P}{P\star - P}\right]\Big[(C_{P,D_2O,g} - C_{P,D_2O,\ell})\Delta\theta + L\Big] \\
& -k'_R\left[1 - \frac{(1+\lambda)It}{2FM^0}\right][(\theta_{bath} + \Delta\theta)^4 - \theta^4_{bath}]
\end{aligned}
\tag{12}
$$

Approximate analytical solutions of equation (12) give the thermal balance at a point just before the application of the calibration pulse, $t = t_1$, Fig 7, and this balance is determined by the heat transfer coefficient[3,10], $(k'_R)_4$.

[†]The values of $(k'_R)_{11}$ as determined for blank experiments can be used to obtain precise values of the "lower bound rates of excess enthalpy generation, $(Q_f)_{11}$".

$$
\begin{aligned}
(k'_R)_4 \;=\; & \Big\{\Delta Q \\
& - \frac{3I}{4F}\Big[\frac{P(t)}{P^* - P(t)}\Big]\Big[(C_{P,D_2O,g} - C_{P,D_2O,\ell})\Delta\theta_2(t_2) + L_{D_2O}\Big] \\
& + \frac{3I}{4F}\Big[\frac{P(0)}{P^* - P(0)}\Big]\Big[(C_{P,D_2O,g} - C_{P,D_2O,\ell})\Delta\theta_1(t_2) + L_{D_2O}\Big] \\
& \frac{-C_{P,D_2O,\ell}\; M^\circ\Big(\frac{d\Delta\theta}{dt}\Big)_{\Delta\theta_2,t_2} + C_{P,D_2O,\ell}\; M^\circ\Big(\frac{d\Delta\theta}{dt}\Big)_{\Delta\theta_1,t_2}\Big\}}{[(\theta_{bath} + \Delta\theta(t))^4 - (\theta_{bath} + \Delta\theta(0))^4]}
\end{aligned}
\tag{13}
$$

The excess enthalpies calculated by using $(k'_R)_2$,$(Q_f)_2$, are virtually identical to those calculated using $(k'_R)_4$, $(Q_f)_4$, a fact which has not been understood[21]‡. We note here that the term

$$
\Big[C_{P,D_2O,\ell}M^\circ(\frac{d\Delta\theta}{dt})_{\Delta\theta_2,t_2} - \Big[C_{P,D_2O,\ell}M^\circ(\frac{d\Delta\theta}{dt})_{\Delta\theta_1,t_2}\Big]
$$

was not included in the analysis developed by the group at General Electric ie their analysis was based on the steady-state approximation (i) rather than (ii). The omission of that term is sometimes within the limits of the experimental errors of $(k'_R)_2$ or $(k'_R)_4$§. However, in general, it is not permissible to omit the rate of change of the enthalpy content of the calorimeter $C_{P,D_2O,\ell}M^\circ\Big(\frac{d\Delta\theta}{dt}\Big)$, (eg in the calculation of $(k'_R)_{11}$) and this is especially true for calorimeters modelled by equations such as (12) where no steady-state is reached.

The relative standard deviations of $(k'_R)_2$ or $(k'_R)_4$ are in the range 1-2% of the mean and these standard deviations are measures of the accuracy which can be achieved by making the thermal balances at a single point. There are two major reasons for the $\sim$ order of magnitude difference between the precision and accuracy of the calibrations. The first is the fact that the denominators of equations (11), (13), (14), and (15) are determined by the difference of two large quantities whereas that of equation (10) is determined by one of

‡We focussed attention on $(Q_f)_4$ rather than $(Q_f)_2$ for three major reasons. Firstly, because the mathematical analysis shows that the thermal balance should be made at that point; secondly, because $(Q_f)_2$ is slightly smaller than $(Q_f)_4$ (and because we have always attempted to make conservative estimates); thirdly, because we chose to avoid drawing attention to the fact that there is positive feedback in the system.

§At sufficiently low temperatures (say $\theta_{cell} < 40°C$) it is also permissible to omit the differences in the rates of evaporative cooling at $\Delta\theta_2$ and $\Delta\theta$. so that we obtain the approximate values of the heat transfer coefficients

$$
(k'_R)_2 = \frac{\Delta Q - [E_{cell}(\Delta\theta_1, t_2) - E_{cell}(\Delta\theta_2, t_2)]I}{(\theta_{bath} + \Delta\theta_2)^4 - (\theta_{bath} + \Delta\theta_1)^4} \tag{14}
$$

$$
(k'_R)_4 = \frac{\Delta Q}{(\theta_{bath} + \Delta\theta_2)^4 - (\theta_{bath} + \Delta\theta_1)^4} \tag{15}
$$

the quantities alone. The second reason is that high accuracy cannot be achieved by making a thermal balance at a single point[¶]. The ultimate limit of the achievable accuracy can only be reached by fitting the integrals of the differential equations to the experimental data sets[‡‡].

Although the accuracy of $(k'_R)_2$ and $(k'_R)_4$ is perfectly adequate to assess whether or not there is excess enthalpy generation in the Pd/D_2O system, we regarded the disparity between the precision and accuracy of the measurements to be unsatisfactory. In the normal course of events the development of the data processing would have moved sequentially through the procedures (ii)-(v) listed above. However, owing to the pressure of events at the time, we moved directly to (v). There were several reasons which dictated this choice, the principal one being the fact that the equation governing the behaviour of the calorimeters, equation (12), is not well-suited for the application of linear or multi-linear regression methods[‖].

We will not discuss the use of non-linear regression techniques in this paper beyond noting that the accuracy of the heat transfer coefficients derived is in the range 0.1-0.2% of the mean ie the accuracy which can be achieved by using the integrated equations is comparable to the precision which can be achieved by making thermal balances at single points in time. The question of the precision and accuracy of the measurements can be more conveniently assessed by using the methods delineated in the next Section. We note here that we have been unable to develop the non-linear regression methods to the point where they are suitable for routine applications to large numbers of data sets. The principal reason is that these methods are iterative and therefore require extensive computation (especially as it is necessary also to integrate equation (9) numerically). Instead, we now rely on simple linear regression which has the advantage of "working at first shot". However, as we shall see, the particular way of implementing linear regression has been strongly influenced by our experience with non-linear regression procedures.

Methods of data processing in current use

The first step in our current approach to the data processing is the reimplementation of the analysis based on the "lower bound heat transfer coefficient $(k'_R)_{11}$". There are four major reasons for our return to this particular method: in the first place, it is independent of any method of calibration which might be adopted for calibrating the cells; secondly, it is quite sufficient in order to make a rapid assessment of the question: "is there or is there not a generation of excess enthalpy in the $Pd\text{-}D_2O$ system?" and, furthermore, to give a "lower bound estimate of the rate of excess enthalpy generation, $(Q_f)_{11}$"; thirdly, the method is particularly suitable for incorporating in spreadsheet calculations and, therefore, for dealing with the large volume of data generated by our experimental programme; fourthly, related to the first and second aspects, the method is well suited for assessing the results of other research groups, especially of those research groups which concluded that there is no such excess enthalpy generation (where this conclusion has been based on inadequate or

[¶]This is a situation which is well understood in the field of chemical kinetics where it has long been known that one must fit the integrated rate equations to the experimental data in order to achieve accurate values of the rate constants. The comparison of this case to the fitting of equations (9) and (12) will be self-evident.

[‡‡]Alternatively, we can change the experiment design and use Fourier Transform techniques. This is a topic which we will discuss elsewhere[3].

[‖]We were unable to implement the change to the cell design, Fig 5, before October 1989. This change removed the time-dependence of the heat transfer coefficients (compare equations (10) and (12)) and, thereby, also the need to implement (v).

even incorrect calibration of the cells used).

We can illustrate the utility of the method by considering the application to the Pd-H_2O and Pd-D_2O systems. For the former there is a marked decrease of $(k'_R)_{11}$ at short times which is due to the excess enthalpy generated by the absorbtion of hydrogen in the lattice (the effect is so large that $(k'_R)_{11}$ is initially negative [15,16]). However, at long times $(k'_R)_{11}$ is again equal to $(k'_R)_2$ (more exactly, it is equal to the heat transfer coefficient determined by non-linear regression fitting, $(k'_R)_5$, or to the heat transfer coefficient derived by linear regression fitting, $(k'_R)_{22}$, see below). We conclude that there is no generation of excess enthalpy at long times in the Pd/H_2O system.

The situation is entirely different for the Pd/D_2O system. Here $(k'_R)_{11}$ is also initially negative due to the heat of absorption of deuterium in the lattice. However, $(k'_R)_{11}$ never reaches the true value $(k'_R)_2$, $(k'_R)_5$ or $(k'_R)_{22}$ because a new source of excess enthalpy develops, the source of enthalpy which we have attributed to nuclear processes in the lattice. This source of excess enthalpy increases to such an extent that $(k'_R)_{11}$ again becomes negative on the last day of operation as the cell boils dry (which terminates the experiment[15,16]).

Although $(k'_R)_{11}$ never reaches the true value of the heat transfer coefficient ($(k'_R)_2$, $(k'_R)_5$ or $(k'_R)_{22}$), the maximum value reached can be used to estimate a lower bound of the rate of excess enthalpy generation, $(Q_f)_{11}$. The judgement that there is such an excess enthalpy generation in the Pd-D_2O system can be made at the semi-quantitative level quite independently of the calibration of the cells[15,16].

However, we clearly require the true value of the heat transfer coefficients, an assessment of their accuracy and a means of implementing these evaluations rapidly as part of a spreadsheet procedure. At the same time such an evaluation should provide a means of assessing the validity (or otherwise) of the modelling of the "Black Box" as represented by the relevent differential equation. In developing the procedures in current use, which are based on linear regression fitting (iii), we have been guided by our experience of the application of non-linear regression procedures specifically, the need to fit the integrals of the differential equations to the experimental data.

We consider first of all a means of increasing the precision of the "lower bound heat transfer coefficient" while at the same time providing a means of assessing the validity of the modelling, equation (9). Although we cannot obtain a generally valid analytical solution of this equation, we can integrate the left and right hand sides over a chosen interval 0 to t to give

$$C_{P,D_2O,\ell}\ M^{\circ}[\Delta\theta(t) - \Delta\theta(0)]$$

$$= \int_0^t [Enthalpy\ input(\tau)]d\tau\ +\ \Delta Qt\ -\ \int_0^t [\Delta H_{evap}(\tau)]d\tau$$

$$-(k'_R)_{31}\ \int_0^t [(\theta_{bath} + \Delta\theta(\tau))^4 - \theta_{bath}^4]d\tau \qquad (16)$$

In this equation we have designated the "lower bound heat transfer coefficient" by $(k'_R)_{31}$ rather than $(k'_R)_{11}$ to denote that it is derived by using the integral of equation (9) rather than by the equation itself (which leads to the definition of $(k'_R)_{11}$, equation (10), and which

contains the differential $d\Delta\theta/dt$). In the evaluation it is convenient to set the time origin at the start of the heater calibration pulse, eg see Fig 8. It is normally sufficient to use the trapezium rule to evaluate the integrals in equation (16); in exceptional circumstances (very rapid changes of the kernel with τ), Simpson's rule can be used (eg see[18]). Having derived the various terms in equation (16), we can rearrange this equation to

$$\frac{\left\{\int_0^t [Enthalpy\ input(\tau)]d\tau + \Delta Qt\ -\ \int_0^t [\Delta H_{evap}(\tau)]d\tau\right\}}{\int_0^t [(\theta_{bath}+\Delta\theta(\tau))^4 - \theta_{bath}^4]d\tau} =$$

$$(k'_R)_{31} + \frac{C_{P,D_2O,\ell}\ M^\circ[\Delta\theta(t)-\Delta\theta(0)]}{\int_0^t [(\theta_{bath}+\Delta\theta(\tau))^4 - \theta_{bath}^4]}d\tau \qquad (17)$$

and plot the left-hand-side (which is derived from the experimental data) versus

$$\frac{\Delta\theta(t)-\Delta\theta(0)}{\int_0^t [\theta_{bath}+\Delta\theta(\tau))^4 - \theta_{bath}^4]d\tau}$$

(which is also known), Fig 9. The slope then gives $C_{P,D_2O,\ell}M^\circ$ (which is required to achieve optimum precision, see below) while the intercept gives $(k'_R)_{31}$. Exact evaluations use linear regression which automatically gives also the correlation coefficient. These correlation coefficients are typically in excess of 0.9999 indicating the adequacy of the modelling, equation (9).

We observe next that we can also evaluate $(k'_R)_{31}$ by using

$$(k'_R)_{31} = \frac{\left\{\int_0^t [Enthalpy\ input(\tau)]d\tau + \Delta Qt - \int_0^t [\Delta H_{evap}(\tau)]d\tau - C_{P,D_2O,\ell}\ M^\circ[\Delta\theta(t)-\Delta\theta(0)]\right\}}{\int_0^t [(\theta_{bath}+\Delta\theta(\tau))^4 - \theta_{bath}^4]} \qquad (18)$$

Such evaluations only require values of $C_{P,D_2O,\ell}M^\circ$ of reasonable accuracy provided they are carried out at long times (of the parameters determining the performance of the calorimeters, $C_{P,D_2O,\ell}M^\circ$ is the most difficult to determine accurately; however, at long times $(k'_R)_{31}$ is insensitive to changes in $C_{P,D_2O,\ell}M^\circ$). Repeated applications of equation (18) show that the standard deviation is $\sim 0.01\%$ of the mean ie the application of the integrated form (18) of equation (9) decreases the standard deviation by $\sim$1 order of

magnitude. Fig 10 gives an illustration of the precision for one such set of measurements.

Similar considerations apply to the determination of the accuracy of the heat transfer coefficients. In this case let us consider the possible effects of excess enthalpy generation by including the term Q_f in equation (16) viz

$$\begin{aligned} & C_{P,D_2O,\ell}\, M^{\circ}[\Delta\theta(t) - \Delta\theta(0)] \\ & = \int_0^t [Enthalpy\ input(\tau)]d\tau + \int_0^t Q_f(\tau)d\tau + \Delta Qt - \int_0^t [\Delta H_{evap}(\tau)]d\tau \\ & \qquad -(k'_R)_{31} \int_0^t [(\theta_{bath} + \Delta\theta(\tau))^4 - \theta_{bath}^4]d\tau \end{aligned} \tag{19}$$

We can also carry out an integration using the values of $E_{cell}, Q_f, P \text{and} \Delta\theta$ just before the applications of the heater calibration pulse

$$0 = [Enthalpy\ input(0)]t + Q_f(0)t - [\Delta H_{evap}(0)]t - k'_R[(\theta_{bath} + \Delta\theta(0))^4 - \theta_{bath}^4]t \tag{20}$$

With the assumption that $Q_f(t)$ is constant and equal to $Q_f(0)$ (which should be valid over short experiment durations) we can subtract equation (20) from (19) so as to eliminate the unknown rate of excess enthalpy generation. With some rearrangement we obtain

$$\begin{aligned} (k'_R) = (k'_R)_{22} = & \Big\{\int_0^t [Enthalpy\ input(\tau)]d\tau - [Enthalpy\ input(0)]t \\ & - \int_0^t [\Delta H_{evap}(\tau)]dt + [\Delta H_{evap}(0)]t \\ & + \Delta Qt - C_{P,D_2O,\ell}\, M^{\circ}[\Delta\theta(t) - \Delta\theta(0)]\Big\} \\ & \Big/ \Big\{\int_0^t [(\theta_{bath} + \Delta\theta(\tau))^4 - \theta_{bath}^4]d\tau - [(\theta_{bath} + \Delta\theta(0))^4 - \theta_{bath}^4]t\Big\} \end{aligned} \tag{21}$$

As the unknown rates of excess enthalpy generation have been eliminated, the heat transfer coefficient determined from equation (21) becomes the true heat transfer coefficient $(k'_R)_{22}$ (the suffix 22 denotes that the evaluation has been carried out using the integrals of all the experimental quantities). In determining $(k'_R)_{22}$, it is convenient to use the values of $C_{P,D_2O,\ell}M^{\circ}$ derived from the application of equation (17)**. The standard deviations of $(k'_R)_{22}$ are now reduced to $\sim 0.1\%$ of the mean ie the accuracy of $(k'_R)_{22}$ is by an order of magnitude better than that of $(k'_R)_2$. Fig 10 gives an illustration of the accuracy of $(k'_R)_{22}$ compared to the precision of $(k'_R)_{31}$.

**It is also possible to develop an equation analagous to (17) but for the estimation of $(k'_R)_{22}$ and $C_{P,D_2O,\ell}M^{\circ}$ by linear regression fitting viz

Several important conclusions follow from this particular method of data processing[††]. In the first place we see that the simple statistical procedure of linear regression fitting to a straight line, equation (17), is sufficient to achieve accurate evaluations (we will comment elsewhere on the comparison of linear and non-linear regression techniques[3]). Secondly, we see that the accuracy of this form of isoperibolic calorimetry is $\pm 0.1\%$[‡‡]. This accuracy could be improved further by calibrating all the instruments used in the experimentation. We consider it unlikely that other types of calorimetry can exceed the accuracy which is achievable using the simple instrumentation, Fig 5. Thirdly, we note that the comparison of the precision and accuracy of the heat transfer coefficients for "blank cells" sets an upper bound on the rate of reduction of oxygen in the system. Although the magnitude of the difference between the means $\overline{(k'_R)_{31}} - \overline{(k'_R)_{22}}$ is very small ($\sim 0.23\%$ of $\overline{(k'_R)_{22}}$ for the example shown), this difference is nevertheless at the $\sim 33\sigma_{(k'_R)_{31}}$ or $\sim 5.1\sigma_{(k'_R)_{22}}$ level and must therefore be judged to be significant. The most likely explanation is that there is a small source of excess enthalpy in the cells which is neglected in determining the "lower bound heat transfer coefficient, $(k'_R)_{31}$," using equation (18). The magnitude of this source can be estimated to be ~ 2.3 mW for the example illustrated.* Rates of enthalpy generation of this magnitude are negligible compared to the rates of excess enthalpy generation observed in the Pd/D_2O system.

Extensions and Further Simplifications of the Experiments

The procedures which we have outlined here meet the objectives which we have set for our work during the last 3 years. On the one hand we have sought simplification and this

$$\frac{\int_0^t [Enthalpy\ input(\tau)]d\tau + [\Delta Q]t - \int_0^t [\Delta H_{evap}(\tau)]d\tau - [Enthalpy\ input(0)]t + [\Delta H_{evap}(0)]t}{\int_0^t [(\theta_{bath} + \Delta\theta(\tau))^4 - \theta_{bath}^4]d\tau - [(\theta_{bath} + \Delta\theta(0))^4 - \theta_{bath}^4]t}$$

$$= (k'_R)_{22} + \frac{C_{P,D_2O,\ell}\ M^\circ[\Delta\theta(t) - \Delta\theta(0)]}{\int_0^t [(\theta_{bath} + \Delta\theta(\tau))^4 - \theta_{bath}^4]d\tau - [(\theta_{bath} + \Delta\theta(0))^4 - \theta_{bath}^4]t} \qquad (22)$$

The values of $C_{P,D_2O,\ell}M^\circ$ derived using this expression are closely similar to those obtained using (17) and the correlation coefficients exceed 0.99999. Nevertheless the errors in the intercepts, $(k'_R)_{22}$, become appreciable because it is necessary to extrapolate over an appreciable range of the abscissa. We prefer therefore to use equation (21) at long times where the values of $(k'_R)_{22}$ become insensitive to changes in in $C_{P,D_2O,\ell}M^\circ$.

[††]We observe that similar methods should be applicable in other areas of the Natural Sciences. To the best of our knowledge, the method which we have set out here has not been used previously.

[‡‡]Statements that isoperibolic calorimetry is accurate to $\pm 10\%$ (eg see[21]) can be seen to be incorrect by at least two orders of magnitude. It is well-known that most forms of isoperibolic calorimetry are correct to $\pm 1\%$ even without implementing advanced methods of data processing. It is not surprising that detailed evaluations using software implemented methods enhance the accuracy by more than one order of magnitude.

*The fact that there is no appreciable reduction of oxygen should have been evident from the comparison of the precision and accuracy of the heat transfer coefficients contained in our recent publications[15,16]. It is also evident from the fact that the volume of H_2O or D_2O added during the course of the experiment matches that lost by electrolysis and evaporation; furthermore the volume of gas evolved matches that for electrolysis eg see [10]. Nevertheless, the recombination of the electrogenerated gases continues to be advanced as the explanation for the observation of excess enthalpy generation[17,20].

objective has been met in two quite distinct ways: firstly, by our return to our preliminary methods of data evaluation based on the "lower bound heat transfer coefficient". This method does not require any calibration of the cells and can give semi-quantitative values of the rates of excess enthalpy generation; it is particularly well suited to the analysis of data obtained with the cell design Fig 5, since the heat transfer coefficients are independent of time. The second way in which we have sought simplification is via the substitution of linear regression procedures for the non-linear regression method which we used in our earlier work[10].

At the same time we have sought an increase in the precision and accuracy of our methods of data analysis. This has again been achieved by adopting the methods which we have described in this paper, due mainly to the application of statistical analysis of the integrals of the experimental data. The underlying objective has been simple: an increase in the level of significance of the derived rates of excess enthalpy generation.

There are, however, two additional ways in which we have been able to simplify the investigations. In the first of these we use the protocols based on the concepts outlined in the first part of this paper to produce high rates of excess enthalpy generation and thereby to drive the cells to the boiling point[15,16], the cells then being allowed to boil to dryness. The main mode of heat flow from the cell is then that due to evaporation/boiling; the rate of excesss enthalpy generation under these extreme conditions can be estimated by measuring the time required to evaporate/boil out the cell contents[15,16]. The second way is based on the measurement of the cooling curves following the interruption of the polarisations and, under extreme conditions, following the boiling to dryness of the cells. The extremely simple conditions which can be achieved in this way are described in a further paper presented at this Meeting[22] (see especially the "Black Box" model, Fig 1 of [22].

Discussion

In the first part of this paper we have given one possible description of the State Variables which may control excess enthalpy generation in the Pd/D_2O system. We have found this type of description useful for several reasons. In the first place, it focusses attention on factors which might otherwise be ignored such as the rôle of the primary, secondary and tertiary current distributions, the influence of stationary or non-stationary diffusion and of migration etc. Secondly, it leads to the search for and recognition of phenomena which have an important influence on the excess enthalpy generation eg the influence of phase changes/reversal in the heat of absorption. Thirdly, it leads to the delineation of experiments which have not so far been attempted. However, the most immediately important factor is that it guides the choices of methodology and experimental protocols.

It goes without saying that the subject is still in its infancy. Thus many of the terms in the State Vector will be interrelated and, in due course, the extent of these interrelations will be revealed by the off-diagonal elements of the matrix representations of the linearised models†. Such an initial characterisation will undoubtedly lead to more detailed characterisation by using the relevant Transfer Functions.

Equally, we must take note of the fact that similar approaches should guide the investigation of the weak nuclear signatures leading to the interrelation of the various signatures. The overall objective, naturally, is to discern the nature of the process or processes which lie at the root of the observed State Vectors.

† However, it will be apparent that there are also markedly non-linear terms in this model.

In the second part of this paper we give first of all an account of the methodology we used in our investigations up to October 1989. The reason why it is still necessary to present such an apologia is because the basis of our conclusions has been misunderstood and misrepresented, a phenomenon which continues to this day. A major aspect of our work in the succeeding phases has been the search for simplicity (both of the instrumentation and data analysis) and for accuracy (so as to raise the statistical significance of our observations). This aspect is also described in the second part of this paper; our aim here has been to show that high accuracy can, indeed, be achieved by adopting appropriate data processing strategies while at the same time retaining the flexibility of the simple instrumentation. The achievement of these twin objectives has allowed us to install an adequately large number of experiments which has allowed us to explore an appreciable part of the parameter space. In turn, this has led to two significant results: high levels of the specific rate of excess enthalpy generation at intermediate temperatures (temperatures required to generate "low grade heat") and the phenomenon of "Heat after Death" with is described in a further paper presented at this meeting[18].

Glossary of Symbols Used

The meaning of additional suffices is defined in the text.

$C_{P,D_2O,g}$	is the heat capacitance of the D_2O vapour.	[J(g Mole)$^{-1}$K^{-1}]
$C_{P,D_2O,\ell}$	is the heat capacitance of liquid D_2O.	[J(g Mole)$^{-1}$K^{-1}]
E_{cell}(t)	is the measured cell voltage at time t.	[V]
$E_{thermoneutral,\ bath}$	is the cell voltage at which the electrolysis of D_2O neither generates heat nor absorbs heat from the surroundings.	[V]
F	is the Faraday.	[coulombs (g Mole)$^{-1}$]
$f_0 - f_6$	are the functions of the stated variables.	
$H(t-t_1)$	$= 0\ for\ t < t_1$ is a Heaviside unity shift function $= 1\ for\ t > t_1$	
$H(t-t_2)$	$= 0\ for\ t < t_2$ is a further Heaviside unity shift function $= 1\ for\ t > t_2$	
ΔH_{evap}	is the rate of evaporative cooling.	[W]
I	is the cell current.	[A]
k'_R	is the radiative heat transfer coefficient from the cell to the surroundings.	[W K^{-4}]
L_{D_2O}	is the latent heat of evaporation of D_2O.	[J (g mole)$^{-1}$]
$M°$	is the heavy water equivalent expressed as the number of Moles of D_2O of the calorimeter at time t=0 (normally chosen to coincide with the refilling of the cell to make up for D_2O losses due to electrolysis and evaporation)	[Moles]
P	is the vapour pressure of D_2O at the cell temperature.	[bar]

P^*	is the atmospheric pressure.	[bar]
P_{D_2}	is the pressure of deuterium.	[bar]
$P_{hydrostatic}$	is the hydrostatic pressure.	[bar]
Q_f(t)	is the rate of generation of excess enthalpy in the cell.	[W]
ΔQ	is the rate of injection of Joule heat into the calibrating resistor.	[W]
t	is the time.	[s]
X	is the charging ratio H/Pd or D/Pd.	
z	is a coordinate.	[cm]
$\Delta\theta$	is the difference in temperature between the cell and the water bath.	[K]
θ_{bath}	is the temperature of the water bath.	[K]
θ_t	is the cell temperature.	[K]
λ	is a parameter characterising the decrease of k'_R with t.	[Mole]
μ	is the chemical potential.	[J]
$\overline{\mu}$	is the electrochemical potential.	[J]
τ	is a time.	[s]
ϕ	is the Galvani potential.	[V]
χ	is the surface potential.	[V]
ψ	is the Volta potential.	[V]

References

1. M. Fleischmann, S. Pons and M. Hawkins, J. Electroanal. Chem., 261 (1989) 301; for corrections see J. Electroanal. Chem., 263 (1989) 187.

2. M.L. Oliphant, P. Harteck and Lord Rutherford, Nature, 133 (1934) 413.

3. To be published.

4. A. Coehn, Z. Elektrochem., 35 (1929) 676.

5. Claudia Bartolomeo, M. Fleischmann, G. Larramona, S. Pons, Jeanne Roulette, H. Sugiura and G. Preparata, "Alfred Coehn and After: the α, β, γ of the Palladium - Hydrogen System" Paper M 1.2 presented at the 4th International Conference on Cold Fusion, Maui, Hawaii, USA (December 6-9, 1993).

6. W.S. Gorsky, Phys. Z. Sowjetunion, 8 (1935) 457.

7. P.W. Bridgeman, "The Physics of High Pressure", Bell and Sons Ltd., London (1949).

8. Lange and Miscenko, Z. Phys. Chem., 149 (1930) 1.
Lange, Z. Elektrochem., 55 (1951) 76.

9. G. Preparata "Cold Fusion '93: Some Theoretical Ideas," paper No. T1.2 presented at the 4th International Conference on Cold Fusion, Maui, Hawaii (December 6-9 1993).

10. M. Fleischmann, S. Pons, M.W. Anderson, L.J. Li and M. Hawkins, "Calorimetry of the palladium–deuterium–heavy water system." J. Electroanal. Chem., 287 (1990) 293.

11. E. Storms, "Review of Experimental Observations about the Cold Fusion Effect"", Fusion Technology 20 (1991) 433.

12. M.C.H. McKubre, S. Crouch-Baker, A.M. Riley, S.I. Smedley and F.L. Tanzella, "Excess Power Observations in Electrochemical Studies of the D/Pd System; the Influence of Loading" in *Frontiers of Cold Fusion* Ed. H. Ikegami, Proceedings of the 3rd International Conference on Cold Fusion, Nagoya October 21-25, 1993, Universal Academy Press Inc., Tokyo, 1993 page 5; ISSN 0915-8502.

13. K.Kunimatsu, H.Hasegawa, A. Kubota, N.Imai, M. Ishikawa, H.Akita and Y. Tsuchida, "Deuterium Loading Ratio and Excess Heat Generation during Electroloysis of Heavy Water by a Palladium Cathode in a Closed Cell Using a Partially Immersed Fuel Cell Anode." in *Frontiers of Cold Fusion* Ed. H. Ikegami, Proceedings of 3rd International Conference on Cold Fusion, Nagoya October 21-25, 1993, Universal Academy Press Inc., Tokyo, 1993 page 31; ISSN 0915-8502.

14. T.B. Flanagan and J.F Lynch, J. Phys. Chem., 79 (1975) 444.

15. Martin Fleischmann and Stanley Pons in: *Frontiers of Cold Fusion: Proceedings of the Third International Conference on Cold Fusion*, Nagoya, Japan (21-25 October 1992), ed. H. Ikegami, Frontiers Science Series No. 4 (FSS-4) p.47.

16. Martin Fleischmann and Stanley Pons, "Calorimetry of the Pd–D_2O system: from simplicity via complications to simplicity." Physics Letters A 176 (1993) 118.

17. D. Morrison, Messages on the Electronic Mail Networks.

18. S. Pons and M. Fleischmann, "Heat after Death" Paper C 2.12 presented at the 4th International Conference on Cold Fusion, Maui, Hawaii, USA (December 6-9), 1993).

19. M. Fleischmann and S. Pons, "Some Comments on the paper Analysis of Experiments on Calorimetry of LiOD/D_2O Electrochemical Cells, R.H. Wilson et al., J. Electroanal. Chem., 332 (1992) 1." J. Electroanal. Chem., 332 (1992) 33.

20. Douglas R.O. Morrison, "Comments on Claims of Excess Enthalpy by Fleischmann and Pons using Simple Cells made to Boil." to be published in Physics Letters A.

21. R.H. Wilson, J.W. Bray, P.G. Kosky, H.B. Vakil and F.G. Will, "Analysis of Experiments on Calorimetry of LiOD/D_2O Electrochemical Cells," J. Electroanal. Chem., 332 (1992) 1.

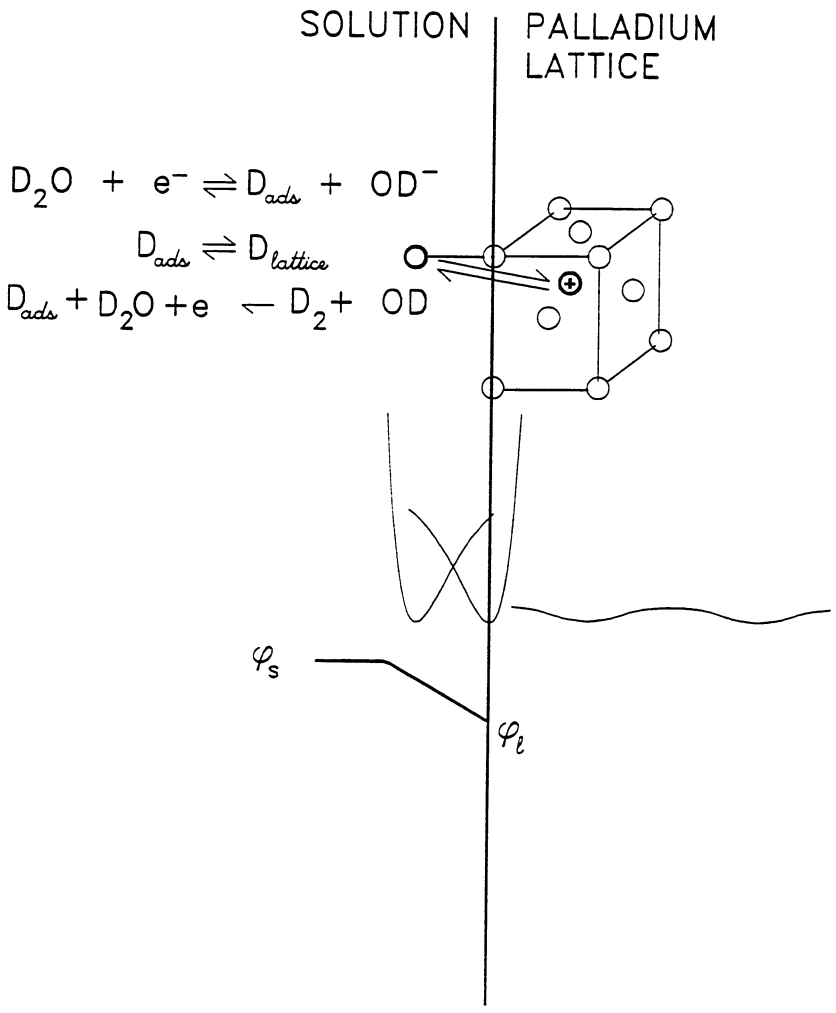

Fig 1. The electrochemical charging of a Pd–cathode.

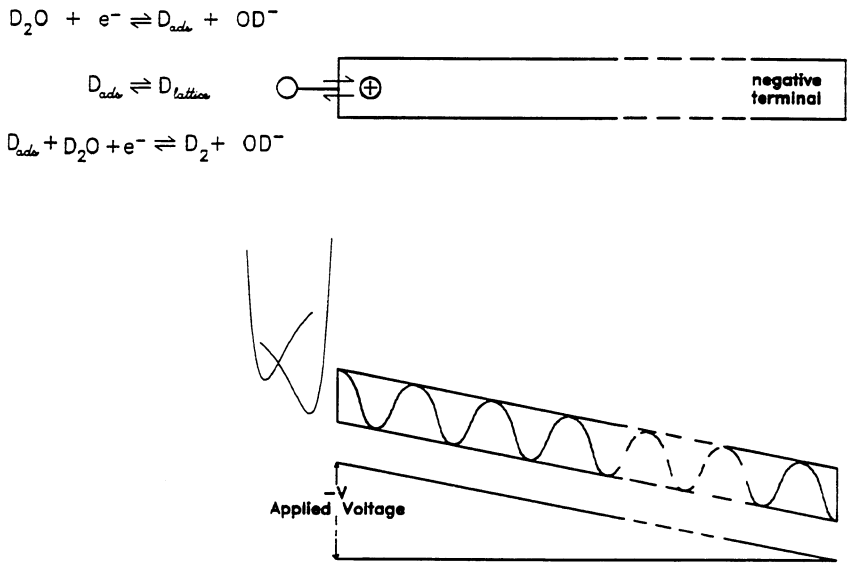

Fig 2. The electrodiffusion of D^+ in a Pd-wire.

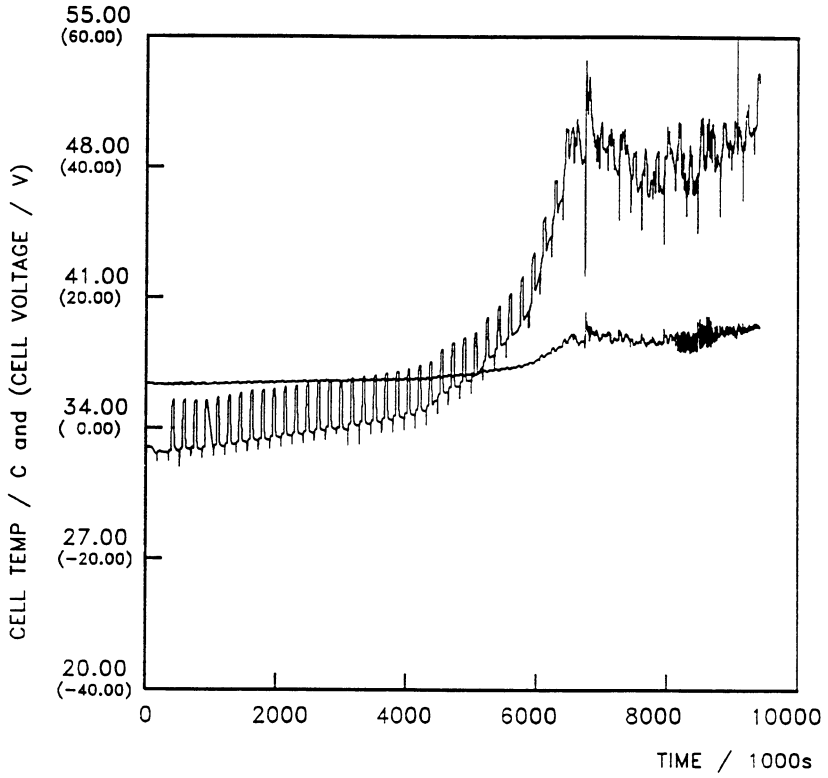

Fig 3A. Temperature–time and Cell Potential–time curves for the polarisation of a 1 mm diameter by 12.5 mm length Pd-10% Rh cathode in 0.1M LiOH in H_2O; Cell current: 0.200 A.

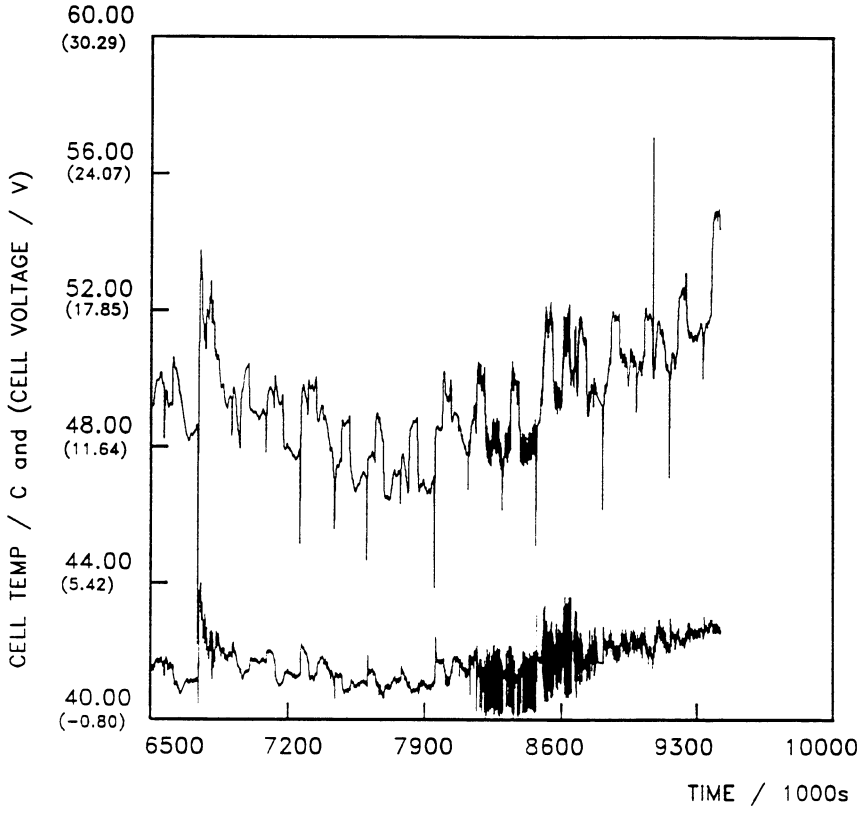

Fig 3B. Expanded section of Fig 3A.

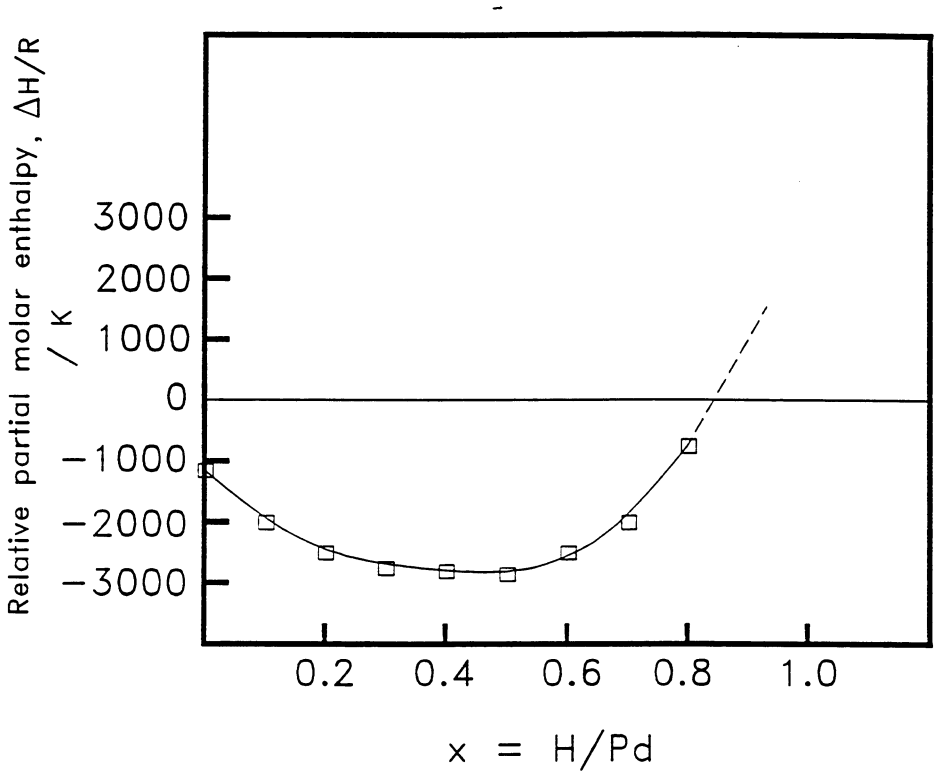

Fig 4. The variation of the relative partial molar enthalpy of hydrogen in Palladium with the charging ratio.

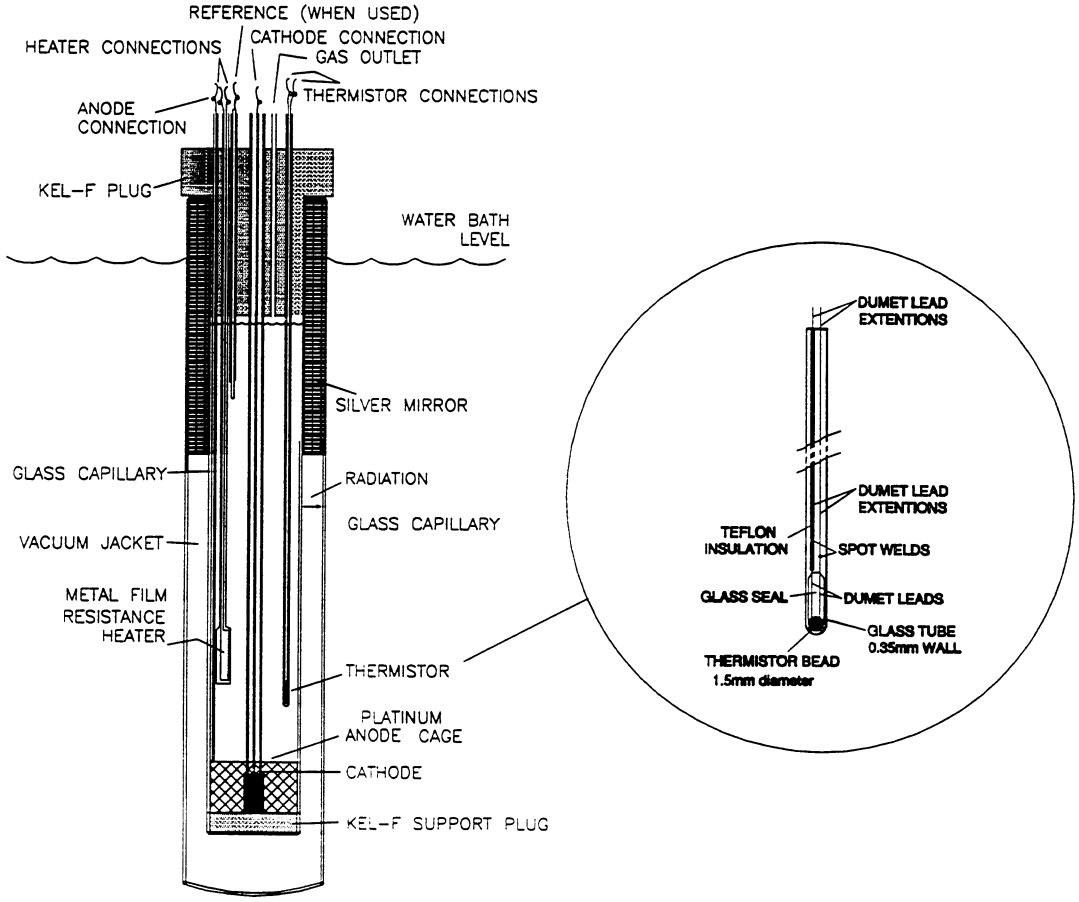

Fig 5. The calorimetric cell; inset: the thermistor assembly.

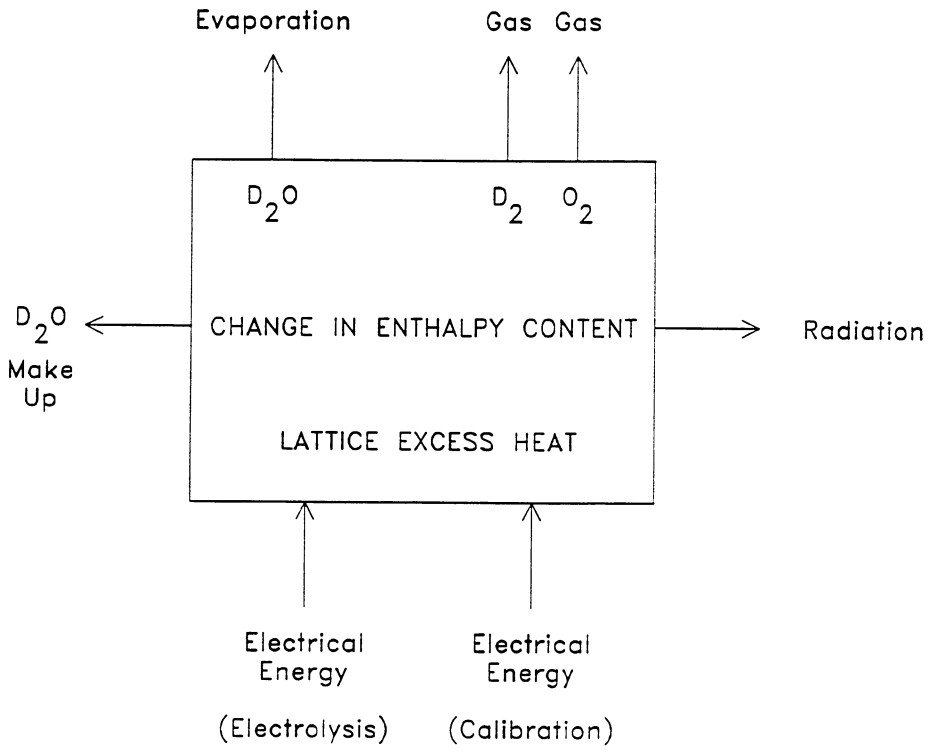

Fig 6. The "Black Box Model" of the Calorimeter.

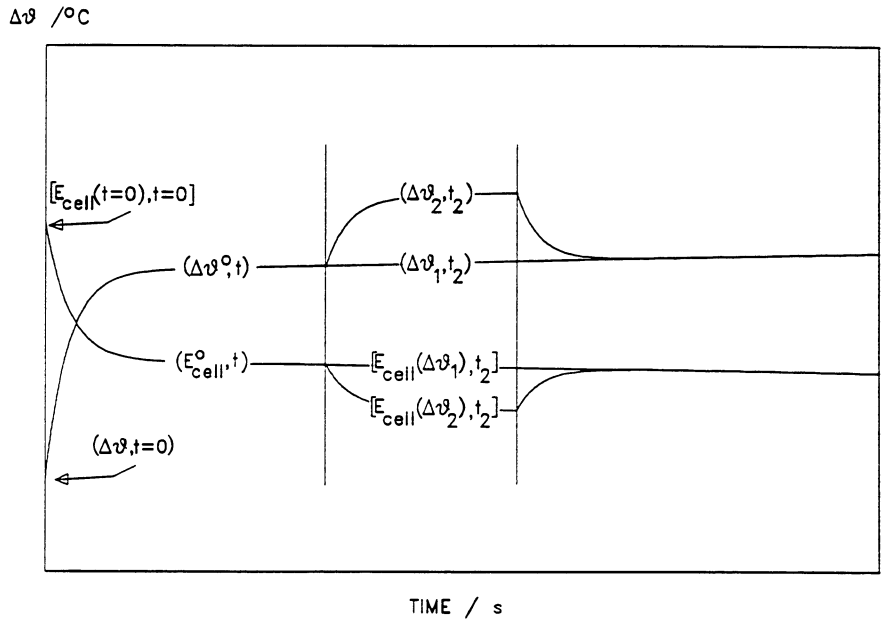

Fig 7. Schematic diagram of the methodology used in the calculations.

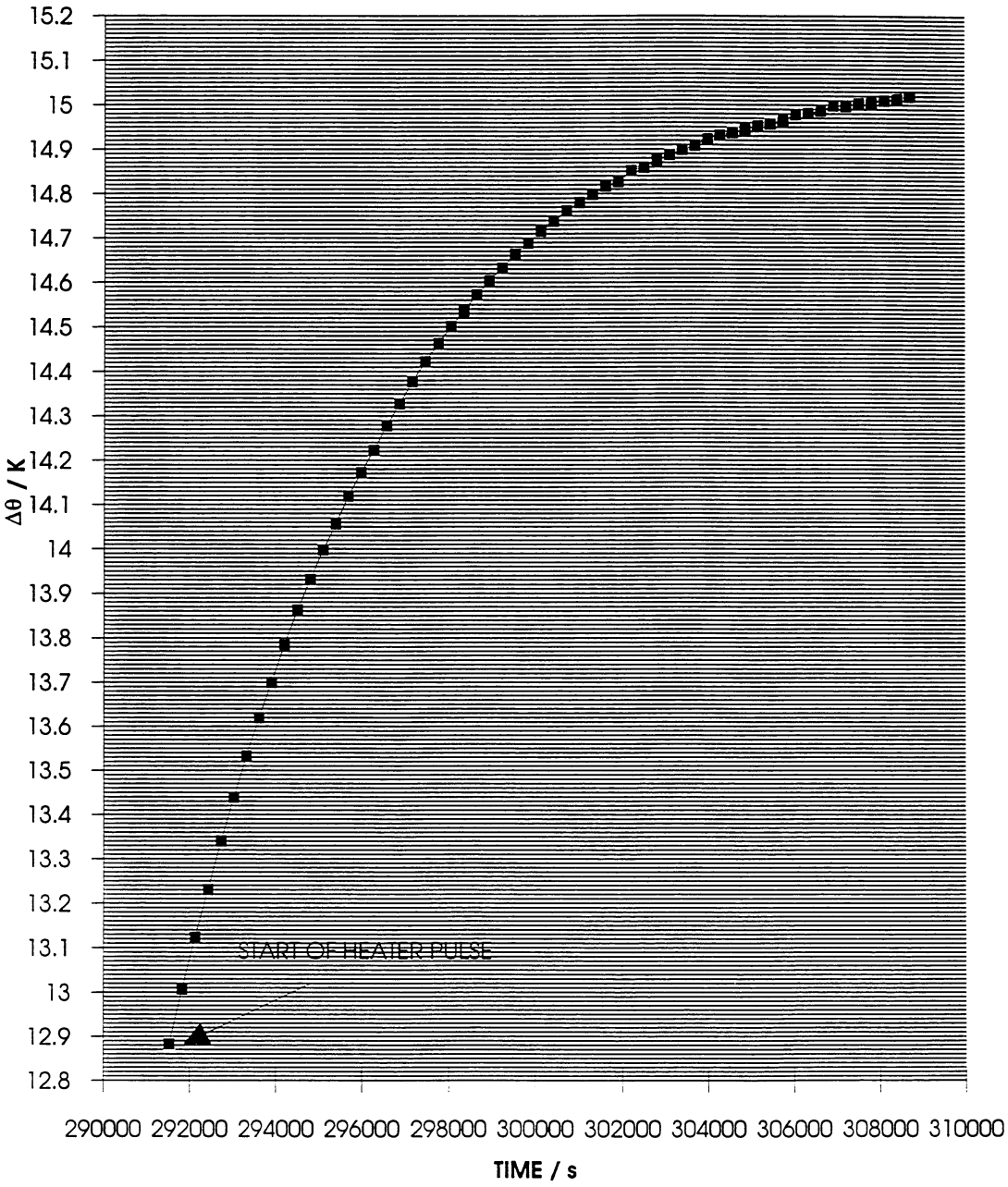

Fig 8. Graph showing the temperature–time curve following the application of a 0.250 W heater pulse to a calorimeter containing a 4 mm diameter, 12.5 mm Pd cathode polarised in 0.1 M LiOH in H_2O; cell current 0.250 A.

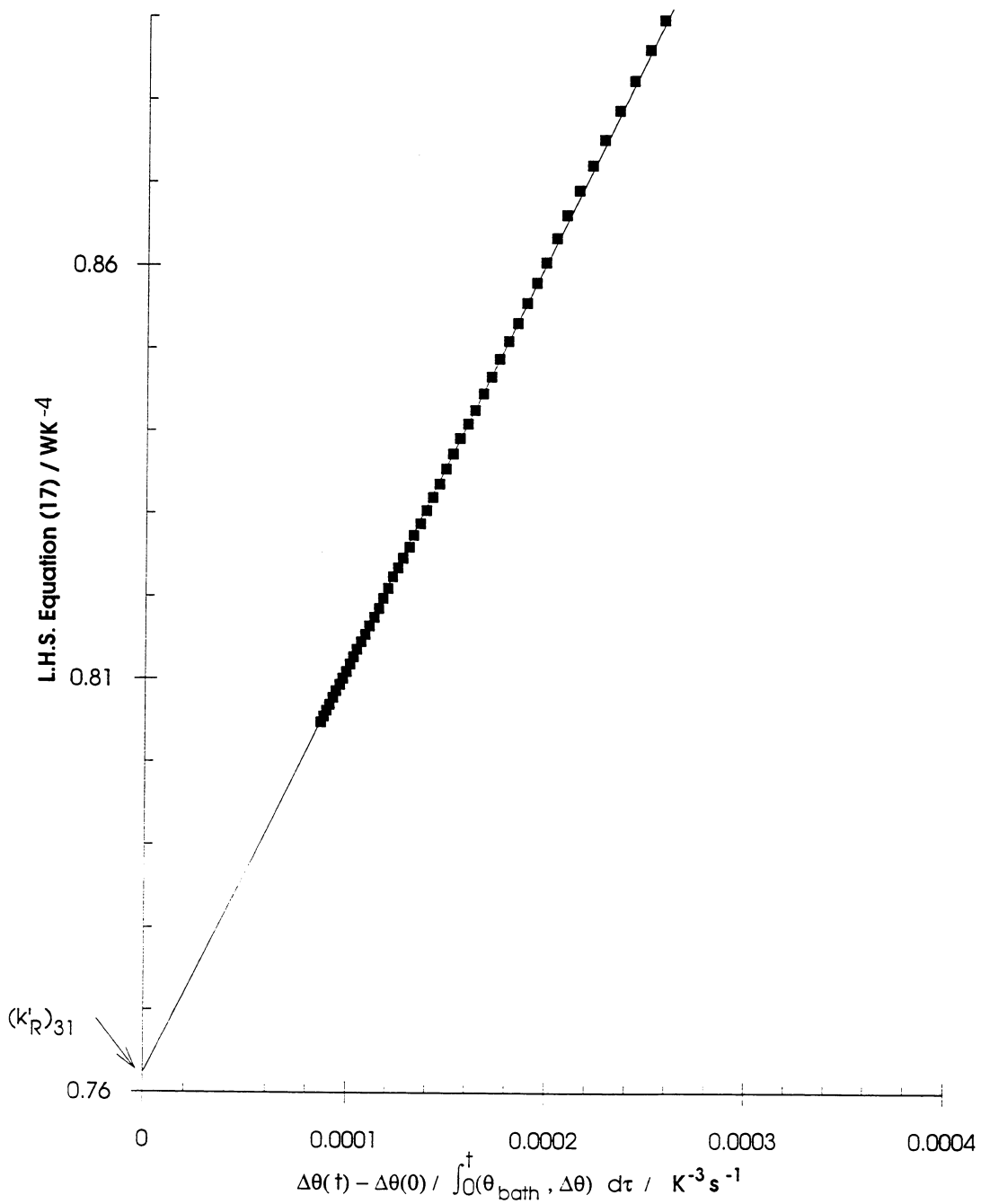

Fig 9. Graph showing the L.H.S. of equation 17 plotted versus the independent variable $[\Delta\theta(t) - \Delta\theta(0) \ / \ \int_0^t [(\theta_{bath} + \Delta\theta(\tau))^4 - \theta_{bath}^4] d\tau$.

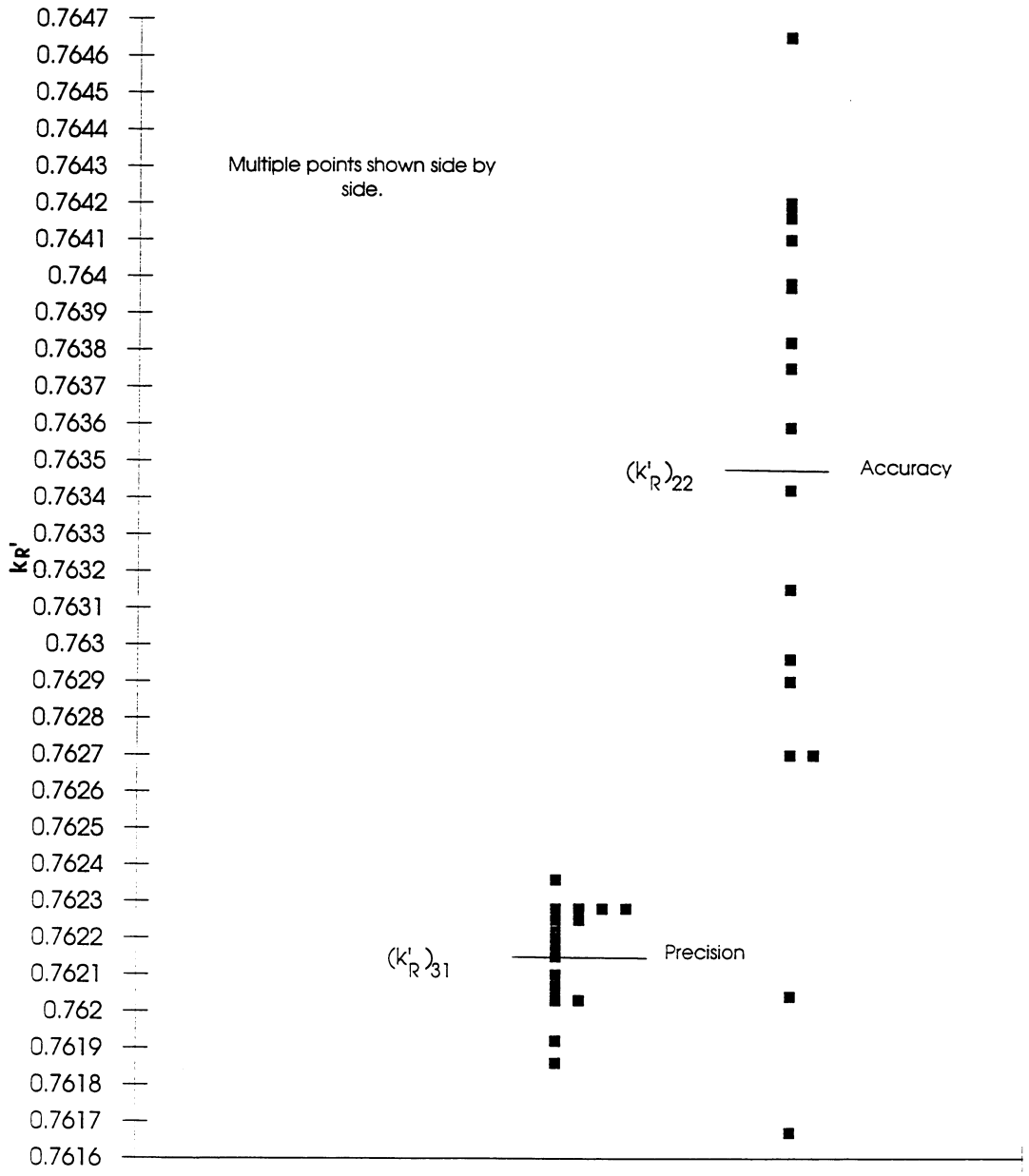

Fig 10. The precision and accuracy of the heat transfer coefficients $(k'_R)_{31}$ and $(k'_R)_{22}$.

EXCESS HEAT AND NUCLEAR PRODUCT MEASUREMENTS IN COLD FUSION ELECTROCHEMICAL CELLS

D. Gozzi[1] , R. Caputo, P.Luigi Cignini[2], M.Tomellini[3]
Dipartimento di Chimica, Università *La Sapienza*, P.le Aldo Moro 5, 00185 Roma, Italy

G. Gigli, G. Balducci
Dipartimento di Chimica, Università *La Sapienza*, P.le Aldo Moro 5, 00185 Roma, Italy

E. Cisbani, S. Frullani, F. Garibaldi, M. Jodice[4], G.Maria Urciuoli[4]
Laboratorio di Fisica, Istituto Superiore di Sanità, V.le Regina Margherita 299, 00161 Roma

Abstract

We present the results of a new experiment with our multicell set-up implemented with mass spectrometric measurements of ^4He and a highly improved neutron detector. The excess heat measured is *in linea* with the our previous results as well as with other laboratories while no neutrons, and a tritium excess lower than expected from power excess were found. ^4He has been measured in the electrolysis gases and a tentative correlation of ^4He with excess power is presented and discussed.

Introduction

Since 1989, in various countries around the world, continuous efforts have been done to investigate the nature of the excess heat found in electrochemical experiments of loading palladium or palladium alloys by deuterium. Five years about of such as experiments carried out by several groups, by using different techniques and procedures indicate that the heat power excess findings, up to 3.7 kW/cm^3 of Pd (**1**), cannot be attributed to artifacts and their magnitude appears well beyond the power that any expected chemical process could release. If adequate protocols are used, heat generation is found and quite definite progress

[1]To whom any correspondence should be addressed
[2]CNR-Centro di Termodinamica Chimica alle Alte Temperature, c/o Dipartimento di Chimica, Università *La Sapienza*
[3]Dipartimento di Scienze e Tecnologie Chimiche, Università *Tor Vergata*, Via della Ricerca Scientifica, 00133 Roma
[4]National Institute for Nuclear Physics (INFN) sez.Sanità, V.le Regina Margherita 299, 00161 Roma

has been made towards its reproducibility though it is still difficult to adequately control its onset, duration and magnitude. Because these features are the primary conditions for developing any type of technologically exploitable energy-producing device, efforts for improving them are in progress, expecially by private companies, mostly in Japan.
On the side of nuclear *ashes* recovery, the overall picture is more intriguing. At present time one thing is very well confirmed: the generation rate of neutrons and tritium nuclei, coming from the *d,d* reaction channels, *thought* as occurring in plasma physics, are of several order of magnitude lower, if compared with the rate values expected from heat power excesses measured by calorimetry. Therefore, in condensed matter, other nuclear byproducts of *d,d* reaction have to be invoked and searched. In this two-body reaction, only another channel can exist: the ^{4}He channel. Since the beginning, various measurements (**2-8**) to detect ^{4}He both in Pd cathodes and in the gas phase escaping from the electrochemical cells were reported but only a few of them are accounted for in detail. Up to now only one electrochemical cells experiment has been reported (**3**) where evidence is given of heat excess roughly correlated with ^{4}He measured in the gas phase. The air contamination which could have possibly occurred in this experiment was later discussed (**5**). Gas loading experiments in a high vacuum assembly have clearly shown the release of ^{4}He when deuterium is confined in Pd between blocking interfaces (**6**).
From the theoretical point of view, there are at least two great problems to solve for explaining this experimental scenario: *i.* Coulomb barrier for *d,d* reaction between low energy nuclei; *ii.* the energy release to Pd lattice of the α-particle produced. In terms of plasma physics, for both these problems there is not a solution. On the other hand these problems have been attacked with promising results by some theories (**9-12**). Their main feature is the attempt to overcome the schemes of the high energy physics believed to be not fully apt to treat a different physical situation such as that of the condensed matter.
All this is a bird-view emerging from four International Conferences (**13-16**), specialized International Meetings (**17-18**) and several hundreds of publications on Journals.
Starting from 1989, our group, where competences of physical chemistry and nuclear physics are present, is with continuity involved in making multicell experiments providing calorimetric and nuclear (neutrons, tritium, ^{4}He, gammas) measurements as well as a little bit of Materials Science applied to Pd cathodes preparation (**19-27**). Scope of the present paper is to show a part of the results obtained in the last multicell experiment in which the feature of the quantitative measurement of ^{4}He was added.

Experimental

Overview

The basic idea in designing our experimental set-up was to have a multicell system, up to ten equal cells, in which the unique difference among them was in the cathode in terms of material or geometry or preparation. One or more cells can be blank cells having the cathode made of a material not D (H) absorbing such as Pt or Au or made of Pd but in a D free electrolyte. All the cells are connected in series and electrolysis is carried out in galvanostatic mode (each cell can be excluded or inserted at any time in the electrical series circuit by a home-

made device controlled in manual or by computer mode). This allows the rate of all the electrochemical processes be the same in each cell. This condition produces a certain number of important facts related to the calorimetry; as an example, the flow-rate of the electrolysis products, D_2 (g) and O_2 (g), is, according to the Faraday's law, equal in each cell[5] so that the heat transported by the escaping gases and the heat necessary to saturate the gases themselves by D_2O (H_2O) are also the same in each cell provided the temperature of the solution be the same.

Because each cell is a non-adiabatic calorimeter, it is important that the way the heat is exchanged with the sorroundings is the same for all the cells. As expected, this has to occur mostly through the conductive path localized in the cell glass wall between the eletrolyte solution and the thermostated stream of circulating water. This is obtained by positioning all the cells simmetrically in a torus-shaped bath thermostated by circulating water kept at constant temperature (generally 21.0 ± 0.1 °C) by a high quality thermostat. The room temperature is maintained close to this value.

The torus (50 cm outer diameter and 30 cm innermost diameter) is contained in a large neutron counter designed by us and manufactured by Jomar-Canberra, Los Alamos (see below).

To easier understand what is monitored, what is done in each cell and how the signal are processed, we report in Fig. 1 the complete flow-chart (24).

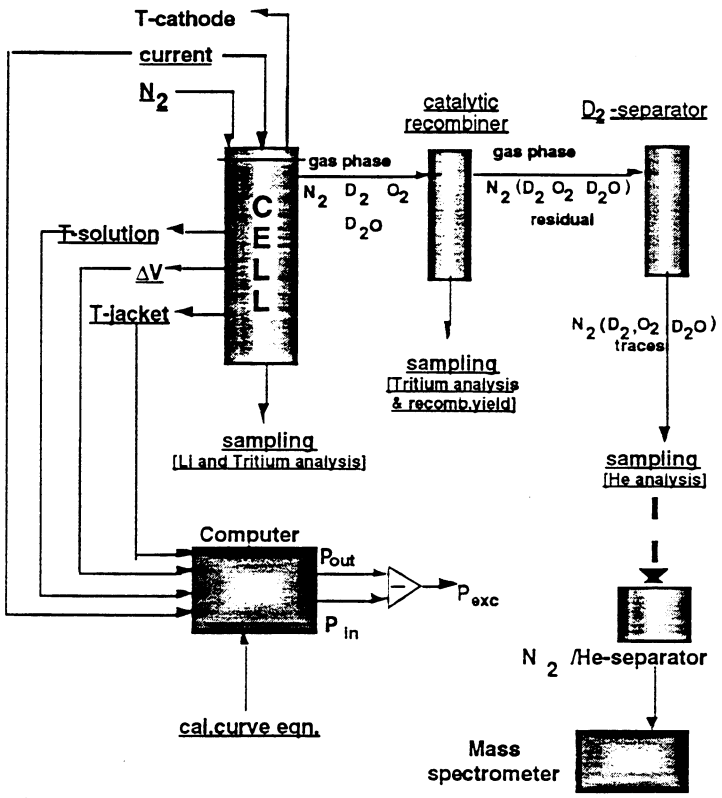

Figure 1
Flow-chart of the operations performed on each cell

[5]To be correct this is exactly true when the rate of D (H) absorpion by the cathode is zero. For practical purposes, this condition is fulfilled quite soon after the starting of electrolysis

All the cells are treated according to this flow chart. As it is shown in figure 2, our cells are open-type cells with external recombination. The external recombinator joined to the D_2 (H_2) separator is an efficient D_2 (H_2) cutting system (see below).
^4He measurement by a magnetic type mass spectrometer (28) is not an on-line measurement and the gas line is sampled discontinuously by filling a 500 ml steinless steel (SS) cylinder. At sampling stage, as it will be shown later on, the gas composition is given by N_2 with D_2 (H_2), O_2 and D_2O (H_2O) traces and ^4He if any. At certain stage of the experiment ^{20}Ne measurements have been initiated as a marker of a supposed air contamination.
In the followings, we shall describe, except for the ^4He measurement procedure reported elsewhere (28), the single parts of the experimental set-up as well as the adopted procedures, making use of what was already reported (24-26) while describing in details the new features and the reliability of the various methods adopted.

Electrochemical Cells and Calorimetry
i. Electrochemical cell.
The present most recent version of the electrochemical cell is reported in Fig. 2. This cell was modified with respect to the previous version (26) essentially to make it impervious to the air contamination in view of ^4He measurements. In fact, particular care has been reserved to all the feedthroughs in the cap in making them tight by high precision machining of the crossing holes as well as in selecting the feedthrough material. Nylon 66 or SS tubes were adopted for the lines because, as we tested (28), they are not ^4He permeable. Connections in the lines were done by Swagelock fittings and where this was not possible, as in the case of SS-Pyrex joints, we made them by soldering SS tube and Pyrex by epoxy resin adhesives (of the types used in high vacuum technology). To carry ^4He up to the sampling cylinder, due to the deuterium cutting system , we have to use a stream of N_2 coming from a LN_2 tank. This ensures a practical null background of ^4He (28).
The cell geometry (inner diameter 22 mm x 245 mm height) was designed to maximize the heat transfer in the radial direction by taking also into account the combined effect of the carrier and electrolysis gases bubbling which jointly allow the thermal gradient to be localized on the plane orthogonal to the z-axis of the cell. The effective volume of the cell to be filled with the electrolyte solution is about 53 ml. Small deviations from this value may exist from cell to cell if the cathodes are different in size.
Three K-type thermocouples are present in the cell to measure the temperature of the cathode, solution and just outside the cell in a massive copper ring immersed in the thermostated bath. Automatic and computer controlled refilling of D_2O (H_2O) is operated by the liquid sensor level positioned in the lateral tube.
To ensure a good and permanent coaxial positioning of the electrodes, both the cathode and anode are partially inserted in a properly machined Teflon piece which also acts as N_2 scrubber in its bottom part.
The anode is made of a 1 mm diameter Pt wire shaped as coil having 12 mm inner diameter and height comparable to that of the cathode.

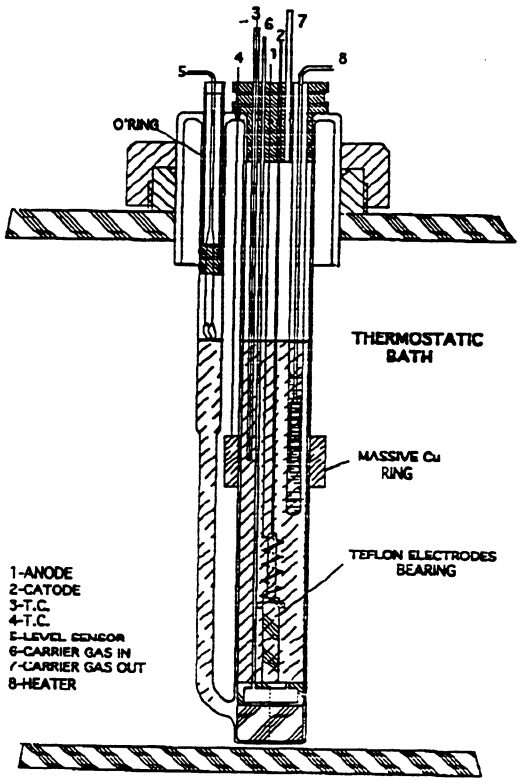

Figure 2
Scheme of the electrochemical cell

The electrolyte solution is 0.2 M solution of LiOD in 99.99% D_2O (from ISOTEC, USA) at low tritium content (≈ 1Bq/ml or 60 dpm/ml). The ICPAES (Inductively Coupled Plasma Atomic Emission Spectroscopy) analysis of the starting solution did not detect any alkaline or heavy metal above the detection limit which is generally ≤ 10 ppb.
In Table I are reported some of the features of the cells tested in this experiment. All the Pd cathodes were prepared starting from Johnson & Matthey (UK) rods.

Table I. Details of the electrochemical cells used in this experiment

# cell	cathode size [mm x mm] ø x h	Treatment	Gas line material	Remark
1	Pt 1 x 23	as received	SS	blank
2	Pd 2 x 25	as received	Nylon	
4	Au/Pd 6 x 23	HV at mp of Au	SS	D_2 Confinement experiment (32)
7	Pd 2 x 21	screw dislocated	Nylon	switched on from 675 to 930 hrs
8	Pd 3 x 22	screw dislocated	Nylon	
10	Pd 3 x 23	as received	Nylon	

ii . Calorimetry

The calorimetric excess heat measurements are based on the comparison of the actual value of temperature of the solution at a given input power with the calibration curve. The calibration curve is obtained by increasing or decreasing in step-fashion the input power. This can be done either in thermal mode, by the inner heater, or in electrochemical mode by using Au or Pt cathodes exactly in the same conditions in which the experiment is subsequently carried out. A detailed discussion about those procedures has been already reported in literature (25-26), therefore we limit ourselves to give in Table II the calibration curves equations for the cell used in this experiment.

Table II. Calibration curves: $P_{in} = (a_i \pm \Delta a_i) + (b_i \pm \Delta b_i)\Delta T_i$

Cell/i	a_i /W	Δa_i/W	b_i/WK^{-1}	Δb_i/WK^{-1}	r	$P_{exc,i}^{min}$/W
1	0.7	0.5	7.0	0.1	0.9983	1.7±0.7
2	0.3	0.7	5.8	0.1	0.9985	1.2±0.8
4	0.06	0.60	5.5	0.1	0.9979	0.9±0.7
7	0.5	0.3	5.06	0.07	0.9993	1.3±0.3
8	-0.6	0.4	5.21	0.09	0.9991	0.2±0.4
10	-0.5	0.9	6.3	0.2	0.9968	0.4±0.9

All the curves are practically straight-lines with high correlation factor r having the general equation form as: $P_{in} = (a_i \pm \Delta a_i) + (b_i \pm \Delta b_i)\Delta T_i$ where $\Delta T_i = \left(T_s - T_s^0\right)_i - \left(T_{tb} - T_{tb}^0\right)_i$ with T_S and T_{tb}, respectively, the temperature of the solution and of the thermostated bath just outside the cell and measured in the copper ring. T_s^0 and T_{tb}^0 are the respective values of T_S and T_{tb} kept at P_{in} =0. P_{in} is the input power equal to IxV or Ix (V - V_{th}) depending on whether the cell is powered in thermal or electrochemical mode. V_{th} = $\Delta H°/2F$ is the thermoneutral potential being $\Delta H°$ the enthalpy of decomposition of D_2O (H_2O) and F the Faraday constant. The adopted value of V_{th} for D_2O is 1.5367 V (29). V_{in} and I are, respectively, the electrical potential difference at leads read closest to the heating resistor, when in thermal mode, or electrodes, when in electrochemical mode and current measured through the voltage drop at leads of a high precision 100 mΩ resistor. The overall uncertainty in measuring P_{in} is 0.01%. The heat power excess, P_{exc}, of a given cell i, is given by:

$$P_{exc,i} = P_{out} - P_{in} = a_i + b_i \Delta T_i - P_{in} \qquad (1)$$

where ΔT_i is now the value measured in the experiment. The overall error on P_{exc} has been evaluated to be less than ±10% (25). The minimum heat power excess detectable is given by $P_{exc,i}^{min} \geq (a_i \pm \Delta a_i) + (b_i \pm \Delta b_i)\Delta\Delta T_i$ where, $0.1 < \Delta\Delta T_i \leq 0.2$ °C, is the minimum temperature change appreciable by the K-type thermocouples used. In Table II, the $P_{exc,i}^{min}$ column was calculated assuming $\Delta\Delta T_i$= 0.15 °C. Note that due to the definition of ΔT_i, the systematic error on this quantity is practically zero.

The energy balance of such a calorimeter during a calibration input power step is given by:

$$P_{in} = m_s C_s \frac{\partial \Delta T_i}{\partial t} + \frac{\pi d k_{Pyrex}}{l} h \Delta T_i(t) + \frac{k_{Rad}}{\pi d h}\left\{\left[T_{tb} + \Delta T_i(t)\right]^4 - T_{tb}^4\right\} + \\ + \left(\frac{3I}{4F} + \frac{P}{RT_r} f_{N_2}\right)\left[\frac{p(t)}{P - p(t)}\right]\left[\left(C_g - C_l\right)_{D_2O} \Delta T_i(t) + \Lambda_{D_2O}\right] \quad (2)$$

where the four terms on the right side represent, respectively, the rate of enthalpy change of the solution, the rate of heat transfer from solution to the thermostated bath by conduction through the Pyrex wall, the rate of heat transfer by radiation to the thermostated bath and rate of heat transfer from solution to the gases (produced by electrolysis + N_2 carrier) escaping from the cell and saturated with D_2O (H_2O) at the temperature of solution. Consult Appendix A for the meaning of symbols in Eqn. 2. Due to the continuous heat transfer to the thermostated bath, ΔT_i, contrarily to an adiabatic calorimeter (1), is generally below 15 °C, and therefore also the vapor pressure of D_2O (H_2O) is low with respect to the atmospheric pressure and the term $\left[\frac{p(t)}{P - p(t)}\right] \approx 2\text{x}10^{-2}$. The sign of the last contribution to the sum of the right side member of Eqn. 2 depends on the sign of the term $\left[(C_g - C_l)_{D_2O} \Delta T_i(t) + \Lambda_{D_2O}\right]$ which is always > 0 in the useful working temperature range (it becomes < 0 at $\Delta T_i(t) = -\frac{\Lambda_{D_2O}}{(C_g - C_l)_{D_2O}} > 906.5$ °C !!) whereas the overall magnitude can be evaluated close to ≈ 4.5 mW for I < 1A and $f_{N_2} = 5.4 \text{ x } 10^{-7}$ $m^3 s^{-1}$ at stp (see below).

The radiative term $\frac{k_{Rad}}{\pi d h}\left\{\left[T_{tb} + \Delta T_i(t)\right]^4 - T_{tb}^4\right\}$, for the same above considerations on ΔT_i, is evaluated ranging around 3 mW and, therefore, for practical purposes Eqn. 2 can be written as

$$P_{in} \equiv m_s C_s \frac{\partial \Delta T_i}{\partial t} + \frac{\pi d k_{Pyrex}}{l} h \Delta T_i(t) \quad (3)$$

It is important to point out that in the case of determination of P_{exc}, Eqn. 2 might be put in the form:

$$P_{exc,i}(t) = m_s C_s \frac{\partial \Delta T_i}{\partial t} + \frac{\pi d k_{Pyrex}}{l} h \Delta T_i(t) + \Phi\left[\Delta T_i(t)\right] - P_{in,i}(t) \quad (4)$$

where, in the term $\Phi\left[\Delta T_i(t)\right]$ are now considered the sum of both the terms previously neglected. It is esay to verify that the elimination of $\Phi\left[\Delta T_i(t)\right] > 0$ from Eqn. 4 always produces an underestimate of P_{exc}.

The integration of Eqn. 3, in the case of a calibration step of input power, gives:

$$\Delta T_i = \frac{\tau P_{in}}{\zeta}\left(1 - e^{-\frac{t}{\tau}}\right) = \Delta T_{i,(t\to\infty)}\left(1 - e^{-\frac{t}{\tau}}\right)$$
$$\tau = \left(\frac{\pi dhk_{Pyrex}}{l\zeta}\right)^{-1};\ \zeta = m_s C_s;\ \Delta T_{i,(t\to\infty)} = \left(\frac{\pi dhk_{Pyrex}}{l}\right)^{-1} P_{in} \qquad (5)$$

where the term $\left(\frac{\pi dhk_{Pyrex}}{l}\right)^{-1}$ is the slope of the calibration curve which corresponds to the $(b_i)^{-1}$ parameters shown in Table II. The theoretical time constant value is $\tau = \frac{\zeta}{b_i} = \frac{\rho_l V^\circ C_l}{b_i M} \cong \frac{280}{b_i}$ s. Higher values (350-400 s) of τ are experimentally found due to the fact that the ζ term should be more correctly written as $\zeta = m_s C_s + \sum m_k C_k$ where the summation runs on all the masses present in the cell. If a set of points is obtained in stationary condition of ΔT_i associated each time to a different P_{in} value, provided h is kept constant by a level sensor, this set has to be, within the experimental errors, on a straight-line of slope $\left(\frac{\pi dhk_{Pyrex}}{l}\right)^{-1}$ since this vahue depends only on constant quantities. This is just what we in fact obtained, as shown in Table II. To check the validity of the treatment above, one can obtain k_{Pyrex} from the slope of the calibration curve . The averaged value obtained is 0.9 ± 0.1 $Wm^{-1}K^{-1}$ which is in agreement with the value reported in literature (30) (see Appendix B).

Deuterium cutting system

It is composed by two parts connected in series by SS (inner diam. 1.5 mm) or Nylon66 (inner diam. 3 mm) tubing: *i* . catalytic recombinator and *ii* . Pd sponge trap. This operation allows to measure tritium in the electrolysis gas phase (see below) and eliminate D_2 from the gas stream before sampling for ^4He analysis.

i . ***Catalytic recombinators.***

They are described elsewhere (25). Their yield η is calculated by the following equation:

$$\eta = \frac{V_{rec}}{V_{cons}} = \frac{V_{meas} - f_{cond}\Delta t}{\frac{\bar{V}}{2F}\int_{\Delta t} Idt} \qquad (6)$$

measuring the recombined volume of D_2O in the time interval Δt. The correction for the condensation of D_2O contained in the gas stream was measured to be 3.75×10^{-6} cm^3s^{-1}. The recombination yield value averaged on 10 recombinators is about 92%.

The partial pressure values of D_2 at the recombinator inlet and outlet are given by the equations:

$$P_{D_2}^{in} = \frac{\frac{I}{2F}}{\frac{P}{RT_r} f_{N_2} + \frac{3I}{4F}} P;\quad P_{D_2}^{out} = \frac{\frac{I}{2F}(1-\eta)}{\frac{P}{RT_r} f_{N_2} + \frac{3I}{4F}(1-\eta)} P \qquad (7)$$

Supposing, for instance, I = 1A, $\eta \approx 0.9$ and using data in Appendix B. $P_{D_2}^{in}$ and $P_{D_2}^{out}$ are, respectively, equal to 1.74×10^{-1} P and 2.28×10^{-2} P. This last value is the D_2 partial pressure of the gas stream entering in the Pd sponge trap.

*ii . **Pd sponge trap***

Two equal traps, working alternatively and continuously fluxed under N_2 carrier, when in regeneration, are made of a SS cylinder with an inner coaxial SS tube. The path of the gas mixture inside the trap is a such to have the largest contact surface area with the Pd sponge. In each trap are contained 150 g about of Pd sponge from Johnson & Mattey (UK).

If we suppose the absorption reaction

$$Pd(s) + \frac{y}{2} D_2(g) = PdD_y(s) \qquad (8)$$

completely shifted on the right side, we can define the nominal capacity of the trap as $C_{trap} = \frac{y w_{Pd}}{2 M_{Pd}}$, therefore, the residual capacity of the trap with respect to the initial capacity, as a function of D_2O consumed, is given by:

$$C_r = 1 - \frac{1-\eta}{\bar{v} C_{trap}} v_{cons} \qquad (9)$$

It is easy to see that to exhaust a Pd trap, in the case of $\eta = 0$, would be sufficient the electrolysis of just 8.5 cm^3 of D_2O. Because in our case $\eta \approx 0.90$, to exhaust completely the trap it would be necessary to make electrolysis of a D_2O quantity ten times higher.

The minimum partial pressure of D_2 in the gas stream at outlet of the Pd trap should be equal to the activity of $D_2(g)$ in the gas phase in thermodynamic equilibrium with the condensed phase at a certain activity of D according to reaction 8. This value can be calculated by the following equation (**31**):

$$\ln a_{D_2} = \left[-\frac{\Delta H_{abs}(y)}{RT_r} \right] + 2 \ln\left(\frac{y}{1-y} \right) + \frac{\Delta S^0_{abs}}{R} \qquad (10)$$

As it is reported elsewhere (**32**), the background pressure of D_2 at the outlet of the Pd trap, measured by mass spectrometry, has been found to be $\approx 5 \times 10^{-10}$ atm which, by Eqn. 10 corresponds, to $y \approx 0.2$. Therefore, the overall cutting factor of D_2, present in the N_2 carrier at the outlet of the electrolysis cell, is 10^8 about. This remarkable result joined to the high resolution power of the mass spectrometer allows to be very confident on the quantitative determinations both of ^4He and D_2.

Measurements of Nuclear Byproducts

i. **Tritium.**

To prevent any air contamination, contrarily to the past, we did not make tritium tests in the electrolytic solutions of the cells but only in D_2O produced by the catalytic recombinators. The experimental procedure adopted to measure tritium was described elsewhere (24) as well as the calculation to evaluate the tritium electrolytic enrichment in the solution. In this experiment, because the tritium measurement is done on the recombined gases and a gas carrier is present in addition to the electrolysis gases, to evaluate correctly the effects of the electrolysis on the tritium concentration in the gas stream it is necessary to modify the mathematical treatment we utilized in the past.

Considerations based on the mass balance of tritium in our cells lead to the following differential equation:

$$\frac{dx}{dt} = n_{D_2O}\left[x_f f_{D_2O} - \frac{I}{2F\alpha_E}x - \frac{p}{\alpha_V(P-p)}f_G x - x\frac{dn_{D_2O}}{dt}\right] \qquad (11)$$

As we stated before, in the previous section, the volume of electrolyte has to be constant, therefore, the term $\frac{dn_{D_2O}}{dt} = 0$, and so the D_2O feed, must be such as to compensate D_2O consumed by the electrolysis and D_2O evaporated in the gas stream escaping from the cell. If, as it normally occurs, the molar fraction of DTO in the D_2O feed is the same as in the D_2O initially present in the electrolytic solution, the integration of eqn. 11 gives:

$$q = q_{\lim} - \left(q_{\lim} - \frac{1}{\alpha_E}\right)e^{-\frac{v_{cons}(I,t)}{V^*}} \qquad (12)$$

where the quantity $q = \frac{x_g}{x^\circ}$ represents the expected change, due only to the electrolysis, of tritium atomic fraction in the gas phase with respect to the initial atomic fraction of tritium in the electrolyte. In eqn. 12 the terms $q_{\lim}$ and V * are, respectively, obtained by the equations below:

$$q_{\lim} = \frac{1+\left(\frac{3}{2}+\frac{2FPf_{N_2}}{RT_rI}\right)\left(\frac{p}{P-p}\right)}{1+\frac{\alpha_E}{\alpha_V}\left(\frac{3}{2}+\frac{2FPf_{N_2}}{RT_rI}\right)\left(\frac{p}{P-p}\right)} \qquad (13);\ V^* = \frac{\alpha_E V^\circ}{1+\frac{\alpha_E}{\alpha_V}\left(\frac{3}{2}+\frac{2FPf_{N_2}}{RT_rI}\right)\left(\frac{p}{P-p}\right)} \qquad (14)$$

In Fig. 3 is reported the $q_{\lim}$ surface in the plane V*, α_E. Combining eqns. 13 and 14, it is easy to show that only the values of V* satisfying the condition $\left(\frac{V^\circ}{V^*} - \frac{1}{\alpha_E}\right) \geq \frac{3}{2\alpha_V}\left(\frac{p}{P-p}\right)$ can be selected in the above plot. In fact the left side term in the inequality has to be positive being the right side term always a

positive quantity. As it appears in fig. 3, the values of the $q_{lim} \geq 1$ correspond to V* and α_E values which are without physical meaning.
At fixed temperature and carrier gas flow-rate, an important difference between eqn. 12 and eqn. 2 of ref. 24 (obtained for the tritium enrichment in the electrolyte) is that, q_{lim} and V* are also function of the electrolysis current whereas the corresponding terms α and β are constant quantities. By inspection of eqns. 12 through 14, the following remarks can be drawn:

a) at $v_{cons} \to 0$, $q = \frac{1}{\alpha_E}$;

b) at $v_{cons} \to \infty$, $q = q_{\lim} \Rightarrow$

$$\begin{cases} f_{N_2} = 0 \Rightarrow \dfrac{1}{\alpha_E}\left[\dfrac{1+\dfrac{3}{2}\left(\dfrac{p}{P-p}\right)}{\dfrac{1}{\alpha_E}+\dfrac{3}{2\alpha_V}\left(\dfrac{p}{P-p}\right)}\right] \cong \dfrac{1}{\alpha_E}\alpha_E \cong 1 \\ I = 0 \quad \Rightarrow \quad \dfrac{\alpha_V}{\alpha_E} \cong \dfrac{1}{\alpha_E} \end{cases} \qquad (15)$$

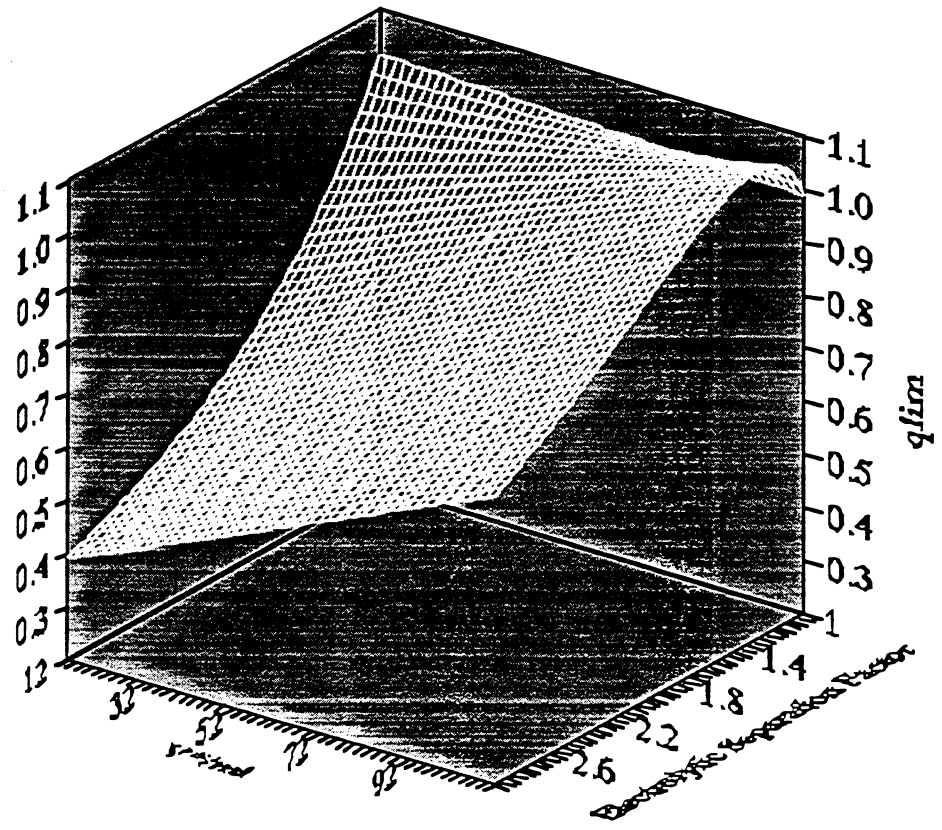

Figure 3
Calculated surface of q_{lim} term in eqn. 12 as function of V* and electrolytic separation factor between deuterium and tritium on a Pd cathode.

Therefore, the expected q *vs* v_{cons} curve starts from $\frac{1}{\alpha_E}$ and remains, of course, at this value if I=0 or tends to 1 in the case of electrolysis without any carrier gas stream, whatever is the I value. Since α_E depends mostly from the nature of the cathode, on Pd α_E =1.8 (**24-25**), it is expected that the q limits will be in the range from $\approx\frac{1}{2}$ to 1. In this experiment, $f_{N_2} \neq 0$ and kept always constant whereas I was changed and in some cases put off for a certain period of time, as it will be shown in the results section. Therefore, we have to expect that throughout the experiment, if tritium is not generated in the cell by a nuclear reaction, the value of q must be within the range $\frac{1}{\alpha_E} \leq q < 1$. Further aspects will be treated in the discussion section.

ii . Helium-4

See in this book the paper by the same authors concerning the quantitative mass spectrometric measurements of ^4He.

iii . Neutrons

A description of our more recent system for neutron detection was already reported (**26**). However, for the sake of a better understanding of the results, a cross-section of the detector-cell system assembly is shown in Fig. 4.

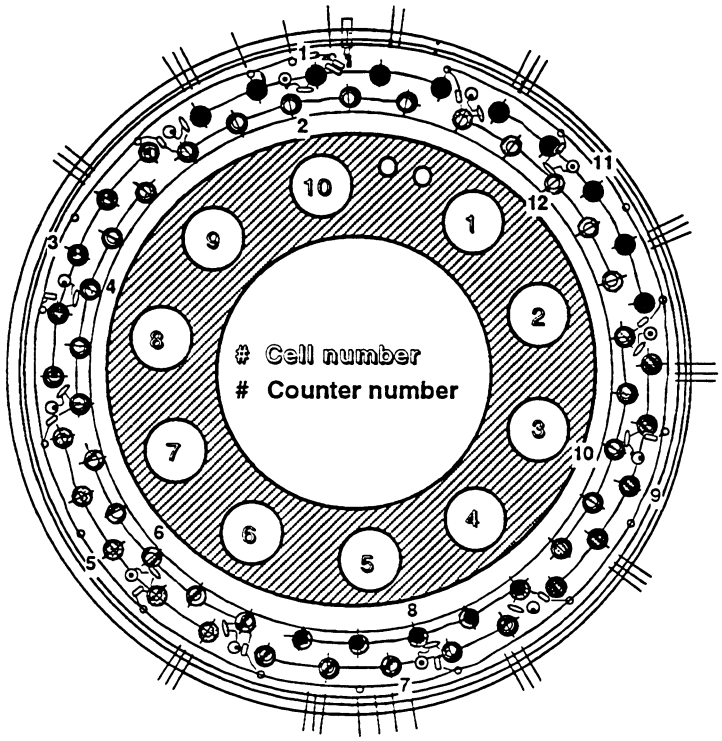

Figure 4.
Cross section of the neutron detector assembly. Dashed area is the torus containing the electrochemical cells. Black circles represent the ^3He tubes. Each counting group is constituted by five tubes.

iiii . Data Aquisition System

Two separate data acquisition systems are now at work [only one in the past (24)] in our experiments both based on the network Macintosh Computer ⇔ IEEE-488&RS-232 Interfaces ⇔ Instruments. They are dedicated the first to the neutron acquisition (see before and ref. 26) and the second to the acquisition and control (24) of all the other devices and sensors of the experimental set-up (mostly through a data logger). The programs running on each of the two systems were home-made both realized on the software LabVIEW 2.1.1 from National Instruments (Austin,TX). All the temperature, voltage, current and other analog signals go to the analog input channels of the data logger (Orion 3531 D, Schlumberger,UK) and logged at fixed scan intervals. Generally the scan interval time is set at 300 s but it can change automatically to 5 s if an alarm occurs on one of the logged channels. The alarm feature is based on a preset threshold. All the channels connected to the cathode and solution thermocouples of each cell as well as the counter channel connected in parallel to the TTL logic OR of the neutron counter are set to generate alarms. The primary file (the program generates also other ancillary files as for example those containing dating and volumes of D_2O refillings of each cell) of every piece of data acquisition is constituted of a matrix of 1000 rows x 60 columns which is build by append mode on both the RAM and removable hardisks. A real time plotting of all the channels is at the hand on the computer screen.

Finally, as already mentioned, since the system of all the cells is positioned inside the neutron detector, a B/W TV camera, connected to a videorecorder, is placed in the center of the torus, and operated both in manual and automatic remote control (by data logger), to have a more direct control of the status of each cell.

Results

Calorimetric and ^{4}He data

All the data that will be presented throughout the text are to be intended as obtained according to the step-wise patterns of the electrolysis current as showed in fig. 5 for all the cells tested.

In the four next figures which follow (figs. 6 to 9), two graphs each are reported which represent the ^{4}He and calorimetric results throughout the experiment for some cells. Each figure shows in the upper part the ^{4}He concentration, given in ppb, compared with the ^{4}He concentration in the blank cell and, in the bottom part, the input power (left scale) and heat power excess (right scale). Heat power excess has been calculated according to eqn. 1 and Table II and the related error has to be considered conservatively equal to ±10% of the value while the error on the input power is, as already mentioned, negligible. Because of the high number of points composing each curve (>10^4), in order to obtain a better readability, the errors bars are not reported in the bottom graphs. To facilitate a comparison of the energy quantities involved both the scales have the same limits. Furthermore, the lack of heat excess results in some parts of the related curve is due to a conservative choice we adopted in not considering those data which were acquired in experimental conditions not exactly equal to the ones in which the calibration curve had been obtained[6]. The error on ^{4}He concentration

[6]Connected to some electrical pertubations induced during the D_2 confinement experiment on cell #4 (32)

has been estimated equal to ± 13% of the value (28) Cells #1 and #7 did not show any excess of heat power within the experimental error. For cell #1, this is as expected because it is the blank cell. Cell #7 was switched on in the final part of the experiment essentially having the scope (any particular attention was reserved to the charging protocol) to obtain other elements to understand the effect of a change of gas composition, due to electrolysis, on the mechanism of a supposed contamination by air. In fact, in this case, the line was continuously

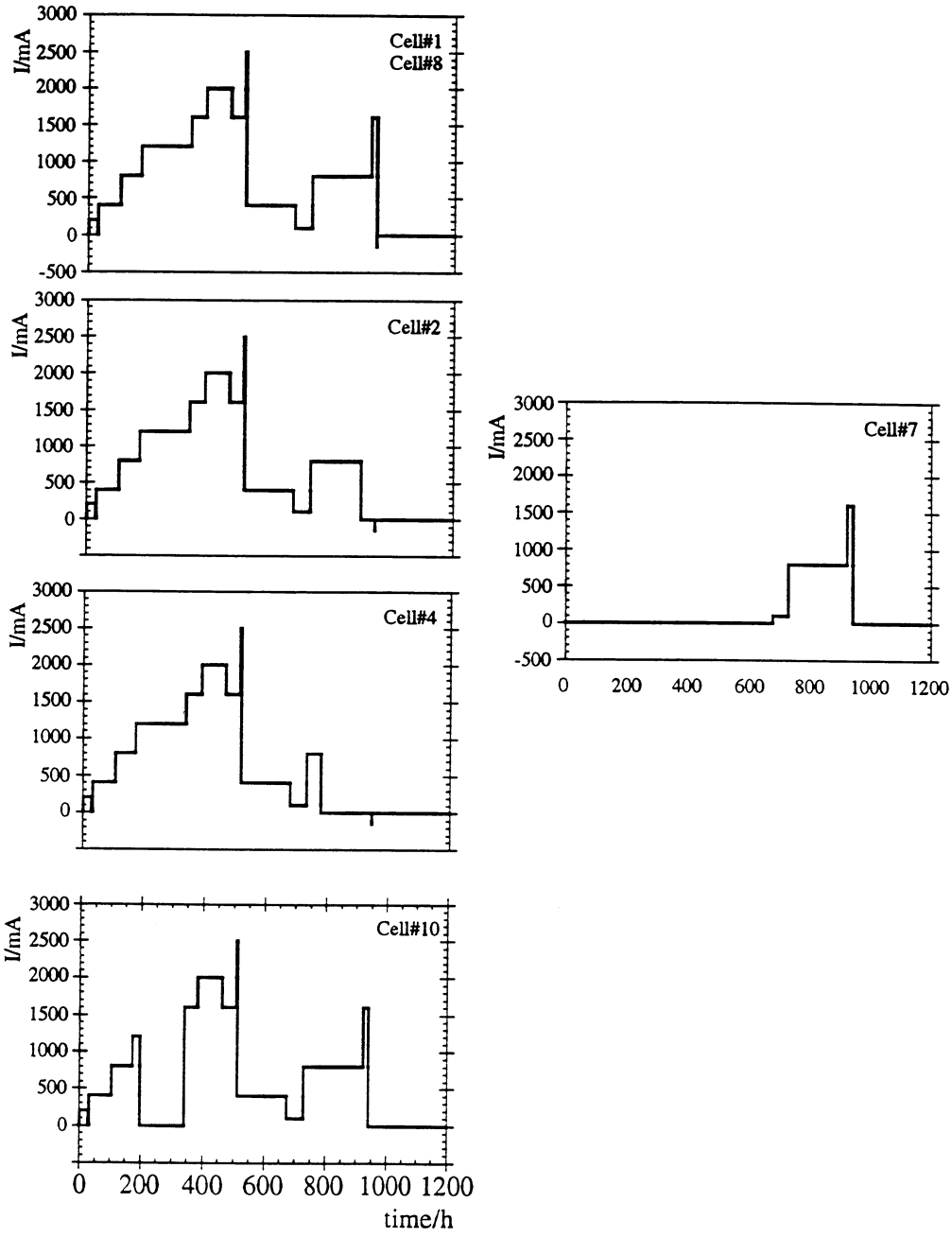

Figure 5
Time chart of the electrolysis current applied to the cells reported in Table I

fluxed by the carrier gas since more than 700 h. ^{4}He data of cell #7 are shown elsewhere in this book (28). The maximum value of heat power excess in each cell was found in the range from 2 to 19 W (± 10%) and the ratio $\Gamma = \frac{\text{excess power}}{\text{input power}}$ ranging from 0.13 to 0.70. These figures and other ones extracted from the plots above are reported in Table III.

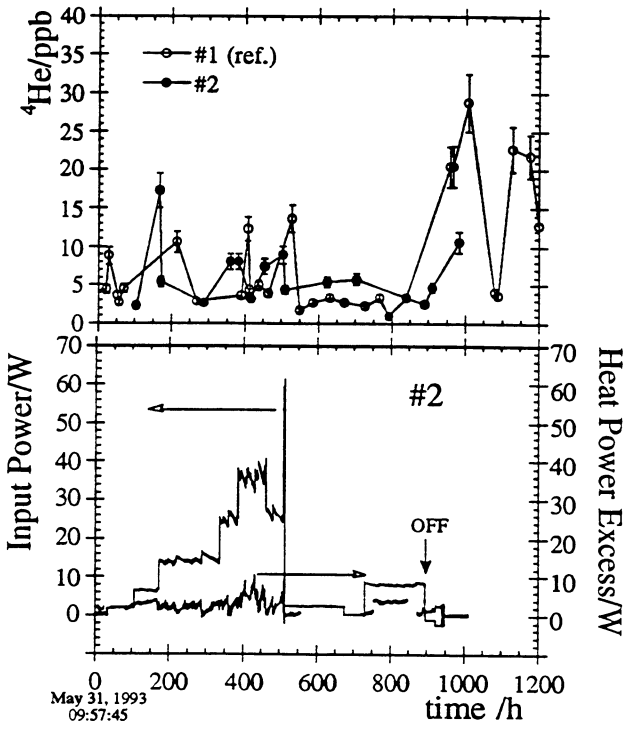

Figure 6 : Cell #2
Upper figure. ^{4}He concentration in the gas stream of cell #2 and reference cell #1
Bottom figure. Left ordinate: input power; Right ordinate: heat power excess

Table III. Summary of the calorimetric results

Cell #	Cathode diameter m m	Treat-ment	*Current density mAcm^{-2}	&Excess Power W	Vol.Exc Power Wcm^{-3}	Surf.Exc. Power Wcm^{-2}	Γ
2	2	no	1280	10.0±1.0	111	6.4	0.26
4	6	yes	460	2.0±0.2	3	0.46	0.13
8	3	yes	947	15.0±1.5	79	7.1	0.43
10	3	no	905	19.0±1.9	100	8.6	0.70

*Current density at the maximum excess power
&Maximum excess power

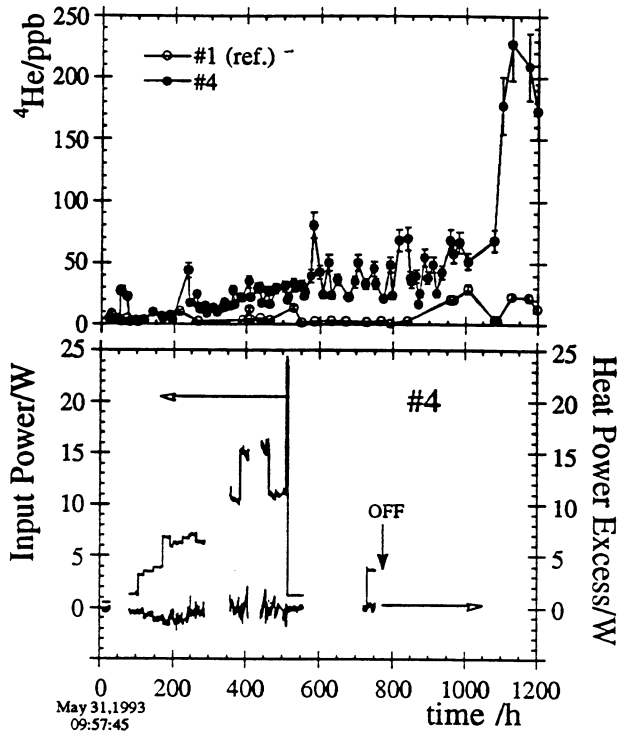

Figure 7: Cell #4
Upper figure. ^{4}He concentration in the gas stream of cell #4 and reference cell #1
Bottom figure. Left ordinate: input power; Right ordinate: heat power excess

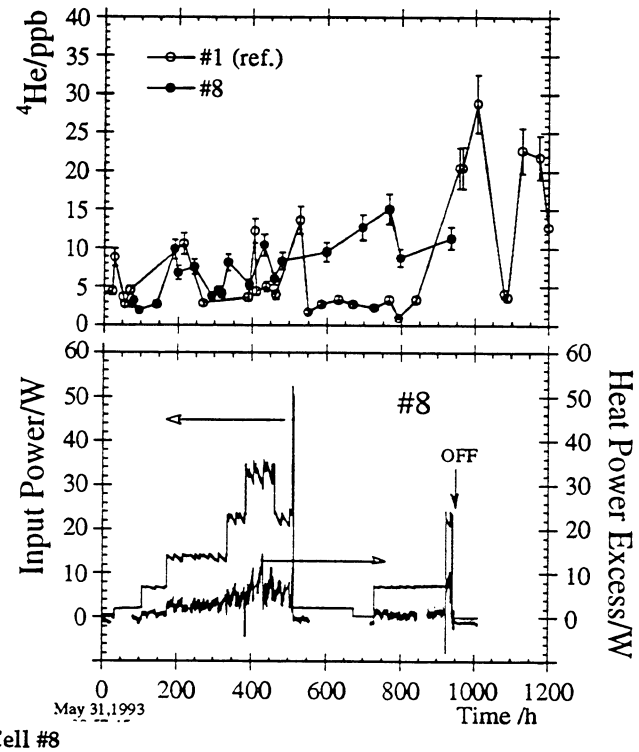

Figure 8: Cell #8
Upper figure. ^{4}He concentration in the gas stream of cell #8 and reference cell #1
Bottom figure. Left ordinate: input power; Right ordinate: heat power excess

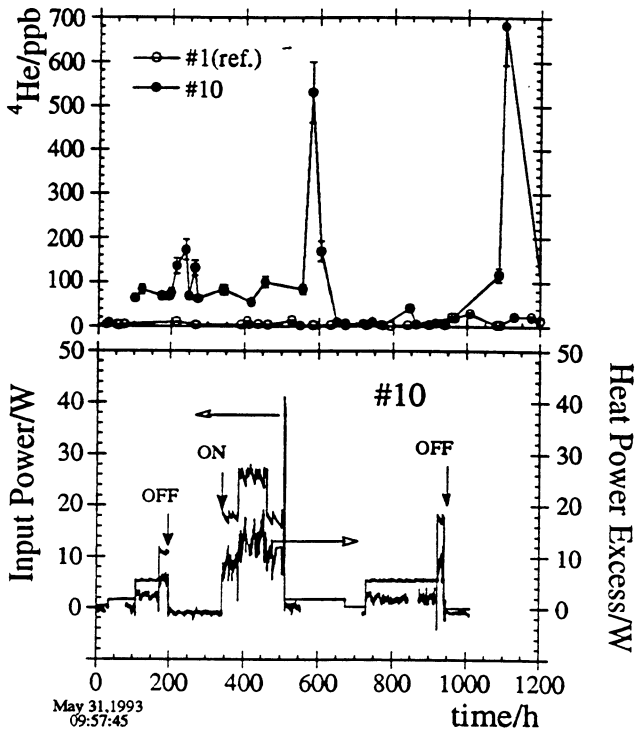

Figure 9: Cell #10
Upper figure. ^{4}He concentration in the gas stream of cell #10 and reference cell #1
Bottom figure. Left ordinate: input power; Right ordinate: heat power excess

Tritium data

Tritium data are reported in figs.10 and 11. In both fig. 11 five equal graphs are reported in which each of them gives $q^{\#}_{th}$, as calculated by eqn.12, $q^{\#}_{exp}$ measured in the recombined gases (we remind that $q^{\#}_{exp} = \frac{x^{\#}_g}{x^\circ}$) and only the values of the difference $\left(q^{\#}_{exp} - q^{\#}_{th}\right)$ satisfying the condition $\left(q^{\#}_{exp} - q^{\#}_{th}\right) \geq \frac{\Delta x_g}{x^\circ} = \frac{5}{80} = 6.25 \times 10^{-2}$, where Δx_g is the experimental error on the measurement, given in dpm ml^{-1}, of the atomic fraction of tritium in the recombined D_2O. In considering the plot of cell#1, it has to be taken into account that the theoretical equation has been calculated by assuming $\alpha_E(Pt) = \alpha_E(Pd)$. Since, notwhitstanding the criterion adopted before in discriminating $\left(q^{\#}_{exp} - q^{\#}_{th}\right)$ values, some $(q^{1}_{exp} - q^{1}_{th})$ values were still found > 0, to be conservative, the quantity of tritium atoms in excess in the electrolytic solution of each cell was obtained by subtracting the averaged data $(q^{1}_{exp} - q^{1}_{th}) > 6.25 \times 10^{-2}$. To calculate the integral curve of the excess of tritium atoms, the following equation was then used:

$$\int_0^t {}^3H\, dt = 9.17 \times 10^6\, \alpha_E x^\circ V^\circ \left\{ \int_0^t \left[(q^{\#}_{exp} - q^{\#}_{th}) - \overline{(q^{1}_{exp} - q^{1}_{th})} \right] dt \right\} \qquad (16)$$

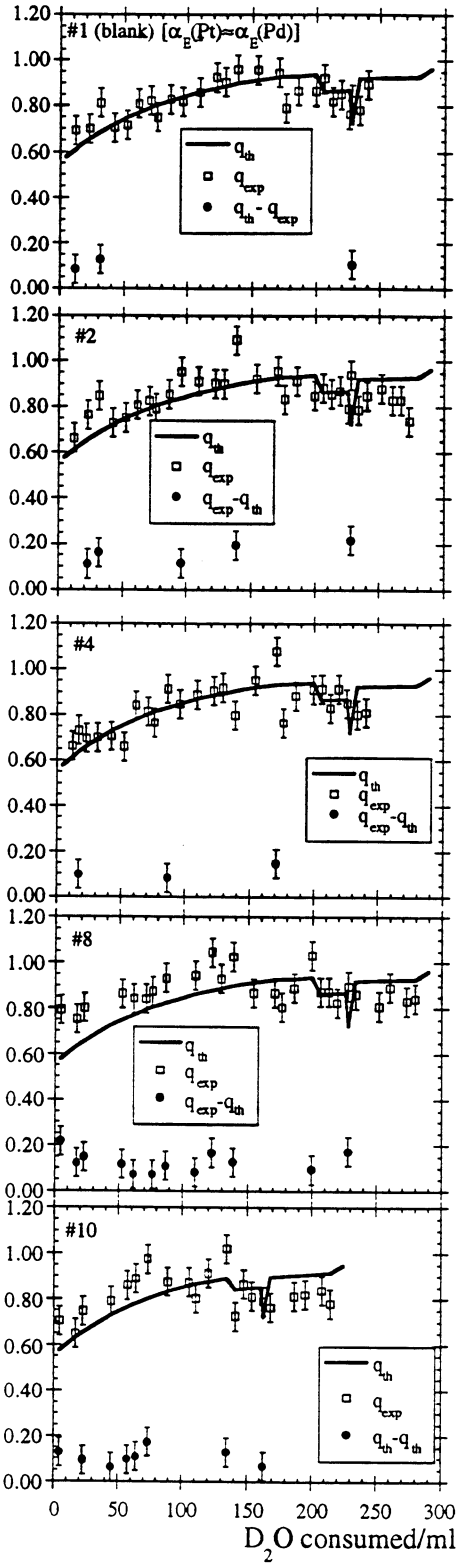

Figure 10
Tritium in recombined gases. Values of q_{th}, q_{exp} and (q_{th}-q_{exp}) for cells #1,#2, #4, #8 and #10.

by considering first that the combination of α_E and q allows to write $x^{\#} = \alpha_E x^{\circ} q^{\#}$ (see also the list of symbols and constant). As it clearly appears in fig. 11, through the procedure adopted, excess of tritium is present only in cells #2 and #8.

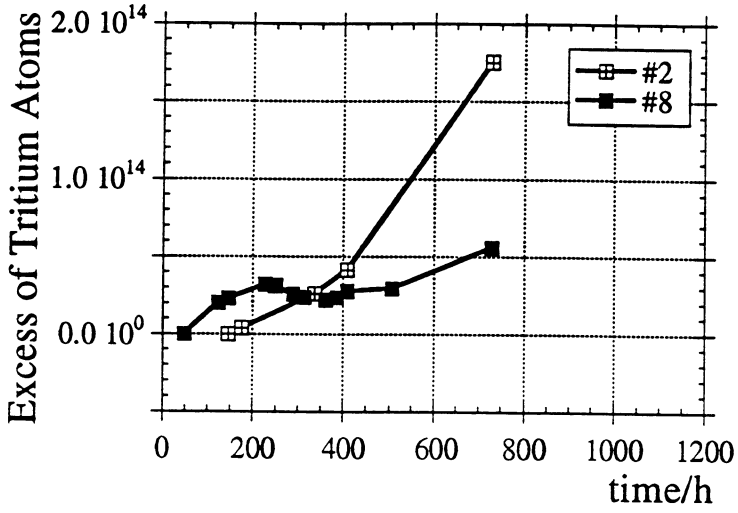

Figure 11
Excess of tritium atoms for cells #2 and #8

Neutrons data

In this experiment, there was no statistical evidence of neutron emission from the cells. Fig. 12 shows the number of neutrons detected each ten minutes by the groups of tubes no. 1, 3, 6, 11, 12 before and during the experiment.

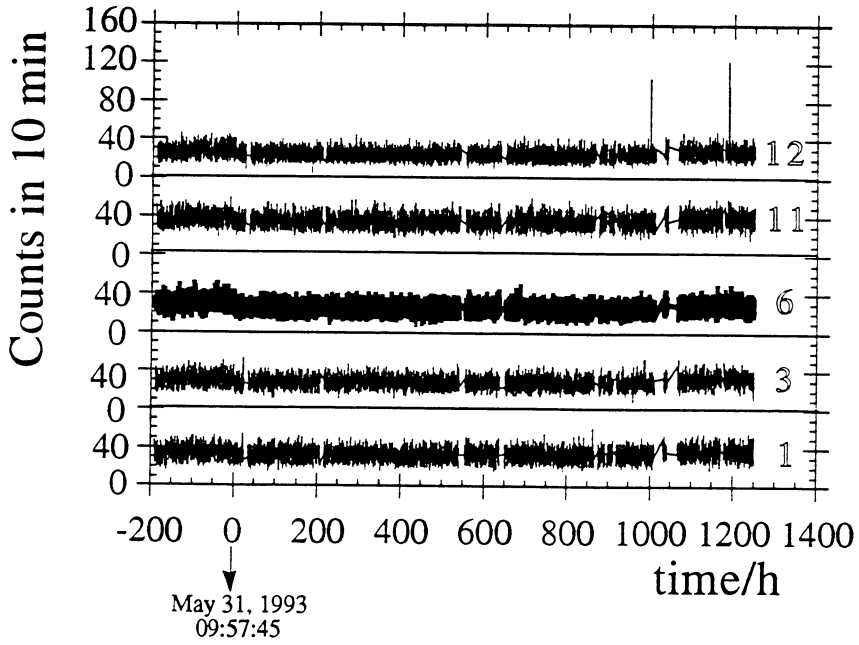

Figure 12
Counts in 10 min of 5 counting groups out of 12 before and after the starting of the experiment. For checking the positioning of the counting groups, see figure 4

The neutron countings vs time graphs of the other groups are not shown for readability purposes, but they show similar characteristics and trend. As shown in the figure, there is no statistical difference between the number of neutrons detected when the electrolysis was in progress and the background. Apparent exceptions are the two large countings of the group 12, which occurred beween ~ 900 and ~ 1200 hours. Howewer, simple considerations about the settlement of the experimental apparatus together with the check, by the oscilloscope, of the pulses coming from the groups of tubes, showed that the two great enhancements of the neutron counting rate of the group 12 (as well other enhancements detected by other groups not showed in fig. 12 and having the same characteristics), were not generated by neutrons. In fact:

- As shown in fig. 4, the presence of two rings of groups of tubes surrounding the toroid embedding the cells, assures that a bunch of neutrons coming from whichever cell (and also from the region outside the detector) must hit at least one group in each ring. Enhancements of the neutron counting of group 12, if generated by real neutrons, must hence be simultaneous to other enhancements of at least one of the outer ring groups. Particularly, the group 11 is bounded to detect an enhancement too;
- The normal shape of the analogical signal coming from a group hit by a neutron, as checked by the oscilloscope, is a peculiar negative shape (see fig. 6 of ref. 24). The two enhancements of the neutron counting detected by the group 12 were instead generated by anomalous pulses, in which a sudden, very large, negative drop of the signal was followed by oscillations around zero.

Discussion

Due to the absence of significant amount of neutrons and low excess of ^3H atoms with respect to the excess power measured we will try in the followings to consider the nuclear reaction

$$d + d = {}^4\mathrm{He} + 23.8\ \mathrm{MeV(lattice)} \qquad (17),$$

as originating the observed power excess. Therefore the most important comparison to be made is that between the power excess and the ^4He found assuming the above reaction as the source of both these quantities.

In order to compare the excess power data reported in figures 6 to 9 with ^4He found, it is necessary to evaluate the minimum sampling time, *mst*, defined as the time required to fill our sampling cylinder of volume V_S at the gas flow-rate J_G at the sampling stage (after the catalytic recombination). The *mst* quantity is given by:

$$mst = \frac{V_s}{J_G} = \frac{PV_s}{\left[\frac{P}{RT_r} f_{N_2} + \frac{3}{4F}(1-\eta)I\right] RT_r} \qquad (18)$$

The quantity so calculated corresponds to the time which would be spent by an ideal piston moving at constant velocity from the bottom to the top of the sampling cylinder. This is like to say that the entering gas moves pushing out the pure N_2 initially present in the cylinder. Under this hypothesis, the composition

of the gas trapped in the cylinder at sampling is representative of the gas composition during the last *mst* seconds before the sampling independently of the fluxation time. In fig. 13 (right scale), the equation 18 is reported *vs* the electrolysis current at different values of η. It appears that in the range of our experimental conditions the *mst* value is confined within a short range of variability and, in any case, is at least 12 times lower than the sampling time we effectively adopted because of the reasons shown elsewhere (28). As expected from eqn. 18, for $\eta \rightarrow 1$, *mst* is independent of the electrolysis current value. Therefore, if the heat power excess is measured in the gas phase, by considering the mass flux balance in the cell it is possible to calculate the expected ^{4}He concentration, $x_{^4He}$, produced through reaction 17, in the sampled gas stream by the equation below:

$$x_{^4He} = \frac{\frac{q_r}{N_A}\int_0^t P_{exc}\,dt}{\frac{P}{RT_r}f_{N_2}t + \frac{3}{4F}(1-\eta)\int_0^t I\,dt + \frac{q_r}{N_A}\int_0^t P_{exc}\,dt} \cong \frac{\frac{q_r}{N_A}P_{exc}}{\left[\frac{P}{RT_r}f_{N_2} + \frac{3}{4F}(1-\eta)I\right]} \qquad (19)$$

The approximate term implies P_{exc} constant on time in the integration interval and the contribution of ^{4}He flux negligible with respect the sum of the other fluxes. From eqn. 19, one sees that the ^{4}He concentration measurable in the gas stream depends on some experimental parameter which is mandatory to keep under control. In fig. 13 (left scale), the quantity $\frac{\partial x_{^4He}}{\partial P_{exc}}$, derived from eqn. 19, is plotted against the electrolysis current. For $\eta \rightarrow 1$, also the specific ^{4}He concentration becomes independent from I.

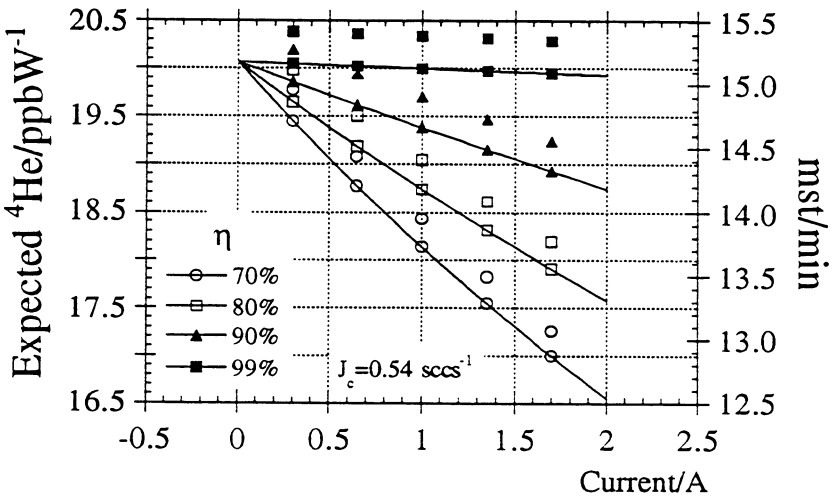

Figure 13

Left scale: Specific ^{4}He expected to be measured in the electrolysis gases per 1 W of excess power as function of electrolysis current at different values of η.

Right scale (scatter plots): Minimum sampling time, *mst*, as function of the electrolysis current η is the recombination yield

To convert the experimental concentration values (in ppb) of ^4He into excess power, the following equation was used:

$$\overline{P_{exc}} = 10^{-9}\, e\, n_{tot}\, q_r \frac{x_{^4He}}{mst} = 46.9788 \frac{x_{^4He}}{mst} \qquad (20)$$

where $n_{tot} = \frac{N_A P V_s}{R T_r}$ is the total number of molecules in the sampling cylinder. $\overline{P_{exc}}$ calculated by eqn. 20 has to be intended averaged on *mst*.. In fig. 14, we give in separate plots for cell #4 and #10, respectively, top and bottom part of the figure,

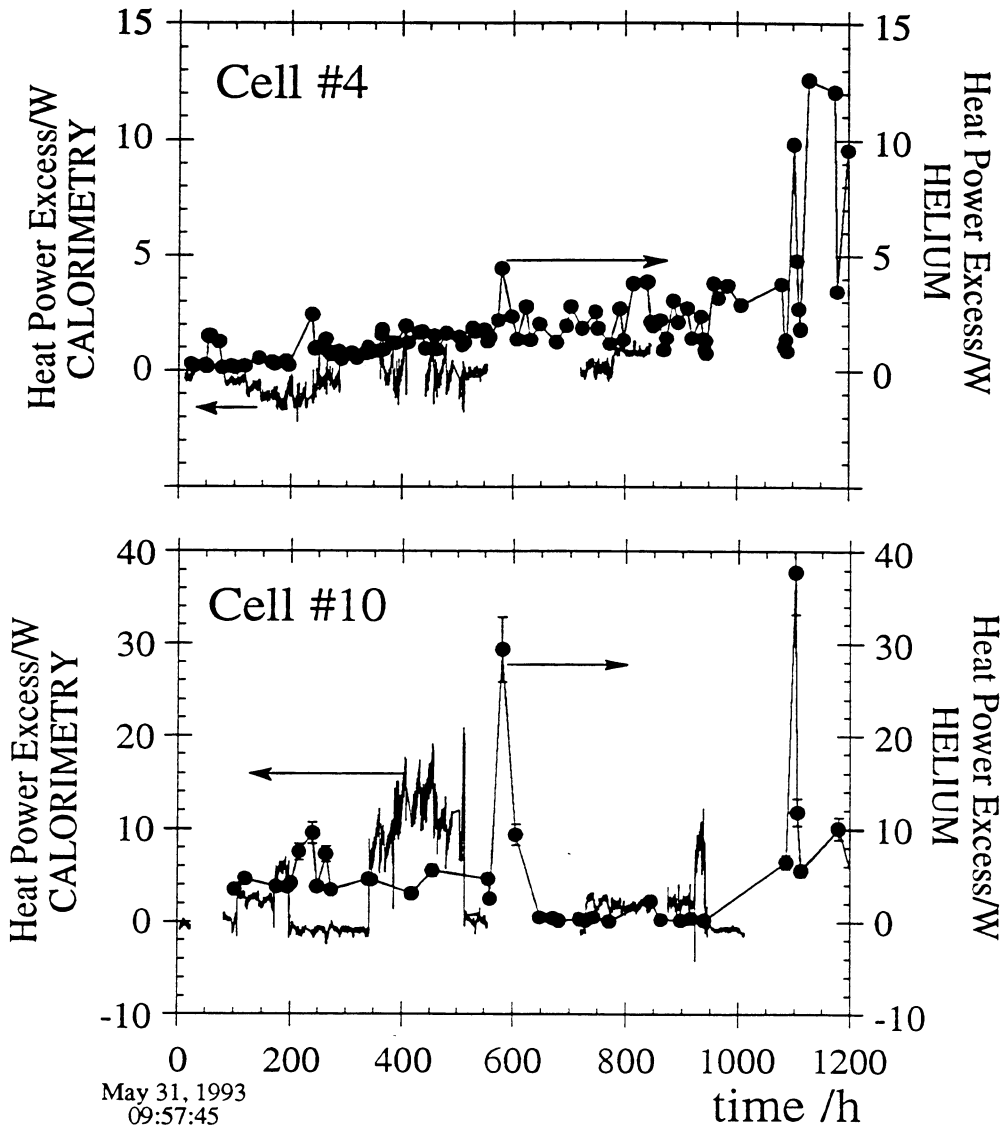

Figure 14
Upper figure: cell #4; Bottom figure: cell #10
Left ordinate: Heat power excess as measured by calorimetry. Continuous line
Right ordinate: Heat power excess calculated by ^4He data (reaction 17 and eqn.20). Circle points

the heat power excess, as obtained by calorimetry, left scale, (see figs. 7 and 9 bottom plots right scales), and on the right scale the heat power excess calculated by eqn. 20 through ^4He data (see figs. 7 and 9 upper plots). It is important to observe that in each plot of fig. 14 the two heat power excess quantities, obtained in a completely independent way, are comparable (note that the limits of the ordinate scales are the same in each plot). It is evident by examining fig. 14 that two different processes are at work and in both cases the ^4He concentrations are clearly higher than the respective ^4He backgrounds before the start of the experiment (not for cell #10 because we have not background) other than the background found in the blank cell #1. If we limit to the time interval where electrolysis is still on (see fig. 5), we observe for cell #4 a progressive increase of the heat power excess from ^4He, HPEH, to compare with a quite constant and low heat power excess from calorimetry, HPEC. This trend is clear even if the error bars are considered for both the quantities, though, quite at any time, (HPEH $\pm$ ΔHPEH) $\approx$ (HPEC $\pm$ ΔHPEC) holds. In cell #10, the result (HPEH $\pm$ ΔHPEH) > (HPEC $\pm$ ΔHPEC) is always found only when the electrolysis current was drastically decreased or off. In all other cases, HPEC prevails. What is impressing is that ^4He recovering is systematically found after generation of excess heat. Concerning the evaluation of ΔHPEC, this was already treated in the experimental section while the evaluation of ΔHPEH originates immediately from eqn. 20 being this quantity proportional to the error in the ^4He determination (28). The application of eqn. 20 to the ^4He data of cells #2 and #8 (figs. 6 and 8, respectively) leads to HPEH values lower than 0.6 $\pm$ 0.1 W after subtracting the ^4He background before the starting of the electrolysis. This value is in any case better (but comparable to) than the calorimetric detection limit as shown in Table II. According to fig. 13 and the maximum HPEC found, the corresponding maximum values of the ^4He concentration expected for cells #2 and #8 should be, respectively, 195 and 292 ppb. This is far enough from the experimental findings. A similar reasoning better matches for cell #10 and partially also for cell #4. Therefore, apparently, we are left with the dilemma of one cell which shows a ^4He concentration in the gas phase of the correct order of magnitude (with respect to the heat excess) while others, cell #2 and cell #8, do not. On the other hand it must be pointed out that before drawing any particular conclusion two central questions are to be answered: *does it exist a time relation between the heat generation and ^4He release out from the surface* ? and, if yes, *is the delay a function of how the source is deep inside with respect to the electrode surface* ?

To our knowledge, there are not yet experimental evidences to answer satisfactorily to these questions. On the other hand some pieces of general information on this argument comes only from the experiments carried out for studying the effect of the ^3He, as product of tritium decay, on mechanical and physical properties of materials candidate for hot fusion reactors (33). However, our hypothesis on the behaviour of helium in Pd when it is generated *in situ* is based on the fact that being highly insoluble, it nucleates everywhere a point or linear defect exists. The transformation from a cluster of a few atoms to microbubbles depends on the extension of the defects and/or to the possibility of migration of defects. The probability for a bubble to reach the surface is in any case very low and increases on decreasing the distance between the nucleation

centre and the surface. If this distance becomes greater than 10 nm (see M.W. Lee in ref. 16), the calculated time required for ^4He to reach the surface could be as long as 14 years (34). Up to this point we believe this scheme applicable to all the metals and alloys, but things could seriously change in the case of a Pd specimen subject to a process where defects are continuously generated and propagate quite randomly in the metallic matrix due to D charging. In this case, the pattern for ^4He to reach the surface could be through the defects (sometimes so extended that they collapse generating fractures) produced by D loading. If so, we can expect any time correlation between the time of heat generation and ^4He release, except be made when the site of the nuclear reaction is the surface itself or some monolayers below. It appears that the recovery of ^4He in the gas phase of different electrodes (, and therefore different microstructures,) is far from being expected to occur at any definite and predictable rate. Therefore, under this hypothesis, all the results of heat excess and ^4He we showed keep their own consistency.

For the above considerations, we have to expect that the condition HPEH ≤ HPEC should be commonly found. An experimental evidence consistent with the reasoning above comes from the literature (3) in which the energy associated to ^4He was found more or less an order of magnitude lower than the energy found by calorimetry.

The integration of HPEH and HPEC data of cell #10 given in fig. 14 is reported in fig. 15 where throughout the experiment the heat excess from ^4He is found comparable with the heat excess measured by calorimetry, though, the former is, in extended interval of time (from 200 to 500 h and from 600 to 1050 h), greater than the latter.

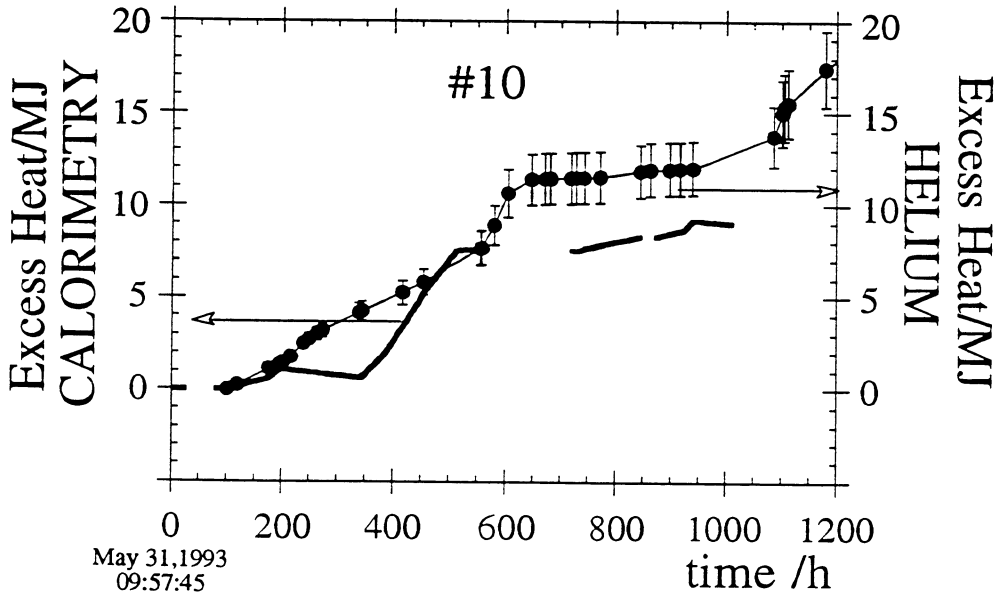

Figure 15: Cell #10
Left ordinate: Heat excess obtained by integration on time of heat power excess as measured by calorimetry (fig. 9 bottom figure right ordinate)
Right ordinate: Heat excess obtained by integration on time of eqn.20

According to the reasoning above this is not allowed and we have to introduce in the discussion the possibility of another source of ^4He, likely, air contamination in some extent as it appears from the ^{20}Ne detection[7] (28). Concerning the error bar on solid curve of fig. 15, the same considerations given before for the other curves containing calorimetric data still hold.
Concerning tritium data it should be noted that in the plots of fig.10 and 11 there are a few number of experimental points, $q^{\#}_{exp}$, not only exceding the expected value, $q^{\#}_{th}$, over the experimental error, but ≥ 1. It is easy to demonstrate from eqn 13 that the condition $q_{lim} \geq 1$, in absence of tritium generation, would produce the result $\frac{\alpha_E}{\alpha_V} \leq 1$ which is clearly impossible due to the fact that α_E must be >1 and $\alpha_V \cong 1$. This constitutes a strong rigorous support in favor of generation of tritium, even if, this seems to occurs at low level and sporadically. On the other hand, it is important to remind that the tritium measurement is not an on-line measurement and since it is done on the recombined D_2O, the minimum time interval between two samplings is the time necessary to produce at least 1 ml of D_2O which is the suitable volume to perform the tritium determination. This time is given by $\frac{2F}{\bar{\nu} I \eta}$. By considering the current plots (see fig . 5), the time required varies from ≈1 (at I=2.5 A) to ≈33 (at I=0.1A) hours. For practical reasons is not possible for us to perform the tritium test every 1 ml of D_2O produced, expecially at the highest current values, so very often the sampling (of 1 ml) is made on a higher volume of D_2O. In the case of spike-wise release of tritium in the cell, as it is likely expected, this implies to loose this time structure because of the dilution effect which flats the concentration profile. Further key point to take into consideration, often not sufficiently stressed in discussing tritium measurements, is the distribution of tritium generated, if any. It is our opinion, also supported in literature (35,36), that tritium should be mostlty searched in the cathode and/or in the gas phase. In fact, if tritium is produced in the bulk of the cathode, it can be trapped and/or released on time as DT (g). If generated at the surface, the DT molecules go directly in the gas phase. According to the general adopted mechanism (37) of H (D) electrolytic reduction on a cathode, *Me*, the H_2 (D_2) formation step can follow two different processes:

$$D_{ads}(Me) + D_{ads}(Me) = D_2\,(g) \qquad (21A)$$

and/or

$$D_{ads}(Me) + D_2O + e(Me) = D_2\,(g) + OD^- \qquad (21B)$$

If tritium atoms, *T*, are produced, at the *Me* surface, reactions 21 become:

$$D_{ads}(Me) + T_{ads}(Me) = DT\,(g) \qquad (22A)$$

and/or

$$T_{ads}(Me) + D_2O + e(Me) = D_2\,(g) + OT^- \qquad (22B)$$

---

[7]Without invoking the concurrent release of both ^4He and ^{20}Ne

Through step 22B, it is possible to keep tritium in the solution as really found and reported previously (20,24,25). There is not other process allowing to tritium to remain in the solution in significative extent being the solubility of DT in D_2O and the catalyzed reaction of T at the cathode with dissolved oxygen in solution to give DTO, very negligible processes. Therefore, a complete balance of tritium would require its measurement in both the Pd cathode and the solution. Furthermore, as we did, the tritium is measured in the gas phase via the external catalytic recombination two factors does exist which concurr to give a result in defect: *i*) the isotopic effect on the catalytic recombination which increases the rate of the D_2O formation with respect to DTO; *ii*) the stoichiometric ratio $\frac{D_2}{O_2}$, fixed by the electrolysis and good for the recombination, is no more strictly satisfied in the recombinator when tritium is generated.
From fig. 11, it appears that a net production of tritium atoms, significatively out of the experimental errors (we remind the procedure showed in the results section) only occurs in the cells #2 and #8. Incidentally, in these cells ^4He was found to be very low and not comparable with the excess heat.
If the channel of tritium of the plasma fusion *d,d* reaction is invoked, we can calculate that the energy released throughout the experiment in the case of cell #2, for instance, is 115 J, whereas, a rough evaluation of the integrated heat excess measured by calorimetry in the same cell (see fig. 6) is more than four order of magnitude higher. By the same reasoning, we should expect an excess of neutrons with respect to the background equal to the number of tritium atoms. This would imply a maximum averaged rate of $\approx 7 \times 10^7$ ns^{-1}. This rate value other than to be very dangerous, it would be easily detectable whereas, as shown in fig. 12 no excess of neutrons above the background was measured.

Conclusions

Our calorimetric results show excess power quite *in linea* with the other positive results reported up to now. In particular, if one considers the power excess per unit electrode surface area as a function of the current density, a fair agreement is found with the general behaviour first pointed out by Storms (38) by considering many calorimetric measurements on the Pd- D_2O electrolysis carried out at room temperature in different laboratories with different calorimetric devices and procedures were used. As concerns the nuclear products, in the present experiment, a lack of neutrons and a low tritium excess on two cells out of four has been observed contrarily to what expected on the basis of *d,d* reactions . Also, under this respect our results do confirm the previous findings which exhibited such a large unbalance. As for the ^4He measurements in the escaping gases, the detection of ^{20}Ne (28), prevents to draw definite conclusions from the comparison with the calorimetric data. However it cannot be left unnoticed the notable commensurate amounts of ^4He and heat excess found in the case of cell #10. Quite striking is also the time pattern of the amount of ^4He recovered which, shifted in time, does match the power excess time pattern observed. The different quantities of ^4He recovered from different cells (e.g. #8 and #10) where power excesses of same order of magnitude have been observed, if understandable by invoking different kinetics of the ^4He release, highlight the

usefulness of being able to perform a complete energy and mass balance by taking into account also the ^4He content of the electrodes.

Acknowlegments
The financial supports of the National Research Council (CNR), the National Institute of Nuclear Physics (INFN) and the Physics Laboratory of the Istituto Superiore di Sanità are gratefully acknowledged.
We are grateful to Dr. M. Achilli and Prof. E. Cardarelli for the chemical analyses by ICPAES and to Dr. D. Ferro for the skilful SEM analysis on the cathodes.

References

1. M. Fleischmann and S. Pons, Physics Letters A, **176** (1993) 118
2. D. Albagli et al., J. Fusion Energy, 9 (1990) 133
3. B.F. Bush, J.J. Lagowski, M.H. Miles and G.S. Ostrom, J. Electroanal. Chem., **304** (1991) 271
4. N. Lewis et al., Nature, **340** (1989) 525
5. M.H. Miles, R.A. Hollins, B.F. Bush, J.J. Lagowski and R.E. Miles, J. Electroanal. Chem., **346** (1993) 99
6. E. Yamaguchi and T. Nishioka, ICCF3, 3rd International Conference on Cold Fusion, Nagoya, October 21-25, 1992, Proc. in Frontiers of Cold Fusion, Edited by H. Ikegami, Frontiers Science Series no.4, Universal Academy Press Inc., Tokyo (1993), p.179
7. J. O'M. Bockris, C.C. Chien, D. Hodko and Z. Minevski, Proc. in Frontiers of Cold Fusion, Edited by H. Ikegami, Frontiers Science Series no.4, Universal Academy Press Inc., Tokyo (1993), p.231
8. B.Y. Liaw and P.L. Tau, J. Electroanal. Chem., **319** (1991) 161
9. P.L. Hagelstein, J. Fusion Energy, 9 (1991) 451; see also ICCF4 ref. 16
10. G. Preparata, in: Common Problems and Ideas of Modern Physics, Eds. T. Bressani, B. Minetti and A. Zenoni, (World Scientific, 1992); G. Preparata, in: The Science of Cold Fusion: Proc. Second Annual Conf. on Cold Fusion, ACCF2, Como, Italy, 29 June - 4 July 1991, Eds. T. Bressani, E. Del Giudice and G. Preparata, vol.33 of the Conf. Proc. of the Italian Physical Society , (Bologna, 1991), p. 453
11. J. Schwinger, Z. Phys.D, **15** (1990) 21; Z. Naturforsch. A, **45** (1990) 756; see also ICCF4 ref. 16
12. H. Rambaut and J.P. Vigier, Physics Letters A, **142** (1989) 447; **148** (1990) 229; **163** (1992) 335
13. Proc. First Annual Conf. on Cold Fusion, ACCF1, Salt Lake City, Ut, 28-31, March 1990
14. Proc. Second Annual Conf. on Cold Fusion, ACCF2, Como, Italy, 29 June - 4 July, 1991, Eds. T. Bressani, E. Del Giudice and G. Preparata, The Science of Cold Fusion, vol.33 of the Conf. Proc. of the Italian Physical Society , (Bologna, 1991)
15. Proc. Third Int. Conf. on Cold Fusion, ICCF3, Nagoya, 21-25 October, 1992 , Frontiers of Cold Fusion, Ed. H. Ikegami, Frontiers Science Series no.4, (Universal Academy Press Inc., Tokyo 1993)
16. Proc. Fourth Int. Conf. on Cold Fusion, ICCF4, Lahaina, Hawaii, Dec. 6-9, 1993, (EPRI Proc.), to be published

17. Workshop on Cold Fusion Phenomena, Santa Fe, NM, May 22-25, 1989, Proc. on J.Fusion Energy, **9** (1990)
18. Anomalous Nuclear Effects in Deuterium/Solid Systems, Provo, UT, October 22-24, 1990 AIP Conference Proceedings **228**, (Eds. S. Jones, F. Scaramuzzi and D.Worledge), American Institute of Physics (New York) 1991
19. D. Gozzi, P.L. Cignini, L. Petrucci, M. Tomellini, G. De Maria, S. Frullani, F. Garibaldi, F. Ghio and M. Jodice in: Understanding Cold Fusion Phenomena, Eds. R.A. Ricci, E. Sindoni and F. De Marco, vol. **24** of The Conf. Proc. of the Italian Physical Society , (Bologna, 1989), p.
20. D. Gozzi, P.L. Cignini, L. Petrucci, M. Tomellini, G. De Maria, S. Frullani, F. Garibaldi, F. Ghio and M. Jodice, Nuovo Cimento, **103A** (1990) 143-154
21. M. Tomellini and D. Gozzi, J. Mat.Science Lett., **9** (1990) 836-838
22. D. Gozzi, P.L. Cignini, L. Petrucci, M. Tomellini, G. De Maria, S. Frullani, F. Garibaldi, F. Ghio, M. Jodice and E. Tabet, J. Fusion Energy, **9** (1990) 241-247
23. D. Gozzi, P.L. Cignini, L. Petrucci, M. Tomellini, S. Frullani, F. Garibaldi, F. Ghio, M. Jodice and G.M. Urciuoli in: Anomalous Nuclear Effects in Deuterium/Solid Systems, Eds. S. Jones, F. Scaramuzzi and D.Worledge, AIP Conf. Proc. vol. **228**, (American Institute of Physics, New York, 1991), p. 481
24. D. Gozzi, P.L. Cignini, M. Tomellini, S. Frullani, F. Garibaldi, F. Ghio, M. Jodice and G. M. Urciuoli, Fusion Technol., **21** (1992) 60
25. D. Gozzi, P.L. Cignini, M. Tomellini, S. Frullani, F. Garibaldi, F. Ghio, M. Jodice and G. M. Urciuoli in: The Science of Cold Fusion: Proc. Second Annual Conf. on Cold Fusion, ACCF2, Como, Italy, 29 June - 4 July 1991, Eds. T. Bressani, E. Del Giudice and G. Preparata, vol.**33** of the Conf. Proc. of the Italian Physical Society , (Bologna, 1991), p. 21
26. D. Gozzi, P.L. Cignini, R. Caputo, M. Tomellini, G. Balducci, G. Gigli, E. Cisbani, S. Frullani, F. Garibaldi, M. Jodice and G. M. Urciuoli in: Frontiers of Cold Fusion, Ed. H. Ikegami, Frontiers Science Series no.**4**, (Universal Academy Press Inc., Tokyo 1993), 155
27. D. Gozzi et al., submitted to J. Electroanal.Chem.
28. D. Gozzi et al., *Helium-4 Quantitative Measurements in the Gas Phase of Cold Fusion Electrochemical Cells*, companion paper in this book
29. J. Balej and J. Divisek, J. Electroanal. Chem., **278** (1989) 85
30. Handbook of Physics and Chemistry , 60th Edition, R.C. Weast Ed., CRC Press Inc. (1980)
31. Hydrogen in Metals, Edited by G. Alefeld and J. Völkl, Springer-Verlag, Heidelberg, vol. II p.95 (1978)
32. D. Gozzi et al., *Electrochemical Confinement of Deuterium in Palladium*, paper in preparation
33. E. Ruedl et al.; F. Carsughi et al.; P. Gondi, Proc. of Research, Development and Technology of Fusion Reactor Materials, ENEA, Frascati, Dec. 4-6, 1990
34. G.J. Thomas and J.M. Mintz, J. Nucl.Mat., **116** (1983) 336
35. F. G. Will, K. Cedzynska and D.C. Linton, ICCF4, 4th International Conference on Cold Fusion, Lahaina, Hawaii, December 6-9, 1993, EPRI Proceedings to be published
36. K. Cedzynska, S.C. Barrowes, H.E. Bergeson, L.C. Knight and F.G. Will, Anomalous Nuclear Effects in Deuterium/Solid Systems, Provo, UT, October 22-24, 1990 AIP Conference Proceedings **228**, (Eds. S. Jones, F. Scaramuzzi and

D.Worledge), American Institute of Physics (New York) 1991, p. 463; Fusion Technol., 20 (1991) 108; Fusion Techñol., 22 (1992)156
37. J. 0'M. Bockris and A.K.N. Reddy, Modern Electrochemistry, vol. 2 ch.10, Plenum Press, New York (1974)
38. E. Storms, Fusion Technol. 20 (1991) 433

APPENDIX A

List of Symbols

α_E	electrolytic separation factor $\equiv \frac{x_g}{x}$	
α_V	isotopic separation factor in the vaporization $\equiv \frac{x_g}{x}$	
a_{D_2}	activity of D_2 in the gas phase	
a_i	intercept of the calibration curve of the i-th cell	W
b_i	slope of the calibration curve of the i-th cell	W °C^{-1}
C_g	heat capacity of D_2O vapour	J (mol K)$^{-1}$
C_l	heat capacity of D_2O liquid	J (mol K)$^{-1}$
C_r	relative capacity of Pd sponge trap	
C_s	heat capacity of solution	J (mol K)$^{-1}$
C_{trap}	nominal capacity of Pd sponge trap for D_2	mol
d	deuterium nuclei	
d	inner diameter of cell	m m
f_{D_2O}	feed of D_2O to the cell	moli s^{-1}
f_G	gas flow-rate of the gas mixture	moli s^{-1}
f_{N_2}	N_2 flow-rate	scm^{3}s^{-1}
f_{cond}	correction for D_2O condensation in recombinator	cm^{3}s^{-1}
Γ	ratio of excess power on input power	
h	height of the solution level in the cell	m m
h	recombination yield	
I	electrolysis current	A
k_{Pyrex}	heat conductivity constant of Pyrex	W (m K)$^{-1}$

k_{Rad}	Stefan Boltzmann constant	Wm^2K^{-4}
L	heat of evaporation of D_2O	J mol^{-1}
l	thickness of Pyrex wall of the cell	m m
M	molar mass of D_2O	g mol^{-1}
M_{Pd}	atomic mass of Pd	g mol^{-1}
m_S	mass of solution	mol
mst	minimum sapling time	s
n_{D_2O}	number of moles of D_2O in V°	
n_{tot}	total number of molecules in V_S	
P	Atmospheric pressure	kPa
p	vapour pressure of D_2O	Pa
p_{D_2}	$D_2(g)$ partial pressure	Atm
$P_{exc,i}$	excess of heat power of the i-th cell	W
P_{in}	input power	W
P_{out}	output power	W
q_r	energy released by reaction 17	MeV
r	correlation factor in linear regression	
ρ_l	density of D_2O	kgm^{-3}
t	time constant	s
T_r	temperature of room	°C
T_S	temperature of solution	°C
T_s^0	temperature of solution at P_{in} =0	°C
T_{tb}	temperature of thermostated bath	°C
T_{tb}^0	temperature of thermostated bath at P_{in} =0	°C
V	voltage of the cell	V
v_{cons}	volume of D_2O consumed by electrolysis	cm^3
v_{rec}	volume of D_2O recombined	cm^3
$\bar{v}$	molar volume of D_2O	$cm^3\,mol^{-1}$
V_S	volume of the sampling bottle	cm^3
V_{th}	thermoneutral potential	V
V°	volume of solution in the cell	cm^3
w_{Pd}	weight of Pd sponge in the trap	g
x	atomic fraction of DTO in D_2O	
x_f	atomic fraction of DTO in D_2O feed	
$x_{^4He}$	atomic fraction of ^4He in the gas mixture	
x_g	atomic fraction of T in the gas mixture	
x°	starting atomic fraction of DTO in the electrolyte	
y	D/Pd atomic ratio	
ΔH°	standard enthalpy change of formation of D_2O_l	kJ mol^{-1}
ΔH_{abs}	enthalpy change of reaction 8	kJ mol^{-1}
ΔS_{abs}^0	standard entropy change of reaction 8	J $mol^{-1}K^{-1}$
ΔT_i	$\Delta T_i = \left(T_s - T_s^0\right)_i - \left(T_{tb} - T_{tb}^0\right)_i$	°C

APPENDIX B

List of constants

α_E	electrolytic separation factor	1.8	
α_V	isotopic separation factor in vaporization	≈1	
C_g	heat capacity of D_2O vapour	44.500	J (mol K)$^{-1}$
C_l	heat capacity of D_2O liquid	84.349	J(mol K)$^{-1}$
C_{trap}	nominal capacity of Pd sponge trap	≈0.47	D_2 moles
d	inner diameter of cell	22.0	m m
e	elementary charge	1.60219x10^{-19}	C
F	Faraday constant	96484.6	C mol^{-1}
f_{N2}	N_2 flow-rate	0.54	scm^{3}s^{-1}
h	height of the solution level in the cell	≈ 180	m m
k_{Pyrex}	heat conductivity constant of Pyrex	0.878	W (m K)$^{-1}$
k_{Rad}	Stefan Boltzmann constant	5.6703x10^{-8}	Wm^{2}K^{-4}
L	heat of evaporation of D_2O	41.673	kJ mol^{-1}
l	thickness of Pyrex wall of the cell	2	m m
M	molar mass of D_2O	20.02748	g mol^{-1}
M_{Pd}	atomic mass of Pd	106.42	g mol^{-1}
N_A	Avogadro number	6.02205x10^{23}	mol^{-1}
P	Atmospheric pressure	101.3 (nominal)	kPa
p	vapour pressure of D_2O	7.83x10^{2}exp(5.143x10^{-2}T$_S$)	Pa
p_{DTO}	vapour pressure of DTO	7.66x10^{2}exp(5.165x10^{-2}T$_S$)	Pa
q_r	energy released by reaction 17	23.8	MeV
R	ideal gas constant	8.31441	J (mol K)$^{-1}$
r_l	density of D_2O	1.1055	gcm^{-3}
T_r	temperature of room	20±1	°C
T_{tb}	temperature of thermostated bath	21.0±0.1	°C
$\bar{v}$	molar volume of D_2O	18.116	cm^3 mol^{-1}
V_s	volume of the sampling bottle	500	cm^3
V_{th}	thermoneutral potential	1.53668	V
V°	volume of solution in the cell	≈53	cm^3
$x°=x_f$	starting atomic fraction of DTO in the electrolyte	80	[8]dpm ml^{-1}
y	D/Pd atomic ratio (at 298 K, $p_{D_2} = P$)	0.67	
ΔH°	standard enthalpy change of formation of D_2O_l	296.53	kJ mol^{-1}
ΔH_{abs}	enthalpy change of reaction 8	$\Delta H_{abs}(y) = 95.5 - 89.96y$	kJ mol^{-1}
ΔS^0_{abs}	standard entropy change of reaction 8	106.3	J mol^{-1}K^{-1}

[8][1 dpm = 1 disintegration per min =9.17x10^6 atomi T min^{-1} = 4.50x10^{-7} μCi]

OBSERVATION OF EXCESS HEAT DURING ELECTROLYSIS OF 1M LiOD IN A FUEL CELL TYPE CLOSED CELL

N. Hasegewa, N. Hayakawa, Y. Tsuchida, Y. Yamamoto, and K. Kunimatsu
IMRA JAPAN CO. LTD.
3-6 Techno Park 2 cho-me, Shimonopporo Atsubetsu-ku
Sapporo, 004 Japan

Abstract

Measurements of electrolytic deuterium loading into Pd and Pd-Rh alloy cathodes and excess heat during electrolysis in 1M LiOD have been conducted simultaneously in closed cells with a fuel cell anode pressurized by deuterium gas. The excess heat up to 4-5W/Pd cc has been reproduced by using Pd rod cathodes from various sources. Excess heat increases with electrolysis current density higher than ca 0.1-0.2 A/cm^2, cathode overvoltage and D/Pd higher than 0.80-0.84, but its dependence on D/Pd or D/M appears to be specific to each cathode material in the region of high cathode loading, where the current density or overvoltage appears to be a more important parameter to control the amount of excess heat than the cathode loading.

Introduction

In our previous paper presented at ICCF3[1,2] we reported our first data to show the excess heat generation as a function of deuterium loading ratio, D/Pd, as well as the electrolysis current density. The data showed existence of the threshold loading ratio and the current density around 0.84 and 100 mA/cm^2, respectively, and suggested generation of the higher excess heat if we could extend our measurements into the region of D/Pd higher than 0.90. However, we could not realize the experimental condition to have D/Pd higher than 0.88 for the Pd cathode in 1M LiOD even at high current densities close to $1A/cm^2$.

The aim of the present investigation is in two folds: firstly to reproduce the previous data to show the dependence of the excess heat generation on D/Pd in 1M LiOD, and secondly to investigate the dependence in the region of D/Pd higher than 0.9. In order to obtain the higher D/Pd, however, we had to employ new approaches by modifying the Pd cathode surface with a surfactant, thiourea, and by employing a new cathode material, Pd–Rh alloys.

Surfactants such as thiourea are known to inhibit Tafel step of the hydrogen evolution reaction at hydrogen electrodes, and Enyo and Maoka[3] showed that hydrogen loading ratio for a given current density at a palladium cathode increases a few percent in 1M H_2SO_4 in the presence of 10–5M thiourea. We firstly investigated effect of thiourea on the hydrogen and deuterium loading for Pd in 1M LiOD as function of current density and conducted excess heat measurements in the presence of 0.6 mM thiourea. It should be noted that surface modification of the Pd cathode by organic surfactants such as thiourea is possible only in electrolysis cells utilizing fuel cell anodes the potential of which is not high enough to oxidize thiourea electrochemically during electrolysis, while oxygen evolving anodes can easily destroy such organic substances due to its high working potentials. This is probably one of the reasons why inorganic substances such as aluminum, silicon and boron are employed for the purpose of surface modification of the Pd cathode in electrolysis cells utilizing oxygen evolving anodes [4].

The Pd–Rh alloys are known to have higher D/M(Pd+Rh) under high hydrogen pressures than palladium, where M represents the total number of Pd and Rh atoms in the alloy. D/M = 1.01 was reported for the alloy with 30 atomic % rhodium [5]. The crystal structure of the Pd-Rh alloys is the same as Pd, fcc, and its lattice constant is smaller than Pd and decreases with increasing Rh content . It is expected, therefore, to have much higher deuterium density in the Pd–Rh alloys than Pd because of the higher D/Pd ratio combined with the smaller lattice constants. The Pd–Rh alloys look very attractive as cathodes for excess heat generation for which the higher deuterium density in the cathode lattice is believed to play an important role.

Experimentals

The excess heat measurements were carried out in 1M LiOD in closed cells with fuel cell anodes, the details of which were described elsewhere. The deuterium loading ratio, D/M, were measured simultaneously during the measurements to find its role in the excess heat generation. The determination of D/M is conducted by measuring pressure of hydrogen or deuterium gas in the cell, the decrease of which from its initial value is related to D/M by the following equation:

$$D/M = -2V(P_o/T_o - P/T)/n_M R$$

where V is the internal gas phase volume of the cell, n_M the total mols of metal atoms in the cathode, R the gas constant, P and T pressure of deuterium gas in the cell and temperature in the gas phase, P_o and T_o are their initial values before electrolysis. The D/Pd values have been corrected for the following effects: temperature dependence of the vapor pressure of heavy water, temperature and pressure dependence of solubility of deuterium gas in water as well as PTFE used in the cell. The corrections due to these effects are usually small, i.e., at most a few percent. After the ICCF4 we found an small error in the determination of the internal volume, which is typically ca 200 cc. The correct value has turned out to be ca 7cc smaller and this has reduced the D/M value by a few percent according to the above equation.

The reproduction of our previous excess heat measurements have been done firstly in cells with the same structure using the Pd cathodes made from the same batch of Pd rods as before. Secondly Pd rods from different sources were compared in cells with a new structure which is shown schematically in Fig. 1. The inner wall of the cell body containing electrolyte, 1M LiOD, is coated by a ceramic film, while a thick PTFE cap was encased in the cell body in the previous cell design. It was realized later, however, that slow hydrogen/deuterium absorption into a thick PTFE caused serious problems in the accurate determination of D/Pd, and the cells shown in Fig. 1 have been employed in most of the current experiments. The cell was totally submerged in the water bath regulated at 10°C during the measurements. But the loading experiments was conducted without the outer vessel 2 of the cell shown in Fig. 1 to keep the electrolyte temperature at 10°C even at high current densities, at which, however, the electrolyte temperature did go up to ca 20°C and the cathode loading was reduced by the temperature rise as shown later.

The excess heat measurements were conducted by measuring temperature in the cathodes, Ni and Pd or Pd-Rh alloys, for which Ni served as a reference to make a calibration curve in 1M LiOD. The measurements have been done on Pd and Pd-Rh alloys rods of 4mm diameter and 20–25 mm long from various sources such as IMRA Materials, Johnson Matthey and Tanaka Kikinzoku. The Pd and Pd-Rh alloy electrodes were degassed in vacuum at 200°C for three hours before the experiments. Other experimental details have been described elsewhere [1,2].

Hydrogen or deuterium overvoltage at the cathode was determined by measuring the potential difference between the cathode and the RHE or RDE, reversible hydrogen or deuterium electrode in the same solution placed close to the cathode as shown in Fig. 1. The overvoltage has been corrected for the IR drop between the cathode and the reference electrode which has been determined by the galvanostatic pulse method.

RESULTS AND DISCUSSION

1. Reproduction of the previous excess heat measurements

The excess heat data presented at ICCF3 was accompanied by two more data sets taken in different cells but using the Pd cathodes made from the same batch of Pd rods supplied by IMRA Materials during the same period.

The cell structure used for the measurements was the one with a thick PTFE cup encased, the details of which has been described before [1,2]. Figure 2 shows all the excess heat data obtained in the three cells plotted as a function of D/Pd. The data are rather scattered probably due to the experimental errors in the determination of D/Pd in a cell of this type as described before. When plotted as a function of current density, however, the data becomes much less scattered as shown in Fig. 3. The current density between 100mA/cm^2 and 200 mA/cm^2 seems to be the threshold for excess heat generation. We plotted the excess heat data as a function of another experimental parameter, i.e., cathode overvoltage, in Fig. 4, which shows almost linear increase of excess heat with overvoltage but with different slope for each cell. The data presented in Figs. 2 and 3 show good reproducibility of our previous results as far as we follow the same procedure of the excess heat measurements.

2. Excess heat measurements with Pd cathodes from various sources

2.1 Blank experiments in 1M LiOH

The calorimetry was conducted in a new cell shown in Fig. 1 firstly for the light water system, Ni, Pd/1M LiOH, to test its performance in the blank experiments. Figure 5 shows the relation between the input power and the temperature rise in the cathode observed with Ni and Pd respectively. Difference in the temperature rise between the two cathodes is very small in the input range examined which is up to 1 A/cm^2 in terms of the electrolysis current density. From the difference between Ni and Pd shown in Fig. 5 we calculated "excess heat" on the Pd cathode as a function of input power as well as current density as shown in Figs. 6A

and 6B. These data show that the error in the excess heat measurement is ca. +0.5W and no excess heat is observed on Pd in light water within the experimental error.

2.2 Excess heat measurements in 1M LiOD with Pd cathodes

We have conducted excess heat measurements using Pd cathodes from various sources. Figure 7 is a typical data to show the temperature rise in a Pd cathode compared with Ni as a function of input power. The difference between the Ni and Pd cathodes is analyzed as indicative of excess heat generation, which increases at the higher input power. The data obtained for various Pd cathodes are plotted as a function of D/Pd and current density in Figs. 8 and 9, respectively. The Pd rods supplied by IMRA Materials (I/M) have two kinds of lot numbers, 9112 and 9209, and one of the three excess heat data sets for Pd(I/M 9112) in 1M LiOD is the one which was reported at ICCF3. The Pd(TNK type-C) rod is a cold-worked material manufactured at Tanaka Kikinzoku by drawing under liquid nitrogen temperature and has a high Vicker's hardness value of ca 140 while the other Pd materials have the value between 90 and 110.

The data shown in Fig. 8 shows evolution of excess heat between D/Pd=0.8 and 0.84 but dependence of excess heat on D/Pd is rather scattered and sharp to know its functional form in this region. It is important therefore to extend the excess heat measurements into the higher D/Pd region to characterize its significance in excess heat generation. Systematic dependence of the excess heat on current density is seen in Fig. 8 which shows steady increase of excess heat at the higher current densities than 0.1-0.2 A/cm^2. The results presented in Figs. 8 and 9 show that the previous data presented at ICCF3 by our group is essentially reproduced by using Pd materials manufactured and processed in different ways at various sources.

It is important to point out that the Pd(TNK) gave the maximum D/Pd of 0.78 in this particular experiments which is much lower than obtained commonly in loading as well as excess heat measurements. In this experiments no excess heat was observed within the experimental error up to 0.8 A/cm^2 which is much higher than the critical current density between 0.1 and 0.2 A/cm^2 for Pd. This is a good example to show

importance of achieving the critical loading between 0.8 and 0.84 for the excess heat generation.

We have replotted the data in Fig. 8 with respect to cathode overvoltage in Fig. 10 in an attempt to find the dependence of excess heat on another important experimentally observable parameter. The dependence of excess heat on the cathode overvoltage presented in Fig. 10 looks almost linear and much more systematic than the dependence on D/Pd and current density. It should be noted that the cathode overvoltage observed on one of the Pd(I/M 9112) is much higher than the others, and this is the reason why the dependence of the excess heat on overvoltage is extended up to -1.5 V for this Pd cathode. The higher cathode overvoltage on this particular Pd electrode is seen more directly in the plot of overvoltage *vs* log i(A/cm^2) compared to all the other electrodes as shown in Fig. 11. We do not know, however, why this particular Pd gave much higher cathode overvoltage than others.

2.3 Excess heat measurements on modified Pd cathodes by chemisorbed thiourea, $(NH_2)_2C=S$

We have shown that surface modification of Pd cathodes by chemisorbed thiourea, although we do not know its surface coverage under hydrogen evolution condition, leads to improved cathode loading by hydrogen as well as by deuterium and gives rise to the maximum H/Pd and D/Pd of 1.0 and 0.91 at 10°C respectively [6,7]. We conducted excess heat measurements in 1M LiOD containing 0.6mM thiourea in an attempt to see effect of surface modification by chemisorbed molecules.

Figures 12A and 12B show results plotted as a function of D/Pd and current density respectively, which did not give as much excess heat as observed without thiourea despite the fact that D/Pd up to 0.88 was achieved and the current density was extended up to 0.5A/cm^2. The maximum D/Pd value lower than obtained before in the loading experiments is due to rise in electrolyte temperature which is inevitable in the excess heat measurements while temperature was kept below 20°C in the loading experiments to minimize the temperature effect on D/Pd [7]. Comparison between the poor performance presented in Fig. 12 and the

results without thiourea shown in Fig. 8 may imply that surface modification or blocking the surface atomic sites by chemisorbed molecules is not good for the excess heat generation. This may lead to further discussion on the nature of the excess heat generating process, i.e., if it is surface or bulk process, but we would certainly need more information on the nature of the adsorbed species which modify the surface atomic layer of the Pd cathode to go into such discussion.

2.4 *D/M and Excess heat on Pd-Rh alloys in 1M LiOD*

Measurements of D/M and excess heat have been conducted with Pd–Rh(5, 10 atm%) cathodes in 1M LiOD in an attempt to investigate their relation in the higher D/M region than realized for Pd cathodes. The D/M on these alloy cathodes are shown in Fig. 13 as a function of current density [8]. In these measurements temperature of the electrolyte was kept 10^{o} C except at high current densities at which electrolyte temperature went up to ca 20^{o}C due to the high input power. The D/M on these alloys are 5–15 % higher than Pd for a given current density, the maximum values being 0.91 and 0.97 for 5atm% and 10atm% Rh–Pd alloy respectively. The tendency to show decrease of D/M at higher current densities commonly observed for Pd and Pd–Rh alloys is due to the electrolyte temperature rise mentioned above.

Dependence of excess heat on D/M on these alloy cathodes were observed in different experiments and the results are shown in Fig. 14. It is rather unexpected to see much smaller excess heat than Pd cathodes and decrease of excess heat with increasing D/Pd on the Pd–Rh alloys. However, when plotted with respect to current density as shown in Fig. 15, we see a systematic increase of excess heat with increasing current density, although the critical current density for the excess heat generation appears to be higher than Pd and lies between 0.2 and 0.4 A/cm^2. In Fig. 15 we plotted also the D/M observed during the excess heat measurements as a function of current density. The D/M decreases with increasing current density due to the electrolyte temperature rise, which is shown in Fig. 16, and this is the reason why the excess heat looks as if it decreases with increasing D/M. We interpret the data in Fig. 14 in the way that the excess heat is decreasing not because D/M increases but because the current

density is a more important factor controlling the excess heat generation in this high D/M region.

We plan to conduct D/M and excess heat measurements for 20 and 30 atm% Rh–Pd alloys in order to extend our investigation up to the full loading, D/M=1.0, which is likely to be achieved on these alloys with higher rhodium content.

4. Factors controlling excess heat

The dependence of excess heat on Pd and Pd-Rh alloys upon D/M, current density and cathode overvoltage reported in the present study strongly suggest that there is a critical cathode loading by deuterium which lies between 0.8 and 0.84 and critical current density between 0.1 and 0.2 A/cm^2 on Pd cathodes. The role of the critical current density is clearly to load the cathode by deuterium to the critical value and maintain it. Once having reached the critical cathode loading, however, it seems as if the excess heat depends more systematically on current density and cathode overvoltage than D/M as demonstrated clearly by the data on the Pd-Rh alloys. Unfortunately, however, current density and overvoltage are not independent from each other and it is difficult to discuss the role of these two parameters separately on Pd and Pd–Rh alloy cathodes. However, comparison of the cathode overvoltage for a given current density and dependence of excess heat on current density between Pd and Pd–Rh alloy cathodes as shown in Figs. 17 and 18 respectively indicates that the cathode overvoltage of the Pd–Rh alloys is always higher while the excess heat on the alloys is more less comparable or smaller than Pd for a given current density. This implies that the higher overvoltage on the Pd–Rh alloy cathodes is not in fact contributing effectively to the excess heat generation.

The comparison between Pd and Pd–Rh alloys can be summarized as follows: the excess heat on the Pd–Rh alloy cathodes for a given current density is comparable or smaller while D/M and cathode overvoltage is higher than Pd cathodes. This suggests that the current density is the most important parameter controlling excess heat generation among the three experimental parameters above a critical cathode loading. It would be

important to conduct excess heat measurements for other cathode materials and for Pd cathodes with modified surface and in other electrolytes, which would make it possible to investigate the significance of D/Pd, current density and cathode overvoltage in the excess heat generation in more comprehensive ways.

There are some more experimental parameters considered significant in the excess heat generation such as length of time to hold the D/Pd higher than the critical value often mentioned by the group at SRI [4], temperature as suggested by Fleischmann and Pons in their excess heat measurements at electrolyte boiling [9], the third element present in the electrolyte and possibly incorporated into or onto the Pd cathode such as B^+ and Li^+, and micro crystal structure of the Pd cathode lattice which could affect the achievable electrolytic cathode loading by hydrogen and deuterium. However, we have not been able to investigate effect of these parameters in a systematic way so far and hope to conduct such investigation in near future.

REFERENCES

1) K.Kunimatsu, N.Hasegawa, A.Kubota, N.Imai, M.Ishikawa, H.Akita and Y.Tsuchida: Frontiers of Cold Fusion, Proceedings of ICCF3(1992) p31.
2) N. Hasegawa, K. Kunimatsu, T. Ohi, T. Terasawa: ibid., p377.
3) T. Maoka and M. Enyo, Electrochimica Acta, 26(1981)607.
4) M.C.H.Mckubre, S.Crouch-Baker, A.M.Riley, S.I.Smedley and F.L.Tanzella., Frontirs of Cold Fusion, Proceedings of ICCF3(1992)p5.
5) B. Baranowski, S. Majchrzak and Ted B. Flanagan, J. Phys. Chem., 77(1973)35.
6) H. Akita, Y. Tsuchida, T. Nakata, A. Kubota, A. Kubota, M. Kobayashi, Y. Yamamoto, N. Hasegawa, N. Hayakawa and K. Kunimatsu, Proceedings of ICCF4, submitted.
7) Y. Tsuchida, H. Akita, T. Nakata and K. Kunimatsu, to be published.
8) N. Hasegawa, Y. Yamamoto, N. Hayakawa and K. Kunimatsu, to be published.
9) M. Fleischmann and S. Pons, Frontiers of Cold Fusion, Proceedings of ICCF3(1992)p47.

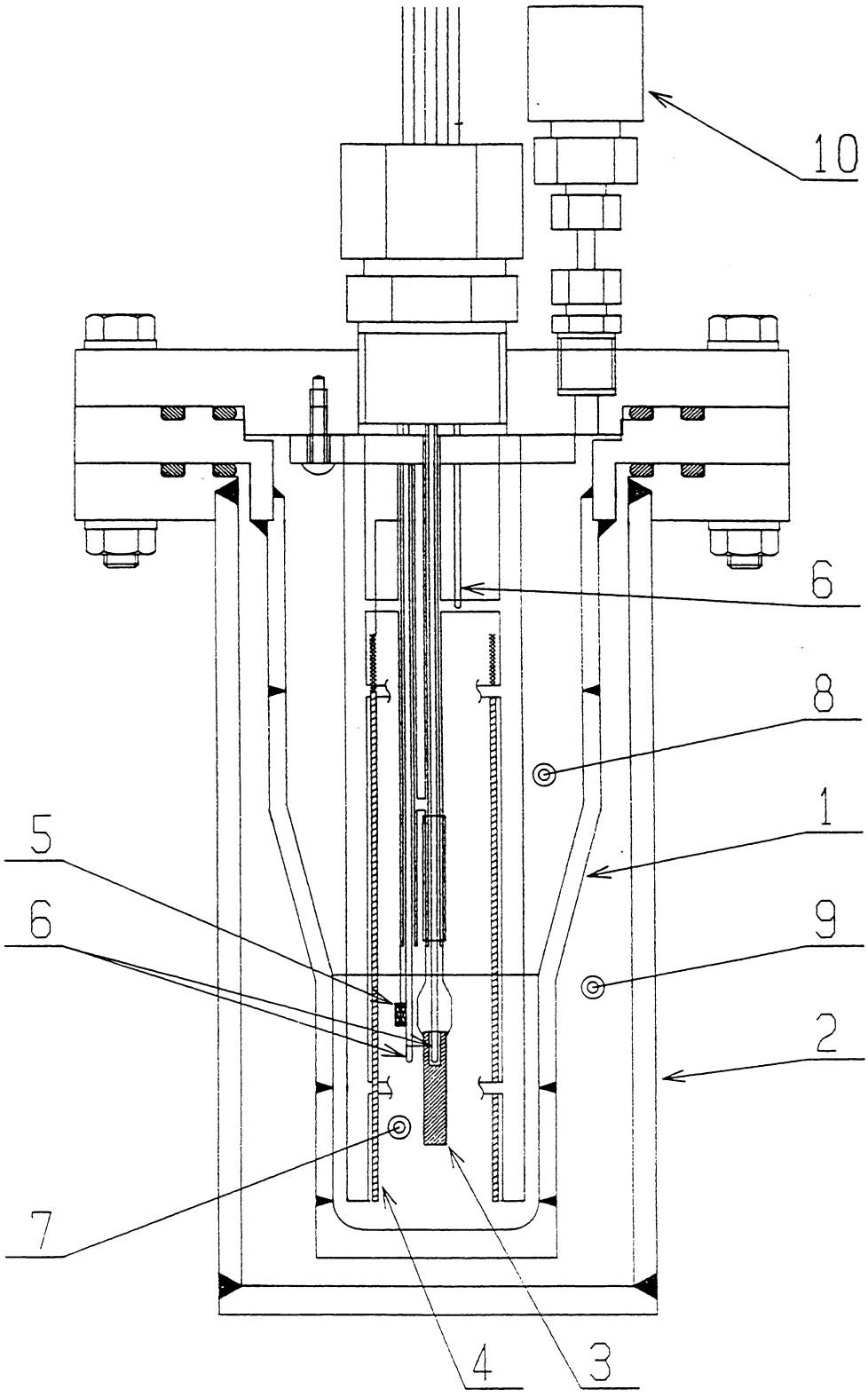

Fig.1 Closed Electrolysis Cell with Fuel Cell Anode for D/Pd and Excess Heat Measurement

1.Pressure Vessel (SUS316) 2.Vessel (SUS316) 3.Pd Cathode
4.Fuel Cell Anode 5.RHE(Pt/Pt) 6.Thermocouple 7.1M LiOD
8.D_2 (5–10kg/cm^2) 9.Air 10.Pressure Sensor

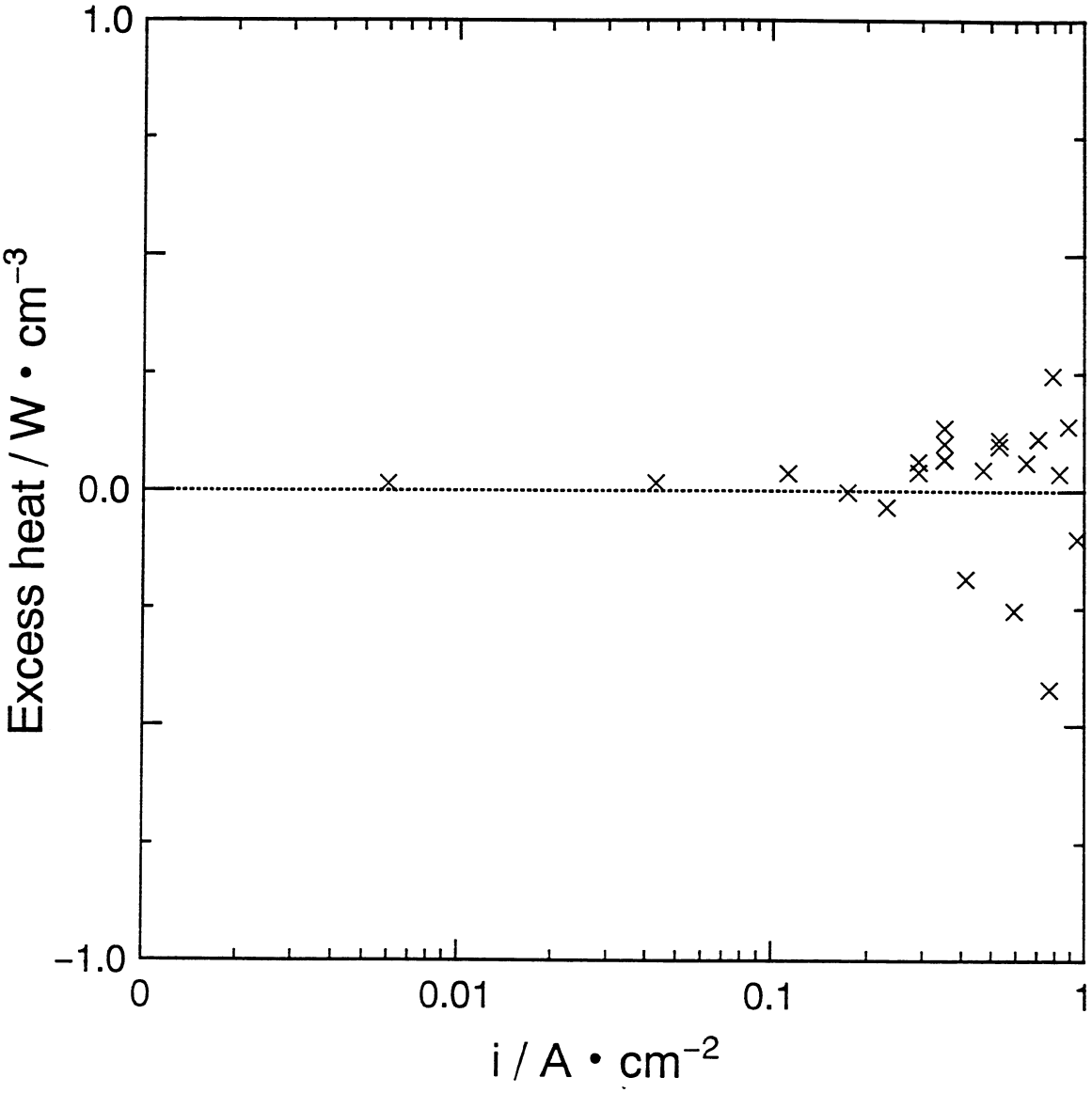

Fig.6B Calculated excess heat vs. current density for Pd in 1M LiOH

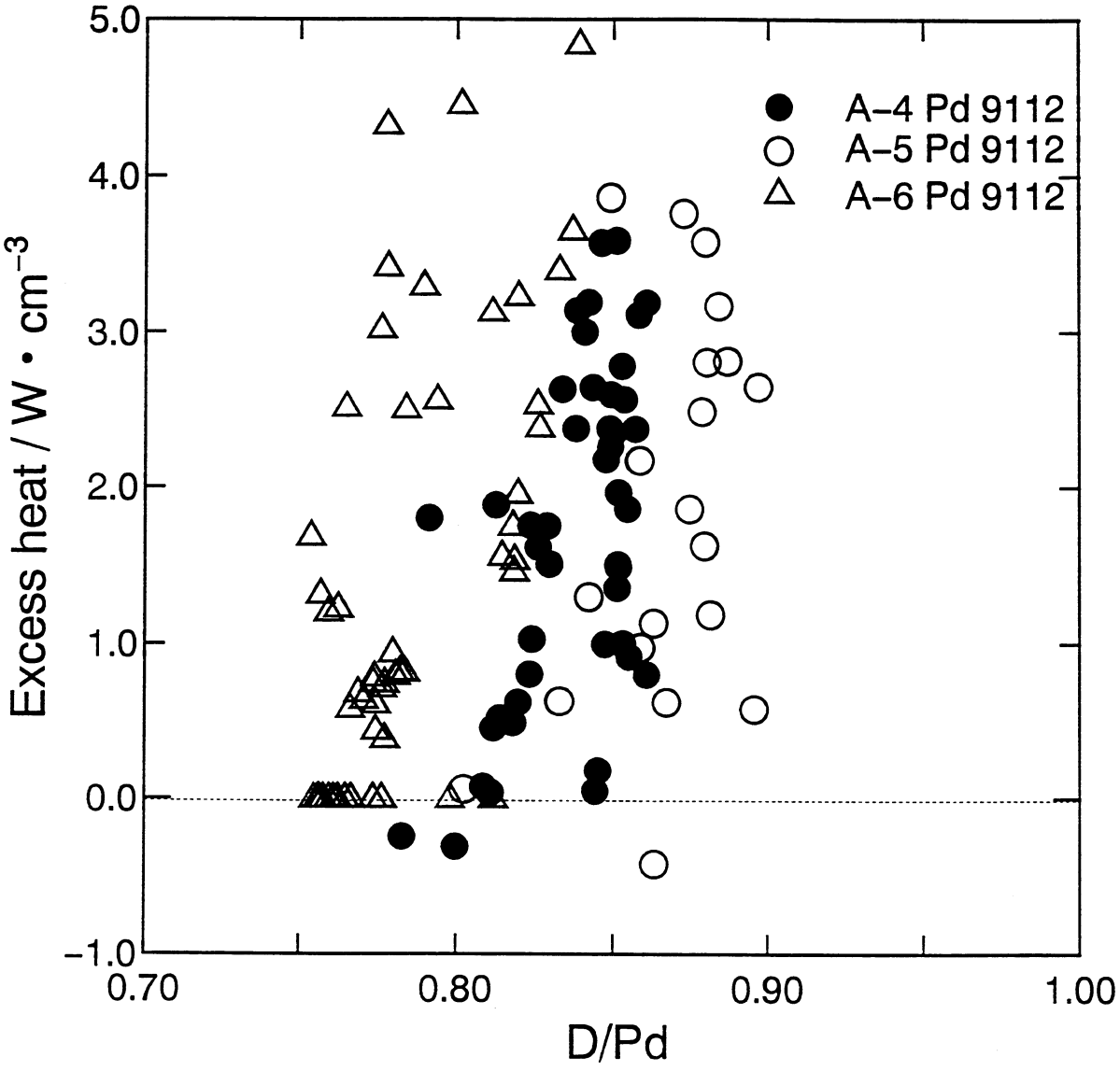

Fig.2 Excess heat vs D/Pd for three Pd(IM9112)rod electrodes in 1M LiOD.

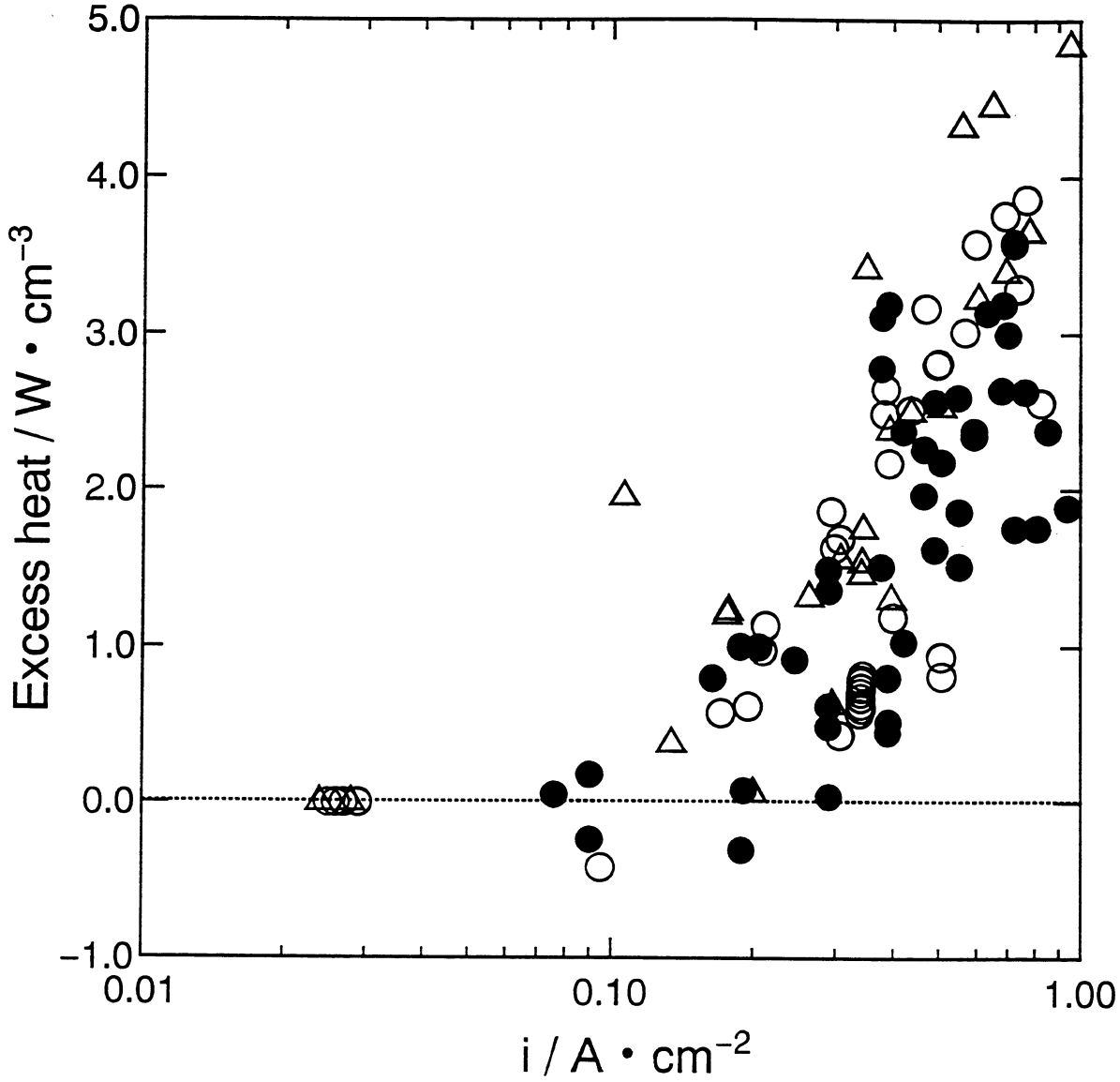

Fig.3 Excess heat vs current density for three Pd(IM9112) rod electrodes in 1M LiOD

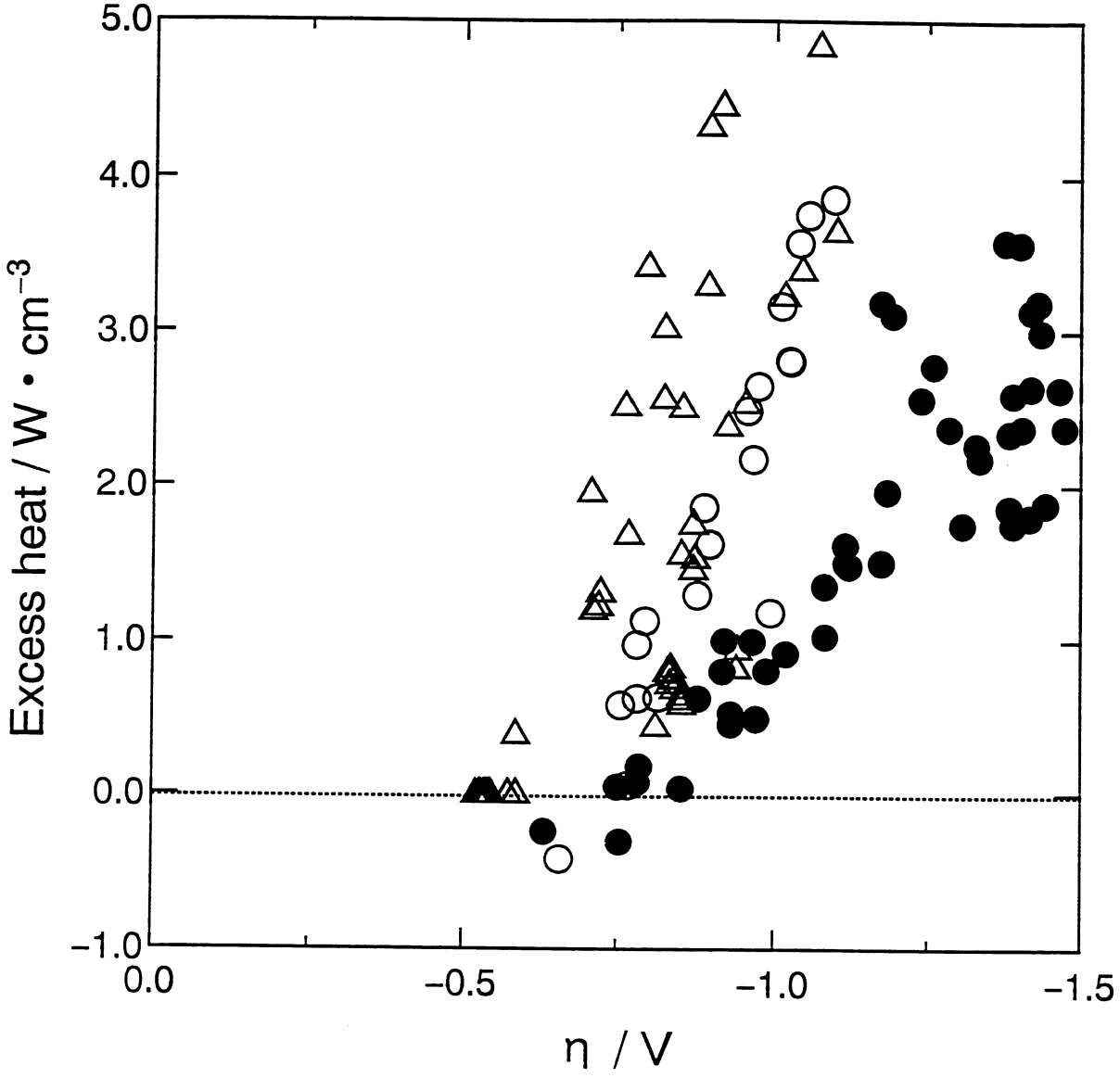

Fig.4 Excess heat vs cahtode overvoltage for three Pd(IM9112) rod electrodes in 1M LiOD

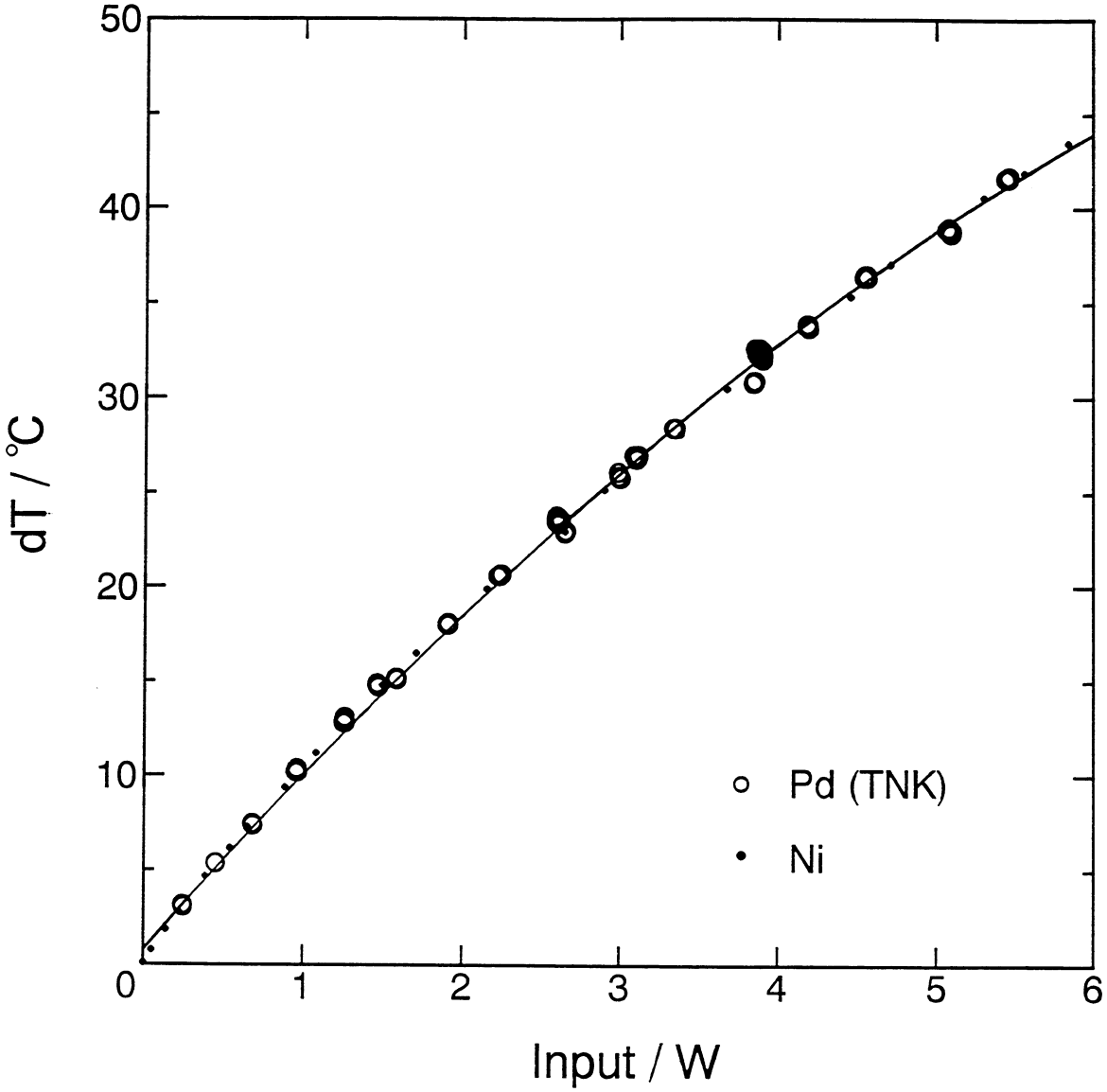

Fig.5 Change of electrode temrerature with input power for Pd and Ni cathodes in 1M LiOH.

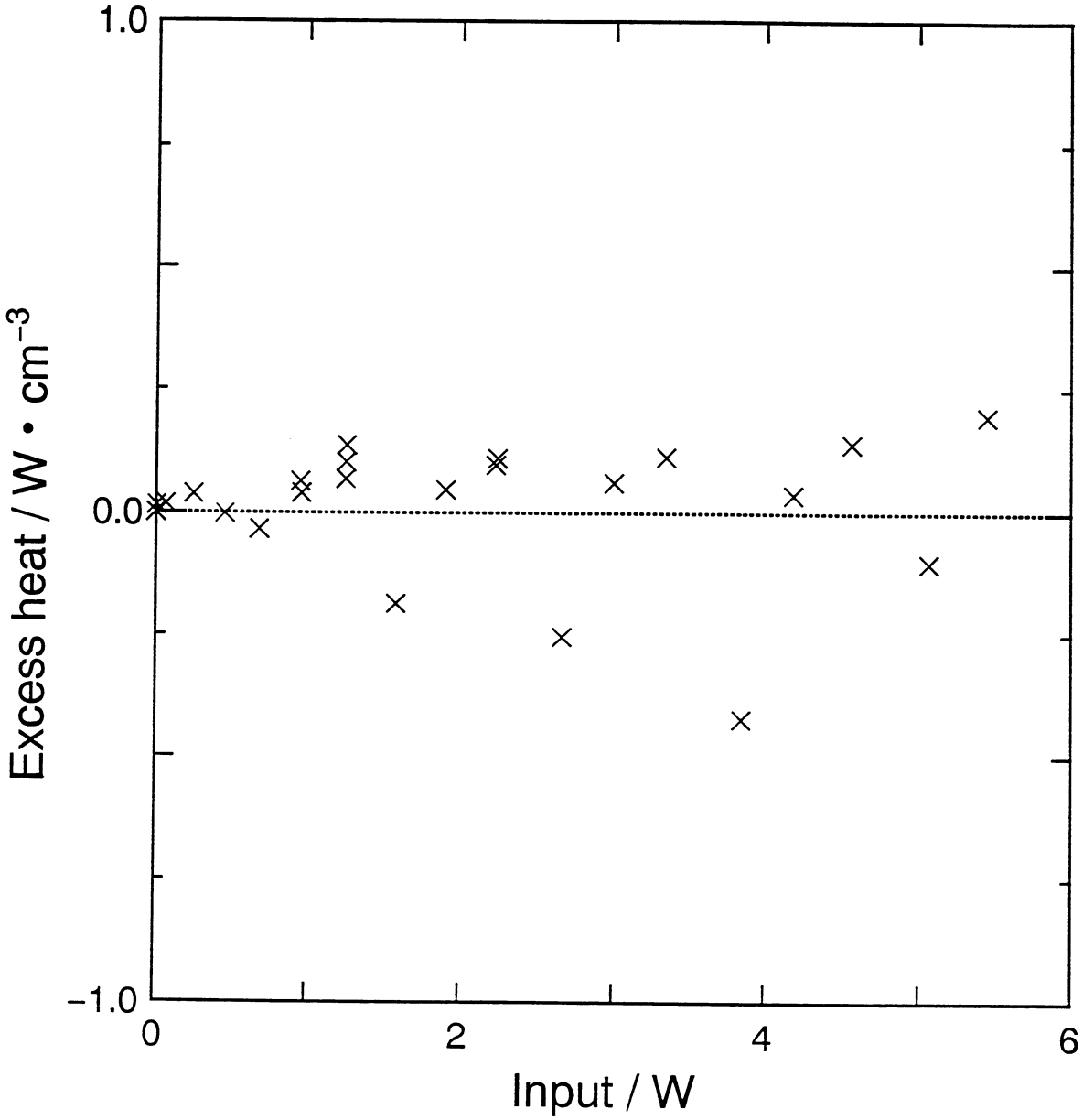

Fig.6A Calculated excess heat vs input for Pd in 1M LiOH.

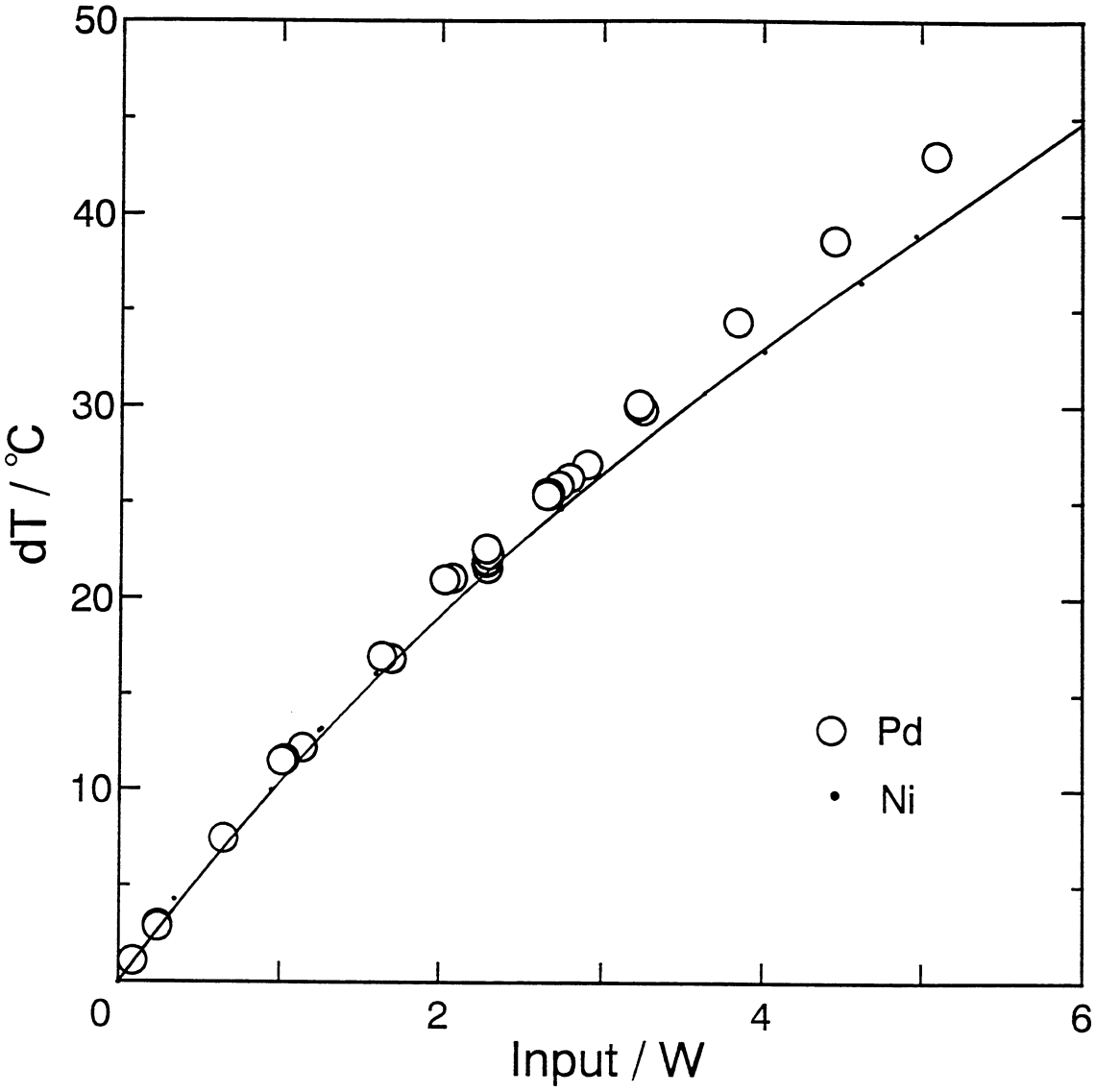

Fig.7 Cathode temperature change vs input power for Pd(IM9209) in 1M LiOD.

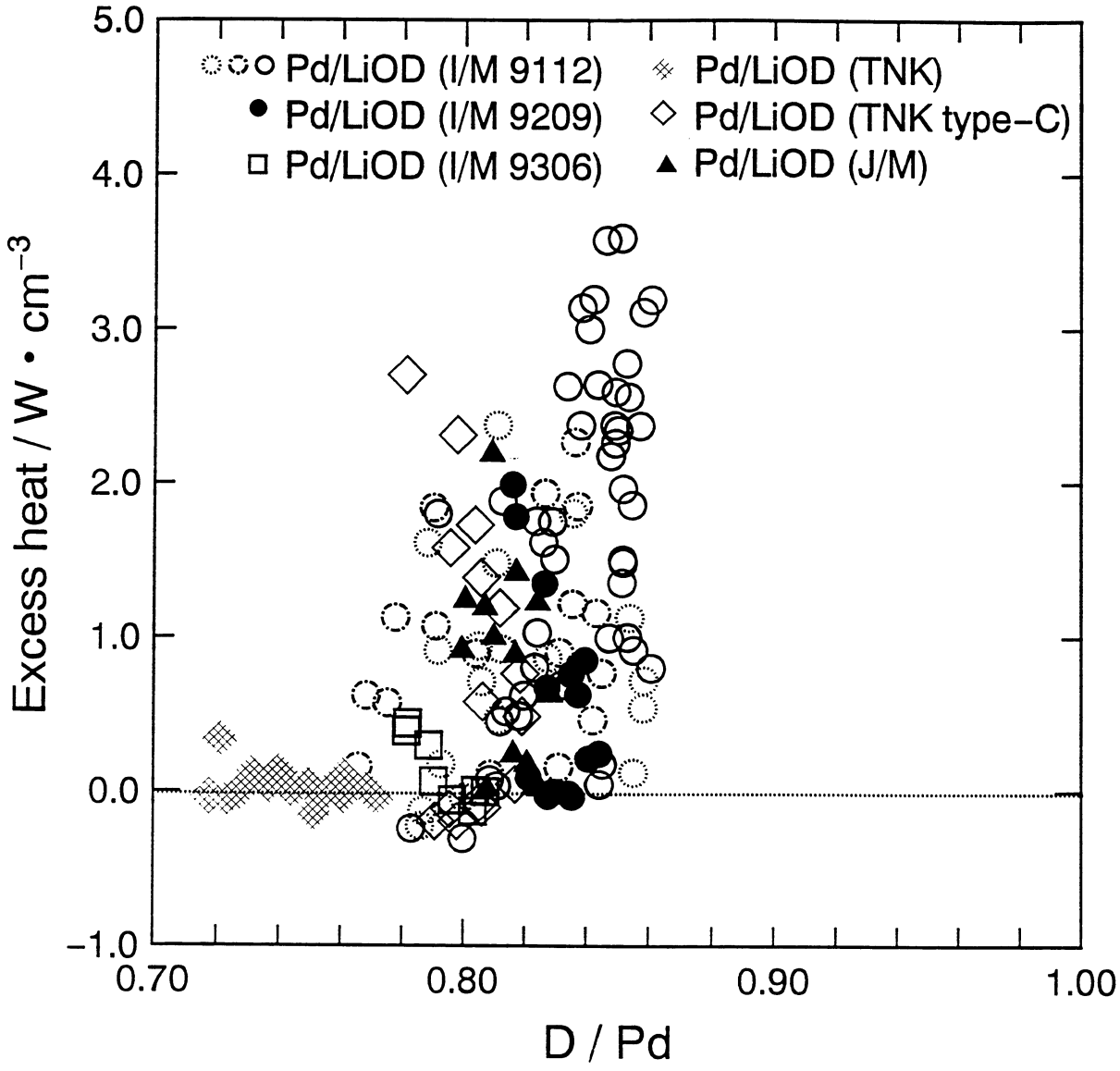

Fig.8 Excess heat vs cathode loading for Pd cathodes in 1M LiOD.

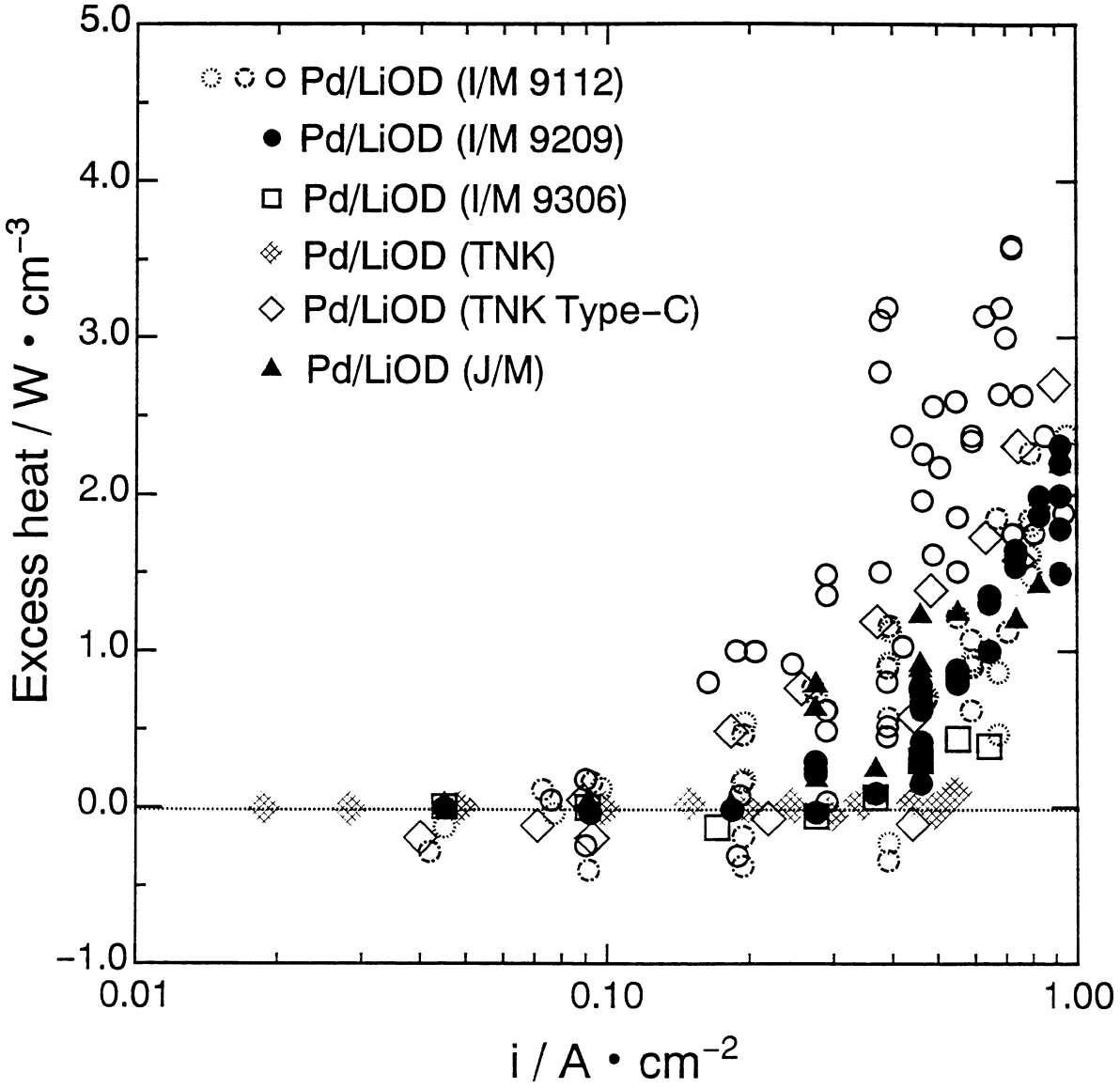

Fig.9 Excess heat vs current density for various Pd cathodes in 1M LiOD.

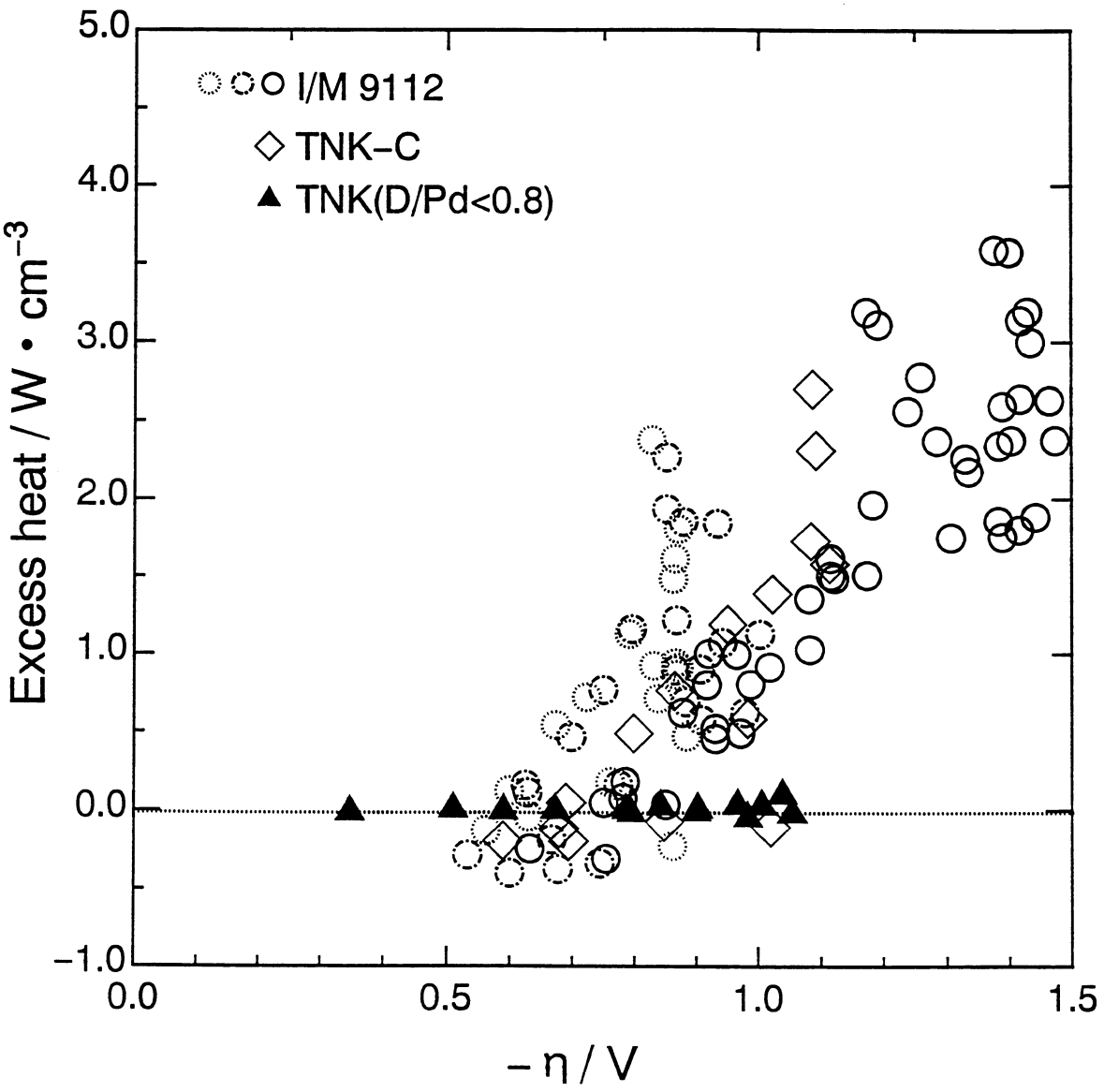

Fig.10 Excess heat vs overvoltage for various Pd cathodes in 1M LiOD.

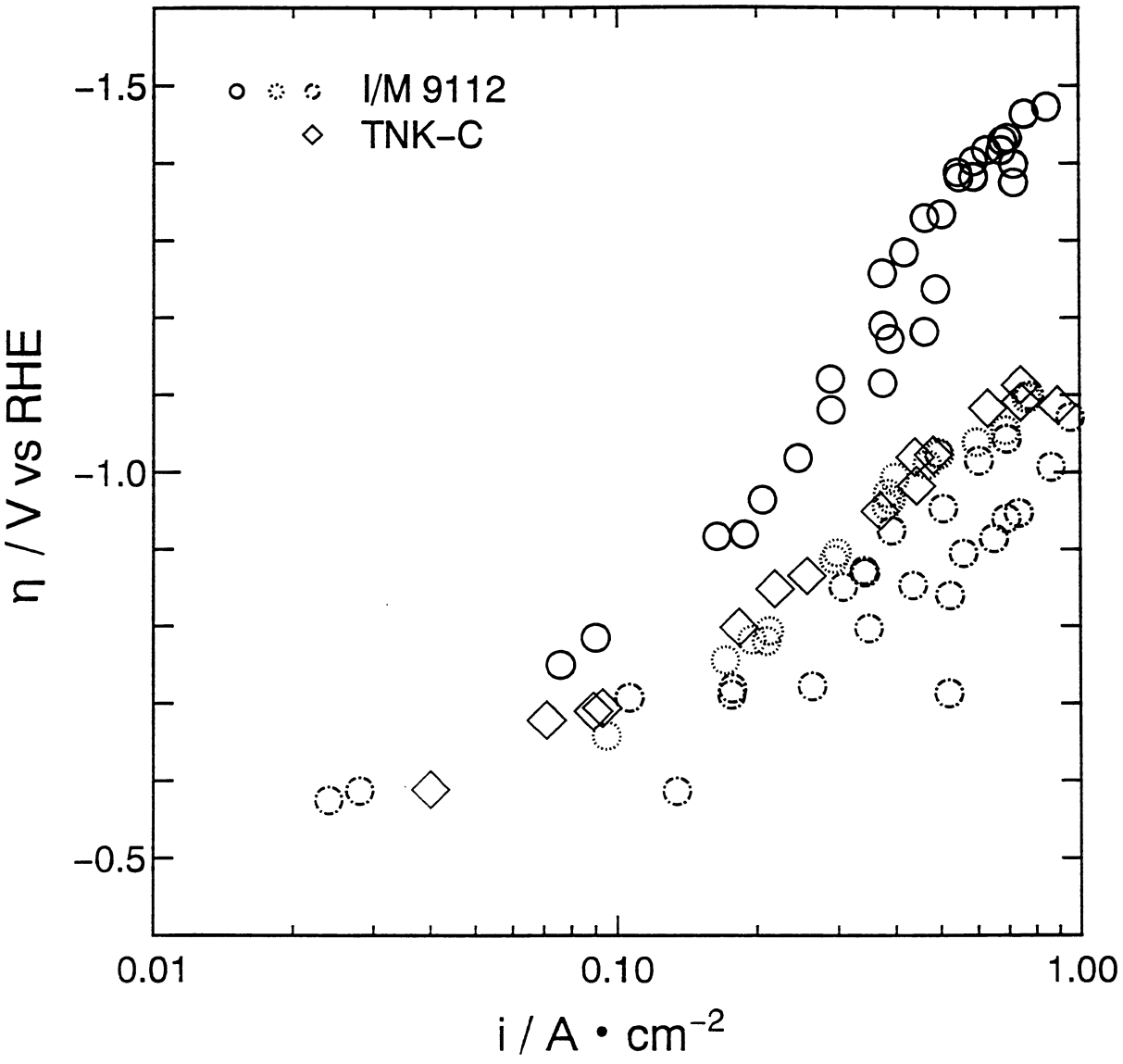

Fig.11 Cathode overvoltage vs current density on Pd in 1M LiOD at 10℃.

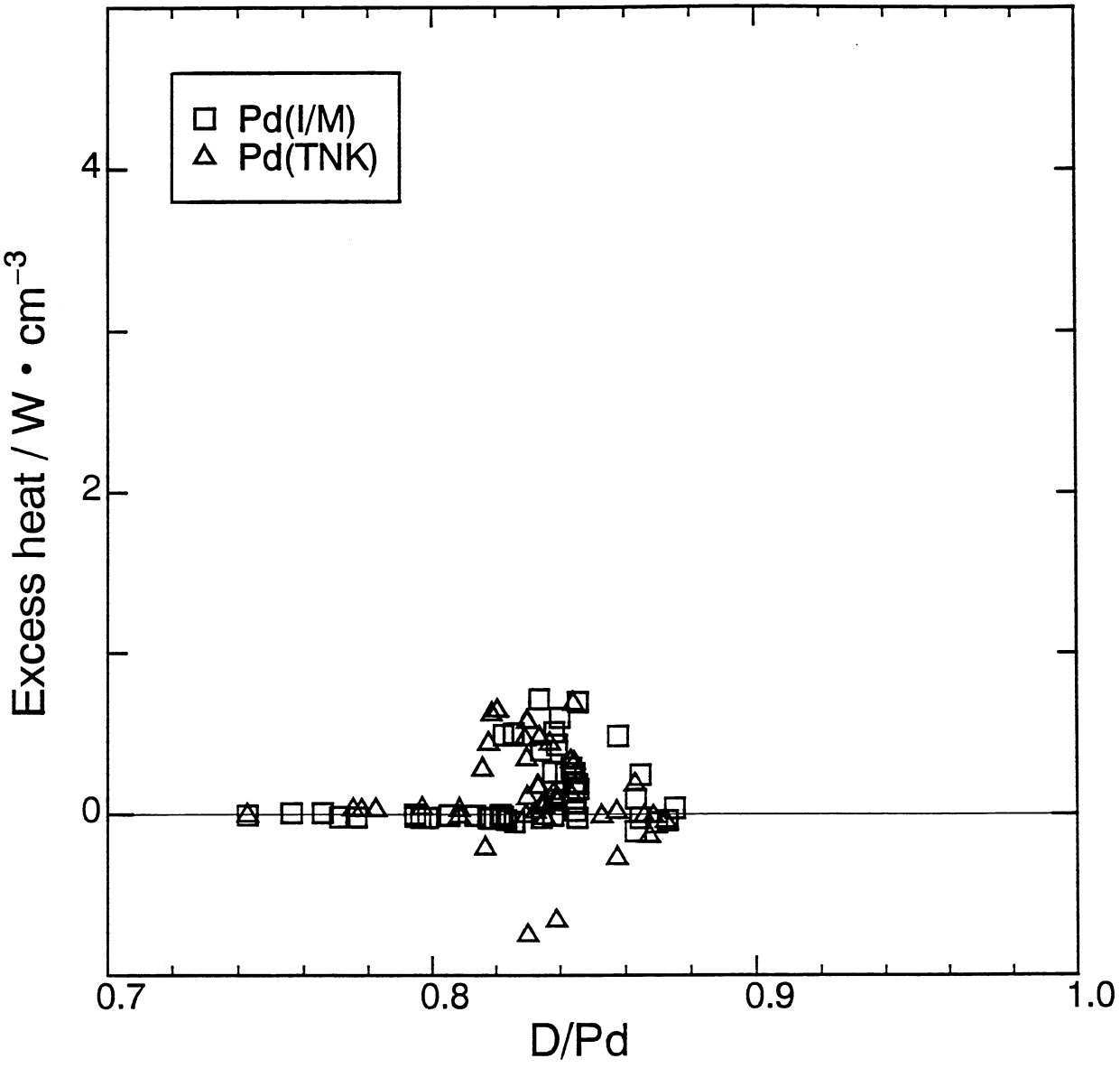

Fig.12A Excess heat vs. D/Pd for ϕ 4Pd in 1M LiOD+0.6mM thiourea.

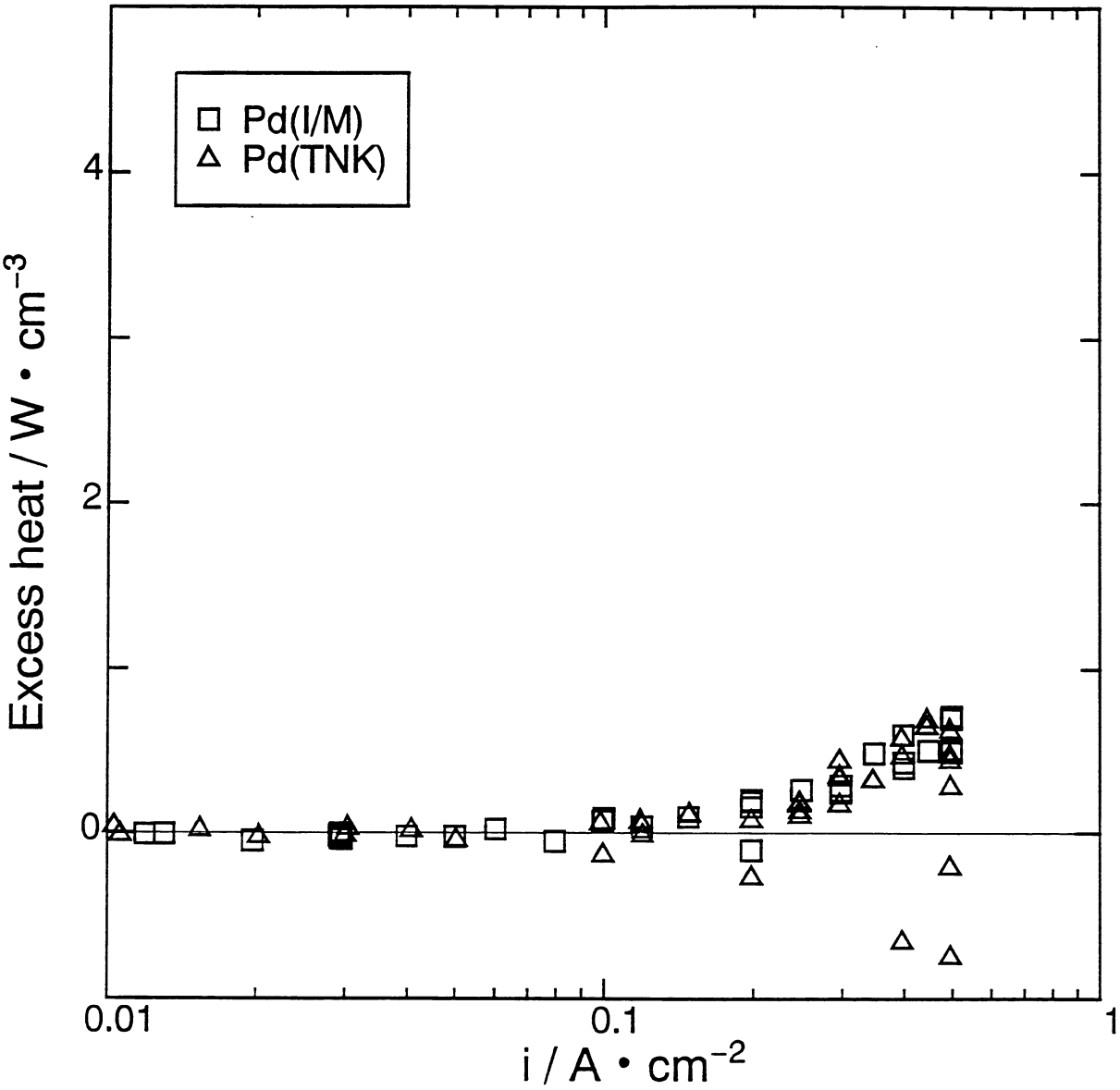

Fig.12B Excess heat vs. current density for ϕ4 Pd in 1M LiOD+0.6mM thiourea.

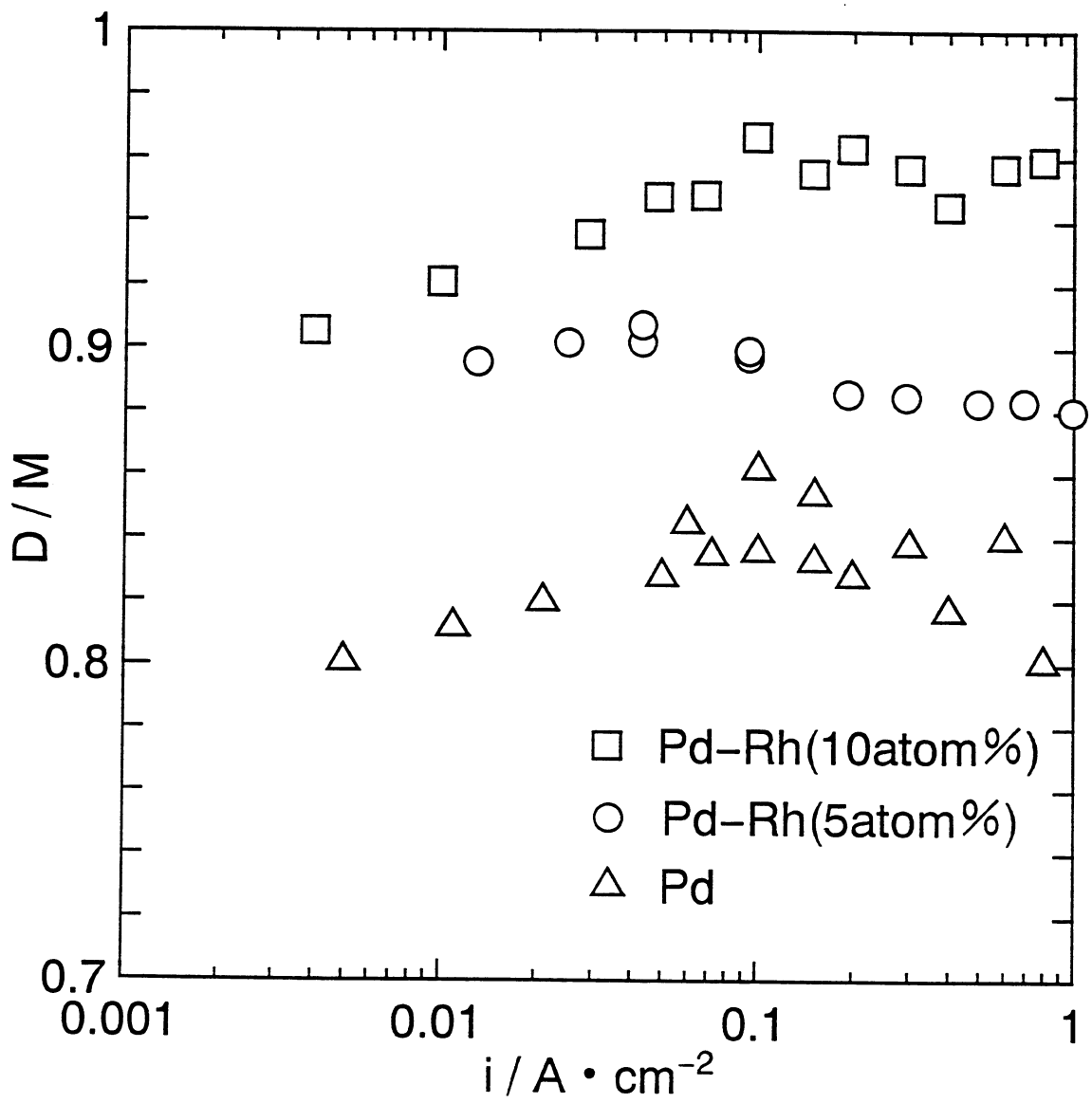

Fig.13 Dependence of D/M on current density for Pd and Pd–Rh alloy cathodes in 1M LiOD at 10℃.

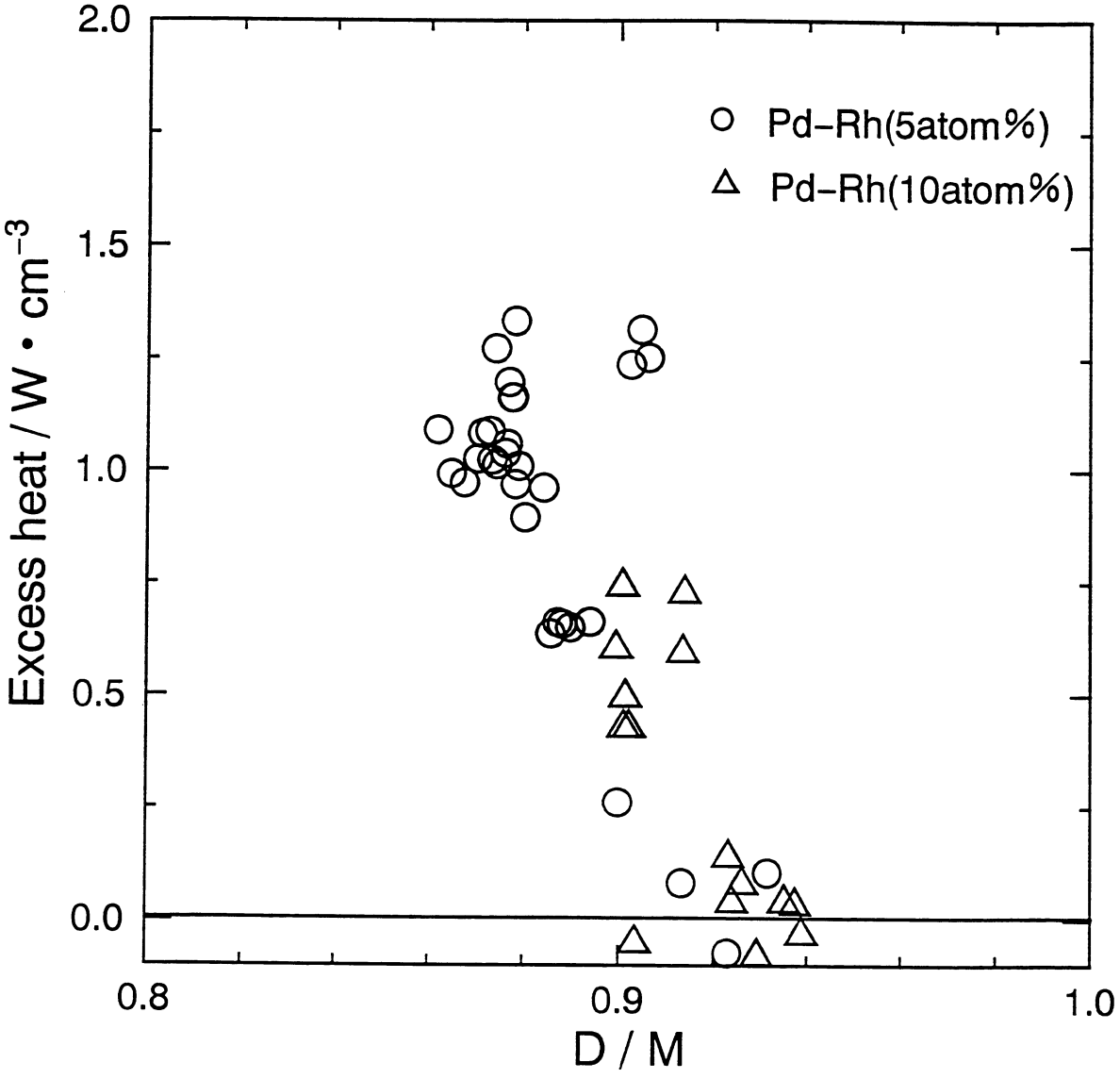

Fig.14 Excess heat vs. D/M on Pd-Rh(5atom%) and Pd-Rh(10atom%) cathodes in 1M LiOD.

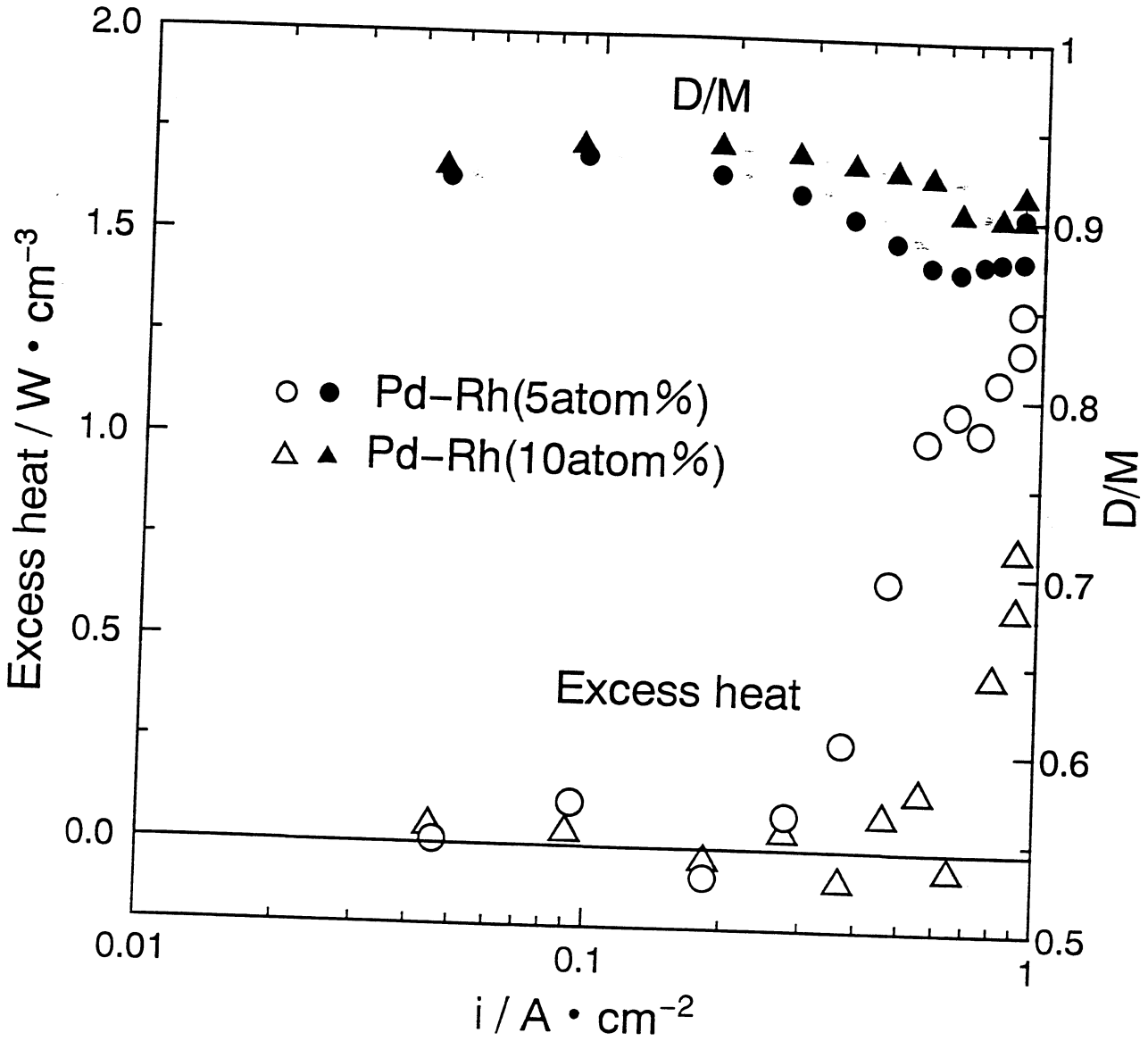

Fig.15 Excess heat and D/M vs current density on Pd–Rh(5atom%) and Pd–Rh(10atom%) in 1M LiOD.

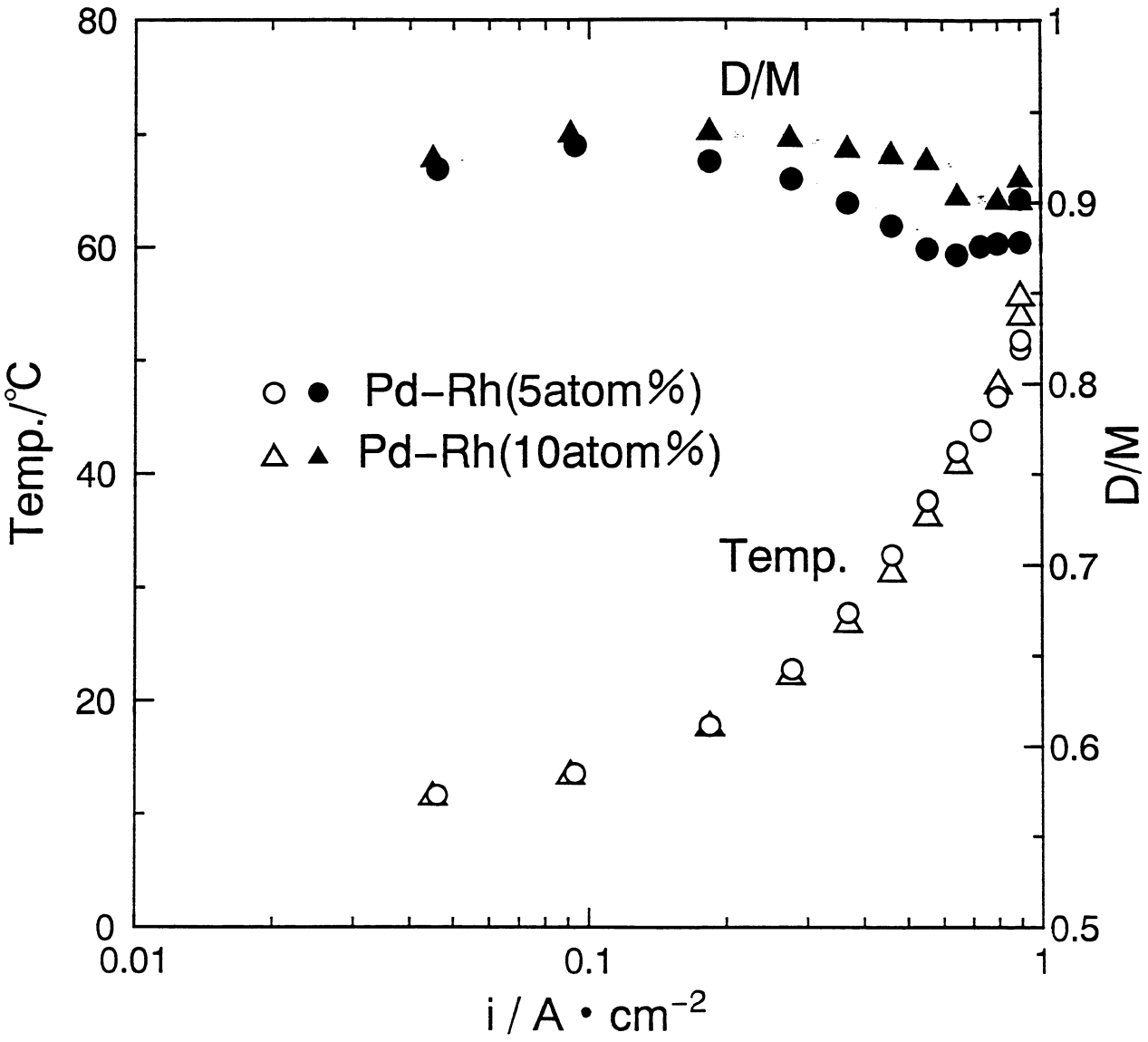

Fig.16 D/M and electrolyte temperature vs current density during excess heat measurement on Pd–Rh(5atom%) and Pd–Rh(10atom%) in 1M LiOD.

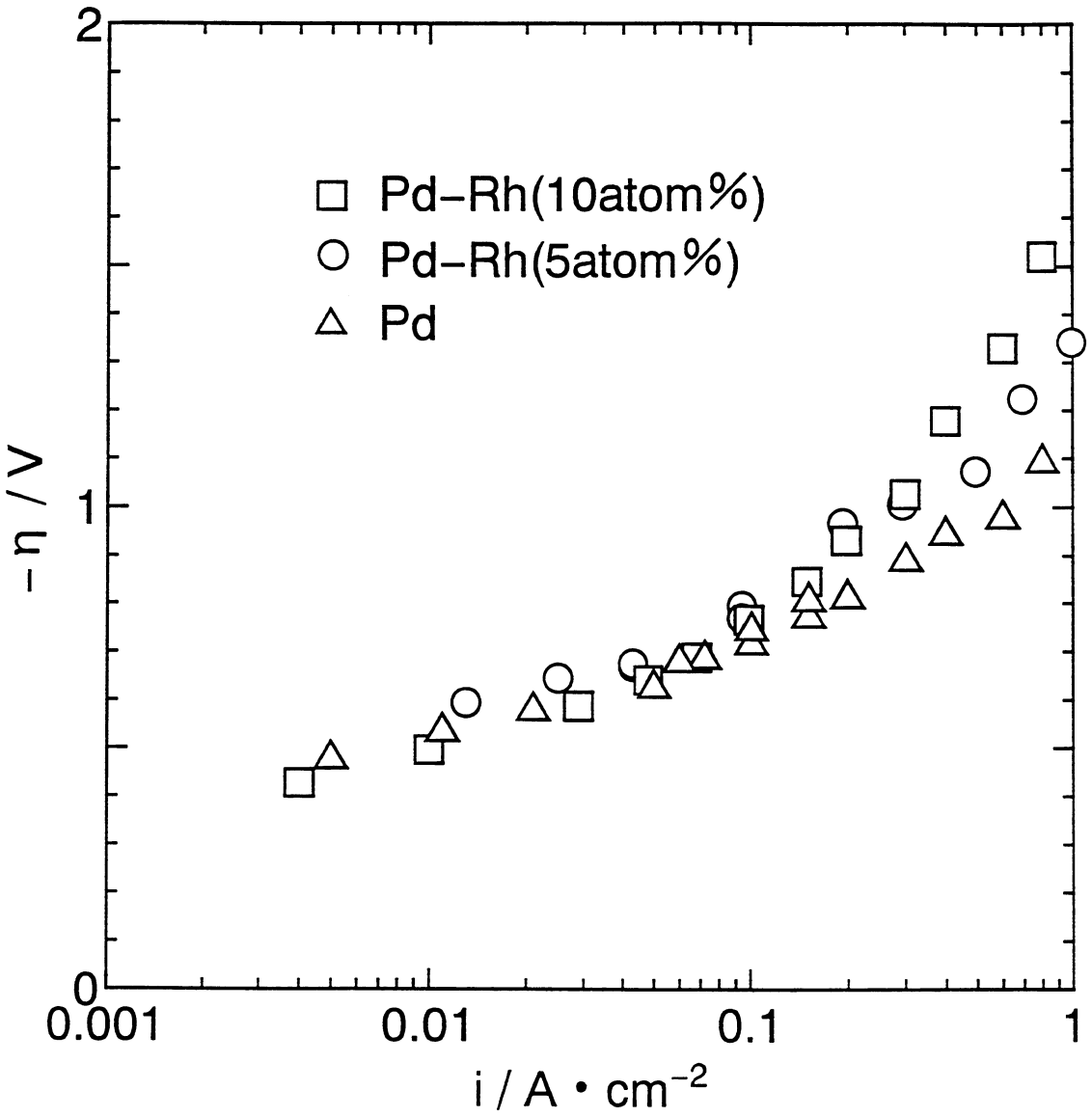

Fig.17 Cathode overvoltage vs current density for Pd and Pd–Rh alloy cathodes in 1M LiOD at 10℃.

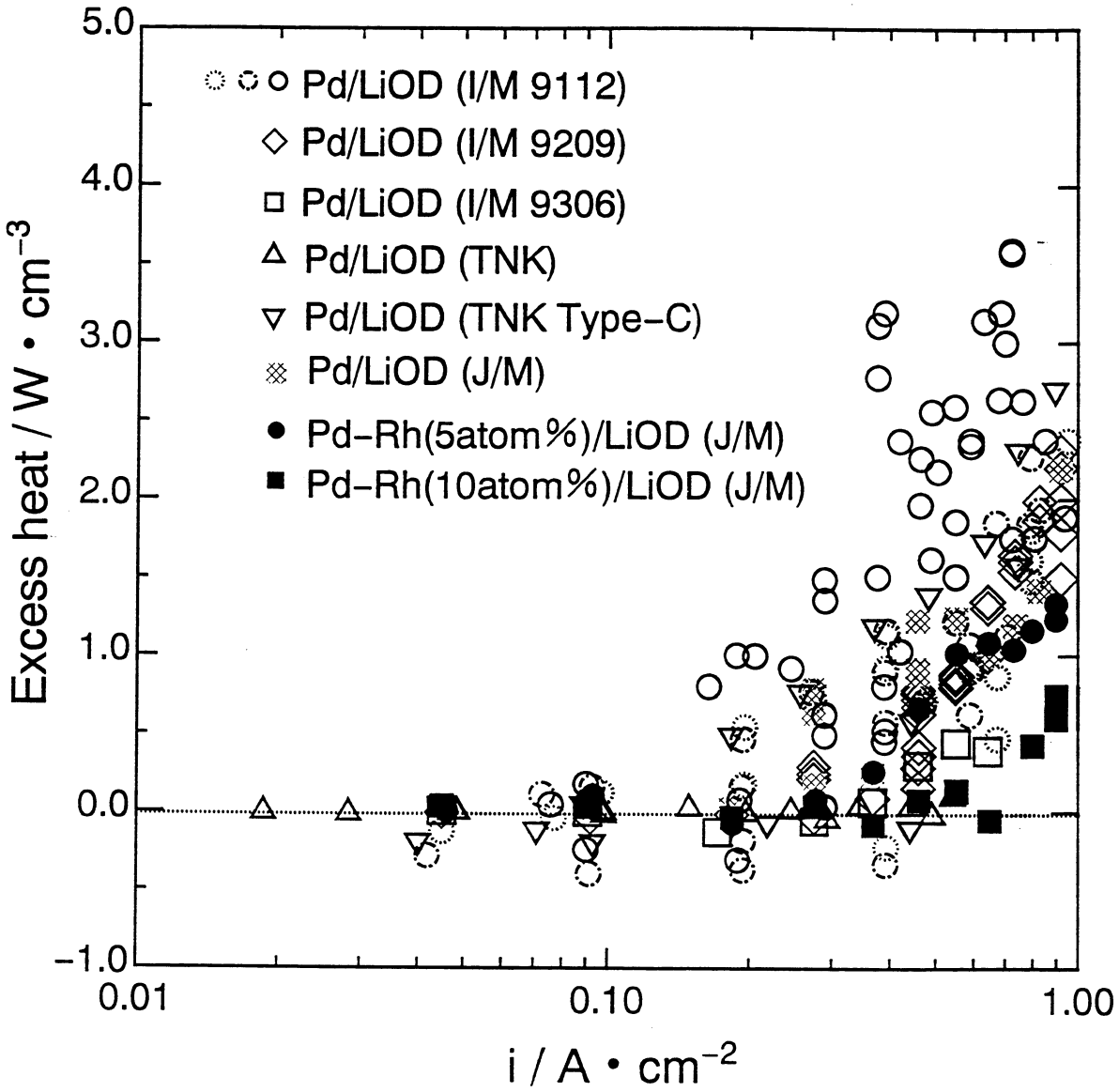

Fig.18 Excess heat vs current density for various Pd and Pd-Rh alloy cathodes in 1M LiOD.

FSSCI/FUSFRE28

BEHAVIOUR OF A Pd MEMBRANE DURING DEUTERIUM ELECTROCHEMICAL LOADING: EXCESS HEAT PRODUCTION

L. Bertalot[a], F. De Marco[a], A. De Ninno[b]
R. Felici[c], A. La Barbera[d], F. Scaramuzzi[b],
V. Violante[a]

CRE ENEA, via E. Fermi 27, I-00044 Frascati, Italy

1. INTRODUCTION

At ICCF3 a new approach to the study of the dynamics of D in Pd had been presented, with the concurring evidence of heat excess production (1). The method consisted in the use of an electrolytic cell with a special configuration, with the cathode acting as a membrane between the electrolyte and an ambient in which gaseous D_2 could be collected. The permeation of D through the membrane could be related to the appearance of heat excess production. In 1993 new experiments have been performed with the same kind of apparatus, and are reported here: a further evidence of heat excess has been detected, and a correlation between the pressure of D_2 on the gas-side of the cathode and the phase of the palladium deuteride is proposed.

The same type of apparatus is used in two other experiments:

- in the first one, in collaboration with ISM/CNR of Frascati, the surface of the cathode immersed in the electrolyte is investigated during electrolysis with the help of a X-ray spectrograph, in order to study the variation of the cell parameter, and thus to follow in real time the D-charging (see the same authors, this Conference).

- another experiment, which will be started at the beginning of 1994, will be performed in collaboration with a Group of INFN of Bologna. The measurement of the heat excess (and related parameters) in one of our cells will be performed while the cell is sitting inside a quite sophisticated neutron detector mounted in the Gran Sasso National Laboratory of INFN, where the level of neutron background is 10^3 times less than at the sea level (2): the possible correlations between charging of D in Pd and heat excess production on one side and the emission of neutrons on the other side will be investigated, with the expectation of giving a clear answer to this still obscure issue in Cold Fusion research.

2. THE EXPERIMENT

We will recall here the main features of the experimental apparatus. In Fig.1 a schematic drawing of the cell/calorimeter is shown. The cathode (a) is immersed on one side in the electrolyte, while the other side faces a vacuum-tight ambient: the measurement of the deuterium gas pressure in this ambient monitors the flow of deuterium through the cathode, thought of as a membrane. The glass coil (f) is the main feature of the calorimeter: a constant flow of thermoregulated water takes away most of the heat produced in the cell, and the measurement of the temperature difference between its inlet and outlet (ΔT_C) permits to deduce accurately the power outlet (± 50 mW). A better insulation of the cell from the outer ambient has been obtained, by inserting the cell in a thermoregulated chamber (ΔT = 1°C). Accurate calibrations, for powers up to 50 W

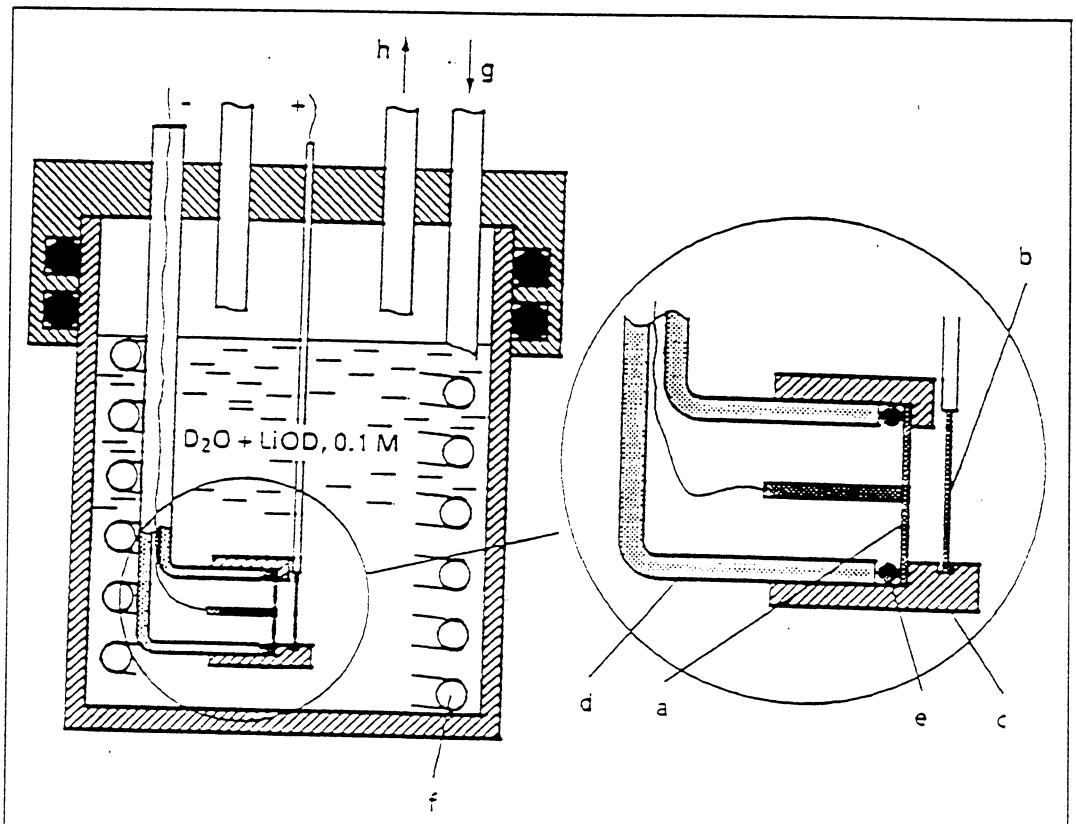

Fig.1 Schematic drawing of the cell/calorimeter: (a) is the Pd cathode and (b) the anode. The O-ring (e) allows a vacuum-tight connection between the cathode and the glass container (d) in which D_2 gas can be collected. A constant flow of thermoregulated water is circulated through the glass coil (f). Measuring the temperature difference ΔT_C between the inlet (g) and the outlet (h) the power produced in the cell can determined.

and at outside temperatures ranging from 30 to 50°C, have been performed, taking also into account the effect of gas

bubbling during the electrolysis; as a result, a linear relation between power output and ΔT_c was found up to 30 W. Accurate monitoring of the flow of the evolved gas permitted a check of the efficiency of the electrolysis, which was always better than 98%, well within the error of the measurement.

The measurement of the D_2 pressure in the gas ambient behind the cathode has provided interesting information, which permits to correlate these measurements with the state of the deuteride at the surface facing the gas. In Table 1 the results of the gas flow measurements through the cathode in four runs, one of which of 1992 (1), are correlated to the different phases of the deuteride: it can be seen that in the α-phase and in the $(\alpha+\beta)$-phase the flow is definitely lower than in the β-phase. Note that in the 92/3 run, while heat excess was produced, a negative flow could be measured, showing that D was flowing <u>into</u> the cathode from the gas ambient: it is as if a new phase, and the corresponding phase transition, is envisaged when heat excess is produced. This effect could not be seen in the only run of 1993 in which we saw heat excess (93/2), because of a CO poisoning of the surface, by us purposely produced. Note also that, even though the general trend described above is confirmed, the absolute values of the flow are widely different, showing once more that one electrode is different from the other, due both to differences in the sample itself and in the laboratory preparation procedures before starting electrolysis. Another way of looking at this phenomenon is presented in Fig.2, where for one of the runs quoted above (CNR/NOV), the absolute pressure behind the cathode is shown as a function of time. We have tried to determine on this graph the corresponding stages of deuterium charging, taking into account the phase-diagram of palladium deuteride, and thus the D/Pd ratio at the gas-side of the cathode. Starting from this datum, with a reasonable hypothesis on the dependence of the diffusion coefficient on the D/Pd ratio, it is possible to evaluate the D/Pd ratio at the other surface of the cathode, the one immersed in the electrolyte.

TABLE 1 The flow of D through the cathode in different experiments and different phases of the palladium deuteride (in 10^{15} atoms/s.cm^2)

Experiment / Phase	CNR/NOV	CNR/OCT	92/3	93/2
alfa	1.00	-	-	-
alfa+beta	0.80	0.60	-	-
beta	3.89	2.18	1.00	0.30
heat excess	-	-	-0.50	-

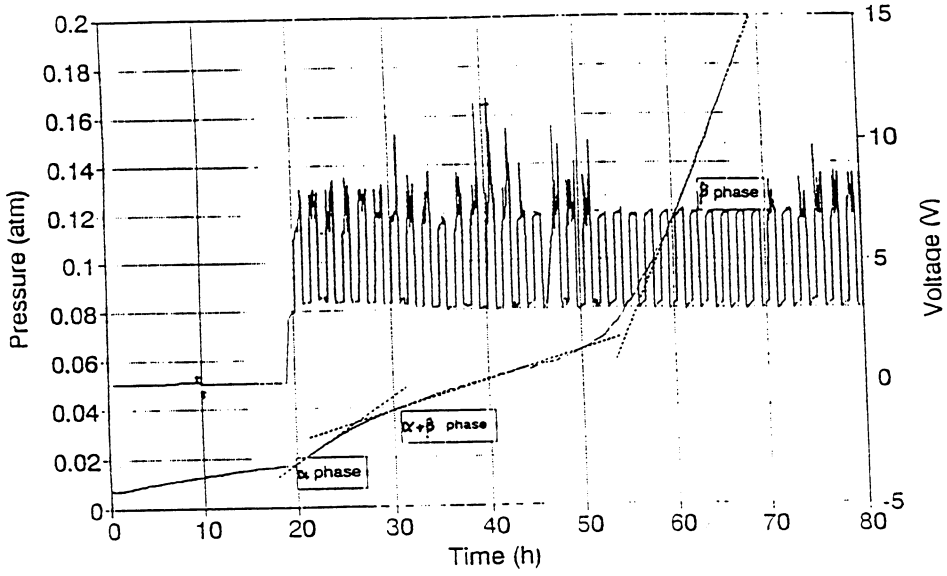

Fig.2 The pressure in the D_2 gas behind the cathode, as a function of time. Different phases of the palladium deuteride are shown, in correspondence of different slopes of the curve (i.e., different gas flows: see Table 1).

In Fig.3 the only positive event with the production of excess heat is shown. Power in excess, with a maximum of 4.5 W (9% of the heat inlet), was obtained, for a total time of about 20 hours, and a total heat excess larger than 200 kJ.

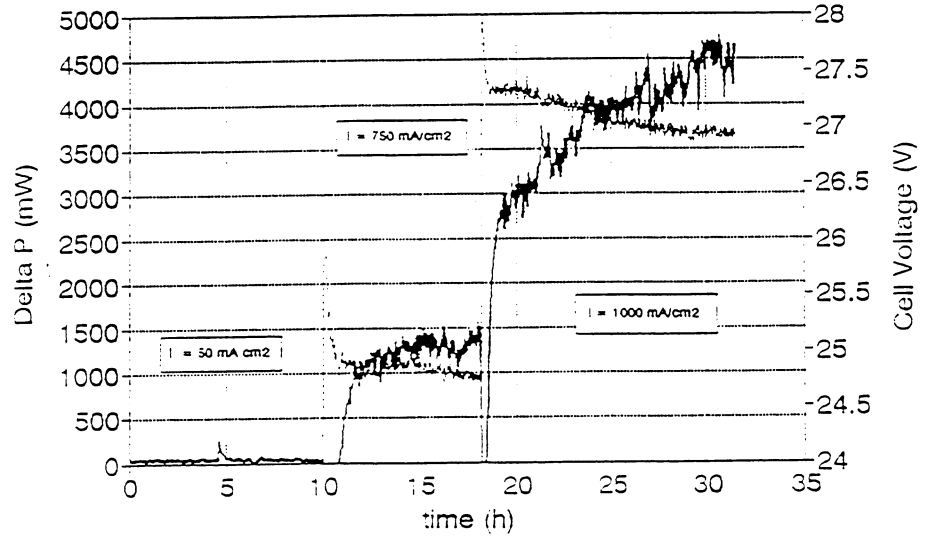

Fig.3 The power excess measured in experiment 93/2. The total amount of heat excess produced amounted to more than 200 kJ. The thicker sign is the power excess, the thinner is the cell voltage.

3. CONCLUSIONS

The geometry chosen for our cell seems to show a very interesting route to study the dynamics of D in Pd, which is, in our opinion, the main feature to investigate, in order to understand the phenomenology of Cold Fusion. This will require a more systematic investigation, aimed to better understand the relations between the pressure behind the cathode (and its time derivative, i.e., the gas flow) and the parameters characterizing the palladium deuteride at that surface. Thermodynamic modeling of the D-flow in the Pd-lattice (which has been undertaken by three of us, ADN,ALB,VV) could help finding the best conditions to obtain reproducibly the production of heat excess. This is one of the purposes of our future experiments.

Another important issue to be addressed is the set of material science features that clearly affect the reproducibility of D-charging in Pd. This, we hope, could be the aim of a common effort with other laboratories and industries.

REFERENCES

(a) ENEA Frascati, ERG/FUS
(b) ENEA Frascati, INN/FIS
(c) CNR Frascati, ISM
(d) ENEA Casaccia, INN/NUMA
1. L. Bertalot et al., Frontiers on Cold Fusion, Proceedings of ICCF3, Universal Academy Press, Inc., Tokyo, Japan, 365 (1993)
2. A. Bertin et al., Il Nuovo Cimento, 105A, 751 (1992)

LOADING, CALORIMETRIC AND NUCLEAR INVESTIGATION OF THE D/Pd SYSTEM

SRI International, Menlo Park, California

Michael McKubre

Ben Bush

Steven Crouch-Baker

Alan Hauser

Nada Jevtic

Stuart Smedley

Mahadeva Srinivasan

Francis Tanzella

Mark Williams

Sharon Wing

Electric Power Research Institute, Palo Alto, California

Thomas Passell

Work Sponsored by: **The Electric Power Research Institute**

Palo Alto, California, USA

Presented at the ICCF4 - December 6, 1993

Hypothesis 1

"There is an unexpected and unexplained source of heat in the D/Pd system, which may be observed when deuterium is loaded electrochemically into the palladium lattice, to a sufficient degree".

Experiments

- **Loading (R/R°)**
- **Calorimetry**

Results

Excess heat and excess temperature observed in mass flow and heat flow calorimeters

Not consistent with known chemistry or with any artifact we have considered

Loading is necessary but not sufficient

Current (density)

Temperature

Initiation (other elements?)

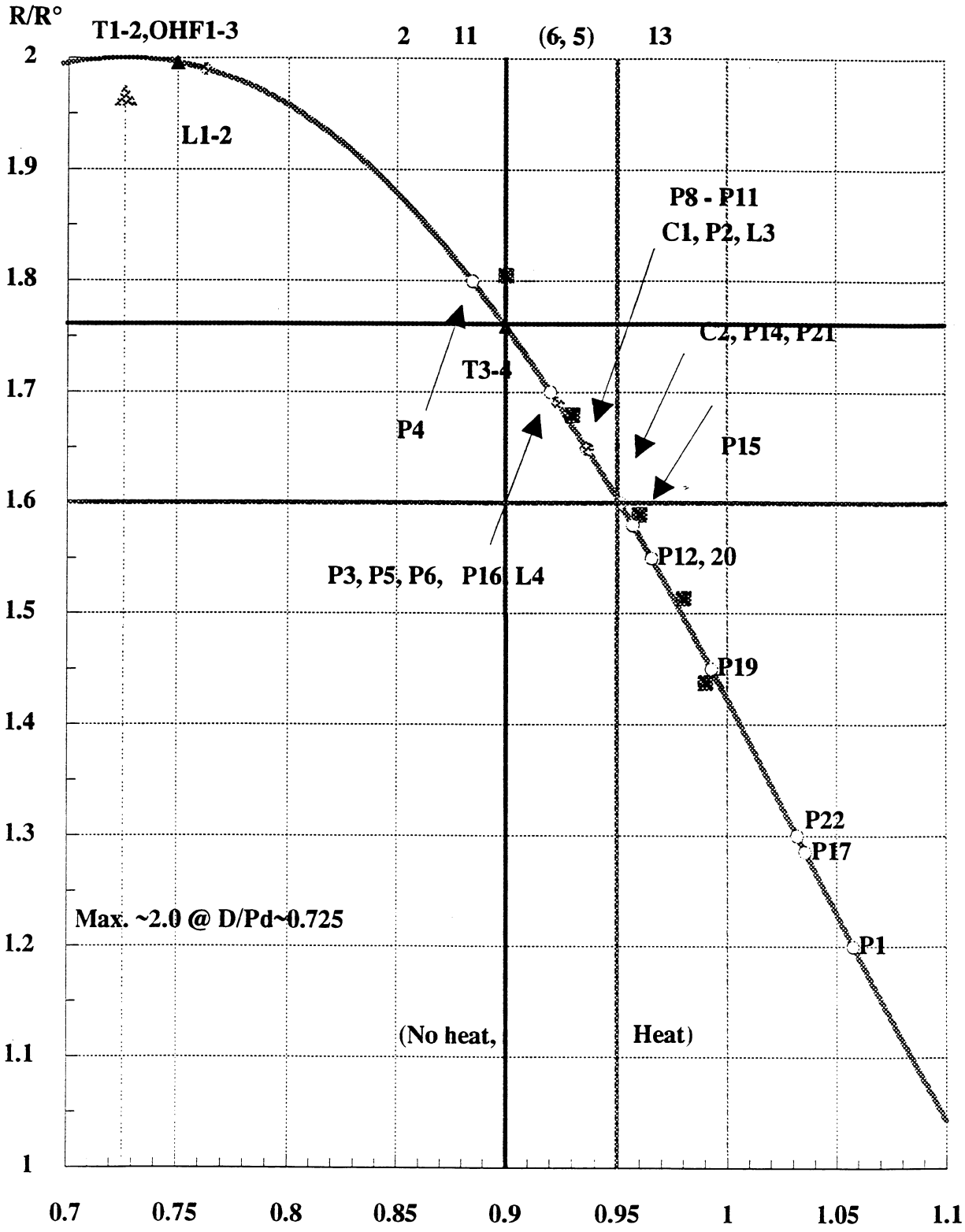

Figure 1 Maximum loading, D/Pd, attained in experiment; determined by R/R°.

Hypothesis 2

"The excess heat originates from an unexpected and unexplained nuclear process"

Experiments

Establish a quantitative and/or temporal correlation between excess heat and nuclear products:

- **Gamma and X-ray spectrometer**
- **Neutron spectrometer**
- **(Charged particle double telescope)**
- **Tritium**
- **Helium**
- **Isotope shifts**

Results

Nuclear process not (presently) confirmed
Separate systems difficult to optimize jointly
Difficult to search for more than one potential product per calorimeter

NUCLEAR

Attempt to:

- **Optimize one system at a time**
- **Define accurate lower bounds on the production rates in all potential nuclear channels**
- **Make accurate determination of product energies to aid mechanistic understanding**

Gamma- and X-ray

Pb passive shield 2' dia., 3 ' high, 4" wall

NaI Compton suppression annuli, 16" dia., 16" high

- **3" diameter bore**
- **5" diameter hole**

Ge detectors: mounted coaxially

- **52.5% extra low background, 0.5 mm Be window**
  Capability down to 3 keV
  FWHM 1.85 keV @ 1332 keV (Co-60)
- **47.5% low background capsule resolution 2 keV**

Background 10 keV - 2.5 MeV

Low *BG*/No Compton suppression ~ 6-7 c/s

Extra low *BG*/Compton suppression ~ 1 c/s

Detection Capability /100,000 s

~ 10^{-3} c/s @ 30 keV

~ 10^{-4} c/s @ 1300 keV

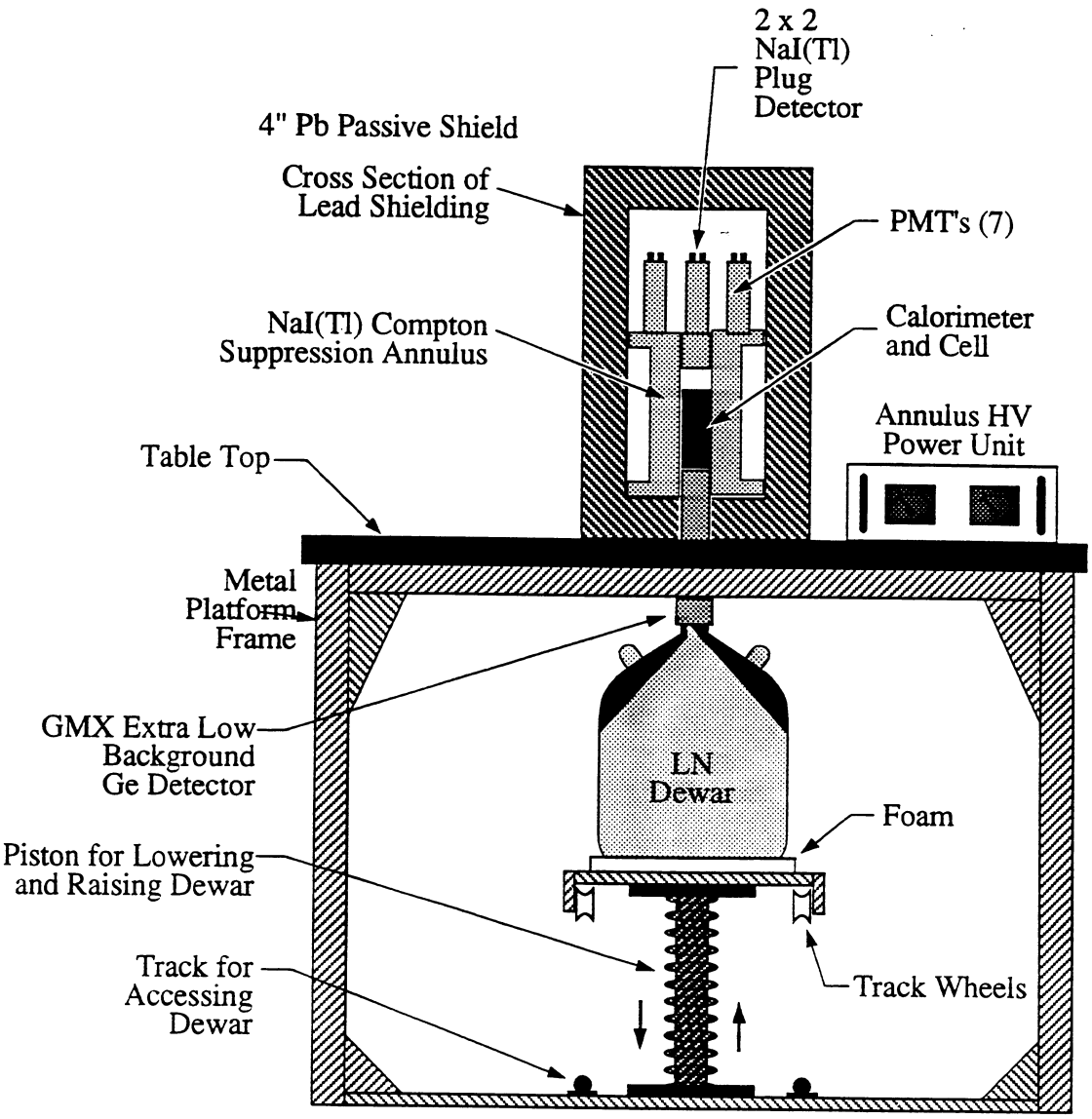
2 x 2
NaI(Tl)
Plug
Detector
4" Pb Passive Shield
Cross Section of
Lead Shielding
PMT's (7)
NaI(Tl) Compton
Suppression Annulus
Calorimeter
and Cell
Annulus HV
Power Unit
Table Top
Metal
Platform
Frame
GMX Extra Low
Background
Ge Detector
LN
Dewar
Foam
Piston for Lowering
and Raising Dewar
Track for
Accessing
Dewar
Track Wheels

CM-4035-016

Neutron

6 active 40x70 cm plastic scintillator cosmic ray shields

4" polyethylene passive shield

2 - 5x3" NE-213 liquid scintillators

Pulse shape discrimination between n° and γ

Event-by-event data

1 MeV - 5 MeV

Efficiency ~ 2%

Charged Particles

Triple Si surface barrier detector

Event-by-event mode operation as two δE/E telescopes with noise rejection

Tritium

***Ex-situ* electrolyte analysis: 10 pCi/ml sensitivity, 20% Absolute Efficiency**

Helium

Extrel # C50

- ***Ex-situ* real time analysis ~ 1 ppm sensitivity**
  separate D_2 and He

Bureau of Mines, Helium Field Operations, Texas

- **< 1 ppb ^4He**
- **< 30 ppt ^3He**

Isotopes

Mass spectroscopy (SIMS/SALI)

- **Depth profiling for solid samples**
- **Molecular interferences with light elements present**
- **Sampling problems for highly localized changes**

PGAA (Prompt γActivation Analysis)

CNDP (Cold Neutron Depth Profiling)

Electrochemical Investigation of the Pd-H/D System

EXPERIMENTAL APPROACH

Assess degree of loading (DoL) employing *in-situ* resistance measurements with:

- "Farm" of ten electrolytic cells
- "Movable-Wire" electrode apparatus

  - Batch Differences
  - Anode Selection
  - Surface Modifying Agent
  - Alternating Polarity
  - Annealing Conditions

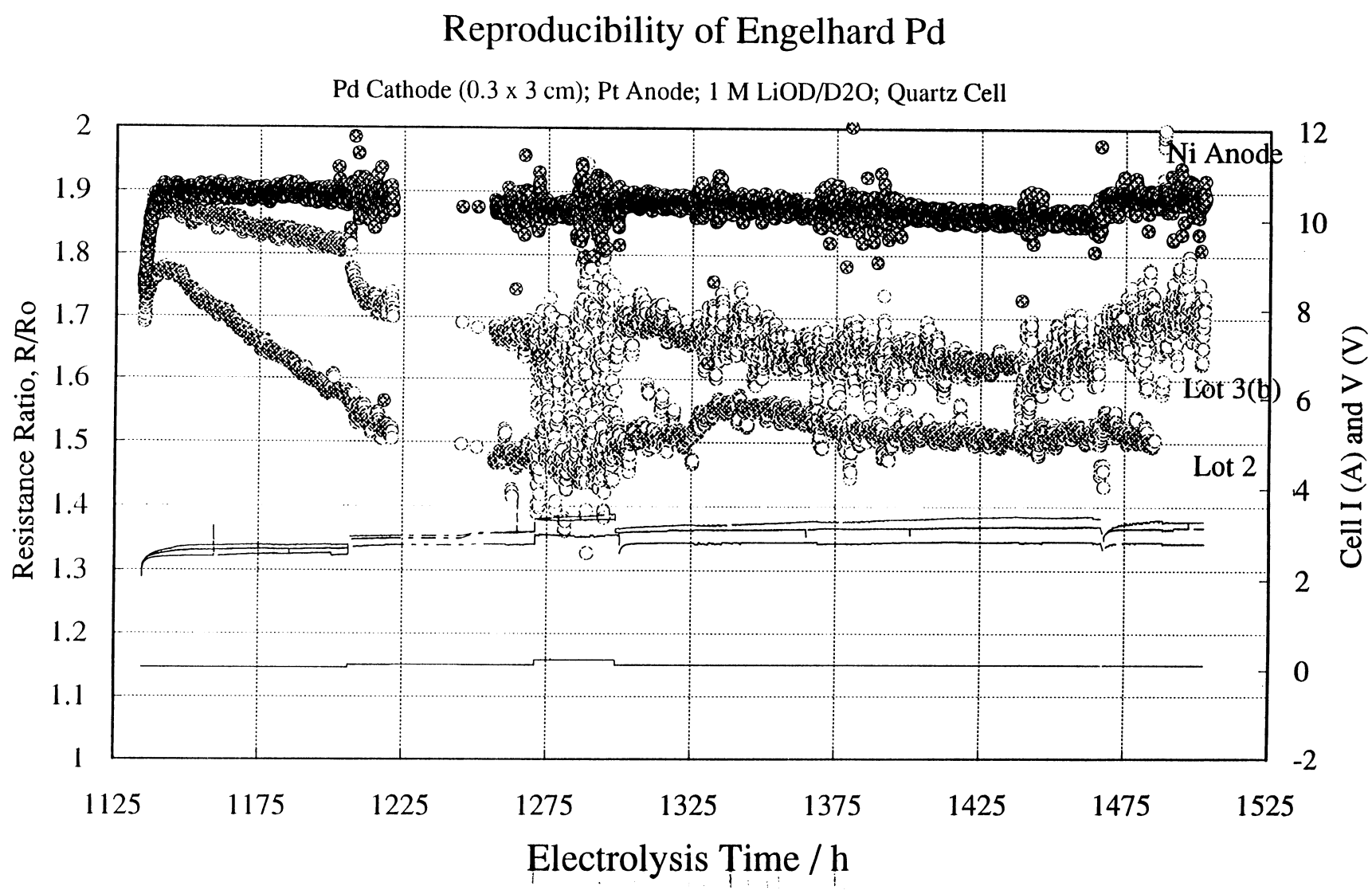
Reproducibility of Engelhard Pd
Pd Cathode (0.3 x 3 cm); Pt Anode; 1 M LiOD/D2O; Quartz Cell
Resistance Ratio, R/Ro
Cell I (A) and V (V)
Electrolysis Time / h
Ni Anode
Lot 3(b)
Lot 2
2
1.9
1.8
1.7
1.6
1.5
1.4
1.3
1.2
1.1
1
12
10
8
6
4
2
0
-2
1125
1175
1225
1275
1325
1375
1425
1475
1525

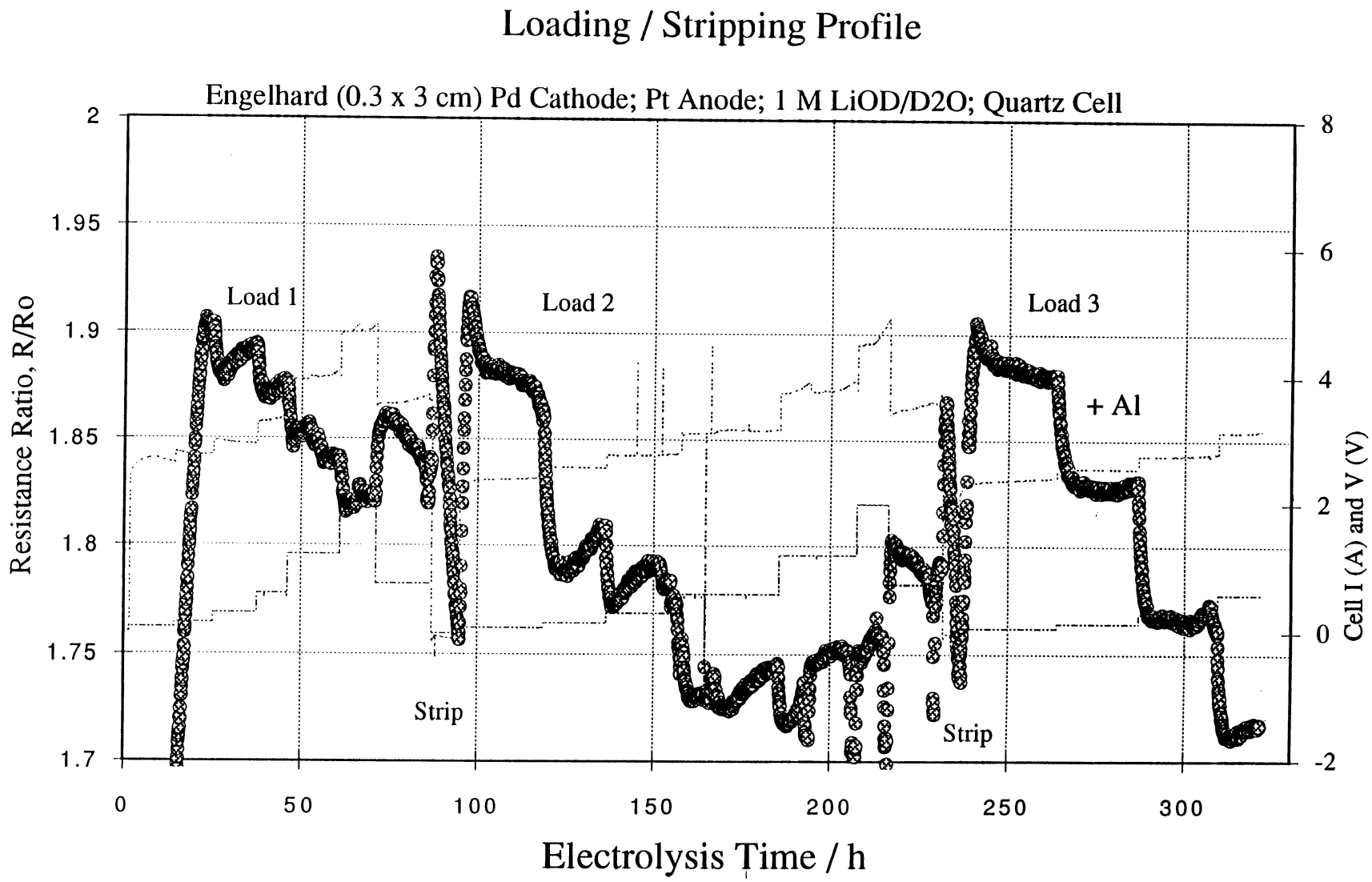
Loading / Stripping Profile
Engelhard (0.3 x 3 cm) Pd Cathode; Pt Anode; 1 M LiOD/D2O; Quartz Cell
Resistance Ratio, R/Ro
Cell I (A) and V (V)
Electrolysis Time / h
Load 1
Load 2
Load 3
+ Al
Strip
Strip
2
1.95
1.9
1.85
1.8
1.75
1.7
8
6
4
2
0
-2
0
50
100
150
200
250
300

Effect of Surface Modifying Agent on Loading

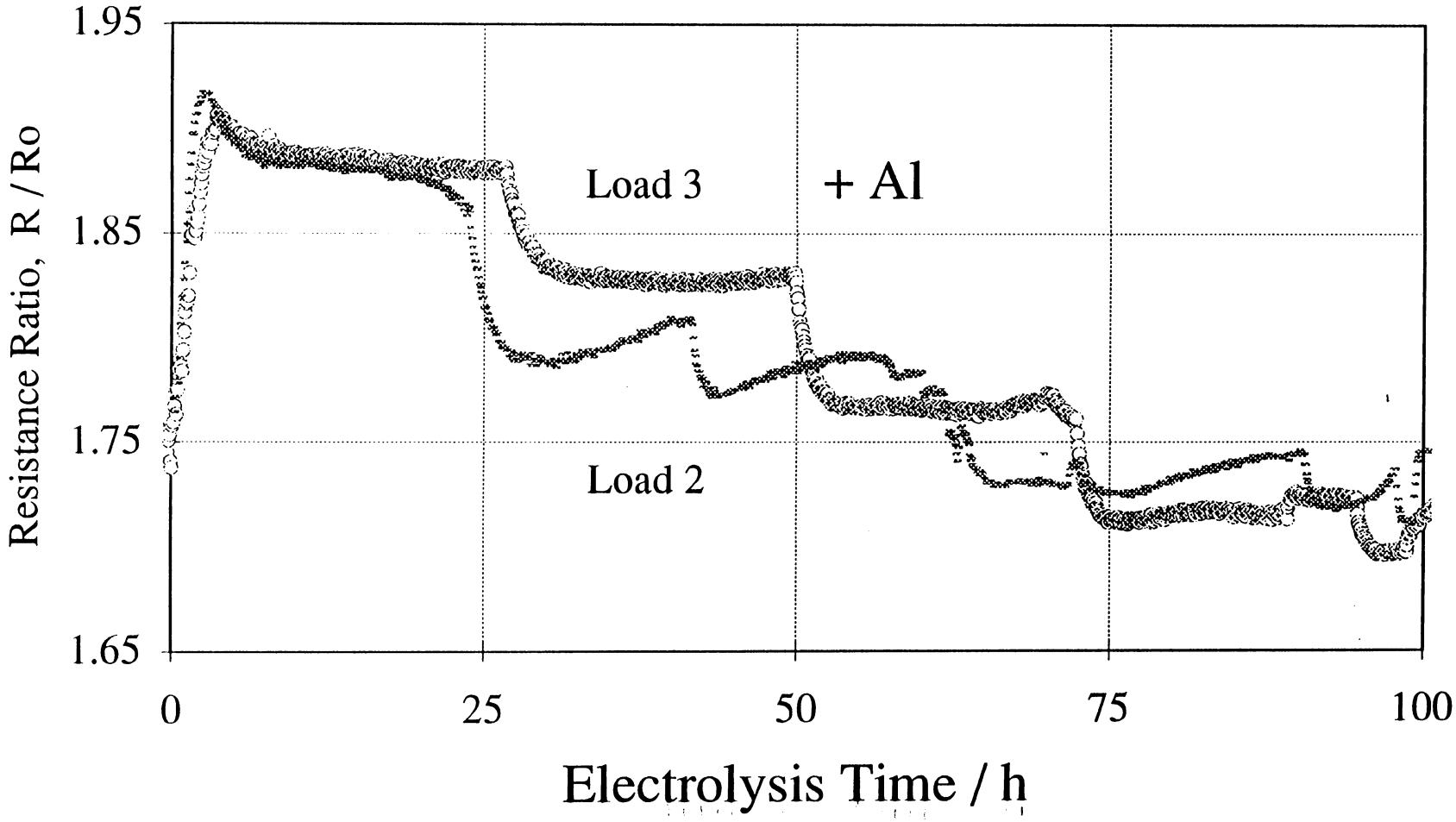

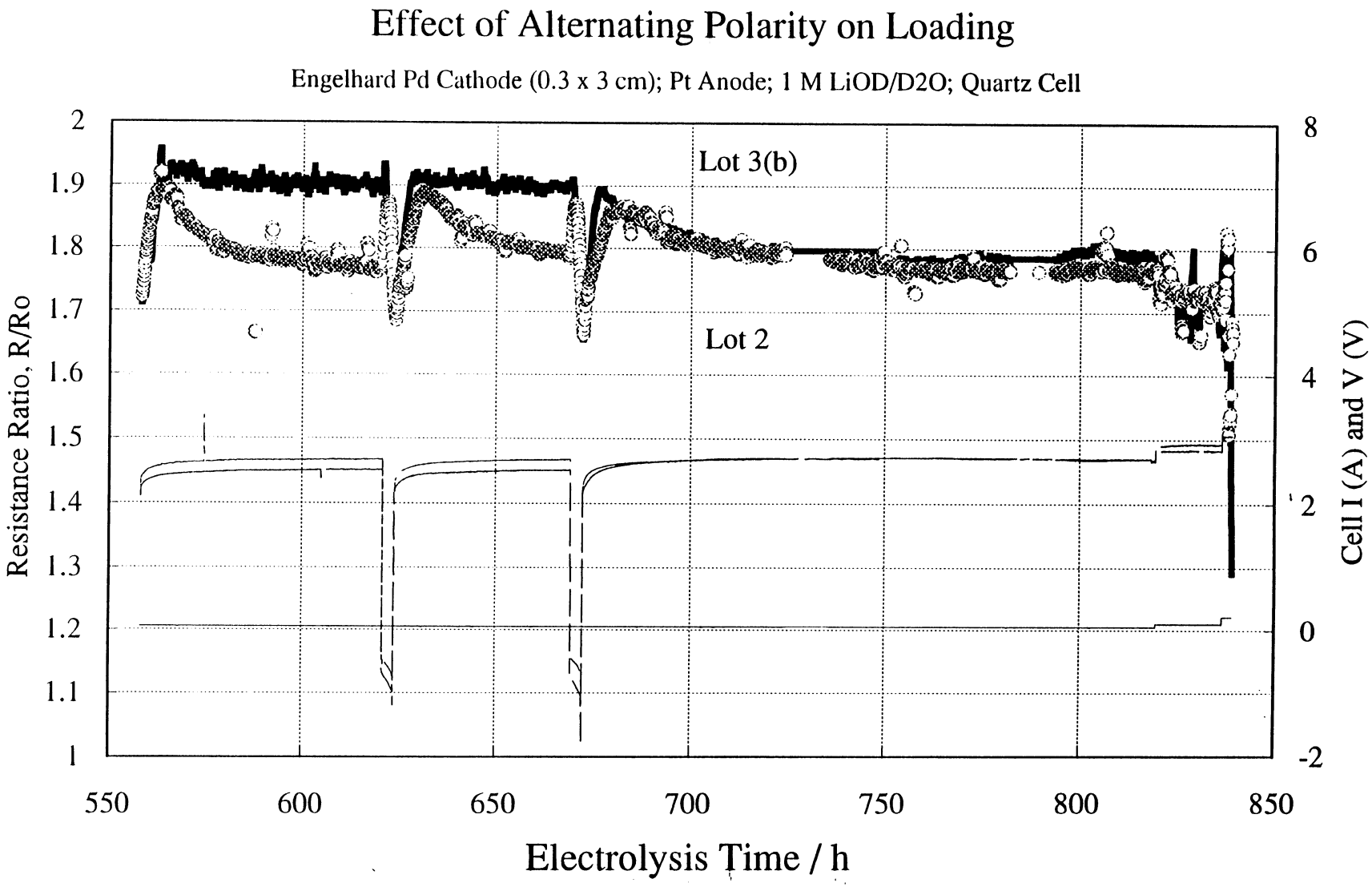
Effect of Alternating Polarity on Loading
Engelhard Pd Cathode (0.3 x 3 cm); Pt Anode; 1 M LiOD/D2O; Quartz Cell
Lot 3(b)
Lot 2
Resistance Ratio, R/Ro
Cell I (A) and V (V)
Electrolysis Time / h
2
1.9
1.8
1.7
1.6
1.5
1.4
1.3
1.2
1.1
1
8
6
4
2
0
-2
550
600
650
700
750
800
850

Effect of Time of Annealing at 850 C on Loading

Engelhard Lot 3 Pd Cathode (0.3 x 3 cm); Pt Anode; 1 M LiOD/D2O; Quartz Cell

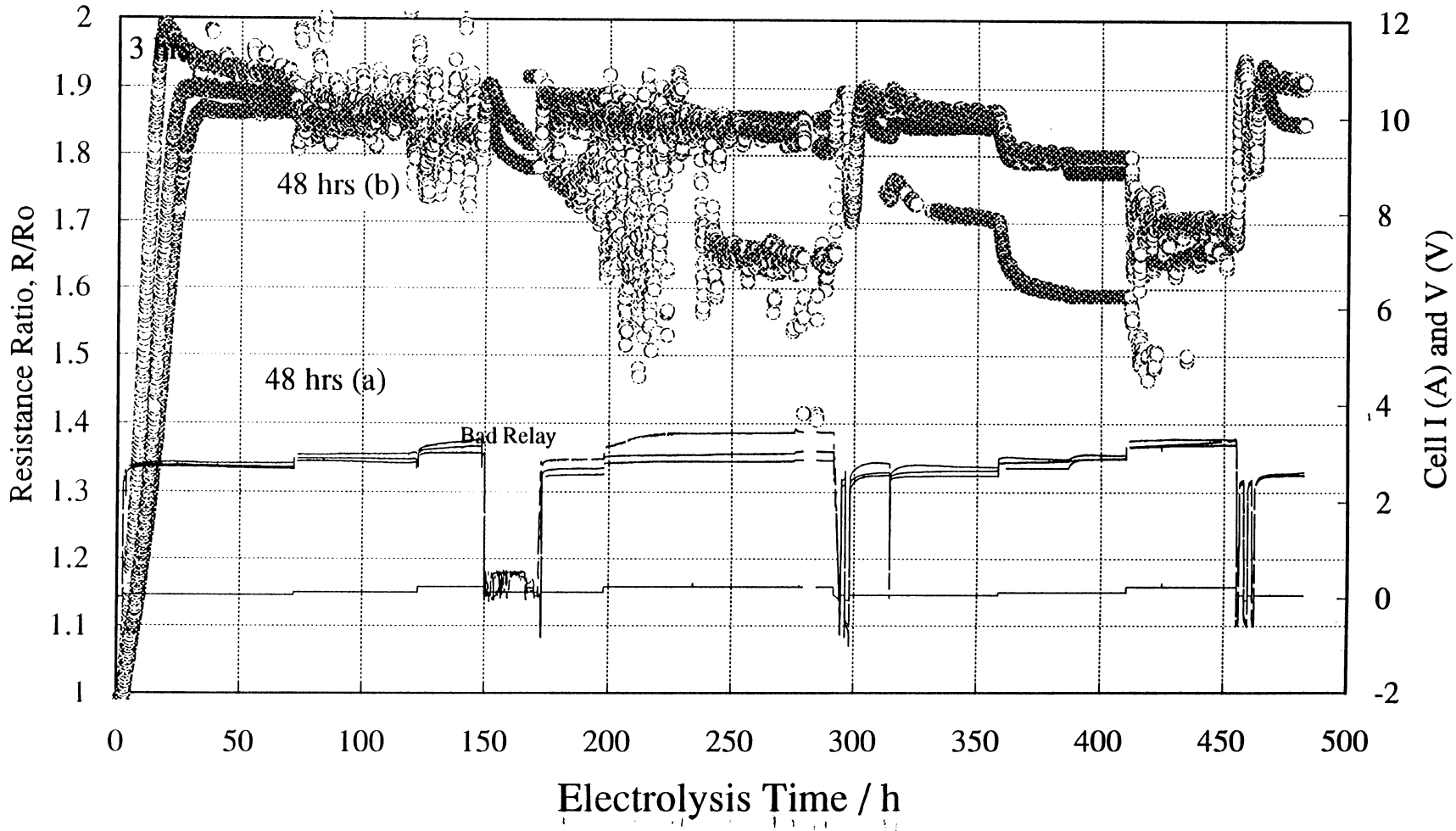

CALORIMETRY

Mass Flow: L, M

Thermodynamically closed

Maintain high accuracy over wide input/output power range

Long term stable operation needed to integrate potential products

Heat Flow

Thermodynamically open

Sensitivity (°/W, τ)

Flexibility (Geometry, optical detectors)

Redundancy of method

- **Isoperibolic: T, HF, D, F, G**
- **Seebeck: OHF, HH**
- **Lateral: LHF**

LABYRINTH CALORIMETERS

All: 1.0 M LiOD + 200 ppm Al

3mm dia. x 3 cm long Engelhardt Pd

Four Pt wire contacts for R/R°

	L1	L2	L3	L4	
Anode	**Ni**	**Pt/Nb**	**Pt**	**Pt**	
Cathode	**3**	**3**	**2**	**2**	**batch**
i_{max}	**1.1**	**1.1**	**1.6**	**1.1**	**A cm^{-2}**
X_{max}	**0.76**	**0.76**	**0.94**	**0.92**	**D/Pd**
Duration	**1600**	**900**	**2500**	**2500**	**h**
P_{xs}	**0 ± 50**	**0 ± 50**			**mW**

"Boil On"

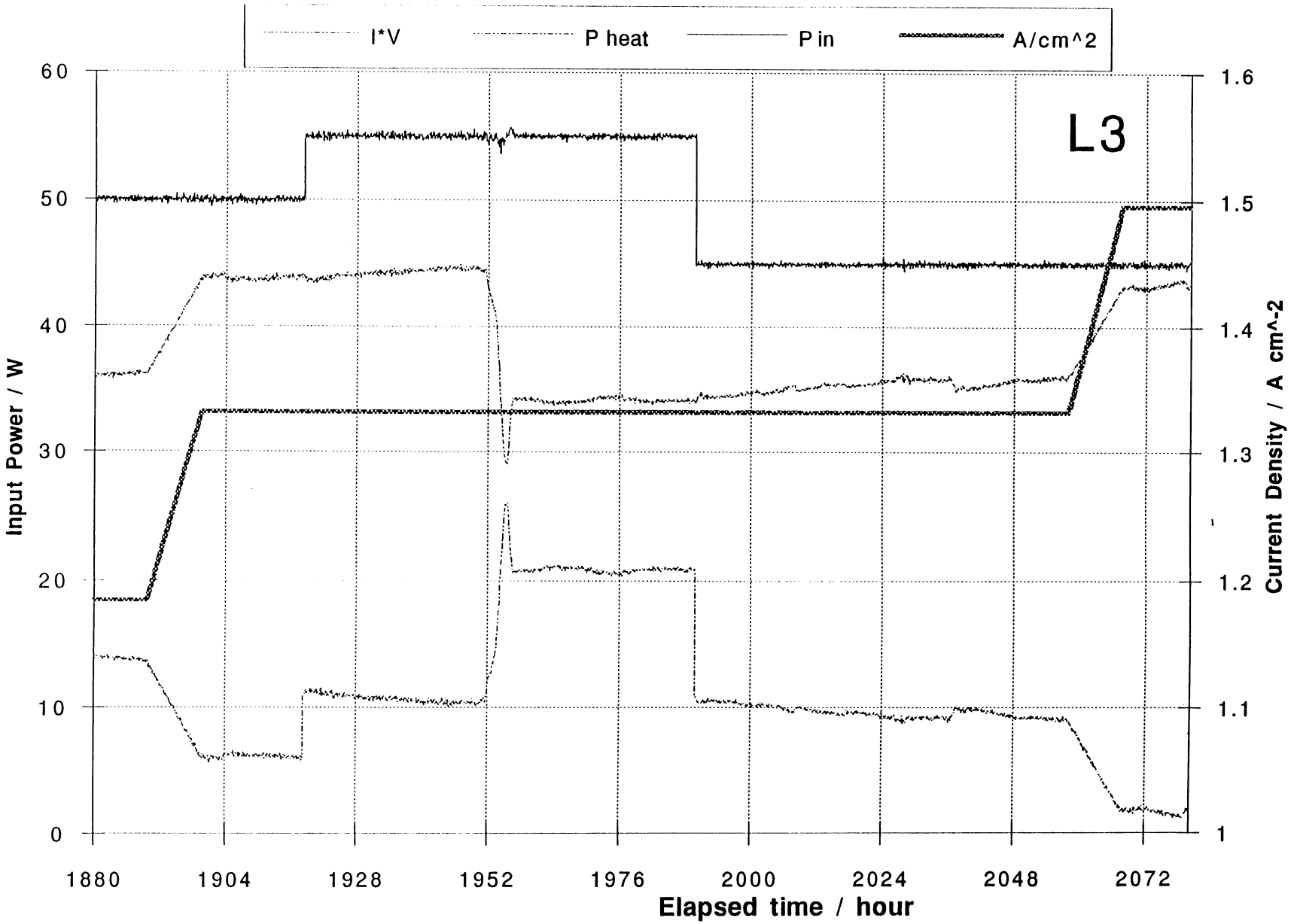

Exp. started 8/3/93 15:43

3/11/94

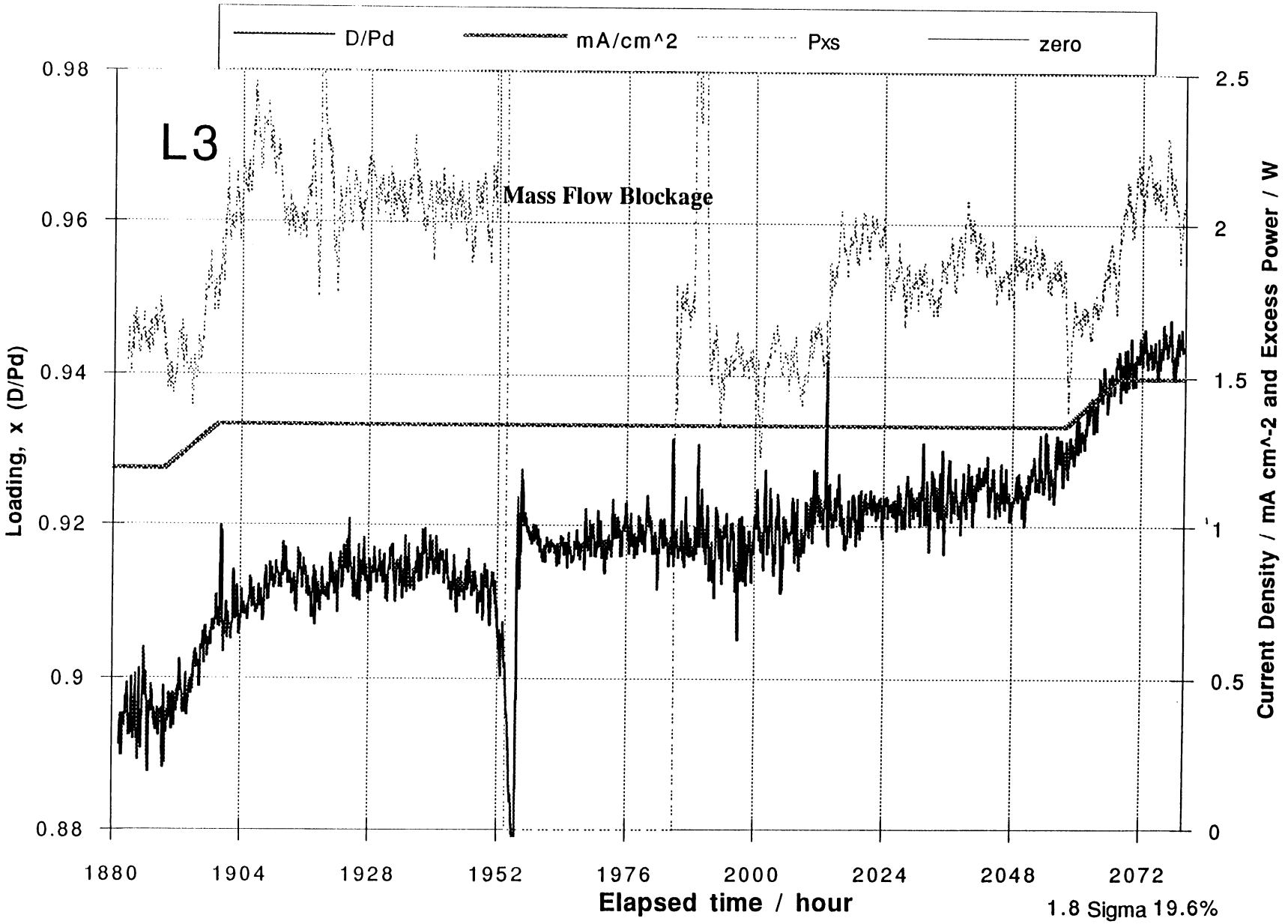

Exp. started 8/3/93 15:43

3/11/94

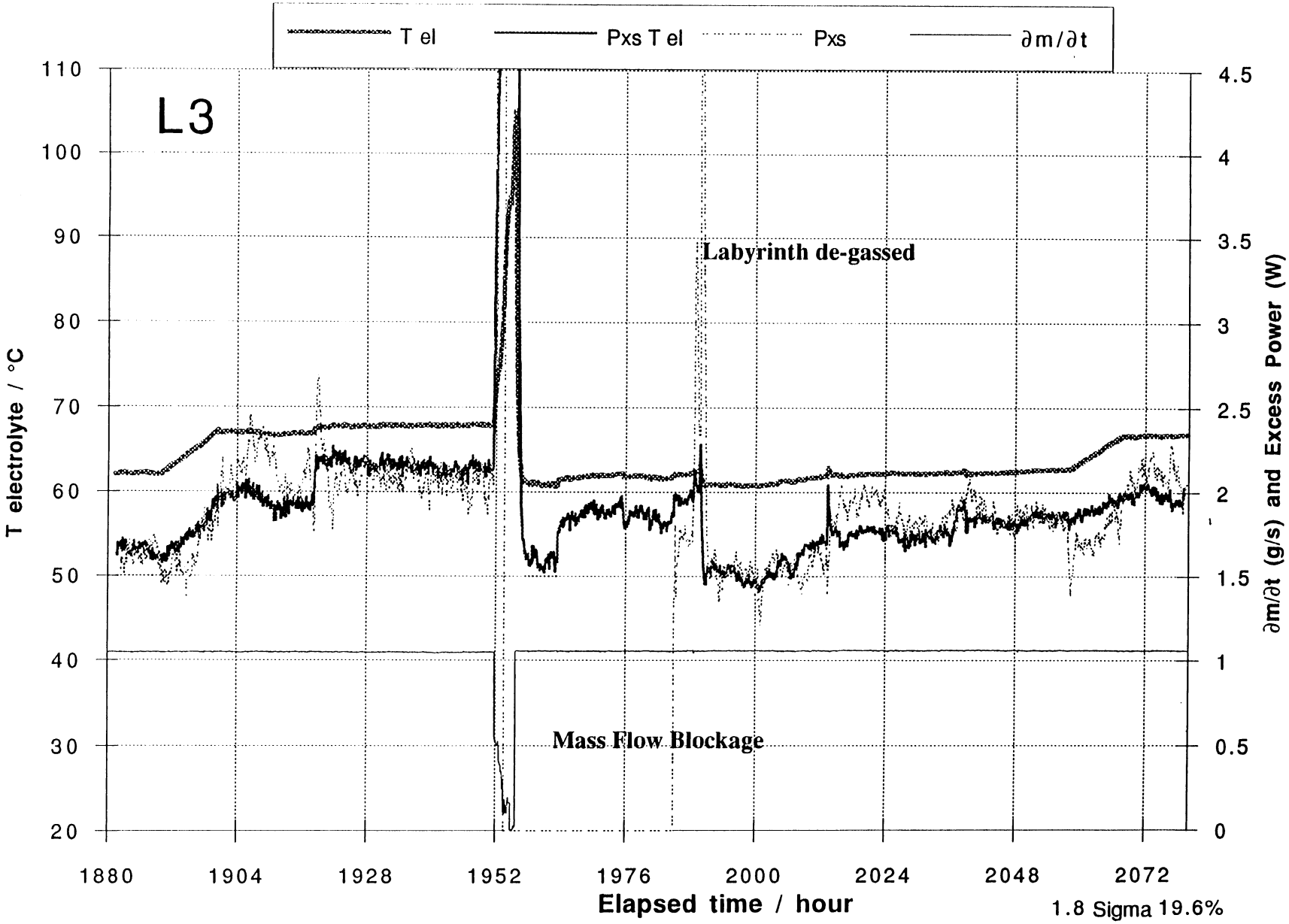

Exp. started 8/3/93 15:43

3/11/94

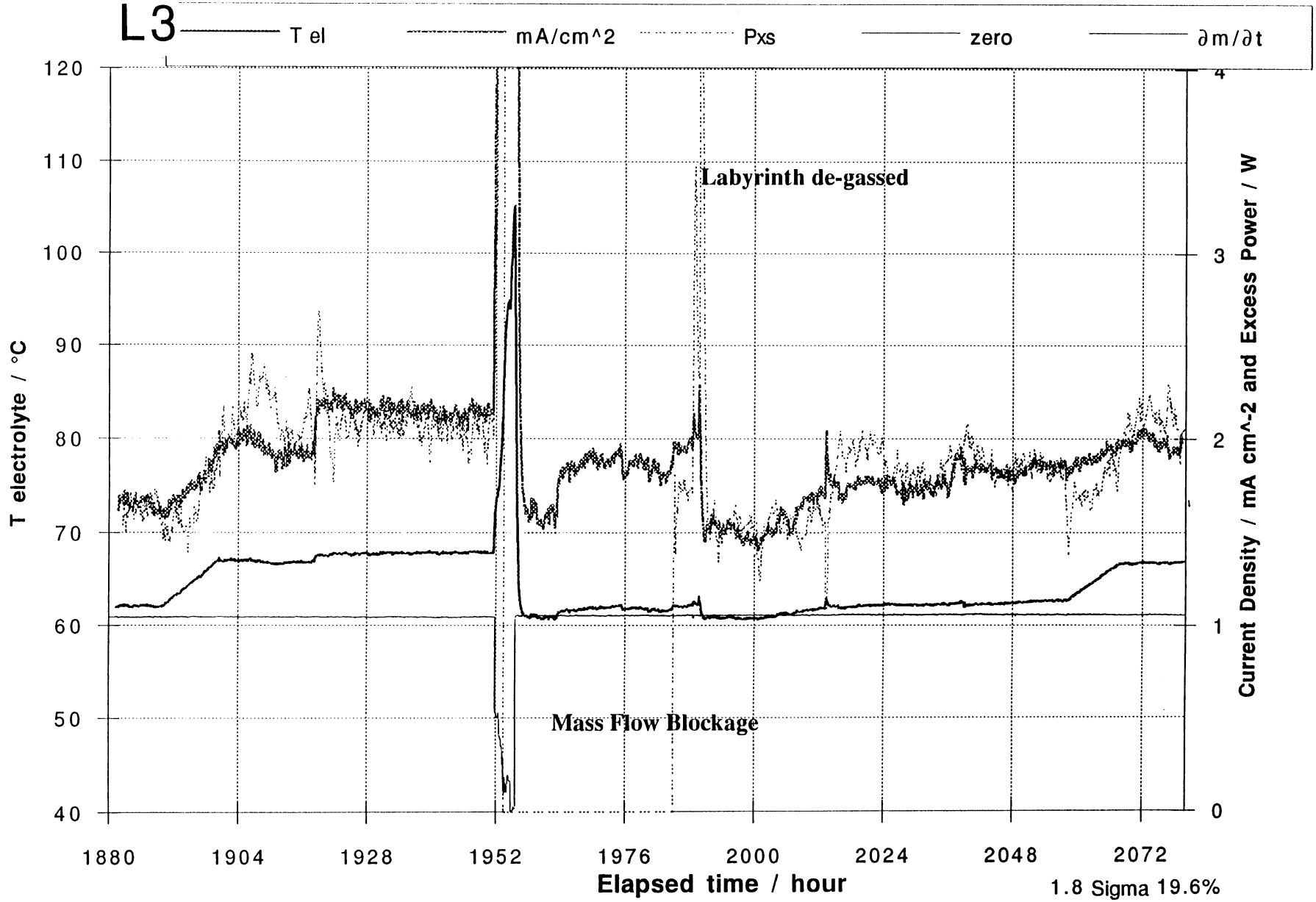

Exp. started 8/3/93 15:43

3/11/94

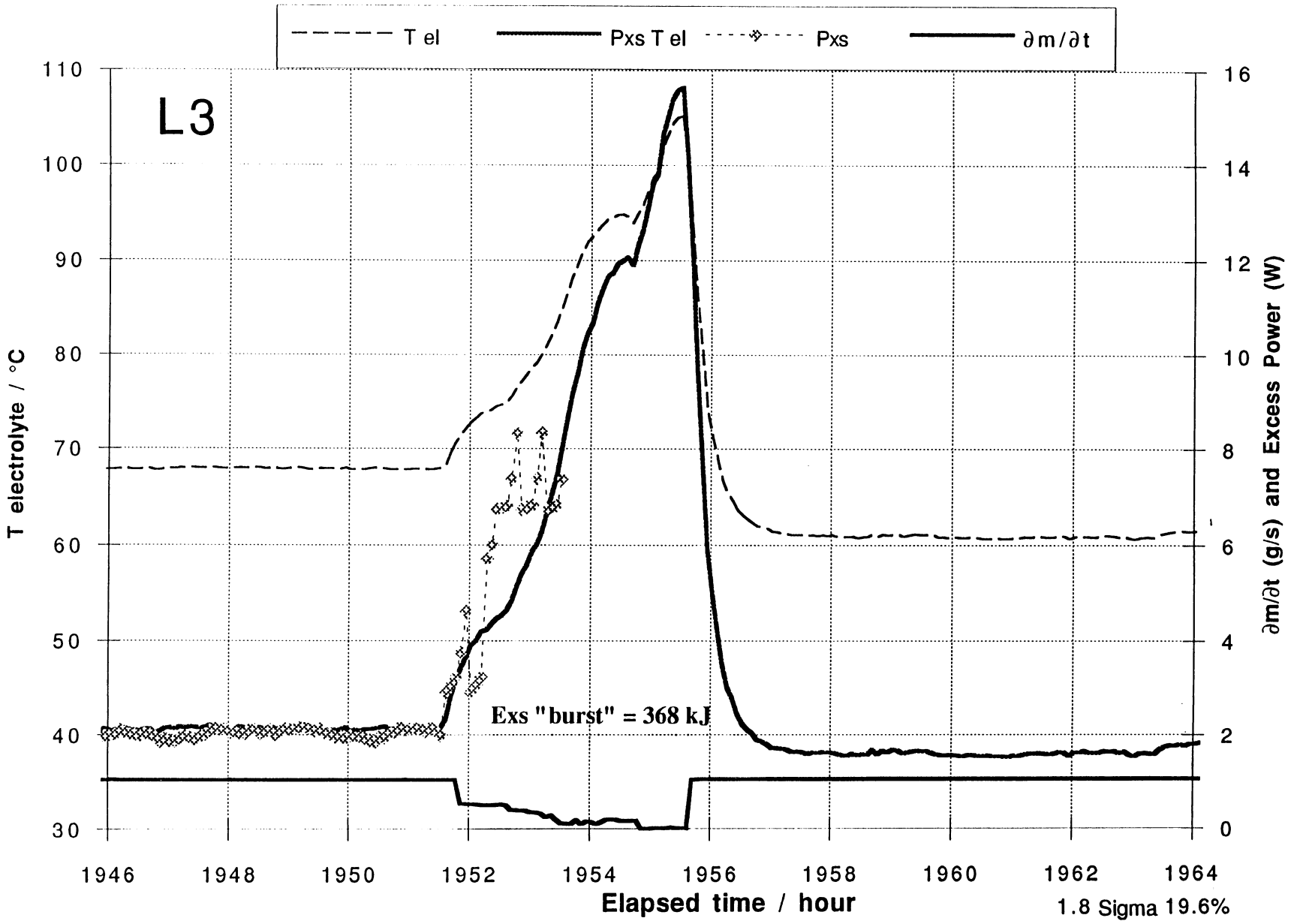

Exp. started 8/3/93 15:43

3/11/94

"Heat After Life"

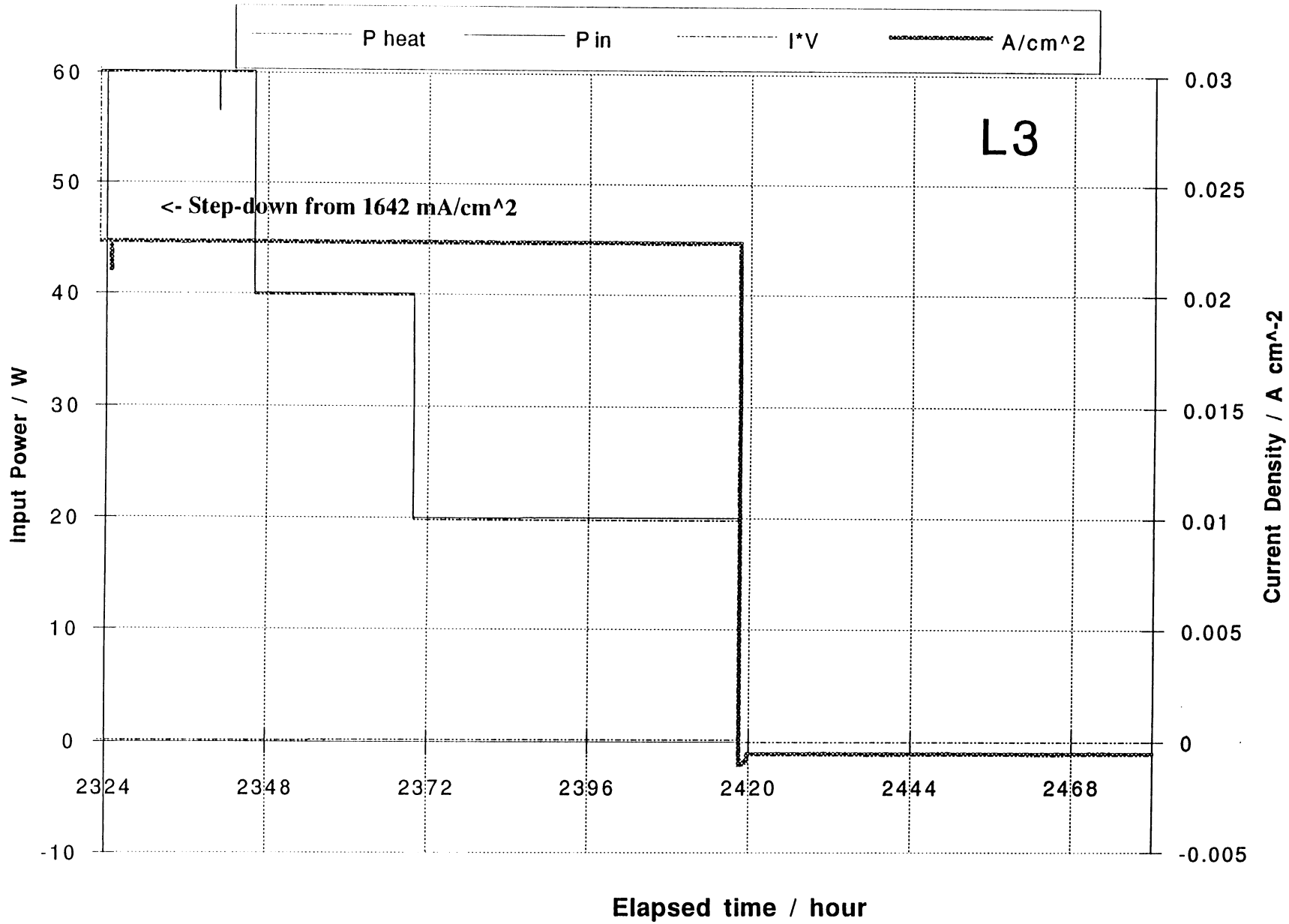

Exp. started 8/3/93 15:43

3/11/94

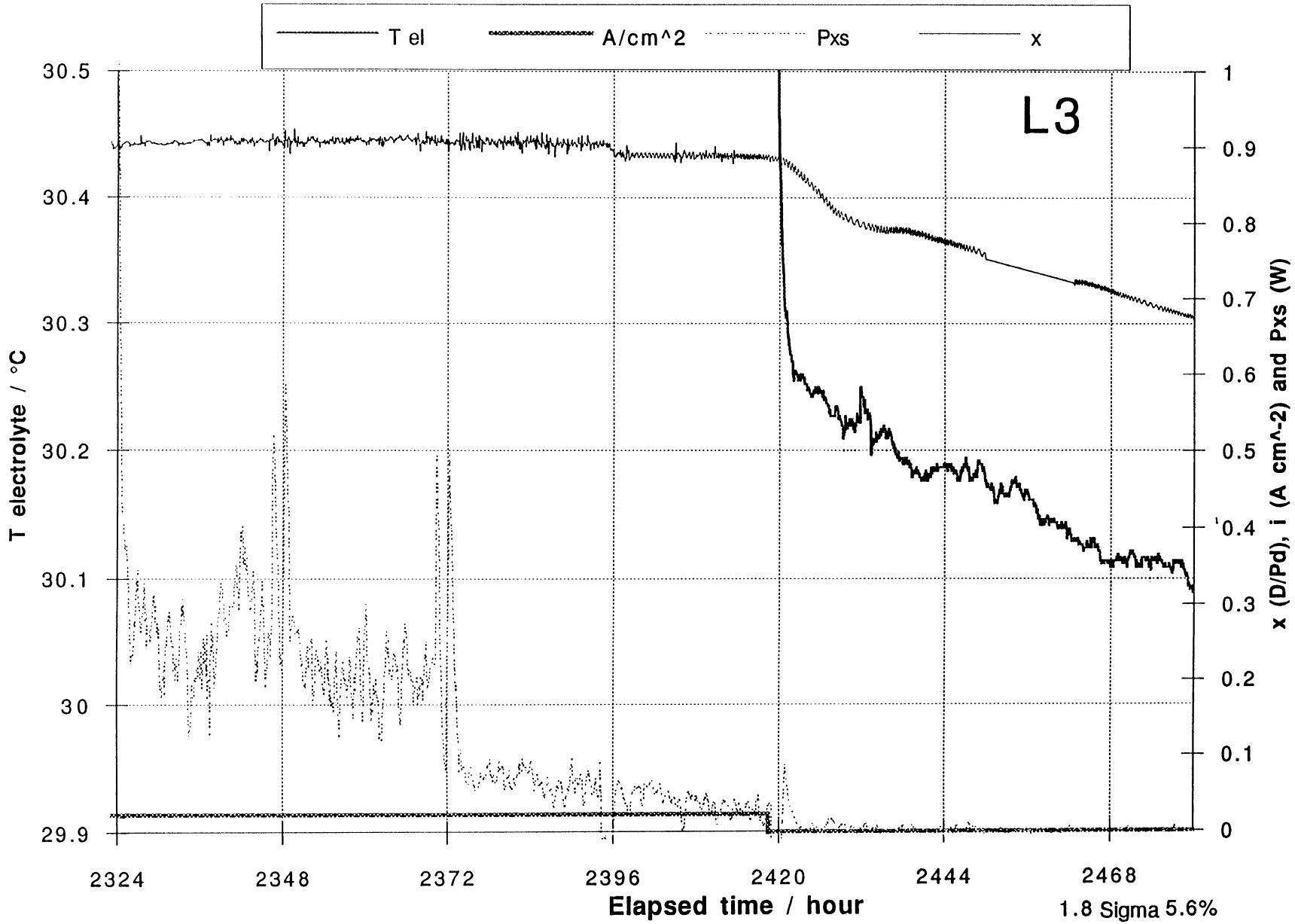

Exp. started 8/3/93 15:43

3/11/94

"Loss of Resistance"

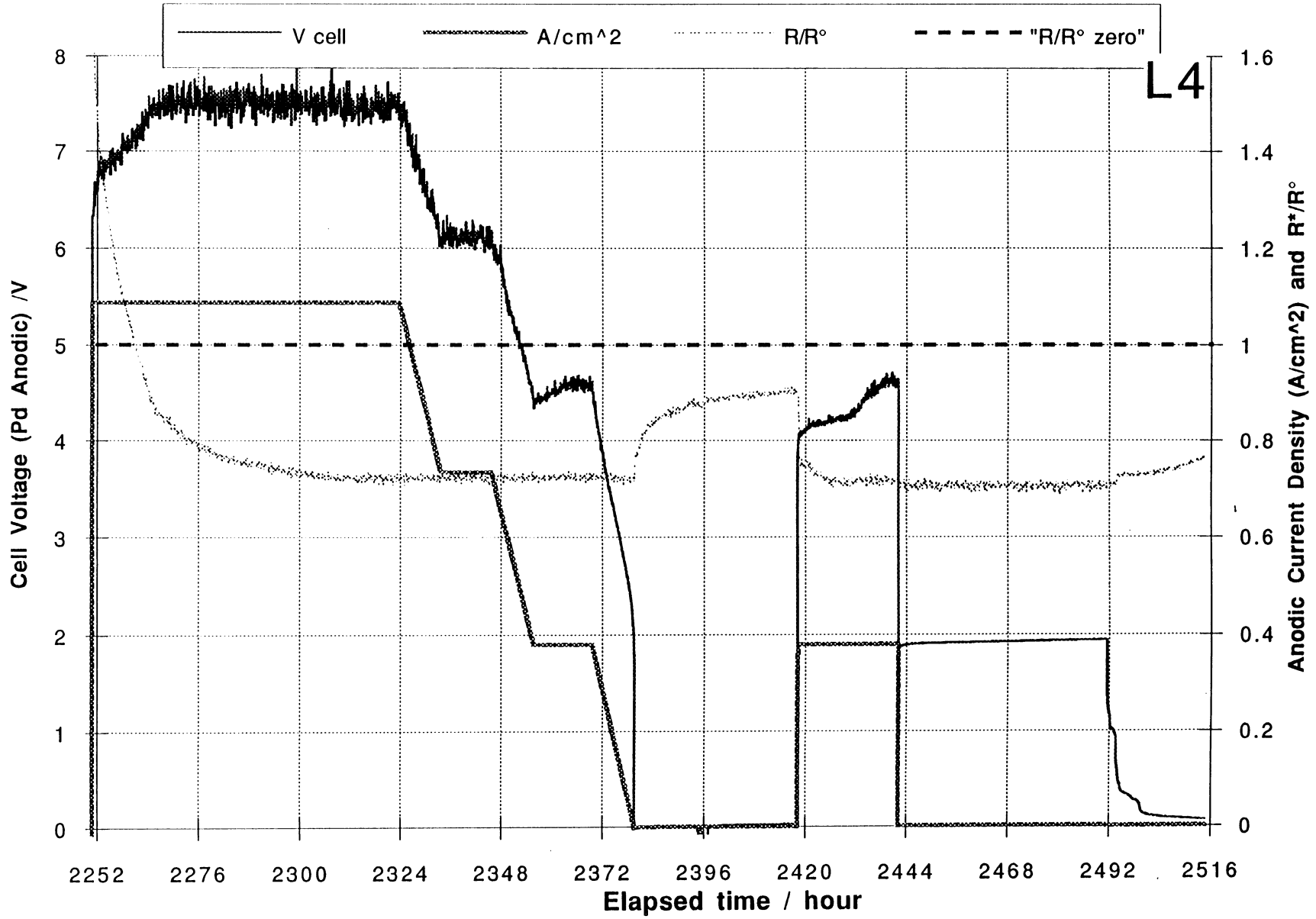

Exp. started 8/3/93 15:43

3/11/94

HELIUM-4 QUANTITATIVE MEASUREMENTS IN THE GAS PHASE OF COLD FUSION ELECTROCHEMICAL CELLS

D. Gozzi, R. Caputo, P. L. Cignini* , M. Tomellini#
Dipartimento di Chimica, Universita' *La Sapienza*,
P.le Aldo Moro 5, 00185 Roma, Italy

G. Gigli, G. Balducci
Dipartimento di Chimica, Universita' *La Sapienza*,
P.le Aldo Moro 5, 00185 Roma, Italy

E. Cisbani, S. Frullani, F. Garibaldi, M. Jodice°, G.M. Urciuoli°
Laboratorio di Fisica, Istituto Superiore di Sanita',
V.le Regina Margherita 299, 00161 Roma, Italy

Abstract

The quantitative determination of the ^4He content in the gaseous products of a cold fusion Pd-D_2O electrolysis experiment lasting 1200 hours is reported. The details of the mass spectrometric method, which allows a sub ppb detection limit, are described. In order to check air contamination the ^{20}Ne content has also been, nearly simultaneously, measured. The method employed, while involving an off-line determination on collected samples, nevertheless allowed to collect an amount of data capable of providing a description of the time dependence of the phenomena.

Introduction

In the last years our experimental facilities devoted to the calorimetric and nuclear studies of the Pd - D_2O systems electrolysis have been steadily improved[1-5] with the aim to both ameliorate sensitivity and reliability of the original heat power excess and neutron emission measurements and increase the number of the possible nuclear signatures monitored. Recently, on the side of the nuclear ashes detection, it has been added the capability to perform an off-line mass-spectrometric quantitative measure of ^4He amount in the electrolysis gases. We are here giving a

* CNR - Centro di Termodinamica Chimica alle Alte Temperature, Dipartimento di Chimica, Universita' La Sapienza

Dipartimento di Scienze e Tecnologie Chimiche, Universita' di Tor Vergata, via della Ricerca Scientifica, 00133 Roma

° INFN sezione Sanita', V.le Regina Margherita 299, 00161 Roma

detailed description of the method used and of the results obtained. The complete experiment lasting ≈1200 hours is reported in a separate paper in this same meeting [6]. Here it is useful to recall that 5 cells (Pd cathode, 0.2 M LiOD in D_2O, in our notations cells #2,4,7,8,10) were used while one cell (Pt cathode in the same solution, cell#1) provided the blank.

With the magnetic mass spectrometer at our disposal, the effort here described had the aim to measure, during the electrolysis experiment and with adequate sensitivity, a number of the collected gaseous samples large enough to provide a picture of the time dependence of the phenomena, if any, occurring. Indeed this capability was, by necessity, much reduced in the experiments already reported in the literature [7-11] where the collected gaseous samples were, as a rule, shipped to the best specialised laboratories by taking advantage of the better detection limits there attainable.

Experimental

The mass spectrometer, originally built by Nuclide Analysis Associates (now PATCO, Premier American Technologies Co.), is a single focusing 12" 60° magnetic instrument equipped with a Nier type electron ion source. It has been designed for and is currently used, in the field of high temperature chemistry, coupled to a Knudsen effusion molecular source. The resolving power used, as a compromise between sensitivity and discrimination capabilities, was 660 (measured by single peak half height width on mass ^4He). The detector is an electron multiplier operated at a gain, measured on mass 28, equal to 3 10^5. The operating conditions were as follows: 1 mA emission current, 100 eV ionising electron energy, accelerating voltage ≈ 4500 V. A magnetic scan across mass 4 is shown in fig. 1 where it is shown how readily D_2 and He peaks are baseline resolved with a magnetic instrument.

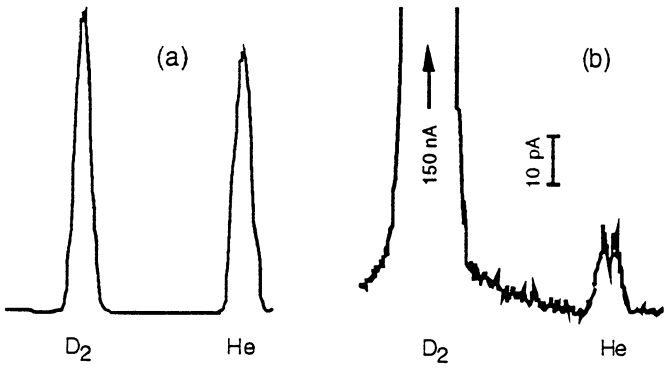

Figure 1 Magnetic scans across nominal mass 4 for nearly equal a) and largely different b) amounts of Deuterium and Helium

On the other hand another, related but not identical, property of the mass spectrometer can be important in this type of measurement. Indeed in the electrolysis gases one is sometime looking for the very low signal of helium on the tail of a large deuterium signal. With respect to this property, sometime called the abundance sensitivity, an idea of our experimental conditions is given in the same fig. 1 where, at the typical operating ion source pressure, while measuring the samples, of roughly 10^{-5} torr, and for the case of a synthetic mixture, helium is measured, by a magnetic scan, on the residual tailing of a much larger deuterium peak.

A general scheme of the collection lines, together with the materials employed in these lines, is shown in fig. 2. Boil off nitrogen has been used as a carrier gas to sweep the electrolysis cells. Each of the cells was connected in series to his specific D_2/O_2 external recombiner while the stream of gas coming from the different cells could, by a manifold valve system, be made to pass through a Stainless Steel (SS) trap filled with Pd sponge and a SS collecting vessel 500 cm^3 in volume. Two of these traps and vessel system were available in order to be able to flush directly with the only carrier gas one of the two when it was necessary to do so as well as when the Pd sponge had to be regenerated. The passage through the recombiner and the Pd sponge greatly reduced the deuterium content in the gas reaching the collecting vessel.[6]

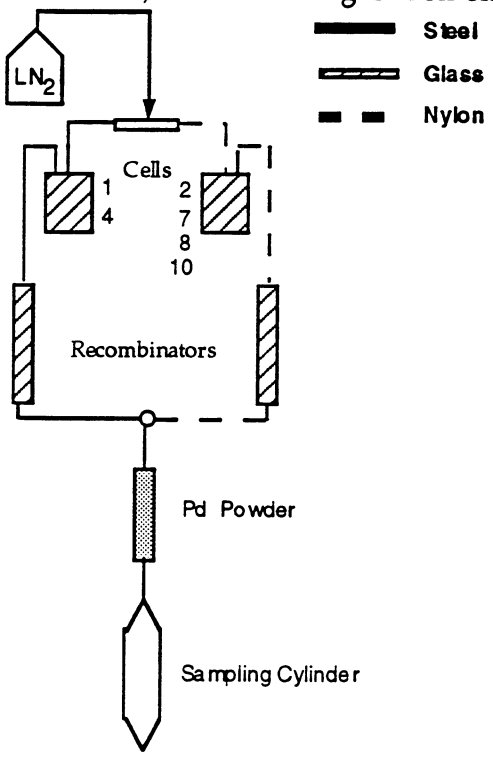

Figure 2 Scheme of the collecting lines and their type of materials

Pyrex glass was used for the cells and the recombiners. Nylon 66 (cell lines #2,7, 8 and 10) or SS (cell lines #1 and 4) tubes were adopted; indeed for both materials a relatively low ^4He background was measured. Connections in the lines were done by Swagelock fittings and where this was not possible, as in the case of SS-Pyrex joints, by soldering SS tube and Pyrex by epoxy resin adhesives (of the type used in high vacuum technology). The SS vessels were, for three times in sequence, evacuated with a fore vacuum pump and filled with boil off nitrogen before connecting it to the collecting line.

For this experiment the Knudsen molecular source assembly has been removed and replaced with an inlet line assembled with conventional small flange KF25 fittings. The inlet line, depicted in fig. 3, was connected to the mass spectrometer ion source

through a Balzers UDV035 dosing valve and a short quartz tubing ending immediately before the first plates of the ion source itself.

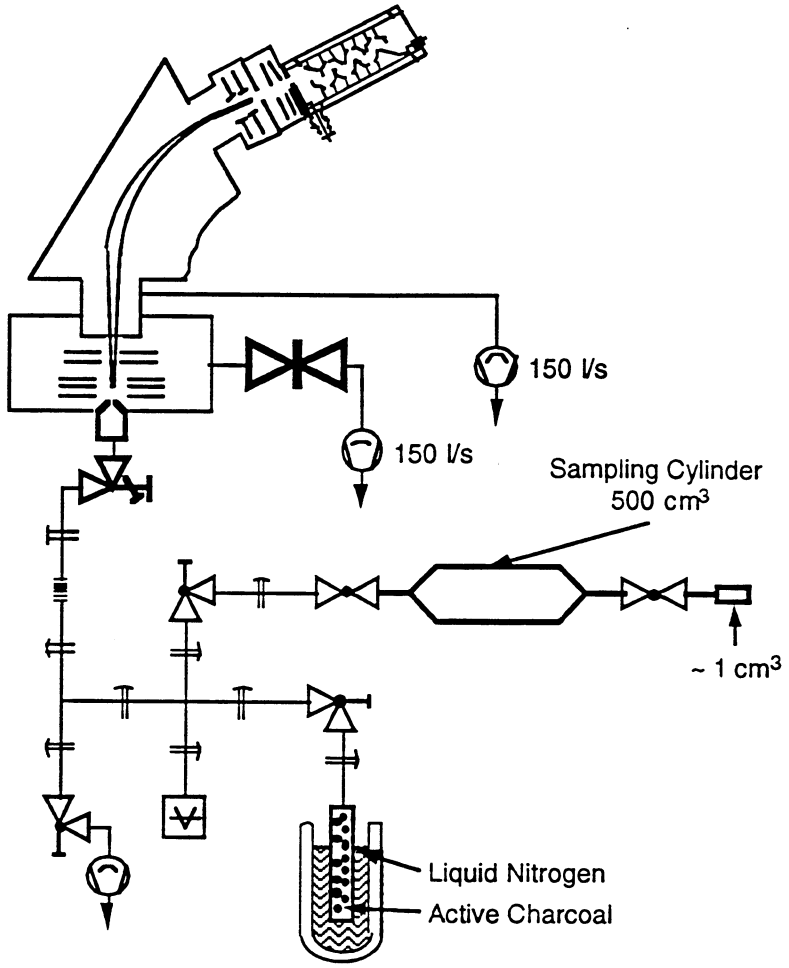

Figure 3 Scheme of the inlet line used.

Helium Measurements

The procedure followed in the measurements is best described with reference to the same fig. 3. The sampling cylinder is brought to the spectrometer and connected to the inlet line which can be evacuated with an auxiliary diffusion pump. After shutting off the pumping the sample is allowed to expand into the line where the nitrogen, in some minutes, is adsorbed by the active charcoal, maintained at liquid nitrogen temperature, down to a pressure of the order of 10^{-2} torr. It is to be said that this *passing* on the active charcoal is not addressed to eliminate the deuterium in the sample both because, as described in the companion paper[6], the sample itself has

been already purified by recombining the electrolysis gases and by passing it through the Palladium sponge and because the mass spectrometer, to a certain extent and as already shown, can detect helium in the presence of fairly large amount of deuterium. What it is looked for, here, is to get rid of the nitrogen in order to be able to open as much as possible the dosing valve and admit the sample to the spectrometer without the nitrogen itself which, otherwise, would make the pressure in the ion source either to raise too much or to severely deteriorate noise and resolution power, and , hence, sensitivity. Therefore this "nitrogen purified" sample is admitted to the mass spectrometer ion source whose pumping has been shut off with the gate valve shown in fig. 3 shortly before the opening of the dosing valve. Due to the differential pumping of the mass spectrometer and the low conductance between the ion source and the analyser section the partial pressure of helium, or of any other admitted gas, will raise on opening the dosing valve and subsequently fall, as a consequence of the pumping through the connection to the analyser, with a kinetics mainly dependent on the mass of the gas itself. This raise and fall of the partial pressure of helium in the ion source is depicted by the plots of the resulting He^+ ion signal shown in fig. 4.

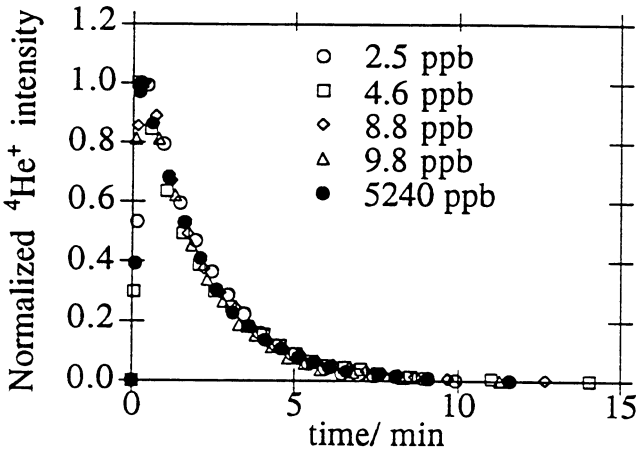

Figure 4 Examples of the $^4He^+$ ion intensity time dependence with various amounts of air admitted (from 500 cm^3 to 0.24 cm^3)

What is important to notice here is that for a quite large variation of the helium content in the sample admitted the kinetics does not show any variation; the normalised time dependence is superimposable so that one can either take the integral of the signal or the maximum value in order to measure the helium content. Both ways were used in preliminary experiments with differences in the range of 2-3 %.

An example of a typical measure recording is shown in fig. 5. Time flows upward in the vertical direction while ion intensity increases to the right. At the beginning of the recording the mass spectrometer is focused on the ^{4}He mass and no scanning is operative. During the very same initial part of the recording, while following the raise and falling down of the helium signal already referred to, the background and the deuterium ion intensity can also be measured. Indeed the focusing conditions are changed, varying the accelerating voltage by discrete amounts, in order to, first, measure the ion intensity in the valley between helium and deuterium, then, move on top of the deuterium peak, and finally, back to the valley and to the helium peak. Actually a discontinuous voltage scan is being made in such a way

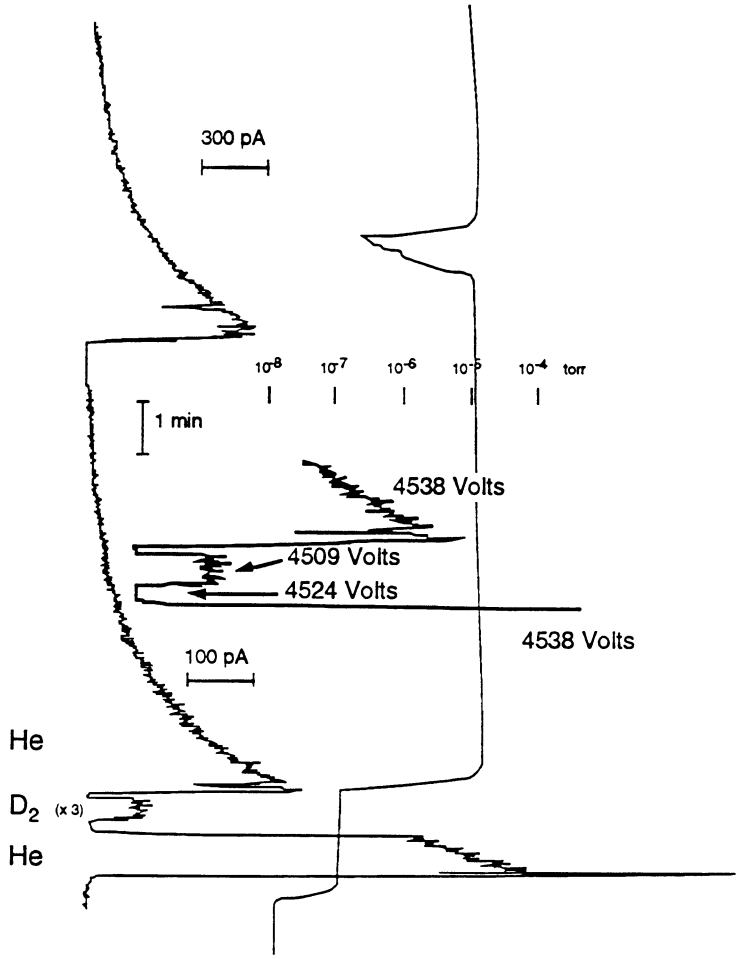

Figure 5 Typical measurement of helium. The trace on the right, shifted in space and not in time, represents the recording of the ion source pressure. The first rise of pressure shown is due to the shutting of the pumping while the admission of the sample causes the second. The enlarged portion shows how performing a discrete voltage scan is possible to check the background between helium and deuterium (at 4524 Volts) and measure the deuterium (at 4509 Volts).

that in addition to check the background for the measure of helium a control of the assignment to the helium mass is performed. Indeed, if for any reason the deuterium ion intensity was being mistakenly recorded as a function of time no signal would have been found at the higher mass focalising conditions realised. The final portion of the recording of fig. 5 is best understood by referring once more to the fig. 3. At the end of the sampling cylinder there is a short portion of tubing used to connect it with the collecting lines. After having removed the cylinder from the line, about 1 cm^3 of air can be trapped in this section by plugging the tubing. When this cubic centimetre of air is allowed to enter into the line and, subsequently, into the mass spectrometer it gives raise to the helium signal shown in fig. 5. By knowing the volume of air admitted and by assuming its content in helium equal the tabulated one (5.24 ppm) the helium content of the sample can be derived. This can be done either deriving a conversion factor between the ion intensity measured and helium admitted or by direct comparison of the peaks maximum intensities or areas. Actually this *in situ* calibration was only used to regularly check the procedure or to control immediately those particular measurements that appeared to be unusual or of any specific interest. On the contrary, in order to have a more conservative estimate of the overall error, the conversion factor to be used in the measurements was derived by performing a number of specific calibrations all through the experiment. The results of various measurements, made with fairly different quantity of helium ranging from ppm to fraction of ppb, are displayed in fig. 6 where it can be seen the absence of time dependence. The

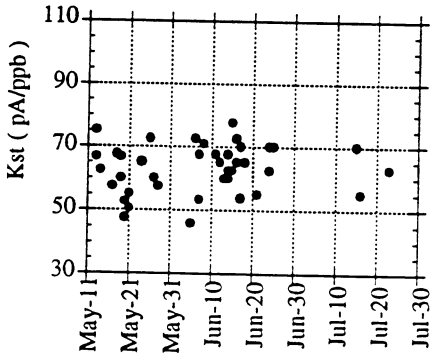

Figure 6 Sensitivity factors for the measurement of helium determined during the experiment.

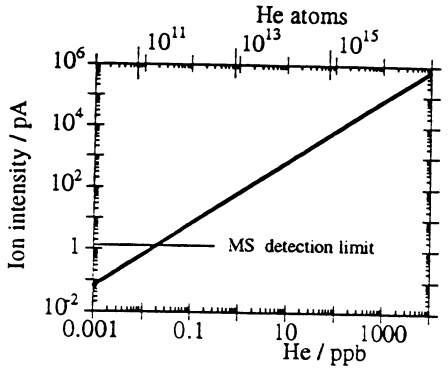

Figure 7 Detection limits attained.

dispersion of the values shown in the plot has been taken as our error in the measurement. This conversion factor, which is the sensitivity (63± 8 pA/ppb) of the method, was found to be fairly linear in the explored range; indeed the average value of this factor evaluated with the sampling cylinder full of air (5.24 ppm) was 56 while with ≈1 cm^3 of air in Nitrogen (10.4 ppb) it was 64.

In fig. 7 is shown the overall detection limit which can be attained with the aforementioned sensitivity. The detection limit shown ($\approx 3x10^{11}$ atoms or $1x10^{-8}$ cm^3 stp or 0.02 ppb in the sampling volume of $500cm^3$) is to be considered an extrapolated one because the handling of air samples smaller than 50 µl ($6x10^{12}$ atoms) was not attempted. The semi-dynamic procedure here used does prevent to reach the lower limits reported by using specialised mass spectrometers operated in fully static vacuum conditions ($\approx 10^8$ atoms) nevertheless, while allowing to comfortably measure the expected ^4He amounts, is much less prone to memory problems.

Always as far as the procedure used is concerned, it must be recalled that at the levels of helium concentration mentioned, one has to be careful in order to avoid any contamination in the handling of the samples. The connection of our sampling cylinders to the lines was a possible source of contamination; indeed between the exit of the line and the valve of the vessel, by making the connection, a small amount of air (less than 1 cm^3) was going to be trapped. While this air could have been removed with a vacuum pump, much care was made in avoiding to have under vacuum any part of the experimental assembly beside those, like the inlet line to the mass spectrometer, which could have been easily checked for leaks with the mass spectrometer itself. Therefore one had to wait enough time, after the connection, in order that the stream of gas coming from the collecting lines would have swept away any gas quantity not fully representative of the cell gas composition. On that point a rather conservative attitude had been taken measuring the helium content of a vessel full of air as a function of the time elapsed after the connection to the carrier gas line. In fig. 8 is reported the final portion of the resulting depletion curve. On the basis of these results at least 2 hours (almost always 3 hours), or overnight periods, were allowed to elapse before the collection was considered to be completed. By operating in such a manner any other possible mutual-contamination between the lines should have also been avoided.

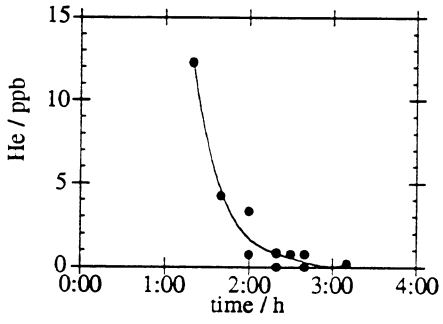

Figure 8 Depletion of the helium content of a sampling vessel, intially full of air, as a function of the time of fluxing with boil off nitrogen.

The background measured for the sole inlet line, by following closely the same procedure used with the samples, was routinely checked and it was always found to be barely measurable.

Helium Results

In fig. 9, as an example, we report the result obtained all over the experiment for the cell # 10. While significant amounts of helium were detected above background it

appears that the larger values were obtained at the end of the experiment. On the other hand, for reasons connected to the neutrons detection, it has been necessary to operate mechanically on the assembly shortly after 900 hours. However carefully it has been done, nevertheless it was the first time the assembly has been even touched. As a matter of fact, up to that point, we were very strict on not inducing any mechanical stress to the apparatus for fear to modify the sealing properties of the various connections. Indeed we were aware from preliminary measurements that the lines used to collect the sample were not perfectly

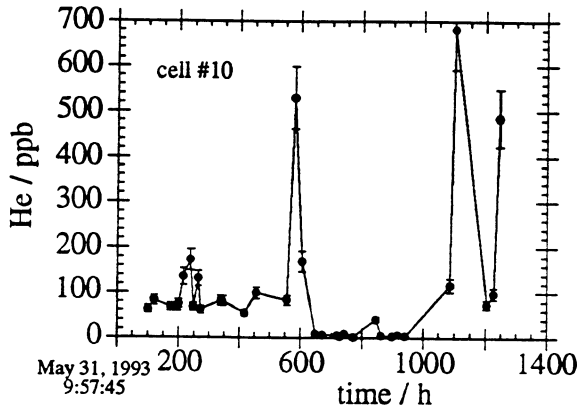

Figure 9 **Helium concentrations measured for cell #10.**

tight. The concentration of helium measured in the sample cylinder, in absence of any electrolysis, was typically of the order of some ppb while, in our experience, the boil off nitrogen, if taken directly from the liquid phase, did show, as a rule, helium concentrations at the level of our detection limit and, always, lower than some tenths of ppb. On the other hand this background, greater than that provided by the carrier gas itself, happened to be of the same order of magnitude irrespective of the collecting line used either those made of stainless steel or those of nylon. Therefore the observed background at the ppb level had to be attributed to the connections between the various portions of the lines. Hence the care which was exercised in not moving any part of the experimental assembly. When, on the contrary, such a manipulation had to be done we looked for any hint of its influence. Indeed on inspecting the values for the reference cell and line shown in fig. 10 a smoothing function fitted to the data indicates an increase of the helium detected after 900 hours. This can be taken as a confirmation of the hypothesis of an influence of the mechanical manipulation. Therefore, also if this evidence pertains to a "parallel" blank we preferred to take a conservative attitude and discard all the helium data taken during the final part of the experiment.

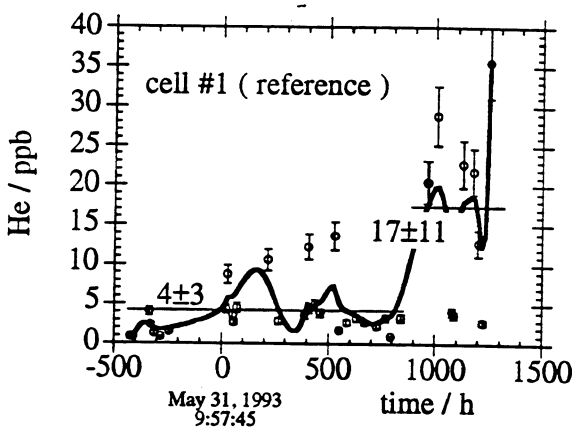

Figure 10 ^{4}He concentrations found for the reference cell #1.

In fig. 11 and 12 the results obtained for the cells 2,7 and 8 and for the cells 4 and 10 respectively are reported as a function of time, up to the mentioned limit of 900 hours, together with the reference cell (#1) measurements.

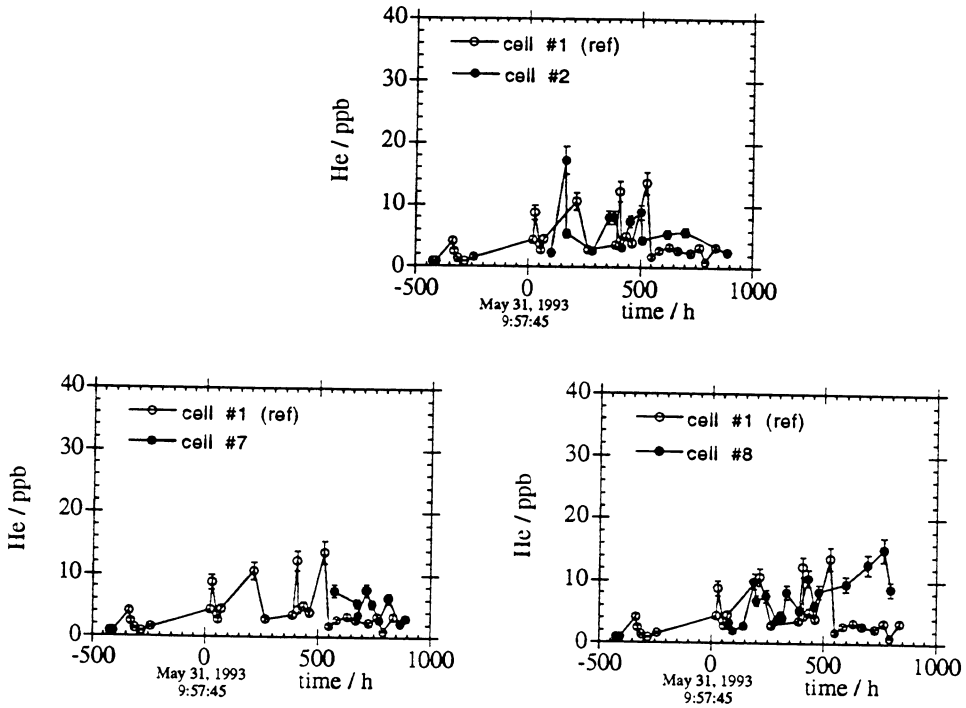

Figure 11 ^{4}He concentrations found for cell #2, #7 and #8 each compared with those of the reference cell#1.

As for cells #2, 7 and 8, if compared with the cell #1 measurements, it appears from fig. 11, that, from the point of view of the sole helium measurements, none of these cells did exhibit amounts large enough to be considered significant with confidence.

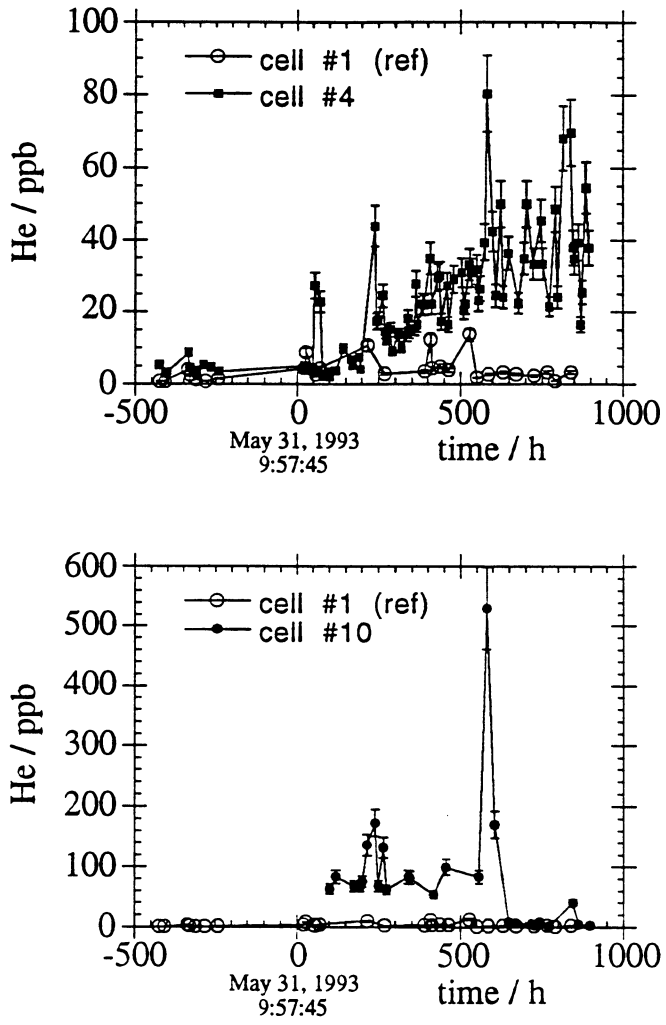

Figure 12 **^{4}He concentrations for cell #4 and #10 each compared with those of the reference cell #1.**

On the contrary, as it is apparent from the data in fig. 12 , significant amounts of helium were detected for the cells #4 and # 10. It can also be noted the very different concentrations ranges used in the two plots. In the case of cell #4 it can be seen the progressive build up of the helium detected with respect to both the background measured for roughly 250 hours before the beginning of the electrolysis and the blank provided by the reference cell #1.

As for cell #10, whose results are shown in the same fig. 12 and for which no comparable background is available before the beginning of the electrolysis, the

much larger values observed and the sudden decrease observed at ≈600 hours did pose the question of the possible occurrence of the spontaneous closing of a leak in the line. Indeed the roughly constant value of ≈70 ppb observed until 600 hours of the experiment and on which two large spikes were recorded was attributed to a large background of that particular collecting line. On the other hand the impressive drop, down to the usual background of a few ppb, which occurred at ≈600 hours could be seen as due to the closure of the leak affecting the line or, deeming not probable this spontaneous modification, could signal that an helium release in the interior came to the end. As a consequence, while up to that point of the experiment we were basically looking for an increase of the amount of ^4He found with respect to the "normal" value, whatever it was, of that particular cell and collecting line without taking into account the spontaneous opening or closure of leaks, then after ≈600 hours we were led to devise a way in order to confirm or prove wrong the hypothesis of the occurrence of air leakage in our lines.

Neon Measurements

Therefore it has been initiated the measurement of the neon content of our samples being neon the only possible marker of an air contamination which was not going to be condensed at liquid nitrogen temperature during the inlet procedure.

As shown in fig. 13 Neon can be measured mass spectrometrically by

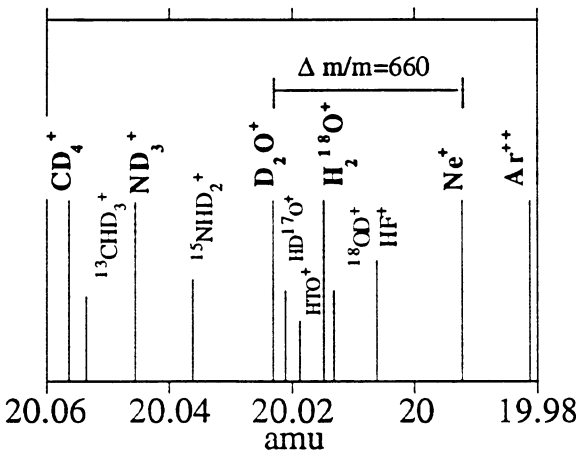

Figure 13 **Possible ions of nominal mass 20.**

discriminating its contribution to mass 20 from the other possible ones. The mass resolving power employed allowed a partial resolution from the higher masses. The doubly ionised Argon peak, which could not have been mass resolved, was avoided by lowering the operating value of the ionising electron energy, at 40 eV, below the onset of this process.

However, as the helium signal lasts only some minutes as shown in fig. 4, it remained to be proved the possibility to perform a nearly simultaneous measurement of both helium and neon. To this end the same type of calibrations which were made by taking advantage of the air helium content were now performed with the neon content of the air. An example of the results is shown in fig. 14. Once more, in spite of the fairly large range of the amounts introduced, the kinetics behaviours monitored were superimposable. On the other hand, as expected from the different mass, the neon lasts in the ion source much more than helium thus allowing to measure, first, the maximum peak value of the helium and, subsequently, the neon ion intensity when it is still sufficiently close to its maximum value to allow a satisfactory back extrapolation. The sensitivity, *id est* the conversion factor between the ion intensity measured and the amount of neon introduced, resulted to be 24 pA/ppb.The procedure followed is best seen in fig. 15 where examples of actual measurements are reported. In these figures, as for the fig. 4, time flows in the vertical direction while ion intensity increases to the right. At the very beginning

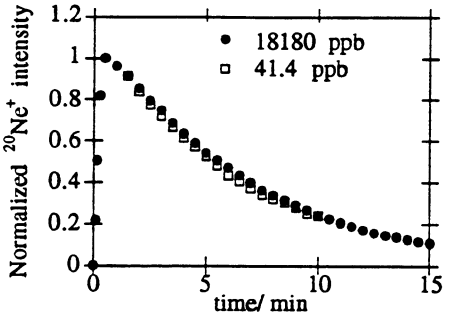

Figure 14 **Examples of the $^{20}Ne^+$ ion intensity time dependence with various amounts of air admitted (from 500 cm^3 to 1.14 cm^3)**

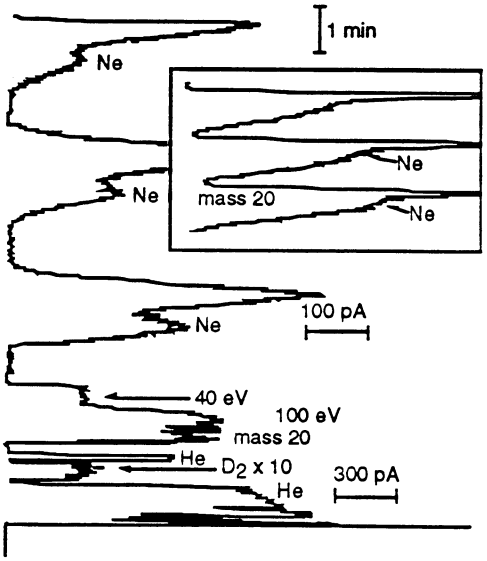

Figure 15 **Example of nearly simultaneous helium and neon measurement. The insert shows a different and rather extreme case where a larger superimposition of masses is apparent.**

the helium ion intensity is being followed up to the peak value while its decrease is recorded only for the time necessary to make the voltage scanning up to the

deuterium peak and allow, when necessary, a back extrapolation to zero time. The nominal mass 20 is, then, quickly focused-and the ionising electron energy is lowered. Subsequently some very low speed magnetic scans across mass 20 are performed. Making use of the known time dependence of the neon inside the ion source (see fig. 14) it is possible to back trace the $^{20}Ne^{+}$ intensity to its initial value. The actual degree of resolution attained, which did depend mainly on the relative amounts of neon and water, both normal and substituted, is shown in fig. 15 and in the insert of the same figure; the latter providing an extreme example of superimposition of peaks. The occurrence of this superimposition led us to assign an estimated uncertainty on the neon content measurements twice that of the helium determinations. In any case , whenever possible, the assignment of the mass 20 peak to neon was checked with an appearance potential determination, always found to be consistent with the tabulated value of neon (21.6 eV), and the isotopic abundance distribution of isotopes 20 and 22 (being the 21 isotope almost always too low in intensity).

Neon Results

Recalling that after 600 hours the only cell with significant amounts of helium was the cell #4, in fig. 16 is reported the ratio He/Ne for this cell

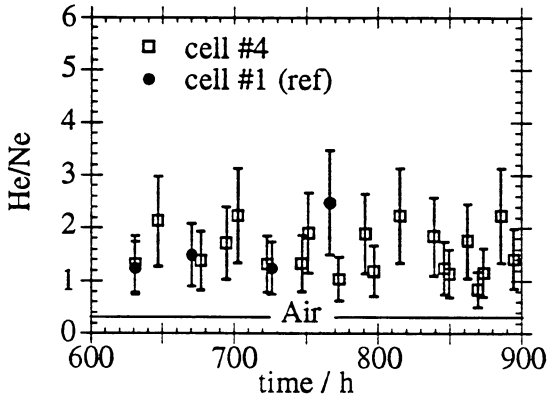

Figure 16 **Helium to neon ratios measured as a function of time for cell #4 and #1.**

together with that measured for the reference cell #1. In spite of being definitely greater than the ratio value found in air, nevertheless cell #4 values are almost superimposable on those of cell #1. Therefore some type of fractionating mechanism had to be at work with a preferential inflow of helium with respect to neon irrespectively of the different flow amount. A simple Knudsen mechanism of preferential inflow of helium with respect to neon, which would lead to a He/Ne ratio, adjusted for the pressure gradient, $[M(^{20}Ne)/M(^{4}He)]^{1/2}\ [\Delta P(^{4}He)/\Delta P(^{20}Ne)] \approx 0.64$, is neither consistent nor fully unconsistent with the data.

However what it must be pointed out is that the situation depicted cannot be ascribed to the materials used: lines #1 and #4 were identical while helium detected was found to be 8 times different; values of helium recorded for cell #10 were up to 50 times larger than those of cell 2,7 and 8 in spite of being identical. If present what we were observing could not be attributed to a permeation through the material of cells or lines but to some sort of leakage in the connections. This conclusion is also supported by the very same sharp variations with time that have been observed.

Moreover the value, constant with time, found for the He/Ne ratio indicates a correlation between the helium and neon concentrations which is much more clear in fig. 17 where the helium detected in all the cells is plotted against the neon observed. Here it is quite apparent that when helium increases neon also increases. A similar behaviour, even if less definite, is found also in the lower range of concentrations shown in the same fig. 17. The correlation shown between helium and neon, different

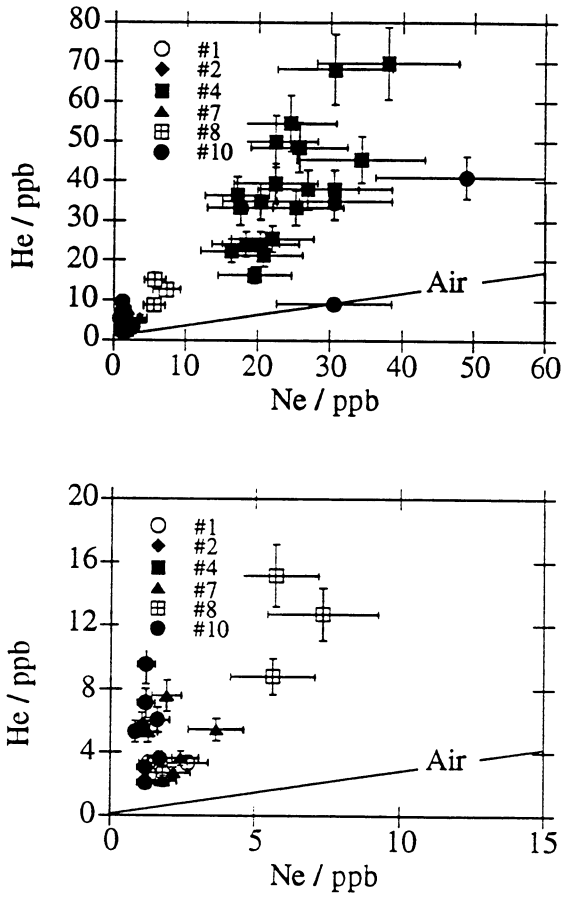

Figure 17 **Helium versus neon detected for all the cells (for readability purposes the data in the low range of concentrations are repeated in the lower graph).**

from what expected for the air, could be interpreted with a combination of mechanisms of leakage or, possibly, with a combination of helium inflow from outside and release in the interior. Indeed some support to this hypothesis does come from fig. 18. Here an increase of the ratio He/Ne with respect of the amount of helium detected can be hypothesised. Unless one invokes an helium inflow mechanism assisted by the helium itself it seems that the simplest explanation of this seemingly increasing trend is a superimposition of two processes: a leakage and a release in the interior.

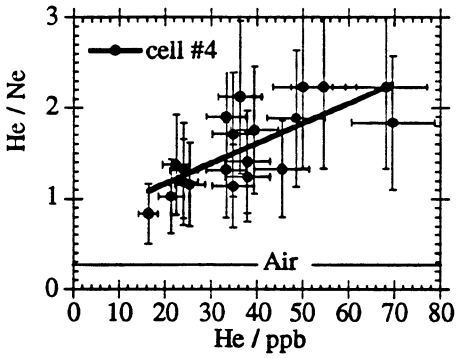

Figure 18 He/Ne versus helium concentrations for cell #4; the time interval is the same of fig. 16.

Discussion

In this discussion we are looking at the sole helium data here presented intentionally avoiding to take into account the concurrently obtained heat power excess results[6]. With the aim of obtaining an independent assessment of the reliability of our present experimental results, we are, in a sense, assuming the attitude of a laboratory providing the helium analysis without a knowledge of the source of the samples.

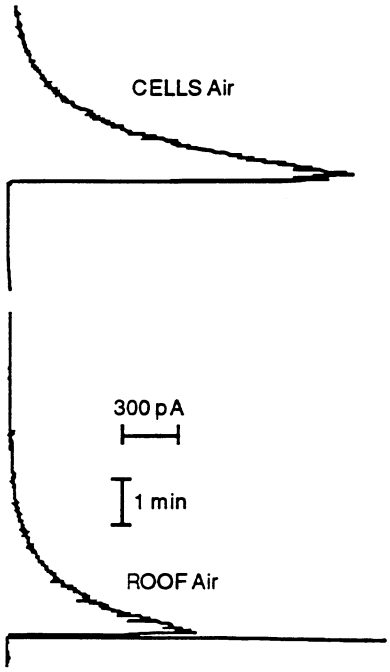

Figure 19 Example of the determinations of the helium concentrations in the air collected in the cells room and on the roof of the building

In the hypothesis of the occurrence of a leakage as the source of the helium found in cells #4 and 10 one should expect that an increase of the helium content in the air surrounding the cells would cause an increase of the helium found in the collected sample. Indeed, since the beginning of the experiment, due to the presence in our department of various possible sources of helium like the NMR machines, the helium content in the air of cells and the mass spectrometer rooms has been, from time to time, checked. The helium content of the air collected, in open air, on the roof of the department building has been used as the reference. These checks were performed in a way entirely similar to that used for the sample the only difference being the much smaller collecting volume employed. An examples of such controls is shown in fig. 19. Simply by comparing the two areas shown and assuming the roof air at the tabulated level the ppm concentration of the air in the cells room could be derived. Indeed quite

large variations in the helium content of the cells room, up to about 4 times the normal one, has been observed. Nevertheless, contrarily to what expected and as shown in fig. 20 , no correlation is apparent, on a reasonable time scale, between the most prominent spike of helium detected in cell 10 and the helium content of the air surrounding the cells.

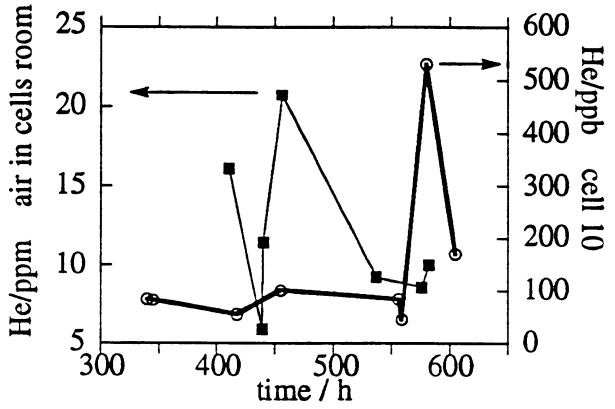

Figure 20 **Concentrations of helium found in the air surrounding the cells and in the cell #10. The lines connecting the measured values are only drawn as an help to the eye.**

With respect to the helium content of the air surrounding the apparatus it can be of interest to other people working in the field the behaviour of the helium concentration in the mass spectrometer room, shown in fig. 21, that happened to be measured in a special occasion. No extraneous potential source on that particular day could be identified. This clearly shows the care one should exercise in these measurements.

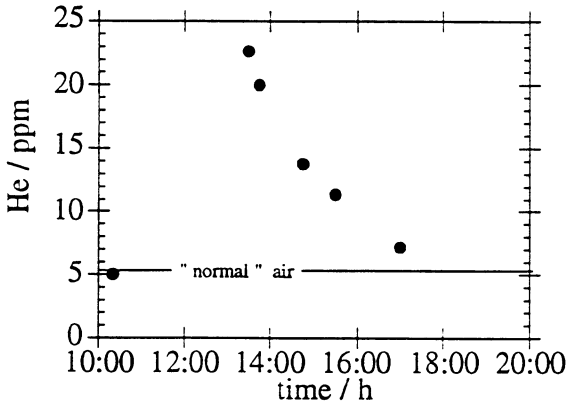

Figure 21 **Time dependence of the helium concentration in the air of the mass spectrometer room measured on June 15,1993.**

It should also be mentioned that, during the experiment, many quite large variations in the composition of the gaseous mixture of the cells were caused by either the electrolysis variations or the occasional shutting off of the recombiners. A complete independence, on this compositional variations, of the helium concentrations measured in the collected samples was observed. Whatever be the helium inflow mechanism, this behaviour seems to be quite unexpected.

In the hypothesis of a genuine release of helium in the interior a drop of the helium detected to background levels after the end of the electrolysis is to be expected. The manipulation performed on the assembly at 900 hours is believed to have caused the failure to observe this clear decrease. If no significance is given to such manipulation, whose influence on the sealing properties of all the lines, and not only the line pertaining to the reference cell #1, is not proved, the failure to observe such a clear drop points towards the occurrence of air contamination.

Spontaneous changes in the sealing properties, on *a priori* basis, seem to be highly unprobable. However if they are believed to have occurred, the evidences of air contamination, provided by the neon data, which have been observed after 600 hours and on cell #4, from a logical point of view, if do suggest this possibility for other cells, do not prove it for the most relevant helium measurements done which pertains to a different cell and different period (cell#10 at $t < 600$ h).

Finally it should be pointed out that the parallel blank of the reference cell #1 did exhibit a fairly low background all through the experiment without any spurious spike.

As a conclusion it can be observed that the overall picture which emerges doesn't seem to fit an unique interpretation which may fully satisfactorily account for all the experimental data. However the various arguments presented must be balanced. It seems clear that the stronger evidence observed was the He vs Ne correlation. This does favour the occurrence of an unexplained air contamination also if an hint, provided by the He/Ne increase with He, suggests the concurrence of both air contamination and helium release.

Acknowlegments
The financial supports of the National Research Council (CNR), the National Institute of Nuclear Physics (INFN) and the Physics Laboratory of the Istituto Superiore di Sanità are gratefully acknowledged.

References

1. D. Gozzi, P.L. Cignini, L. Petrucci, M. Tomellini, G. De Maria, S. Frullani, F.. Garibaldi, F. Ghio and M. Jodice, Nuovo Cimento, 103A (1990) 143-154

2. D. Gozzi, P.L. Cignini, L. Petrucci, M. Tomellini, G. De Maria, S. Frullani, F. Garibaldi, F. Ghio, M. Jodice and E. Tabet, J. Fusion Energy, 9 (1990) 241-247

3. D. Gozzi, P.L. Cignini, M. Tomellini, S. Frullani, F. Garibaldi, F. Ghio, M. Jodice and G. M. Urciuoli, Fusion Technol., 21 (1992) 60

4. D. Gozzi, P.L. Cignini, M. Tomellini, S. Frullani, F. Garibaldi, F. Ghio, M. Jodice and G. M. Urciuoli in: The Science of Cold Fusion: Proc. Second Annual Conf. on Cold Fusion, ACCF2, Como, Italy, 29 June - 4 July 1991, Eds. T. Bressani, E. Del Giudice and G. Preparata, vol.33 of the Conf. Proc. of the Italian Physical Society , (Bologna, 1991), p. 21

5. D. Gozzi, P.L. Cignini, R. Caputo, M. Tomellini, G. Balducci, G. Gigli, E. Cisbani, S. Frullani, F. Garibaldi, M. Jodice and G. M. Urciuoli in: Frontiers of Cold Fusion, Ed. H. Ikegami, Frontiers Science Series no.4, (Universal Academy Press Inc., Tokyo 1993), 155

6. D. Gozzi, R. Caputo,P.L. Cignini, M. Tomellini, G. Gigli, G. Balducci, E. Cisbani, S. Frullani, F. Garibaldi, M. Jodice and G. M. Urciuoli. " Excess heat and nuclear products measurements in cold fusion electrochemical cells " companion paper in this book

7. M.H. Miles and B.F. Bush in this book.

8. M.H. Miles, R.A. Hollins, B.F. Bush, J.J. Lagowski and R.E. Miles. " correlation of excess power and helium production during D20 and H2O electrolysis using palladium cathodes." J. Electroanal. Chem. Vol. 346 , p 99 (1993).

9. M.H. Miles and B.F. Bush, " Search for anomalous effects involving excess power and helium during D2O electrolysis using palladium cathodes", ICCF3, 3rd International Conference on Cold Fusion, Nagoya, October 21-25, 1992, Proc. in Frontiers of Cold Fusion, Edited by H. Ikegami, Frontiers Science Series no.4, Universal Academy Press Inc., Tokyo (1993), p.179

10. M.H. Miles, B.F. Bush, G.S. Ostrom and J.J. Lagowski, " Heat and helium production in cold fusion experiments" in: The Science of Cold Fusion: Proc. Second Annual Conf. on Cold Fusion, ACCF2, Como, Italy, 29 June - 4 July 1991, Eds. T. Bressani, E. Del Giudice and G. Preparata, vol.33 of the Conf. Proc. of the Italian Physical Society , (Bologna, 1991), p. 453

11. B.F. Bush, J.J. Lagowski, M.H. Miles and G.S. Ostrom. " Helium production during the electrolysis of D_2O in cold fusion experiments" J.Electroanal. Chem. Vol. 304, p. 271(1991)

LA-UR 94-

Los Alamos National Laboratory is operated by the University of California for the United States Department of Energy under contract W-7405-ENG-36.

TITLE: TRITIUM EVOLUTION FROM VARIOUS MORPHOLOGIES OF PALLADIUM

AUTHOR(S): D. G. Tuggle, T. N. Claytor, and S. F. Taylor

SUBMITTED TO: Fourth International Conference on Cold Fusion
Maui, Hawaii
December 6 to December 9, 1993
(Paper)
To be published in Fusion Technology

Los Alamos Los Alamos National Laboratory
Los Alamos, New Mexico 87545

FORM NO. 836 R4
ST. NO. 2629 5/81

TRITIUM EVOLUTION FROM VARIOUS MORPHOLOGIES OF PALLADIUM

D. G. Tuggle, T. N. Claytor and S. F. Taylor*

Los Alamos National Laboratory
Los Alamos, NM 87545
***Affiliated with Brigham Young University**

ABSTRACT

We have been able to extend our tritium production techniques to various novel morphologies of palladium. These include small solid wires of various diameters and a type of pressed powder wire and a plasma cell. In the most successful experiments, the amount of palladium required, for an equivalent tritium output, has been reduced by a factor of 100 over our older powder methods. In addition, we have observed rates of tritium production (>5 nCi/h) that far exceed most of our previous results. Unfortunately, the methods that we currently use to obtain the tritium are poorly understood and consequently there are numerous variables that need to be investigated before the new methods are as reliable and repeatable as our previous techniques. For instance, it seems that surface and/or bulk impurities play a major role in the successful generation of any tritium. In those samples with total impurity concentrations of >400 ppm essentially no tritium has been generated by our gas loading and electrical simulation methods.

1. INTRODUCTION

The anomalous appearance of small amounts of tritium has been repeatedly observed in electrolytic and solid state gas loading experiments[1-4]. Some of these results were obtained with gas loaded discharge tubes operated at 25 kV, some with voltages as low as 50 V in electrolytic cells, and some with only cyclic hydriding and dehydriding of metal. The only readily common features in all the experiments are the presence of palladium (or other hydrided metal), deuterium and a disequilibrium condition for the deuterium. We will report on our tritium generation results from various morphologies of palladium subjected to periodic unipolar current pulses. These morphologies include wire, powder wire, and two types of plasma cells. The primary advantages of these experiments are that they are moderately reproducible, they produce readily detectable tritium levels in a few hours or days, and offer the possibility that they could be much more efficient.

In our previous work[1], all tritium data was obtained from 20 g batches of oxidized palladium powder. In these experiments the amount of palladium involved is up to 40 times less and the water vapor problem is eliminated. All of the tritium data was obtained with on-line tritium gas monitors. One experiment was done in the batch mode because it was placed in a neutron counter in an underground laboratory.

Some have criticized the detection of tritium because the signals seem to be insignificant, tritium is ubiquitous, neutrons are not detected commensurate with the tritium generation rate, and the palladium metal is subject to possible tritium contamination. We will briefly discuss the possible avenues for contamination and show that each is negligible, or not a factor, in the experiments described. The magnitude of the signals discussed in this paper are multi-sigma and

are often over a hundred times the tritium background in the supply gas. Furthermore, tritium may be the most sensitive and rapid indicator of anomalous nuclear behavior in deuterided metals. As such, it is well suited for rapid parametric investigations. The lack of a detectable neutron signal[5] is distressing, but only if one assumes that the mechanism for tritium production produces energetic tritions (energies >25 keV).

2. MATERIALS

The detailed analysis of our materials (Pd, Si, H_2, D_2) has been described previously[1]. For this work we used, exclusively Cryogenic Rare Gases deuterium 99.995% that has 90 pCi/l of tritium. The major impurity in the deuterium is H_2 (0.005%) (He <1ppm). A total of 168.8 g of palladium powder was used in our recent experiments described in this paper. This powder has been checked for tritium contamination by three independent methods. Of that amount, 39.4 g was used in various hydrogen control experiments. A total of 20.11 g of palladium foil and wire (>99.99%) from Johnson and Matthey and Goodfellow was used in the wire and plasma cells; 1.63 g of this amount was checked for tritium contamination by heating.

All of the palladium has been subjected to rigorous metallographic and impurity analysis. Major impurities in the Engelhard palladium are oxygen (980 ppm) Chlorine (80 ppm), Nitrogen (65 ppm) and Carbon (47 ppm). All other major impurities are (each) under 35 ppm by weight. The impurity levels for the wires (Johnson Matthey Puratronic) varied from the specification sheet and were in the 150 ppm range (all metals) rather than the quoted values of 5-10 ppm. The Goodfellow wire was analyzed at 66 ppm rather than the <10 ppm listed in the analysis sheet supplied by the vendor. Repeated analysis of the same batch of wire gave up to a 50% variation in total impurity concentration. This is either intrabatch variation or, more likely, random analysis error.

The 220 micron thick foils were always annealed at 850 °C for 2 hours at 10^{-6} torr before use. These foils have been hydrided, run in cells, dehydrided and annealed seven times and show neither a monotonic decrease nor increase in tritium production. The palladium powder was virgin powder and had been oxidized in air at 350 °C for 2 hours. Wire from five batches (lots W13918, W06528, Z0114, NM 35680, GF5140) was obtained from Johnson Matthey and Goodfellow Metals. Only one of these batches (W 13918) showed large (16 to 298 nCi/g) amounts of tritium.

Tritium contamination in the palladium powder was tested by three independent methods: dissolution and scintillation counting, hydriding and dehydriding and measurement[6] of ^3He. By these means we can assign an upper limit on tritium contamination of 0.005 nCi/g (i.e., no tritium detected within experimental error). The Goodfellow wire was tested for contamination (with null results) by analyzing a sequential 0.1 g of wire taken between wire samples shown to produce tritium in the experiments. Also, in an extensive independent[7] investigation of palladium wire, several hundred samples were tested with no contamination present. The purity of the wire used in these experiments also weighs heavily against intrinsic spot contamination.

A total of 29 wire experiments were performed, six of these were powder wire. Separately, a total of four plasma experiments will be discussed. In addition, ten powder layered experiment (eight D_2 and two H_2) were also performed with nominal results, consistent with our previously reported results. However, because the results were obtained in a recently built tritium analysis system with a lower intrinsic background and no prior history of tritium contamination we consider these to be a positive confirmation of our previous results.

3. APPARATUS

Shown in Figure 1 is the stainless steel gas analysis loop containing a three liter ion gauge and a 310.9 cc calibration volume. The three pressure gauges (0.2%), ion gauge and sample and room temperatures (0.1 °C) are recorded on a computer log at 60 s intervals. In operation, a solid state or plasma cell would be attached to the loop and hydrided in situ with deuterium or hydrogen or a mixture of gas. The pressure drop during hydriding or the resistivity of the wire was used as indicators of the stochiometry of the PdD_x. The environmental chamber also enables us to heat (500 K) and cool (200 K) the sample allowing various levels of stochiometry.

The Femtotech ion gauge rejects pulse type radioactive events that effectively discriminate against radon and cosmic ray ionization. Prior to this study, the Femtotech background (system 1) was usually between 1.8 and 2.2 nCi/l (due to particulate and tritium exposure of previous cold fusion cells) and had a relatively low drift rate, initially (0.006 nCi/l-hr). After exposure to the cells described in this paper, the drift rate was considerably higher (often up to 0.1nCi/l-hr) and was difficult to return to the baseline rate. Partway through the study a second system was built with a new Femtotech. The background with this new system (system 2) is near zero ± 0.2 (at 600 torr) and it has a negligible drift rate (<0.001 nC/l-hr).

The new loop is improved over our original loop because the Femtotech is heated at a constant temperature, there is an integral cold trap, and there is valving to allow the pressurization of the cell independent of the loop. Two 2 micron filters are installed at the inlet of the ion gauge and at the outlet of the cell to eliminate spurious responses due to particulates. A pressure gauge at the Femtotech also directly measures the ionization gauge pressure even with flow in the loop.

A hydrogen oxidation system was built to act as a backup test for tritium using a scintillation counter (Packard 9600). Calibration D_2 gas with 25 nCi/l of tritium was used to test the two Femtotechs and the oxidation system. The two ionization systems agree to within 5% of each other while the scintillation results were about 30% lower than the Femtotechs. Not enough runs have been completed with the oxidation system to optimize the tritium collection as a function of gas flow at this time.

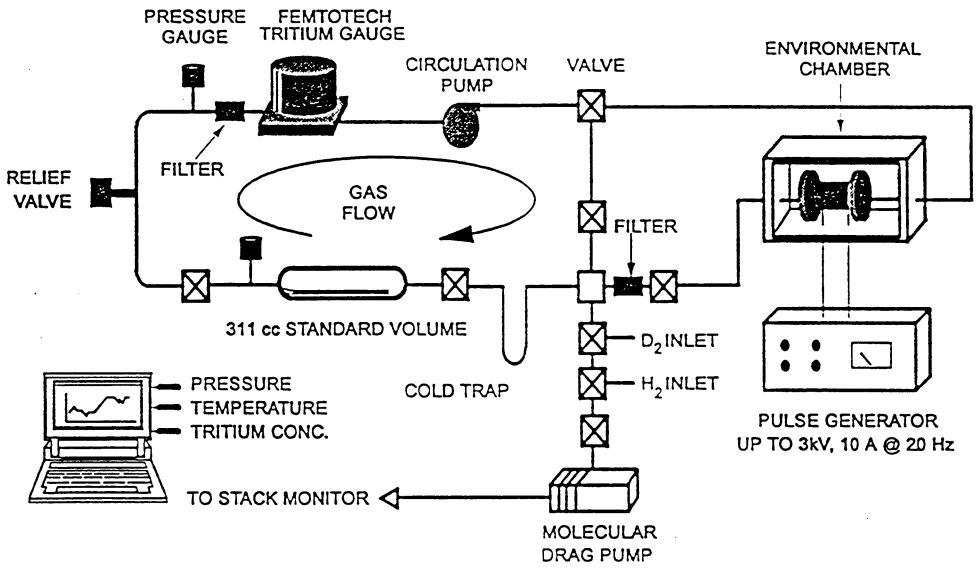

Figure 1. The new tritium analysis system (system 2) used in the second half of this study.

4. PROCEDURE

The procedure for hydriding a wire or Pd-Si cell was to first fill the 3.1 liter loop with deuterium gas at 600 to 1200 torr and measure the background tritium concentration, if possible. The gas would then be circulated around the loop for 12- 24 hours to determine the background drift rate. With the loop drift rate measured, fresh deuterium was introduced into the loop and the cell hydrided slowly with the deuterium flowing in the loop. With the system 2, the drift rate is so low that these steps can be eliminated.

After a cell had been hydrided, the gas was circulated with the cell in place from 15 minutes to several days to ensure that no tritium was evolving from the palladium and to allow the palladium to fully hydride. With wire cells it was a simple matter to measure the resistance of the wire to determine the hydride state. With the plasma cells, a wait of 24 hours was used to ensure the foils and wires were hydrided. As received (100 micron) wires would typically hydride in 12-18 hours, wires that had been cleaned with alcohol and by scraping with a Al_2O_3 plastic polishing cloth (3 micron) took about 6 to 8 hours to hydride. Wires that had been cleaned and then annealed (350 °C for 2 h in air), hydrided within 15 to 30 minutes.

To dehydride the wires, a large dc current (0.6 to 0.8 A) was run through the wire, or the whole cell was heated to over 150 °C. Powder samples were dehydrided by heating to 473 K with the environmental chamber. A final dehydride could be accomplished by closing off the cell, evacuating the loop, and then opening the hot cell to vacuum. The last 6-10% of the deuterium could be recovered by this method. The plasma cells were dehydrided by simply evacuating the loop and drawing off as much deuterium from the plasma cell as possible at room temperature.

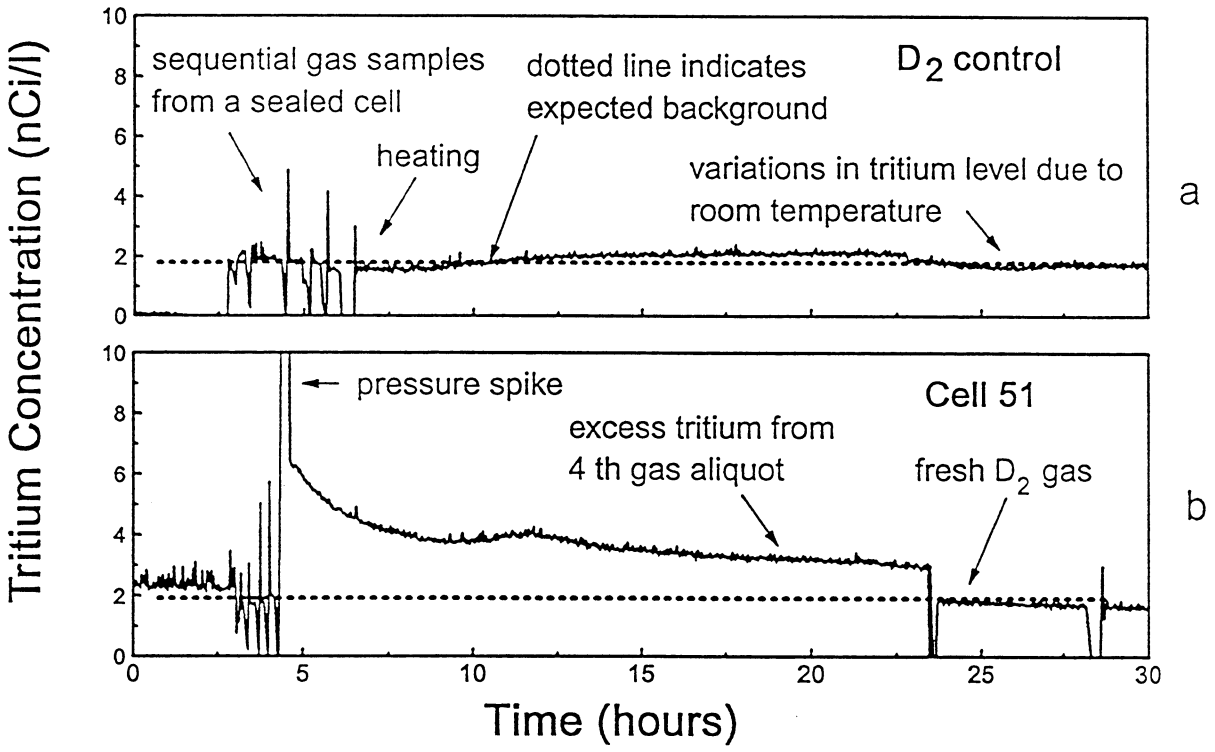

Figure 2. Comparison of background and foreground results with a Pd-Si layer powder type cell.

5. RESULTS

A summary of the various experiments is as follows. There were a total of 29 wire and powder wire experiments, 4 plasma cell experiments as well as ten Pd-Si powder cell experiments. These are grouped by type but it should be understood that, generally, the wire and powder-silicon types were run near the beginning of this series of experiments and some of the earlier experiments were done with system 1.

Pd-Si Cells

Two of the Pd-Si cells were run underground at BYU; the first cell shorted and gave only 1± 0.3 nCi, the tritium results for the second cell are shown in Figure 2 with a background. The largest tritium output (for this cell type), in the series of cells run with the clean system was with cell 56 that gave 13.5 nCi as compared to background runs of either hydrogen or deuterium that gave 6.5 ± 0.2 nCi. The tritium evolution rates were commensurate with the rates obtained in system 1 (0.05 to 0.3 nCi/hr) for active cells.

Shown in Figure 2 is a dehydride of cell 51 (Compact 51 in ref. 5) that was run for about 105 hours in the BYU tunnel in a sealed sample chamber with 4 atm. deuterium pressure. As indicated in the figure, 600 torr aliquots of gas were removed from the sample cell after an initial 600 torr fill from the original D_2 cylinder was used to check the response of the system. Also shown in Figure 2a is a sample of palladium powder of the same batch as cell 51 that was put in the sample chamber and deuterided and dehyrided with the same pressure as cell 51. The control sample was not pulsed. It is seen that after the control sample is heated to dehyride the palladium, a decrease in the apparent tritium level is observed. This is due to the quenching effect of water on the ionization current. Sample 51 shows a completely different behavior, when heated. The apparent tritium level increases and then decreases, presumably due to mixing. We attribute this to the presence of tritiated water vapor from the cell. The fact that the tritium level is still dropping at the end of the test when the deuterium is pumped out created an uncertainty in the measured level. The other revealing feature of cell 51 is that the tritium level, in the first three aliquots increases with each sample, slightly, whereas, the samples from the inactive cell decrease with each sample due to an increased concentration of water vapor in the latter samples.

The total amount of tritium evolved from cell 51 is only 5.1 ±1.5 nCi. To put this number in perspective with the rest of our measurements, it should be noted that about 28% of the cells produced tritium >15 nCi, while about 34% of the samples give reading of between 0 and 5 nCi. The result from cell 51 is entirely consistent with data taken over two years ago with a completely different ionization gauge and deuterium with a tritium concentration of up 100 nCi/l. In the recent experiment and in the historical cases, most of the tritium was evolved when the palladium was dehydided. For these most recent experiments the sensitivity and accuracy of the measurements far exceeds the prior data because the intrinsic tritium level (90 pCi/l) is inconsequential and consequently the separation factor is negligible.

Solid Wire Cells

Of the 29 wires that were run, 7 of these were of the powder type (Figure 3c), the rest were bare palladium wire wrapped on a grooved macor ceramic spool. Of the wires, only one batch (W13918) from Johnson and Matthey showed consistent tritium production over 0.1 nCi/hr. All of this wire came from one spool, and another, supposedly identical batch, from another spool

did not show any significant production in system 2. The rest of the solid wires, whether they were run in system 1, system 2 or in a sealed pressure vessel were rather unproductive, for instance, wire ten gave 4.2 nCi total in system 2 after 380 hours of pulsing at high currents (11 amps peak). All other wires we ran gave an average of 1.0 nCi after 133 hours of operation. Most of the wires were 100 microns in diameter, but wires were fabricated with diameters of 112, 152, 203 and 254 microns in lengths of 100 to 500 cm. For a given material and length of wire, the smaller wires produced more tritium than the larger diameters even though they contained much less material. Most of the wire was run in the as received condition, but one wire was run after being annealed in air at 600 °C. This procedure did not noticeably affect the tritium generation rate. Another wire was contaminated with chlorine on the surface and did not hydride or produce any tritium.

Most of the batches (excluding batch W13918) of wire showed considerable contaminants including microscopic (100x) carbon deposits on the wire. To illustrate just how deleterious this might be, we electrically heated one batch (W06528) to about 500 °C in air and witnessed a visible smoke from the wire. A yellow-brown residue was left on the otherwise white ceramic spool after this episode. Sections (~ 0.1 g) of the Johnson and Matthey and Goodfellow wires have been heated (280 °C) in deuterium, in the tritium analysis loop, in an attempt to drive out tritium contamination. No tritium contamination has been found in the wire by this procedure to within 0.2 ± 0.1 nCi..

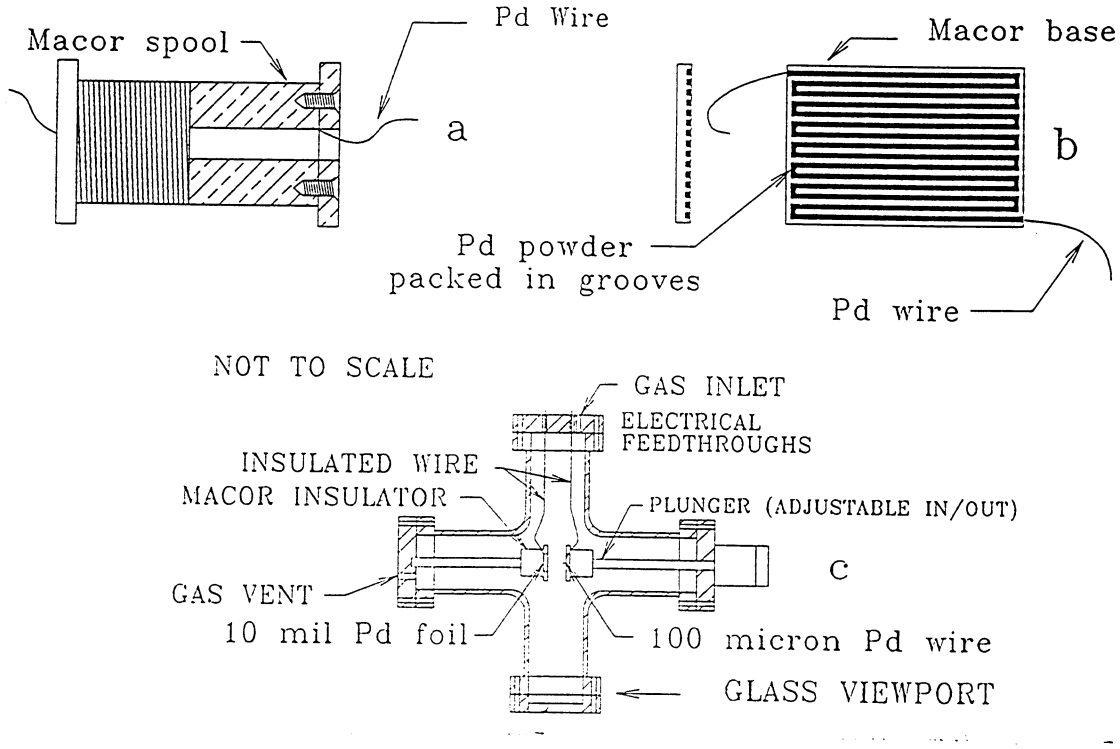

Figure 3. Diagram of the cell types used in this study.

The wire experiment with the largest tritium yield (batch W13918) is shown in Figure 4. It can be seen that the tritium level in the cell increases over the background drift rate at pulsed peak currents of greater than 3 amps. The background drift rate was measured prior to the placement of the cell in the loop and is for D_2 gas, unfortunately the drift rate was rather high due

to residual tritium contamination from a previous cell. Even so, the rates of tritium evolution from this wire exceed the background drift rate by a factor of 4.5. Other runs with this wire gave similar rates even though they were run in closed cells. Heating the wire to 100 °C prior to the current pulsing did not produce significant tritium over the background, but heating the wire after a run did produce significant evolution of the tritium. For instance, in the wire shown in Figure 4, 19.5 nCi was evolved during the time the current was on but an additional 52 nCi was released during the post heating of the cell.

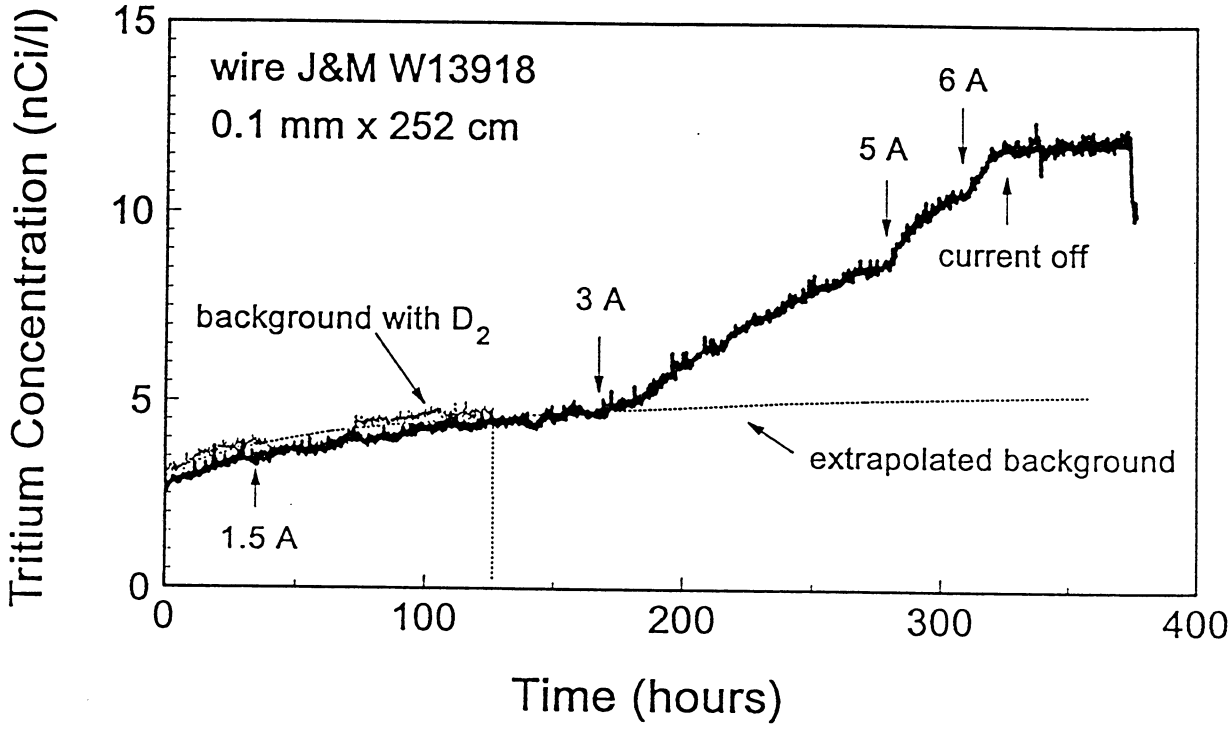

Figure 4. Tritium evolution from a Johnson Matthey wire.

One other wire was of note, and that was a Goodfellow 0.152 mm diameter wire. This wire was run in system 2 and produced 1.8 nCi at a rate of 0.085 nCi/h before a pump and power failure terminated the experiment. This particular batch of wire was not as clean as the J&M W13918 batch but was cleaner than other J&M batches based on the amount of residue left on the ceramic spool.

Powder Wire

The seven powder wires were difficult to fabricate and run consistently. The largest result is shown in Figure 5 and occurred when an arc was apparently formed in the track. This produced an immediate and sudden rise in the tritium level as shown in the upper curve of Figure 5. The rate of tritium production (~ 5 nCi/hr) during this episode far exceeds anything we have seen from the other types of cells. Unfortunately, none of the other cells could be made to arc in this way or produce much more than a few nanocuries as shown by the lower results in Figure 5 for cells 14 and 15. The three powder track cells that were taken to BYU produced only an

average of about 0.4 ± 0.3 nCi.

While these cells were not reproducible, they did indicate that arcing was important. Therefore, we attempted to produce a plasma or an arc between plates and wires as described below.

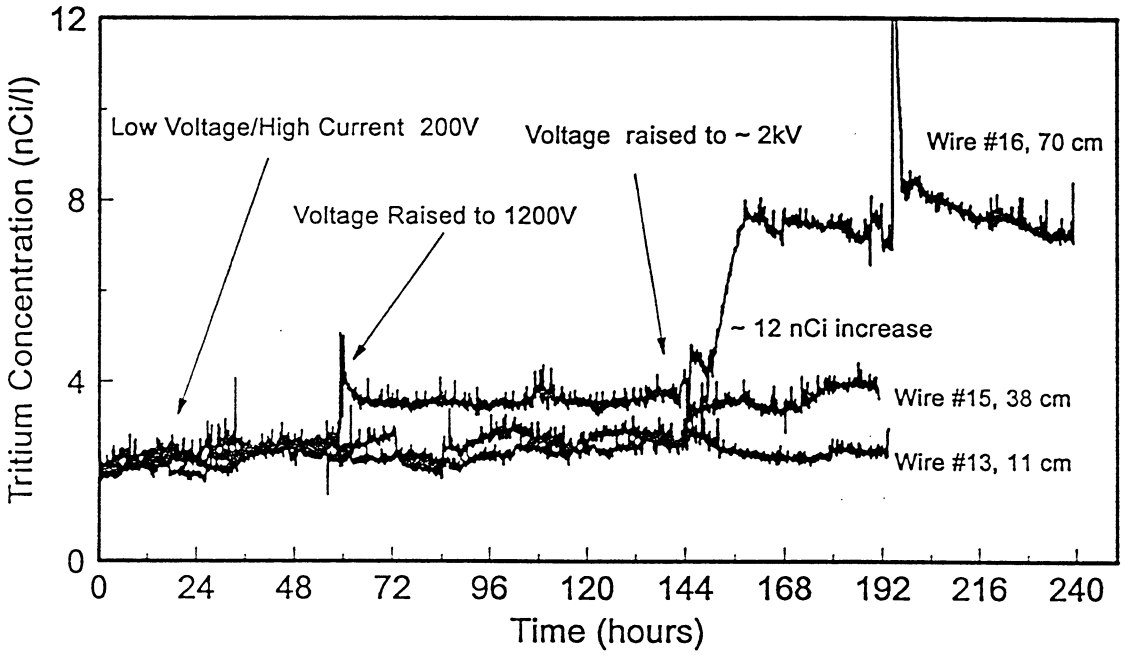

Figure 5. Tritium evolution from three powder wire cells. The conditions that produced the large, sudden, increase in tritium level in cell 16 have not been reproduced.

Plasma Cells

Of all the cells constructed, the most prolific and (seemingly) reproducible were the four plasma cells (Figure 3c). The basic cell design of plasma 1, 3, and 4 was palladium plates (0.25 mm thick by 19mm dia.) opposite palladium wires. Plasma cell 2 was constructed with two opposing palladium plates and exhibited a stable plasma but produced no tritium. These cells are similar to those reported by the Russian[8,9] and French[10] researchers. Plasma one used J&M 0.1mm dia. wire while 3 and 4 used the Goodfellow 0.25mm wire. The wire was pulsed negatively, 1 μs pulse width at 500 Hz, with respect to the plate. Peak currents of up to 12 A were used; voltages were from 2700 V (initiating the plasma) to 400 - 800 V (sustaining voltage).

Figure 6 shows the results for plasma 1 and plasma 2. Plasma one was only run for about 5 hours and produced about 0.6 nCi during the time indicated. The rest of the time the plasma was activated it was arcing between the wall of the containment vessel and a connector. The expected signal level from the Femtotech for this plasma cell (based on pressure) is shown as the dotted line. It should be noted that the cell did not produce any tritium at 20 torr. The production only began after the pressure was increased to 80 torr. Similarly, the plate-plate cell produced a stable plasma at 20 torr but did not produce any tritium. It also did not produce any tritium at 600 torr where a spark was produced for several hundred hours resulting in copious amounts of fine palladium black on the inside of the vacuum chamber. As shown in Figure 6 after plasma 2 was

run, the loop was pumped out and fresh D_2 at 600 torr was introduced into the loop. The Femtotech level is seen to be approximately the same as during the period of arcing.

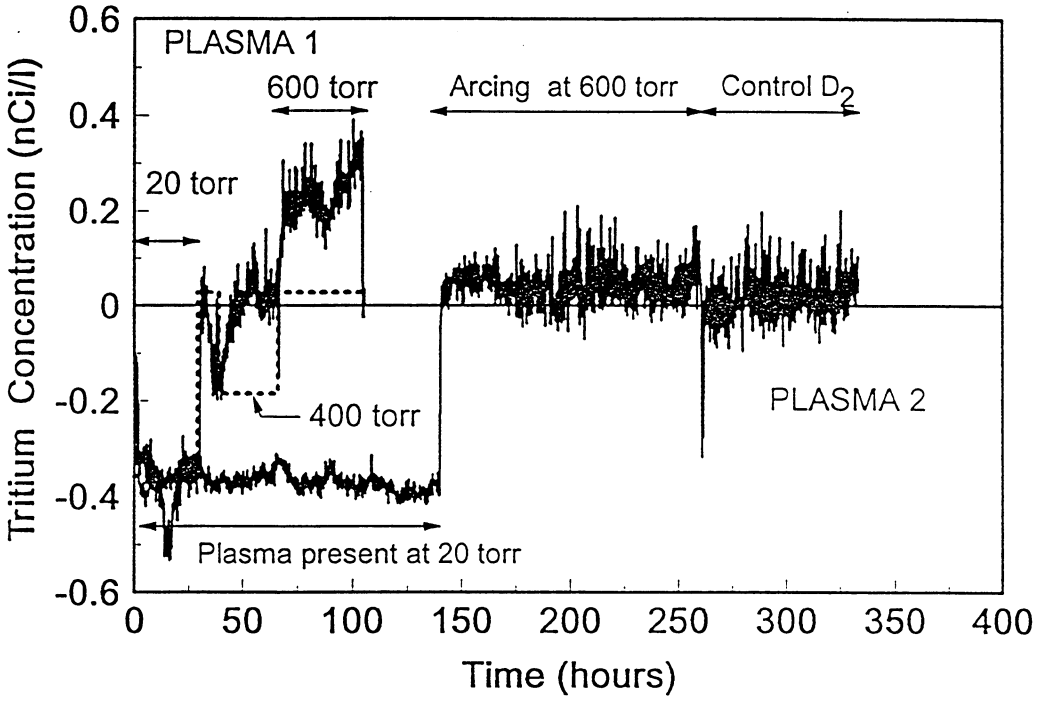

Figure 6. Results from the first two plasma experiments.

Since the plate-plate arrangement did not produce tritium, two attempts were made to replicate the wire-plate experiment. Both of these were very successful. Plasma 3 produced about 30 nCi total and Plasma 4 produced nearly 102 nCi. For clarity, only the result for Plasma 3 is shown in Figure 7 although the result from plasma 4 is very similar. Wire and plate from the same batch were used for all of the plasma experiments described here.

The protocol for these cells is somewhat complicated, but in general, they were hydrided (120 torr) in the loop for a minimum of 24 hours then started with a peak current of > 4 A, later the currents would be increased. The wire was charged negative during the pulse. Near the end of the runs the peak currents were on the order of 12 A. The tritium generation rate was dependent on current, but was not linear with current and seemed to be saturating at currents over 8 A. A 5% efficient ^3He slab neutron detector was placed directly under the cells and did not show any counts over background (~ 2.3 counts/s).

After a certain length of time, the dead volume in back of the plate was flushed. This resulted in the immediate release of a significant amount of tritium. This jump in tritium is labeled in Figure 7 as (a). Later, another flush and a final flush were given to the system. These are labeled (b) and (c). After the experiment the plates and wire were separately heated. The wire released about 12 nCi of tritium while the plate had no measurable release. In Figure 7 the two dotted lines indicate the tritium release rate for two peak currents (5 and 6.5 Amps). Also plotted in Figure 7 are the two previous plasma run that indicate the stability and magnitude of the result from plasma 3.

6. DISCUSSION

Tritium has been detected in Pd-D systems when excited by unipolar electrical pulses. There are five plausible sources for the excess signal. The tritium could be contamination in the palladium, the tritium could be hiding in the loop, the tritium could be coming out of the sample chamber, the tritium signal could be spurious and finally the tritium could be generated in the palladium by unknown processes.

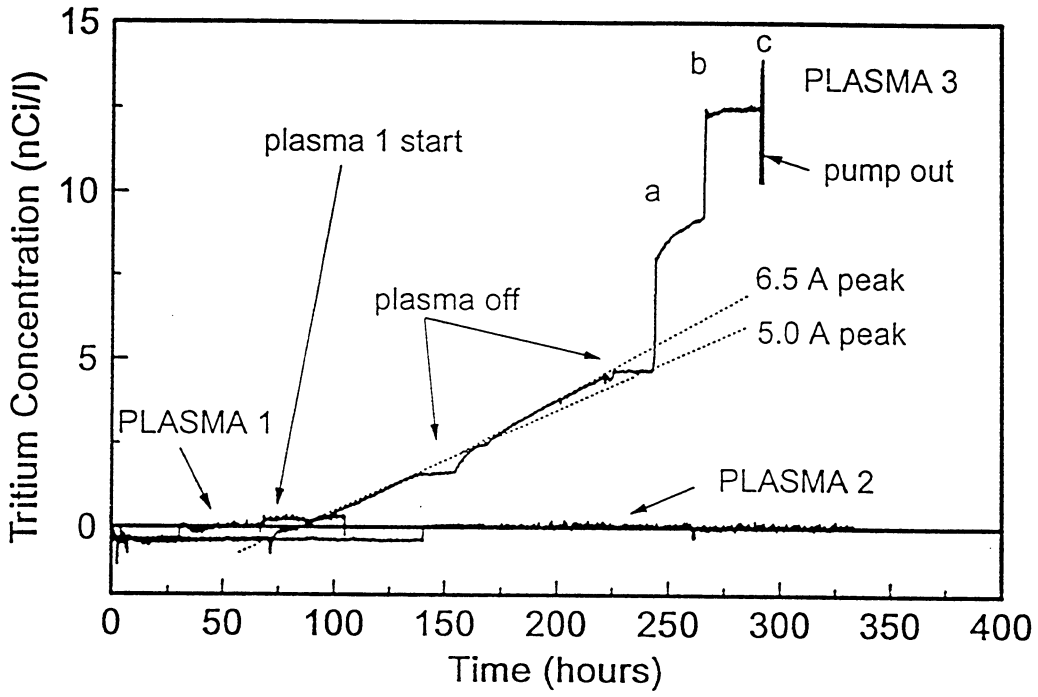

Figure 7. Tritium generation from a wire-plate plasma cell operated at 80 torr.

No tritium could be detected in any of the materials by a number of methods. However, since only samples of the material were used in the impurity analysis, the actual palladium in a sample could be "spot" contaminated. This type of contamination is unlikely to be intrinsic to the material since the materials are of very high "stated" purity. However, palladium wire that is drawn has to be lubricated either with oil or water and is usually fabricated from a thick right cylinder. Any spot contamination would tend to be drawn out and smeared throughout the length of the wire. Therefore, contiguous sections of wire should be cross contaminated. We attribute the residue and smoke seen from some of the wires to entrained lubricant. Tritium contaminated oil should be detected in all sections of the wire.

Spot contamination extrinsic to the wire, such as an oil residue left after opening the wire but before placing the wire in the container is a possible type of spot contamination. This is unlikely to occur in our samples since all parts are handled with new gloves and cleaned with ethanol prior to assembly.

Given the relatively large amounts of tritium seen in some of the samples, tritium should have been displaced from the wire by the hydriding process. As shown in Figures 4 and 7 there is no indication that the tritium would be evolved prior to running at high current densities. Post test, it was found that the tritium in the samples was more difficult to remove than expected,

requiring temperatures on the order of 250 °C for 10 hours. Peak temperature rise over ambient in the wire due to the current pulses is only 40 °C.

Finally, some wires and constituents of the plasma cells were heated at 80 °C, in the analysis loop, for 12-24 hours prior to the activation of the cell. Tritium was evolved during the subsequent current pulsing rather than during the quasi-static heating. Similarly, the cell bodies and other constituent parts were heated to 200 °C for 24 h in an attempt to drive out any adsorbed tritium. No excess tritium could be detected in these tests.

The next most likely source of excess tritium is from hideout and tritium adsorption in the loop itself. System number one has been previously exposed to tritium for calibration purposes and previous cells have generated copious amounts of tritium that may have diffused into various parts of the system. Loop one has also been exposed to a volatile binder and trace amounts of pump oil that may have back diffused and could possibly trap tritium. It has been suggested that heated palladium would act as a catalyst and decompose the oil or binder contaminated with tritium. However, if the contaminated species can migrate to the palladium, it could also migrate to the ion chamber where it would give a direct reading.

System number one has been disassembled and the inside of the loop was swiped for tritium. A brownish deposit was found in some of the stainless tubing and this deposit was contaminated. We estimate, based on the swipes, that the system contained about 180 nCi of adsorbed tritium. This amount of adsorbed tritium could seriously skew our results, but could not account for all the tritium seen in the largest of the events. In addition, tests were run where the cells were closed and only opened to the loop briefly to dehydrided the cells or where the cells were shut from the loop and then opened later with a resulting increase. We attribute the contamination to, primarily, the loop piping rather than the Femtotech because in one test, (during the cleanup after cell 42) the Femtotech was valved off from the rest of the loop and showed a low drift (< 0.02 nCi/h) but when the valves were opened to the loop, the apparent tritium level immediately rose and the drift rate increased to 0.12 nCi/h. The loop was heated to 423 K for this test to promote cleanup. While the contamination in the loop makes certain experiments more difficult to analyze, it does not negate the results since an overall total of 42 cells were run in closed cells.

Another possibility is that the ionization gauge may be directly affected by some agent originating in the cell such as water vapor, CO_2, carbon or palladium black caused by the arcing. It is very unlikely that there would have been enough of a change in the composition of the gas to change the ionization efficiency by any significant amount since additions of CO_2 (1 to 5 torr out of 1200 torr) are undetectable by the ion chamber. The fact that the chamber did not drift with the valves closed yet the system was drifting indicates that contamination of the ion chamber itself is not the primary factor. Furthermore, it is apparent that the ion chamber can be quenched by the presence of water, but we have no evidence that leakage current due to adsorbed water on the probe insulator will give anything other than a negative reading. A high steady reading due to a cloud of small particulates is unreasonable in view of the two filters in the system and because the tritium signal does not decrease whenever the gas flow was halted. The effect of particulates can be seen in Figure 5 where at about 194 hours the Femtotech reading goes off scale for a few hours but returns to normal after the transient. This is typical of the response of the instrument to particulates.

From what has been discussed above it should be apparent that the loop contains various reservoirs for TDO hideout and storage. We believe the storage is of TDO rather than TD based

on our extensive experience with similar systems that have been exposed to high levels of gaseous tritium. Adsorbed TDO is released slowly over a period of days as it exchanges with normal water or is deadsorbed from the surfaces of the loop by flushes of hydrogen deuterium or air. The difference in background drift rate is illustrated by the drift seen in Figure 4 versus the drift rate much later after multiple cleanings as shown in Figure 5 for the powder wire cell 13.

Because of the drift rate, tritium hideout, and water vapor effects make the powder cells difficult to interpret, we have concentrated on the wire, powder wire and plasma cells. These recent systems are very clean since they do not contain a volatile binder or any significant amount of water vapor. System 2 was also built to replace System 1 so that there would be no question as to the source of the tritium that was detected.

Most of the wire experiments have been done in situ in system 2 and have shown small or no amounts of tritium. The largest tritium release occurred from a 0.15 mm Goodfellow wire. Sections of this wire have been heated in deuterium with no release of tritium noted. All of the plasma experiments have been run in System 2 and have generated over 130 nCi of tritium in a very clean system that over a period of months showed no increase over background with other types of cells.

The wire and the plasma experiments have confirmed the measurements made earlier on the powder cells that indicated the tritium output depended on current. In the wire, there appears to be a threshold current density, while in the plasma it there is a low current threshold and also saturation at high currents.

No significant neutron emission has been measured in these experiments or those at BYU using our materials and cells. Based on the tritium output and our previous neutron results, we would not expect to have detected any significant emission given the paucity of tritium found in the cells run at BYU. All of the samples have been subjected to gamma analysis both before during and after the experiments. No anomalous gamma lines, of any significance, have been detected.

7. CONCLUSIONS

Several methods of tritium production with palladium deuteride systems have been demonstrated. The tritium output depends on the current applied to the cells. Yet, the tritium yield is found to depend strongly on the type of palladium metal used (powder, foil or wire) and the type of experiment powder wire, wire, plasma. Various tests for tritium contamination confirm that there is no initial tritium contamination in the powder, foil, wire or other materials used in this study.

Annealing of the palladium seems to be necessary to reactivate foils after a deep dehydride. Lower values of stochiometry or lower gas pressures are less efficient for the generation of tritium. It is probably necessary to have at least a stoichiometry of 0.55 in the palladium.

The purity of palladium has varied in our experiments, with the wire experiments, it appears that very pure palladium is more effective that impure palladium in producing tritium. We also must conclude that we do not fully understand the full impact of impurities. We think this is partially a morphological or metallurgical issue since we have seen output from annealed as well as received palladium. However, palladium that been hydrided must always be annealed.

We do not expect that the nuclear process responsible for the tritium occurs in the plasma or that it is conventional two body d-d fusion. The plate-plate experiment produced a stable

plasma with no indication of tritium or neutron generation.

The success of these experiments relies on a non equilibrium condition existing in beta phase deuterated palladium. The plasma, arcing, and pulse heating are means to achieve this condition. We believe that the uncontrolled purity and metallurgical condition of most palladium electrodes is a major factor in explaining the unreproducible nature of many experiments.

8. ACKNOWLEDGMENTS

Many people were involved in a direct way with the experiments described here. Some of these were Ken Griechen, Roy Strandberg, Royce Taylor, Marie Bissett, and Steve Jones. We gratefully acknowledge the use of the first plasma cell from Dan Phelps and Ted Lautzerhiser of AMOCO.

9. REFERENCES

1. Claytor, T. N., Tuggle, D. G., Taylor, S. F.; **Evolution of Tritium from Deuterided Palladium Subject to High Electrical Currents,** Frontiers Science Series No. 4, Proceedings of the Third International Conference on Cold Fusion., October 21-25 Nagoya Japan., Ed. H. Ikegami, Universal Academy Press Tokyo Japan., 1993, p217.

2. Bockris, J. O'M., Chien, C-C., Hodko, D., Minevski, Z., **Tritium and Helium Production in Palladium Electrodes and the Fugacity of Deuterium Therein,** Frontiers Science Series No. 4, Proceedings of the Third International Conference on Cold Fusion., October 21-25 Nagoya Japan., Ed. H. Ikegami, Universal Academy Press Tokyo Japan., 1993, p231.

4. Wada, N. and Nizhizawa, K., 1989, **Nuclear Fusion in Solid,** Japanese Journal of Applied Physics, Vol. 28, No. 11, p L 2017.

5. Taylor, S. F., Claytor, T. N., Tuggle, D. G., and Jones, S. E., **Search for Neutrons from Deuterated Palladium Subject to High Electrical Currents**, See these procedings.

6. Pohts, J., INC-6, LANL, December 1992, private communication.

7. Cedzynska, K., Barrowes, S. C., Bergeson, H. E., Knight, L. C., and Will, F. W., 1991, **Tritium Analysis in Palladium With an Open System Analytical Procedure**, Fusion Technology, Vol 20, No 1, p 108, and private communication.

8. Karabut, A. B., Kucherov, Ya.R., Savvatimova, I.B., **Nuclear Product Ratio for Glow Discharge in Deuterium**, Physics Letters A, 170, 1992, p265.

9. Romodanov, V., Savin, V., Skuratnik, Ya. Timofeev, Yu., **Nuclear Fusion in Condensed Matter**, Frontiers Science Series No. 4, Proceedings of the Third International Conference on Cold Fusion., October 21-25 Nagoya Japan., Ed. H. Ikegami, Universal Academy Press Tokyo Japan., 1993, p307 .

10. DuFour, J., **Cold Fusion by Sparking in Hydrogen Isotopes**, Fusion Technology, Vol 24, 1993, p205.

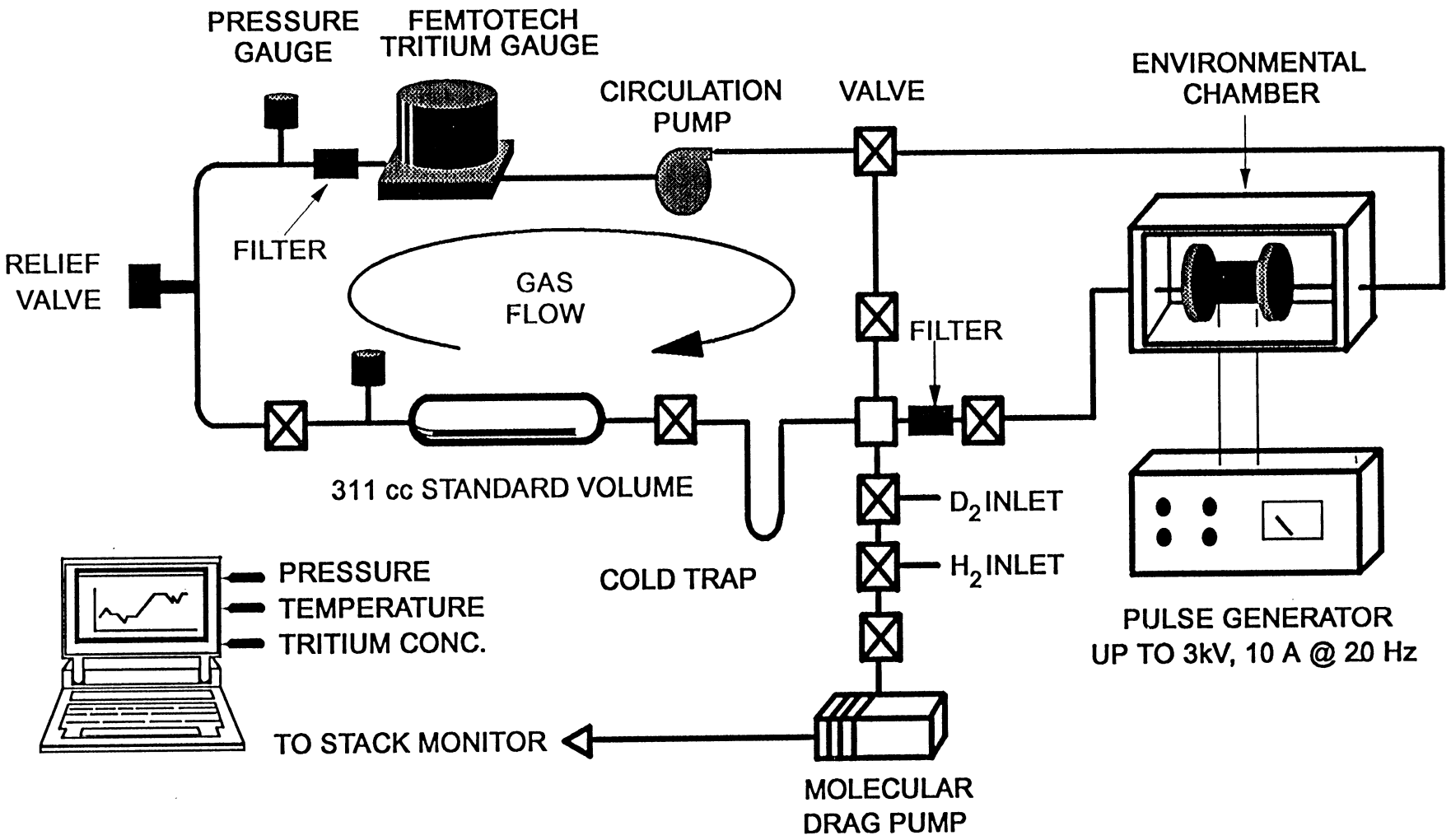
PRESSURE GAUGE
FEMTOTECH TRITIUM GAUGE
CIRCULATION PUMP
VALVE
ENVIRONMENTAL CHAMBER
RELIEF VALVE
FILTER
GAS FLOW
FILTER
311 cc STANDARD VOLUME
D_2 INLET
H_2 INLET
COLD TRAP
PRESSURE
TEMPERATURE
TRITIUM CONC.
PULSE GENERATOR
UP TO 3kV, 10 A @ 20 Hz
TO STACK MONITOR
MOLECULAR DRAG PUMP

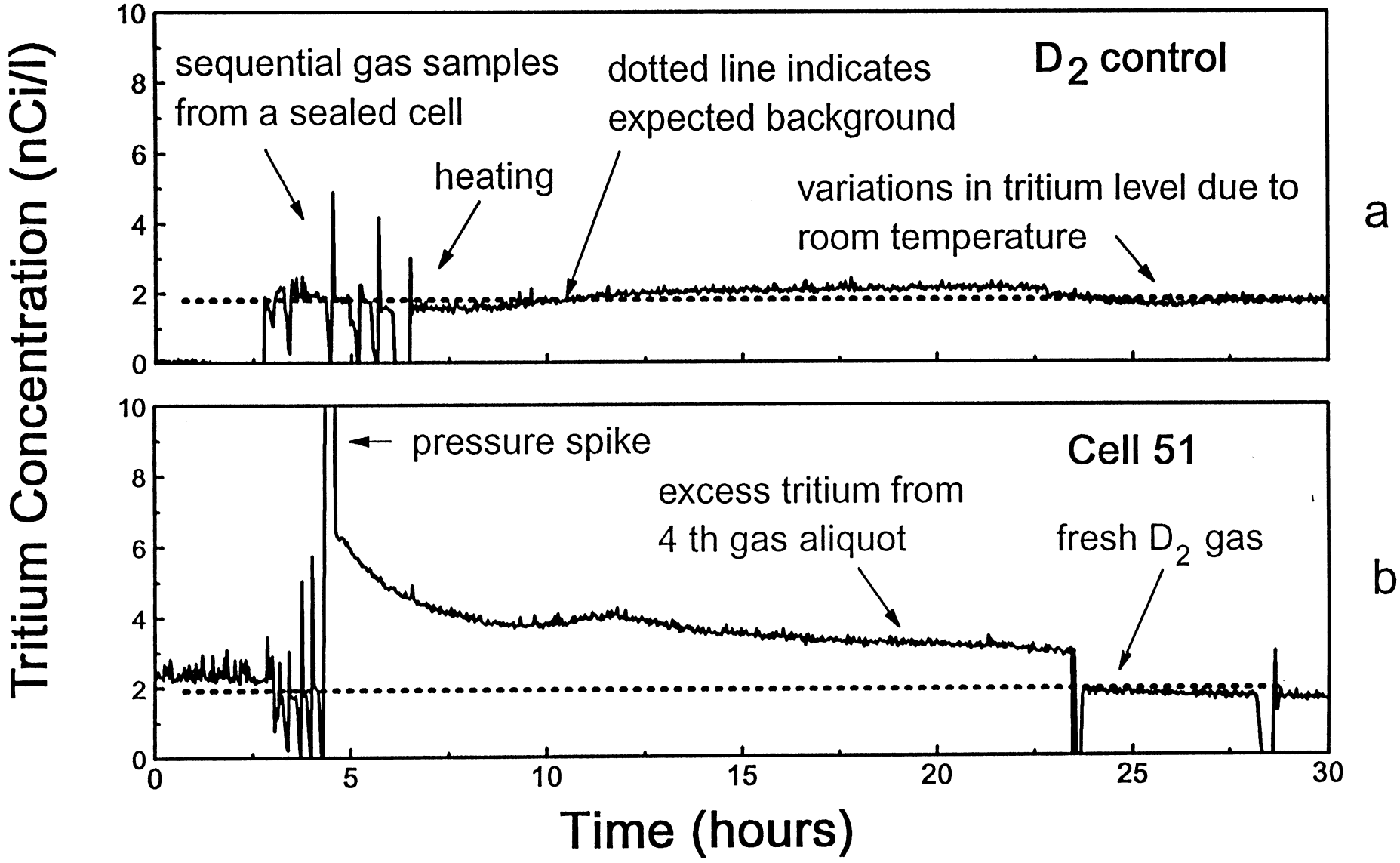
Tritium Concentration (nCi/l)
10
8
6
4
2
0
sequential gas samples
from a sealed cell
heating
dotted line indicates
expected background
D2 control
variations in tritium level due to
room temperature
a
pressure spike
Cell 51
excess tritium from
4 th gas aliquot
fresh D2 gas
b
0
5
10
15
20
25
30
Time (hours)

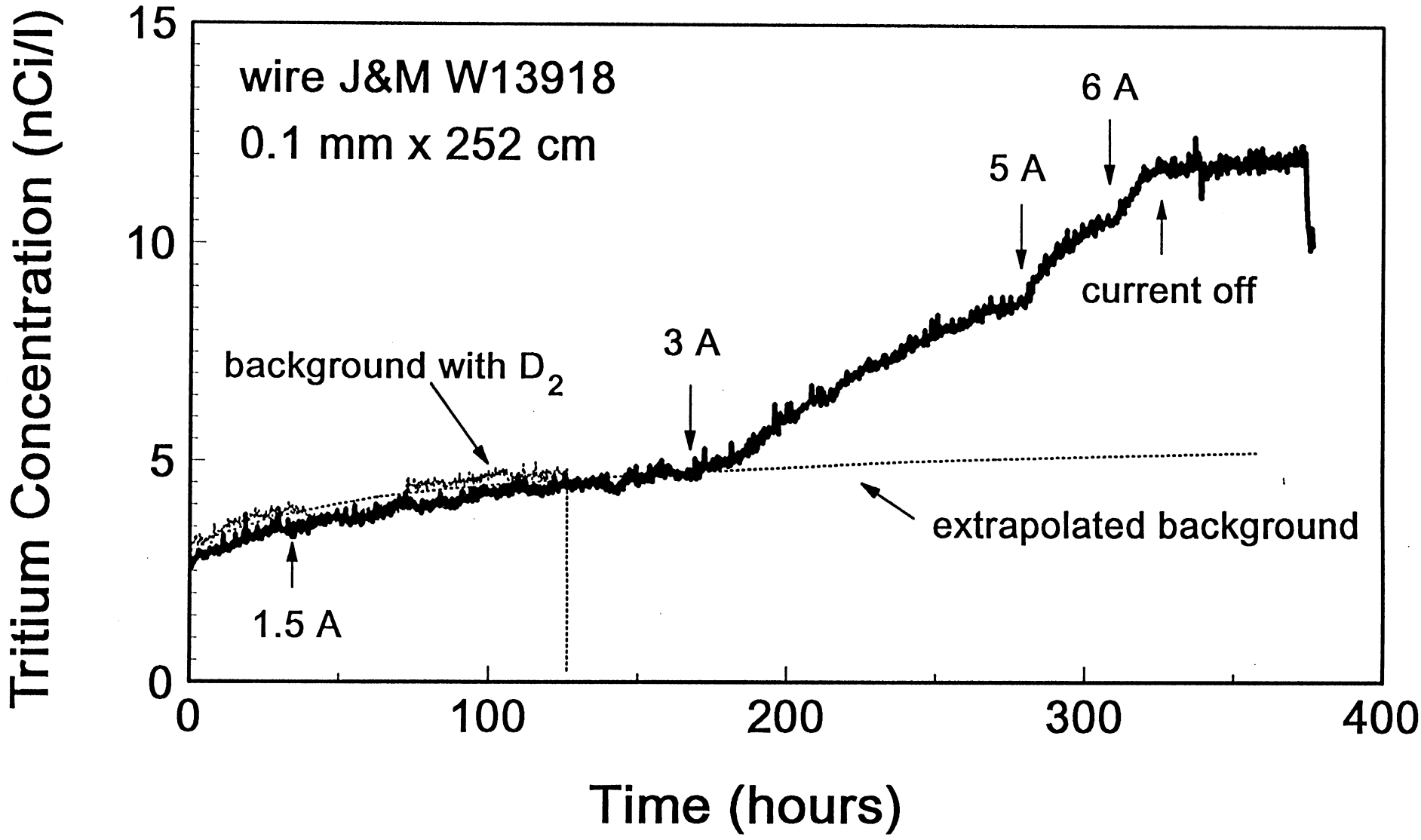
wire J&M W13918
0.1 mm x 252 cm
6 A
5 A
current off
3 A
background with D_2
extrapolated background
1.5 A
Tritium Concentration (nCi/l)
Time (hours)
0
5
10
15
0
100
200
300
400

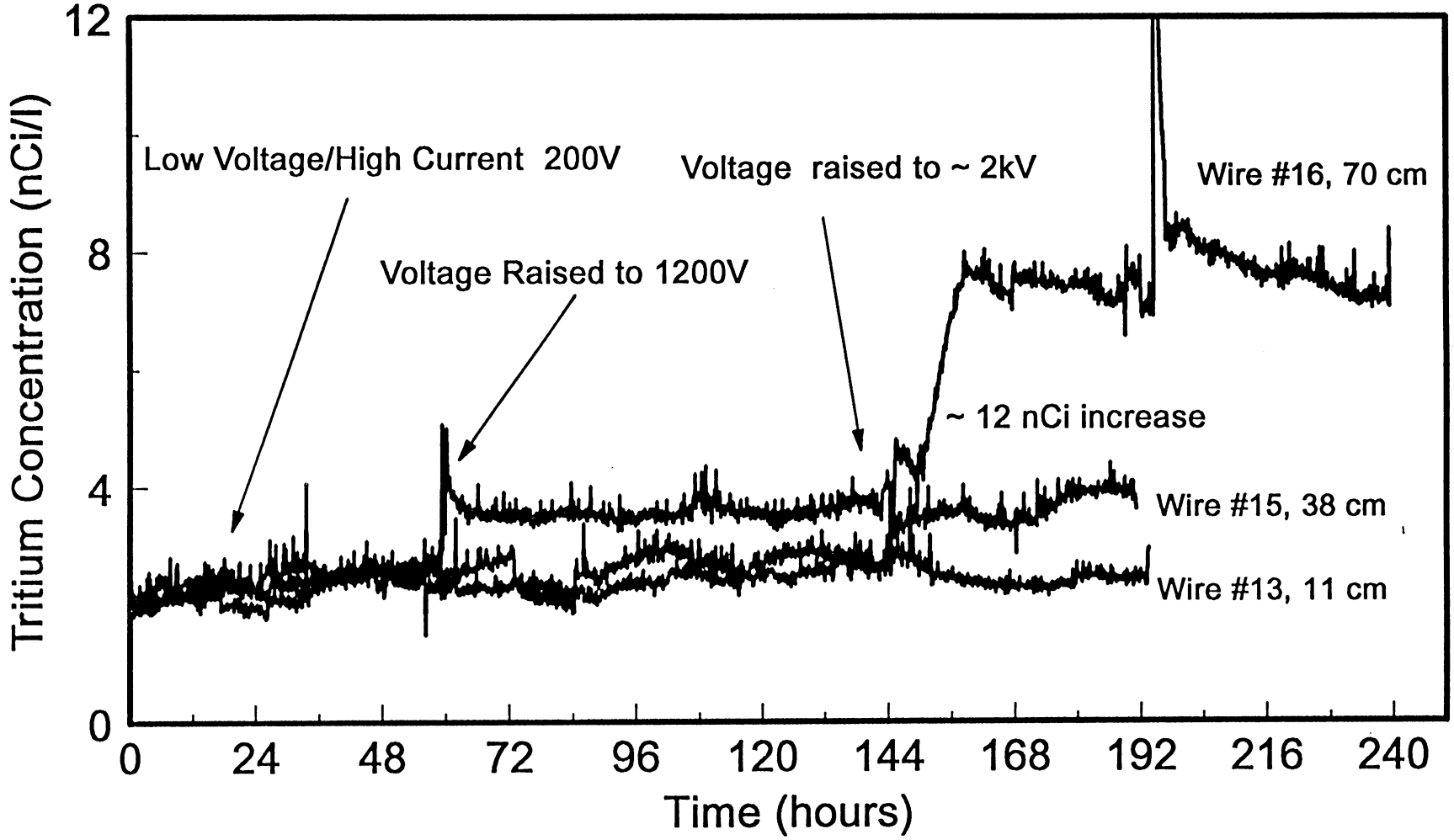
Tritium Concentration (nCi/l)
12
8
4
0
0
24
48
72
96
120
144
168
192
216
240
Time (hours)
Low Voltage/High Current 200V
Voltage Raised to 1200V
Voltage raised to ~ 2kV
~ 12 nCi increase
Wire #16, 70 cm
Wire #15, 38 cm
Wire #13, 11 cm

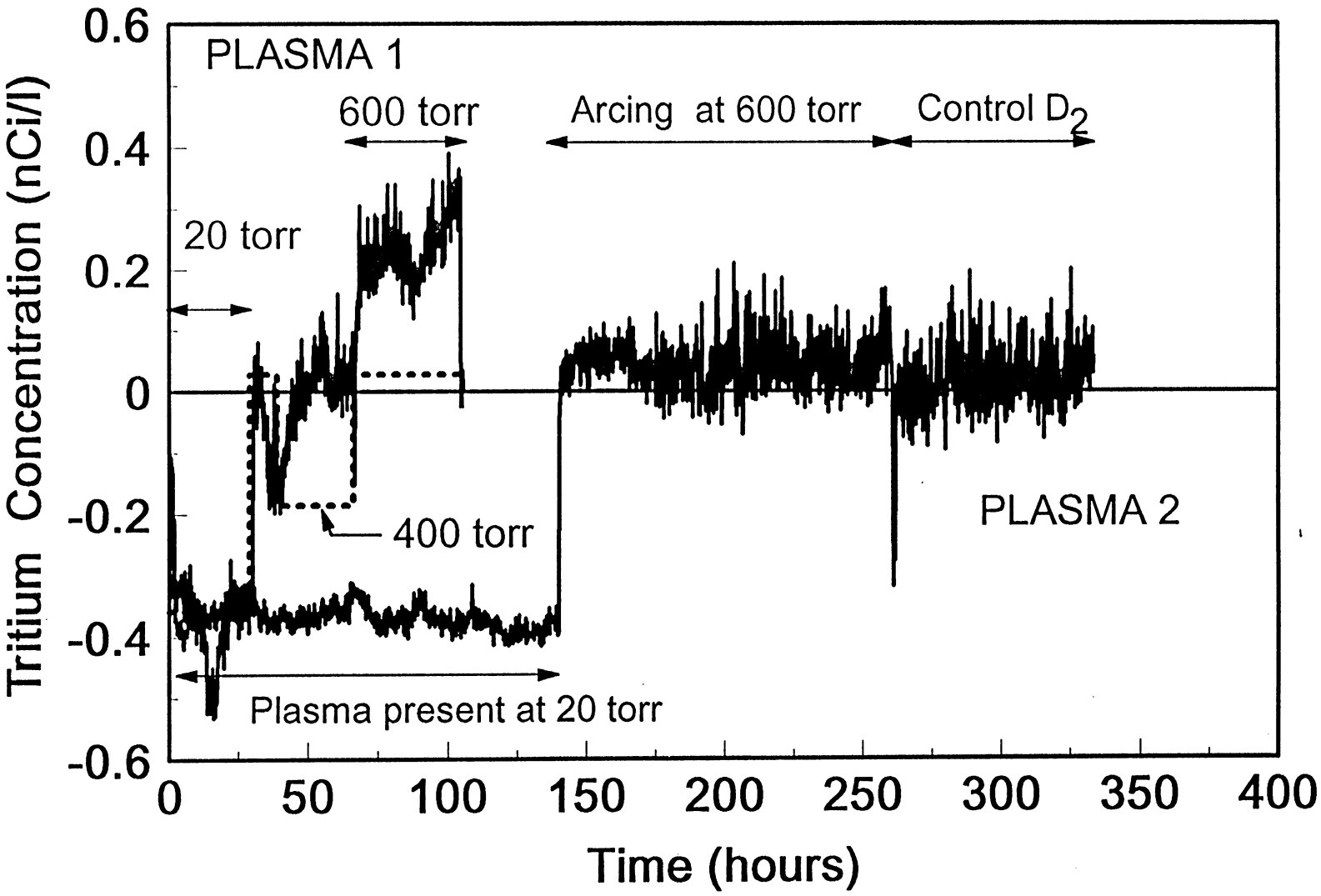
PLASMA 1
600 torr
Arcing at 600 torr
Control D_2
20 torr
400 torr
PLASMA 2
Plasma present at 20 torr
Tritium Concentration (nCi/l)
0.6
0.4
0.2
0
-0.2
-0.4
-0.6
0
50
100
150
200
250
300
350
400
Time (hours)

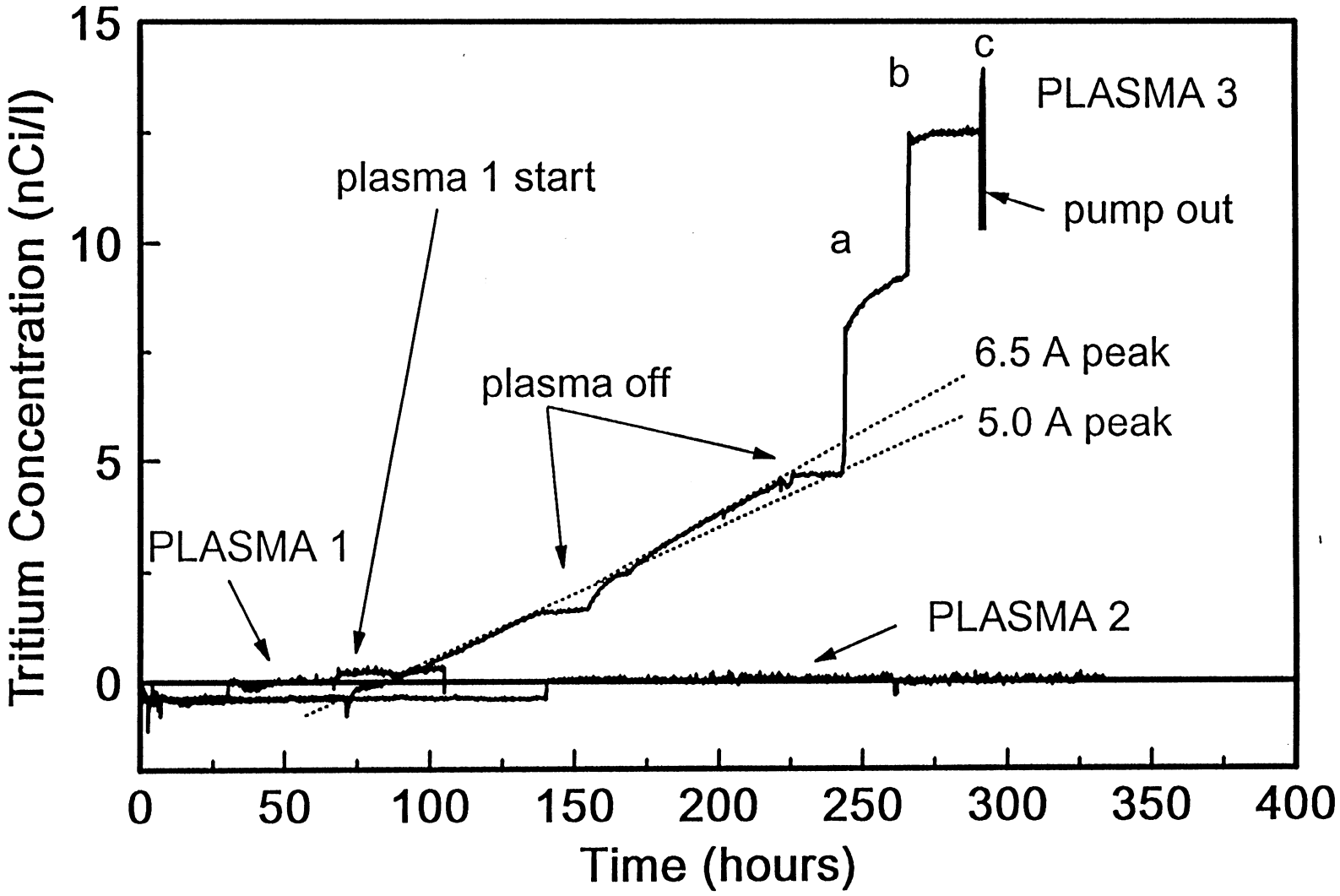
Tritium Concentration (nCi/l)
15
10
5
0
0
50
100
150
200
250
300
350
400
Time (hours)
plasma 1 start
plasma off
PLASMA 1
PLASMA 2
PLASMA 3
a
b
c
pump out
6.5 A peak
5.0 A peak

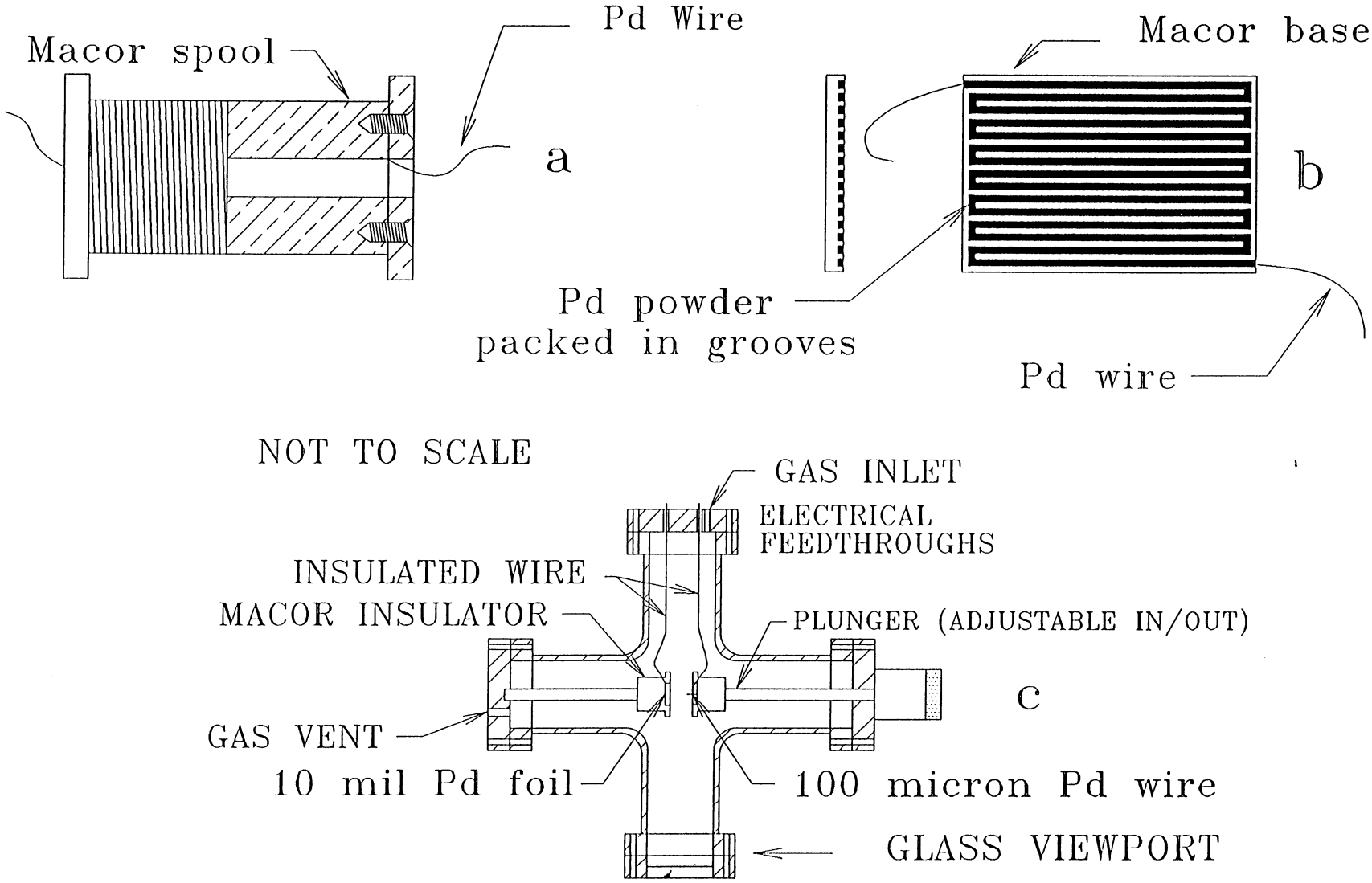
Macor spool
Pd Wire
a
Macor base
b
Pd powder
packed in grooves
Pd wire
NOT TO SCALE
GAS INLET
ELECTRICAL
FEEDTHROUGHS
INSULATED WIRE
MACOR INSULATOR
PLUNGER (ADJUSTABLE IN/OUT)
c
GAS VENT
10 mil Pd foil
100 micron Pd wire
GLASS VIEWPORT

TRITIUM GENERATION IN PALLADIUM CATHODES WITH HIGH DEUTERIUM LOADING

Fritz G. Will*
Department of Chemical and Fuels Engineering
University of Utah
Salt Lake City, UT 84112

Krystyna Cedzynska
Institute of General Food Chemistry
Technical University of Lodz
90-924 Lodz, Poland

Denton C. Linton
Department of Physics
University of Utah
Salt Lake City, UT 84112

Abstract

Tritium up to fifty times background has been observed upon electrolyzing 1N D_2SO_4 in four out of four cells when using Pd cathodes "of a certain type". No tritium was detected in four control cells, containing H_2SO_4 in H_2O, employing Pd cathodes cut from the same wire spool. Tritium amounts were from 7×10^{10} to 2.1×10^{11} atoms, corresponding to average generation rates from 1×10^5 to 4×10^5 atoms/sec/g Pd. In all cases, D/Pd and H/Pd loadings of 1 ± 0.05 were attained. A cyclic loading/unloading regime rather than the usual continuous constant current regime was applied to attain these high loadings. Tritium analysis was performed in Pd, electrolyte and the gas head space of the sealed cells. Maximum tritium concentrations of 8.9×10^{10} atoms/g Pd, 180 times the detection limit, were found in the D-loaded Pd cathodes, none in the H-loaded Pd. Also, no tritium within detection limit was found in 150 unused Pd pieces. Of these, 13 were cut randomly from the same wire spool as the four D-loaded Pd cathodes. The probability that the tritium in the latter was due to random spot contamination is computed as 1 in 2,380. It is concluded that the tritium was generated by nuclear reactions in the Pd. However,

---

* Present address: Electric Power Research Institute, Palo Alto, CA 94304

no tritium was detected in four D-loaded Pd cathodes of a different type in spite of attaining loadings D/Pd = 1. Different metallurgical history and impurity contents may play an important role.

Introduction

Low-level tritium generation during D_2O electrolysis with Pd cathodes, was first reported by Fleischmann and Pons [1], followed by many others [2], but has proven sporadic and irreproducible. It has been suggested [3] that the tritium found in these types of experiments is not due to nuclear reactions in the Pd cathodes but to spot contamination of the as-manufactured Pd. This paper reports on the results of studies aimed at (1) exploring the conditions leading to the reproducible generation of tritium, (2) minimizing the chances for accidental contamination during the experiments and (3) evaluating the statistical probability of spot contamination of the Pd prior to the experiments, that is, in their as-manufactured condition.

Experimental

All experiments were performed in tightly closed two-compartment glass cells in which the Pd cathode (wire of 2 mm diameter and 2.6 cm length) was surrounded by a fritted glass cylinder and a platinized Pt cylinder anode. A Pt-catalyzed fuel cell electrode was positioned in the gas head space above the anolyte and served as D_2-O_2 recombination catalyst. The gas spaces above anolyte and catholyte were connected with glass tubing.

The electrolytes were 1N D_2SO_4 or 1N H_2SO_4, the cathodes 99.9% pure Pd wire, as-drawn, supplied by Hoover & Strong and the gases in the pre-evacuated headspaces D_2 (0.05–0.14 nCi/l) or pre-purified H_2.

Cell temperature was maintained at 27 ± 0.02°C. Cathode and anode temperatures were monitored with thermistors, bonded to the electrodes, with a precision of ± 0.02°C. Charge and discharge currents were controlled by a precision constant current source.

A volumetric technique, using water-filled manometers to measure the occluded D_2 or H_2 volume [4,5], was employed to determine the D/Pd or H/Pd loading ratio continuously to a precision of ± 0.05. Tritium analysis was performed with a Beckman LS 5000 TD liquid scintillation counter with a sensitivity of 1×10^7 tritium atoms [6]. Pd was analyzed for tritium, employing an acid digestion technique, followed by distillation and catalytic hydrogen isotope oxidation in a closed system [7].

The following experimental procedure was employed: two cells, one containing 1N D_2SO_4 and the other 1N H_2SO_4 as a control, were always run in one experiment at the same time in electrical series connection. Four experiments, lasting from 164 to 484 hours, were conducted. All eight Pd cathodes of 2.6 cm length each were cut randomly from the same spool of 2 mm diameter wire and 60 cm total length. Nine control pieces of ~3 mm length each were also cut from the same spool, with locations adjacent to the Pd cathodes, and analyzed for tritium in their

as-manufactured state. The Pd cathodes were palladized (~1 μm Pd black layer) and gas-preloaded in 1 atm D_2 or H_2 gas, just prior to starting electrolytic loading with D or H. The D_2 gas in the head space and the electrolyte (D_2SO_4 and H_2SO_4) were analyzed for tritium before and after an experiment. Pd control pieces were analyzed before and the actual Pd electrodes after an experiment.

Results and Discussion

Hydrogen Loading

When charging Pd wires in D_2SO_4 or H_2SO_4 continuously with a constant current, loading ratios generally between 0.6 and 0.7 were observed. This is in agreement with the results of an extensive study [8] in which only 15 out of 62 experiments, spontaneously and unpredictably, yielded loading ratios close to 1.

However, when repeatedly loading (charging) and unloading Pd with low current densities, we were able to attain loading ratios of 1 ± 0.05 reproducibly on 16 out of 16 Pd electrodes [9,10]. The results of such cyclic loading are shown in Fig. 1 for the case of D and H in Pd; loading ratios of 0.96 were achieved in the seventh loading event. Unloading was performed to a cut-off cell voltage of 0.8V, thus avoiding the formation of Pd surface oxides or molecular oxygen. Also, deep discharge into the α-phase region is avoided, thereby minimizing lattice strain.

Similar results as shown in Fig. 1 were obtained in three other D_2SO_4 and H_2SO_4 cells. Saturation of the loading near values of D/Pd or H/Pd = 1 was usually observed [10].

Tritium Yield

The tritium yields for the four heavy water cells, after D_2SO_4 electrolysis with Pd cathodes, are comprised of the sum of the tritium amounts in the gas head space, the electrolyte and the Pd. The amounts in the head space is negligible, whereas the electrolyte contained between 2 and 10 times more tritium than the Pd. Electrolysis was always terminated with a charging event.

The tritium yields were found to lie in a relatively tight band from 7×10^{10} to 2.1×10^{11} tritium atoms. This corresponds to specific tritium yields from 8.4×10^{10} to 2.1×10^{11} T atoms/g Pd. No tritium was found in any of the four light water control cells, within the detection limit of the analytical method, that is, 4×10^9 T atoms. The tritium generation rates, referred to the time of D/Pd >0.8, were between 1×10^5 and 4×10^5 atoms/sec/g Pd.

Compared to our values from 8.4×10^{10} to 2.1×10^{11} T atoms/g Pd, the results of ten other groups run from about 3×10^9 to 1×10^{15} T atoms/g Pd [9], with the majority (seven groups) reporting values from about 2.5×10^{10} to 6×10^{12} T atoms/g Pd.

Tritium in Palladium and its Identification

Scintillation counting of the clear neutralized aqueous solutions, resulting from the distillation and catalytic hydrogen isotope oxidation of the acid-digested Pd [7], yielded values in the range of up to 1.6×10^{10} to 4.7×10^{10} T atoms/g dissolved Pd, compared to a detection limit of 5×10^8. T/D atomic ratios were found [9] to be 37 to 223 times larger in the metal than in the electrolyte.

If the two phases, metal and liquid, were in equilibrium, the T/D ratios would be 2 to 5 times smaller in the metal [9]. This was taken as evidence [9] that the tritium had been generated inside the Pd and had insufficient time to equilibrate with the electrolyte. These findings rule out any possibility of accidental or deliberate contamination of the electrolyte (or the gas) as source of the observed tritium.

For identification of tritium as being the source of the observed scintillation counts, beta spectra were recorded of (1) pieces of Pd cathodes after use in D_2SO_4 electrolysis; (2) a secondary tritium standard prepared in-house; and (3) a commercial tritium standard (Beckman). The secondary standard was prepared by adding 1 ml of tritiated light water (activity 1000 decompositions/min-DPM) to 10 ml scintillation cocktail (Beckman pseudocumene/xylene). The primary standard had been supplied by the manufacturer of the scintillation counter (Beckman); it consisted of a tritium-containing organic solution (toluene) of scintillation-grade fluors.

Figures 2–4 show the relevant spectra in plots of counts (detected in five-channel increments) versus channel number. The relationship

$$N = 72 + 280 \log E\ [\text{keV}] \qquad (1)$$

permits conversion from channel number N to kinetic energy of the electrons.

The standard method for identifying an unknown beta emitter from its spectrum is to determine its end point energy by producing a Fermi-Kurie plot [11] of the data and comparison with table values. For spectra obtained with scintillation counters, this technique is not reliable, due to the quenching of the electrons by the scintillation fluid. The end point energies determined from the plots in Figs. 2–4, using equ. (1), lie in the range from 17.5 to 20.6 keV (channels 420 to 440), compared with a table value of 18.6 keV. Among all known beta emitters, only Pb^{210} (15 keV) and Pu^{241} (21 KeV) have endpoint energies close to this range.

Comparison of the spectra of Pd cathodes with the spectra of tritium standards was applied in the present paper for identification of tritium in the Pd cathodes. Fig. 5 shows a superposition of the spectra of Fig. 2–4, normalized to the maximum number of counts. The maxima of the three curves for the primary standard, secondary standard and Pd cathode occur at channel numbers 238, 220 and 218, respectively, corresponding to energies of 3.9, 3.4 and 3.3 keV. There is good correspondence of the curves between secondary standard and Pd cathode. The shift of both curves toward lower energies as compared to the primary standard is caused by the additional quenching of the electrons by the 1 ml water added to the scintillation liquid. No water is present in the primary standard, hence, there is less quenching. The spectra of Pu^{241} and especially of Pb^{210} are sufficiently different from the spectra in Fig. 5 to rule out Pb^{210} with confidence and Pu^{241} with high probability as being the sources of the observed beta emission from Pd cathodes.

Probability of Accidental Tritium Contamination

To evaluate the statistical probability that the tritium observed in all four D_2SO_4 cells employing 2 mm diameter Pd cathodes from Hoover & Strong could have been caused by chance contamination of the as-manufactured Pd wire rather than by nuclear reactions in the Pd, a

number of controls from the same wire spool were also analyzed for tritium. In addition, a large number of as-manufactured Pd samples from other wire lots were analyzed.

All eight Pd cathodes (four for D_2SO_4 cells (D) and four for H_2O control cells (H)) and nine as-made Pd control pieces were cut from the same 60 cm long, 2 mm diameter Pd wire. Cathodes were about 2.6 cm, control pieces about 0.26 cm long. They accounted for a total of 23.1 cm length. D cathodes and H cathodes were always cut alternately and control pieces were always cut adjacent to the cathodes. This meant that D cathodes, H cathodes and control pieces each *originated from various parts of the wire* rather than the D cathodes all from one part, etc. This *random cutting* is important for the statistical evaluation of the analysis results.

Average tritium concentrations from 35 to 94 times the detection limit (5×10^8 atoms/g Pd) of the analytical technique was found in all four D cathodes. No tritium was found in any of the four H cathodes or in any of the nine as-made Pd control pieces. If the tritium in the four D cathodes would have been due to chance contamination of the as-received material, the probability of having selected all four correctly out of 17 Pd pieces total may be calculated by two methods, depending on the assumptions made.

If it is assumed that potential tritium contamination is uniformly distributed along the entire wire, then the chance for randomly cut pieces to contain tritium is just as large as the chance not to contain tritium. The probability of correctly predicting the presence or absence of contamination is therefore ½ for each piece, identically for all pieces. The overall probability of making all predictions correctly for 17 pieces is thus $(\frac{1}{2})^{17}$ or 1 in 131, 072.

If random spot contamination is assumed, then for the presence of four T-contaminated Pd pieces in a total of 17 pieces, the probability of selecting these four pieces in four attempts is $\frac{4}{17} \times \frac{3}{16} \times \frac{2}{15} \times \frac{1}{14}$ = 1 in 2,380.

Thus, while chance contamination of the as-made Pd wire cannot be ruled out with certainty, the likelihood that the tritium observed in the four heavy water Pd cathodes is due to chance contamination is exceedingly small.

Wolf et al. [3] reported finding tritium spot contamination in two out of 45 unused Pd pieces cut from one particular spool of as-made 1 mm Pd wire from Hoover & Strong. No tritium was found in 45 Pd pieces from a different lot of 1 mm Hoover & Strong or in 160 Pd pieces from other sources. In addition, Wolf et al. [3] reported finding tritium in 2 out of 50 LiOD and 3 out of 50 LiOH electrolytic cells. While the findings of Wolf et al. could be due to rare spot contamination of some of the as-received Pd, radioactive contamination during handling and experimentation cannot be ruled out, especially since (1) vented electrochemical cells were used which had to be topped off with D_2O daily for many weeks, (2) the tritium analysis in the Pd samples were carried out in open cells and (3) the laboratory was located near the cyclotron with a variety of radiation sources present. Concerns regarding false positive tritium readings in the open system analytical technique used have been expressed previously[6]. By comparison, our results presented here and previously [7,9], employing closed electrochemical cells and closed-system analytical techniques, show no tritium in any of 150 unused Pd samples, comprised of wires from three different manufacturers as well as several foils and powders. More than 100 Pd

samples originated from Hoover & Strong. In addition, no tritium was found in ten H_2O control cells, either in the electrolyte or in the Pd electrodes. We found tritium exclusively in the electrodes and electrolytes of four D_2O cells with highly D-loaded Pd cathodes. While rare spot contamination cannot be excluded as a possible source for the observed tritium, the probability for this is exceedingly low.

Conclusions

Tritium generation has been found in four out of four heavy water cells, employing Pd cathodes which had attained loading ratios D/Pd = 1 by applying a cyclic loading/unloading technique. The tritium concentrations ranged up to 50 times background in the electrolyte and up to 180 times in the Pd cathodes. No tritium was found in light water control cells or in a large number of unused Pd samples. Tritium was identified as such by analyzing the beta emission spectra and comparing them to controls. Four heavy water cells with Pd wires from a different supplier showed no tritium. This may be due to the different impurity content and metallurgical history. Statistical evaluation of the data yields a probability of only 1 in 2,380 that the observed tritium is due to random spot contamination rather than to nuclear reactions in the highly D-loaded Pd cathodes. While the type of nuclear reactions resulting in the observed tritium is as yet unknown, cold fusion of deuterium atoms in the Pd lattice has to be ruled out due to the observation of a very small neutron signal[12].

Acknowledgments

The authors acknowledge the help of X. Du, J. Yuan, B. Namski and J. Peterson in the tritium analysis and the financial support of the State of Utah.

References

1. M. Fleischmann, S. Pons and M. Hawkins, "Electrochemically Induced Nuclear Fusion of Deuterium", *J. Electroanal. Chem.*, Vol. 261, p. 301 (1989); errata, Vol. 263, p. 187 (1989).

2. E. Storms, "Review of Experimental Observations About the Cold Fusion Effect", *Fusion Technol.*, Vol. 20, p. 433 (1991).

3. K.L. Wolf, L. Whitesell, H. Jabs and J. Shoemaker, "Tritium and Tritons in Cold Fusion", AIP Conference Proceedings "Anomalous Nuclear Effects in Deuterium/Solid Systems", Provo, UT, 1990, p. 552.

4. R. Clamroth and C.A. Knorr, "Ueber die verschiedenen Anteile der Wasserstoffueberspannung an Palladium", *Z. Elektrochem.*, Vol. 57, p. 399 (1953).

5. A.M. Riley, J.D. Seader, D.W. Pershing and C. Walling, "An In-Situ Volumetric Method for Dynamically Measuring the Absorption of Deuterium in Palladium During Electrolysis", *J. Electrochem. Soc.*, Vol. 139, p. 1342 (1992).

6. K. Cedzynska, S.C. Barrowes, H.E. Bergeson, L.C. Knight and F.G. Will, "Tritium Analysis in Palladium with an Open System Analytical Procedure", *Fusion Technol.*, Vol. 20, p. 108 (1991).

7. K. Cedzynska and F.G. Will, "Closed-System Analysis of Tritium in Palladium", *Fusion Technol.*, Vol. 22, p. 156 (1992).

8. A.M. Riley, J.D. Seader, D.W. Pershing, D.C. Linton and S Shimizu, "Measurement of Absorption of Deuterium in Palladium During Electrolysis of Heavy Water", Final Report, National Cold Fusion Institute, Univ. of Utah, Vol. 2, p. 2–135, June 1991.

9. F.G. Will, K. Cedzynska and D.C. Linton, "Reproducible Tritium Generation in Electrochemical Cells Employing Palladium Cathodes with High Deuterium Loading", *J. Electroanal. Chem.*, Vol. 360, p. 161 (1993).

10. K. Cedzynska, D.C. Linton and F.G. Will, "Method for Consistent Reproduction of High Deuterium Loading and Tritium Generation in Palladium Electrodes", U.S. Patent Application, U-1967, Nov. 12, 1991.

11. G. Friedlander, J.F. Kennedy and J.M. Miller, "Nuclear and Radiochemistry", John Wiley & Sons, New York, 1981, pp. 239–53.

12. F.G. Will, K. Cedzynska, M.-C. Yang, J.R. Peterson, H.E. Bergeson, S.C. Barrowes, W.J. West and D.C. Linton, Proc. 2nd. Annu. Conf. on Cold Fusion, Italian Nuclear Society, Como, Italy, June 29-July 4, 1991, p. 373.

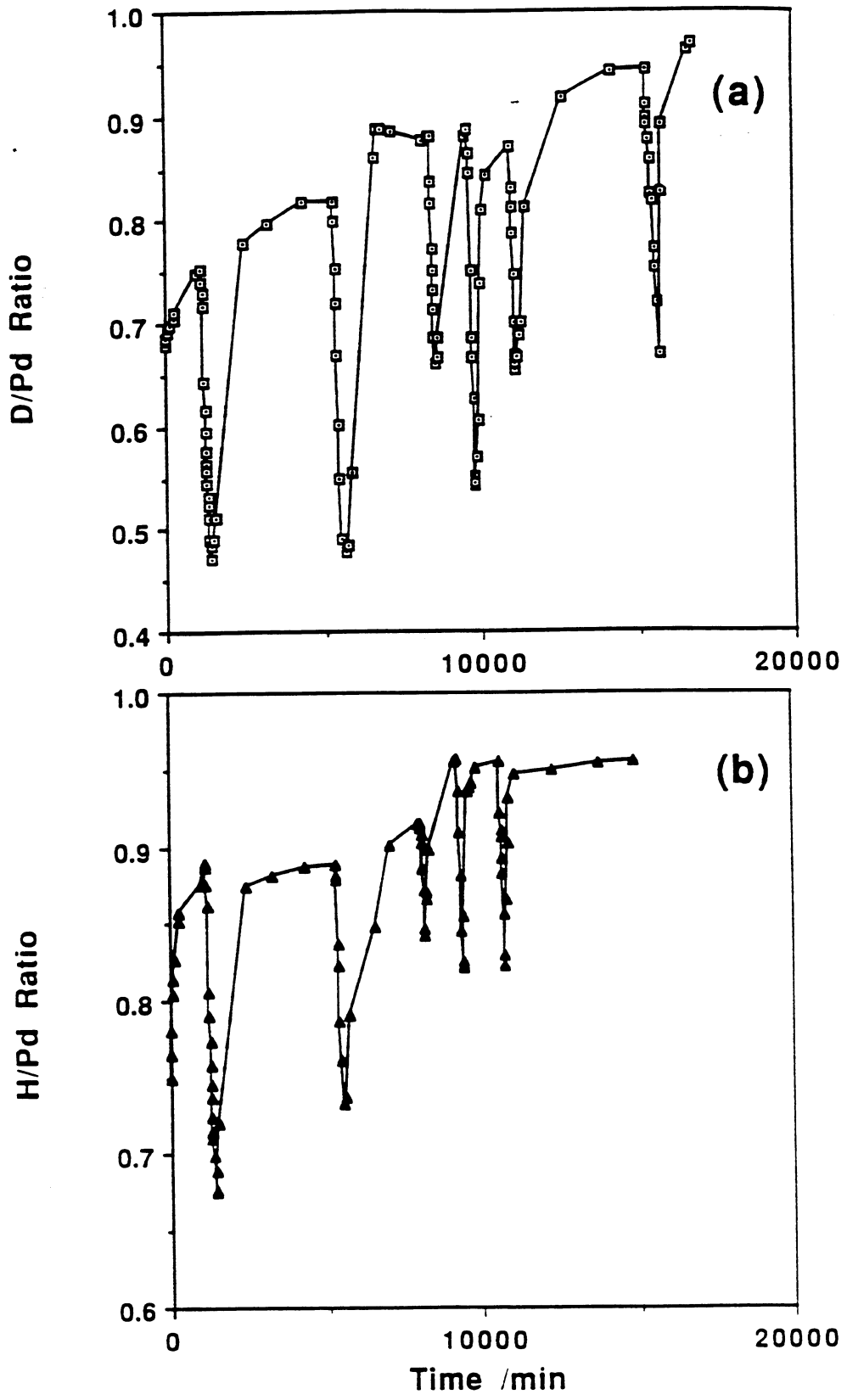

Fig. 1. D/Pd (a) and H/Pd (b) loading ratio as a function of time. Charging with 10 to 30 mA; discharging successively at 30, 20 and 10 mA. Electrode area ~2 sq cm.

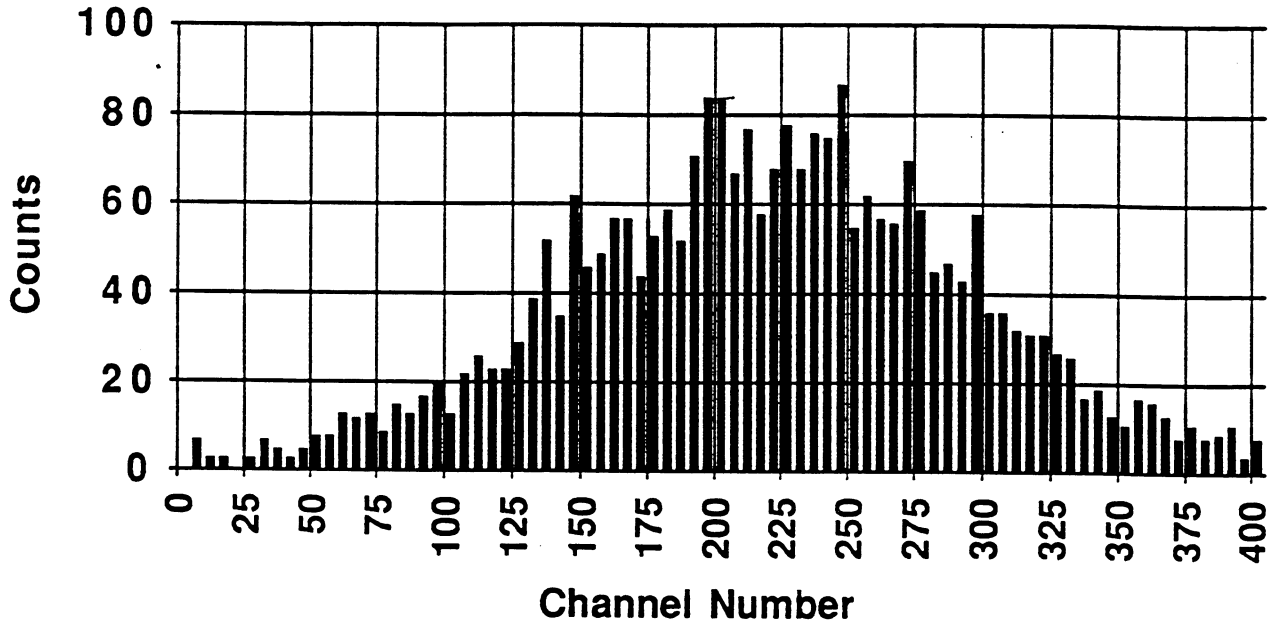

Fig. 2. Beta spectrum of Pd cathode piece after D_2O electrolysis and application of closed-system analytical method [6]. Ordinate: Incremental counts per 5-channel interval in 20 minutes.

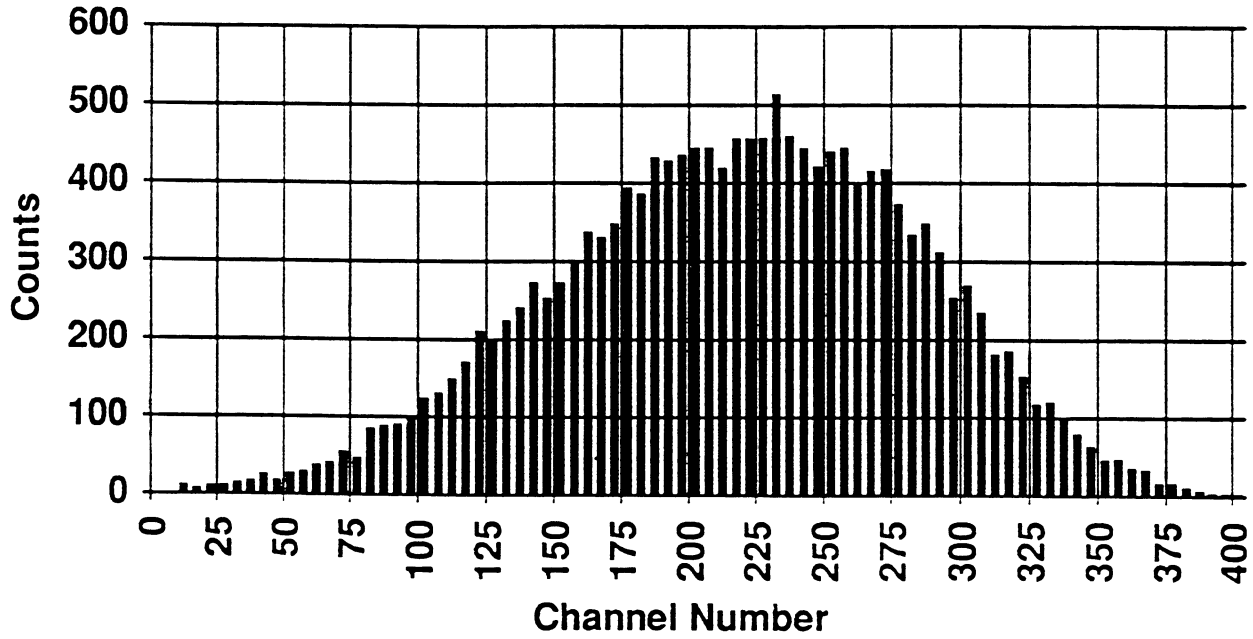

Fig. 3. Beta spectrum of secondary tritium standard: Tritiated H_2O (1000 dpm) in Beckman scintillation cocktail. Ordinate: Counts per 5 channels per minute.

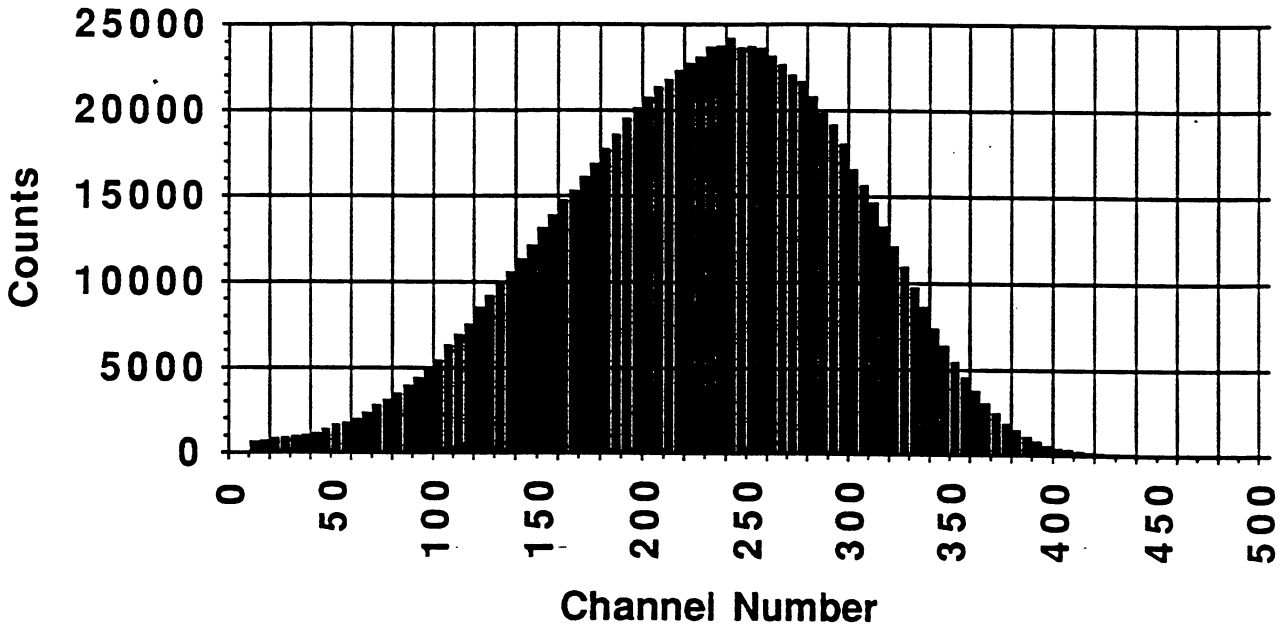

Fig. 4. Beta spectrum of water-free primary tritium standard supplied by Beckman. Ordinate: Counts per 5 channels per minute.

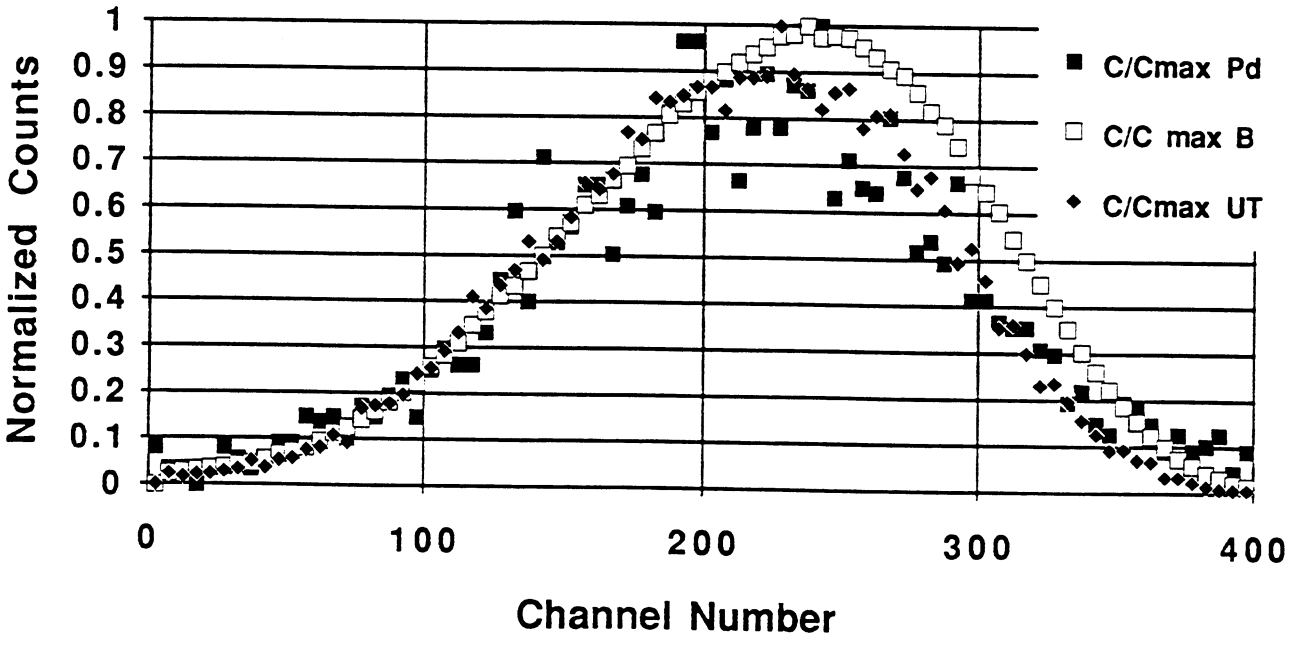

Fig. 5. Beta spectra of Pd cathode piece, primary (B), and secondary (UT) tritium standard, normalized to maximum number of counts.

COLD FUSION BY SPARKING IN HYDROGEN ISOTOPES. ENERGY BALANCES AND SEARCH FOR FUSION BY-PRODUCTS. A STRATEGY TO PROVE THE REALITY OF COLD FUSION

by
J.Dufour
SRSA/CNAM 292 Rue St Martin
75003 Paris FRANCE

J.Foos
CNAM 292 Rue St Martin
75003 Paris FRANCE

J.P.Millot
CNAM 292 Rue St Martin
75003 Paris FRANCE

NOVEMBER 29, 1993

Abstract

A strategy is proposed to firmly establish the reality of cold fusion. This strategy is based on a simple hypothetical mechanism that could trigger these reactions : 3 body collisions (through the formation of virtual poly-neutron states), between an hydrogen isotope, an electron and a third nucleus (a second hydrogen isotope or a nucleus present in the host metal).

The consequences of possible successive reactions of that type have been examined. The conclusion of this analysis is that a variety of nuclear ashes can be expected, most of them having already been identified experimentally. The drawback is that they may appear in small quantities and in rather great number, rendering their detection difficult. It thus seems necessary to have an experiment yielding a sufficiently high level of excess energy, so as to use detection methods well above their limits.

We propose to use a reactor (based on ozoniser type discharge) able to generate an excess power of tens of watt on several weeks. Experimental results are given, on preliminary trials with the ozoniser type of discharge.

Nuclear ashes detection methods are proposed, that meet the required signal/noise ratio

Introduction

Proving the reality of a new phenomenum is not an easy task. On the one hand, the enthousiasm of the pionneers can lead to over selling and excess of imagination. On the other hand, the rigour that is necessary in all scientific field, can lead to the undue rejection of a major discovery. One of us[1], has been active since the beginning, in the so-called "cold fusion" field and has experienced for several years these 2 conflicting but complementary tendancies. Patents were filed by the company he is working for (Shell), because the technical approach proposed was original and because Shell is acting in the field of energy.

But, at a certain moment in time, it became apparent that the only way of getting a sound evaluation of the interesting results obtained, was to involve critical but objective and open-minded scientists, experts in the fields relevant to "cold fusion". After some unsuccessful trials, such a team of scientists was found in the "Conservatoire National des Métiers" (CNAM) and a research agreement was signed between the CNAM and Shell. The research work (financed by Shell) is thus now carried out in the CNAM. This paper presents the strategy that has been jointly defined and gives indications on some preliminary results.

How to prove the reality of cold fusion

Cold fusion will became a reality, only when it will be recognized as such by the scientific community and for that, we think 3 conditions are required :

1. The excess energy production must be reproducible, of long duration (weeks) in a steady state situation and able to generate an excess power of sufficient size (tens of watt).

2. A possible and plausible nuclear reactions scheme has to be proposed, that explains experimental facts already observed.

3. The products of these reactions (nuclear ashes) have then to be traced, taking into account possible artifacts and eliminating them. As there seems to be a great variety of these products but at low concentrations, a high excess energy production is needed to have measurements well above the detection limits of the analytical methods used.

When this nuclear ashes hunting has proven successful, the theory of the phenomenum can be improved on a reliable basis, but cold fusion is then already accepted as a reality.

We shall describe how we are planning to try to meet these three conditions, first recalling some main characteristics of the technical approach we follow.

Main features of the "High transient electrical field" approach

As explained[1], we think that "cold fusion" reactions in hydrogen loaded metals are triggered by high transient electrical fields that develop in these metals under various electrical situations. Sparks, ozoniser discharges and high current density pulses in hydrogen loaded metals can create these situations [1,2,3].

Sparks and ozoniser discharges also generate high amounts of atomic hydrogen, able to locally increase the hydrogen/metal ratio. We shall give some new results obtained with ozoniser discharges that are likely to be easier to upscale than spark discharges and could thus answer point 1 of our strategy.

Results with ozoniser type discharge. Excess power increase

The so-called ozoniser type discharge, occurs at high gas pressures (1 bar and higher), when an AC high voltage is set between two metal electrodes, isolated by dielectric barrier(s). When two dielectric barriers are present (one on each electrode), the discharge never sees the metal electrodes. We shall call this situation double barrier ozoniser discharge. When only one dielectric barrier is present, the discharge is very comparable, but sees one metallic electrode. We shall call this situation single barrier ozoniser discharge. The difference between double and single barrier ozoniser, thus allows a comparison to be made between two similar discharges in an hydrogen isotope, the former seing no metal electrode and the latter one.

The macroscopic aspect of this ozoniser type of discharge is different from a spark discharge and looks like a low pressure glow discharge. But on the microscopic scale, the ozoniser discharge consists of a great number of very small sparks, the development of which to full scale sparks, being prevented by the presence of the dielectric barrier(s). They thus, also cause high current densities at there impact on a metal electrode (when it is present).

The calorimetric equipment previously described[1] was used to study these two types of ozoniser discharge. The reactor was slightly modified (see Fig.1 and Fig.2) and the ozonizer built around a 4 cm diameter pyrex tube welded to the upper part of the reactor. The outer electrode was made from a copper foil. When the single barrier ozoniser was used, the inner electrode was a palladium cylinder, (10 mm diameter, 23 mm height and 0.5 mm thick) supported by a stainless steel electrode holder. When the double barrier ozoniser was used, the palladium tube was removed and a pyrex tube (1cm diameter and 10 cm long) was placed on the stainless steel electrode holder, acting as the inner electrode (see Fig.1 and 2). In order to prevent any possible ozoniser discharge to take place between the outer copper electrode and the metallic surroundings of the

reactor, and thus influencing the results, the part of the reactor outside the 4 cm pyrex tube was filled with air. It was carefully checked that the reactor so modified had the same thermal behaviour as the previous one. Several calibrations yielded the same calibration curve as for the spark approach[1], and this was true whether the reactor was filled with hydrogen or with air (due to the position of the calibration resistance, the heat losses through the electrode holder are in both cases very comparable).

Three experiments were run using deuterium and palladium as the metal electrode in a single barrier ozoniser discharge and 4 were run using deuterium in a double barrier ozoniser discharge. Each experiment was run after the calorimetric system had reached a complete steady state. Their duration varied between 48 and 72 hours.The results are given in the following table :

	Single barrier ozon.		Double barrier ozon.	
	Power in React. (w)	Excess Pow out (w)	Power in React. (w)	Excess pow out (w)
	3.00	1.62	2.46	0.21
	3.67	1.84	2.75	0.43
	2.66	2.75	2.94	0.54
			2.75	-0.90
Mean value	3.11	2.07	2.73	0.07
Stand.dev.	0.42	0.49	0.17	0.57

From these datas, it can be concluded that the excess power production is significantly higher for the single barrier discharge than for the double barrier one and that for the latter, the excess power production is very close to 0. Thus, under essentially similar discharges conditions in the deuterium gas, excess power is only produced when palladium is in contact with the discharge. The reaction yielding the excess power is thus likely to take place in the palladium.

We are planning to use this type of discharge to increase the excess power generation (to tens of watt), as it is likely to be easier to upscale than the spark discharge.

Possible nuclear reactions scheme

The standard model of the sun, includes a 3 body reaction between 2 protons and an electron, yielding deuterium with the emission of a neutrino :

$$(1) \qquad {}_1{}^1H + {}_1{}^1H + e^- = {}_1{}^2H + \nu$$

The coulomb barrier problem is solved by the presence of the electron, giving a virtual neutron state with one proton, which can react with the other proton; the rate of this reaction is very low under the sun conditions. Reaction (1) was envisaged[4], as an alternative hypothesis to the TRM model. We had proposed[1], that this reaction could be the prototype of possible successive 3 body reactions between an hydrogen isotope, an electron and a second hydrogen isotope or a nucleus present in the metal. We have taken into account those reactions that are exothermal, which is the case of the great majority of them. These reactions have the four main following features :

1. The Coulomb barrier is avoided by an indirect transition of second order approximation.

2. The daughter nucleus is neutron rich and, if unstable, will preferentially stabilize through beta- emission.

3. The final products of the reactions are likely to be complex mixtures resulting from the various possible (and successive) reactions between hydrogen isotopes and their corresponding virtual neutron states. Because of the successive reactions occuring, the composition of these mixtures is likely to be very dependent on the time of sampling in the course of an experiment. Besides, other nuclei present in the metal can react with virtual neutron states.

4. Most of the fusion energy released is carried away by neutrinos and is thus definitively lost. Only the recoil energy of the daughter nuclei is left in the reactor (together with the energy resulting from the possible subsequent nuclear deactivation of these daughter nuclei when they are instable).

We have analysed in detail the consequences of the successive reactions scheme presented[1], and arrived at the conclusions that will now be described.

Hydrogen chain

Starting from hydrogen, the sequence we envisage is :

(1) $\quad {}_1{}^1H + {}_1{}^1H + e^- = {}_1{}^2H + \nu$

(2) $\quad {}_1{}^1H + {}_1{}^2H + e^- = {}_1{}^3H + \nu$

(3) $\quad {}_1{}^1H + {}_1{}^3H + e^- = {}_1{}^4H + \nu$

(3') $\quad {}_1{}^2H + {}_1{}^2H + e^- = {}_1{}^4H + \nu$

(4) $\quad {}_1{}^2H + {}_1{}^3H + e^- = {}_1{}^5H + \nu$

In these reactions, virtual neutron ($_1{}^1H + e^-$), di-neutrons ($_1{}^2H + e^-$), or tri-neutrons ($_1{}^3H + e^-$) states can be formed, that can react with any hydrogen isotope. $_1{}^4H$ and $_1{}^5H$ are hypothetical hydrogen isotopes of very short life time. A life time of 10^{-17} s has been measured for $_1{}^4H$. $_1{}^5H$ is not known experimentally.

The final product of reactions (1) to (4) is thus $_2{}^4He$, $_1{}^2H$ and $_1{}^3H$ being intermediate products, likely to be found in very small amounts (determined by the relative rates of the successive (1) to (4) reactions). $_2{}^3He$ should be present in even smaller amounts, being produced during the beta decay of $_1{}^3H$ formed by reaction (2). Note that small variations in the yields of intermediate products, could be caused by the deuterium always present in hydrogen samples.

Reaction (4), although likely to yield only small amounts of $_1{}^5H$, is of interest in that sense it can rationnalize a (small) production of neutrons through the reactions :

$$(5) \qquad {}_1{}^5H = {}_2{}^5He + \beta^- + \bar{\nu}$$

$$(6) \qquad {}_2{}^5He = {}_2{}^4He + {}_0{}^1n$$

The amount of energy released by the sequence of reactions (1) to (4), comprises the recoil energy of the daughter nuclei of these reactions and their decay energy when this decay is of short half-life (short compared to the duration of the experiment). Likely to be in this category are reactions (5) and(6) together with(7), the beta decay of $_1{}^4H$ formed in (3) :

$$(7) \qquad {}_1{}^4H = {}_2{}^4He + \beta^- + \bar{\nu}$$

Reaction (7) should have a very short life time, so the detailled steps of the overall reactions (3_T) and ($3_T'$) involving $_1{}^4H$, would have to be elucidated and the repartition of the total energy released (some 20 MeV), between the daughter nucleus, the neutrinos and the beta emitted should be determined and a theoretical explanation should be given:

$$(3_T) \qquad {}_1{}^1H + {}_1{}^3H + e^- = {}_2{}^4He + \beta^- + \nu + \bar{\nu}$$

$$(3_T') \qquad {}_1{}^2H + {}_1{}^2H + e^- = {}_2{}^4He + \beta^- + \nu + \bar{\nu}$$

The sequence (4), (5) and (6) should also be very fast and the amount of energy deposited in the reactor by the overall reaction (4_T) should be determined :

$$(4_T) \qquad {}_1{}^2H + {}_1{}^3H + e^- = {}_2{}^4He + \beta^- + \nu + \bar{\nu} + {}_0{}^1n$$

The conclusion on the hydrogen chain is that the part of the energy staying in the reactor is likely to be several MeV, mainly coming from reactions (3_T) and ($3_{T'}$).

Deuterium chain

Should absolutely pure deuterium be used, only the overall reaction ($3_{T'}$), would take place:

$$(3_{T'}) \quad {}_1{}^2H + {}_1{}^2H + e^- = {}_2{}^4He + \beta^- + \nu + \bar{\nu}$$

But, as hydrogen together with tritium are always present, in varying amounts, in any deuterium sample, we should expect all (1) to (4) reactions to take place, yielding similar products pattern as the hydrogen chain, with minor variations in the yields (depending on the exact composition of the sample processed).

The energy left in the reactor by reaction ($3_{T'}$) should also be the major part of the energy released by the deuterium sequence.

Thus hydrogen and deuterium should yield comparable amounts of energy.

Reactions between virtual neutron states and nuclei present in the metal lattice

Many reactions of virtual neutron states can be envisaged, either with nuclei trapped in the lattice (such as He or K for instance), or with the host metal itself (palladium, nickel ...). We shall give some examples of the 2 categories.

Reactions with nuclei trapped in the metal lattice.

- The first example is the reaction with He. ${}_2{}^4He$ being the end product of reactions (1) to (4), builds up in the metal lattice during the course of an experiment. Such reactions as the following, can thus take place :

$$(9) \quad {}_1{}^2H + {}_2{}^4He + e^- = {}_2{}^6He + \nu$$

followed by : $$(10) \quad {}_2{}^6He = {}_3{}^6Li + \beta^- + \bar{\nu}$$

prototype of reactions which would rationalize Lithium production, that can become important as the experiment lenghthens and can decrease the final amount of He. (Note that the corresponding reaction to (9) with ${}_1{}^1H$ is endothermal). This production of ${}_3{}^6Li$ might alter the isotopic ratio of Lithium present in palladium.

- The second example is the reaction with K, which we choose because it can rationnalize results obtained in [4,5]. Reactions with K trapped in a nickel lattice can be :

$$(11) \quad {}_1{}^1H + {}_{19}{}^{41}K + e^- = {}_{19}{}^{42}K + \nu$$

(12) $$ {}_1{}^{2}H + {}_{19}{}^{40}K + e^- = {}_{19}{}^{42}K + \nu $$

(13) $$ {}_1{}^{3}H + {}_{19}{}^{39}K + \bar{e}^- = {}_{19}{}^{42}K + \nu $$

followed by:

(14) $$ {}_{19}{}^{42}K = {}_{20}{}^{42}Ca + \beta^- + \bar{\nu} $$

which explains the appearance of Ca in experiments above mentionned.Other reactions between virtual neutron states and potassium isotopes would yield stable potassium isotopes, altering the isotopic composition of the potassium.

Reactions with the host metal itself.
Virtual neutron states can also react with the host metal itself, according to the following general reaction scheme:

(15) $$ {}_1{}^{n}H + {}_Z{}^{A}Me + e^- = {}_Z{}^{A+n}Me + \nu $$

where n = 1,2 or 3.

(15) is, in due case, followed by the nuclear decay of ${}_Z{}^{A+n}Me$, which can, depending on Me, yield a variety of nuclear decay types (EC, IT or beta- emission). Isotopic variations in the metal composition can also be observed, together with the appearance of new nuclei. As an exemple, the case of palladium is given in Table 1.

Conclusion on the proposed nuclear reactions scheme.
If the concept of virtual neutron states (hydrogen isotopes + electron) is accepted, most of the experimental observations made so far in cold fusion can be rationalized, by considering successive reactions between them and other nuclei. It is thus of great interest to firmly and quantitatively trace all the by-products obtained. The analysis we have made above shows that it is a difficult task. This is why we think it absolutely necessary to run experiments with a sufficiently high excess energy production (at least 10 watt) and of long duration, in order to obtain signals well above the background and to be able to study the changes of by-products pattern with the evolution of the experiment in time.

When we succeed in this approach, some modifications in the theory might be necessary to justify the reaction rates that are required to fit the experimental datas. Such a modification has been proposed[6] (the neutrino should have a mass round 0.1 eV). Should this explanation be correct, a modification of the theory on a very precise point, that has so far never been proven experimentally (the zero mass of the neutrino), would allow the rationalization of cold fusion (not to speak of other important and currently unsolved problems).

Tracing nuclear by-products
In order to start with a simple case, we have chosen to first run experiments with hydrogen ($_1{}^1H$) and palladium (Johnson Matthey, Grade 1 , foils 0.5 mm thick, that are formed in a cylinder fitting the electrode holder).

As a step between the current level of excess power (1 to 2 watt) and the high excess power ozoniser type of reactor that is under study, we are increasing the excess power of our present reactor[1] to 6/8 watt (by minor modifications on the electrical alimentation).

Starting from palladium electrodes that have been activated by sparking for periods varying from 5 days to 4 weeks, following investigations are in progress or in preparation

Information on active species present in the reactor just atfer activation by sparking
We described[1] observations of low intensity currents passing through the gaseous gap between the electrodes, when these electrodes were polarized by a DC voltage, after cut-off of the AC voltage that had generated the sparks during the activation period.

We have analysed (oscilloscope Philips PM 3320A) this current, that stabilizes after 5 to 6 days to a steady state value.For a DC polarization voltage of 3500 V, it is composed of pulses, with frequency 2 to 3 Hz and electrical charge 0 to 10^{-11} Coulomb/pulse. These pulses have a time constant of the same order as the RC constant of the circuit we use (0.15 ms).

We have started the analysis of the repartition in amplitude of these pulses, using a TMCA2 Card and associated software (Aries Target System Electronic). First results are encouraging, since the spectrum obtained shows characteristics of a beta- spectrum. Before any firm conclusion can be drawn, following steps have to be achieved :

1. Calibrating the reactor/counter which we plan to do by introducing a $_{48}{}^{109}Cd$ source close to the electrodes.

2. Checking the influence of the hydrogen pressure in the reactor and/or of the polarization voltage.

3. Checking the influence of possible air leakage into the reactor.

4. Running blank experiments using fresh hydrogen and virgin electrodes (this experiment yields a zero current value and no pulses should appear, except electronic noise).

5. Running blank experiments using fresh hydrogen and the electrodes having been used for the activation, to

eliminate spurious peaks that could be due to a modification of the electrodes by the sparks.

If we can confirm by another analysis (see below), that the spectrum we observe with the reactor/counter, after stabilisation, is indeed tritium, this will validate this way of counting and we shall use it to identify short life species that seems to be present just after sparking cut-off (e.g active Pd isotopes, see table 1) and that would otherwise be difficult to identify.

Tritium, helium and lithium measurement

Two ways are implemented to measure tritium, helium and lithium that may be present in the palladium electrodes after an experiment:

1. The electrode will be melted, by induction heating in an alumina crucible contained in a silica tube, through wich a flow of oxygen will be passed. The resulting water (and tritiated water), will be trapped in a liquid nitrogen trap. The remaining oxygen containing helium, will then be analysed by GC/MS to identify helium. This type of analysis is likely not to see lithium.

2. The electrode will be melted in a tungsten crucible by an electron beam under ultra-high vacuum and the gases will be analysed by high resolution mass spectrometry. The presence of lithium might be detected by this approach.

Neutron measurements

In experiments were activation of the electrode is done by sparks, we shall use a track-etching method as described[1], in order to avoid perturbations due to the sparks.

In experiments using the ozoniser discharge approach, we shall use a BF_3 proportionnal counter, as electrical perturbations are likely to be very low with this type of discharge.

Detection of products resulting from reaction of virtual neutron states with the host metal

As these products are likely to be in trace amounts (except for very long duration experiments), we are planning to identify them by the method described above (information on active species present in the reactor)

For those products that would seem to be in measurable amounts, methods such as SIMS, XPS or microprobe with electron microscopy, will be tried.

Conclusion

The strategy we propose to prove the reality of cold fusion, is based on 2 simple hypothesis, which, for the time being, we postulate, without trying to give any in depth theoretical justification:

1. Virtual neutron (and poly-neutrons) states ($_1{}^nH + e^-$) can be formed, having a sufficient life time to react with a nucleus present in the metal and then giving an overall exothermal reaction.

2. Successive and fast reactions can take place between these virtual neutron (and poly-neutrons) states and the daughter nuclei of previous reactions and/or nuclei present in the metal.

Taking into account these 2 simple hypothesis, allows a rationalization of most of the experimental facts found in cold fusion:

- low amounts of tritium, neutrons and $_2{}^3He$
- variable amounts of $_2{}^4He$
- appearance of "transmuted nuclei" : Ca from K, Sr from Rb, Li, isotopic variations in metal ...

When we succeed in correctly identifying all by-products formed, it will remain to explain in details the formation of virtual neutrons states and the way that part of the energy released by the reactions is left in the reactor.

If all this is an indication of the huge potentialities of cold fusion, it also shows the problems we are faced with to prove its reality.

We wish this paper can be a contribution to this difficult but fascinating and firing with enthusiasm task.

References

1. J.Dufour, "Cold fusion by sparking in hydrogen isotopes," *Fusion Technology*, 24, 205, (1993)

2. J.Dufour, "Energy Source System," Patent application WO91/01036 (1991).

3. J.Dufour, "Energy Source System II," Patent application T6176EPC, filed 26/10/1992.

4. R.T. Bush, "A light water excess heat reaction suggests that "cold fusion" may be "alkali-hydrogen fusion"," *Fusion Technology*, 22, (301), (1992)

5. R.Notoya, "Cold fusion by electrolysis in a light water-potassium carbonate solution with a nickel electrode," *Fusion Technology*, 24, 202, (1993)

6. J.Russel, "Virtual Electron Capture in Deuterium," *Ann. Nucl. Energy*, 18, 2, 75 (1991)

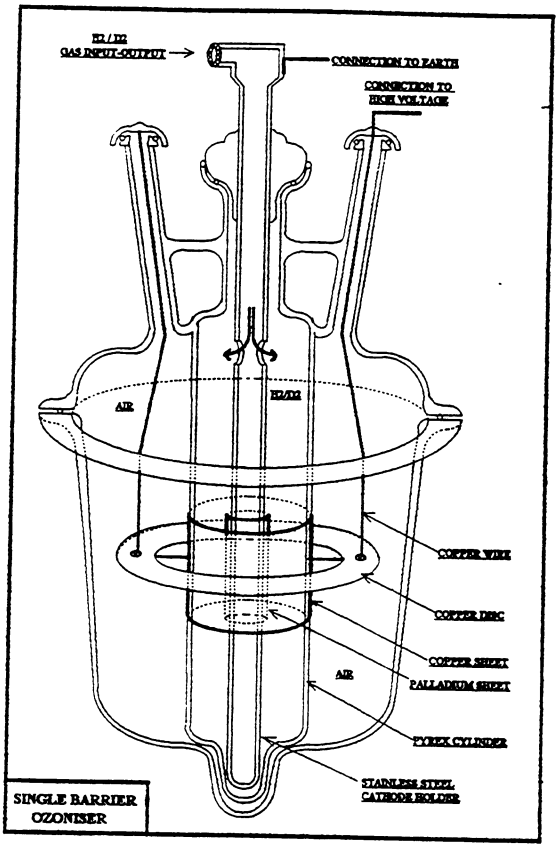

Figure 1

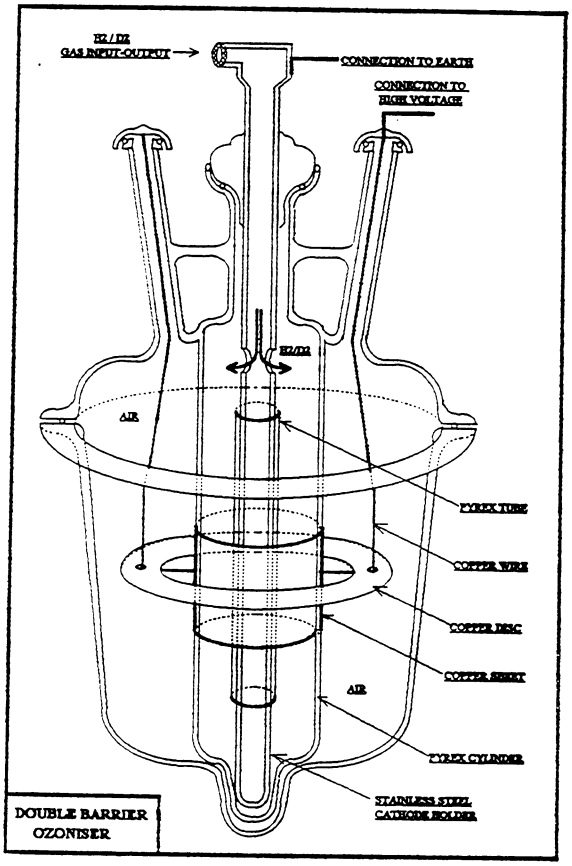

Figure 2

TABLE 1

Possible reactions of $^{1}_{1}H + e$ with PALLADIUM isotopes

Atomic mass A	Isotopes	Abundance (%)	Energie of ❶ (MeV) ❶ $^{A-1}_{46}Pd + ^{1}_{1}H + e \rightarrow ^{A}_{46}Pd + \nu$	Recoil energy of ❶ (KeV)	Decay of daughter nuclide from ❶			
					Energy (Kev)	Type	1/2 life	Final product
102	$^{102}_{46}Pd$	1.02						
103	$^{103}_{46}Pd$		6.08	0.77	576	EC	16.97 days	$^{103}_{45}Rh$
104	$^{104}_{46}Pd$	11.14	9.27	1.77		STABLE		
105	$^{105}_{46}Pd$	22.33	6.34	0.8		STABLE		
106	$^{106}_{46}Pd$	27.33	8.82	1.57		STABLE		
107	$^{107}_{46}Pd$ m		?	?	215	IT	20.9 sec.	$^{107}_{46}Pd$
107	$^{107}_{46}Pd$		?	?	33	β^-	$6.5\ 10^6$ years	$^{107}_{47}Ag$ (IT)
108	$^{108}_{46}Pd$	26.46	?	?		STABLE		
109	$^{109}_{46}Pd$ m		?	?	189	IT	4.68 min.	$^{109}_{46}Pd$
109	$^{109}_{46}Pd$		5.41	0.57	1116	β^-	13.47 hours	$^{109}_{47}Ag$ (IT)
110	$^{110}_{46}Pd$	11.72	8.04	1.26		STABLE		
111	$^{111}_{46}Pd$ m		?	?	172	IT	5.5 hours	$^{111}_{46}Pd$
111	$^{111}_{46}Pd$		4.99	0.47	2200	β^-	22 min.	$^{111}_{48}Cd$ (IT, β^-, IT)
112	$^{112}_{46}Pd$		7.63	1.11	290	β^-	21.03 hours	$^{112}_{48}Cd$ (β^-, β^-)

NEUTRON TRANSFER REACTIONS

Peter L. Hagelstein and Sumanth Kaushik

Massachusetts Institute of Technology
Research Laboratory of Electronics
Cambridge, Massachusetts 02139

ABSTRACT

A new model is proposed to treat configuration mixing between bound and continuum neutron states in a lattice; the Hamiltonian for this model is of the form of the Anderson Hamiltonian. In condensed matter physics, the Anderson model describes (among numerous other effects) electron hopping in semiconductors; the neutron model presented here predicts neutron hopping in lattices containing a mixture of isotopes. This result is new.

The Anderson model treats the mixing between localized states embedded in a continuum. In the neutron model, the localized states are energetically far removed from the continuum; consequently, the neutron model treats a much simpler mathematical problem.

Brillouin-Wigner theory is applied to a restricted Fock space version of the model containing states with 0 and 1 neutrons free. This leads to perturbative results that describe the effects of continuum neutron mixing to lowest order. The resonant scattering of virtual neutrons is predicted to lead to neutron delocalization, as long as the interaction perturbs either the linear momentum or total angular momentum of the nucleons.

Delocalized neutrons can be captured, with the reaction energy going into gammas and other incoherent decay products; such reactions are predicted by this model. Delocalized neutrons can be captured accompanied by energy exchange with the lattice. Formulas describing this type of reaction are derived, and the resulting rates estimated.

1. Introduction

During the last several years, there have been numerous reports of the observation of excess heat in electrochemical experiments following the initial announcement by Pons and Fleischmann of the

effect in 1989.[1–4] The magnitude of the claimed effect is very large, with net energy production in some experiments reported to be in excess of 100 eV per atom of cathode material. This level of excess energy cannot be of chemical origin; if it is correct, then it must be due to a nuclear process.

These experiments have proven to be difficult to verify, and there is doubt on the part of most members of the scientific community as to whether there even exists an effect. Theoretical arguments given early on as to what the origin of the effect might be were easily dismissed. The seeming absence of any compelling theoretical reason as to why there should be any effect at all, together with the rather poor signal to noise ratio of the initial experimental data, combined with the seeming irreproducibility of the effect, has led to the general rejection of the effect outright by the scientific community. Noted skeptics are now quick to bring up the topic of UFOs when discussing research on the Pons-Fleischmann effect.

The question of whether or not there is an effect is ultimately an experimental one; clearly the work reported here was motivated towards seeking theoretical explanations of the effect under the assumption that an effect exists. Hopefully, the experimental issues will be settled soon, although it is clear that the work is hard and progress has been slow.

When the effect was first reported, there were speculations as to possible origins of the effect. Most speculations centered around the possibility that *dd*-fusion was somehow responsible for the heat. The fusion of deuterons in quantities commensurate with the claimed heat production would lead to large tritium production and lethal neutron generation rates; neither is observed in the experiments. Even now, the majority of theorists who continue to work in this area are focusing their attentions on fusion mechanisms, for explaining heat or other effects.[5–7] Some popular current proposed explanations postulate that a new fusion channel exists that leads to ^{4}He production, with the energy excess going into the lattice.

We have focused instead on novel reaction mechanisms involving the proposed exchange of neutrons between distant nuclei in a lattice.[8–10] The basic proposed effect is a neutron analog of electron hopping in semiconductors, with energy exchange with the lattice taking place through the frequency shifting of highly excited phonon modes; this mechanism will be discussed in the present work, and discussion of lattice energy transfer appears elsewhere.[8–11]

There are two principal difficulties in the proposal of neutron transfer reactions as a candidate reactions to account for heat production. The neutron transfer was proposed to take place through virtual neutron states, and it is well known that the range of virtual neutrons near an isolated nucleus is measured in fermis rather than Angstroms; this is the first difficulty. Virtual neutrons must somehow be delocalized before any reactions can take place. Last year we noted that delocalization can be induced through scattering, we evaluated delocalization effects due to Bragg scattering; we also proposed that resonant scattering of virtual neutrons might lead to observable

effects. We proposed last year[10] that the resonant scattering be mediated through electromagnetic interactions; these are found to be too weak, and here we propose that resonant scattering mediated by strong force interactions is a far more likely route.

The second fundamental difficulty with heat generation through neutron transfer reactions is the problem of coupling nuclear energy with the lattice. It can be shown that direct recoil effects are not capable of mediating the requisite large energy transfer without the presence of fast (MeV) nuclei. We instead proposed that very large energy transfer can be mediated through changes in the basic structure of the phonon modes.[8,9,11] In a sense, energy transfer through the creation or destruction of phonons doesn't work; energy transfer through the modification of pre-existing phonons does work, at least theoretically.

There exists no currently generally accepted experimental evidence supporting the proposal that neutron hopping can occur in a lattice. We will argue here that neutron hopping is somewhat analogous to electron hopping, and argue further that the Anderson model[12] used for electron band mixing calculations can, with modifications, be used for neutron problems.[13] This statement is in fact the primary result reported in this work. A key feature of the Anderson model is the presence of localized states that are embedded in a continuum of free states; the neutron localized states are several MeV below the continuum states, so that although mathematically similar to the Anderson model, the neutron model is very much simpler.

Having posed the model, we begin the task of analyzing the model to extract reaction rates. The field of Anderson model studies is by now relatively mature; variational methods, perturbation theory and canonical transformation approaches have proven to be very successful is analyzing solutions for the Anderson Hamiltonian. We have attacked the problem using infinite order Brillouin-Wigner theory, which leads directly to a perturbation expansion that is relatively easy to understand; the evaluation of the resulting formulas is less easy. We propose here rather crude estimates of reaction rates; this is perhaps appropriate, since this work is the first publication on the neutron lattice Anderson model.

The formulas appear to show that neutron hopping can occur at fast rates that would not have been anticipated if either phonon exchange or total angular momentum exchange occurs during a single site-to-site transfer. This is a key result of the present work.

2. Neutron Transfer Reactions

In previous publications, we have worked towards the development of a theory for neutron transfer reactions in a lattice mediated by electromagnetic E1 and M1 interactions.[8–10] In the present work, this theory is developed further, and extended to include effects mediated by the strong force.

We have explored a model including the lattice, nuclei, and free neutrons. In the absence of recoil effects, the resulting model is mathematically equivalent to the periodic Anderson model in condensed matter physics; our application of the Anderson model to describe neutrons, rather than electrons, is new. Electron hopping effects are well-known in condensed matter physics, and can in certain limits be described using the periodic Anderson model; applied to neutrons, our model describes neutron hopping, an effect unknown prior to our studies.

The periodic Anderson model has been analyzed using a variety of techniques. It has been solved approximately using the Schrieffer-Wolff rotation;[14–17] it can be solved exactly in certain limits through the use of a canonical transformation.[18] In the limit that essentially no neutrons are free, we can simplify the problem by truncating Fock space to include only zero- and one-neutron subspaces; the resulting equations can be solved approximately using Brillouin-Wigner theory, which leads to estimates for free neutron densities and reaction rates.

Upon evaluating the resulting formulas, we find that no coherence factors appear. In previous publications,[10] we had speculated that coherence factors should appear by analogy with the coherence factors that occur in Dicke superradiance. This speculation is found to be in error, for rather fundamental reasons associated with the fermionic statistics associated with the neutron transfer and bosonic statistics associated with photon emission.

Furthermore, we find that in the absence of coherence factors, the effects associated with electromagnetic E1 and M1 transitions are trivially small, and can not by themselves lead to any observable new effects. The relative weakness of the electromagnetic effects comes about due to the smallness of external electric or magnetic fields applied to the nucleus. A significantly larger effect is possible through the use of the strong force interaction, and we find that neutron hopping rates and neutron transfer reaction rates may become important when mediated by the strong force.

There are a variety of neutron transfer reactions that are possible in this model. A bound neutron that couples to continuum states will most often not stray more than a few fermis from the parent nucleus: this effect appears as the lowest order effect in all solutions to the model, and is also present in the isolated nucleus problem. The neutron will occasionally become delocalized; in the theory, this appears as a result of the possibility of scattering of the free (virtual) neutrons. Delocalized neutrons can "hop" from nucleus to nucleus. A large rate is estimated for the resonant

process where a delocalized neutron hops between equivalent nuclei, such that the total isotopic distribution is unchanged (so-called "null" reactions); although of great theoretical interest, these reactions are not easily observable, except possibly through isotopically-sensitive self-diffusion experiments. However, delocalized neutrons that hop onto a nonequivalent nucleus can result in gamma or alpha emission, as well as the creation of radioactive species.

If a delocalized neutron hops onto a nonequivalent nucleus, and if the lattice can provide or accept the energy defect, then a large reaction rate is predicted. We have discussed previously the conditions under which significant energy exchange during a neutron transfer reaction can occur with the lattice; energy transfer can occur if a highly excited phonon mode changes frequency by jumping across a phonon band gap. In this case, the process becomes resonant, and the associated reaction rates are calculated to be very large. The end result of such reactions can in principle be the generation (or absorption) of net energy, modification of pre-existing isotopic ratios, or the production of new isotopes.

We must now consider how this theory might address some of the outstanding experimental claims. In the case of the Pons-Fleischmann experiments, the heat-producing reaction with the smallest energy defect is the transfer of a neutron from ^{105}Pd to ^{6}Li, with an energy mismatch of 156 KeV. The symmetry of the Pd transfer involves *d*-wave neutrons, which results in small interaction matrix elements. Perhaps more promising are neutron transfers between ^{11}B (*p*-wave) and ^{29}Si (*s*-wave), with an energy mismatch of 849 KeV; and neutron transfers between ^{29}Si as donor and ^{29}Si as acceptor, with and energy mismatch of 2.14 MeV. In the light water heat experiments,[19–20] there occurs a relatively close match (12 KeV) for neutron transfers from ^{62}Ni (*p*-wave) and ^{29}Si (*s*-wave). Tritium production in this model could come about due to neutron transfers from a number of materials to deuterium; examples are given in Tables I and II in Section 9.

3. The Periodic Anderson Model

The proposed neutron transfer reaction in metal hydrides is in many ways analogous to the problem of electron hopping in solids. Before discussing the neutron problem further, it seems appropriate to first review briefly the electron version of the problem. The most relevant condensed matter model are variants of what is termed the Anderson model, following the initial treatment by Anderson of the *s-d* mixing of an iron-group metal impurity in a host metal.[12] This Anderson model treats the coupling between an isolated localized impurity electronic state that is embedded in a conduction band. This model has been generalized to treat multiple impurity states in a metal, and further generalized to apply to mixing between valence and conduction bands in a lattice.[23–28]

Whereas the neutron analog of the single impurity problem is simpler (since the bound state is so far removed from the continuum states), the neutron analog of the lattice model will be of great interest in what follows.

In the non-degenerate version of the periodic Anderson model, the Hamiltonian can be written as

$$\hat{H} = \sum_{\mathbf{k},\sigma} \epsilon_{\mathbf{k}} \hat{c}^{\dagger}_{\mathbf{k},\sigma} \hat{c}_{\mathbf{k},\sigma} + \sum_{i,\sigma} \epsilon_d \hat{d}^{\dagger}_{i,\sigma} \hat{d}_{i,\sigma} + \frac{1}{2} U \sum_{i,\sigma} \hat{n}_{i,\sigma} \hat{n}_{i,-\sigma} + \sum_{i,\mathbf{k},\sigma} [V_{\mathbf{k}} e^{-i\mathbf{k}\cdot\mathbf{R}_i} \hat{c}^{\dagger}_{\mathbf{k},\sigma} \hat{d}_{i,\sigma} + V^{*}_{\mathbf{k}} e^{i\mathbf{k}\cdot\mathbf{R}_i} \hat{d}^{\dagger}_{i,\sigma} \hat{c}_{\mathbf{k},\sigma}] \tag{3.1}$$

where $\hat{n}_{i,\sigma} = \hat{d}^{\dagger}_{i,\sigma} \hat{d}_{i,\sigma}$. This Hamiltonian includes individual Hamiltonians for the conduction band $\sum_{\mathbf{k},\sigma} \epsilon_{\mathbf{k}} \hat{c}^{\dagger}_{\mathbf{k},\sigma} \hat{c}_{\mathbf{k},\sigma}$ (which are the s-orbitals of the s-d model), the localized valence states $\sum_{i,\sigma} \epsilon_d \hat{d}^{\dagger}_{i,\sigma} \hat{d}_{i,\sigma}$ and the valence correlation energy $\frac{1}{2} U \sum_{i,\sigma} \hat{n}_{i,\sigma} \hat{n}_{i,-\sigma}$. The last term on the right hand side mixes the valence band and the conduction band. The spin dependence of $V_{\mathbf{k}}$ has been suppressed, following a convention used in much of the literature.

Numerous variants of this model appear in the literature. In the limit that the correlation energy U is taken to be zero, the Hamiltonian can be diagonalized exactly. In the alloy analog approximation,[23] the correlation term is omitted, and a site-dependent valence energy is introduced. In many cases, the correlation energy U is very large, so that only two valence configurations are present. In this case, the problem can be restated in terms of more complicated transition operators that prevent inclusion of unwanted configurations in the problem. For example, the degenerate periodic Anderson model sometimes appears as[29–33]

$$\hat{H} =$$

$$\sum_{\mathbf{k},\sigma} \epsilon_{\mathbf{k}} \hat{c}^{\dagger}_{\mathbf{k},\sigma} \hat{c}_{\mathbf{k},\sigma} + \sum_{i,\lambda} \epsilon_{\lambda} \hat{X}_{\lambda,\lambda}(i) + \sum_{i,\mu} \epsilon_{\mu} \hat{X}_{\mu,\mu}(i) + \sum_{i,\mathbf{k},\sigma,\mu,\lambda} [V^{\mathbf{k},\sigma}_{\lambda,\mu} e^{-i\mathbf{k}\cdot\mathbf{R}_i} \hat{c}^{\dagger}_{\mathbf{k},\sigma} \hat{X}_{\mu\lambda}(i) + V^{\mathbf{k},\sigma}_{\mu,\lambda} e^{i\mathbf{k}\cdot\mathbf{R}_i} \hat{X}_{\lambda\mu}(i) \hat{c}_{\mathbf{k},\sigma}] \tag{3.2}$$

where the $\hat{X}$ operators are Hubbard operators; these are more complicated operators that are made up of products of single particle creation and annihilation operators.

Sakai et al[34] have used a model Hamiltonian to study mixed valence states of rare earth ions; this Hamiltonian was written in the interesting form

$$\hat{H} = \sum_{\mathrm{l},\sigma_l} |f\mathrm{l}\sigma_l > E_f(\sigma_l) < f\mathrm{l}\sigma_l| + \sum_{\mathbf{k},\sigma} |c\mathbf{k}\sigma > E_{\mathbf{k}} < c\mathbf{k}\sigma| + \frac{1}{\sqrt{N}} \sum_{\mathrm{lk}\sigma} v[|f\mathrm{l}\sigma > e^{i\mathbf{k}\cdot\mathrm{l}} < c\mathbf{k}\sigma| + \mathrm{h.c.}] \tag{3.3}$$

In this formula, $|fl\sigma_l>$ refers to an f state at lattice site $\vec{l}$. The occurence of projection operators is explicit in this notation. Recognizing that equations (3.2) and (3.3) describe the same basic model perhaps helps to make clear the role of the Hubbard operators.

There are many papers that have obtained approximate solutions for these models, however, it is generally recognized that the appearance of the more complicated transition operators greatly complicates the algebra associated with the solutions. The slave-Boson model was developed to address this issue.[35] Since the predominant effect of the correlation term is to restrict multiple occupancy of the localized valence sites, simple fermionic creation and annihilation operators could be employed (without the correlation term) if the creation of unwanted electrons could be restricted by the addition of a new degree of freedom. The basic idea of the slave-Boson model is then to treat the valence sites approximately using simple fermionic operators (which by themselves could produce multiple occupancy) supplemented by a simple Bosonic degree of freedom that more or less acts as a switch to turn off further electron creation once a site is singly occupied. This model is implemented in the slave-Boson Hamiltonian

$$\hat{H} = \sum_{\mathbf{k},\sigma} \epsilon_{\mathbf{k}} \hat{c}^{\dagger}_{\mathbf{k},\sigma} \hat{c}_{\mathbf{k},\sigma} + \sum_{i,\sigma} \epsilon_d \hat{d}^{\dagger}_{i,\sigma} \hat{d}_{i,\sigma} + \sum_{i,\mathbf{k},\sigma} [V_{\mathbf{k}} e^{-i\mathbf{k}\cdot\mathbf{R}_i} \hat{c}^{\dagger}_{\mathbf{k},\sigma} \hat{d}_{i,\sigma} \hat{b}^{\dagger}_i + V^{*}_{\mathbf{k}} e^{i\mathbf{k}\cdot\mathbf{R}_i} \hat{d}^{\dagger}_{i,\sigma} \hat{c}_{\mathbf{k},\sigma} \hat{b}_i] \tag{3.4}$$

In order to enforce single occupancy at a site, the following auxiliary constraint is imposed

$$\sum_{\sigma} \hat{d}^{\dagger}_{i,\sigma} \hat{d}_{i,\sigma} + \hat{b}^{\dagger}_i \hat{b}_i = 1 \tag{3.5}$$

This version of the periodic Anderson model has proven to be rather successful, being easier to analyze and providing answers that are close to the original model.[18,35–37]

4. An Anderson Model for Neutrons

A lattice that contains an element that has two isotopes differing only by one mass leads to a neutron analog of the mixed valence problem. In this case, the valence bands are composed of highly localized bound neutron states corresponding to the different isotopes, and the conduction band is composed of free neutrons states. The neutron valence bands will be very narrow, corresponding perhaps more closely to the premise of the Anderson model than the electronic valence states in mixed valence problems.

There will also be significant differences between the neutron and electron Anderson models. For example, the nuclear binding energies are measured in MeV, rather than in eV, and the conduction

orbitals are very nearly free neutron states. The Anderson model in condensed matter was developed originally to model discrete states that are embedded in a continuum, and most modern applications and interesting physics associated with the model arise due to this intimate coupling; in the nuclear problem, the neutron bands will always be well-separated from the conduction band. Because of this, the neutron version of the problem is fundamentally much simpler.

The neutron is much heavier than an electron; consequently, recoil effects will be much more important. The motion of free electrons in a metal is reasonably benign; a single electron can scatter, contibute to a magnetic susceptibility, and interact with phonons, none of which by itself leads to observables that are easily discernable from the outside. A single free neutron, if captured, will likely produce gamma radiation that can on average be observed from the outside with high efficiency.

The electron Anderson models discussed in the last section may be adopted almost directly for use in analyzing neutron mixing and dynamics. For example, the periodic Anderson model of equation (3.1) will lead to

$$\hat{H} = \sum_{\mathbf{k},\sigma} \epsilon_{\mathbf{k}} \hat{c}^{\dagger}_{\mathbf{k},\sigma} \hat{c}_{\mathbf{k},\sigma} + \sum_{i,\sigma} \epsilon_d \hat{d}^{\dagger}_{i,\sigma} \hat{d}_{i,\sigma} + \frac{1}{2} U \sum_{i,\sigma} \hat{n}_{i,\sigma} \hat{n}_{i,-\sigma} + \sum_{i,\mathbf{k},\sigma} [V_{\mathbf{k}} e^{-i\mathbf{k}\cdot\hat{\mathbf{R}}_i} \hat{c}^{\dagger}_{\mathbf{k},\sigma} \hat{d}_{i,\sigma} + V^{*}_{\mathbf{k}} e^{i\mathbf{k}\cdot\hat{\mathbf{R}}_i} \hat{d}^{\dagger}_{i,\sigma} \hat{c}_{\mathbf{k},\sigma}] \tag{4.1}$$

In this model, the creation and annihilation operators now will refer to neutron orbitals, and ϵ_d now will be on the order of MeV. The matrix element $V_{\mathbf{k}}$ will generally also be spin-dependent, though this dependence is suppressed in the notation. Recoil and lattice effects will be important, and this can be included by taking the nuclear center of mass coordinates to be phonon operators $\hat{\mathbf{R}}_i$. The neutron Anderson Hamiltonian should be augmented by a lattice Hamiltonian; this we will attend to elsewhere. For now, we may include phonon effects approximately by including them in matrix elements where appropriate.

The generalizations of the electronic Anderson Hamiltonian discussed in the last section also will serve as generalizations of the neutron Anderson Hamiltonian, with modifications as discussed above. This connection between the two problems is important because it allows, in principle, the use of the particular methods, solutions, and physical effects known for the electronic problem to be used for the neutron problem. For example, we may use the Schrieffer-Wolff transformation, or the various Green's function methods, or even apply the slave-Boson model.

5. Configuration Interaction Mixing

The interaction Hamiltonian that mixes the valence and conduction band in the case of the electronic Anderson model is the one-electron part of the site Hamiltonian[12]

$$V_{\mathbf{k}}^{*} = \frac{1}{\sqrt{N}} \int \phi_d^{*}(\mathbf{r}) H_{HF}(\mathbf{r}) \sum_n e^{i\mathbf{k}\cdot\mathbf{R}_n} a(\mathbf{r}-\mathbf{R}_n) \tag{5.1}$$

where $a(\mathbf{r}-\mathbf{R}_n)$ is the band Wannier function. The Hartree-Fock approximation at a site produces solutions that are stationary against mixing with all configurations involving the promotion of only a single electron at that site, so that there would be no mixing were it not for the fact that the Wannier functions from neighboring sites spill over, leading to

$$V_{\mathbf{k}}^{*} = \frac{1}{\sqrt{N}} \sum_{\mathbf{R}_n \neq 0} e^{i\mathbf{k}\cdot\mathbf{R}_n} V_d(\mathbf{R}_n) \tag{5.2}$$

Our attention must now turn to the interaction in the case of neutron band mixing. Since bound neutrons are strongly localized around their parent nuclei, the associated Wannier functions will also be localized. The mixing brought about from neighboring site overlaps is exponentially damped; consequently, the normal one-electron Anderson interaction matrix elements vanish in the analog neutron Anderson model.

In our previous works on the neutron transfer model, we focused on one-neutron matrix elements mediated by electromagnetic E1 and M1 interactions.[8–10] In this case there is no question that an appropriate one-neutron interaction arises, and that a neutron Anderson model would result. Unfortunately, this interaction is simply not sufficiently strong to lead to interesting consequences, as will be clear shortly. In the absence of any other mixing effects, this problem would be uninteresting.

But we have so far neglected two-nucleon matrix elements in this discussion. Consider the mixing between a ground state nuclear wavefunction $|\Phi_0,(J)^{\pi}>$ and the free state built up of the ground state $\overline{\Phi}_0$ of the parent nucleus and a free neutron ϕ_k to give $|\overline{\Phi}_0\phi_{\mathbf{k}},(J)^{\pi}>$, with both total states containing equivalent numbers of neutrons and protons. In a multiconfigurational Hartree-Fock approximation, these states would mix. In a nonorthogonal Hartree-Fock approximation, the states would be mixed directly; in the standard Hartree-Fock method, the free state would be orthogonalized against the ground state before mixing.

Depending on the details of the calculation, mixing would occur between the states arising from two-nucleon interactions, although only one neutron is free in the excited state admixture. Two-nucleon matrix elements would be expected to arise naturally due to rearrangement effects in the parent nucleus. This mixing would normally lead to relatively minor adjustments in the ground

state energy of $|\Phi_0,(J)^\pi>$. It could be argued that in a lattice model based on a collection of "exact" isolated nuclear wavefunctions (using known experimental energies), that this configuration interaction is already included in the states and their energies.

The configuration interaction energy due to configurations containing one free neutron could be estimated by assuming a variational trial wavefunction of the form

$$\Psi = d|\Phi_0,(J)^\pi> + \sum_{\mathbf{k},\sigma} c_{\mathbf{k},\sigma}|\overline{\Phi}_0\phi_{\mathbf{k}},(J)^\pi> \tag{5.3}$$

where d and $c_{\mathbf{k},\sigma}$ are scalars. In the general problem, we would also sum over all parent nuclei, a complication that we forgo here. The trial energy for this wavefunction is

$$E = \epsilon_d d^* d + \sum_{\mathbf{k},\sigma} \epsilon_{\mathbf{k}} c^*_{\mathbf{k},\sigma} c_{\mathbf{k},\sigma} + \sum_{\mathbf{k},\sigma}[V_{\mathbf{k}} c^*_{\mathbf{k},\sigma} d + V^*_{\mathbf{k}} d^* c_{\mathbf{k},\sigma}] \tag{5.4}$$

subject to the constraint

$$|d|^2 + \sum_{\mathbf{k},\sigma} |c_{\mathbf{k},\sigma}|^2 = 1 \tag{5.5}$$

The interaction matrix element is

$$V_{\mathbf{k}} = <\overline{\Phi}_0\phi_{\mathbf{k}},(J)^\pi|V_s|\Phi_0,(J)^\pi> \tag{5.6}$$

where V_s is the strong force interaction. In the OPEP (One Pion Exchange Model) interaction,[38] V_s is

$$V_s = \sum_{i<j} \frac{1}{3}\frac{g^2}{\hbar c} m_\pi c^2 (\tau_i \cdot \tau_j) \left\{ (\sigma_i \cdot \sigma_j) + \left[1 + \frac{3}{\mu r_{ij}} + \frac{3}{(\mu r_{ij})^2} \right] S_{ij} \right\} \frac{e^{-\mu r_{ij}}}{\mu r_{ij}} \tag{5.7}$$

The strong force coupling constant is $g^2/\hbar c = 0.081$, the mass of the pion is m_π, the τ vectors are isospin operators, the σ vectors are nuclear spin operators, and the extinction coeficient is $\mu = m_\pi c/\hbar = (1.4 \text{ fm})^{-1}$. The term proportional to S_{ij} is the tensor part of the interaction.

The trial energy is easily minimized; to lowest order the energy is

$$E = \epsilon_d - \sum_{\mathbf{k},\sigma} \frac{|V_{\mathbf{k}}|^2}{\epsilon_{\mathbf{k}} - \epsilon_d} \tag{5.8}$$

Correlations from continuum states to total nuclear energies are generally small compared to the neutron binding energy; for example, neutron binding energies are typically 5-10 MeV, and the correlation energy may be on the order of a hundred KeV or greater.

In the Anderson model for electrons, the interaction matrix element is often taken to be constant, and estimates for (5.8) then follow. In the nuclear problem, a similar approximation leads to a divergence. If we assume that $V_{\mathbf{k}}$ mixes continuum s-orbitals, and if we introduce a Gaussian cut-off at high momentum, then we may parametrize $V_{\mathbf{k}}$ through

$$|V_{\mathbf{k}}|^2 = \frac{V_n}{V}|v_0|^2 e^{-|\mathbf{k}|^2/k_0^2} \tag{5.9}$$

V_n is the nuclear volume, V is the lattice volume, and k_0 is a cut-off momentum. The correlation energy ΔE_c becomes

$$\begin{aligned}\Delta E_c &= -\sum_{\mathbf{k},\sigma} \frac{|V_{\mathbf{k}}|^2}{\epsilon_{\mathbf{k}} - \epsilon_d} \\ &= -\int_0^\infty \frac{|V_{\mathbf{k}}|^2}{\epsilon_{\mathbf{k}} - \epsilon_d}\rho(k)dk \end{aligned} \tag{5.10}$$

Using $\rho(k) = (2k/\pi)^2 V$, we obtain

$$\Delta E_c = -\left[\frac{2}{\pi}\right]^2 V_n k_0^3 \frac{|v_0|^2}{|\epsilon_d|}\int_0^\infty \frac{a^2 y^2 e^{-y^2}}{y^2 + a^2}dy \tag{5.11}$$

where

$$a = \frac{|\epsilon_d|}{\hbar^2 k_0^2/2M_n} \tag{5.12}$$

The integral can be estimated

$$\int_0^\infty \frac{y^2 e^{-y^2}}{y^2 + a^2}dy \approx \frac{\sqrt{\pi}}{2}\frac{1}{1 + a + a^2/2} \tag{5.13}$$

leading to

$$\Delta E_c = -\frac{2}{\pi^{3/2}} V_n k_0^3 \frac{|v_0|^2}{|\epsilon_d|}\frac{a^2}{1 + a + a^2/2} \tag{5.14}$$

The various constants that appear in (5.14) are together of order unity, and the reduced interaction strength is on the order of an MeV

$$|v_0|^2 \sim |\epsilon_d \Delta E_c| \tag{5.15}$$

The free neutron in this case is localized. Whereas each individual free neutron orbital goes like $e^{i\mathbf{k}\cdot\mathbf{r}}$, the coefficients $c_{\mathbf{k},\sigma}$ are slowly varying with $\mathbf{k}$. The free neutron wavefunction in this case can be constructed from the mixing coefficients

$$\psi_\sigma(\mathbf{r}) \sim \sum_{\mathbf{k}} c_{\mathbf{k},\sigma} e^{i\mathbf{k}\cdot\mathbf{r}} \longrightarrow Ce^{-\alpha|\mathbf{r}|} \tag{5.16}$$

It is the destructive interference between the waves that leads to the short range of the virtual neutron.

Configuration mixing in the case of a lattice will generally be similar, except that since the continuum orbitals extend over the lattice, each nucleus mixes with a common set of orbitals. Before doing any computations, we would immediately expect that the energy of the N neutrons that are being mixed should be on the general order of

$$E = N\left[\epsilon_d - \sum_{\mathbf{k},\sigma} \frac{|V_{\mathbf{k}}|^2}{\epsilon_{\mathbf{k}} - \epsilon_d}\right] \tag{5.17}$$

with lattice effects contributing terms at higher order.

If we assume that at each occupied site we have a contribution from a ground state nuclear wavefunction $d_i|\Phi_0(i),(J)^\pi>$, and the continuum orbitals are filled with probability $c_{\mathbf{k},\sigma}$, the we might expect the total energy to be

$$E = \sum_i \epsilon_d d_i^* d_i + \sum_{\mathbf{k},\sigma} \epsilon_{\mathbf{k}} c_{\mathbf{k},\sigma}^* c_{\mathbf{k},\sigma} + \sum_{\mathbf{k},\sigma}\sum_i [V_{\mathbf{k}} e^{-i\mathbf{k}\cdot\mathbf{R}_i} c_{\mathbf{k},\sigma}^* d_i + V_{\mathbf{k}}^* e^{i\mathbf{k}\cdot\mathbf{R}_i} d_i^* c_{\mathbf{k},\sigma}] \tag{5.18}$$

subject to the constraint

$$\sum_i |d_i|^2 + \sum_{\mathbf{k},\sigma} |c_{\mathbf{k},\sigma}|^2 = N \tag{5.19}$$

It is not hard to show that the optimization of this energy leads to equation (5.17) to lowest order. In the optimization, we find that

$$c_{\mathbf{k},\sigma} = -\sum_i \frac{V_{\mathbf{k}} e^{i\mathbf{k}\cdot\mathbf{R}_i} d_i}{\epsilon_{\mathbf{k}} - \epsilon_d} \tag{5.20}$$

This has an interesting interpretation; suppose that the phases of all of the ground state nuclei were the same ($d_i \approx 1$), then only the neutron states with wavevectors matching the reciprocal lattice vectors contribute. In retrospect this is obvious, since the localized free neutron contribution around each wavefunction would be in phase, and these could only be made up of continuum waves that are matched with the lattice.

From the discussion above, it is clear that states containing free neutron orbitals will mix with nuclear ground states, that the free neutron contribution is localized to lowest order, and that this mixing in the lattice does involve many localized nuclei mixing with a common continuum.

Consequently, the lattice Anderson model is appropriate to describe this mixing. The energy formulas above are similar in form to some of the terms appearing in the Anderson Hamiltonian (the U-correlation terms are absent due to the choice of the variational wavefunctions), and this is not an accident.

From the arguments given above, it is clear that the energy eigenvalues of the neutron lattice Anderson Hamiltonian should be renormalized to remove the equivalent one-free-neutron isolated nucleus correlation energy. Our focus will be on that part of the free neutron wavefunction that is delocalized, which has no analog in the isolated nucleus problem.

6. One-Neutron Approximation

Our immediate goal is the computation of reaction rates for neutron transfer reactions. If we had solutions to the Anderson model, then we could in principle use these solutions to obtain estimates of the reaction rates. We will argue below that if interactions with the phonons are neglected in the neutron Anderson model described in the last two sections, which corresponds to the situation most often treated in the literature, then no reactions occur to lowest order. If phonon interactions are included, then reactions become allowed. We are not aware of any solutions to the Anderson model that include the full recoil interaction, although recent works have appeared that include phonon interactions to lowest order.[42–44] If the neutron Anderson model is further modified to include a more complicated group structure, then reactions also become allowed due to the exchange of angular momentum, even if no phonon exchange occurs. We introduce the one-neutron approximation and Brillouin-Wigner theory below to address the general problem of estimating reaction rates.

The coupling between the neutron valence band and conduction band is sufficiently weak that to lowest order all neutrons are tightly bound, assuming that no free neutrons have been injected into the lattice. To first order, perhaps there may be a few free neutrons present; we propose to use this to our advantage by considering only excited states containing only a single free neutron. The advantage of this approach is that the structure of the resulting Hamiltonian is much simpler, and this allows us to apply perturbation theory algebraically. The important results in this section are formal; the perturbation theory is used to begin a discussion of reaction rates in the following section.

We may implement this approximation by restricting Fock space to include 0-neutron and 1-neutron subspaces only. In this case, the projected Anderson Hamiltonian takes the form

$$\hat{H} = \begin{bmatrix} \hat{H}_0 & 0 \\ 0 & \hat{H}_1 \end{bmatrix} + \begin{bmatrix} 0 & \hat{V} \\ \hat{V}^\dagger & 0 \end{bmatrix} \tag{6.1}$$

where $\hat{H}_0$ operates on the 0-neutron states, and so forth.

The time-independent Schrodinger equation may be solved formally using infinite order Brillouin-Wigner theory (this is closely related to the approach of Ref. 39); we assume a solution of the form

$$\Psi = \begin{bmatrix} \Phi_0 \\ 0 \end{bmatrix} + \begin{bmatrix} \hat{Q}\Psi_0 \\ \Psi_1 \end{bmatrix} \tag{6.2}$$

where Φ_0 is an exact solution of the 0-neutron problem

$$\hat{H}_0\Phi_0 = E_0\Phi_0 \tag{6.3}$$

The projection operator $\hat{Q}$ is given by

$$\hat{Q} = 1 - |\Phi_0 >< \Phi_0| \tag{6.4}$$

It can be shown that the energy E can be written as

$$E =< \Phi_0|\hat{H}_0|\Phi_0 > + < \Phi_0|\hat{V}|\Psi_1 > \tag{6.5}$$

The equation for $\hat{Q}\Psi_0$ is

$$(E - \hat{H}_0)\hat{Q}\Psi_0 = \hat{V}\Psi_1 + (\hat{H}_0 - E)\Phi_0 \tag{6.6}$$

Since $(\hat{H}_0 - E)\Phi_0 = (E_0 - E)\Phi_0 = -\Phi_0 < \Phi_0|\hat{V}|\Psi_1 >$, this form of solution leads to two coupled time-independent Schrodinger equations

$$(E - \hat{H}_0)\hat{Q}\Psi_0 = \hat{Q}\hat{V}\Psi_1 \tag{6.5}$$

$$(E - \hat{H}_1)\Psi_1 = \hat{V}^\dagger\hat{Q}\Psi_0 + \hat{V}^\dagger\Phi_0 \tag{6.6}$$

The two equations can be combined to yield an equation for the 1-neutron wavefunction

$$\left[E - \hat{H}_1 - \hat{V}^\dagger(E - \hat{H}_0)^{-1}\hat{Q}\hat{V}\right]\Psi_1 = \hat{V}^\dagger\Phi_0 \tag{6.7}$$

This result is interesting because it contains explicitly the scattering potential of the free neutrons. A recursive formula is obtained for the energy E

$$E =< \Phi_0|\hat{H}_0|\Phi_0 > + < \Phi_0|\hat{V}\left[E - \hat{H}_1 - \hat{V}^\dagger(E - \hat{H}_0)^{-1}\hat{Q}\hat{V}\right]^{-1}\hat{V}^\dagger|\Phi_0 > \tag{6.8}$$

We consider first the problem of configuration interaction of an isolated nucleus; in this case there is no resonant scattering of the free neutrons, and we may solve for Ψ_1

$$\Psi_1 = (E - \hat{H}_1)^{-1}\hat{V}^\dagger\Phi_0 \tag{6.9}$$

The denominator is the difference of the bound state energy and the free neutron energy, which will be several MeV; Ψ_1 will consequently be quite insensitive to the mixing since $E - E_0$ will be small. This leads to an energy E equal to

$$E =< \Phi_0|\hat{H}_0|\Phi_0 > + < \Phi_0|\hat{V}(E - \hat{H}_1)^{-1}\hat{V}^\dagger|\Phi_0 > \tag{6.10}$$

which is to lowest order

$$E = \epsilon_d - \sum_{\mathbf{k},\sigma}\frac{|V_\mathbf{k}|^2}{\epsilon_\mathbf{k} - \epsilon_d} \tag{6.11}$$

in agreement with the results of section 5.

Neglecting free neutron scattering in the case of the lattice case leads again to

$$E =< \Phi_0|\hat{H}_0|\Phi_0 > + < \Phi_0|\hat{V}(E - \hat{H}_1)^{-1}\hat{V}^\dagger|\Phi_0 > \tag{6.12}$$

which evaluates to lowest order to

$$E = N\left[\epsilon_d - \sum_{\mathbf{k},\sigma}\frac{|V_\mathbf{k}|^2}{\epsilon_\mathbf{k} - \epsilon_d}\right] \tag{6.13}$$

Fortunately, the infinite-order Brillouin-Wigner solution leads naturally to a convenient approximation scheme that has a rather clear interpretation.

We are now in a position to examine the effects of resonant scattering using perturbation theory. To second order, we obtain for Ψ_1

$$\Psi_1 = (E - \hat{H}_1)^{-1}\hat{V}^\dagger\Phi_0 - (E - \hat{H}_1)^{-1}\hat{V}^\dagger(E - \hat{H}_0)^{-1}\hat{Q}\hat{V}(E - \hat{H}_1)^{-1}\hat{V}^\dagger\Phi_0 \tag{6.14}$$

The first term is local; we seek neutron delocalization in the second order correction. Two of the denominators involve $(E - \hat{H}_1)$, which evaluates to the binding plus free energy, which is on the order of several MeV. The other denominator involves $(E - \hat{H}_0)$, and is resonant.

If the lattice is composed of nuclei with only a single isotope present, then this term does very little; in this case, a neutron that originates from site i must land on site i, which (in the absence

of phonon generation) would give back the ground state (which is excluded by the $\hat{Q}$ operator. Far more interesting is the mixed valence problem where the lattice is composed of near equal amounts of the ground state $|\Phi_0,(J)^\pi>$ nuclei and the parent $|\overline{\Phi_0},(J')^{\pi'}>$ nuclei. With the addition of many equivalent parent nuclei, there are now a very large number of resonant sites where the free neutron can scatter. A neutron originating from site i now can "hop" to the many possible sites j, in each case with a resonant denominator $(E-\hat{H}_0)$ occuring.

Under the assumption that the scattering involves free neutron states of low energy, the off-resonant denominators are well-approximated by the neutron binding energy. Identifying the parts of Ψ_1 that are local and due to scattering

$$\Psi_1 = (\Psi_1)_{\text{local}} + \delta\Psi_1 \tag{6.15}$$

we may write for the second order term

$$\delta\Psi_1 = -\frac{1}{\epsilon_d^2}\hat{V}^\dagger(E-\hat{H}_0)^{-1}\hat{Q}\hat{V}\hat{V}^\dagger\Phi_0 \tag{6.16}$$

The renormalized energy shift to lowest order is

$$\delta E = <\Phi_0|\hat{V}|\delta\Psi_1> \tag{6.17}$$

which is approximately

$$\delta E = -\frac{1}{\epsilon_d^2} <\Phi_0|\hat{V}\hat{V}^\dagger(E-\hat{H}_0)^{-1}\hat{Q}\hat{V}\hat{V}^\dagger|\Phi_0> \tag{6.18}$$

7. Reaction Rates for Incoherent Neutron Transfers

Delocalized neutrons may be captured by other nuclei with lower binding energies, accompanied by the emission of gammas or other decay products. An approximate formal expression for this decay rate can be estimated from the above formulas, by taking advantage of the free neutron density operator

$$\begin{aligned}\hat{\rho}_c(\mathbf{r}) &= \sum_{\mathrm{k.k'},\sigma} \phi^*_{\mathrm{k},\sigma}(\mathbf{r})\phi_{\mathrm{k'},\sigma}(\mathbf{r})\hat{c}^\dagger_{\mathrm{k},\sigma}\hat{c}_{\mathrm{k'},\sigma} \\ &= \frac{1}{V}\sum_{\mathrm{k.k'},\sigma} \hat{c}^\dagger_{\mathrm{k},\sigma}\hat{c}_{\mathrm{k'},\sigma}e^{i(\mathrm{k}-\mathrm{k'})\cdot\mathrm{r}}\end{aligned} \tag{7.1}$$

We obtain the incoherent reaction rate for neutron capture to be

$$\Gamma_{in} = \int < \Psi_1 | \hat{\rho}_c(\mathbf{r}) | \Psi_1 > \sum_{\alpha} N_{\alpha}(\mathbf{r}) < \sigma_{\alpha} v >_0 \, d^3\mathbf{r} \tag{7.2}$$

where $N_{\alpha}(\mathbf{r})$ is the density and $< \sigma_{\alpha} v >_0$ is the below threshold incoherent neutron capture rate coefficient of isotopes denoted by α. Local neutrons from one set of isotopes will have no overlap with the nuclei of other isotopes in the lattice; delocalized neutrons will have overlaps and will be incoherently absorbed.

8. Lattice-Assisted Neutron Transfers

In the case that the lattice is able to absorb (or provide) the reaction energy, through the frequency shift (across a phonon band gap) of a very highly excited phonon mode, during a neutron hop from one isotope to a nonequivalent isotope, the reaction rate can be found to lowest order through

$$\Gamma = \frac{2\pi}{\hbar} | < \Phi_f | \hat{V}' | \Psi_1 > |^2 \rho(E_f) \tag{8.1}$$

where Φ_f is the final state, and where $\hat{V}'$ transfers a neutron to nonequivalent isotopes. We note that this formula is specific for neutron delocalization of donor neutrons; there is an analogous formula for acceptor neutron delocalization. Using equation (6.16), this becomes

$$\Gamma = \frac{2\pi}{\hbar} \frac{1}{\epsilon_d^4} | < \Phi_f | \hat{V}' \hat{V}^{\dagger} (E - \hat{H}_0)^{-1} \hat{Q} \hat{V} \hat{V}^{\dagger} | \Phi_0 > |^2 \rho(E_f) \tag{8.2}$$

It may appear to be surprising that $\hat{V}'$ should be expected to transfer tens to hundreds of KeV during a single neutron transfer. Nevertheless, in the presence of very highly excited phonon modes, the frequency shift of an excited continuum phonon mode is accompanied by an energy transfer ΔE_L of

$$\Delta E_L = N_m \hbar \delta \omega_m \tag{8.3}$$

where N_m is the number of phonons and where $\delta\omega_m$ is the phonon band gap that is crossed. The frequency shift can be on the order of meV; if N_m is of the order of 10^8, the resulting energy transfer will be on the order of 10^5 eV, which is sufficient to make up the energy mismatch between neutron binding energies of the ground states of different isotopes.

9. Reaction Rate Estimates

The neutron lattice Anderson model is new, consequently there remains considerable work in analyzing and understanding the theory. One approach to estimating rates would be to obtain a ground state solution for the Anderson problem, and then develop rate estimates from the resulting delocalized neutron densities. A number of variational ground state solutions for the electron problem have been described in the literature; with some work, it might be possible to adapt these solutions for reaction rate estimates. In the case of the slave-Boson model, there now exists ground state solutions for the decoupled valence and conduction bands; it is very likely that these solutions will apply to the neutron Anderson model being considered here. But these projects for now must remain for future work.

Our goal in this section is to begin examining the rates predicted from the one-neutron approximation discussed in the last section, and to obtain rather rough esimates. It happens that there is no delocalization in the case of zero phonon exchange with the normal spin-conserving interaction Hamiltonian; this is discussed below.

In the neutron Anderson model described above, a bound neutron with spin σ is coupled into a continuum state with momentum $\mathbf{k}$ and spin σ, leaving behind a hole of momentum $\mathbf{k}$. If the neutron is captured back with no change in momentum or spin, then no delocalization occurs. In order to achieve delocalization, the virtual neutron must be captured with either an altered linear momentum or an altered total angular momentum. The interaction with phonons can change the linear momentum, but the energy exchange that accompanies this process makes it non-resonant by the phonon exchange energy.

The structure of the lattice can result in nonconservation of angular total momentum during a neutron hop. Since the lattice is not rotationally invariant around a nucleus, a free neutron with orbital angular momentum relative to an initial nucleus will not generally preserve that angular momentum when captured by a translated nucleus. This effect allows free neutrons to access degenerate nonequivalent states, which is very important within Brillouin-Wigner theory as discussed below.

We begin the discussion by working with the conventional Anderson model adapted to the neutron problem, and show that resonant interactions do not occur. We then discuss phonon and total angular momentum modifications of the model.

We begin by noting that the $\hat{V}$ and $\hat{V}^\dagger$ operators that occur in previous sections are given by

$$\hat{V} = \sum_i \sum_{\mathbf{k}\sigma} V_{\mathbf{k}}^* e^{i\hat{\mathbf{k}}\cdot\hat{\mathbf{R}}_i} \hat{d}_{i,\sigma}^\dagger \hat{c}_{\mathbf{k},\sigma} \tag{9.1}$$

$$\hat{V}^\dagger = \sum_i \sum_{\mathbf{k}\sigma} V_{\mathbf{k}} e^{-i\hat{\mathbf{k}}\cdot\hat{\mathbf{R}}_i} \hat{c}^\dagger_{\mathbf{k},\sigma} \hat{d}_{i,\sigma} \tag{9.2}$$

The operator $\hat{V}^\dagger$ creates a continuum neutron, leaving behind a hole; $\hat{V}$ destroys both. Inspection of the rate formula (8.2) indicates that the product $\hat{V}\hat{V}^\dagger$ takes the initial state to other states that are nearly-degenerate with the initial state Φ_0. The part of $\hat{V}\hat{V}^\dagger|\Phi_0>$ that is proportional to Φ_0 is projected out.

Since Φ_0 contains no neutrons, and $\hat{V}\hat{V}^\dagger|\Phi_0>$ also contains no neutrons, we find that

$$\hat{V}\hat{V}^\dagger|\Phi_0> = \sum_{ij} \sum_{\mathbf{k}\sigma} |V_{\mathbf{k}}|^2 e^{i\mathbf{k}\cdot(\hat{\mathbf{R}}_i - \hat{\mathbf{R}}_j)} \hat{d}^\dagger_{i,\sigma} \hat{d}_{j,\sigma} |\Phi_0> \tag{9.3}$$

At this point, the operator nature of $\hat{\mathbf{R}}_i$ becomes important. At low temperature ($T \to 0$), it may be that very few phonons will be created or destroyed on average for low momentum continuum neutrons. If we examine the 0-phonon part of $\hat{V}\hat{V}^\dagger$, we find that

$$<0|\hat{V}\hat{V}^\dagger|0> \approx \sum_{ij} \sum_{\mathbf{k}\sigma} |V_{\mathbf{k}}|^2 e^{i\mathbf{k}\cdot(\mathbf{R}^0_i - \mathbf{R}^0_j)} e^{-2W_D(\mathbf{k})} \hat{d}^\dagger_{i,\sigma} \hat{d}_{j,\sigma} \tag{9.4}$$

where the notation $<0|\hat{V}\hat{V}^\dagger|0>$ implies zero neutrons present in initial and final states, and zero phonons generated. The equilibrium center of mass position at site i is $\mathbf{R}^0_i$. The expression is approximate in that we have assumed that there is no correlation between sites i and j in the calculation of the Debye-Waller factor $e^{-W_D}(\mathbf{k})$ at each site. If we define

$$\hat{d}_{\mathbf{k},\sigma} = \frac{1}{\sqrt{N}} \sum_i e^{-i\mathbf{k}\cdot\mathbf{R}^0_i} \hat{d}_{i,\sigma} \tag{9.5}$$

then it follows that

$$<0|\hat{V}\hat{V}^\dagger|0> \approx N \sum_{\mathbf{k}\sigma} |V_{\mathbf{k}}|^2 e^{-2W_D(\mathbf{k})} \hat{d}^\dagger_{\mathbf{k},\sigma} \hat{d}_{\mathbf{k},\sigma} \tag{9.6}$$

This result indicates that the hole that is created will be the same hole that is destroyed. In this equation, the operator $\hat{d}_{\mathbf{k},\sigma}$ is taken to be the same as $\hat{d}_{\mathbf{k}+\mathbf{G},\sigma}$, where $\mathbf{G}$ is a reciprocal lattice vector.

To within an excellent approximation, it follows that there is no free neutron delocalization at all in the limit described above; for example, if $\hat{V}^\dagger$ creates a matched neutron and hole pair, both with momentum $\mathbf{k}$, and then $\hat{V}$ destroys the same matched pair, then there is no change in the state of the system. In this case

$$< 0|\hat{V}\hat{V}^{\dagger}|0 > \Phi_0 \sim \Phi_0 \tag{9.7}$$

and

$$\hat{Q} < 0|\hat{V}\hat{V}^{\dagger}|0 > \Phi_0 = 0 \tag{9.8}$$

No change in state means no net scattering, which results in no net effects. This mathematical statement corresponds to the physical arguments given above that the virtual neutron must in some way be "scattered" in order to be delocalized. We now turn our discussion to this problem.

One approach to the problem is to investigate phonon exchange. It would be possible at this point to begin an examination of the transition matrix elements, considering first 1-phonon matrix elements, then 2-phonon matrix elements, et cetera. Some work along these lines has been done recently by Azzam.[45] It may be possible to obtain some advantage by working at the outset with operators devoid of the zero-phonon contributions; for example, $\hat{Q}\hat{V}\hat{V}^{\dagger}$ could be replaced with the non-zero-phonon piece

$$\hat{Q}\hat{V}\hat{V}^{\dagger} \longrightarrow \hat{V}\hat{V}^{\dagger} - < 0|\hat{V}\hat{V}^{\dagger}|0 > \tag{9.9}$$

Further work will clarify the issue.

We wish now to obtain rough estimates of the reaction rates in the case of neutron transfer reactions. At high temperature, many phonons will be present, and we will assume that continuum neutron creation and distruction will be accompanied by free phonon exchange. We assume additionally that there are numerous equivalent sites for a scattered continuum neutron to be reabsorbed.

In the presence of phonon generation, continuum neutrons and holes will be generated with disparate momenta; the product of the $\hat{V}$ operators now becomes of the form

$$\hat{V}\hat{V}^{\dagger} - < 0|\hat{V}\hat{V}^{\dagger}|0 > = \sum_{\mathbf{k}\neq\mathbf{k}'} \sum_{\sigma} v_{\mathbf{k},\mathbf{k}'} \hat{d}^{\dagger}_{\mathbf{k},\sigma} \hat{d}_{\mathbf{k}',\sigma} \tag{9.10}$$

This operator now creates a neutron hole at one momentum, and then destroys a hole at a different momentum, with about the same basic interaction strength as in the case discussed above. If we term the ground state and parent nuclei as donors, with total numbers in the lattice volume V of N_D ground state nuclei and $N_{D'}$, then we approximate

$$\hat{Q}\hat{V}\hat{V}^{\dagger} \longrightarrow |v_D|^2 \frac{N_B V_n}{V} \sqrt{N_D N_{D'}} \tag{9.11}$$

where N_B is the number of free neutron Brillouin zones that contribute.

The arguments for the product $\hat{V}'\hat{V}^\dagger$ are basically similar, except that now the energy exchange must be included. We know that Φ_f has no free neutrons, so that

$$\hat{V}(\hat{V}')^\dagger|\Phi_f>=\sum_{ij}\sum_{\mathbf{k}\sigma}V_{\mathbf{k}}(V'_{\mathbf{k}})^* e^{i\mathbf{k}\cdot(\hat{\mathbf{R}}_i-\hat{\mathbf{R}}_j)}\hat{f}^\dagger_{i,\sigma}\hat{d}_{j,\sigma}|\Phi_f> \tag{9.12}$$

where $\hat{f}_{i,\sigma}$ refers to the nonequivalent isotope. If net energy transfer occurs, it must be accompanied by a change in the lattice phonon structure. Consider the matrix elements of the phonon operators over the lattice phonon states

$$M =< \Psi_i^{(L)}(\{\mathbf{R}\})|e^{i\mathbf{k}\cdot(\hat{\mathbf{R}}_i-\hat{\mathbf{R}}_j)}|\Psi_f^{(L)}(\{\mathbf{R}\})> \tag{9.13}$$

Upon rewriting this matrix element in terms of phonon mode amplitudes q_m, we find

$$M = C < \Psi_i^{(L)}(\mathbf{q}_i)|e^{i\mathbf{k}\cdot(\hat{\mathbf{R}}_i-\hat{\mathbf{R}}_j)}|\Psi_f^{(L)}(\mathbf{q}_f)> \tag{9.14}$$

where C is a normalization constant originating from the fact that the initial lattice and final lattice have a different mode structure and frequencies. Making use of Duschinsky[40,41,8–11] operators $e^{-i\hat{S}_D}$ allows us to recast this matrix element in terms of initial state phonon amplitudes $\mathbf{q}_i$; we obtain

$$M =< \Psi_i^{(L)}(\mathbf{q}_i)|e^{i\mathbf{k}\cdot(\hat{\mathbf{R}}_i-\hat{\mathbf{R}}_j)}e^{-i\hat{S}_D(i)}e^{-i\hat{S}_D(j)}|\Psi_f^{(L)}(\mathbf{q}_i)> \tag{9.15}$$

Only the few modes that jump a phonon band gap are responsible for the primary energy transfer. Consequently, it is a reasonable approximation to separate the phonon modes into gap-jumping and non-gap jumping parts, neglecting recoil for the gap-jumping modes, and neglecting mode structure changes for the non-gap-jumping modes:

$$M =< \Psi_i^{(L)}(\mathbf{q}_i)|e^{i\mathbf{k}\cdot(\hat{\mathbf{R}}_i-\hat{\mathbf{R}}_j)}|\Psi_f^{(L)}(\mathbf{q}_i)>_m< \Psi_i^{(L)}(\mathbf{q}_i)|e^{-i\hat{S}_D(i)}e^{-i\hat{S}_D(j)}|\Psi_f^{(L)}(\mathbf{q}_i)>_{m^*} \tag{9.16}$$

In this approximation, we will obtain a total reaction rate estimate of the form

$$\Gamma = \frac{2\pi}{\hbar}\frac{1}{\epsilon_d^4}|< \Phi_f|e^{-i\hat{S}_D}||\Phi_0>_{m^*}|^2|< \Phi_f|\hat{V}'\hat{V}^\dagger(E-\hat{H}_0)^{-1}\hat{Q}\hat{V}\hat{V}^\dagger|\Phi_0>_m|^2\rho(E_f) \tag{9.17}$$

This allows us to approximate

$$\hat{V}'\hat{V}^\dagger \longrightarrow v_D v_A \frac{N_B V_n}{V}\sqrt{N_D N_A} \tag{9.18}$$

for the part not involved in lattice energy transfer.

The average energy of the exchanged phonons appears in the resonant denominator; we take

$$(E - H_0)^{-1} \sim (\delta\epsilon_m)^{-1} \tag{9.19}$$

where $\delta\epsilon_m$ depends on the details of the phonon exchange. In the case of a thermal phonon distribution near room temperature, this energy will be on the order of kT.[45] In the presence of strong phonon excitation of nearly degenerate phonon modes, this energy can be much smaller.

The density of states is dominated by the lattice energy exchange; we take

$$\rho(E_f) \sim \frac{1}{\sqrt{N_m}} \frac{1}{\hbar\omega_m} \tag{9.20}$$

which is appropriate for a highly excited classical phonon state. If number states were somehow generated, then the spread could be lower by several orders of magnitude.

These approximations leads to a total rate crudely estimated to be

$$\Gamma \sim \frac{2\pi|v_A|}{\hbar} \frac{|v_D|^4}{\epsilon_d^4} \frac{|v_D|^2}{\delta\epsilon_m^2} N_S N_D^2 N_{D'} N_A \left[\frac{N_B V_n}{V}\right]^4 \frac{|v_A|}{(\Delta E_L \hbar\omega_m)^{1/2}} \tag{9.21}$$

where N_S is the number of regions in the lattice that can transfer an energy ΔE_L from the lattice to drive a reaction.

Whether this theory leads to net reaction rates that are observable depends on the numbers, and we can use equation (9.21) to obtain crude estimates. There are several different situations to be considered; we consider first transitions mediated by thermal phonons. In this case, the largest reaction rates will be produced by donors and acceptors both of which interact with s-wave continuum neutrons. These are listed in Table I. We choose for a numerical example here silicon, which may be both donor and acceptor (^{29}Si as donor and ^{29}Si as acceptor).

The interaction matrix elements are parametrized by the volume-reduced quantities v_D and v_A; we assume here that $|v_D| \sim |v_A| \sim 10^6$ eV. We take $\epsilon_d \sim -9$ MeV. The nuclear volume V_n for a mass 30 nucleus is on the order of $V_n \sim 1.2 \times 10^{-37}$ cm^3. The ratio $N_D N_B/V$ is on average the inverse atomic volume to which the donor nuclei are localized: this can be made to be on the order of $(8 \times 10^{-27})^{-1}$ cm^{-3}. The maximum number of phonon regions capable of transferring about $\Delta E_L = 2.1$ MeV is about $N_S = 10^{12}$ per cm^3. The optical phonon energy $\hbar\omega_m$ is assumed to be on the order of 0.035 eV.

Isotope	Neutron Binding Energy (MeV)
^{2}H	2.2244
^{3}H	6.2570
^{119}Sn	6.4870
^{113}Cd	6.5420
^{125}Te	6.5718
^{129}Xe	6.9081
^{123}Te	6.9379

Isotope	Neutron Binding Energy (MeV)
^{117}Sn	6.9453
^{111}Cd	6.9752
^{115}Sn	7.5462
^{29}Si	8.4740
^{114}Cd	9.0431
^{120}Sn	9.1055
^{126}Te	9.1139

Isotope	Neutron Binding Energy (MeV)
^{130}Xe	9.2555
^{118}Sn	9.3263
^{112}Cd	9.3980
^{124}Te	9.4204
^{116}Sn	9.5629
^{30}Si	10.6099
^{4}He	20.5817

Table I: Binding energies of neutrons of stable nuclei (and tritium) that will have configuration mixing with stable parents and s-wave continuum neutron orbitals.

In the case of reactions driven by thermal phonons, the resonant energy is on the order of $\delta\epsilon_m \sim 0.025$ eV. This yields a total reaction rate that is on the order of 7×10^4 sec^{-1} cm^{-3}.

The large energy transfer with the lattice is driven by the presence of an optical phonon field with a very high modal occupation. If that phonon field is sufficiently strong locally to compete against the thermal field, then phonon interactions with significantly lower dispersion can occur. If so, we may take $\delta\epsilon_m \sim \hbar\omega_m/Q$, where Q is the phonon quality factor, which we assume to be on the order of 10^3. This results in a reaction rate that is on the order of 4×10^{10} sec^{-1} cm^{-3}.

We have assumed that the energy transfer with the lattice is mediated by classical states, rather than by phonon number states. It may be that neutron transfer reactions would generate phonon number states (speculation at this point); if so, rates two to three orders of magnitude higher would be produced.

There remain other sources of considerable uncertainty. The assumption of $|v_A| \sim |v_D| \sim 10^6$ eV is at this point a rough guess; the answer is sensitive to this quantity to the eighth power. The nuclear potential is known to be able to effectively modify the magnitude of the normalization V_n considerably (as is well known in the case of neutron capture on protons).

The level shift predicted by equation (6.18) evaluates to

$$\delta E \sim \frac{|v_D|^2}{|\epsilon_D|}\left[\frac{N_D N_{D'} N_B^2}{V^2}\right]^{1/2} V_n \tag{9.22}$$

using the crude approximations outlined above. Using the numbers for our example, this energy shift is about 1.7 μeV, which is small compared to the width $\delta\epsilon_m$. We may check for the breakdown of perturbation theory; for example, the use of only the first term in the Taylor series expansion for Ψ_1 given in equation (6.14) requires that

$$\frac{\hat{V}\hat{V}^\dagger}{\epsilon_d \delta\epsilon_m} \longrightarrow \frac{|v_0|}{\epsilon_d}\frac{|v_0|}{\delta\epsilon_m}(N_D N_{D'})^{1/2}\frac{N_B V_n}{V} \tag{9.23}$$

be less than unity in magnitude. It is observed that this is equivalent to the condition

$$\frac{\delta E}{\delta\epsilon_m} < 1 \tag{9.24}$$

which is satisfied in this example.

We consider a second example in which the acceptor nuclei interacts with p-wave continuum neutron orbitals, and orthogonality is circumvented by phonon interactions. This example is potentially interesting since the number of nuclei that interact with s-wave neutrons is rather small. Nuclei that interact with p-wave free neutron orbitals are given in Table II.

Isotope	Neutron Binding Energy (MeV)	Isotope	Neutron Binding Energy (MeV)	Isotope	Neutron Binding Energy (MeV)
^{13}C	4.9463	^{7}Li	7.2499	^{188}Os	7.9607
^{195}Pt	6.1051	^{208}Pb	7.3682	^{172}Yb	8.0203
^{183}W	6.1918	^{184}W	7.4120	^{200}Hg	8.0287
^{201}Hg	6.2299	^{77}Se	7.4195	^{156}Gd	8.5373
^{187}Os	6.2914	^{57}Fe	7.6458	^{54}Cr	9.7194
^{157}Gd	6.3594	^{202}Hg	7.7548	^{58}Fe	10.0454
^{155}Gd	6.4349	^{61}Ni	7.8200	^{78}Se	10.5009
^{171}Yb	6.6147	^{196}Pt	7.9225	^{62}Ni	10.5978
^{199}Hg	6.6640	^{158}Gd	7.9383	^{15}N	10.8344
^{207}Pb	6.7376	^{53}Cr	7.9393	^{11}B	11.4548

Table II: Binding energies of neutrons of stable nuclei (and tritium) that will have configuration mixing with stable parents and p-wave continuum neutron orbitals.

Unfortunately, the interaction matrix elements for p-wave transitions will be suppressed by a factor of kR relative to analogous s-wave matrix elements, where k is the continuum neutron wavenumber and where R is the nuclear radius. If a p-wave transition is paired with an s-wave transition, either as donor or acceptor, in a phonon-assisted reaction as described above, then the resulting rate will be smaller by a factor of $(kR)^2$ which is about 10^{-8}. Transitions involving d-wave or higher order interactions will be further suppressed relative to s-wave transitions.

Rather than seeking modifications in linear momentum of the continuum neutrons as occurs in the case of phonon exchange as formulated above, we next examine the destruction of orthgonality through nonconservation of angular momentum. In this case, we consider delocalization of virtual neutrons by p-wave transitions in the absence of phonon exchange. The basic mechanism was outlined briefly above; a donor nucleus with quantum numbers $(J)^\pi$ and M_J couples through the strong interaction to a continuum state with identical quantum numbers. If the neutron is resonantly captured by an equivalent parent nucleus at another site that is translated in space, the capture can produce a new nucleus with quantum numbers $(J)^\pi$ and M'_J. The change in angular momentum comes about due to the translation; a virtual neutron that has a non-zero angular momentum relative to one site will generally have a different angular momentum relative to a distant site. By definition, this route is unfortunately not available to transitions involving s-wave continuum orbitals, which are initially isotropic, and hence preserve M_J.

Given the terrible price that must be paid for coupling to p-orbitals as discussed above, the question arises as to what new physics might make such an approach worthwhile? Since no phonon exchange occurs, this type of interaction can be truly resonant, and some ground can be made up through the presence of smaller resonant denominators.

In this case, the interaction operator might be taken to be of the form

$$\hat{V} = \sum_i \sum_{\mathbf{k}\sigma\sigma'} V^*_{\sigma,\sigma'}(\mathbf{k}) e^{i\hat{\mathbf{k}}\cdot\hat{\mathbf{R}}_i} \hat{d}^\dagger_{i,\sigma} \hat{c}_{\mathbf{k},\sigma'} \tag{9.24}$$

although it might be more natural to use a Hubbard operator formalism as appropriate to SU(N) models, in which the non-conservation of angular momentum would show up without any modifications. In this case, the projection problem of equation (9.8) no longer occurs. The captured neutron will now produce a degenerate new state that is with finite probability not equivalent to the initial state. The resonant denominator is then determined by whatever shifts and widths are appropriate: for example, nuclear magnetic and crystal quadrupole interactions will broaden the nuclear levels. The level shift predicted by equation (6.18) will be greater than these under conditions where significant reactions are expected.

We consider an example in which virtual neutron delocalization is present in a p-wave system,

and the second pair of the donor and acceptor is an s-wave system. For example, ^{62}Ni (p-wave) donating to ^{29}Si (s-wave) has a very small energy defect of about 12 KeV.

In this case, we assume that $|v_D| \sim 10^{-4}$ MeV, $|v_A| \sim 1$ MeV, and $|\epsilon_D| \sim 10.6$ MeV. The nuclear volume of Ni is $V_n \sim 2.4 \times 10^{-37}$ cm^3, and we retain our earlier crude estimate for $N_D N_B/V$. The ^{61}Ni linewidth is taken to be 10^{-11} eV (this is a guess). Using these numbers, we obtain a rate on the order of 25 sec^{-1} cm^{-3}. The energy shift is small, $\delta E \sim 3 \times 10^{-14}$ eV, and from this we know that $\delta E/\delta\epsilon_m < 1$ implying that perturbation theory does not break down.

If the matrix element v_D were larger, due to possible effects mentioned above, then it might be possible to enter into a nonperturbative regime. With the numbers given, an increase of a factor of 20 in $|v_D|$ would succeed in making $\delta E/\delta\epsilon_m > 1$; such a correction is by no means out of the question given the rough approximations used. Whether the nonperturbative regime leads to a substantial increase in neutron delocalization is unknown, but is a question of great interest. The perturbative rate in this case would be about 10^9 sec^{-1} cm^{-3}. Such a mechanism would be very attractive in accounting for excess heat claims in light water experiments.

We note that the use of electromagnetic E1 or M1 matrix elements in this theory leads to reaction rates below 10^{-50} sec^{-1} per cm^3. The rate depends on the coupling matrix element through v^8, which favors strong force matrix elements.

10. Conclusions and Discussion

The key contributions in this work are: (1) the formulation of a neutron version of the Anderson model to describe configuration interaction effects between neutron valence and conduction bands; (2) the observation that the Wannier overlap from neighboring sites normally responsible for mixing in the Anderson model vanishes, and must be replaced by two-nucleon matrix elements in the neutron Anderson model; (3) the proposal of the one-neutron approximation; (4) the development of infinite-order Brillouin-Wigner theory solutions that give rise to a useful perturbation theory; (5) the development of formal rate formulas for incoherent and lattice-assisted neutron transfers; and (6) the crude estimate of rates in the case of lattice-assisted transfer reactions.

We have developed this model as a candidate theory to account for anomalous heat production in Pons-Fleischmann experiments. In connection with these experiments, this model would fit the reported observations qualitatively much more closely than modified dd-fusion related theories. Although we have not emphasized the point here, the formulas for incoherent neutron capture and lattice-assisted neutron capture strongly favors the lattice-assisted reactions when they can occur; heat production through this mechanism would be relatively clean.

In the case of the Pons-Fleischmann experiments, our earlier suggestions that neutron transfer reactions between ^{105}Pd and ^{7}Li to account for heat production do not appear to survive the selection rule considerations discussed in the present work. Possible alternative reactions include the ^{29}Si to ^{29}Si transfer (leading to ^{28}Si and ^{30}Si) at 2.14 MeV, and the ^{30}Si to ^{10}B transfer at 845 KeV. In the light water experiments, the ^{62}Ni to ^{29}Si transfer at 12 KeV looks most promising.

There remains numerous issues to resolve. The reaction rates discussed in this work are quite sensitive to transition matrix elements that are not currently well known; these matrix elements must be quantified as a high priority for further progress to be made. There is a more subtle issue involving the highly excited phonon modes that must also be considered.

For example, during a single lattice-assisted neutron transfer reaction, the energy transfer occurs through up-shifting a large number of phonons in a gap-jumping mode. If new phonons had to be supplied to the next gap-jumping mode before more reactions could occur, the overall dynamics would be grossly inefficient, and there would be no possibility of reaching the efficiencies claimed in experiments. In our earlier proposals, we have assumed that the phonons could be brought back into position through Raman mixing with lower energy phonons, in essence dumping extra energy by generating phonons at the difference frequency. An alternative approach is to simply decay incoherently back down, since the downward step is exothermic relative to lattice decays which we have described elsewhere.[11]

There remain numerous other issues that are of interest. For example, the progress in heat-producing experiments has not yet lead to a generally accepted quantitative demonstration of reaction product. It is our hope that this work will help to motivate such searches. An alternate test of the theory would be the activation of a host lattice or impurities through nearly-resonant neutron transfers. Detection of neutron hopping in null reactions through an isotopically sensitive self-diffusion experiment would also be of great interest to verify the phenomenon discussed in this work.

Acknowledgements

One of the authors (PLH) would like to acknowledge support from EPRI and from the EE & CS Department at MIT; SK acknowledges support from ENECO. The authors would like to thank L. Smullin and Y. Fukai for valuable conversations.

References

1. S. Pons, M. Fleishmann and M. Hawkins, *J. Electroanal. Chem* **261** 301 (1989).

2. S. Pons and M. Fleischmann *Phys. Lett. A* **176** 118 (1993).

3. M. C. H. McKubre, S. Crouch-Baker, A. M. Riley, S. I. Smedley and F. L. Tanzella, *Frontiers of Cold Fusion*, Proceedings of the Third International Conference on Cold Fusion, Ed. H. Ikegami, Nagoya, Oct. 1992; p. 5.

4. K. Kunimatsu, N. Hasegawa, A. Kubota, N. Imai, M. Ishikawa, H. Akita, and Y. Tsuchida, *Frontiers of Cold Fusion*, Proceedings of the Third International Conference on Cold Fusion, Ed. H. Ikegami, Nagoya, Oct. 1992; p. 31.

5. G. Preparata, this conference.

6. Y. Kim, J.-H. Yoon, A. Zubarev, and M. Rabinowitz, this conference.

7. G. Hale, this conference.

8. P. L. Hagelstein, *Fusion Tech.* **22** 172 (1992).

9. P. L. Hagelstein, *Fusion Tech.* **23** 353 (1993).

10. P. Hagelstein, *Frontiers of Cold Fusion*, Proceedings of the Third International Conference on Cold Fusion, Ed. H. Ikegami, Nagoya, Oct. 1992; p. 297.

11. P. L. Hagelstein, this conference.

12. P. W. Anderson, *Phys. Rev.* **124** 41 (1961).

13. B. H. Brandow, *Phys. Rev. B* **33** 215 (1986).

14. J. R. Schrieffer and P. A. Wolfe, *Phys. Rev.* **149** 491 (1966).

15. C. Lacroix and M. Cyrot, *Phys. Rev. B* **20** 1969 (1979).

16. J. M. Will and B. R. Cooper, *Phys. Rev. B* **36** 3809 (1987).

17. J. K. Freericks and L. M. Falicov, *Phys. Rev. B* **46** 874 (1992).

18. A. E. Tolpin, *J. Low Temp. Phys.* **87** 1 (1992).

19. R. Mills and K. Kneizys, *Fusion. Tech.* **20** 65 (1991).

20. R. Notoya and M. Enyo, *Frontiers of Cold Fusion*, Proceedings of the Third International Conference on Cold Fusion, Ed. H. Ikegami, Nagoya, Oct. 1992; p. 421.

21. T. N. Claytor, D. G. Tuggle and S. F. Taylor, *Frontiers of Cold Fusion*, Proceedings of the Third International Conference on Cold Fusion, Ed. H. Ikegami, Nagoya, Oct. 1992; p. 217.

22. F. Lanza, V. Bertolini, E. Vocino, E. Parnisari, and C. Ronseco, *The Science of Cold Fusion*, Ed. T. Bressani, E. Del Guidice, and G. Preparata, Conf. Proc. Vol. 33, Italian Physical Society, Bologna, 1992; p. 151.

23. H. J. Leder and G. Czycholl, *Z. Phys. B* **35** 7 (1979); *Z. Phys. B***38** 219 (1980); *Z. Phys. B***44** 59 (1981); *Z. Phys. B***48** 67 (1982).

23. T. Yanagisawa, *Physica B* **186-188** 876 (1993).

24. F. D. M. Haldane, *Phys. Rev. Lett.* **40** 416 (1978).

25. L. G. Brunet, M. A. Gusmao, and J. R. Iglesias, *Phys. Rev B* **46** 4520 (1992).

26. T. Venkatappa Rao, R. G. Gangadhar Reddy and A. Ramakanth, *Sol. State Comm.* **81** 795 (1992).

27. M. Roberts and K. W. H. Stevens, *J. Phys. C* **13** 5941 (1980).

28. C. M. Varma and Y. Yafet, *Phys. Rev. B* **13** 2950 (1976).

29. J. H. Jefferson and K. W. H. Stevens, *J. Phys. C* **9** 2151 (1976).

30. Y. Kuramoto, *Z. Phys. B* **40** 293 (1981).

31. N. Grewe and H. Keiter, *Phys. Rev. B* **24** 4420 (1981).

32. D. L. Huber, *Phys. Rev. B* **28** 860 (1983).

33. T. Yanagisawa, *J. Phys. Soc. Jap* **57** 4071 (1988).

34. O. Sakai, S. Seki and M. Tachiki, *J. Phys. Soc. Jap* **45** 1465 (1978).

35. P. Coleman, *Phys. Rev. B* **29** 3035 (1984).

36. K. Miura, T. Matsuura and Y. Kuroda, *Physica C* **179** 411 (1991).

37. Y. Kuroda, Y. Ono, K. Miura, B. Jin, H. Jichu, D. Hirashima, T. Matsura, *Prog. Theor. Phys. Suppl.* 18 173 (1992).

38. A. DeShalit and H. Feshbach *Theoretical Nuclear Physics* John Wiley and Sons, New York (1974).

39. H. Feshbach, *Ann. Phys.* **5** 357 (1958).

40. F. Duschinsky, *Acta Physicochimica U.R.S.S* **7** 551 (1937).

41. T. R. Faulkner and F. S. Richardson, *J. Chem. Phys.* **70** 1201 (1979).

42. Z. Hang, *Phys. Rev. B* **36** 8736 (1987).

43. Z. Hang, *J. Phys. C* **21** 2351 (1988).

44. Z. Hang, *Phys. Rev. B* **38** 6991 (1988).

45. Z. Azzam, *Neutron Transfer Reactions*, MIT SM Thesis, Feb. 1994.

LATTICE-INDUCED ATOMIC AND NUCLEAR REACTIONS

Peter L. Hagelstein

Massachusetts Institute of Technology
Research Laboratory of Electronics
Cambridge, Massachusetts 02139

ABSTRACT

A new theory for a variety of atomic and nuclear reaction mechanisms resulting from the decay of a highly excited lattice is introduced.

In our previous work on neutron transfer reactions, we found that large energy transfer between a lattice and nuclei could occur through the frequency shift of a highly excited continuum phonon mode across a band gap that is caused by the neutron transfer. Here, we generalize the energy transfer mechanism to include impurity continuum phonon modes due to the presence of vacancies; processes that change the number of vacancies can in principle stimulate the transfer of energy with the lattice.

A consequence of this is that a metal hydride lattice with host vacancies that has very high excitation of gap-jumping phonon modes will be unstable against decay by a variety of atomic and nuclear processes. Coulomb-induced recoil reactions of nuclei with electrons and nearby nuclei that cause vacancy production are found to occur with very high predicted reaction rates.

A lattice with a large number of highly excited phonon modes that can decay sequentially will most likely decay with a "burst" of emitted decay products, as a high order multi-step quantum process. A theory for this type of high-order decay is outlined.

The predictions of this theory may apply to many of the anomalous phenomena claimed to occur in experiments performed on metal deuterides, including neutron production, tritium production, gamma emission and host lattice activation.

1. Introduction

Nearly five years have passed sinced the initial announcement by Pons and Fleischmann[1] of the observation of what they and others have termed "cold fusion." During this time, a wide variety

of claims have been made for the observation of anomalous phenomena of one sort or another in PdD, in TiD_2,[2-5] in other metal deuterides,[6,7] and now also in metal hydrides.[8-10] Perhaps most important, if true, is the claimed observation of excess heat; the heat production reported is sufficiently large that if real, it would not be attributable to chemical or other atomic effects.[11] Many in the field hope that this effect, believed to be due to yet unknown nuclear reactions, will eventually be harnessed to provide a new clean source of energy for mankind.

The scientific community has long since grown immune to any reports of such claims. In a sense, the field of "cold fusion" has been judged, the data weighed and found wanting, and the field sentenced to oblivion. The cause: experiments that seem not to be reproducible, data that may suffer from either systematic errors or poor signal to noise ratio, no consistent effect that appears in all experiments, and no compelling theoretical reason to believe that anything anomalous should happen at all. No obvious progress has been made during the past year in effecting a basic change in attitude.

Our research in the area takes as its premise the possibility that some of the experimental results are in fact correct, and seeks to address the question as to what physical mechanisms, if any, could be responsible. Our studies have led us to consider numerous potential nuclear reaction pathways, focussing on possible enhancements in reaction rates that might be brought about by the atomic environment. Due to the large energy required to cause anything nuclear to happen, it is crucial in any such candidate theory for a clear and obvious energy transfer mechanism to be present that is capable of transferring such large energy.

Recently, such a mechanism was identified in the case of reactions that involve neutron transfer.[12] The basic idea is to generate a very large number of phonons into a small number of continuum phonon modes, and then shift the frequency of these phonon modes by transferring a neutron to or from a nucleus in the lattice. The total energy transfer through this mechanisms is

$$\Delta E = n\hbar\delta\omega \tag{1.1}$$

where $\delta\omega$ is the frequency shift, and where where n is the number of phonons present in the frequency-shifting modes.

To arrange for a continuum phonon mode to change its resonant frequency can be accomplished in certain materials that possess an impurity phonon band separated from other phonon modes by a finite band gap; a neutron transfer process that changes the number of impurity atoms also causes a change in the number of impurity phonon modes, which implies that a small number of phonon modes must jump the band gap. To arrange for a large number of phonons to be in a small number of phonon modes essentially implies the presence of a phonon laser.

Recently we have proposed the generalization of this mechanism to a much wider class of processes, some of which are nuclear and some of which are atomic. The key observation is that an impurity band can be due to the presence of vacancies, which implies that mechanisms that alter the number of vacancies of a certain type can in principle cause a large energy transfer to occur.

For example, in a metal deuteride that possesses a large band gap between the acoustic and optical phonon branches, it may occur that impurity bands for those deuterium atoms near a vacancy will form within the band gap. In PdH, for example, the basic hydrogen occupation of octohedral sites persists in lattice cells with a Pd vacancy;[13] we assume that the same is true in PdD. Deuterium atoms next to a Pd vacancy see a softer potential, and consequently oscillate at a lower frequency, than deuterium atoms not next to a vacancy. The frequency of this type of defect vacancy band is presently unknown; we will make the anzatz in this work that these modes in fact lie within the band gap in the case of the metal deuteride PdD (see Figure 1). A change in the number of vacancies will result in a change in the number of vacancy phonon modes; new vacancy modes are formed from the lowest modes above the band gap, which jump down to join the vacancy impurity band.

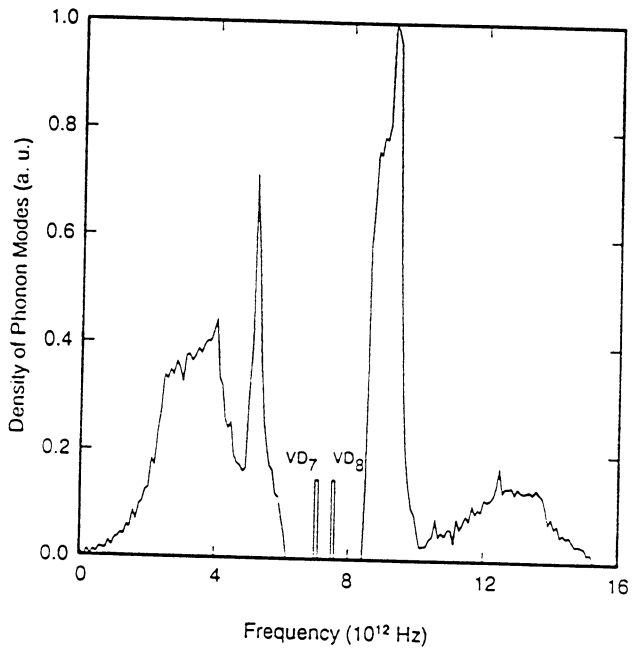

Figure 1: Density of states in PdD (based on the force constants of Ref. 14), augmented with proposed vacancy impurity bands (VD_7 and VD_8). VD_8 indicates modes due to cells with 8 deuterons around a Pd vacancy; VD_7 indicates modes due to 7 deuterons around a Pd vacancy.

In a metal hydride that works in the way outlined above, the generation of a very large number of

phonons in "gap-jumping" phonon modes results in an unstable system that will decay through any mechanism that produces an additional vacancy. For example, the Coulomb interaction between an electron and a nucleus can result in a fast ejected electron, as long as the recoil is sufficient to irreversibly displace the nucleus; in this case the reaction energy is supplied by the lattice through frequency-shifting a large number of phonons, which is caused by the reaction. Coulomb interactions between neighboring nuclei can cause recoil capable at lower energy of ejecting nuclei and causing phonon mode jumps. In the event that the lattice transfers a very large amount of energy, nuclear decay channels become available.

In what follows, we will outline briefly the basic theory for anomlous energy transfer from the lattice, and then review results for various decay channels. Although it is straightforward to compute reaction rates using Fermi's Golden Rule, we find that the rates predicted in this way are much too large for the processes to occur independently; Fermi's Golden Rule breaks down. Consequently, if the processes occur at all, they must occur in bursts as coupled reactions. The generalization of the theory to describe coupled reactions is straightforward formally, but leads to formulas for reaction rates that appear to be difficult to evaluate; we propose a method to extract numerical results from these formula.

2. Lattice-Induced Fast Electron Production

The decay of a highly-excited atomic or nuclear system by Coulomb-mediated fast electron production is well known; in the atomic system the process is known as autoionization, or Auger decay; in the nuclear system, this process is known as internal conversion. A molecule with a very high level of vibrational excitation could in principle decay through electron ejection, although the author is not aware of any examples where this has been observed. The decay of a highly excited lattice by fast electron ejection as a direct process has not been described previously.

A lattice with a highly-excited gap-jumping mode will be able to decay by electron ejection, as long the recoil is sufficiently great for a vacancy to be produced. As an example, we consider lattice decay through ejection of a K-shell electron, in a lattice with very great excitation of the lowest optical phonon modes. The electron recoil in this case must be sufficiently strong to permanently dislodge the nucleus. Our goal in what follows here is to describe a theory for this process that includes explicitly the energy transfer from the lattice, the Coulomb interaction between electron and nucleus, and the resulting nuclear recoil.

In perhaps the simplest possible model for such a decay process, we may start with Fermi's Golden Rule

$$\Gamma = \frac{2\pi}{\hbar} \sum_f \sum_{\mathbf{k}} | < \Psi_i | \hat{V} | \Psi_f > |^2 \delta(I_K + \hbar^2 |\mathbf{k}|^2 / 2m_e + E_f^{(L)} - E_i^{(L)}) \tag{2.1}$$

In this formula, the phonon operator $\hat{V}$ is the Coulomb potential between the nuclei and the K-shell electrons

$$\hat{V} = \sum_j \sum_{j'} \frac{Ze^2}{|\mathbf{r}_{j'} - \hat{\mathbf{R}}_j|} \tag{2.2}$$

where $\mathbf{r}$ refers to the electron coordinate, and where the nuclear center of mass coordinates $\hat{\mathbf{R}}_j$ are taken to be lattice phonon operators. The summations are over all final lattice states f and final electron momenta $\mathbf{k}$. Energy conservation is constrained between the initial lattice energy and final lattice plus electron energy; I_K is the K-shell electron binding energy.

The individual matrix elements that occur in the Fermi's Golden Rule rate formula

$$M = < \Psi_i | \hat{V} | \Psi_f > \tag{2.3}$$

approximately factor into parts that can be individually identified with Coulomb exchange, recoil and mode frequency-shifting, as we will argue below. To do so, we will use the Born approximation for the free electron, and the Born-Oppenheimer approximation for the lattice nuclear motion.

For the computation of an individual matrix element, the initial and final state wavefunctions are taken to be product wavefunctions that are built up from lattice wavefunctions $\Psi^{(L)}$ and single electron orbitals ϕ as follows:

$$\Psi_i = \Psi_i^{(L)} \phi_{1s}(\mathbf{r} - \hat{\mathbf{R}}_j) \tag{2.4}$$

$$\Psi_f = \Psi_f^{(L)} \phi_{\mathbf{k}}(\mathbf{r}) \tag{2.5}$$

This form of initial and final state wavefunctions is appropriate for a rate involving a single electron transfer; had we started with a more complicated many-electron wavefunction, we would find that only one orbital at a time contributes to the total rate. We must keep the total lattice wavefunction at this point, since the vibrational energy that is transferred in the process is not localized.

The integration over an electron coordinate at site j yields

$$\int \phi_{1s}^*(\mathbf{r} - \mathbf{R}_j) \frac{Ze^2}{|\mathbf{r} - \hat{\mathbf{R}}_j|} \phi_{\mathbf{k}}(\mathbf{r}) d^3\mathbf{r} = V(\mathbf{k}) e^{i\mathbf{k}\cdot\hat{\mathbf{R}}_j} \tag{2.6}$$

where

$$V(\mathbf{k}) = Ze^2 \left[\frac{N_{1s}}{V}\right]^{\frac{1}{2}} \left[\frac{Z^3}{\pi a_0^3}\right]^{\frac{1}{2}} \frac{4\pi}{|\mathbf{k}|^2 + (Z/a_0)^2} \tag{2.7}$$

assuming a nonrelativistic $1s$ hydrogenic orbital and a plane-wave $e^{i\mathbf{k}\cdot\mathbf{r}}/\sqrt{V}$ continuum orbital; the number of $1s$ electrons in the K-shell orbital at site j is N_{1s}.

The matrix element for a Coulomb exchange that occurs at site j can now be written as

$$M = V(\mathbf{k}) < \Psi_i^{(L)} | e^{i\mathbf{k}\cdot\hat{\mathbf{R}}_j} | \Psi_f^{(L)} > \tag{2.8}$$

The definitions of the phonon modes may differ between the initial and final lattice states, so that some care must be taken in analyzing this matrix element. In our previous work on energy transfer in the case of neutron capture reactions,[15] we found that correct answers could be obtained most simply by taking equation (2.8) to be defined as involving integrations over nuclear center of mass coordinates

$$M = V(\mathbf{k}) < \Psi_i^{(L)}(\{\mathbf{R}\}) | e^{i\mathbf{k}\cdot\mathbf{R}_j} | \Psi_f^{(L)}(\{\mathbf{R}\}) > \tag{2.9}$$

temporarily dispensing with carats to indicate phonon operators. Considering all terms to be functions of center of mass coordinates removes any such problems because the center of mass coordinates themselves are invariant during Coulomb exchange. The nuclear center of mass coordinates can be expressed in terms of the initial state and final state phonon mode amplitudes q_m through

$$\mathbf{R}_j = \mathbf{R}_j^{0,i} + \sum_m \mathbf{u}_m^{(i)}(j) q_m \tag{2.10}$$

$$\mathbf{R}_j = \mathbf{R}_j^{0,f} + \sum_m \mathbf{u}_m^{(f)}(j) q_m \tag{2.11}$$

where $\mathbf{u}_m^{(i)}(j)$ and $\mathbf{u}_m^{(f)}(j)$ are the lattice displacement vectors for the initial and final lattices.

We need to recast the matrix element M in terms of phonon mode amplitudes in order to analyze frequency-shifting effects. Changing over to phonon amplitudes leads to

$$M = V(\mathbf{k})C < \Psi_i^{(L)}(\mathbf{q}_i) | e^{i\mathbf{k}\cdot\mathbf{R}_j} | \Psi_f^{(L)}(\mathbf{q}_f) > \tag{2.12}$$

The normalization coefficient C is required since the initial and final state phonon amplitudes may not be equivalent. Due to this inequivalence, the matrix element is very difficult to compute in its present form: we would be able to make further progress if we could express Ψ_f in terms of $\mathbf{q}_i$.

As a consequence of the invariance of the center of mass coordinates during Coulomb exchange, there exists a linear relationship between the initial and final state mode amplitudes. From equations (2.10) and (2.11), it is possible to compute individual final state phonon amplitudes in terms of initial state phonon amplitudes; the resulting relation can be summarized as

$$\mathbf{q}_f = \mathbf{A} \cdot \mathbf{q}_i + \mathbf{b} \tag{2.13}$$

in the case of a harmonic lattice. This problem is well known in the case of electronic transitions in polyatomic molecules, and the above relation between initial and final state phonon amplitudes is called a Duschinsky transformation.[16]

Our goal of obtaining the final state wavefunction in terms of the initial state coordinates is accomplished through the use of the Duschinsky operator $e^{-i\hat{S}_D}$,[17] which has the property

$$e^{-i\hat{S}_D}\psi(\mathbf{q}_i) = \psi(\mathbf{A} \cdot \mathbf{q}_i + \mathbf{b}) = \psi(\mathbf{q}_f) \tag{2.14}$$

We may use this to rewrite the matrix element M as

$$M = V(\mathbf{k}) < \Psi_i^{(L)}(\mathbf{q}_i)|e^{i\mathbf{k}\cdot\hat{\mathbf{R}}_j}e^{-i\hat{S}_D}|\Psi_f^{(L)}(\mathbf{q}_i) > \tag{2.15}$$

once again using carats to indicate phonon operators.

There exists a very large number of phonon modes in a macroscopic lattice, but only a few modes can undergo a significant frequency shift during the creation of a single vacancy. Although the frequency-shifting modes will be involved in the recoil, recoil effects will be dominated by the vast majority of the modes that do not undergo any significant frequency shift. This suggests that a separation between recoil effects and frequency-shifting would be a reasonably good approximation, leading to

$$M \approx V(\mathbf{k}) < \Psi_i^{(L)}(\mathbf{q}_i)|e^{-i\hat{S}_D}|\Psi_f^{(L)}(\mathbf{q}_i) >_{m^*} < \Psi_i^{(L)}(\mathbf{q}_i)|e^{i\mathbf{k}\cdot\mathbf{R}_j}|\Psi_f^{(L)}(\mathbf{q}_i) >_m \tag{2.16}$$

where $< \cdots >_m^*$ denotes an average over the gap-jumping modes, and where $< \cdots >_m$ denotes an average over non gap-jumping modes. This result perhaps exhibits most cleanly the physics involved in the proposed decay of a highly excited lattice by electron emission; the Coulomb exchange between nucleus and electron results in $V(\mathbf{k})$; energy transfer of the lattice comes about through frequency shifts in a small number of phonon modes; and the vacancy production required for energy transfer to occur is a simple recoil effect.

The reaction rate for a transition at site j is then given by

$$\Gamma_j = \frac{2\pi}{\hbar}\sum_f\sum_{\mathbf{k}}|V(\mathbf{k})|^2| < \Psi_i^{(L)}(\mathbf{q}_i)|e^{-i\hat{S}_D}|\Psi_f^{(L)}(\mathbf{q}_i) >_{m^*} |^2$$

$$| < \Psi_i^{(L)}(\mathbf{q}_i)|e^{i\mathbf{k}\cdot\mathbf{R}_j}|\Psi_f^{(L)}(\mathbf{q}_i) >_m |^2\delta(I_K + \hbar^2|\mathbf{k}|^2/2m_e + E_f^{(L)} - E_i^{(L)}) \tag{2.17}$$

It is convenient to introduce a function that keeps track of the probability that an energy transfer ϵ occurs, given a recoil momentum $\mathbf{k}$. Such a function may be conveniently defined through

$$p_{j,\mathbf{k}}(\epsilon) = \sum_f | < \Psi_i^{(L)}(\mathbf{q}_i)|e^{-i\hat{S}_D}|\Psi_f^{(L)}(\mathbf{q}_i) >_{m^*} |^2| < \Psi_i^{(L)}(\mathbf{q}_i)|e^{i\mathbf{k}\cdot\mathbf{R}_j}|\Psi_f^{(L)}(\mathbf{q}_i) >_m |^2\delta(\epsilon + E_f^{(L)} - E_i^{(L)}) \tag{2.18}$$

This function may be used to develop a perhaps more intuitive version of the decay rate, given by

$$\Gamma_j = \sum_{\mathbf{k}}\int p_{j,\mathbf{k}}(\epsilon)\Gamma_{j,\mathbf{k}}(\epsilon)d\epsilon \tag{2.19}$$

with

$$\Gamma_{j,\mathbf{k}}(\epsilon) = \frac{2\pi}{\hbar}|V(\mathbf{k})|^2\delta(I_K + \hbar^2|\mathbf{k}|^2/2m_e - \epsilon) \tag{2.20}$$

These formulas suggest a point of view in which there exists a probability p of transferring an energy ϵ from the lattice, and that energy transfer drives a reaction with a partial rate that may be computed essentially without consideration of lattice effects.

The computation of $p_{j,\mathbf{k}}(\epsilon)$ is of course in general quite complicated. As defined, this function is proportional to a lineshape function that might be associated with a process that has an associated recoil and that modifies the underlying phonon mode structure. The recoil term by itself is generally computed by evaluating contributions from 0,1,...,n-phonon pieces; the mode-matching physics is usually treated in perturbation theory. In the case of a thermal lattice, this function would result in a rather standard few-meV wide line that is perhaps shifted by a few-meV. However, if there exist highly excited phonon modes that jump a band gap as a result of modifications to the lattice due to recoil, then the function must shift in energy by an amount $n\delta\omega$ for each mode that jumps, as would a line profile under corresponding circumstances.

In general, there will be a probability that sufficient recoil will occur to cause a gap jumps, as well as a probability that the recoil is insufficient to cause gap jumps. In this case, the function $p_{j,\mathbf{k}}(\epsilon)$ will have two pieces – one that gives energy transfer, and one that does not. Of course, if no energy transfer occurs due to gap-jumping, then the energy transfer from the lattice from thermal recoil effects alone will be too small to drive any of the reactions that we consider below.

Consequently, our interest is focussed only on the part of $p_{j,\mathbf{k}}(\epsilon)$ that corresponds to situations where gap-jumping occurs. Mathematically, the probability $p_{j,\mathbf{k}}(\epsilon)$ will be of the form

$$p(\epsilon) = |T|^2 p_{jump}(\epsilon - \sum n\hbar\delta\omega) + (1 - |T|^2) p_{no\ jump}(\epsilon) \tag{2.21}$$

where $|T|^2$ is the probability that the recoil was sufficient to cause a jump, and where $p_{jump}(\epsilon)$ and $p_{no\ jump}(\epsilon)$ are complicated functions of energy whose precise shapes will be of little concern to us, as long as $p_{jump}(\epsilon)$ is narrow compared to the energy transfer $\sum n\hbar\delta\omega$. In what follows, we will discuss this further. Given that $p_{no\ jump}(\epsilon)$ is of no interest in computing reaction rates for anomalous processes, we will neglect it henceforth.

We have computed previously the line shape for lattice energy transfer as a function of ϵ in the case of neutron capture,[12] under conditions where there was no direct recoil (in this case, the energy transfer occurs through a mass change rather than through the creation of a vacancy). We found that the probability for energy transfer in the case of a single gap-jumping phonon mode initially in a number state was a shifted Gaussian

$$\sum_f | < \Psi_i^{(L)}(\mathbf{q}_i)|e^{-i\hat{S}_D}|\Psi_f^{(L)}(\mathbf{q}_i) >_{m^*} |^2 \sim e^{-\beta(\epsilon - n<\hbar\delta\omega>)^2} \tag{2.22}$$

where ϵ is the actual energy transfer from the lattice, and $n < \hbar\delta\omega >$ is the expectation value of the energy transfer. The line is narrow; $\beta^{-1} \sim n < (\hbar\delta\omega)^2 >$. The spread is due to the range of frequencies of the final state modes into which a single gap-jumping mode projects.

Perhaps more relevant (since it is not clear how to excite a phonon mode to a number state) is the probability distribution in the case of a highly excited gap-jumping continuum phonon that is initially in a classical state. A classical state $|\alpha >$ can be constructed from number states, and it is well known that a Poisson distribution is produced:[18]

$$|\alpha >= e^{-|\alpha|^2/2} \sum_n \frac{\alpha^n}{\sqrt{n!}} |n > \tag{2.23}$$

which leads to

$$| < n|\alpha > |^2 = e^{-|\alpha|^2} \frac{|\alpha|^{2n}}{n!} \tag{2.24}$$

A highly excited classical state is well approximated by a shifted Gaussian around the mean number of phonons $< n >= \alpha^2$, and with a variance $< \Delta n^2 >=< (n - < n >)^2 >=< n >$. For an energy transfer of 1 MeV, on the order of 10^8 or more phonons must be present, which implies a narrow probability distribution $\sqrt{< \Delta n^2 >}/ < n > \sim 10^{-4}$. Consequently, both for number states and for classical states, it will be an excellent approximation to take

$$p(\epsilon) \approx \delta(\epsilon - \sum_{m^*} < n_{m^*} >< \hbar\delta\omega_{m^*} >) \tag{2.25}$$

Here we must extend our analysis to include recoil effects in the probability function. In the case of electron ejection the recoil is relatively weak, and the essential effect that occurs is that the transfer of energy is prevented unless the recoil energy is sufficiently strong to permanently dislodge the nucleus.

For most of the values of the lattice energy transfer ϵ that are of potential interest, the recoil momentum is sufficiently great that a vacancy is created with certainty. An accurate calculation of the recoil matrix element requires a model for inter-nuclear potentials in the lattice, and is beyond the scope of this work. In essence, a nucleus that recoils must overcome a potential barrier to land in a new and inequivalent site in order to satisfy the requirement that the phonon modes be irreversibly changed. We assume that the energy of the vacancy plus displaced nucleus lies at an energy E_d relative to the initial configuration, that the barrier energy is E_b, and that the potential barrier is adequately modeled by a parabola over a distance d

$$V_b(x) = E_b - \frac{1}{2}\alpha x^2 \tag{2.26}$$

with $V_b(\pm d/2) = E_d$. We then obtain an estimate of the efficiency for tunneling for $E_d < E_r < E_b$ to be

$$\sum_f | < \Psi_i^{(L)}(\mathbf{q}_i)|e^{i\mathbf{k}\cdot\mathbf{R}_j}|\Psi_f^{(L)}(\mathbf{q}_i) >_m |^2 = |T(\mathbf{k})|^2 \approx \exp\left\{-\frac{\pi}{2}\frac{(E_b - E_r)}{\sqrt{(E_b - E_d)(\hbar^2/2Md^2)}}\right\} \tag{2.27}$$

where E_r is the recoil energy of the Pd nucleus $\hbar^2|\mathbf{k}|^2/2M$. For $E_r < E_d$, a vacancy is not created, and we take $T = 0$; for $E > E_b$ we assume that the decay occurs freely, and $|T|^2 = 1$.

We have found that the frequency-shift of gap-jumping phonon modes leads ultimately to the appearance of an isolated system reaction rate evaluated at an anomalous energy transfer ϵ; the recoil effects primarily cuts off the reaction rate at low energy. Precisely where this cut-off occurs as a function of lattice energy transfer depends strongly on the details of the chemical environment in the vicinity of the nucleus, details that are not easily available at present. The parabolic tunneling model presented here allows us to obtain predictions given "reasonable" estimates of the excitation energies and barriers.

These approximations lead to an estimate of the reaction rate per nucleus given by

$$\Gamma_j = \Gamma_0(\Delta E_L)\ |T(\mathbf{k})|^2 \tag{2.28}$$

where the lattice energy transfer is

$$\Delta E_L = \sum_{m^*} < n_{m^*} >< \hbar\delta\omega_{m^*} > \tag{2.29}$$

and where the rate $\Gamma_0(\epsilon)$ is obtained by summing over $\mathbf{k}$ to yield

$$\Gamma_0(\epsilon) = \frac{2\pi}{\hbar}|V(\mathbf{k})|^2\rho(E_f) \tag{2.30}$$

where $\mathbf{k}$ is evaluated at $\hbar^2|\mathbf{k}|^2/2m_e = \epsilon - I_K$. Inserting expressions for $V(\mathbf{k})$ and for $\rho(E_f)$, we obtain

$$\Gamma_0(\epsilon) = \frac{24N_{1s}}{\pi Z}\frac{I_H}{\hbar}\left[\frac{\epsilon}{I_H}\right]^{\frac{1}{2}}\frac{1}{[1+(\epsilon/Z^2I_H)]^2} \tag{2.31}$$

where I_H is 13.6058 eV.

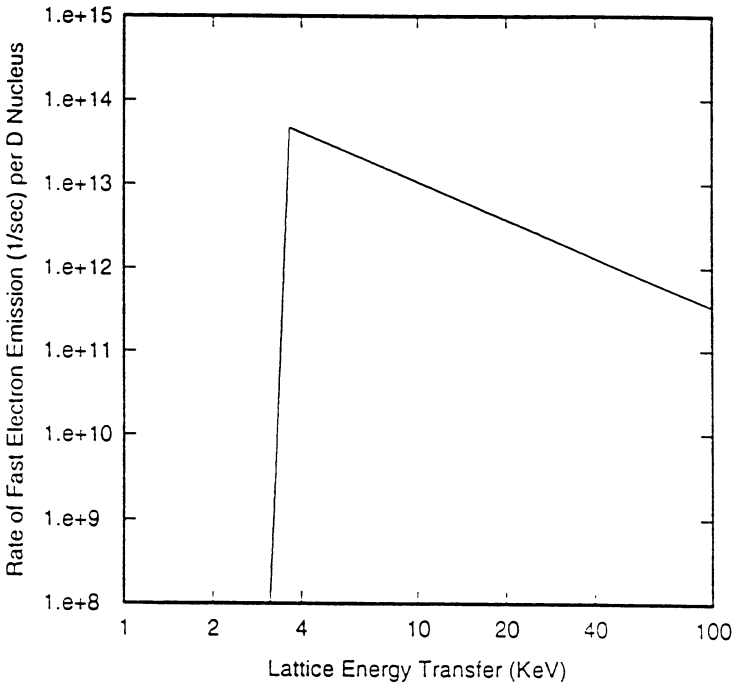

Figure 2: Predicted fast electron emission rate from deuterons as a function of lattice energy transfer.

Results for K-shell ejection from deuterium and from Pd in PdD are shown in Figures 2 and 3. The threshold for emission of fast electrons occurs when the recoil energy of the nucleus becomes equal to the barrier energy for vacancy creation; this occurs in the nonrelativistic limit at

$$\Delta E = 1835\ A\ E_d \tag{2.32}$$

In the case of Pd vacancy production, we have used $E_d = 6eV$ and $E_b = 10eV$ as our "reasonable" estimates of energies required to irreversibly create a vacancy. In the case of deuterium, we have selected the parameters $E_{=}0.7eV$, $E_b = 1.0eV$ and $d = 1a_0$; while the excitation to nearby octohedral or tetrahedral sites will occur with energies below 0.3eV, 1 eV should be sufficient to move the deuterium to a more remote local. Relativistic formulas have been used to estimate the recoil energy in the Figures.

It should be noted that the phonon modes that jump a band gap are different for these two processes. We have discussed gap-jumping in the case of Pd vacancy creation above; this process should occur with strong excitation of the lowest optical phonon modes. In the case of deuterium vacancy creation, we rely on a postulated set of isolated vacancy impurity modes that correspond to cells with different numbers of deuterons in the vicinity of a host metal vacancy.

The decay rates per nucleus for these processes are seen to be very large, consequently the total lattice decay rates will be so great that it must be questioned under what conditions the model will be valid. We will examine this question in the following section.

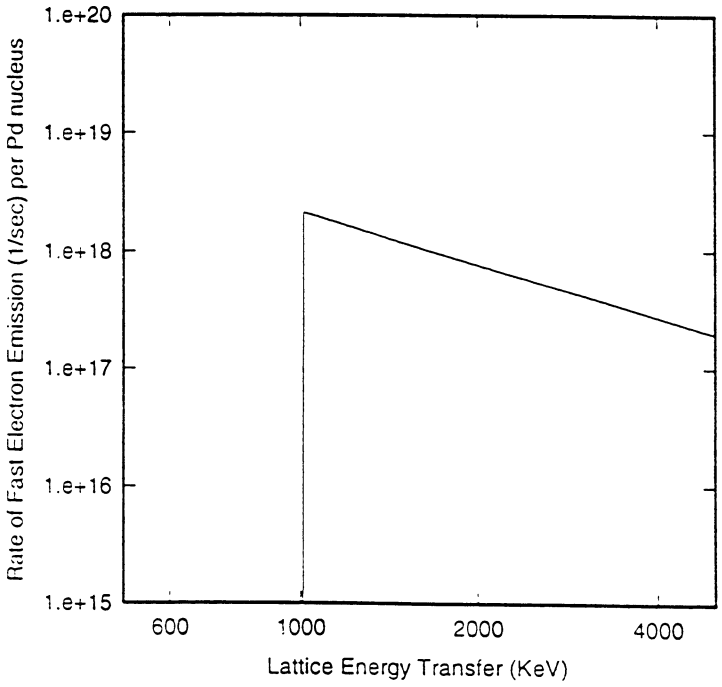

Figure 3: Predicted fast electron emission rate from Pd nuclei as a function of lattice energy transfer.

3. Coupled Reactions

The reaction rate estimates presented in the last section indicates that a lattice with very highly excited gap-jumping phonon modes will decay by fast electron emission very rapidly. The characteristic decay rates can be greater than 10^{10} sec^{-1} per nucleus, which if correct, would perhaps imply a total lattice decay rate between 10^{25} and 10^{30} sec^{-1} for the total volume over which the phonon modes extend; these total rates are much too fast to be physical.

Towards the resolution of this problem, there are a number of issues that must be considered. For example, if the lattice decay rate is so fast, then it becomes problematic how the lattice could have been so highly excited originally. In the process of exciting the gap-jumping modes, a fast decay should have occured once sufficient excitation was present to enable Coulomb decay to occur at all at much slower rates. Under these conditions, the theory described in Section II would apply, and no inconsistencies would be present.

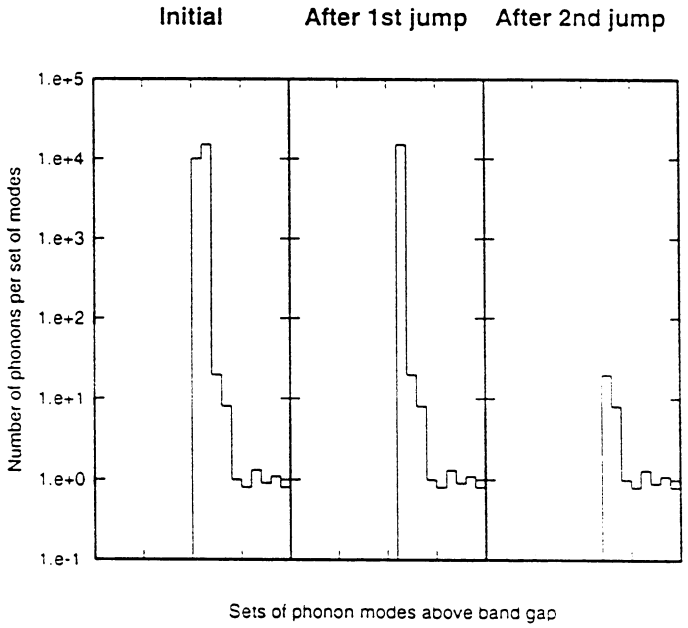

Figure 4: Pictorial of phonon mode excitation near the band gap before and after gap-jumping.

The situation becomes very much more interesting under conditions where the initial moderately-excited modes jump the gap to reveal new gap-jumping modes that are much more highly excited. When downward gap-jumping occurs, it is the lowest phonon modes above the gap that actually jump (see Figure 4). If several jumps occur in succession, it is always the lowest modes that jump in any specific reaction; consequently, phonon modes are stripped away from the bottom in sequence, much like the peeling of an onion.

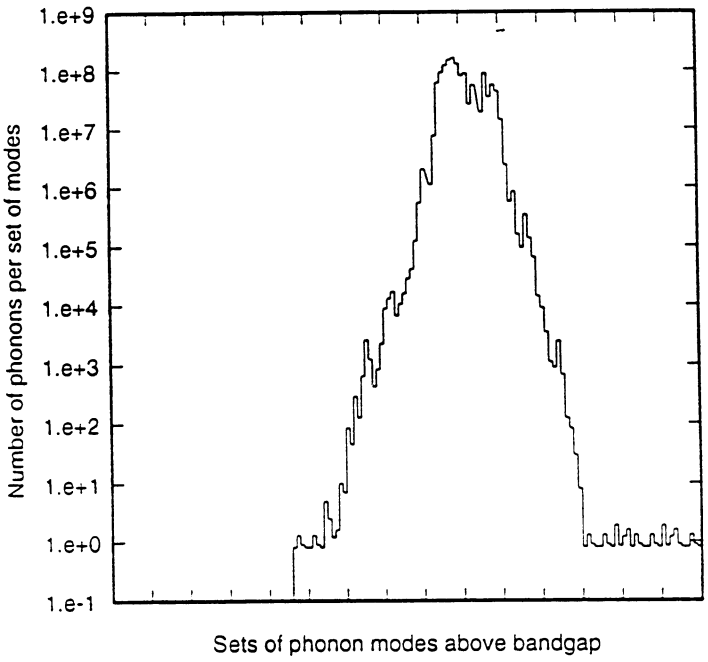

Figure 5: Pictorial of high phonon mode excitation that is shielded from the band gap by modes with low excitation.

Under such conditions, it can no longer be argued that the phonon population could not have built up without provoking a fast Coulomb decay; highly excited modes that are shielded from the gap by unexcited modes are free to build up to very high levels, as illustrated in Figure 5. Nevertheless, we would be certain that if the resulting rate estimate when these modes did finally jump, were on the order of 10^{25} to 10^{30} $\sec^{-1}$, that rate estimate must be in error.

The resolution to this problem is that the two reactions would become coupled together in the Raman sense, and reaction rates must be computed using a theory which fundamentally treats the processes as coupled. The mechanisms that would produce very high phonon populations would however likely not result in such high selectivity as to produce just one or two reactions, rather it is more likely that 10^5 to 10^8 phonon modes would cause reactions at a time. Consequently, we require a theory for bursts of large numbers of reactions.

The starting point for our discussion is the expression for a single isolated event from the last section, recast as

$$\Gamma_j = \frac{2\pi}{\hbar} \sum_{\mathbf{k}} |V(\mathbf{k})|^2 \int d\epsilon \; p_{j,\mathbf{k}}(\epsilon) \delta(I_K + \hbar^2 |\mathbf{k}|^2 / 2m_e - \epsilon) \tag{3.1}$$

Taking the probability function to be sharply peaked in energy, we obtain

$$\Gamma_j = \frac{2\pi}{\hbar}\sum_{\mathbf{k}}|V(\mathbf{k})|^2|T(\mathbf{k})|^2\delta(I_K + \hbar^2|\mathbf{k}|^2/2m_e - < n >< \delta\hbar\omega >) \tag{3.2}$$

We have adopted the notation $< n >< \delta\hbar\omega >$ for $\sum_{m^*} < n_{m^*} >< \delta\hbar\omega_{m^*} >$. This form is most convenient for generalization.

In the case of two coupled reactions, we obtain

$$\Gamma_{j_1,j_2} =$$

$$\frac{\pi}{\hbar}\sum_{\mathbf{k}_1}\sum_{\mathbf{k}_2}\left|\frac{V(\mathbf{k}_1)V(\mathbf{k}_2)T(\mathbf{k}_1)T(\mathbf{k}_2)}{I_K + \hbar^2|\mathbf{k}_1|^2/2M - < n_1 >< \delta\hbar\omega_1 > - i\hbar\gamma} + \frac{V(\mathbf{k}_2)V(\mathbf{k}_1)T(\mathbf{k}_2)T(\mathbf{k}_1)}{I_K + \hbar^2|\mathbf{k}_2|^2/2M - < n_1 >< \delta\hbar\omega_1 > - i\hbar\gamma}\right|^2$$

$$\delta(2I_K + \hbar^2|\mathbf{k}_1|^2/2m_e + \hbar^2|\mathbf{k}_2|^2/2m_e - < n_1 >< \delta\hbar\omega_1 > - < n_2 >< \delta\hbar\omega_2 >) \tag{3.3}$$

The interaction matrix element is now composed of two terms, as is appropriate for a second order process. The relative phases between the various matrix elements will generally be random; when averaged over all pairs of sites in the lattice, the interference terms will not contribute due to cancellation. Consequently, it is of interest to focus on a site-averaged version of the decay rate

$$\overline{\Gamma}_{j_1,j_2} = \frac{2\pi}{\hbar}\sum_{\mathbf{k}_1}\sum_{\mathbf{k}_2}\frac{|V(\mathbf{k}_1)V(\mathbf{k}_2)T(\mathbf{k}_1)T(\mathbf{k}_2)|^2}{(I_K + \hbar^2|\mathbf{k}_1|^2/2M - < n_1 >< \delta\hbar\omega_1 >)^2 + \hbar^2\gamma^2}$$

$$\delta(2I_K + \hbar^2|\mathbf{k}_1|^2/2m_e + \hbar^2|\mathbf{k}_2|^2/2m_e - < n_1 >< \delta\hbar\omega_1 > - < n_2 >< \delta\hbar\omega_2 >) \tag{3.4}$$

To obtain the total decay rate, this formula must be summed over all pairs of nuclei in a domain in which the highly excited phonon modes exist.

Further generalization to larger numbers of coupled reactions is straightforward; we obtain

$$\overline{\Gamma}_N = \frac{2\pi}{\hbar}\sum_{\mathbf{k}_1}\cdots\sum_{\mathbf{k}_N}\frac{|V(\mathbf{k}_1)T(\mathbf{k}_1)|^2\cdots|V(\mathbf{k}_N)T(\mathbf{k}_N)|^2}{\prod_j^{N-1}\left[(jI_K + \sum_i^j \hbar^2|\mathbf{k}_i|^2/2M - \sum_i^j < n_i >< \delta\hbar\omega_i >)^2 + \hbar^2\gamma^2\right]}$$

$$\delta(NI_K + \sum_j^N \hbar^2|\mathbf{k}_j|^2/2m_e - \sum_j^N < n_j >< \delta\hbar\omega_j >) \tag{3.5}$$

This formula, summed over all sets of N nuclei in the domain of the highly excited phonon modes, would give the decay rate for an N-particle "burst".

The appearance of such high order matrix elements in the calculation of reaction rates is rare in the literature. A currently active area of research wherein high order matrix elements are calculated routinely is the area of laser-induced multi-photon ionization.[19] A number of methods have proven to be successful in these calculations, including Floquet theory coupled with R-matrix methods,[20]

and time-dependent Hartree-Fock theory.[21] These types of methods could be used in the present case with some modifications.

It is possible that reliable rates for the present problem could be obtained using a method of steepest descents. The basic idea is as follows: The largest total decay rates would be obtained in the limit that all of the individual steps were resonant; however, many of the transitions will likely take place off of resonance if an adequate degree of phonon excitation is not present – this would be especially true of the earliest decays, which were postulated above to be at best marginal. As a result, excitation energy must be borrowed from those phonon modes that are well above threshold in order for decays to occur with sufficient recoil to cause phonon modes to jump the gap in cases where the phonon excitation is marginal.

Consequently, it should be possible to select an optimum set of decay energies $\{|\mathbf{k}|^2\}$, subject to the constraint that overall energy conservation be maintained, that would give the largest possible value for the product inside the summation of equation (3.5). This optimum would likely have many decays occuring on resonance, with as few decays as possible loaning energy to those decays that are marginal or forbidden. Away from this optimum selection of decay energies, there would be less contribution to the summations; the reduction in the contribution would by definition be second order away from the optimum, and this could be evaluated algebraically using Gaussian integrations.

These arguments imply the following approximation scheme. Define the variational function

$$I[\mathbf{k}_1 \cdots \mathbf{k}_N] = \frac{|V(\mathbf{k}_1)T(\mathbf{k}_1)|^2 \cdots |V(\mathbf{k}_N)T(\mathbf{k}_N)|^2}{\prod_j^{N-1}\left[(jI_K + \sum_i^j \hbar^2|\mathbf{k}_i|^2/2M - \sum_i^j < n_i >< \delta\hbar\omega_i >)^2 + \hbar^2\gamma^2\right]}$$
$$-\lambda(NI_K + \sum_j^N \hbar^2|\mathbf{k}_j|^2/2m_e - \sum_j^N < n_j >< \delta\hbar\omega_j >) \tag{3.6}$$

where λ is a Lagrange multiplier. Compute the optimum distribution of decay energies through

$$\frac{\partial}{\partial k_i} I[\mathbf{k}_1 \cdots \mathbf{k}_N]\Big|_{\{\mathbf{k}\}_0} = 0 \tag{3.7}$$

Next, develop a Gaussian model around the optimum set of decay energies

$$J(\mathbf{k}_1 \cdots \mathbf{k}_{N-1}) = J_0 e^{-(\mathbf{k}-\mathbf{k}_0)^T \cdot \mathbf{G} \cdot (\mathbf{k}-\mathbf{k}_0)} \tag{3.8}$$

where we have adopted a notation $\mathbf{k}$ for a very large vector composed of all individual components for $\mathbf{k}_1 \cdots \mathbf{k}_{N-1}$; the optimum for the momenuta is now denoted by $\mathbf{k}_0$. The partial sum $J(\mathbf{k}_1 \cdots \mathbf{k}_{N-1})$ is defined by

$$J(\mathbf{k}_1 \cdots \mathbf{k}_{N-1}) = \sum_{\mathbf{k}_N} \frac{|V(\mathbf{k}_1)T(\mathbf{k}_1)|^2 \cdots |V(\mathbf{k}_N)T(\mathbf{k}_N)|^2}{\prod_j^{N-1} \left[(jI_K + \sum_i^j \hbar^2 |\mathbf{k}_i|^2/2M - \sum_i^j < n_i >< \delta\hbar\omega_i >)^2 + \hbar^2\gamma^2 \right]}$$

$$\delta(NI_K + \sum_j^N \hbar^2 |\mathbf{k}_j|^2/2m_e - \sum_j^N < n_j >< \delta\hbar\omega_j >) \tag{3.9}$$

The matrix G is obtained by matching second derivatives around the optimum. Finally, the total decay rate is computed using

$$\overline{\Gamma}_N = \frac{2\pi}{\hbar} \sum_{\mathbf{k}_1} \cdots \sum_{\mathbf{k}_{N-1}} J_0 e^{-(\mathbf{k}-\mathbf{k}_0)^T \cdot \mathbf{G} \cdot (\mathbf{k}-\mathbf{k}_0)} \tag{3.10}$$

taking advantage of algebraic Gaussian integration formulas.

We have not carried out any computations for the rates of "bursts" yet with this model; this project is left for future work. There is little question that the excitation of many low-lying modes will result in decays that occur through bursts, and in principle we will be able to estimate rates for the bursts, either with the formulas presented above or through other routes. It is of interest to inquire as to what distribution of decay products would be expected within a burst, assuming that more than one possible decay channel occurs. The theory for bursts presented above is readily generalized in the case of multiple decay channels, with little change in essential physics. The distribution of decay products would be determined in principle by performing sets of burst rate calculations with slightly different sets of decay channels around whatever set of decay channels maximizes the total burst rate.

As these models have not yet been studied, we cannot say at this point with certainty what distribution of decay products should be expected in general. Nevertheless, the appearance of each individual decay process occurs in the total burst rate formula through terms that are very much like those that occur in the single-event version of Fermi's Golden Rule rate. One might postulate that the burst rate fraction f_j for a single decay channel could be estimated by computing the ratio of the single-event rate with the total of all possible single-event rates for all available decay channels dependent on the same phonon modes

$$f_j = \frac{\Gamma_j}{\sum_i \Gamma_i} \tag{3.11}$$

Such a formula might be useful in a "low rate" limit, corresponding to the I^n dependence observed for n-photon absorption in the low intensity regime. Whereas the muiti-photon rates saturate at high I, a non-perturbative treatment of the bursts would likely show "saturation effects". In this limit, a weak channel competing with a stronger channel would have a lower fraction f_j, but it

is not clear at this point by how much. In the sections that follow, lacking more precise tools to quantify reaction rates, we will continue to calculate Fermi's Golden Rule rates for the various channels as single events, keeping in mind that these estimates are only qualitative indicators of actual rates and fractions.

4. Deuteron Acceleration and Neutron Production

Another dominant decay mechanism for a lattice that possesses very highly excited gap-jumping phonon modes is Coulomb-induced nucleus-nucleus recoil. For example, if two Pd nuclei in PdD recoil off of each other with 50 eV energy input from the lattice, at least two Pd vacancies will be created; depending on the details of the outcome, this process could self-consistently lead to energy transfer from the lattice caused by highly excited optical phonon mode jumping a band gap to increase the number of "vacancy" optical phonon models.

Perhaps the most interesting example of this process is lattice decay by deuteron recoil off of other nuclei, for the reason that fast deuterons produced in this way could in principle fuse with other deuterons in the lattice resulting in *dd*-fusion neutrons at 2.45 MeV. We have estimated decay rates for deuteron-deuteron recoil as a function of lattice energy, and used these rates to estimate neutron production rates; the results are quite interesting, and are not inconsistent with some of the experimental claims for the production of neutrons.

Fermi's Golden Rule applied to lattice-induced deuteron-deuteron recoil gives rise to the following rate estimate

$$\Gamma = \frac{2\pi}{\hbar} \sum_f \sum_{\mathbf{K}} | < \Psi_i | \hat{V} | \Psi_f > |^2 \delta(2I_D + \hbar^2 |\mathbf{K}|^2 / 2\mu + E_f^{(L)} - E_i^{(L)}) \tag{4.1}$$

where I_D is the binding energy of a deuteron, $\hbar^2|\mathbf{K}|^2/2\mu$ is the relative kinetic energy of the two deuterons that have recoiled away from each other, and the potential $\hat{V}$ is the Coulomb interaction

$$\hat{V} = \sum_{j<j'} \frac{e^2}{|\hat{\mathbf{R}}_j - \hat{\mathbf{R}}_{j'}|} \tag{4.2}$$

The arguments of Section II can be used here when the energy transfer from the lattice is dominated by the frequency shift of highly excited gap-jumping phonon modes. We focus on the matrix element in the case of the recoil of two specific neighboring deuterons, in which case the Coulomb matrix element can be written in terms of phonon amplitudes

$$< \Psi_i | \hat{V}_{j,j'} | \Psi_f > = < \Psi_i(\mathbf{q}_i) | \hat{V}_{j,j'} e^{-i\hat{S}_D} | \Psi_f(\mathbf{q}_i) > \tag{4.3}$$

where the Duschinsky operator takes into account modifications in the phonon mode structure. As before, the matrix element separates approximately into a piece responsible for the primary energy transfer, and a piece containing the majority of non-gap-jumping phonon modes that are involved in the recoil process

$$< \Psi_i(\mathbf{q}_i)|\hat{V}_{j,j'}e^{-i\hat{S}_D}|\Psi_f(\mathbf{q}_i) > \approx < \Psi_i(\mathbf{q}_i)|e^{-i\hat{S}_D}|\Psi_f(\mathbf{q}_i) >_{m^*} < \Psi_i(\mathbf{q}_i)|\hat{V}_{j,j'}|\Psi_f(\mathbf{q}_i) >_m \qquad (4.4)$$

The initial and final states $\Psi_i(\mathbf{q}_i)$ and $\Psi_f(\mathbf{q}_i)$ have the same energy, and total energy is conserved in this type of recoil reaction. Following the arguments of the last two sections, the Duschinsky matrix element will be sharply peaked around an energy transfer of $< n >< \hbar\delta\omega >$ for the m^* phonon modes that jump the gap. Because of energy conservation, this energy becomes available for the local Coulomb repulsion between two nuclei. We obtain

$$\Gamma_{j,j'} = \frac{2\pi}{\hbar}\sum_f\sum_{\mathbf{K}} | < \Psi_i(\mathbf{q}_i)|e^{-i\hat{S}_D}|\Psi_f(\mathbf{q}_i) >_{m^*} |^2 | < \Psi_i(\mathbf{q}_i)|\hat{V}_{j,j'}|\Psi_f(\mathbf{q}_i) >_m |^2$$
$$\delta(2I_D + \hbar^2|\mathbf{K}|^2/2\mu + E_f^{(L)} - E_i^{(L)}) \qquad (4.5)$$

which evaluates approximately to

$$\Gamma_{j,j'} = \frac{2\pi}{\hbar}\sum_f\sum_{\mathbf{K}} | < \Psi_i(\mathbf{q}_i)|\hat{V}_{j,j'}|\Psi_f(\mathbf{q}_i) >_m |^2\delta(2I_D + \hbar^2|\mathbf{K}|^2/2\mu - < n >< \hbar\delta\omega >) \qquad (4.6)$$

This formula assumes that the recoil is sufficiently great to insure that deuterons are truly irreversibly removed from their cells so that the m^* phonon modes jump a bandgap. Our neglect of the tunneling factor in this formula will mean that our results will be valid only for an energy transfer exceeding 2-3 eV.

The local Coulomb repulsion matrix element is strongly dependent on the local chemical environment, since a large recoil can only occur when the deuterons are close together. Focusing on the interesting case of large momentum transfer, we have approximated the relative probability amplitudes of deuterons in the lattice using the molecular D_2 ground state wavefunction:

$$< \Psi_i(\mathbf{q}_i)|\hat{V}_{j,j'}|\Psi_f(\mathbf{q}_i) >_m \approx < \Psi_{D_2}(\mathbf{r})|\frac{e^2}{|\mathbf{r}|}|\Psi_{\mathbf{K}}(\mathbf{r}) > \qquad (4.7)$$

In this formula. the final state $\Psi_{\mathbf{K}}(\mathbf{r})$ represents a dissociated molecule with a relative momentum between the deuterons of $\hbar\mathbf{K}$. This type of approximation has been used by many authors to provide molecular estimates of *dd*-fusion rates thought to be relevant to the problem of fusion rates in PdD. While the applicability of this type of model in the case of fusion reactions may be

questionable, it is very likely a much better approximation in the case of recoil, since the recoil matrix element samples phase space at larger inter-deuteron separations; the recoil matrix elements appear to be far less sensitive to variations in the potential.

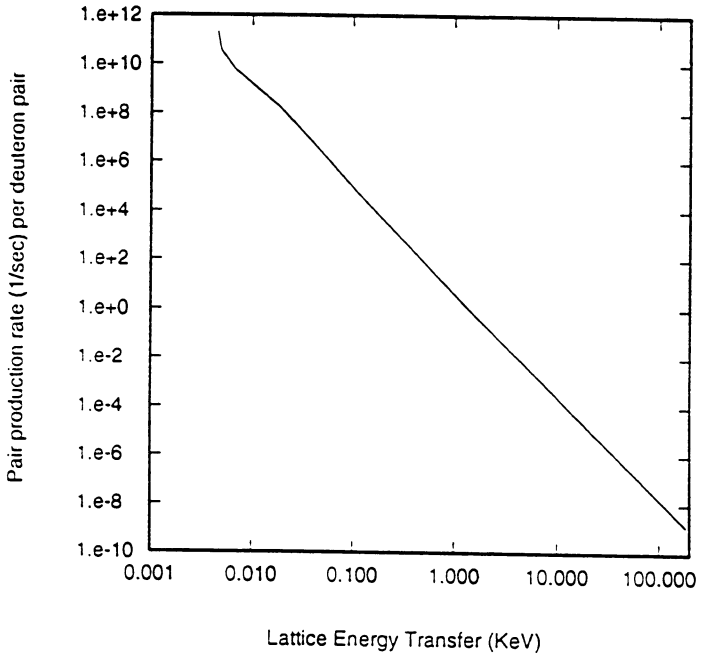

Figure 6: Decay rate per deuteron pair for lattice-induced Coulomb recoil.

It was convenient for us to evaulate the reaction rate using a coupled-channel model, which is an improvement over the approximations discussed above. In this model, the unperturbed ground state radial wavefunction was computed by solution of the unperturbed radial Schrodinger equation

$$EP_o(r) = -\frac{\hbar^2}{2\mu}\frac{d^2}{dr^2}P_o(r) + V(r)P_o(r) \tag{4.8}$$

using the parameterization[22]

$$V(r) = e^{-\alpha r}\left[\frac{e^2}{r} - b\right] \tag{4.9}$$

with $\alpha = 0.886/a_0$ and $b = 2.630 I_H$. The continuum channel was computed using

$$\frac{\hbar^2|\mathbf{K}|^2}{2\mu}P(r) = -\frac{\hbar^2}{2\mu}\frac{d^2}{dr^2}P(r) + V(r)P(r) + \frac{e^2}{r}P_o(r) \tag{4.10}$$

subject to the boundary condition

$$P(r) \longrightarrow f(\mathbf{K})e^{i|\mathbf{K}|r} \tag{4.11}$$

The decay rate is obtained by integrating the outward flux over a sphere at large r; this results in

$$\Gamma_{j,j'} = \frac{\hbar|\mathbf{K}|}{\mu}|f(\mathbf{K})|^2 \tag{4.12}$$

The results of this calculation are shown in Figure 6.

Predicted by this theory are fast deuterons that can in principle fuse with neighboring deuterons. Taking the results of the deuteron-deuteron recoil calculation discussed above, we combined the production rate of fast deuterons with the neutron yield (including the energy loss of the deuterons on the host palladium nuclei) to produce an estimate of the *dd*-fusion neutron rate. The results are shown in Figure 7. Keeping in mind the discussion of Section 3, this process will compete with fast electron production at lattice transfer energies above a few kilovolts, which will have the ultimate effect of essentially eliminating this channel. In metal hydrides with deeper deuteron potentials (such as TiD_2), this competition will be put off to higher lattice transfer energy, resulting in larger neutron production rates.

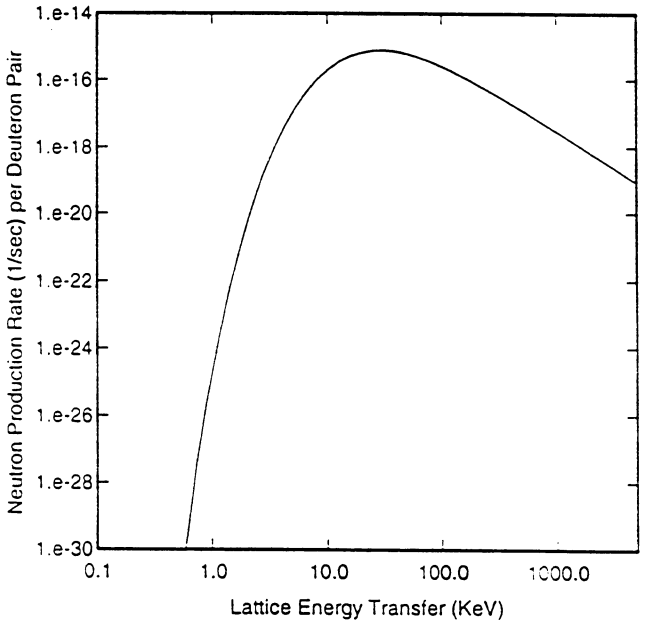

Figure 7: Production rate of *dd*-fusion neutrons through deuteron-deuteron recoil followed by fusion.

For completeness, we estimated reaction rates for the rare process in which the Coulomb exchange causes the two initial recoiling deuterons to fuse with each other. The resulting rate is observed to increase by about thirty orders of magnitude over the ground state D_2 fusion rate, but in our calculations did not compete with the deuteron-other-deuteron fusion rate given above.

5. Lattice-induced Bēta Decays

We have thus far discussed the decay of a highly excited lattice through atomic decay channels. The lattice may also decay through available nuclear channels, subject to the constraints discussed above, and in competition with other open channels such as electron recoil. In this section, we examine lattice-induced reactions mediated by the weak force.

The basic theory for lattice-induced electron capture reactions and beta decays follows immediately from the theory outlined in Sections 2 and 3. The Fermi's Golden Rule estimate for a lattice-induced decay is

$$\Gamma = |T(\mathbf{k})|^2 \Gamma_0(\Delta E_L) \tag{5.1}$$

where $|T|^2$ is the probability that the recoil is sufficient to irreversibly create a vacancy, and where $\Gamma_0(\Delta E_L)$ is the rate computed assuming that an energy ΔE_L is transferred from the lattice. We have computed lattice-induced decay rates according to this estimate based on the $f\tau$ theory discussed in Ref. 23.

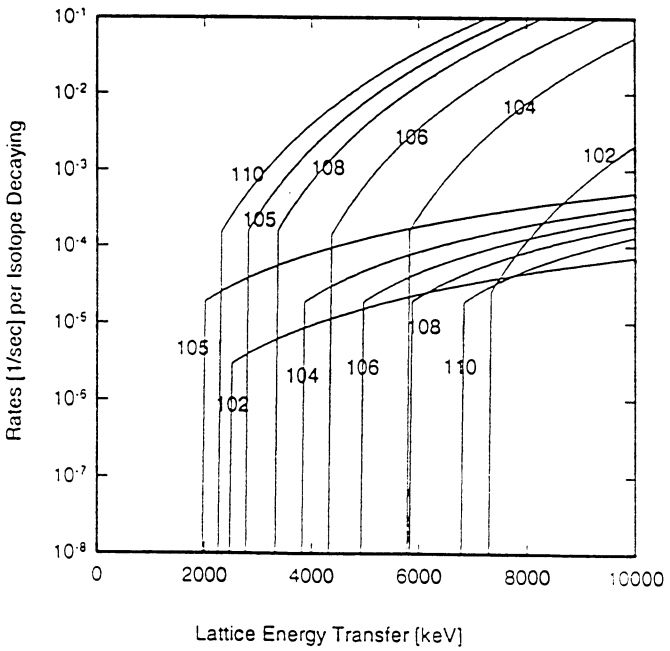

Figure 8: Lattice-induced electron capture and beta decay rates for the Pd nuclei. Curves that continue to rise are e^- decay; curves that are lower are electron capture.

As a function of lattice energy transfer, the first decay to occur is electron capture from ^{105}Pd to ^{105}Rh. This may be interesting, in that the first two excited states of ^{105}Rh occur at 129.6 KeV

and at 149.1 KeV; emission at these energies is claimed to have been observed in glow discharge experiments at Luch. Gamma lines produced by the decay of ^{105}Rh back to ^{105}Pd have also been claimed in these experiments.[7] In Figure 8 is shown estimates of the lattice-induced electron capture rates and beta decay rates for the stable Pd nuclei.

Isotopes that are already unstable against beta decay can decay more rapidly with extra energy input from the lattice. We studied the enhancement of the beta decay of ^{107}Pd to ^{107}Ag through this mechanism. As expected, no enhancement occurs until the recoil becomes sufficiently great to cause a vacancy to be formed. With the model of Section 2, this does not occur until about 950 KeV. At this energy, one would expect to observed characteristic gamma emission from excited ^{107}Ag at 93 KeV.

Tritium decay can be enhanced through this type of mechanism, and lattice-induced electron capture on ^{3}He can in principle produce tritium, although precisely which vacancy impurity bands ^{3}He decay would involve is not clear at this point. The rates for these processes are shown in Figure 9.

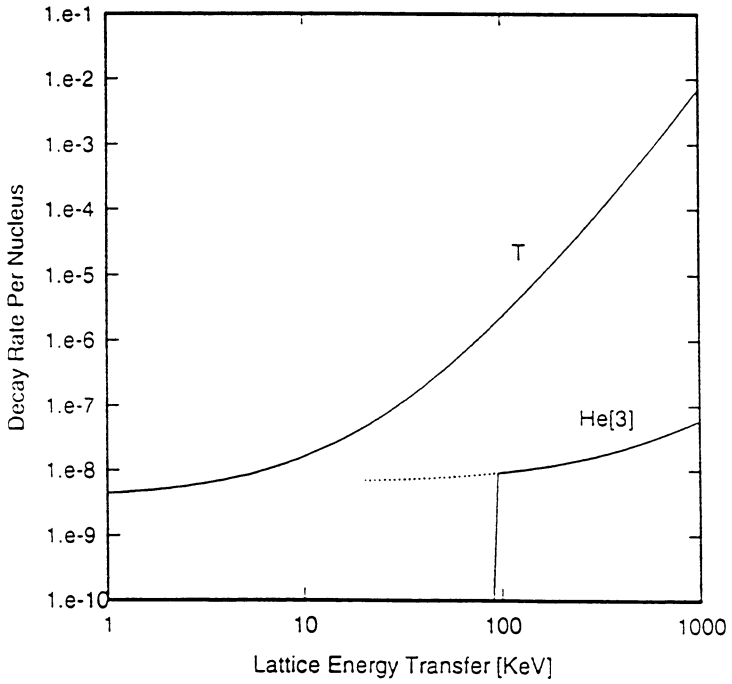

Figure 9: Lattice-enhanced tritium beta decay; lattice-induced ^{3}He electron capture to make tritium.

6. Lattice-Induced Alpha Decay

If the energy transfer is sufficiently great, alpha decay becomes an available decay channel. The analysis of lattice-induced alpha decay is particularly simple, in that the decay always provides sufficient recoil for local vacancy formation. We have calculated the rate for lattice-induced alpha decay of Pd nuclei; the results are shown in Figure 10. The first isotope to decay as a function of energy is ^{102}Pd; energy transfers in excess of about 5 MeV are required for this process.

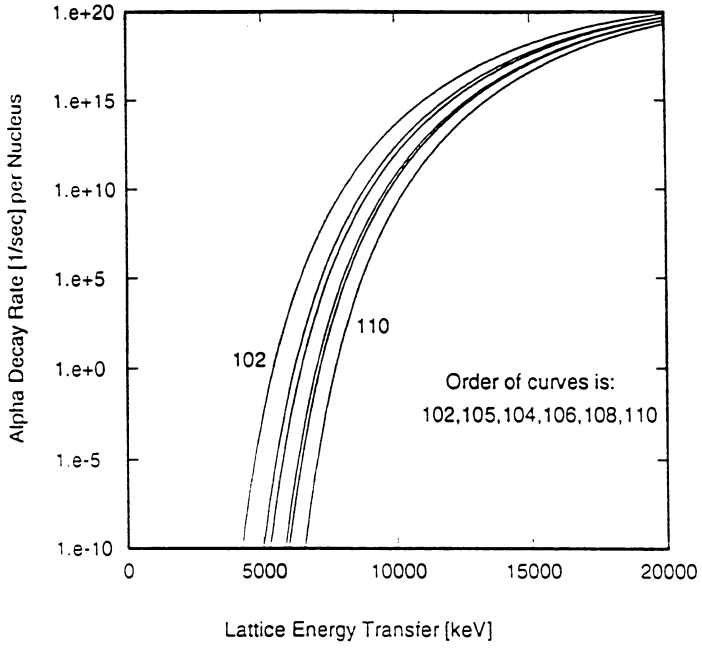

Figure 10: Lattice-induced alpha decay of the Pd isotopes.

Larger energy transfers can lead to more complicated decay channels; for example, proton and neutron decays turn on near 10 MeV lattice energy transfer. We have examined reaction rates for a wide variety of fission decay channels; these will be discussed further elswhere. Qualitatively, the rates for these decays go something like those for alpha decay, but require significantly more energy; from 20 MeV to more than 50 MeV of energy transfer will lead to a wide range of open lattice-induced fission channels. At such large energy transfer where alpha and fission decay processes are allowed, these reactions are predicted to be the dominate decay channels.

7. Discussion and Conclusions

We have presented a new theory for lattice-induced reactions, which a predicted to be driven by highly excited gap-jumping phonon modes. The reaction mechanisms discussed in this work were motivated by the many recent claimes of observations of anomalies in PdD, in other metal deuterides, and in metal hydrides.

At low energy transfer, the dominant lattice decay mechanisms are the Coulomb-mediated nucleus-nucleus recoils; in the case of deuteron-deuteron recoils, *dd*-fusion at low levels is predicted. The reaction rates computed for this process are of the correct order of magnitude to be consistent with the claimed experimental neutron emission, at low lattice energy transfer below that at which fast electron decay channels open.

Fast electron emission through Coulomb induced recoil is predicted to be a dominant process, at lattice energy transfer where the nuclear recoil is strong enough for vacancy creation. There are currently relatively few reports of the observation of fast electrons in cold fusion expriments. Fast electron emission is predicted starting at relatively low energy transfer (a few KeV) from deuteron recoil, and at energies starting near 1 MeV for recoil from Pd. In the case of the stable Pd isotopes, this process competes with all beta decay reactions.

We have studied neutron transfer reaction mechanisms elsewhere[12,24,25] as a route to heat production. Although we have examined neutron transfers from ^{105}Pd to ^{6}Li, with an energy mismatch of 156 KeV, a more recent analysis suggests that this reaction will be suppressed due to selection rules affecting the Pd transition. There are new candidate reactions that are perhaps more promising relative to the selection rules: neutron transfer from ^{29}Si to ^{29}Si (producing ^{28}Si and ^{30}Si) at 2.14 MeV; and neutron transfer from ^{30}Si to ^{10}B at 845 KeV. In the case of the light water experiments, neutron transfer from ^{62}Ni to ^{29}Si has a mismatch of 12 KeV.

The generation of high phonon densities has not yet been addressed. We are considering seriously the possibility that D_2 desorption from the metal deuteride interface produces phonon gain when exothermic. In the case of PdD, the desorption is exothermic at high loadings,[26] which is correlated well with the proposed requirement of high PdD loading for heat production in Pons Fleischmann experiments. The quantum theories that have been developed for desorption[27,28] certainly contain all the essential physics for optical phonon gain, although this appears not to have been realized yet in the desorption literature. We will discuss this further elsewhere.

Acknowledgements

The author would like to acknowledge support from EPRI and from the EE & CS Department at MIT. This work was stimulated by discussions with Y. Kucherov, I. Savvatimova, and A. Karabut. The author would like to thank S. Kaushik, L. Smullin and Y. Fukai for many valuable conversations.

References

1. S. Pons, M. Fleishmann and M. Hawkins, *J. Electroanal. Chem* **261** 301 (1989).

2. S. Jones, E. P.Palmer, J. B. Czirr, D. L. Decker, G. L. Jensen, J. M. Thorne, S. F. Taylor and J. Rafelski *Nature* **339** 737 (1989).

3. M. C. H. McKubre, S. Crouch-Baker, A. M. Riley, S. I. Smedley and F. L. Tanzella, *Frontiers of Cold Fusion*, Proceedings of the Third International Conference on Cold Fusion, Ed. H. Ikegami, Nagoya, Oct. 1992; p. 5.

4. H. O. Menlove, M. M. Fowler, E. Garcia, A. Mayer, M. C. Miller, R. R. Ryan and S. E. Jones, *Fusion Tech.* **9** 215 (1990).

5. T. N. Claytor, D. G. Tuggle and S. F. Taylor, *Frontiers of Cold Fusion*, Proceedings of the Third International Conference on Cold Fusion, Ed. H. Ikegami, Nagoya, Oct. 1992; p. 217.

6. F. Lanza, V. Bertolini, E. Vocino, E. Parnisari, and C. Ronseco, *The Science of Cold Fusion*, Ed. T. Bressani, E. Del Guidice, and G. Preparata, Conf. Proc. Vol. 33, Italian Physical Society, Bologna, 1992; p. 151.

7. A. B. Karabut, Ya. R. Kucherov, I. B. Savvatimova, *Phys. Lett. A* **170** 265 (1992).

8. R. L. Mills and S. P. Kneizys, *Fusion Tech.* **20** 65 (1991).

9. R. Notoya and M. Enyo, *Frontiers of Cold Fusion*, Proceedings of the Third International Conference on Cold Fusion, Ed. H. Ikegami, Nagoya, Oct. 1992; p. 421.

10. M. Srinivasan, A. Shyam, T. K. Sankaranaranyanan, M. B. Bajpai, H. Ramamurthy, U. K. Mukherjee, M. S. Krishnan, M. G. Nayar and Y. P. Naik, *Frontiers of Cold Fusion*, Proceedings of the Third International Conference on Cold Fusion, Ed. H. Ikegami, Nagoya, Oct. 1992; p. 123.

11. S. Pons and M. Fleischmann *Phys. Lett. A* **176** 118 (1993).

12. P. Hagelstein, *Fusion Tech.* **23** 353 (1993).

13. Y. Fukai and N. Okuma, *Jpn. J. Appl. Phys.* **32** L1256 (1993).

14. A. Rahman, K. Skold, C. Pelizzari and S. K. Sinha, *Phys. Rev. B* **14** 3630 (1976).

15. P. Hagelstein, presented at ICAME'93; proceedings to appear in *Hyperfine Interactions.*

16. F. Duschinsky, *Acta Physicochimica U.R.S.S* **7** 551 (1937).

17. T. R. Faulkner and F. S. Richardson, *J. Chem. Phys.* **70** 1201 (1979).

18. R. Loudon, *The Quantum Theory of Light*, Clarendon Press, Oxford, (1973).

19. G. Mainfray and C. Manus, *Rep. Prog. Phys.* **54** 1333 (1991).

20. M. Dorr, M. Terao-Dunseath, J. Purvis, C. J. Noble, P. G. Burke and C. J. Joachain, *J. Phys. B* **25** 2809 (1992).

21. A. L'Huillier, P. Balcou, S. Candel, K. J. Schafer, and K. C. Kulander, *Phys. Rev. A* **46** 2778 (1992).

22. A. A. Frost and B. Musulin, *J. Chem. Phys.* **22** 1017 (1954).

23. P. Marmier and E. Sheldon, *Physics of Nuclei and Particles*, Academic Press, New York (1969).

24. P. Hagelstein, *Frontiers of Cold Fusion*, Proceedings of the Third International Conference on Cold Fusion, Ed. H. Ikegami, Nagoya, Oct. 1992; p. 297.

25. P. Hagelstein and S. Kaushik, presented at the Fourth International Conference on Cold Fusion, Maui, 1993.

26. Y. Fukai, *Frontiers of Cold Fusion*, Proceedings of the Third International Conference on Cold Fusion, Ed. H. Ikegami, Nagoya, Oct. 1992; p. 265.

27. Z. W. Gortel, H. J. Kreuzer and R. Teshima, *Can. J. Phys.* 58 376 (1980).

28. J. Harris, *Surface Sci.* **221** 335 (1989).

MITH 94/2

COLD FUSION '93: Some theoretical ideas *

Giuliano Preparata
Dipartimento di Fisica dell'Università di Milano
and
INFN, Sezione di Milano, via G. Celoria 16, 20133 Milano, Italy
(E-mail: preparata@mi.infn.it)
(Maui, December 1993.)

Abstract

The status of the theoretical research on the Cold Fusion phenomenology of the Fleischmann-Pons system is reviewed within the framework of coherent QED. A particular emphasis is put on the description of the possible complex phenomena that occur at the Pd-catode during the electrolysis of heavy water

I. INTRODUCTION

In spite of the heavy charges of being pathological science, the "scientific fiasco of the century" and "too hot to handle", Cold Fusion has managed to survive for the fourth year, and I come to the enchanted island of Maui to draw a balance of the past years of struggles and achievements. For struggles there were many, and even serious ones but, as it has been amply shown at this Conference, they have not been in the way of a slow but steady progress towards first to establish the reality and the modalities of the phenomena announced by Fleischmann and Pons [1], and second to appreciate the deep implications of these phenomena for our understanding of condensed matter and the physical laws that are at work in it.

The consequences of the ongoing "quiet revolution" of Cold Fusion today appear still limited to the devoted activity of a (relatively) small scientific community, that is pursuing with determination a research, which is surrounded by an almost universal and often rabid hostility; however there are some signs that we may be very close to an epochal change, whose outcome is still beclouded, but its *grandeur* in shaping new scenarios in both science and society can hardly be doubted.

This talk is about the application to the Cold Fusion (CF) phenomena of the Fleischmann-Pons type (heavy water electrolysis with a Pd-cathode) of a set of new ideas

---

*Invited Talk at the IV International Conference on Cold Fusion (ICCF4), Maui (Hawaii, USA) Dec. 6-9 1993— Milano, January 1994.

about the working of Quantum Electro Dynamics (QED) in the deep recesses of Condensed Matter [2]. The general attitude toward such ideas is still far from enthusiastic, but I am confident that the reality of CF phenomena will finally prove their being indispensable also for a deep, general understanding of many other poorly understood behaviours of condensed matter systems, including life itself.

II. PROBLEMS AND FRAMEWORK

As I have already mentioned, this talk will uniquely concern the Fleischmann-Pons (FP) system, i.e. the Pd/D system at high concentration $x = \frac{D}{Pd}$. From all that has been so far established, the problems one must solve are of two kinds:

(α) The QED dynamics of D's in the host Pd-lattice, which leads to the following explicit questions:

(α_1) Why and how does the process

$$D_2|_{gas} \rightarrow D + D|_{lattice} \tag{II.1}$$

proceed?

(α_2) why and how, in the lattice

$$D|_{lattice} \rightarrow D^+ + e^-, \tag{II.2}$$

D^+ and e^- enjoying a different, independent dynamics?

(α_3) why is D^+ so mobile at high x?

(α_4) what are the problems of Pd/d? [1]

(α_5) what happens during electrochemical loading?

(α_6) why one observes "Heat after death"? [2]

and

(β) the mechanisms of CF in the highly loaded Pd/D system, which leads to the further explicit questions:

(β_1) how can one overcome the Coulomb barrier?:

(β_2) which is the main DD-fusion dynamics?:

(β_3) can we understand rarer processes: n,T,,X-rays...?

---

[1] see Fleischmann's talk, these Proceedings

[2] see Pons' talk, these Proceedings

In the following I shall attempt to answer all the above questions within the theoretical framework of QED-coherence in condensed matter (QEDCM) [2] that fully recognizes the essential rôle played by the electrodynamical interactions in determining the structure and the properties of the innumerable systems of Condensed Matter. On the other hand one must stress that in the generally accepted condensed matter physics (GACMP) such interactions are totally disregarded, based on a number of faulty arguments that P. W. Anderson [3] borrowed, unwarrantedly [4], from laser physics. When such misgivings are removed and the correct QED dynamics is recognized, GACMP, which is (almost) universally adopted in the theoretical analysis of physical systems such as the one which forms the object of our analysis, is found severely hampered.

According to the correct QEDCM one may look at condensed matter as comprising a set of **plasmas**, i.e. ensembles of identical charges of charge e and mass m, oscillating around their equilibrium positions with a typical frequency, the plasma frequency ω_p

$$\omega_p = \kappa\omega_0 \qquad \omega_0 = \frac{e}{(m)^{1/2}}(\frac{N}{V})^{1/2} \tag{II.3}$$

κ being a factor $O(1)$, representing the deviation of the particular plasma from the ideal one, whose plasma frequency is ω_0.

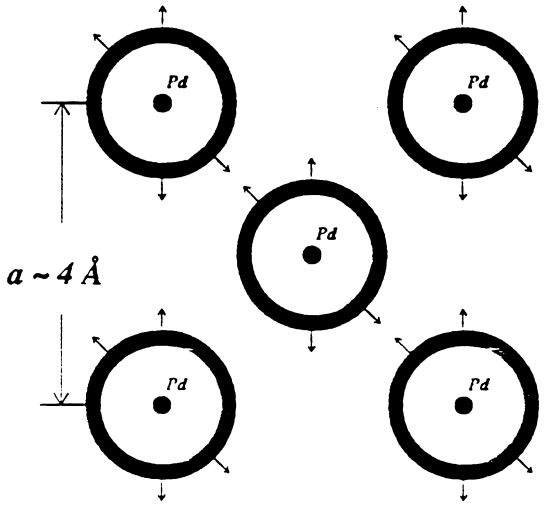

FIG. 1. The electronic d-shells of Pd as seen slicing the lattice along the (1,0,0)-plane.

Let us analyze in detail the plasmas of the Pd/D system that are relevant for Cold Fusion:

(γ_1) the plasma of the d-electrons [5].

We can visualize this plasma (see Fig. 1) as consisting of charged shells of charge $n_d e$ ($n_d = 10$ for Pd) of radius $r_d = 1$Å and thickness a fraction of one Ångstrom, which at this time we need not specify precisely. In order to estimate the deviation of the plasma

frequency of the d-shell ω_{ed} from the ideal value $\omega_{ed}^{(0)} = \frac{e}{(m_e)^{1/2}}(\frac{n_d N}{V})^{1/2}$, we remark [6] that the neutralizing charge of the plasma is not homogeneously distributed in space, but is rather concentrated over the atomic volume. A simple geometrical argument yields

$$\omega_{ed} = (\frac{6}{\pi})^{1/2}\omega_{ed}^{(0)} = 1.38\ \omega_{ed}^{(0)} \simeq 41.5eV, \tag{II.4}$$

a rather high value. As for the maximum oscillation amplitude $\xi_d \simeq 0.5\mathring{A}$ appears as a reasonable estimate. [2]

(γ_2) the plasma of delocalized s-electrons

These electrons are those which enter the lattice to neutralize the absorbed D^+'s. These electrons will be essentially delocalized, however, due to the Pauli principle and Coulomb repulsion. The volume to them V_a available to them (see Fig. 2) will be just ($\frac{N}{V}$ is the Pd density; $\frac{N}{V} \simeq 6.3 \cdot 10^{22} cm^{-3}$)

$$V_a = V[1 - \frac{N}{V}V_{Pd}] = \lambda_a V, \tag{II.5}$$

V_{Pd} being the volume effectively occupied by the Pd-atom and its oscillating d-shell.

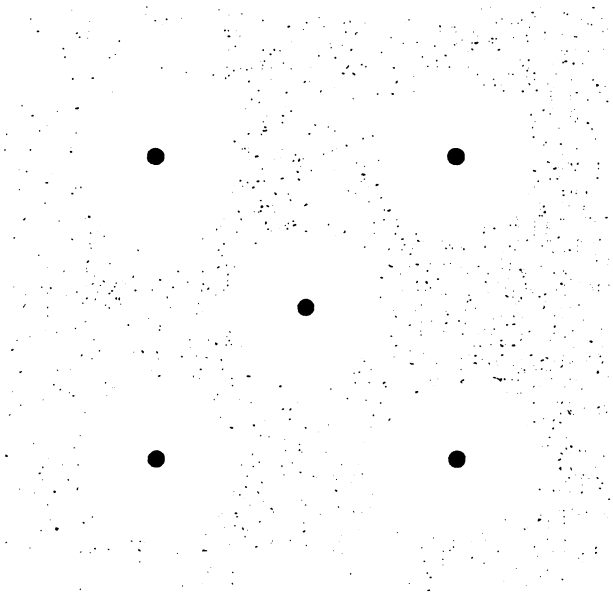

FIG. 2. The region occupied by the s-electrons that enter the lattice together with the positive D-ions.

---

[2] A "real" calculation of ξ_d requires a careful consideration of the (short-range) interaction of the d-shell with the Pd-core.

Note that setting $R_{Pd} \simeq 1.3\mathring{A}$ we obtain $\lambda_a \simeq 0.42$, i.e. about 40% of the metal volume can be occupied by the s-electrons. The parameter λ_a plays an important role in the energetics of the s-electrons' plasma for their plasma frequency is just

$$\omega_{se} = \frac{e}{(m_e)^{1/2}}(\frac{N}{V})^{1/2}\frac{x^{1/2}}{\lambda_a^{1/2}}, \tag{II.6}$$

and the effective coupling [6] g, which controls the gap of the coherent plasma is given by

$$g = (\frac{2\pi}{3})^{1/2}, \tag{II.7}$$

while the gap itself is given by:

$$\delta = -\frac{(g^2 - g_c^2)}{2g^2 g_c^2}\omega_{se}, \tag{II.8}$$

$g_c \simeq (\frac{16}{27})^{1/2}$ being the critical coupling constant. The "superradiant" gain is in part balanced by the "Pauli energy" (N is the number of Pd-atoms)

$$\frac{E_{Pauli}}{Nx} = \frac{3}{10}\frac{(3\pi^2)^{3/2}}{m_e}(\frac{N}{V})^{2/3}\frac{1}{\lambda_a^{2/3}}x^{2/3}, \tag{II.9}$$

arising from the filling of the electron states in the available volume. Putting (II.8) and (II.9) together we may write for the chemical potential

$$\mu_{se} = \epsilon_p x^{2/3} - \epsilon_s x^{1/2}, \tag{II.10}$$

where for $\lambda_a = 0.45$, one computes

$$\epsilon_p = 6.45eV, \quad \epsilon_s = 4.61eV. \tag{II.11}$$

The interest of the Eq. (II.10) lies in the fact that for very small x and for $\lambda_a \simeq 0.4$ the negative term arising from QED coherence predominates over the positive Pauli-term, while for larger values of x μ_{se} becomes positive. In Fig. 3 μ_{se} is plotted for $\lambda_a = 0.425$, which appears experimentally favoured (see later).

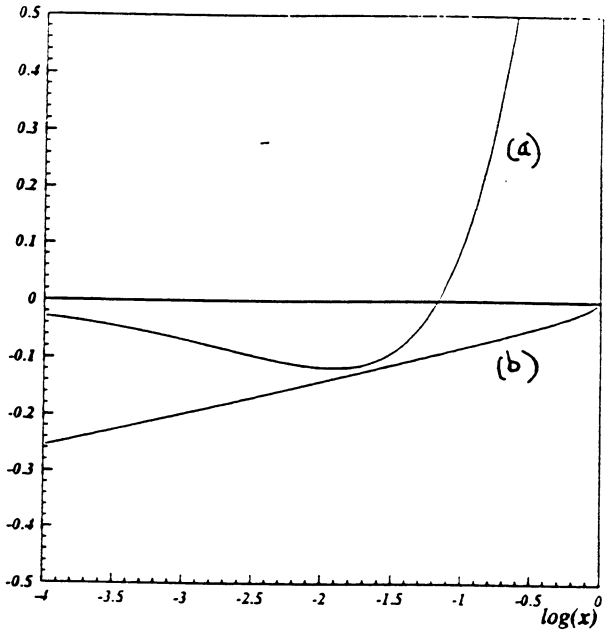

FIG. 3. The chemical potentials μ_{se} (a), compared with μ_{CE} (see Eq. (III.5)) as a function of x.

(γ_3) The plasmas of D^+'s in the octahedral sites

We shall now analyze the conditions for and the energetics of the coherent plasma of deuterons that enter the lattice and get localized in the octahedral sites (Fig. 4). The basic quantities that characterize a coherent plasma are [6] the plasma frequency and the coupling constant. As for the plasma frequency we write:

$$\omega_{D\beta} = \bar{\omega}_{D\beta}(x + x_0)^{1/2} \tag{II.12}$$

where

$$\omega_{D\beta} = \frac{e}{(m_D)^{1/2}}(\frac{N}{V})^{1/2}\frac{1}{\lambda_a} = \frac{0.15}{\lambda_a^{1/2}}eV, \tag{II.13}$$

is the renormalized plasma frequency for $x \simeq 1$, and $x_0 \simeq 0.05$ reproduces the measured value at very low x-values. Note that for larger x-values (II.12) yields the expected $x^{1/2}$-behaviour of a pure (renormalized) plasma oscillation.

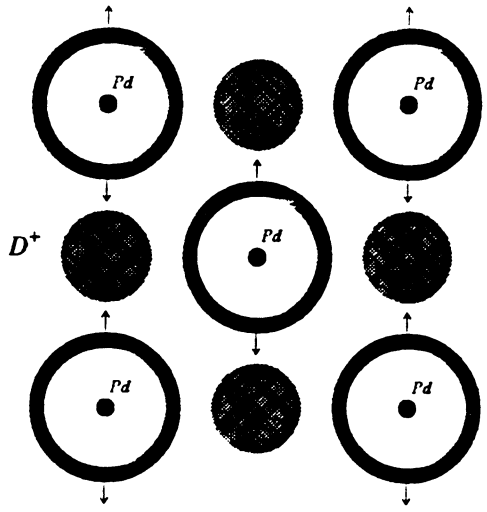

FIG. 4. The octahedral sites in the (1,0,0)-plane of the Pd lattice.

The coupling constant g_β can be written ($V_{D\beta} = \frac{4}{3}\pi\xi_{D\beta}^3$)

$$g_\beta = (\frac{2\pi}{3})^{1/2}\lambda_a^{1/2}(\frac{x}{x_0+x})^{1/2}[1-(\frac{N}{V})V_{D\beta}\frac{x}{\lambda_a}], \qquad \text{(II.14)}$$

where the last factor is particularly noteworthy, originating from the screening of the D^+-charge smeared in the oscillation volume V_D ($\xi_{D\beta}$ is the maximum oscillation amplitude of the D^+'s in the octahedral sites); $\xi_{D\beta} \simeq 0.5\mathring{A}$, but its precise value depends on the careful evaluation of the interaction of the s-electrons with both the d-shell and the D^+-ions. The chemical potential $\mu_{D\beta}$ for $\lambda_a = 0.425\mathring{A}$ and $\xi_{D\beta} \simeq 0.6\mathring{A}$ summed with the s-electrons' chemical potential μ_{se} [Eq. (II.10)] is plotted in Fig. 5.

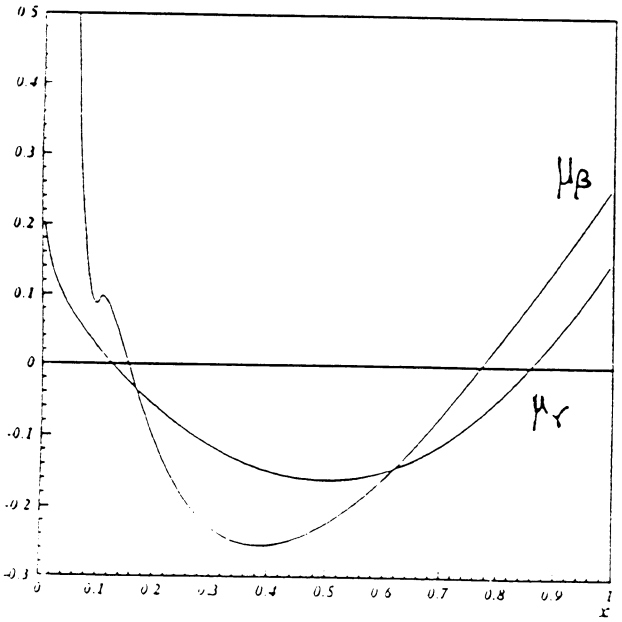

FIG. 5. The chemical potential μ_β of the β-phase (octahedral sites), compared with μ_γ of the γ-phase (tetrahedral sites), as a function of x.

(γ_4) The plasma of D^+'s in the tetrahedral sites

Besides the octahedral sites the plasma of D^+'s can occupy the thin disks that encompass two tetrahedral sites, as depicted in Fig. 6. Differently from the octahedral sites, the tetrahedral sites present to the D^+'s a barrier, whose height can be computed as follows: in the direction $\vec{n}$ of Fig. 6 a repulsive force is exerted by the Pd-ion, of effective charge $Z_{eff} \simeq 10$ at a distance $y_0 \simeq 1.4\mathring{A}$. Note in fact that the electrons of the d-shell oscillate past the equilibrium distance y_0 thus embedding the D^+'s in a static "cloud" of negative charge, whose screening of the D^+-Coulomb barrier will prove essential for the Cold Fusion phenomena [7] (see Section IV). A simple electrostatic calculation yields for the potential of these repulsive forces ($\alpha = \frac{1}{137}$ is the fine-structure constant)

$$V_{rep} \simeq \frac{2Z_{eff}\alpha}{y_0}(1 + \frac{y^2}{y_0^2}), \tag{II.15}$$

whose associated harmonic oscillator frequency ω_{rep} can be calculated from

$$\frac{1}{2}m_d\omega_{rep}^2 = \frac{2Z_{eff}\alpha}{y_0^3}, \tag{II.16}$$

to yield

$$\omega_{rep} = (\frac{4Z_{eff}\alpha}{m_D y_0^3})^{1/2} \simeq 0.65eV. \tag{II.17}$$

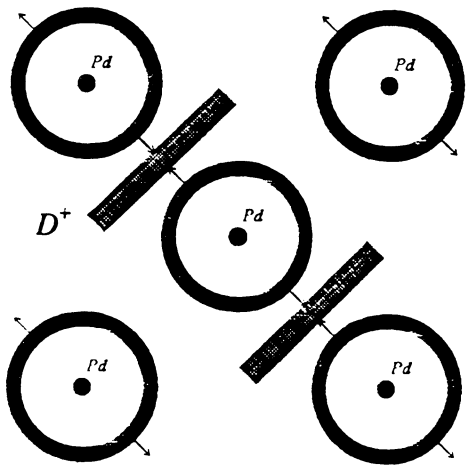

FIG. 6. The thin disks of the tetrahedral sites in the section along the (1.0.0)-plane of the lattice.

Thus the barrier to the access of the D^+'s to the tetrahedral sites is nothing but the zero-point energy of the harmonic oscillator in the $\vec{n}$-direction, i.e. $\frac{\omega_{rep}}{2} \simeq 0.33eV$. We can also estimate the thickness $\Delta = 2t$ of the "tetrahedral disk" from the relation

$$\frac{1}{2}m\omega_{rep}^2 t^2 = \frac{\omega_{rep}}{2}, \tag{II.18}$$

corresponding to the classical turning point. Thus we get

$$\Delta = \frac{2}{(m_D\omega_{rep})^{1/2}} \simeq 0.12\mathring{A}. \tag{II.19}$$

The coupling constant g_γ of this plasma can be written

$$g_\gamma = (\frac{2\pi}{3})^{1/2}\lambda_a^{1/2}[1 - (\frac{N}{V})\frac{\pi}{\lambda_a}\xi_{D\gamma}^2 x\Delta]\frac{e_{eff}}{e}, \tag{II.20}$$

where the only new element (note that the term in square brackets arises from the screening of the s-electrons, $\xi_{D\gamma} \simeq 1\mathring{A}$ is the maximum amplitude of the plasma oscillations of D^+'s in the tetrahedral disk) is the effective charge e_{eff} of the D^+'s embedded in the d-electrons' "cloud". In order to estimate $e_{eff} = e - \Delta e$, Δe is computed geometrically by first evaluating the overlap of a d-shell of thickness $\delta \simeq 0.1\mathring{A}$ and radius $r_d \simeq 1\mathring{A}$ and constant density $\rho = \frac{10e}{4\pi r_d^2 \delta}$, with the "tetrahedral disk" of thickness Δ and radius $\xi_{D\gamma} \simeq 1\mathring{A}$. One obtains $\frac{e_{eff}}{e} \simeq 0.9$ By using for the chemical potential the formula

$$\mu_{D\gamma} \simeq -\frac{e^2 x}{\lambda_a}(\frac{N}{V})\xi_{D\gamma}^2 2\sqrt{3}(g_\gamma - g_c), \tag{II.21}$$

that can be derived from the theory of coherent plasmas of maximum amplitude $\xi_{D\gamma}$ and $g_\gamma \simeq g_c = (\frac{16}{27})^{1/2}$, for $\lambda_a = 0.425$, $\xi_{D\gamma} = 1\mathring{A}$ we obtain for the total chemical potential μ_gamma the curve plotted in Fig. 6.

I am now going to use these theoretical tools and ideas to answer the questions I have formulated at the beginning of this Section. But before doing this I would like to enphasize the still rather semiquantitative nature of the theory so far developed, nevertheless for the purpose of <u>understanding</u> the nature of the phenomena occurring in the Fleischmann-Pons system, as we shall see, this theory turns out to be perfectly adequate <u>and</u> essentially indispensable.

III. THE PD/D SYSTEM

I shall now try and answer all questions of type (α) posed in the preceding Section. The framework is QEDCM and some preliminary work in this direction can be found in Ref. [5].

Let's take up the first questions which, for convenience, I shall repeat here:

(α_1) Why and how does the process

$$D_2|_{gas} \stackrel{-}{\to} D + D|_{lattice} \tag{III.1}$$

proceed?

(α_2) why and how in the lattice

$$D|_{lattice} \to D^+ + e^-, \tag{III.2}$$

D^+ and e^- enjoying different, independent dynamics?

We must envisage the dynamics of D_2 absorption in the lattice as comprising three steps (see Fig. 7). Step (i), in which the D_2-molecule is brought in contact with the Pd-surface: this step is fully governed by the chemical potential of the D_2-gas which can be written (we use the natural units $\hbar = c = k_B = 1$)

$$\mu_{D_2} = -\frac{T}{2}[19.3 + \frac{3}{4}\log\frac{T}{T_0} - \log\frac{p}{p_0}], \tag{III.3}$$

where $T_0 = 300K$ and $p_0 = 1$ Atm. Please note that this formula is the standard result for the perfect gas of a diatomic molecule. Step (ii) describes the interaction of the D_2-molecule with the Pd-surface. as emphasized in [5] in the QEDCM framework the most important process in this step is by far the interaction with the evanescent coherent electromagnetic field, associated with the various plasmas that we have discussed in the previous Section. As a result the D_2-molecules, immersed in strong coherent fields, have a good chance to tunnel through the electrostatic barrier (about $30eV$ high!) undergoing the dissociation process

$$D_2 \to 2D^+ + 2e^-, \tag{III.4}$$

with no energy expenditure. This is what Quantum Mechanics in presence of a strong coherent e.m. field predicts [6], and if you think this hard to believe you should give a harder look at the Debye-Hückel theory of electrolytic dissociation in water. You certainly do not believe that the macroscopic, static dielectric constant of water can be responsible for the overcoming of barriers several eV's high.

Finally in step (iii) the "shattered" D_2-molecule enters the lattice with its D^+- and e^--components subject to independent dynamics. This much for question (α_1) and (α_2).

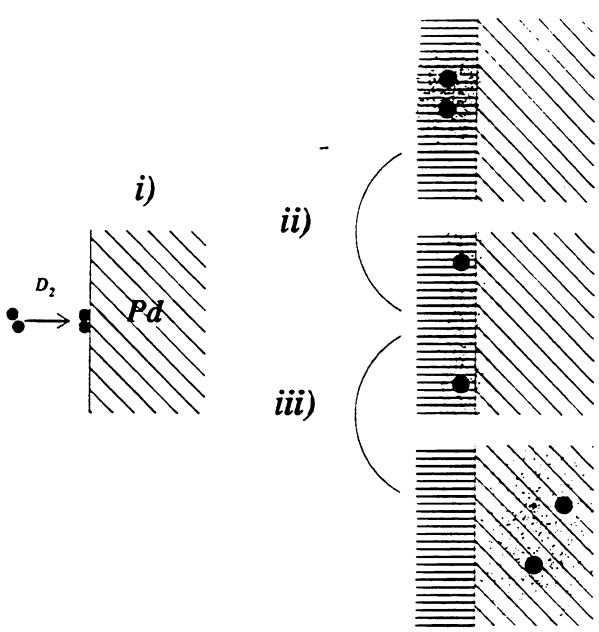

FIG. 7. The three steps of D_2 absorption by the Pd-lattice.

By following through the independent dynamical evolutions of D^+'s and e^-'s we can now answer two more questions:

(α_3) why is D^+ so mobile at high x?;

(α_4) what are the phases of Pd/D?.

For, as we have seen in the preceeding Section the e^-'s access a coherent plasma state whose chemical potential μ_{se} [Eq. (II.10)] is plotted in Fig. 3. For very low x, as we have also seen in the preceeding Section, the D^+'s that must occupy the octahedral sites (for, in order to occupy the "tetrahedral disk", they must overcome the barrier $\frac{\omega_{reo}}{2}$, see Eq. (II.17) and the following discussion) find themselves in a disordered state, with a chemical potential only determined by the configurational entropy of the system, i.e.

$$\mu_{CE} = -T[\log\frac{1-x}{2} - \frac{1}{x}\log(1-x)]. \tag{III.5}$$

This phase of the Pd/D system whose chemical potential is

$$\mu_\alpha = \mu_{se} + \mu_{CE}, \tag{III.6}$$

is the well known α-phase, and is in thermodynamical equilibrium with the gas when

$$\mu_{D_2} = \mu_\alpha. \tag{III.7}$$

It is clear from the behaviour of μ_{D_2} and μ_α as a function of T, p and x, that the α-phase can be stable only for very low x ($x \leq 0.1$); and this is just what is experimentally observed (see Fig. 8). On increasing p and decreasing T, i.e. on decreasing the absolute value of the negative chemical potential μ_{D_2}, a new phase at higher x can be accessed where the D^+ are in the "octahedral plasma".

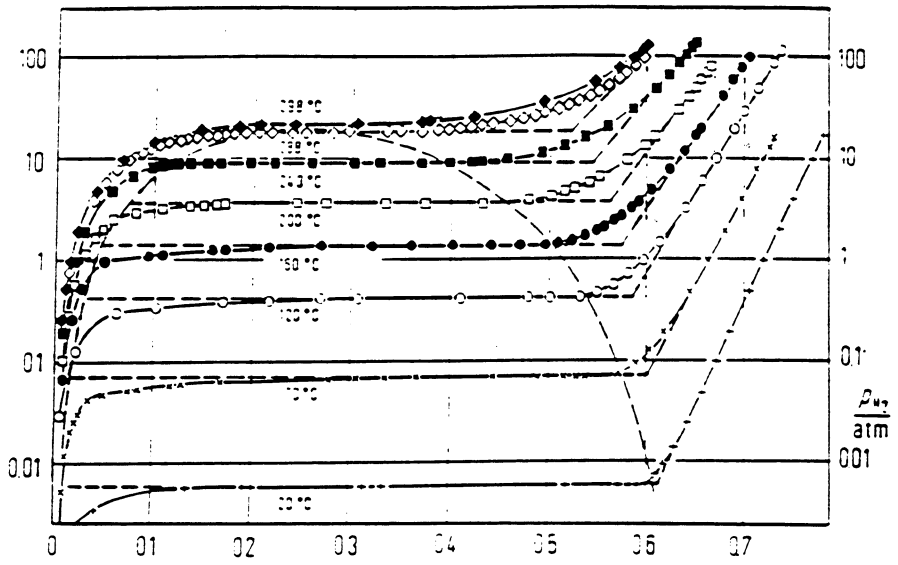

FIG. 8. The $p - x$ phase plane for the Pd/H system.

The chemical potential of this new phase, the well known β phase, is accordingly

$$\mu_\beta = \mu_{es} + \mu_{D\beta}, \tag{III.8}$$

while if the D^+'s are in the "tetrahedral disk" one gets the chemical potential

$$\mu_\gamma = \mu_{es} + \mu_{D\gamma}. \tag{III.9}$$

I have plotted both potentials in Fig. 5, which is remarkable for more than one reason. First it shows that at appropriate values of the thermodynamical variables there is indeed a first order phase transition to a high x-state which has first the features of the β-phase and then, for smaller absolute values of μ_{D_2} at $x = x^* \simeq 0.7$ it undergoes a second-order phase transition to the new phase that we can naturally call the γ phase.

I should remind you that the evidence of this new phase was actually predicted [8] on the grounds that Cold Fusion cannot take place in the β-phase, for

(i) the D^+'s are too far away;

(ii) only the tetrahedral sites can accomodate more than one D^+;

(iii) only in the tetrahedral sites the d-electrons can effectively screen Coulomb repulsion.

Is there any direct evidence? It is a fortunate coincidence that in the summer of 1993 a very nice work was published by a Padova group [9] that seems to support the theoretical evidence. The measurement of the diffusion coefficient of D's in Pd at different concentrations, which can be represented as:

$$D = \sigma x \frac{\partial \mu}{\partial x}, \tag{III.10}$$

where σ is the Einstein mobility, yields the experimental behaviour a fit of which is reported in points in Fig. 9, which clearly suggests a discontinuity around $x^* = 0.7$. As shown in Fleischmann's talk, by a simple parametrisation of the diffusion coefficients of D in both the $\beta-$ and the $\gamma-$phases one can get a good quantitative understanding of recent experiments carried out at IMRA-Europe. We may thus conclude that the γ-phase is a reality and that the QEDCM approach passes here a difficult and important test.

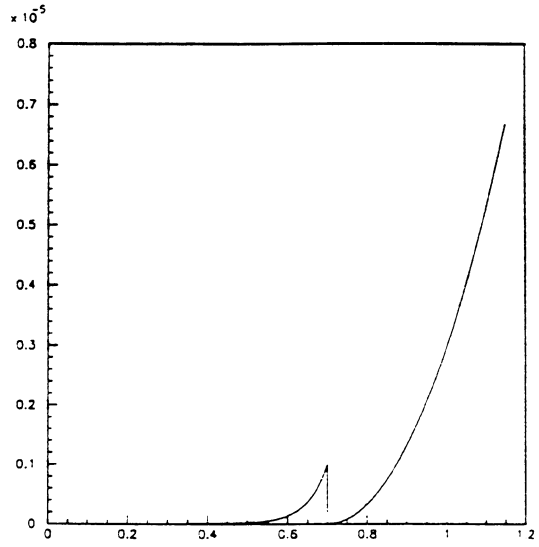

FIG. 9. The measured diffusion coefficients (Ref. [[8]]) for different values of H/Pd and different electrolytes.

We may now come to the last two questions:

(α_5) what happens during electrochemical loading?;

(α_6) why one observes "heat after death"?

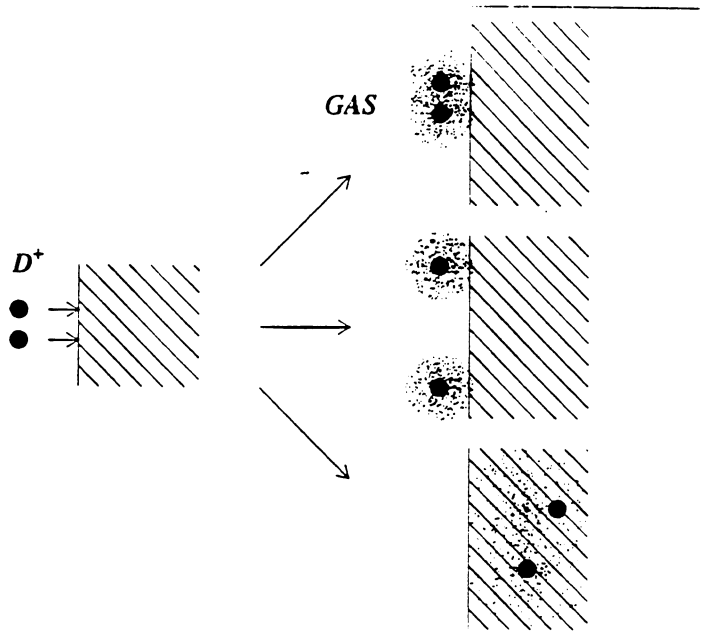

FIG. 10. The different fates of D^+'s arriving at the Pd-cathode.

The fact that through prolonged electrolysis one could drive the system off the thermodynamical equilibrium (the β-phase), to high values of x, was known to M. Fleischmann since a long time and most likely lies at the basis of the FP's "fantasy" that perhaps high loadings could induce two deuterons to fuse inside the Pd-lattice. However, as far as I can make out from the extant literature, how can this happen is still a mystery. Let us see whether and how the new ideas of QEDCM can lift the veil. It should be clear that the electrolysis device is nothing but a means to deploy a definite number of D^+'s per second (the electrolysis current) at the surface of the Pd-cathode. Once on the surface any two D^+'s (see Fig. 10) can do one of three things:

1. by diffusing on the surface they get within a molecular range (at distance $d \leq 1\mathring{A}$), and they combine with the ingoing electrons (that the electrolysis lends to the cathode) according to the process

$$2D^+ + 2e^- \rightarrow D_2. \tag{III.11}$$

The D_2-molecule thus formed will bubble out into the surrounding atmosphere. One can estimate that in order for the process (III.11) not to exhaust the incoming D^+-current i (in Ampère units) for the surface diffusion coefficient D_s one must have:

$$D_s < i\ 10^{-9}\ cm^2/sec. \tag{III.12}$$

a very low value that, most likely, can only be achieved through the deposition of some kind of "muck" on the Pd-cathode surface. Such small D_s's as required by (III.12) can also conceivably be obtained through some smart "poisoning" of the Pd-surface. In any case this appears as the most tricky aspect of the FP-system, one that can discriminate between successful and unsuccessful loadings and therefore determine the degree of reproducibility of FP Cold Fusion phenomena.

2. the D^+'s stay on the surface becoming members, together with the neutralizing electrons, of a double layer whose chemical potential shall be denoted by μ_s;

3. the D^+'s enter, (almost) independent of their neutralizing electrons, the Pd-lattice and load it at a bulk-chemical potential μ_B.

Little reflection is needed to convince ourselves that in order for processes (1) and (3) to lead to high x-values two very strange phenomena must occur:

(i) a negative surface-chemical potential μ_s must arise at high x;

(ii) the bulk chemical potential

$$\mu_B = \mu_\gamma + e\Phi_{ec} \tag{III.13}$$

due to a new electrochemical component $e\Phi_{ec}$ must also become negative at high x, differently from the predicted behaviour of μ_γ reported in Fig. 5.

It is remarkable that in QEDCM one can explain both phenomena in terms of the ponderomotive forces that the different evanescent coherent e.m. fields on the Pd-surface exert upon the charged particles: e^- and D^+. Taking the z-axis normal to the Pd-surface, directed in the outward direction, the evanescent e.m. field can be written

$$\vec{A} = \vec{A}(0)\cos\omega_r t e^{-\omega_0 z} \tag{III.14}$$

where ω_r is the renormalized frequency and $\omega_0 = \frac{2\pi}{\lambda}$ ($\lambda \simeq 10^{-4}$ cm for the D^+ plasmas) is the original frequency of the coherent process ($\omega_0 > \omega_r$). The static ponderomotive potential acting on the charged particle of charge e and mass m is

$$V_{pm} = e\left\langle \frac{\vec{A}(0)^2}{2m} \right\rangle = e\frac{|\vec{A}(0)|^2}{4m}e^{-2\omega_0 z}. \tag{III.15}$$

For the D^+-plasma in the "tetrahedral disks" one estimates a ponderomotive electric field for the electrons

$$E_{pm} = -\frac{\partial V_{pm}}{\partial z} \simeq 2.4 \cdot 10^8 V/cm \cdot x^{3/2}, \tag{III.16}$$

$4 \cdot 10^4$ times larger than for D^+'s. Please note the x-behaviour of (III.16). Giving the potential V_e that binds the electrons to the Pd-surface the simple harmonic representation:

$$V_e = -V_0[1 - \frac{z^2}{z_0^2}], \tag{III.17}$$

where V_0 is the work function and $z_0 \simeq 1\text{Å}$ (a typical atomic dimension), for the width $\bar{z}$ of the double layer one gets

$$\bar{z} = \frac{z_0^2}{2V_0}E_{pm} \simeq 2.4 \cdot 10^{-9} x^{3/2} cm. \tag{III.18}$$

where for the work function V_0 we have taken $5eV$, a reasonable value.

It can be ascertained without much ado that the formation of the double layer has two main consequences:

(i) it induces a negative surface chemical potential

$$\mu_{pm} = -V_0(\frac{\bar{z}}{z_0})^2 = -Ax^3, \tag{III.19}$$

with $A \simeq 0.3eV$, according to the previous estimates;

(ii) it induces a bulk electrochemical potential

$$e\Phi_{ec} = -B\lambda x^{3/2}, \tag{III.20}$$

where $B \simeq 5.5eV$, again from the previous estimates.

One of the most remarkable features of these consequences in their strong dependence on x, we shall now see that this may explain completely the strange phenomena alluded to above.

Indeed , we can write the thermodynamical equilibrium equation for the electrolysis:

$$\mu_s = \mu_{Pd}, \tag{III.21}$$

where the surface chemical potential is

$$\mu_s = \mu_{pm} - \frac{T}{T_0}[0.0875 + 0.025 \log \frac{1}{\lambda} + 0.025 \log \frac{T}{T_0}]eV, \tag{III.22}$$

where the second term ($T_0 = 300K$) stems from the chemical potential of the surface D^+ modeled as a two-dimensional perfect gas; as for the bulk chemical potential one may write:

$$\mu_{Pd} = \mu_\gamma + e\Phi_{ec}, \tag{III.23}$$

where the γ-phase chemical potential can be represented (at least for x not much bigger than 1) as

$$\mu_\gamma \simeq (-0.14 + 5.2(x - x^*)^3)eV, \tag{III.24}$$

where, as usual, $x^* \simeq 0.7$.

Solving Eq. (III.21) for $\lambda = \lambda(x)$ one obtains the curves reported in Fig. 11.

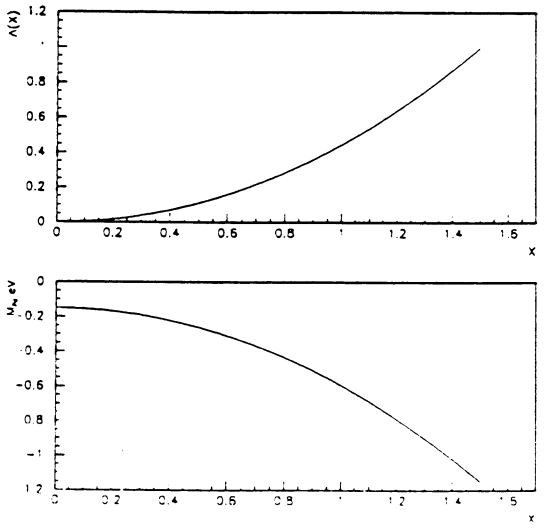

FIG. 11. The behaviour of $\lambda(x)$ and $\mu_\gamma(x)$ from Eqs. (3.19)-(3.22).

Thus it is clear that to achieve high x, fundamental for significant Cold Fusion rates, one must be able to achieve high values of the surface covering λ, and the electrolysis protocol must be optimized to obtain high values of λ.

Also, the events of "heat after death" presented at this Conference by S. Pons, [1] can be readily understood in the framework just presented.

IV. COLD FUSION

On the theoretical understanding of the mechanisms of Cold Fusion proper there has not been much progress since last year [5], and as a matter of fact there has been very little progress since the initial theoretical work [7]. Indeed the phenomenology is still basically the one outlined in the original Cold Fusion paper [7], and the new facts (light water electrolysis, nuclear transmutation, etc.) are still too vague and uncertain to warrant a serious theoretical effort to put them in the proper perspective at this time. Thus in this Section I will limit myself to reiterate known answers to the traditional questions of Cold fusion *à la* Fleischmann-Pons. As reminded in Section II the first question is:

(β_1) how can one overcome the Coulomb barrier?

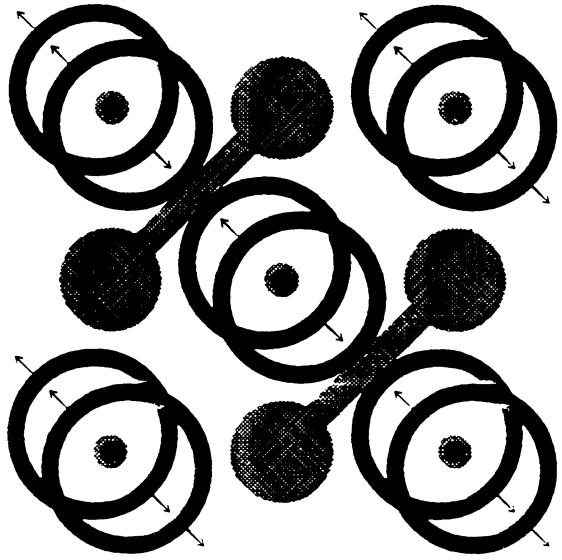

FIG. 12. The oscillating d-shells "fill" the tetrahedral "disks" with a static negative charge.

---

[1] See Pons'talk at this Conference

The answer is (since 1989 [7]) given pictorially in Fig. 12, which implies that, due to large plasma oscillations of the d-elections' shell, in the disk-like tetrahedral region (where the γ-phase D^+'s are located) a high density negative charge condenses statically giving rise to a screening potential V_0 whose profile is reported in Fig. 13. For $x > 1$ (naturally within a single coherence domain of the γ-phase), for below this threshold no D^+ will stably occupy a tetrahedral site that is already occupied, the Gamow amplitude for D-D fusion is given by

$$\eta_G \sim \exp -(2\mu)^{1/2} \int_{r_N}^{r_0} dr' [V(r') - E]^{1/2}, \tag{IV.1}$$

where r_0 is the classical turning point (for which $V(r_0) = E$), r_N is a typical nuclear distance $r_N \leq 10$ F (10^{-12} cm), μ is the reduced mass ($\mu = \frac{m_D}{2}$) and the screened potential $V(r)$ is given by:

$$V(r) = V_0 + \frac{\alpha}{r}. \tag{IV.2}$$

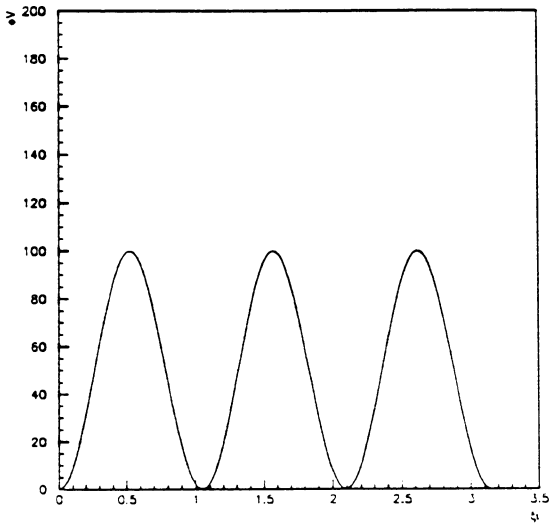

FIG. 13. The electrostatic potential as seen by the D^+'s along the tetrahedral disks.

Note that for $V_0 \simeq -85\ eV$ and $E \simeq 0$ (cold fusion), one obtains $r_0 \simeq 0.16\mathring{A}$ much smaller than the average distance of the D_2-molecule, $r_{D_2} \simeq 0.75\mathring{A}$. This is enough to increase the infinitesimal $\eta_G(D_2) \simeq 10^{-51}$ to $\eta_G(Pd) \simeq 10^{-22\pm1}$ for two D^+'s in the tetrahedral disk.

Thus we may conclude that Coulomb screening is well understood, and that it leads to fusion rates of "Jones' type", about ten orders of magnitudes lower than required by the excess heat observed by Fleischmann and Pons. Indeed for "incoherent fusion" one gets:

$$\Gamma_{INC} = |\eta_G|^2 \Gamma_{NUCL} \simeq 10(x-1)\ fusions/sec\ cm^3. \tag{IV.3}$$

if one takes for $\Gamma_{NUCL} \simeq 1MeV$, a typical nuclear rate. This, then, leads us to the other question:

(β_2) which is the main DD-fusion dynamics?

We should recall that D^+'s that pack the Pd-lattice are in strong coherent e.m. fields. For instance the coherent field associated to the plasma oscillations to the Pd-ions (i.e. the Pd-atoms, deprived of the electronic d-shell, according to QEDCM follow their own quantum plasma dynamics) can be written

$$\vec{A}^{(N)} = a_N \vec{u} \cos \omega_r t, \tag{IV.4}$$

where one estimates $a_N \simeq 3.2 \cdot 10^6$eV and $\omega_r \simeq 0.1eV$. In such field the process:

$$D_e D_\gamma \rightarrow Nuclear\ State, \tag{IV.5}$$

(where D_e is the excess ($x > 1$) deuteron, D_γ is the γ-phase deuteron, and *Nuclear State* (NS) denotes any of the accessible nuclear states) is governed by the interaction Hamiltonian:

$$H_{INT} = e \int_{\vec{x}} \vec{A}^{(N)}(\vec{x}, t) \vec{J}(\vec{x}, t), \tag{IV.6}$$

where the e.m. current operator can be represented as:

$$\vec{J}(\vec{x}, t) = \int_{\vec{\xi}} \Psi^\dagger_{NS}(\vec{x}, \vec{\xi}; t) \vec{J} \Psi_D(\vec{x}, \vec{\xi}; t) \eta_{D_e}(\vec{x}, \vec{\xi}; t). \tag{IV.7}$$

Here $\Psi^\dagger_{NS}(\vec{x}, \vec{\xi}; t)$ is the quantum wave-field describing the plasma oscillations of the (doubly charged) NS, of amplitude $\vec{\xi}$ around the equilibrium position $\vec{x}$, $\Psi_D(\vec{x}, \vec{\xi}; t)$ the quantum field of the D^+ in the γ-phase, and $\eta_{D_e}(\vec{x}, \vec{\xi}; t)$ the wave field of the excess D^+. Diagrammatically the interaction Hamiltonian is given in Fig. 14.

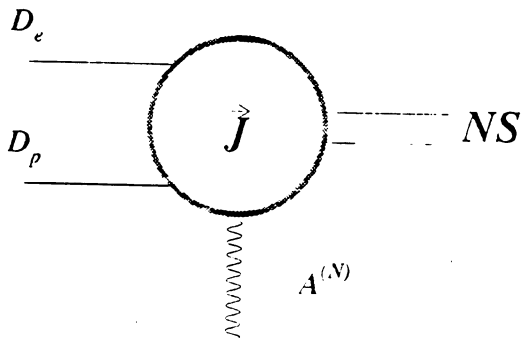

FIG. 14. Diagram for the interaction Hamiltonian [Eqs. (IV.6)-(IV.7)].

The e.m. current J_k, appearing in (IV.7), has the expression:

$$J_k(t) = \langle NS(t)|j_k|D_e D_p\rangle = \eta_G \langle NS(t)|j_k|NS(t)\rangle, \tag{IV.8}$$

where $|NS(t)\rangle$ obeys the Schrödinger equation:

$$i\frac{\partial}{\partial t}|NS(t)\rangle = (H_N + e\vec{A}^{(N)} \cdot \vec{j})|NS(t)\rangle, \tag{IV.9}$$

H_N is the nuclear Hamiltonian and j_k is the nuclear current operator. We simplify the problem by restricting the nuclear states to the three states reported in Fig. 15. Writing

$$|NS(t)\rangle = c_0(t)e^{-i\omega_0 t}|0\rangle + c_1(t)e^{-i\omega_1 t}|1\rangle + c_2(t)e^{-i\omega_2 t}|2\rangle, \tag{IV.10}$$

with $c_0(0) = 1$ and $c_1(0) = c_2(0) = 0$, the Shrödinger equation (IV.9) yields the following result:

$$\begin{aligned} c_0(t) &\simeq 1, \\ c_1(t) &= \frac{e a_N V_{01}}{\omega_0 - \omega_1}(e^{-i(\omega_0-\omega_1)t} - 1), \\ c_2(t) &= \frac{e^2 a_N^2 V_{01} V_{12}}{2(\omega_0-\omega_1)(\omega_1-\omega_2)}(e^{-i(\omega_0-\omega_1)t} - 1)(e^{-i(\omega_1-\omega_2)t} - 1), \end{aligned} \tag{IV.11}$$

where we have set

$$\begin{aligned} V_{01} &= \langle 1|\vec{j}\vec{u}|0\rangle \\ V_{12} &= \langle 2|\vec{j}\vec{u}|1\rangle \end{aligned} \tag{IV.12}$$

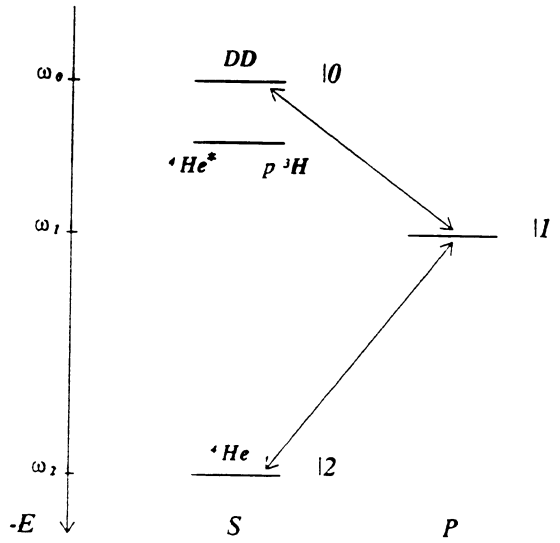

FIG. 15. The level diagram for the states in the dynamical evolution described by (IV.9) Also reported is Schwinger's-^{4}He* state.

We must now compute the transition amplitude over the time $T = \frac{2\pi}{\omega_r}$ (ω_r is the renormalized frequency of the Pd-plasma oscillations), which has been estimated [6] as the time needed for the collective plasma excitation to relax their excess energy to the lattice, that will finally appear as heat. One has

$$A(D_eD_p \to NS,T) = -i\int_0^T dt'\langle NS|H_{INT}|D_eD_p\rangle \simeq -iT\eta_G\frac{2e^2a_N^2}{\omega_0-\omega_1}|V_{01}|^2N_{CD}, \quad \text{(IV.13)}$$

where the factor $N_{CD} \simeq 10^{12}$ – the number of deuterons in a coherence domain of the plasma of deuterons – is especially noteworthy. From (IV.13) we compute the rate

$$R(D_eD_p \to NS,T) \simeq \frac{|A(D_eD_p \to NS,T)|^2}{T} = \quad \text{(IV.14)}$$

$$= |\eta_G|^2\frac{4e^4a_N^2}{(\omega_0-\omega_1)^2}|V_{01}|^2\frac{2\pi}{\omega_r}N_{CD}^2. \quad \text{(IV.15)}$$

In order to evaluate the average energy that the fusion process "dumps" onto the lattice, we first notice that under the action of the e.m. field $\vec{A}^{(N)}$ the nuclear state $|NS\rangle$ will very rapidly go to the ground state consisting of a coherent state ^{4}He which will progressively decay into α-particles that migrate out of the lattice.

We have now all elements to estimate the power W_{CD} that in each coherence domain is produced by the fusion of the excess $(x-1)N_{CD}$ deuterons with the deuterons of the γ-phase. We obviously have:

$$W_{CD} = (x-1)N_{CD}R(D_eD_p \to NS)|\omega_{DD}-\omega_{^4He}| \simeq 10|V_{01}|^4(x-1)Watt/CD \quad \text{(IV.16)}$$

where we have set $|\omega_{DD}-\omega_1| \simeq 10$ MeV. By the further estimates $|V_{01}| \simeq 10^{-2}$ and $(x-1) \simeq 10^{-1}$ we get the very rough evaluation

$$W_{CD} \simeq 10^{-8}Watt/CD \quad \text{(IV.17)}$$

and, considering that in one cm^3 there are $\frac{1}{(2\cdot10^{-4})^3}$ CD's, we obtain:

$$W \simeq 1.25kW/cm^3, \quad \text{(IV.18)}$$

a very large power, of the magnitude reached by Fleischmann and Pons.

As for the final question

(β_3) can we understand rarer processes: n,T,X-rays...?

We note that there can be other fusion routes which may become important in regions where the e.m. field amplitudes a_N are smaller (for instance at the boundary of CD's or around dislocation, plasma vortices etc.). Indeed the transition route (see Fig. 15) $DD \to P \to state \to ^4$He is in general more complicated including the excited ^{4}He-state lying 3.8 MeV below the DD-state [2]. Where a_N is weakened the dominant e.m. energy

---

[2] As enphasized by Schwinger [10] this state will be able to decay into the pT- but not into the n^3He-channel.

producing process, that leads to the ground state ^{4}He, may find some competition from a pure nuclear process such as

$$^4He^* \rightarrow pT, \tag{IV.19}$$

which would explain the anomalous ratio

$$\frac{n}{T} \simeq 10^{-6}. \tag{IV.20}$$

But, how about strange nuclear products that have been announced in the literature, such as:

- high energy neutrons
- Pd X-ray lines
- High energy charged particles
- nuclear transmutation
- ... ?

A possible explanation could be worked out along the following line: as we have seen the main fusion rate is the coherent process

$$D_eD_p \rightarrow^4 He + \delta a^{(N)}, \tag{IV.21}$$

whereby a coherent wave of ^{4}He is produced along with an excited state of the coherent e.m. field $\vec{A}^{(N)}$ (of amplitude $a^{(N)} + \delta a^{(N)}$). This excited state will most probably relax its excess energy to the lattice in the form of heat, however over "nuclear times" ($T_N \simeq \frac{2\pi}{\omega_N} \simeq 10^{-6} \div 10^{-7}\frac{2\pi}{\omega_r}$) and with a branching ratio of order $\frac{T_N}{T}$ the excited field may induce all kind of "coherent" photonuclear reactions, including the photodissociation of deuterons and the successive capture of the neutrons by the Pd-nuciei. This would then provide a realistic physical realization of the neutron transfer mechanisms that have been considered and studied by P. Hagelstein. [1]

But, of course, a decent understanding of these complex issues requires much more theory and experiment!

---

[1] P. Hagelstein, contribution at this Conference

REFERENCES

[1] M. Fleischmann and S. Pons, *Electrochemically Induced Nuclear Fusion of Deuterium*, J. Electroanal. Chem. **261**,301,(1989).

[2] For a review see e.g. G. Preparata, *Coherence in QCD and QED*, in *Common Problems and ideas of Modern Physics*, T.Bressani, B. Minetti and A. Zenoni eds, World Scientific (1992).

[3] P. W. Anderson, *Basic Notions of Condensed Matter Physics*, (Benjamin-Cumunings, California, 1984).

[4] G. Preparata, *Coherence in QCD and QED*, in *Common Problems and ideas of Modern Physics*, T.Bressani, B. Minetti and A. Zenoni eds, World Scientific (1992).

[5] G. Preparata, *Towards a theory of Cold Fusion phenomena*, Proc. Rome Workshop of Cold Fusion in Italy, B. Stella ed., (Roma, 1993).

[6] G. Preparata, *Quantum Electrodynamical Coherence in Matter*, Chapter 5, (to appear).

[7] T. Bressani, E. Del Giudice and G. Preparata, Nuovo Cimento **101A**, 845, (1989).

[8] G. Preparata, Proc. Ist Annual Conf. on Cold Fusion, Salt Lake City, Utah, March 28-31, (1990) p. 91.

[9] G. Mengoli, M. Fabrizio, C. Manduchi,G. Zannoni J. Electroanal. Chem. **350**,57,(1989).

[10] J. Schwinger, Proc. Ist Annual Conf. on Cold Fusion, Salt Lake City, Utah, March 28-31, (1990) p. 130.

DEUTERON-INDUCED FUSION IN VARIOUS ENVIRONMENTS

G. M. Hale
T. L. Talley
Theoretical Division, Los Alamos National Laboratory
Los Alamos, New Mexico 87545, USA

Abstract

The theory of deuteron-induced fusion will be discussed, first in free space, then in muonic molecules where the Coulomb repulsion is highly screened. It will be shown how a consistent description of the d+t reactions can be obtained in these environments using *R*-matrix theory. We compare fusion rates obtained from time-dependent scattering theory with those implied by the partial widths of the resonance associated with muon-catalyzed d-t fusion. Finally, some speculative comments are made about how the d+d reactions might proceed in other media, such as metallic lattices. The unusual properties of states associated with "shadow" poles might account for some of the strange results seen in cold fusion experiments. We emphasize that the same methods can, and should, be used to describe this situation as well as the other two well-established phenomena.

R-Matrix Properties

Wigner's *R*-matrix [1] is an exceptionally useful tool for describing nuclear reactions in free space. If the data are good enough, it can be used to parametrize the behavior of all the reactions of a multichannel system in minute detail and with great precision. At the same time, *R*-matrix theory automatically builds in all known analytic properties of the multichannel *S*-matrix (*e.g.*, causality, generalized unitarity, cut structure, *etc.*), which have a particularly strong influence on the structure of its poles in the complex plane. As we shall see later, these complex-energy *S*-matrix poles play a central role in the expansion of the time-dependent wave function. Finally, and perhaps most importantly, the theory is easily modified to describe nuclear reactions in media other than free space, as will be illustrated by the application to nuclear fusion in muonic molecules (μCF).

The *R*-matrix as Wigner defined it can be expressed as

$$R^{B}_{c'c} = (c'|\left[H + \mathcal{L}_B - E\right]^{-1}|c) = \sum_{\lambda} \frac{(c'|\lambda)(\lambda|c)}{E_\lambda - E} \qquad (1)$$

in which the channel-surface projections of the Green's operator for the total system hamiltonian H become simple pole terms due to the spectral expansion of the resolvent operator in terms of the eigenfunctions $|\lambda)$ and eigenvalues E_λ of the operator $H + \mathcal{L}_B$. The addition of $\mathcal{L}_B$, the so-called "Bloch operator",[2] to H restores its hermiticity on the finite region enclosed by the channel surface (*i.e.*, the "nuclear" region), thereby allowing the spectral expansion to be made, and makes its spectrum discrete by imposing fixed boundary conditions (B) on the logarithmic derivatives of the solutions of H at the channel surface.

Wigner's *R*-matrix can be transformed to one associated with the outgoing-wave Green's operator that is a central quantity in scattering theory,

$$R^L_{c'c} = (c'|\left[H + \mathcal{L}_L - E\right]^{-1}|c) = -(c'|G^+(E)|c) \tag{2}$$

in which the boundary values in the Bloch operator are taken to be the elements of L, the diagonal matrix of logarithmic derivatives of the outgoing-wave solutions for the long-ranged external potentials that act between fragments in the channel region. In free space, these are just the repulsive Coulomb potentials between the charged nuclear ions. In a muonic molecule, the electrostatic attraction of the μ^- to the positive ions must also be included. However, the form of the R^L-matrix and of the scattering matrix,

$$S = 2iO^{-1}R^LO^{-1} + O^{-1}I \ , \tag{3}$$

remains the same in both cases. It is simply a matter of using the incoming- (I) and outgoing- (O) wave solutions associated with the appropriate external potential. In this way, the nuclear information contained in an R-matrix determined by analyzing data for reactions in free space can be transformed to one that describes the nuclear reaction at short distances in a muonic molecule. This idea can be generalized to any environment in which the interaction between the nuclear particles outside the range of nuclear forces can be represented by an effective two-body potential, forming a system that we will describe as being "composite".

Resonance Poles

The poles of the composite-system S-matrix (which are identical with the poles of R^L) contain the effects of both the long-ranged external hamiltonian and the short-ranged internal hamiltonian. Near one of its poles, the S-matrix has the form

$$S_{c'c} = i\frac{\Gamma^{\frac{1}{2}}_{c'\mu}\Gamma^{\frac{1}{2}^T}_{\mu c}}{E_\mu - E}, \tag{4}$$

with

$$\Gamma^{\frac{1}{2}}_{c\mu} = \sqrt{2}O_c^{-1}(c|\mu\rangle \tag{5}$$

the partial-width amplitude in channel c. The solutions $|\mu\rangle$ for the complex energies E_μ, together with their adjoints $|\tilde{\mu}\rangle$, form a normalizable, bi-orthogonal set in all space. The pole energy

$$E_\mu = E_r - \tfrac{1}{2}i\Gamma_\mu \tag{6}$$

occurs on an unphysical sheet of the many-channel Riemann energy surface in the case of a resonance or virtual state, and on the real axis of the physical sheet in the case of a bound state.

We shall see in a later section that the complex-energy (momentum) poles of the S-matrix make important contributions to the time-dependent wave function. These are "quasi-stationary" terms whose time dependence is given by $\exp[-iE_\mu t]$. Only the poles having $\Gamma_\mu > 0$, associated with decaying states, contribute to the wave function for $t > 0$. In terms of momenta (essentially the square root of the energy), this means that the real and imaginary parts must have opposite sign. Therefore, all channel momenta $k_{c\mu}$ associated with a decaying-state pole must lie in quadrants (Q) II or IV.

The complex-momentum states, including their exponential time factors, actually correspond to traveling waves in the channel regions. The type of traveling wave depends on the location of the pole in the complex k_c plane, as is shown in Fig. 1. If the channel momentum $k_{c\mu}$ associated with the pole is in Q II, it corresponds to a confined, ingoing-wave solution. In Q IV, it corresponds to an unconfined, outgoing-wave solution. Most visible resonances are caused by poles that have

outgoing waves in all open channels (*i.e.*, above the second bisector in Q IV) and ingoing waves in all closed channels (above the second bisector in Q II). These "conventional" poles are the only kind discussed in many articles and textbooks on resonance phenomena, giving the impression that there are no other possibilities for *S*-matrix singularities.

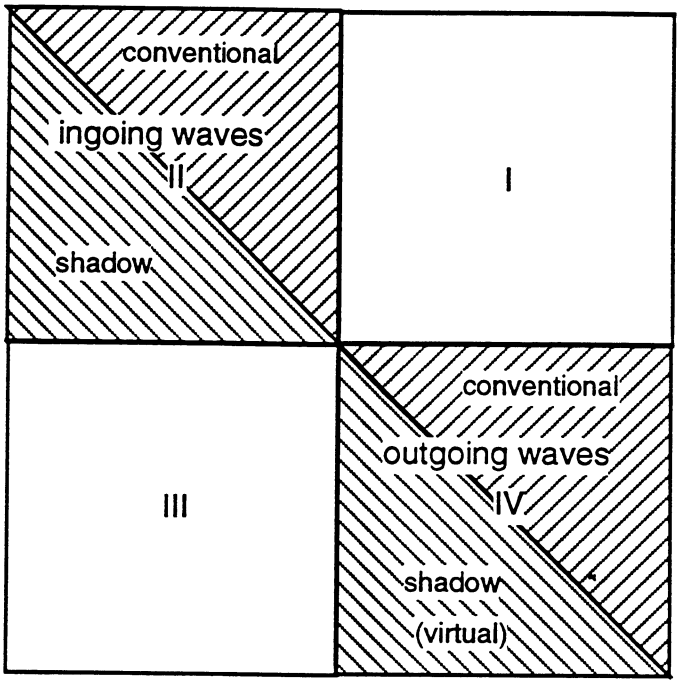

Fig. 1. Allowed regions for decaying-state poles in the complex momentum plane, and their characteristics as traveling waves.

However, it is possible for a pole to have outgoing waves in closed channels, or ingoing waves in open channels, as long as it has outgoing waves in at least one channel so that Γ is greater than zero. Such poles were discussed a number of years ago by Eden and Taylor,[3] who named them "shadow" poles. A shadow pole of the first type can occur in single-channel scattering, in which case it is called "virtual", or "antibound". A shadow pole of the second type can occur only in multichannel systems because of the restriction that it be outgoing in at least one channel. Perhaps for that reason, the existence of states with confined, ingoing waves in open channels is not yet widely recognized. The experimental evidence[4-6] for them has come to light only in recent years, and the physical consequences of such singularities in scattering theory are only beginning to be explored. The first example of such a pole in a nuclear reaction[6] was found in the ^{5}He system, which is the subject of the next section.

The ^{5}He System

This system contains one of the most famous resonances in nuclear physics: the $J^{\Pi}=3/2^+$ resonance responsible for the large ^{3}H(d,n)^{4}He reaction cross section that peaks at E_d=108 keV. Values of the cross section at energies below the resonance are useful in a variety of fusion applications, and at higher energies, the differential cross section is of interest as a neutron source reaction.

The channels and data included in our analysis of the ^{5}He system for excitation energies up to 21.5 MeV are summarized in Table 1. In addition to the physical two-body channels d+t and n+α, an effective n+^{4}He*(0$^+$) channel was added to represent the effects of deuteron breakup (n+p+t). More than 2600 data points from 23 different types of measurements (cross sections, polarizations, *etc.*) were described in terms of 108 free *R*-matrix parameters that give a minimum in chi-square space for which χ^2 per degree of freedom is 1.48. We note that a generalized phase-shift fit would require 89 real parameters to achieve the same sort of description at a single energy.

Table 1. Channel configuration and data summary for the ^{5}He system analysis.

Channel	l_{max}	a_c (fm)
d+t	4	5.1
n+^{4}He	4	3.0
n+^{4}He*	1	5.0

Reaction	Energy Range	# Observable Types	# Data Points	χ^2
^{3}H(d,d)^{3}H	E_d=0-8 MeV	6	704	1164
^{3}H(d,n)^{4}He	E_d=0-8 MeV	14	1121	1379
^{3}H(d,n)^{4}He*	E_d=4.8-8 MeV	1	10	26
^{4}He(n,n)^{4}He	E_n=0-28 MeV	2	793	1150
Totals:		23	2628	3719

Examples of fits to some of the integrated cross-section data are shown in Fig. 2. At the left side of the figure are shown the fits to the reaction cross section (top) and neutron total cross section (bottom) over the whole energy range of the analysis. The right side of the figure shows essentially the same data enlarged over the region of the resonance. One sees that the calculations generally represent the data within their error bars, which, particularly in the case of the LEFCS measurements,[7] are reasonably small.

The energy dependence of the calculated *S*-matrix elements for J^Π=3/2$^+$ that are related directly to the reaction (σ_R) and total (σ_T) cross sections are shown over the resonance in Fig. 3. Unlike the behavior that would be expected for an isolated conventional resonance, the squared amplitudes corresponding to σ_R and σ_T do not peak at the same energy, and have a different energy dependence for the high-energy tail. Our analysis[6] shows that this behavior results from a two-pole structure of the resonance. One of the poles is a conventional pole that occurs on the (-,-)* Riemann sheet, and the other is a shadow pole on the (+,-) sheet. The total cross section is affected more by the conventional pole, shown as a circled "x" at the bottom left of Fig. 3, while the reaction cross section is influenced more by the shadow pole, shown by the same symbol near the real axis at 80 keV.

The resonance parameters for the poles are given in Table 2. The real and imaginary parts of the pole positions give the resonance energies E_r and total widths Γ, respectively, while the partial widths are defined in terms of the residues.[6] Note that for the conventional pole, the partial widths sum approximately to the total width, while for the shadow pole, the sum of the partials greatly exceeds the total. That is another manifestation of the unconventional character of a shadow pole,

---

*The Riemann sheets are labeled by the signs of the imaginary parts of the momenta in the d+t and n+α channels, respectively.

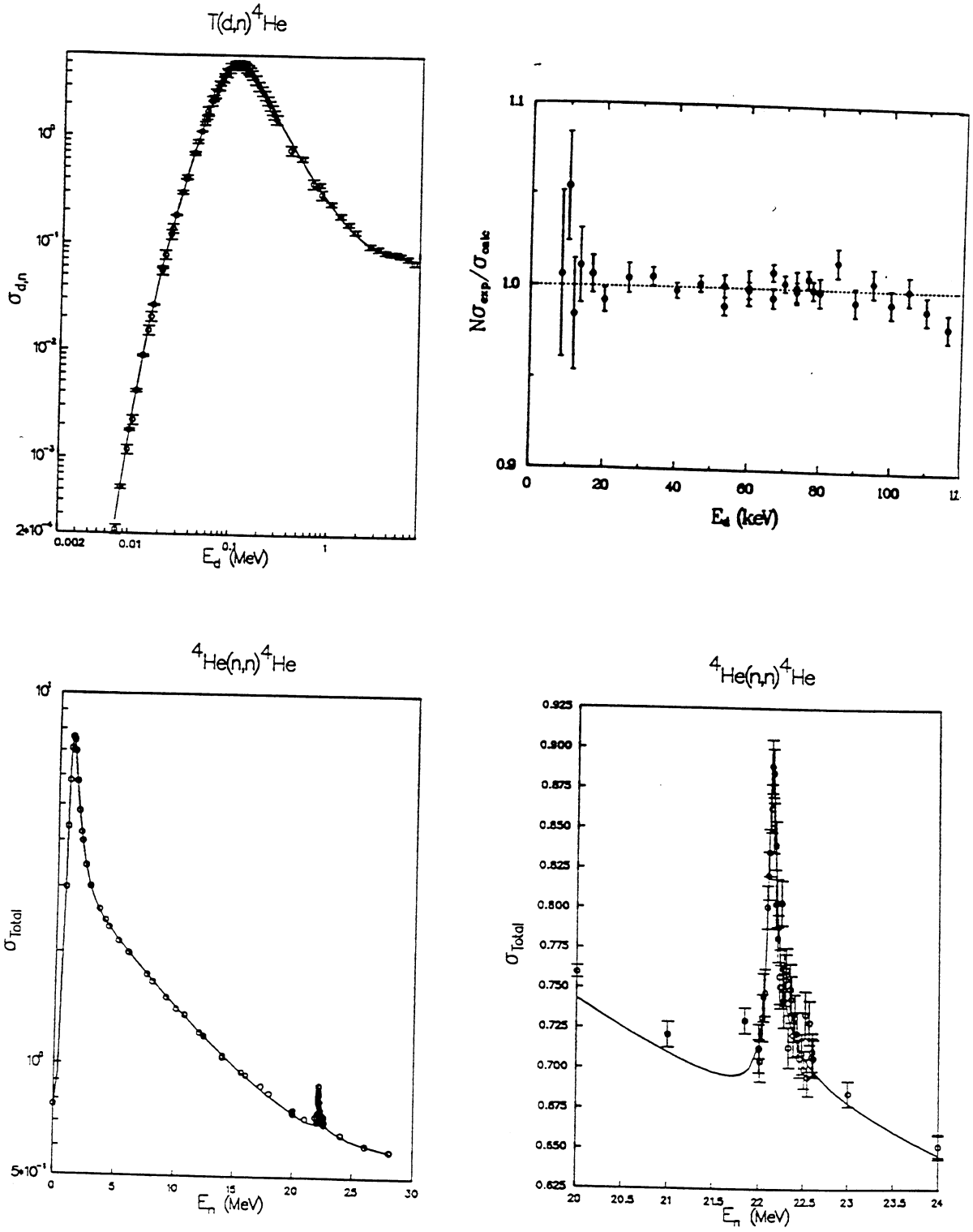

Fig. 2. Data for reaction (top) and neutron total (bottom) cross sections in the ^{5}He system compared with the R-matrix calculations. At the left of the figure, data are shown over the full range of the analysis; at the right they are shown in the region of the $J^\Pi = 3/2^+$ resonance, the upper part being the ratio of measured[7] to calculated values of the reaction cross section over the resonance.

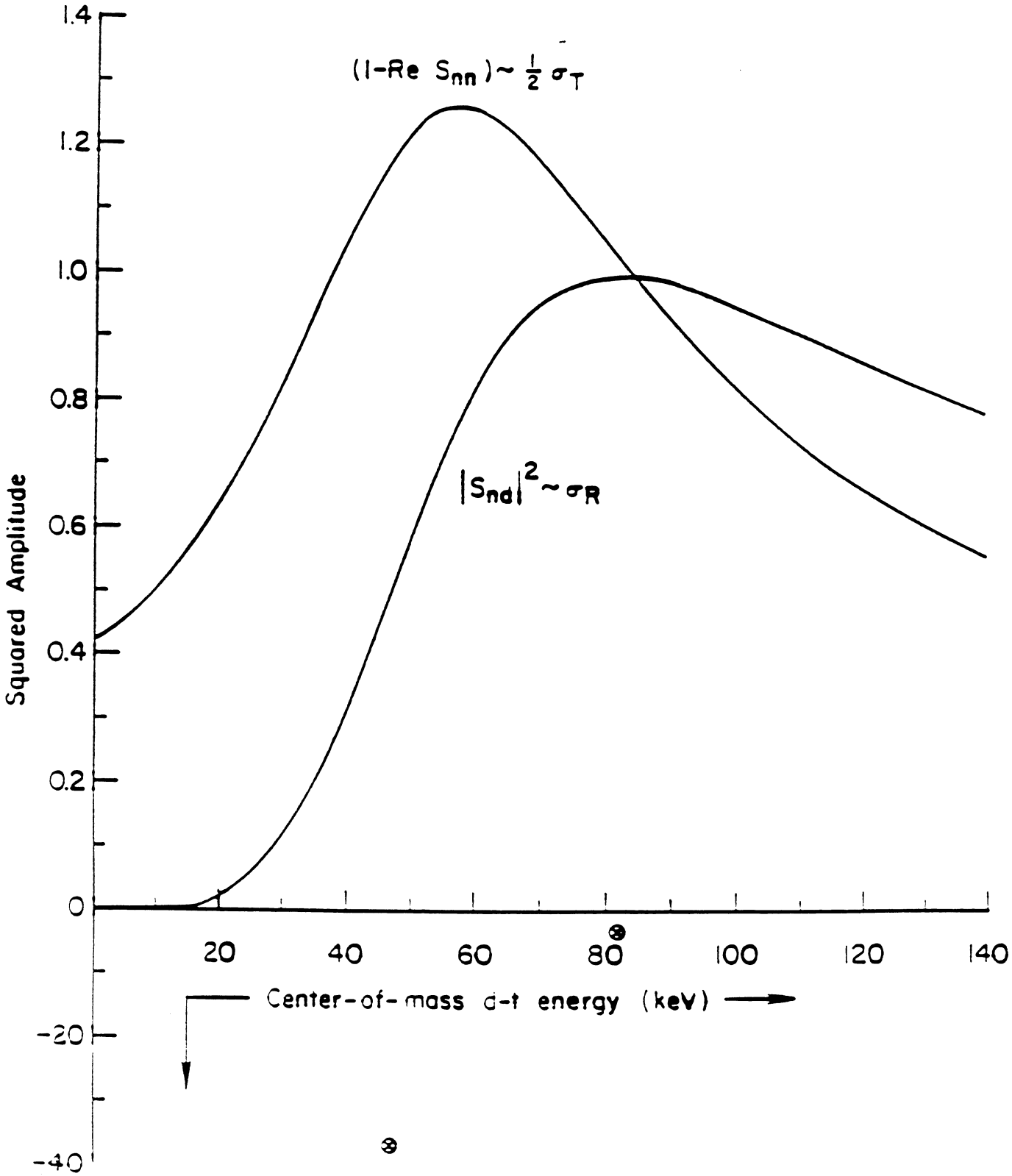

Fig. 3. S-matrix element's energy dependence for J^{Π} =3/2$^+$ that are proportional to the n+α total cross section and the ^{2}H(d,n)^{4}He reaction cross section. The conventional pole is shown by the small "x" at the lower left of the figure, and the shadow pole by the one at the real axis near 80 keV.

and indicates that its small value of Γ does not produce any narrow structure in the cross sections. This scattering state has the unusual asymptotic behavior of confined, ingoing waves in the open d+t channel, acting in some respects as if it were bound in that channel. Indeed, the partial width Γ_d has in that case the significance of a bound-state asymptotic normalization constant, rather than that of a "decay" width.

Table 2. Pole parameters for the $J^\pi=3/2^+$ ^{5}He resonance.

Sheet: (d,n)	(+,+)	(+,-)	(-,-)	(-,+)
E_r (keV)		81.57	46.97	
Γ (keV)		7.28	74.20	
Γ_d (keV)		2861.6	25.10	
Γ_n (keV)		68.77	39.83	

Time-Dependent Theory

In principle, the time-dependent description of a scattering process is the only valid one. Even for a steady-state process, the rates can only be properly derived starting from a time-dependent description. The time-dependent wave function is given in terms of the retarded Green's function at time $t \geq 0$,

$$G^+(t) = -\frac{1}{2\pi i}\int_{-\infty}^{\infty} dE e^{-iEt} G^+(E) \quad [=0 \text{ for } t<0], \tag{7}$$

and the initial wave function $\psi(0)$ by

$$\psi^+(t) = G^+(t)\psi(0)\,. \tag{8}$$

We have developed a somewhat different approach to evaluating the inverse Fourier transform in Eq. (7), which can be illustrated by considering a 2-channel system in which channel 1 has the lowest threshold. First of all, the integration path is taken in momentum (k), rather than energy (E), variables. By choosing a contour that encloses the poles in the lower half of the k_1 plane, one obtains the expansion

$$G^+(t) = \sum_\mu e^{-iE_\mu t}|\mu\rangle\langle\tilde{\mu}| + \int_{-\infty}^{0} dE_1 e^{-iE_1 t}|\psi_1^+\rangle\langle\tilde{\psi}_1^+| + \int_0^{\infty} dE_2 e^{-iE_2 t}|\psi_2^+\rangle\langle\tilde{\psi}_2^+|, \tag{9}$$

that is equivalent to the usual expansion in terms of the physical bound and scattering states of the system. Although the first two terms of the expansion above involve states that are "unphysical" because they diverge at large distances in channel 1, the sum of these terms always leads to a time-dependent wave function in which the divergences cancel, so that it is properly regular in all space. The advantage of using this expansion instead of the usual one is that it makes explicit the contribution of some of the resonances in the time-dependent wave function. The poles enclosed are outgoing in channel 1 and ingoing in channel 2, so that those below the channel-2 threshold are conventional, but those above it are the lesser-known type of shadow pole described in the second section, of which the ^{5}He shadow pole is an example.

If the initial state $\psi(0)$ has no appreciable overlap with the positive-energy channel-2 scattering states, then the time-dependent wave function in the channel-1 region ($r_1 > a_1$) is given in the case of S-waves with no Coulomb by

$$\psi_1(t) = \frac{1}{2}\sum_\mu \alpha_\mu e^{-iE_\mu t}|\mu,1\rangle \mathrm{erfc}(z_{\mu 1}), \tag{10}$$

with

$$z_{\mu 1} = \left(\frac{m_1}{2it}\right)^{\frac{1}{2}}\left(r_1 - a_1 - \frac{k_{1\mu}t}{m_1}\right),$$

$$(r_1|\mu,1\rangle = \left(\frac{m_1\Gamma_{1\mu}}{4\pi k_{1\mu}}\right)^{\frac{1}{2}}\frac{O_{1\mu}(r_1)}{r_1},$$

and

$$\alpha_\mu = \langle\tilde{\mu}|\psi(0)\rangle.$$

In these equations, m_1 is the reduced mass of the two particles in channel 1. The *rate* at which normalization builds up in the channel-1 region can be calculated from the equation of continuity,

$$\frac{\partial}{\partial t}|\psi_1(t)|^2 = \nabla\cdot\frac{1}{m_1}\Im[\psi_1^*(t)\nabla\psi_1(t)], \tag{11}$$

giving an expression

$$\dot{N}_1(t) = \frac{\partial}{\partial t}\int_{a_1}^{\infty} r_1^2 dr_1|\psi_1(t)|^2 = \frac{4\pi a_1^2}{m_1}\Im\left[\psi_1^*(r_1,t)\frac{\partial}{\partial r_1}\psi_1(r_1,t)\right]_{r_1=a_1}, \tag{12}$$

that involves the wave function of Eq. (10) only at the channel surface, since it vanishes asymptotically.

We show in Fig. 4 examples of rates calculated from Eq. (12) for a single resonance in the cases that it has either ingoing or outgoing waves in channel 1. For the outgoing wave case, the rate starts near t=0 at the value expected from the width (Γ= 0.4) of the resonance, and shows approximately exponential decay with time. For the ingoing-wave case, however, the rate is negative at almost all times, meaning that the particles of channel 1 from the reaction would never be observed asymptotically for this type of state.

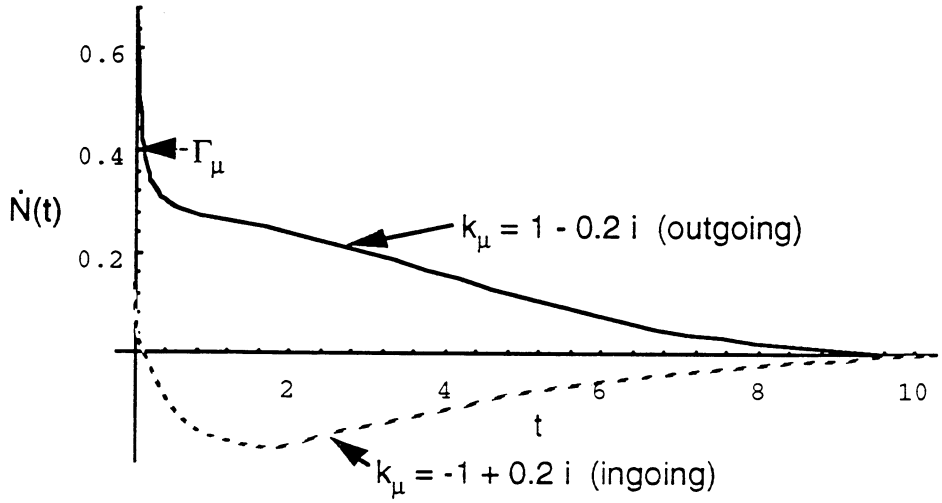

Fig. 4. Time-dependent rates calculated from Eq. (12) for: (a) an outgoing-wave pole (solid line) and (b) an ingoing-wave pole of the same energy (dashed line).

Muon-Catalyzed d-t fusion

In order to apply this sort of approach in the case of muon-catalyzed d-t fusion, one can use the R-matrix parameters for the nuclear ^{5}He system from the analysis described in the third section, but transformed to the outgoing-wave R-matrix of Eq. (2) using the outgoing-wave solutions for the (screened) dtμ potential, rather than those for a purely repulsive Coulomb potential, in the d+t channel. This has been done by Struensee *et al.*[8] for various types of adiabatic dtμ potentials. The most realistic of these is the so-called "improved adiabatic" (IA) potential shown in Fig. 5. The d-t Coulomb repulsion is screened so effectively by the muon that the potential has an attractive well at about 2 muonic atomic units (m.a.u.), or approximately 500 fm, which supports two bound states. The ground-state radial wave function, having rotational-vibrational quantum numbers $L = 0$ and $v = 0$, and its energy, about 317 eV below the mass of d+tμ, are also shown in the figure, but the wave function and energy for the first $L = 0$ excited state, having vibrational quantum number $v = 1$, are not shown.

From the poles and residues of the composite-system S-matrix in Eq. (4) can be determined the resonance parameters of the system. These are given in Table 3 for resonances on the (+,-) sheet, which are the ones that appear in the sum over μ for the time-dependent wave function in Eq. (10). The ro-vibrational bound states of the muonic molecule have been turned into narrow resonances with non-zero widths (Γ_n) for decay into the n+α channel by the nuclear forces at short distances, while the nuclear shadow pole has acquired a substantially different value of asymptotic normalization constant (Γ_d) due to the screened potential in the d+t channel. (Differences in E_r between Tables 2 and 3 for this resonance result mainly from differences in the reference energy, which in Table 3 is the mass of d+tμ, but in Table 2 is the mass of d+t.)

Also given in the table are the neutron rates, $\lambda_n = \Gamma_n/\hbar$, associated with each partial neutron width, and the magnitude of the overlap α_μ of each resonant state with the initial dtμ ground state in the time-dependent wave function. Because these coefficients are so small for all except the $(L,v) = (0,0)$ resonance, the time-dependent neutron rate calculated from Eq. (12) falls off exponentially from the expected value $\lambda_n = 1.29 \times 10^{12}$ s^{-1} at all but the shortest times, where the effect of the shadow pole appears, but probably could never be measured. One sees from the table, however, that a different initial state having strong overlap with the shadow-pole state could produce a neutron rate as much as eight orders of magnitude larger than that initiated from the molecular ground state.

Table 3. ^{5}Heμ Resonances on the (+,-) Sheet in the IA Approximation

(L,v)	(0,0)	(0,1)	shadow pole
E_r (meV)	-317192.6	-31194.1	73281×10^3
Γ (meV)	0.8504	0.7100	7.338×10^6
Γ_d (meV)	1.156×10^9	2.480×10^6	6.172×10^7
Γ_n (meV)	0.8504	0.7100	6.876×10^7
λ_n (s^{-1})	1.29×10^{12}	1.08×10^{12}	1.04×10^{20}
$\lvert\alpha_\mu\rvert$	0.999···	2.9×10^{-6}	1.08×10^{-4}

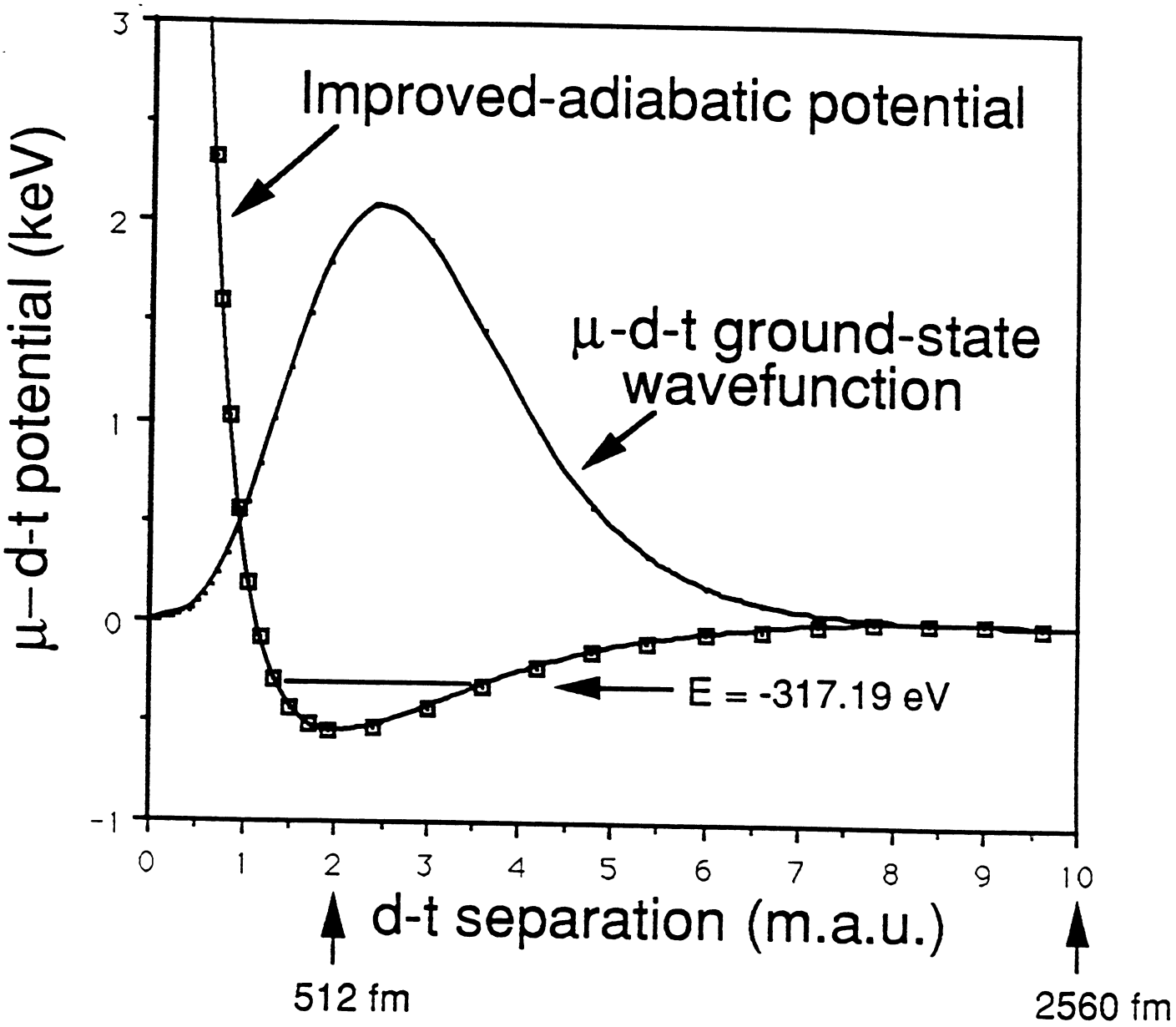

Fig. 5. Improved adiabatic dtμ potential (squares) and ground-state radial wave function (solid line) as functions of d-t separation in muonic atomic units. The ground-state energy of the molecule is also shown relative to the mass of d+tμ.

Summary and Conclusions

We have seen that *R*-matrix theory can give an excellent parametric representation of multichannel nuclear reactions on the real energy axis of the physical sheet, as was illustrated by the reactions in the ^{5}He system. The application to the dtμ system showed how the description can be generalized to a composite system that includes the effects of particles or media other than free space at large distances on the nuclear reactions at small distances. The theory has well-defined continuations into the complex plane that reveal the existence of "shadow" poles in many composite systems. Some of these poles correspond to confined, ingoing-wave states in open channels.

A proper formulation of the composite-system problem involves using time-dependent scattering theory, in which the time-dependent Green's operator gives the possibilities for how the reaction might proceed. For multichannel systems, the shadow poles with ingoing waves in open channels make important contributions to this operator because they are naturally enclosed by the only sensible integration contour that makes resonant effects explicit. Rates based on partial widths have no meaning for ingoing-wave states. In these cases, the time-dependent theory gives mostly negative rates (*i.e.*, particle flux leaving the channel region), and the partial width has the significance of a bound-state asymptotic normalization constant. Therefore, if the initial conditions just prior to the nuclear reaction select such a state in the time-dependent Green's operator, no particles will come out in the ingoing-wave channel, even though that channel is open. This is a situation in which the time-dependent solution is qualitatively different from the stationary (definite-energy) solutions from which it was constructed, allowing the branching ratios for various reaction channels to deviate substantially from the values they have when measured in beam-target scattering experiments.

Now, we turn to some speculative comments directed more specifically at cold fusion phenomena. Although there was no time to discuss it, we have an *R*-matrix description of reactions in the ^{4}He system[9] similar to that for the ^{5}He system, containing the channels p+t, n+^{3}He, and d+d. States exist in the nuclear ^{4}He system for several values of J^π that are outgoing only in the p+t channel, the closest to the d+d threshold being a shadow pole to the (first) excited 0^+ state of the alpha-particle. Perhaps such states also exist in ^{4}He + lattice systems, just as the ^{5}He nuclear shadow-pole state exists in the dtμ molecule. If any of these states has sufficient overlap with the initial d+d confined state in the lattice, the resulting p+t rate could be much larger than the standard rate formulas predict, and there would be no detectable neutron emission, in qualitative agreement with the anomalously low neutron/tritium branching ratios observed in some cold fusion experiments. Furthermore, if the overlap occurs primarily for $J^\pi=0^+$, no gamma-producing transitions are allowed from this state to the ^{4}He ground state, since this would be an electric monopole (E0) transition.

In order to get fusion without any type of particle or γ emission, it is necessary to postulate the existence of 0^+ states that are outgoing only in the E0 channel. No such states have yet been sought or found in the ^{4}He system. However, the search for some type of photon emission should continue, because the amount of energy released in radiationless fusion would be sufficient to excite highly energetic phonon modes in the lattice, with X-rays and possibly high-energy (conversion) electrons accompanying the eventual de-excitation processes.

It is important to realize that the qualitative, speculative statements made above can be made quantitative, using the theoretical framework outlined in this paper. The

first requirement is to know the effective d+d potential in a metal lattice, in analogy with the IA potential in muonic molecules. This is a much more difficult question, however, involving which lattice sites are occupied at high deuterium loading, how the electrons and deuterons participate in screening, periodic and coherence effects, *etc.* The second requirement is to know the initial state of the d+d system in the lattice just prior to fusion. In our view (perhaps not surprising for nuclear physicists), there is now more uncertainty in these quantities than in the properties of the ^{4}He nuclear system near the d+d threshold. Once these quantities are determined, however, the calculation of rates for various outgoing particles can be performed using the expressions developed here. Achieving sufficient accuracy in a multichannel calculation would be a challenging numerical task, but it is likely the only way to answer, once and for all, the theoretical questions about cold fusion to the satisfaction of the scientific "mainstream".

References

1. E. P. Wigner and L. Eisenbud, *Phys. Rev.* **72,** 29 (1947); A. M. Lane and R. G. Thomas, *Rev. Mod. Phys.* **30**, 257 (1958).

2. C. Bloch, *Nucl. Phys.* **4**, 503 (1957); A. M. Lane and D. Robson, *Phys. Rev.* **151**, 774 (1966).

3. R. J. Eden and J. R. Taylor, *Phys. Rev.* **133**, B1575 (1964).

4. A. Herzenberg and D. Ton-That, *J. Phys. B* **8**, 426 (1975).

5. K. L. Au, D. Morgan, and M. R. Pennington, *Phys. Rev. D* **35**, 1633 (1987).

6. G. M. Hale, R. E. Brown, and N. Jarmie, *Phys. Rev. Lett.* **59**, 763 (1987).

7. N. Jarmie, R. E. Brown, and R. A. Hardekopf, *Phys. Rev. C* **29**, 2031 (1984); R. E. Brown, N. Jarmie, and G. M. Hale, *Phys. Rev. C* **35**, 1999 (1987).

8. M. C. Struensee, G. M. Hale, R. T Pack , and J. S. Cohen, *Phys. Rev. A* **37**, 340 (1988).

9. See: D. R. Tilley, H. R. Weller, and G. M. Hale, "Energy Levels of Light Nuclei A=4," *Nucl. Phys.* **A541**, 1 (1992).

NUCLEAR FUSION IN CONDENSED MATERIALS

Setsuo Ichimaru

Department of Physics, University of Tokyo

CONDENSED MATERIALS

DEGENERATE CORES OF WHITE DWARFS

METAL HYDRIDES

ULTRAHIGH-PRESSURE METALLIC HYDROGEN

The rate of nuclear fusion reactions between nuclear species, *i* and *j*, is proportional to $g_{ij}(r_N)$, the value of a

joint probability density $g_{ij}(r)$

for the reacting pairs at a nuclear reaction radius r_N. Either in vacuum or in a condensed material, such a contact probability is given generally as the square

$$|\Psi_{ij}(r_N)|^2$$

of the wave functions that describe scattering between the reacting pairs.

Being a *correlation function*, albeit at short distances, the contact probability may depend quite sensitively on the changes in microscopic, macroscopic, and thermodynamic states of the environment in case it consists of a *condensed material*. Thus the rates of nuclear reactions in condensed materials can differ drastically from those expected in vacuum, due to the *many-body correlation effects*, inherent in such a condensed-matter system.

Enhancement in the rates of nuclear reactions expected from such correlation and thermodynamic effects is investigated for various realizations of the condensed materials in both laboratory and astrophysical settings, such as degenerate cores of white dwarfs, metal hydrides, and ultrahigh pressure metallic hydrogen. Consequently, the subject of

nuclear fusion in condense materials

is viewed as a forum in which an interplay between nuclear physics and statistical physics may be studied usefully *vis-à-vis* the concept of the correlation functions.

OUTLINE

I. RATES OF ELEMENTARY NUCLEAR REACTIONS

(a) The Gamow Rates of Thermonuclear Reactions

(b) Electron-Screened Cold Fusion Reactions

(c) Pycnonuclear Rates in Solids

II. ENHANCEMENT FACTORS

(a) Enhancement by Many-Body Correlation Processes

(b) Electron-Screened Ion Fluids

(c) Thermal Enhancement of Pycnonuclear Rates

III. RATES OF NUCLEAR FUSION REACTIONS

(a) White-Dwarf Progenitors of Supernovae

(b) Metal Hydrides - PdD and TiD_2
equilibrium calculations
possibilities of nonequilibrium states

(c) Ultrahigh-Pressure Liquid-Metallic Hydrogen

THERMONUCLEAR REACTIONS

Schrödinger equation for the s-wave scattering between nuclei, i and j, with relative kinetic energy E :

$$\left[-\frac{\hbar^2}{2\mu_{ij}} \frac{d^2}{dr^2} + W_{ij}(r) - E \right] r\, \Psi_{ij}(r) = 0$$

μ_{ij} : reduced mass between i and j

BARE COULOMBIC REPULSION

$$W_{ij}(r) = \frac{Z_i Z_j e^2}{r}$$

CONTACT PROBABILITY

$$\left| \Psi_{ij}(0) \right|^2 = \frac{\pi \sqrt{\frac{E_G}{E}}}{\exp\left[\pi \sqrt{\frac{E_G}{E}} \right] - 1}$$

$$\rightarrow \pi \sqrt{\frac{E_G}{E}} \exp\left[-\pi \sqrt{\frac{E_G}{E}} \right] \quad (E \ll E_G)$$

NUCLEAR REACTION RATES

(per volume) at E

$$R_{ij}(E) = \frac{2\, S_{ij}(E)\, r_{ij}^{*}}{\pi\left(1+\delta_{ij}\right)\hbar}\; n_i\, n_j \left|\, \Psi_{ij}(0)\right|^2$$

$$\tau_{ij} \equiv 3\left(\frac{\pi}{2}\right)^{2/3}\left(\frac{E_G}{T}\right)^{1/3}$$

GAMOW PEAK $\qquad E_{GP} = \frac{1}{3}\,\tau_{ij}\,T$

RADIUS OF CLASSICAL TURNING POINT

$$r_{TP} = \frac{3\, Z_i\, Z_j\, e^2}{\tau_{ij}\, T}$$

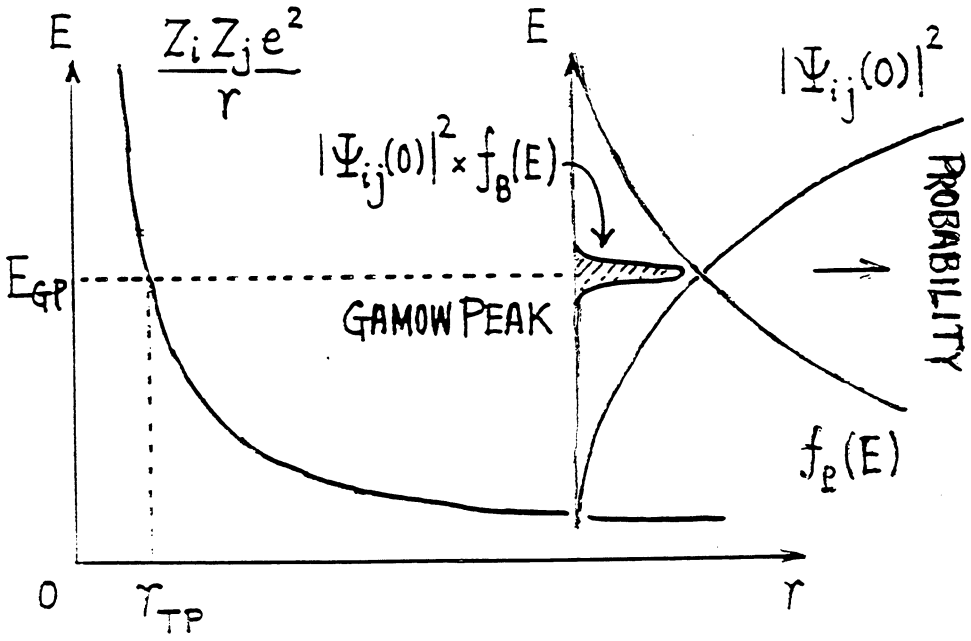

GAMOW ENERGY

$$E_G = \frac{Z_i Z_j e^2}{r_{ij}^*}$$

NUCLEAR "BOHR RADIUS"

$$r_{ij}^* = \frac{\hbar^2}{2 \mu_{ij} Z_i Z_j e^2}$$

CROSS SECTION OF NUCLEAR REACTIONS

$$\sigma_{ij} = \frac{S_{ij}(E)}{E} \exp\left[-\pi \sqrt{\frac{E_G}{E}} \right]$$

$S_{ij}(E)$: nuclear cross-section factor

GAMOW REACTION RATES

$$R_G = \frac{16\, S_{ij}\, r_{ij}^{*}\, n_i\, n_j\, \tau_{ij}^{2}}{3^{5/2}\pi\left(1+\delta_{ij}\right)\hbar}\ \exp\left(-\tau_{ij}\right)$$

(reactions/cm^3/s)

$$\tau_{ij} \equiv 3\left(\frac{\pi}{2}\right)^{2/3}\left(\frac{E_G}{T}\right)^{1/3}$$

♦ ♦ The Gamow reaction rate R_G depends very sensitively on T via the exponential factor, $\exp(-\tau_{ij})$. ♦ ♦

SCREENED COULOMBIC REPULSION

Schrödinger equation

$$\left[-\frac{\hbar^2}{2\mu_{ij}} \frac{d^2}{dr^2} + W_{ij}(r) - E \right] r\, \Psi_{ij}(r) = 0$$

$$W_{ij}(r) = \frac{Z_i Z_j e^2}{r} S(r)$$

$$\rightarrow \frac{Z_i Z_j e^2}{r} - E_S \quad (r \rightarrow 0)$$

$$E_S = \frac{Z_i Z_j e^2}{D_S} \approx 144.0 Z_i Z_j \left(\frac{D_S}{10^{-9}\text{cm}} \right)^{-1} \text{(eV)}$$

SHORT-RANGE SCREENING DISTANCE : D_S

$$S(r) \rightarrow 1 - \frac{r}{D_S} + \cdots \quad (r \rightarrow 0)$$

CONTACT PROBABILITY

$$\left| \Psi_{ij}(0) \right|^2 = \frac{\pi \sqrt{\frac{E_G}{E + E_S}}}{\exp\left[\pi \sqrt{\frac{E_G}{E + E_S}} \right] - 1}$$

$$\rightarrow \pi \sqrt{\frac{E_G}{E + E_S}} \exp\left[-\pi \sqrt{\frac{E_G}{E + E_S}} \right]$$

$$\left(E + E_S << E_G \right)$$

STRONG vs. WEAK ELECTRON SCREENING

STRONG ELECTRON SCREENING

if $E_S > E_{GP}$ or $T < T_S$.

$$T_S = \frac{2}{\pi}\sqrt{\frac{r_{ij}^*}{D_S}}\,\frac{Z_i Z_j e^2}{D_S}$$

$$\approx 5.7\times10^4\sqrt{Z_i Z_j}\left(\frac{2\mu_{ij}}{m_N}\right)^{-1/2}\left(\frac{D_S}{10^{-9}\text{cm}}\right)^{-3/2}\text{(K)}$$

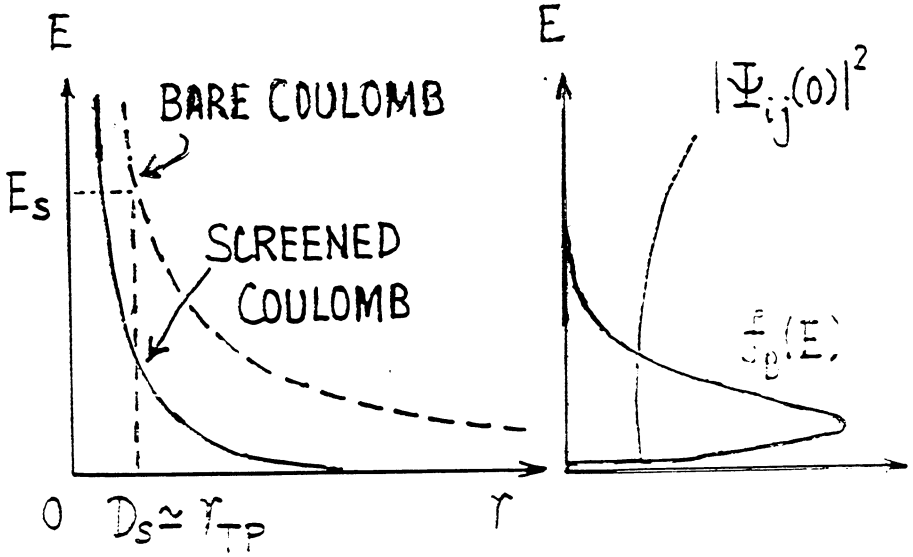

RATES of ELECTRON-SCREENED COLD FUSION

$$R_S = \frac{1.3\, S_{ij}\, r_{ij}^{*}\, n_i\, n_j}{(1+\delta_{ij})\,\hbar} \sqrt{\frac{D_S}{r_{ij}^{*}}}\, \exp\left(-\pi \sqrt{\frac{D_S}{r_{ij}^{*}}}\right)$$

(reactions/cm^3/s)

♦ ♦ R_S increases steeply with **density**, but remains almost independent of **temperature.**

"PYCNONUCLEAR REACTIONS"

A.G.W. Cameron (1959)

TABLE 1 THERMONUCLEAR vs. ELECTRON-SCREENED COLD FUSION

case	Sun	WD	GP	PM
reactions	*p-p*	^{12}C-^{12}C	*p-d*	*p-d*
ρ_m (g/cm^3)	56.2	2×10^9	5.0	20.0
T (K)	1.5×10^7	5×10^7	2×10^4	1.4×10^3
E_G (keV)	49.5	7.7×10^5	66.1	66.1
τ_{ij}	13.7	228	137	154
E_{GP} (keV)	5.9	327	0.078	0.007
D_s (10^{-9}cm)	3.97	0.042	3.2	2.79
E_S (keV)	0.57	1.2×10^2	0.045	0.10
T_s (K)	7.2×10^3	1.1×10^7	8.6×10^3	1.1×10^4

Fundamental reactions are *thermonuclear* for the Sun, white dwarf (WD), and giant planet (GP), and *electron-screened cold fusion* for pressurized liquid-metallic hydrogen (PM).

Enhancement due to *many-body correlations* takes place over the rates of those fundamental reactions.

PYCNONUCLEAR REACTIONS

Schrödinger equation for the s-wave scattering between nuclei, i and j, in a solid:

$$\left[-\frac{\hbar^2}{2\mu_{ij}} \frac{d^2}{dr^2} + W_{ij}^{L}(r) - E \right] r\, \Psi_{ij}(r) = 0$$

LATTICE POTENTIAL $W_{ij}^{L}(r)$:

EFFECTIVE POTENTIAL between a pair of nearest neighbor nuclei. It takes on a minimum at $r = r_{ij}^{m}$, the nearest neighbor distance.

$$W^{L}(r) = -T \ln[g_1(r)]$$

$\Uparrow$

joint distribution for the nearest neighbor pairs

Relaxed lattice model calculation (Salpeter & Van Horn 1969)

Monte Carlo sampling (Ogata et al. 1991)

CONTACT PROBABILITY $|\Psi_{ij}(0)|^2$ **then depends only on the ratio,**

$$\lambda_{ij} = \left(\frac{3}{4}\right)^{1/2} \frac{r_{ij}^*}{r_{ij}^m} ,$$

due to the short-range cusp boundary condition,

$$\lim_{r \to 0} \frac{d \ln \Psi_{ij}(r)}{dr} = \frac{1}{2r_{ij}^*} .$$

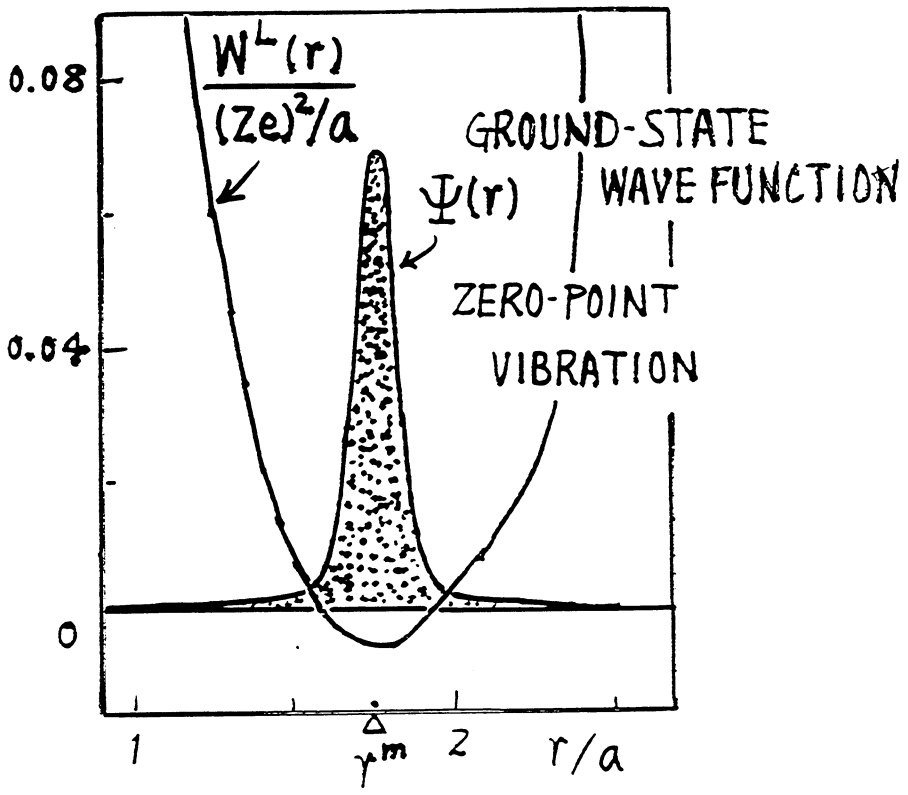

PYCNONUCLEAR RATES

$$R_{PY} = \frac{1.34\times10^{32}}{1+\delta_{ij}} \frac{X_i X_j (A_i + A_j)}{Z_i Z_j (A_i A_j)^2}$$

$$\times S_{ij} \rho_m^2 \lambda_{ij}^{-1.809} \exp\left(-2.460\, \lambda_{ij}^{-1/2}\right)$$

(reactions cm^{-3} s^{-1})

S_{ij} : cross-section factor (MeV barns)

ρ_m : mass density (g cm^{-3})
A_i : mass number
X_i : mass fraction

♦ ♦ R_{PY} increases very steeply with the mass density, since magnitude of its exponent decreases as $\rho_m^{-1/6}$.

$$\exp\left(-2.460\, \lambda^{-1/2}\right) = \exp\left[-278.41 \left(\frac{A}{2}\right)^{2/3} Z\, \rho_m^{-1/6}\right]$$

MANY-BODY CORRELATION PROCESSES

ENHANCEMENT FACTORS A_{ij} **of reaction rates due to** *internuclear many-body correlations* **over the thermonuclear or electron-screened cold-fusion rates**

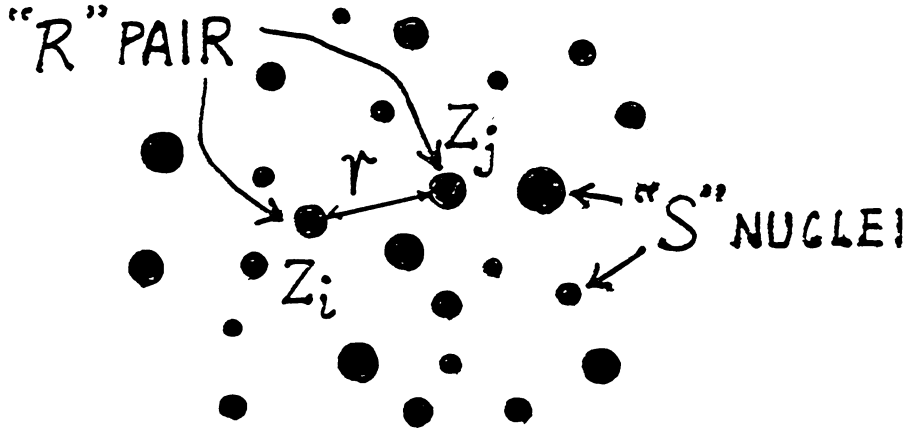

$$A_{ij} = \frac{g_{ij}(r=0\,;\,W)}{g_{ij}(r=0\,;\,0)}$$

$$= \frac{V^2}{\Xi}\left\langle "S" \middle| \exp\left[-\frac{S\{W\}-S\{0\}}{\hbar}\right] \middle| "S" \right\rangle$$

$W(r;"S")$: sum of all the internuclear potentials except one between the reacting "R" pair.

ACTION INTEGRALS

$$S\{W\} = \int_0^{\hbar/T} dt \left[\frac{\mu_{ij}}{2} \left(\frac{dr}{dt} \right)^2 + \frac{Z_i Z_j e^2}{r} + W(r; "S") \right]$$

$$S\{0\} = \int_0^{\hbar/T} dt \left[\frac{\mu_{ij}}{2} \left(\frac{dr}{dt} \right)^2 + \frac{Z_i Z_j e^2}{r} \right]$$

along the trajectories $r(t)$ that minimize S.

The trajectories are taken from the origin back to the origin, in a time interval $\hbar/T$,

in the potential with the reversed sign.

CONFIGURATION INTEGRAL

$$\Xi = \int dr_1 \cdots dr_N \exp\left\{ -\frac{1}{T} \left[\frac{Z_i Z_j e^2}{r} + W(r; "S") \right] \right\}$$

SCREENING POTENTIALS

$$\exp\left\{-\frac{H_{ij}(r)}{T}\right\} = \frac{V^2}{\Xi}\left\langle "S" \left| \exp\left\{-\frac{W(r;"S")}{T}\right\} \right| "S" \right\rangle$$

JOINT PROBABILITY DENSITIES $g_{ij}^{(c)}(r)$ for *reacting "R" pairs* resulting from statistical averages over the CLASSICAL ENSEMBLE of *spectator "S" nuclei*,

$$\Lambda_{ij} < 1.$$

$$\boxed{H_{ij}(r) = \frac{Z_i Z_j e^2}{r} + T \ln\left[g_{ij}^{(c)}(r)\right]}$$

SCREENING POTENTIALS represent the balances between the direct potentials, $Z_iZ_je^2/r$, and the potentials of mean force, $-T \ln g_{ij}^{(c)}(r)$, for *reacting "R" pairs*, and thus measure the extents to which the binary Coulombic repulsion is reduced by the *many-body correlation* effects.

STEPS OF CALCULATIONS

1) Monte Carlo (MC) sampling of $g_{ij}^{(c)}(r)$ at intermediate distances ($0.4 < r/a < 2$)

Metropolis algorithm

2) Short-range Widom (1963) expansion:

$$\frac{H(r)}{T} = \frac{H(0)}{T} - \frac{\Gamma}{4}\left(\frac{r}{a}\right)^2 + h_2\left(\frac{r}{a}\right)^4 \cdots$$

$h_2 \approx 0$ by direct MC sampling

3) INTERPOLATION $\Rightarrow$ FITTING FORMULA

OCP ($5 \le \Gamma \le 180$) $x = r/a$

$$\frac{H(r)}{(Ze)^2/a} = \begin{cases} A - B^2 - \frac{1}{4}x^2, & x \le 2B, \\ A - Bx + \frac{1}{x}\exp\left[C\sqrt{x} - D\right], & 2B < x < 2. \end{cases}$$

$A = 1.356 - 0.0213\ln\Gamma$, $B = 0.456 - 0.013\ln\Gamma$,

$C = 9.29 + 0.79\ln\Gamma$, $D = 14.83 + 1.31\ln\Gamma$.

$$H(r) = \frac{(Ze)^2}{r} + T \ln g^{(c)}(r)$$

$N = 432 \quad c = 1 \times 10^8$

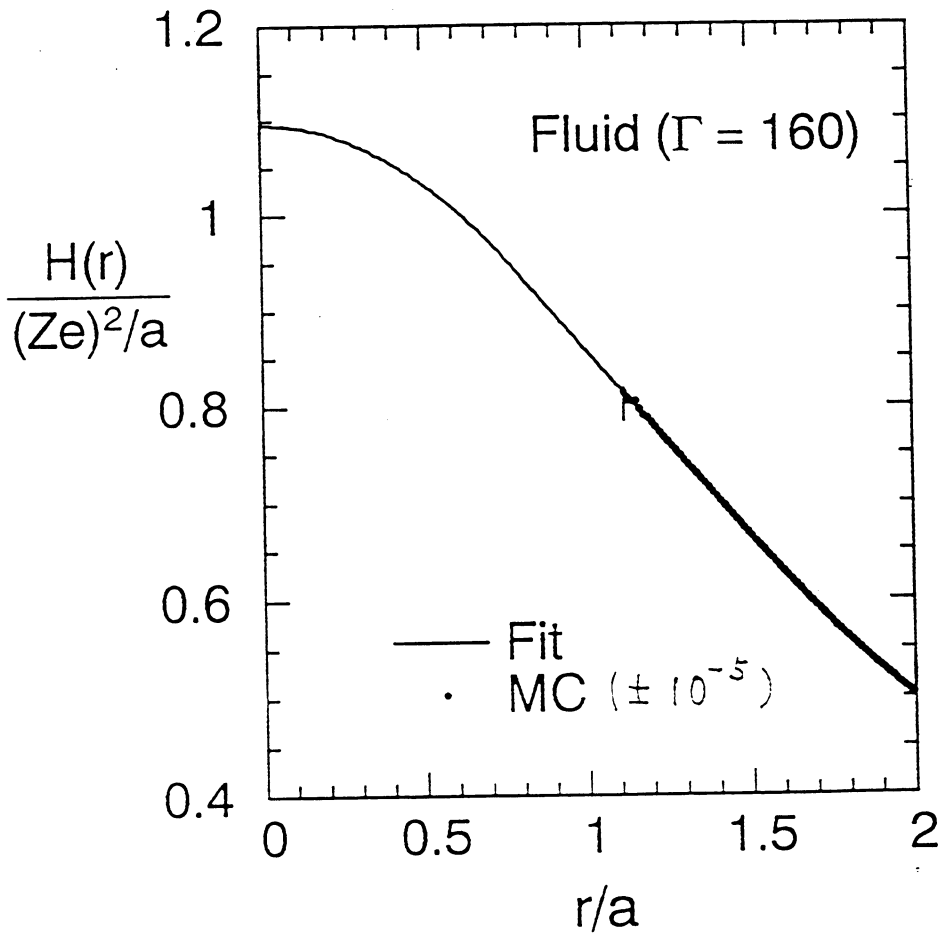

ENHANCEMENT FACTORS

$$A_{ij} = \exp\left[\frac{\langle H_{ij}(r)\rangle_R}{T}\right]$$

$\langle H_{ij}(r)\rangle_R$: path-integral averages of the screening potentials with respect to penetrating wave functions from $r = 0$ to the classical turning point.

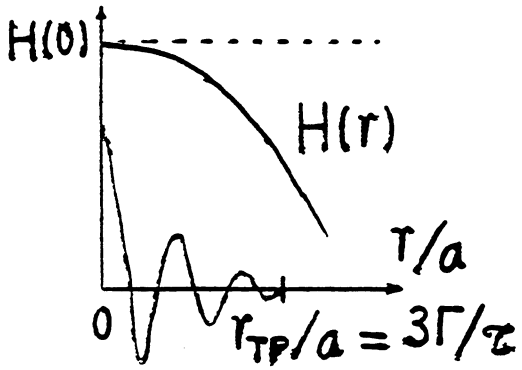

$$\boxed{A_{ij} = \exp(Q_{ij})}$$

$$Q_{ij} = \frac{H_{ij}(0)}{T}$$ (classical contribution)

$$-\frac{5}{32}\Gamma_{ij}\left(\frac{3\Gamma_{ij}}{\tau_{ij}}\right)^2\left[1 + (C_1 + C_2 \ln\Gamma_{ij})\left(\frac{3\Gamma_{ij}}{\tau_{ij}}\right) + C_3\left(\frac{3\Gamma_{ij}}{\tau_{ij}}\right)^2\right]$$

(quantum corrections)

$$H_{ij}(0) = (Z_i Z_j e^2/a_{ij})[1.148 - 0.00944 \ln\Gamma_{ij} - 0.000168(\ln\Gamma_{ij})^2]$$

$C_1 = 1.1858.$ $C_2 = -0.2472.$

$C_3 = -0.07009.$

CHEMICAL POTENTIALS

If $r_{TP} << a_{ij}$, then

$$A_{ij} \approx \exp\left[\frac{H_{ij}(0)}{T}\right].$$

$H_{ij}(0)$: INCREMENTS in the *Coulombic chemical potentials* for the "R" pairs between BEFORE and AFTER the reactions.

OCP

$$H(0) = F_{ex}^{BIM}(N, 0) - F_{ex}^{BIM}(N-2, 1)$$

$F_{ex}^{BIM}(N_1, N_2)$: EXCESS FREE ENERGY of a BIM consisting of N_1 nuclei with charge number Z and of N_2 nuclei with charge number $2Z$.

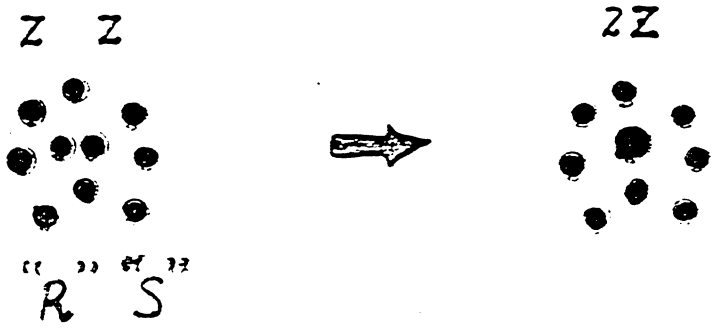

ENHANCEMENT FACTORS

for ELECTRON-SCREENED BIM NUCLEI

$$\boxed{A_{ij}^{(s)} = \exp\left(Q_{ij}^{(s)}\right)}$$

$$Q_{ij}^{(s)} = \frac{H_{ij}^{(s)}(0)}{T}$$

$$- \frac{5}{32}\Gamma_{ij}^{(s)}\left(\frac{D_S}{a_{ij}}\right)^2\left[1 + \left(C_1 + C_2 \ln\Gamma_{ij}^{(s)}\right)\left(\frac{D_S}{a_{ij}}\right) + C_3\left(\frac{D_S}{a_{ij}}\right)^2\right]$$

$$H_{ij}^{(s)}(0)/T = \Gamma_{ij}^{(s)}[1.148 - 0.00944 \ln\Gamma_{ij}^{(s)} - 0.000168(\ln\Gamma_{ij}^{(s)})^2]$$

$C_1 = 1.1858, \qquad C_2 = -0.2472,$

$C_3 = -0.07009.$

Screened Coulomb-Coupling Parameters

$$\Gamma_{ij}^{(s)} = \Gamma_{ij}\, S(a_{ij})$$

$$\approx \Gamma_{ij} \exp\left(-\frac{a_{ij}}{D_S}\right)$$

WHITE DWARFS

case	WD	Sun
reactions	^{12}C-^{12}C	p-p
S_{ij} (MeV·bahn)	8.83×10^{16}	4.07×10^{-25}
Q (MeV)	13.93	13.1
ρ_m (g/cm^3)	4×10^9	56.2
T (K)	1×10^8	1.55×10^7
$\tau_{ij}/\ln 10$	79.0	5.9
$\log_{10} R_G$ (s^{-1})	-43.35	-17.69
Λ_{ij}	0.47	0.023
Γ_{ij}	56.6	0.072
$\Gamma_{ij}^{(s)}$	41.4	0.044
$\log_{10} A_{ij}$	24.57	0.03
$\log_{10} R$ (s^{-1})	-18.65	-17.66
$\log_{10} P$ (W/g)	-8.01	-5.56
Enhancement	HUGE	NONE

METAL HYDRIDES

METALS: Pd, Ti, ···

HYDROGEN NUCLEI: *deuterons*

HYDROGEN IN METAL

- Hydrogen nuclei are strongly screened by valence electrons and by nearly localized electrons in hybridized states.

- The metal atoms situated at *periodic* or *aperiodic* (due to defects) lattice sites create inhomogeneous fields, which act to trap (or localize) the hydrogen nuclei and thereby to alter microscopic features of *short-range correlations*.

- Owing to these influence of the screening electrons and the inhomogeneous lattice fields, hydrogen nuclei in metal hydride bear a *dual* character of itinerant (i.e., fluidlike) and trapped (i.e., solidlike) particles.

METALLIC LATTICES

Pd

d (lattice constant) $\approx$ 4 Å

O-SITES

CURVATURE (Φ'') $\approx$ 1.1 eV/Å^2

BARRIER HEIGHT ($\Delta\Phi$) $\approx$ 0.23 eV

$$V_{\text{Pd-H}}(r) = \frac{22.2\,(\text{eV}\cdot\text{Å})}{r} \exp\left[-\frac{r}{0.42\,(\text{Å})}\right]$$

Ti

d (lattice constant) $\approx$ 4.4 Å

T-SITES

CURVATURE (Φ'') $\approx$ 5.1 eV/Å^2

BARRIER HEIGHT ($\Delta\Phi$) $\approx$ 0.51 eV

$$V_{\text{Ti-H}}(r) = \frac{31.8\,(\text{eV}\cdot\text{Å})}{r} \left\{ \exp\left[-\frac{r}{0.51\,(\text{Å})}\right] + \left[\frac{r}{1.095\,(\text{Å})}\right]^{10.57} \exp\left[-\frac{r}{0.23\,(\text{Å})}\right] \right\}$$

MONTE CARLO SIMULATION OF ITINERANT HYDROGEN NUCLEI IN THE LATTICE FIELDS

MC CELL

500 METAL ATOMS AT FCC SITES WITH THE PERIODIC B. C.

DEFECTS

RANDOM REMOVAL OF 8 METALLIC ATOMS

MC CONFIGURATIONS GENERATED

$c/N_H \geq (1 \sim 3) \times 10^4$

T (K) = (1200), 600, 300, (200)

RANDOM DISPLACEMENTS OF HYDROGEN NUCLEI [N_H = 500 (Pd), 1000 (Ti)] IN THE METROPOLIS ALGORITHM WITH $E_{M\text{-}H} + E_{H\text{-}H}$

REPULSIVE PART OF H-H INTERACTION

$$V_R(r) = \frac{e^2}{\varepsilon_c r}\left[\exp\left(-\frac{r}{D_S}\right) + \left(\frac{r}{r_R}\right)^p \exp\left(-\frac{r}{D_R}\right)\right]$$

ε_c = 1.25(1.36) $\quad D_S$(Å) = 0.19(0.28)

r_R(Å) = 1.04(1.00) $\quad D_R$(Å) = 0.18(0.17)

p = 8.9(10.0)

ENHANCEMENT DUE TO INHOMOGENEOUS LATTICE FIELDS

$$H_R(r) = V_R(r) + T \ln[g_R(r)] \quad \text{(MC sampling)}$$

$$H_R(r) = A + B \exp(-Cr) \quad \text{(FIT)}$$

$$\log_{10} A^{(M)} = H_R(0)/T\ln 10$$

Values of $H_R(0)/T\ln 10$ determined by MC sampling method for hydrogen in metals. [L] means a case with periodic lattice fields; [D], a case with defects.

T (K)	1200	600	300
PdH [L]	2.5	5.5	11.8
PdH [D]	1.9	3.8	5.0
TiH_2 [L]	4.2	9.4	20.9
TiH_2 [D]	7.2	16.5	35.4

ELECTRON-SCREENED COLD-FUSION RATES IN METAL HYDRIDES ENHANCED BY INHOMOGENEOUS LATTICE FIELDS

	PdD		TiD_2	
n_d (cm^{-3})	6.25×10^{22}		9.4×10^{22}	
E_S (eV)	75.79		51.43	
$\log_{10} R_S$ (s^{-1})	-40.79		-51.13	
T (K)	300	600	300	600
Λ	0.45	0.32	0.52	0.37
Γ	356.3	178.2	408.3	204.1
$\Gamma^{(s)}$	0.09	0.05	3.1	1.6
$\log_{10} A^{(MH)}$	10.90	5.39	17.71	9.09
$\log_{10} R$ (s^{-1})	-29.89*	-35.40	-33.42	-42.04
$\log_{10} P$ (W/g)	-20.38	-25.89	-23.29	-31.92
$\log_{10} f_{itin}$	-3.76	-2.43	-7.08	-4.09

* $\approx$ 2~3 reactions/cm^3/year -- consistent with the KAMIOKANDE indications.

POSSIBILITIES OF NON-EQUILIBRIA

- "dynamic" effects -- *already* included !

$$g_{ij}(0) = 1 + \frac{1}{\sqrt{n_i n_j}} \int \frac{dk}{(2\pi)^3} \left[S_{ij}(k) - \delta_{ij} \right]$$

$$= 1 + \frac{1}{\sqrt{n_i n_j}} \int \frac{dk}{(2\pi)^3} \left[\frac{1}{\sqrt{n_i n_j}} \int_{-\infty}^{\infty} d\omega S_{ij}(k,\omega) - \delta_{ij} \right]$$

- **ITINERANT FRACTIONS**

"fluidity"

$$f_{itin} = \exp\left\{ -\frac{1}{T} \left(\Delta\Phi - \frac{3}{2}\hbar \sqrt{\frac{\Phi''}{M_d}} \right) \right\}$$

- *Due to extreme sensitivity of the*

LATTICE ENHANCEMENT FACTOR,

$$\log_{10} A^{(M)} = H_R(0)/T \ln 10,$$

on "lattice defects," the total reaction rates may possibly vary by as much as 10 orders of magnitude !

Opposition and Support for Cold Fusion

M. Rabinowitz
Electric Power Research Institute, P.O. Box 10412, Palo Alto, CA 94303, USA

Y. E. Kim
Department of Physics, Purdue University, West Lafayette, IN 47907, USA

V.A. Chechin and V.A. Tsarev
Lebedev Physical Institute, Russian Academy of Sciences, Russian Federation

Abstract

Situations analogous to the present situation in Cold Fusion (CF) have previously occurred in science. Conventional theory appears so diametrically opposed to the possibility of CF that little room is left for commonality in the theoretical realm. Bifurcation persists because there is still only a sparse experimental meeting ground between the two camps. Experiment should and will be the final arbiter. Nevertheless, a theoretical existence proof i.e. a proof of principle would go far in putting to rest reservations and doubts regarding the reality of CF. Our goal is to see if reasonable answers to the opposition can be given in support of CF.

1. THE CHALLENGE

John Huizenga (1) challenged Cold Fusion (CF) with his three Miracles. In doing so he has made a good, honest, and strong case against CF. Let us explore whether his negative points can be objectively answered with an equally strong case in support of CF. Is there an historical precedent for such a demarcation from the conventional view? What is the basis for the conventional view? What alternative paradigms or models are there? First let's look at his objections.

1.1 Fusion Rate Miracle

The conventionally expected fusion rate at T = 300K is $< 3 \times 10^{-64}$ fusions/sec-dd for r = 0.74 Å as in D_2. Huizenga (1) allows only for r ≥ 1.7 Å in Pd with a considerably smaller fusion rate than in D_2. Sun & Tomanek (2) show that r = 0.94 Å is possible. To account for calorimetiric power levels, $\sim 10^{-9}$ fusions/sec-dd are needed. For r = 0.74 Å, this is 10^{55} higher than expected! To account for the Jones (3) rate, $\sim 10^{-22}$ fusions/sec-dd are needed. This is 10^{42} higher than expected for r = 0.74 Å. So even the modest Jones level appears considerably too high.

1.2 Branching Ratio Miracle

The n & t channels occur about equally with a slightly higher frequency for the t branch. Conventionally t/n ~1. This nearly equal branching ratio is the result of the charge independence of the nuclear force. The $^4He + \gamma$ channel (3) has only a branching ratio $P \sim 10^{-7}$ because of the small ratio of the electromagnetic to the nuclear force. $d + d \rightarrow {}^4He + e^+ + e^-$ has only $P \sim 10^{-9}$.(4) So this reaction is not likely to account for the absense of high energy γs in Cold Fusion (CF), and when the e^+ annihilates with a lattice e^-, two 0.5 Mev γs are emitted. The Problem with CF is that t/n $\sim 10^4$ to 10^8 and no high energy γs have ever been observed. Here are the fusion reactions in question.

$$d + d \rightarrow {}^3He(0.817\ MeV) + n(2.452\ MeV), \quad Q = 3.269\ MeV, \quad P \approx 0.5 \qquad (1)$$

$$d + d \rightarrow p(3.025\ MeV) + t(1.008\ MeV), \quad Q = 4.033\ MeV, \quad P \approx 0.5 \qquad (2)$$

$$d + d \rightarrow {}^4He(7.6\ keV) + \gamma(23.7\ MeV), \quad Q = 23.8\ MeV, \quad P \sim 10^{-7} \qquad (3)$$

1.3 No Nuclear Products Miracle

Huizenga (1) argues that no nuclear products (ash) whatsoever have been validly observed in CF. He feels that the lack of high energy γ detection invalidates any presumed ^{4}He detection. The production of 1 MeV tritium from the d + d $\rightarrow$ p(3.025 MeV) + t(1.008 MeV) reaction implies that there must be a secondary reaction even if the t energy is somehow degraded by dE/dx or otherwise to the ~ 50 keV range.

$$d + t \rightarrow {}^4He(3.52\ MeV) + n\ (14.07\ MeV). \qquad (4)$$

Unfortunately, these 14 MeV neutrons have never been detected.

2. HISTORICAL PRECEDENT

The scientific milieu of our time with Grand Unified Theories and Theories of Everything leads us to think that we have final answers to the mysteries of nature. This has not always been the case in the history of humankind, but neither is it a singular view.

2.1 Napoleonic and Victorian Theories

Perhaps the earliest period with similarly pretentious scientific views was in the early 1800's in France. The chief architect, of what Heilbron (5) calls the Napoleonic Model, was the Marquis de Laplace. The chief ingredients of this theory were fluids. They were the capital feature since every distinct force was supposed to have as its carrier at least one such fluid. There was a postive and negative fluid for electricity; austral and boreal fluids for magnetism. Caloric was the fluid for ordinary heat. Radiant heat was another fluid. The Napoleonic theorists deemed that they had tied together all of astronomy and microphysics. They thought they really understood their fluids; the very large; the very small; and their union. In fact they really didn't know what their fluids were, and in some cases as in the case of Caloric (ordinary heat) the fluid didn't even exist. This theory didn't long survive Napoleon.

In the late 1800's, in Great Britain, Lord Kelvin (Wm.Thompson) was the Chief Architect of what Heilbron (5) calls the Victorian Model. Its chief Ingredients were discrete particles in the ubiquitous, continuous ether. It had many notable successes such as Maxwell's equations and theory of gases, as well as some unheralded ones. For example, Joseph Larmor (6) [better known for his theory of charged particle precession] created a theory of ether knots. He had knotted rings of opposite helicity that he called negative & positive electrons. For him atoms were the rotation of symmetric rings of opposite electrons. His ideas date from the 1890's --before the discovery of the electron and long before the nuclear atom, and were not readily accepted at the time. Despite its many successes, the Victorian theory with its absolute space and time, together with mechanical analogs for the machinery of the ether, was felled by the Energists and Relativity.

Our grand and all encompassing theories today may fare no better than that of the Napoleonic and Victorian theories. These theories produced quantitative results; agreed to some degree with experiment; and enjoyed a wide consensus among scientists of the day. The Defenders of the Scientific Faith considered these theories to be fundamental, universal, and immutable. Though they had many good points, to a large extent both of these theories have long since been abandoned. One might think that these theories were ill-fated because they go back so far in time. Let us examine more recent theories to see such a fate for contemporary paradigms.

2.2 Superconductivity and High Temperature Superconductivity

Onnes discovery of superconductivity in 1911 falls into the realm of something that was totally unexpected by the laws of physics (7). Not long before the 1957 BCS theory of superconductivity, Felix Bloch the founder of solid state theory jokingly said that the only theorem about superconductivity which can be proved is that any theory of superconductivity is refutable. By this he meant that superconductivity appears theoretically impossible because the energy of the current carrying state is higher than the ground state. The Meissner effect, the exclusion of a

magnetic field from the bulk of a superconductor, was not discovered until 1933, some 22 years after the discovery of superconductivity. In that 22 year period the scientific community thought the field would be trapped as predicted by Maxwell's equations. It was then thought that the magnetic field could not be trapped, until Rabinowitz et al (8) demonstrated that it could be.

Although there were many spurious observations of high temperature superconductivity (HTSC) prior to its discovery in 1986, almost the entire scientific community thought that HTSC was impossible. For the last 37 years it has been thought by the scientific community that it is impossible to calculate transition temperatures without knowing the electron pairing interaction and its strength. Yet the transition temperatures for a wide range of superconductors has been accurately calculated (9, 10) without knowledge of the pairing interaction and its strength.

2.3 Superfluidity

Although theory agrees reasonably well with the superfluid transition temperature T_c of 2.17 K for ^{4}He, it has done rather poorly for the T_c of ^{3}He.(11) By analogy with the BCS theory for superconductivity, in 1959-60 top theoreticians throughout the world predicted $T_c \sim 0.1$ K for ^{3}He. When the experimentalists couldn't find ^{3}He superfluidity down to ~ 0.01 K, the theoreticians sharpened up their calculations and predicted $T_c \sim 10^{-6}$ to 10^{-9} K. In 1972, the experimentalists Osheroff, Richardson, and Lee found $T_c = 2.6$ mK, which can be closely calculated by the same interaction-free approach used for HTSC (10, 12).

2.4 Solar Neutrino Problem

The standard solar model helped to predict the abundance of the elements in the universe and in all types of stars including the sun. Although it worked extremely well and the scientific community was thoroughly satisfied with it, Davis ran an experiment that would help to verify predictions of the model in terms of the neutrino flux. After running an experiment from 1968 to 1986, the neutrino flux was found to be 2 to 3 times lower than predicted. This large inconsistency has continued even with recent experiments. We were drawn to the solar neutrino problem in the hope that insight into this hot fusion paradox might also help us understand CF. We think our findings help to solve this problem(13-15). However, it has not led to insight into CF.

3. THEORETICAL ISSUES

3.1 Introduction

Theoretical demonstration of CF "permissibility in principle" would provide an important psychological factor for putting the reported phenomenon into a framework which might lead to its general acceptance. A trustworthy hypothesis would be invaluable if it could correlate observations, make predictions, and stimulate experiments. Theory needs to explain why the calorimetric excess energy is ~10^5 times higher than the fusion tritium energy which is ~ 10^8 times higher than the neutron energy. Experimentally it may be possible to distinguish between cold fusion and hot fusion on an atomic scale (which is the basis of some CF models) by temperature and kinematic broadening and shifting of the characteristic fusion product lines (16). High loading claims (d/Pd > 0.7) must be considered with caution as in some cases this may simply be due to the filling of voids and cracks that are created as the host lattice is forced to expand.

Calculating tunneling probabilities for the Coulomb barrier between two d's, and their sensitivity to shielding can quickly make us aware of one basis for the conventional pessimistic view, followed by optimism with respect to CF. In the context of α-emission, Gamow in 1928 first derived the tunneling (transmission) probability $G = e^{-2\Gamma}$ (Gamow factor) through the mutual Coulomb barrier of two particles of charges Z_1e and Z_2e, when the center of mass (CM) energy E is much less than the barrier height, in esu

$$\Gamma = \frac{1}{\hbar}(\pi Z_1 Z_2 e^2)\sqrt{\frac{\mu}{2E}} \qquad (5)$$

where $\mu = m_1 m_2 / (m_1 + m_2)$ is their reduced mass, and $\hbar$ is $(1/2\pi)$Planck's constant. For two d's taking E ~ (1/40) eV for illustration, G ~ 10^{-2730}; and in free space the classical distance of closest approach would be ~580 Å. G is extemely small yielding pessimism about CF, but also illustrating that electron shielding of the barrier cannot be neglected at low E.

There are many models for shielding (screening potential) in a solid which lead to roughly similar results. Rabinowitz (17-20) developed a model of a spherical shell of radius R of negative charge surrounding each d as the simplest conceptionally as well as computationally since it results in only a shifted Coulomb potential ,

$$V = e^2[(1/r) - (1/R)], \quad r_n \le r \le R, \qquad (6)$$

where r_n is the nuclear well radius. $G' = e^{-2g}$, where

$$g = \frac{\pi e^2}{\hbar}\left[\frac{\mu R}{2(ER + e^2)}\right]^{1/2} \qquad (7)$$

For E ~ (1/40) eV and R = 1Å, G' ~ 10^{-114}, picking up ~2616 orders of magnitude which illustrates one basis for optimism about CF. In the limit as $R \to \infty$, $g \to \Gamma$, yielding the unshielded case for $Z_1 = Z_2 = 1$ here, and in general. A model of a uniform cloud of electrons as well as use of the Maxwell-Boltzmann (MB) deuteron velocity distribution (21,22) would give a significantly higher tunneling and fusion rate but still not enough to account for CF.

3.2 Response to Foremost Theoretical Challenge

Leggett and Baym (L&B) presented the foremost theoretical challenge to CF by calculating a maximum upper limit of $\lambda = 3 \times 10^{-47}$/(sec-dd) for the fusion rate in a lattice (23,24). It is important to bear in mind that the Leggett and Baym argument is an equilibrium argument, and that CF is not necessarily an equilibrium process. Interestingly, R.H. Parmenter and the Nobel Laureate Willis E. Lamb (P&L) do not invoke non-equilibrium in responding to L&B. In their 1st paper (25) they calculate a fusion rate $\lambda = 2 \times 10^{-30}$/(sec-dd), exceeding the L&B limit by 10^{17}. They attribute this to the potential well of the trapping site in the lattice that holds the 2 d's. This was neglected by L & B. They get the L & B limit when the harmonic oscillator potential is disregarded, and only the screening at large distances is kept.

In the 2nd P&L paper (26), the L&B limit is further circumvented by means of a larger effective mass for the conduction electons at wave numbers ≤ the inverse Debye screening length, though they agree that the free electron mass should be used at much larger wave numbers. Their analysis leads to the usual free electron mass for electrons that are close to the deuterons, but finds that at large distances the electrons behave as if they have a larger effective mass ~ 2.6 times the free mass. This increases the fusion rate another factor of 10^7 over the L&B limit for a total factor of 10^{24} allowing them to account for the Jones level of fusion.

The P&L results are controversial. The unfavorable milieu for supportive publications is indicated by their comment (26), "The calculations reported here may be viewed by some as a vain attempt on the part of the authors 'to revive a dead horse,' in view of the recent outpouring of negative publicity concerning cold fusion and the sometimes vicious attacks on its proponents." For them, the low n levels "can be explained without invoking any physics more esoteric than that of screening of positive charges by conduction electrons."

4. THEORETICAL MODELS

Analyzing CF theoretical models is like shooting at a moving target. Some of these models may already be abandoned as new models are created. Nevertheless shortcomings will be presented so that models do not resurface unchallenged. Space limitations only permit looking at a small number of models briefly. We will look at a much larger number of models in depth in a critical review (27). The main problem in CF is overcoming the Coulomb barrier. We shall present at least one model in each category to show how this problem is dealt with.

4.1 Barrier Circumvention

4.1.1 Transmission Resonance (TR)

The presence of only one barrier leads to a very low transmission probability (coefficient) through it. However anti-intuitively, quantum mechanics allows high probability transit for the one-dimensional problem of particle passage through two (or a periodic sequence) of potential energy barriers for certain discrete values of energy (e.g. at which an odd number of quarter wavelengths fit into the well width). This quantum mechanical effect occurs as a result of destructive interference of waves reflected from multiple barriers as lucidly analyzed by Bohm (28), and is called transmission resonance (TR). TR was suggested by Turner (29) for CF, though he apparently did not pursue it further. The idea was further developed by Bush (30).

Critique: There is a basic defect in the TR model. Contrary to Turner, Bush, and Jandel (31), we feel that Bohm's one-dimensional TR model is not applicable to d's in a lattice, as a given d must also get through the nuclear well of another d. Bohm's model applies to electrons, as they do not have a nuclear interaction. Following Bohm, Jandel has presented his objectons to Bush's TR model of CF, but not to the relevance of the model itself.

The TR model of CF has a number of inconsistencies beginning with its basic premise. Although the transmission coefficient can be high (but as we shall show not necessarily in the CF realm), fusion rates can still be extremely low. The build-up of the wave function between the barriers near resonance is a very slow process with time scales ~ the time for alpha decay . As Bohm points out, the process is similar to the building up of an intense standing wave in a resonant cavity --be it acoustic or electromagnetic.

The seriousness of the filling time problem can easily be seen quantitatively. For a system of two barriers, with each described by the potential V(x), the transmission probability (coefficient) as obtained from the WKB approximation is:

$$P' \approx [\, 1 + 4G^{-4} \sin^2\{(\pi - J)/2\}]^{-1}, \qquad (8)$$

where G = exp(-J) is the Gamow factor given in Sec. 3.1.

Let us consider two d's approaching each other through two barriers at room temperature, with E = kT = 1/40 eV. Taking into account screening of the Coulomb potential barriers, G ~ 10^{-100} as shown in Sec. 3.1. If the system is far from the resonant energy E_{res}, $P' \sim G^4 \sim 10^{-400}$. This corresponds to a small fraction of ~ $(G^2)(G^2)$ of the incident d's tunneling through two barriers. At resonance $J = \pi$, and equation (8) gives a unity tunneling probability, i.e. P' =1 for any G. The resonance is related to the existence of a metastable state whose lifetime is $\Delta t \sim \hbar / \Delta E$, where the half-width $\Delta E = E - E_{res}$ for P' = 1/2. Bohm shows that the lifetime is

$$\Delta t = t_t G^{-2} \ , \qquad (9)$$

where t_t is the classical transit time to cross the well and return. For a well width of ~ 1Å = 10^{-8} cm, and a velocity ~ 2 x 10^5 cm/sec, $t_t \sim 10^{-13}$ sec.Thus at resonance, $\Delta t \sim 10^{-13}$ sec $(10^{200}) = 10^{187}$sec. The age of the universe is small in comparison. being only ~15 x 10^9 years = 4.7 x

10^{17} sec. Of course shorter times are possible as E gets further from resonance, but the combination of lifetime and tunneling probability does not appear capable of accounting for CF.

4.1.2 Lattice Induced Nuclear Chemistry (LINC)

The main theme of a series of papers by Chubb and Chubb (32,33) relates to the wave nature of boson particles in a solid. They feel that just as electrons are better described as waves in a solid, deuterons should not be described as particles when they are inside a solid lattice. The position of these authors is, "Overlap of the wave functions necessary to initiate the reaction is ensured by algebraic properties of a many-particle wave function, but not by tunneling which is the basis of conventional nuclear physics." The basic predictions of the LINC model are a high rate of fusion in a lattice, dominance of the production of ^{4}He, and heat release without observable fast nuclear products.

Critique: The authors' premise identifying overlap of the d wave function with fusion in a lattice is erroneous. This is because their wave function is derived from a Hamiltonian which neglects the d-d interaction, and does not minimize the full Hamiltonian of the d system. Their excess energy is due to a neglect of dd Coulomb repulsion, which if included gives a tremendously smaller fusion rate. Furthermore, the factor corresponding to the Astrophysical Function is neglected, i.e. the probability that nucleons will stay in the nuclear well after tunneling into it. Thus their model calculates a higher p-p fusion rate than d-d because this factor is neglected.

4.2 Barrier Reduction

4.2.1 Superradiance (SR)

Bressani et al (34), and Preparata (35,36,37,38) propose that the key to understanding CF lies in superemissive dynamics -- superradiance (SR) -- in a solid. According to these authors, this means that the components of elementary atomic systems to some extent lose their individuality and become part of a kind of collective plasma. This plasma is a medium of charged particles vibrating about their equilibrium positions with plasma frequencies $\omega_p = e\sqrt{n'/m\varepsilon}$, where e and m are the charge and mass of the particles, n' is their number density, and ε is the permittivity of the medium. They have an instability in the quantum electrodynamic (QED) ground state (independent zero-point oscillations). Their minimal energy state is a superradiant one in which all the plasma particles oscillate in phase with the electromagnetic field that is excited coherently from the perturbative ground state of QED. They assert that SR provides a very strong effective screening of the Coulomb dd potential by the electron plasma in Pd.

SR was first presented by Dicke (39), though his work is not referenced in any of these papers; and neither is credit given to previous work (17-20,40) for the shifted Coulomb potential which Preparata borrows freely. Coherence is the key to understanding SR. If we have N particles radiating incoherently, then the total power radiated is the sum of the individual powers. For particles radiating coherently (in phase) in a small enough volume that the phase coherence is not lost from one end to another, then the total electric field E_t is the sum of the electric fields in each of the radiated waves. The total radiated power $\propto E_t^2$. For example, in simple terms, if the individual radiated power is P for each particle, then $P_{incoherent} = NP$, and $P_{coherent} \sim N^2P$.

Critique: Preparata (37) makes a $> 10^2$ numeric error. His r_n=20 fm is too large a value for the deuteron-deuteron nuclear attraction distance. The d radius is small. The d-d nuclear force diameter is < 8 fm, resulting even with his eq.(16) in a tunneling probability $D_T < 10^{-42}$ rather than his 10^{-40} due to the great sensitivity of the tunneling probability on r_n. Consequently, his claim of achieving the Jones level of CF is not supported. His disparity (37) with experiment

increases considerablly more than this factor of 10^2 since as we will show this model has too much shielding. Thus at the top of his p.88 (37) rather than "an enhancement of some 30 orders of magnitude over the tunneling amplitude for molecular deuterium", the resulting number is many orders of magnitude less. His eq.(26) is crucially important (37), but is not derived in detail in any of these papers. Its reliability is thus questionable. For the complex Feynman diagram (Fig. 5) it is not clear what approximations are made for the coupling constants and vertex functions.

In the course of their screening estimate, an assertion is made that Z electrons orbiting in phase about a Pd nucleus look like a sphere of radius δ defined by the dispersion of the plasma oscillations

$$\delta = \left[\frac{\hbar}{2m_e\omega_p}\right]^{1/2} \approx \frac{6.7\times10^{-9}}{Z^{1/4}}\text{cm}. \tag{10}$$

Due to electron oscillations, they assume a d may be covered by a cloud of Z electrons. According to these authors, the screening potential of these electrons takes the form

$$V_{screen} \equiv V_s \approx \frac{Ze^2r^2}{2\delta^3} \text{ for } r \le \delta. \tag{11}$$

$$\text{At } r = r_0 = \delta(2/Z)^{1/2},\ V_s + V_d = 0, \text{ since } V_d = e^2/\delta \text{ at } r = \delta. \tag{12}$$

With this abnormally large amount of screening the tunneling probability $P' = G^2$ is exceedingly high especially for $E_d \sim 0$.

To understand this anomalous result, note that δ is close to the characteristic dimension of a Thomas-Fermi atom of atomic number Z,

$$R_{TF} = \frac{0.885\hbar^2}{me^2Z^{1/3}} = 4.5\times10^{-9}\,\text{cm}/Z^{1/3}\,. \tag{13}$$

Consequently, the arrangement of Z electrons inside the region $r \le r_0 \sim R_{TF}$ is possible only in the Coulomb potential Ze/r of a nucleus of charge Z, but not in the field of a singly charged d. One of the conceptual errors of this model is having Z electrons take part in steady state screening of the d's Coulomb field. Solids would collapse if such close equilibrium screening were possible.

4.2.2 Lattice Vibrations (LV)

Perhaps the most notable theoretical support for CF comes from the Nobel Laureate Julian Schwinger (41,42,43) who contends d's encounter a relatively narrow Coulomb barrier allowing them to fuse into ^{3}He in a highly deuterated lattice. He cites Einstein (1907) as pointing out "that the initial phase of a novel investigation can be hindered by an excess of realism". According to Schwinger the effective potential of the d+d and also p+d interactions are modified due to averaging related to their zero-point oscillations in a solid lattice. In simpler words, the coupled harmonic motion of particles is supposed to lead to a reduction of the Coulomb barrier for fusion. When calculating this effect, one replaces the coordinate $\mathbf{r}$ in the Coulomb potential e/r by $\mathbf{r} + \delta\mathbf{r}$, where the operator addition $\delta\mathbf{r}$ corresponds to d oscillations and has a conventional expansion in terms of phonon degrees of freedom

$$\delta\mathbf{r} = \sum_q \sqrt{\hbar/2m_d\omega_q N}(a_q e^{-i\omega_q t} + a_q^{+} e^{i\omega_q t})\,. \tag{14}$$

Here a_q is the boson operator for phonon production with q momentum; N is the number of d's, $\hbar\omega_q$ is the energy of the q th phonon. When averaged to first approximation in the ground state, the effective potential of interaction for a slowly moving proton with a phonon oscillated d is

$$\langle 0|V(\mathbf{r}+\delta\mathbf{r}|0\rangle \sim e^2/r \text{ for } r >> \Lambda, \text{and } e^2/\Lambda \text{ for } r << \Lambda. \tag{15}$$

Where $\Lambda = \sqrt{\frac{\hbar}{2m_d}\left\langle\frac{1}{\omega_q}\right\rangle}$, and $\left\langle\frac{1}{\omega_q}\right\rangle$ is an average in terms of phonon modes. For $\left\langle 1/(\hbar\omega_q)\right\rangle \sim$ $1/(0.1\text{eV})$, we obtain $\Lambda \sim 10^{-9}$ cm. In the next approximation

$$\delta V \approx -[\nabla V(r)]^2 \sum_q \left[\frac{1}{2m_d N}\left\langle\frac{1}{\omega_q^2}\right\rangle\right] \qquad (16)$$

Assuming $\left\langle\frac{1}{\omega_q^2}\right\rangle \approx \left\langle\frac{1}{\omega_q}\right\rangle^2$ and considering that $2\Lambda \sim 10^3\hbar^2/(m_d e^2)$, Schwinger finds that

$$\delta V = -\frac{e^2}{r}\left(\frac{10\,\Lambda}{r}\right)^3 . \qquad (17)$$

This expression is valid for $r >> \Lambda$. For $r > 10\,\Lambda$, eq. (17) gives a rather marked decrease of the Coulomb potential, e^2/r. Schwinger concludes from this that a substantial suppression of the Coulomb barrier may be possible at the expense of lattice vibrations (LV).

Critique: We have great respect for Schwinger, yet our analysis indicates that there is a limit to what the phonons can do, and that there is not a sufficiently strong effect from LV. To us, Schwinger's LV approach appears applicable only for $\delta V << V$. Accordingly, this implies a small relative correction to the repulsive Coulomb potential rather than the large one he finds. As we showed in Section 2, modest decreases in the width of the Coulomb barrier can have enormous increases in the tunneling probability P' (the more so the lower P' is to begin with). However, the LV decrease in V goes further than seems warranted, and gives too large of an increase in P'. In going from the d+d reaction (41) to the p+d reaction (42,43), the 23.8 MeV γ is avoided and only a 5.5 MeV γ has to be absorbed directly by the lattice. There are also two minor issues that may need resolution for the d+d case. 1) The competing decay channels d+d$\rightarrow$ t+p and d+d $\rightarrow {}^3$He+n normally occur in times ~ 10^{-22}sec. The maximum frequency of the phonons ~ 10^{13}/sec implies a phonon emission time ~ 10^{-13}sec. It is not obvious *a'priori* that these decay channels will not depopulate the d+d scattering state faster than the phonon emission. 2) Schwinger (43) suggests that his model can produce t production rates ~ 10^3/sec -10^{10}/sec. It is not obvious that even with dE/dx energy degradation of ~ MeV t due to electron and ion interactions, that the reaction

$$d + t \rightarrow {}^4\text{He}(3.52\text{ MeV}) + n\ (14.07\text{ MeV}) \qquad (18)$$

cannot take place in measurable quantities. Reaction (18) has not been observed in CF. This issue also applies to other models and experiments which have a large t production. Detailed calculatons by Szalewicz et al (44) and Petrillo et al (45) of the effects of d oscillations in a lattice agree with us. Crawford (46) is even more pessimistic, claiming that "properly treating deuteron motions would lead to smaller calculated p-d fusion than if phonons were neglected."

4.3 Barrier Ascent

4.3.1 Interface Acceleration (IA)

In 1989, Rabinowitz and Worledge (18,20) suggested the following interface acceleration (IA) model based upon an observation of dendrites on electrolytic cathodes.(47) Asperities (sharp microscopic whiskers) grow on electrolytic cathodes, as a way of relieving internal and external stresses in a variety of settings (48). Field enhancement at the tip of the whisker ~height/(tip radius), together with the already present high double-layer electric field, can lead to very high local electric fields ~ 10^7 V/cm even though the macroscopic field is very low (49). A high current density of electrons can be field emitted from a whisker and ionize some D's.

They pointed out (18,20) that if a small number of d's become entrained with the high current density of electrons, the d's would attain the same velocity v as the electrons -- just as a log

in a river attains the velocity of the current in the river. The ratio of the energy of the d's to the energy of the electrons would be the same as their mass ratio

$$\frac{\frac{1}{2}m_d v^2}{\frac{1}{2}m_e v^2} = \frac{m_d}{m_e} = 3670. \qquad (19)$$

Even though the potential difference in a D_2O bubble is only a small fraction of the voltage applied to the cell, they pointed out possible non-equilibrium mechanisms for producing larger transient voltages. Thus for an electron energy ~ 10 eV, the d energy could be as high as 37 keV. Some consequences of the IA model for CF are discussed by Kim (21,22).

In the context of CF experiments produced by gas discharges, IA may be a possible explanation. The experiments of Karabut, Kucherov and Savvatimova (50) do have an incubation period which could be related to whisker growth. Furthermore, low pressure gas discharges are unstable leading to arcing with high L dI/dt voltages. Entrainment of d ions could lead to microscopic hot fusion, and resulting neutrons could cause transmutation of elements. Predictions of the IA model are:

1) Fusion rates at the Jones level and higher.
2) Sporadic character and burst-like nature of the process as whiskers are damaged.
3) Incubation period related to the growth of whiskers.
4) Poor reproducibility of the data related to the irregular behavior of the whisker growth process, and of the occurrence of non-equilibrium discharge conditions.

Critique: Although whiskers can grow due to stress during temperature cycling and rapid phase transitons in Ti, there is no applied electric field in the cycling experiments. Perhaps electron acceleration with entrainment of the d's could be related to field enhancement by whiskers of fracture produced electric fields. The IA model applies more clearly to electrolytic and gas discharge experiments. The same serious criticism that applies to other acceleration models applies to IA that the branching ratio, and rates for the different reactions should be the same as for hot fusion, but appears not to be so.

4.4 Exotic Chemistry

A number of models assume the existence of an exotic chemical system whose occurrence either precedes nuclear synthesis or makes it quite unnecessary. Such systems are assumed to be engendered by electromagnetic or nuclear interactions. The similarity of these postulated models is in their tight binding of electrons in atoms and/or molecules.

Critique: None of these models appears correct. They do not avoid the nuclear ash problem as the tight orbits would lead to apprecialble fusion rates. A simple demonstration of proper spectral lines would constitute proof in all these models, but this has not been done. Detailed analysis on all these models can be found in refs.51 and 52. Let's look at some here.

Maly and Va'vra (53) solve the relativistic Dirac equation for the hydrogen atom and get an electron orbit of ~ 500 keV binding energy, and radius r ~ 5 fm. There is a serious error in their analysis. At the nuclear surface, $r = r_n \neq 0$, which implies both the regular and irregular solutions are simultaneously allowed for $r \geq r_n$. The general solution is a linear combination of both for $r \geq r_n$ making the irregular solution nearly negligible compared to the regular solution. They erroneously assumed that the general solution can be given by just the irregular solution, independent of the regular solution. Their electron orbit radius of ~ 5 fm is 50 times smaller than muonic orbits of 250 fm . If such tight D atoms existed, upon collison, they should produce fusion at a much higher rate than muon catalyzed fusion.

Barut (54), Gryzinsky (55), and Vigier (56) propose a Superbound H_2^+ or D_2^+ with ~ 50 keV binding energy, and r ~ 40 fm for H_2^+ with r ~ 20 fm for D_2^+. Their analysis is predicated on the electron being exactly between the 2 d's which implies that the system is unstable. The tightness of the orbit violates the Uncertainty Principle if the potential is only Coulombic. Their non-relativistic analysis is warranted for H isotopes. However, a non-stationary electron requires a relativistic treatment. Perhaps a full relativistic calculation including spin-spin and spin-orbit coupling may save this model; but this has not been presented as yet. Their electron orbits ~ 20 fm, are 13 times smaller than the 250 fm muonic orbits and upon collison would produce fusion at a much higher rate than muon catalyzed fusion.

5. CONCLUSION

In spite of considerable efforts, no theoretical formulation of CF has succeeded in quantitatively or even qualitatively describing the reported experimental results. Those models claiming to have solved this enigma appear far from having accomplished this goal. Not all of the models are testable. It is imperative that a theory be testable, if it is to be considered a physical theory. The mechanism for anomalous effects in deuterated metals is still unknown.

The issues raised by Huizenga (1) have not yet been fully answered. The most important miracle to answer is Miracle 3: Where are the Nuclear Products? The exotic chemistry solutions are appealing because they completely eliminate this miracle. However, we have not seen a convincing one yet. Miracles 1 and 2 also need to be answered. However, too many historical exceptions weaken Huizenga's attempt to discredit Cold Fusion by reliance on disagreement with conventional fusion theory. Nevertheless, it is important to understand why the tunneling coefficient is so exceptionally high, why the branching ratio is so far from unity, why the secondary reaction d + t is not occurring, and why high energy γ's have not been observed.

Reproducibility of CF claims by an independent qualified laboratory should be given the highest priority to firmly establish the credibility of CF. However, lack of reproducibility is not a just reason for branding CF a "pathological science." Many valid fields of scientific inquiry such as weather, catalysis, regular and ball lightning, earthquakes, and solar storms are not well understood and are far from reproducible. The example of the semiconductor field may be a source of optimism. In 1931, the great physicist Wolfgang Pauli (57) said, "I don't like this solid state physics...though I initiated it. ...One shouldn't work on semiconductors, that is a filthy mess; who knows whether they really exist." Not withstanding this pessimistic view, the semiconductor field became a great success once the important variables were understood and controlled.

REFERENCES

1. J. R. Huizenga, *Cold Fusion: The Scientific Fiasco of the Century*. Rochester, NY: Univ. of Rochester Press, 1992, p.110-114.
2. Z. Sun and D. Tomanek, "Cold Fusion: How Close Can Deuterium Atoms Come Inside Palladium?," *Phys. Rev. Lett.* **63**, 59 (1989).
3. S.E.Jones,E.P.Palmer,J.B.Czirr,et al, "Observation of Cold Nuclear Fusion in Condensed Matter," *Nature* **338**, 737 (1989).
4. W. A.Fowler, "Cold Fusion Results Still Unexplained" *Nature* **339**, 345(1989).
5. J. L. Heilbron, "The Rise of the Standard Model." Proc. 3rd Intl. Symp. History of Particle Phys. Cambridge Univ. Press (1992)
6. J. Larmor.*Aether and Matter*. Cambridge: Cambridge Univ.Press, 1900, pp. 26-28.
7. M. Rabinowitz, "Do the Laws of Nature and Physics Agree on What is Allowed and Forbidden?" *21st Century Science & Technology* **6**,10 (1993).
8. M. Rabinowitz, E.L. Garwin, and D.J. Frankel, "An Investigation of the Very Incomplete Meissner Effect," *Nuovo Cimento Letters* **7**, 1 (1973).
9. M. Rabinowitz and T. McMullen, "Phenomenological Theory of Cuprate Superconductivity," *Applied Physics Letters* **63**, 985 (1993).

10. M. Rabinowitz, "Phenomenological Theory of Superfluidity and Superconductivity," *International Journal of Theoretical Physics* **33**, 391 (1994).
11. M. Rabinowitz, "Basic Connection between Superconductivity and Superfluidity," *International Journal of Theoretical Physics* **32**, 565 (1993).
12. M. Rabinowitz, "Phenomenological Theory for Short Coherence Length Superconductivity," to be published in *Chemical Physics Letters* (1993).
13. Y.E. Kim, M. Rabinowitz, J.H. Yoon, and R.A. Rice, "Conventional Nuclear Physics Explanation of the Solar Neutrino Problem," *Intl. J. of Theoretical Physics* **32**, 301 (1993).
14. Y.E. Kim, J.H. Yoon, and M. Rabinowitz, "Condensed Matter Effects on Fusion Neutrino Production Rates," *Modern Physics Letters B* **7**, 953 (1993).
15. Y.E. Kim, M. Rabinowitz, J.H. Yoon, "Condensed Matter Effects on Nuclear Fusion Rates in Laboratory and Astrophysical Environments,"*Intl. J. of Theo.Physics* **32**, 301 (1993).
16. Y.E. Kim, J.H. Yoon, R.A. Rice, and M. Rabinowitz,"Cluster-Impact Fusion and Effective Deuteron Temperature," *Physical Review Lett.ers* **68**, 373 (1992).
17. M. Rabinowitz, "High Temperature Superconductivity and Cold Fusion," *Mod.Phys. Lett. B* **4**, 233 (1990).
18. M. Rabinowitz and D.H. Worledge, "Possible Mechanisms for Fusion in a Solid Lattice," *Proc. EPRI-NSF Workshop* (Wn.D.C.), 28-1.(1989).
19. M.Rabinowitz, "Cluster-Impact Fusion: New Physics or Experimental Error," *Mod.Phys. Lett. B* **4**, 665 (1990).
20. M. Rabinowitz and D.H. Worledge,"An Analysis of Cold and Lukewarm Fusion," *Fusion Technology* ***17***, 344 (1990).
21. Y.E. Kim, "Surface-Reaction Theory of Cold and Warm Fusion," *Proc.Cold Fusion Conf.* (Salt Lake City), **228**, 807 (1990).
22. Y.E. Kim, "Surface Reaction Mechanism for Deuterium-Deuterium Fusion with a Gas/Sold State Fusion Device" *Fusion Technology* **19**, 558 (1991).
23. A.J. Leggett and G. Baym, "Exact Upper Bound on Barrier Probabilities in Many-Body Systems: Applications to 'Cold Fusion'," *Phys. Rev. Lett.*, **63**, 191 (1989).
24. A.J. Leggett and G. Baym, "Can Solid-State Effects Enhance the Cold-Fusion Rate? " *Nature*, **340**, 45 (1989).
25. R.H.Parmenter & W.E.Lamb,"Cold Fusion in Metals,"*Proc.Natl.Acad.Sci.* **86**,8614(1989).
26. R. H. Parmenter and W. E. Lamb, "Cold Fusion in Palladium: A More Realistic Caculation," *Proc. Natl. Acad. Sci.* **87**, 8652 (1990).
27. V.A.Chechin,T.A.Tsarev,M.Rabinowitz,and Y.E.Kim,"Critical Review of Theoretical Models for Anomalous Effects in Deuterated Metals,"to be published in *Intl.J.Theo.Phys.* 1994.
28. D.Bohm. *Quantum Theory*. New Jersey: Prentice Hall, 1951, pp.286-295.
29. L. Turner, "Thoughts Unbottled by Cold Fusion," *Physics Today* **42**, 140 (1989).
30. R.T.Bush,"Cold Fusion: The Trans.Res.Model Fits Data on Excess Heat, Predicts Optimal Trig.Points, and Suggests Nuclear-Reaction Scenarios," *Fusion Technology* ***19***, 313 (1990).
31. M. Jandel,"The Fusion Rate in the Transmission-Resonance Model," *Fusion Technology* **21**, 176 (1992).
32. T.A.Chubb and S.R.Chubb,"Bloch-Symmetric Fusion in PdD_x,"*Fusion Tech.* **17**,710 (1990).
33. S.R.Chubb and T.A.Chubb, "Lattice Induced Nuclear Chemistry," *AIP Conf. Proc.* (Provo, Utah) **228**, 691 (1990).
34. T. Bressani, E.D. Giudice, and G. Preparata, "First Steps Toward an Understanding of "Cold" Nuclear Fusion," *Nuovo Cimento* **101A**, 845 (1989).
35. G. Preparata et al, "Theoretical Ideas on Cold Fusion,"*Proc.Cold Fus.Conf.* (Salt Lake) 91 (1990).
36. G. Preparata, "Fracto Fusion Revisited," *AIP Conf. Proc.* (Provo, Utah) **228**, 840 (1990).
37. G. Preparata, "Some Theories of Cold Nuclear Fusion:A Review," *Fusion Tech.**20***, 82 (1991).
38. G.Preparata,"Cold Fusion: What do the Laws of Nature Allow and Forbid," *Como Conf.Proc.* **33**,453 (1991).
39. R. H. Dicke,"Coherence in Spontaneous Radiation Processes," *Phys. Rev.* **93**, 99 (1954).

40. M.Rabinowitz, Y.E. Kim, G.S. Chulick, R.A. Rice, "Cluster-Impact Fusion: Bridge Between Hot and Cold Fusion?" *AIP Conf. Proc.* **228**, 846 (1990)
41. J. Schwinger,"Nuclear Energy in an Atomic Lattice,"*Proc.Cold Fus.Conf.* (Salt Lake),130(1990).
42. J. Schwinger, "Nuclear Energy in an Atomic Lattice.1," *Z. Phys.D* **15**, 221 (1990).
43. J. Schwinger, "Cold Fusion: A Hypothesis,"*Z. Naturforsch.* **45a**, 756 (1990).
44. K. Szalewicz, J. Morgan, and H. Monkhorst, "Fusion Rates for Hydrogen Isotopic Molecules of Relevance for Cold Fusion," *Phys. Rev..A* **40**. 2824 (1989).
45. C. Petrillo and F. Sacchetti, "A Possible Mechanism for Bulk Cold Fusion in Transition Metal Hydrides," *Europhys. Lett.* **10**, 15 (1989).
46. O. H. Crawford,"Examination of a Proposed Phonon-Coupling Mechanism for Cold Fusion," *Fusion Technology 21*, 161 (1992).
47. G.Lin, R. Kainthela, N. Packham, J. Bockris,"Electrochemical Fusion: A Mechanism Speculation,"*J. Electroanalytic Chem.* **280**, 207 (1990).
48. M. Rabinowitz and E.L. Garwin. *High Electric Field Effects in a Superconducting Accelerator* . Stanford Linear Accelerator Center. SLAC-TN-68-27. 1968.
49. M. Rabinowitz. *Electrical Conductivity in High Vacuum* . Stanford Linear Accelerator Center. SLAC-TN-68-23. 1968.
50. A.B. Karabut, Y. R. Kucherov, and I.B. Savvatimova, "The Investigation of Deuterium Nuclei Fusion at Glow Discharge Cathode" *Fusion Technology* **20**, 924 (1991).
51. R.A. Rice, Y.E. Kim, and M. Rabinowitz, "Comment on 'Electron Transitions on Deep Dirac Levels I." Accepted for publication in *Fusion Technology* (1994).
52. R.A. Rice, Y.E. Kim, M. Rabinowitz, and A.L. Zubarev "Comments on Exotic Chemistry Models and Deep Dirac States for Cold Fusion," *Intl. Conf. Cold Fus.* (Maui) (1993)
53. J.A. Maly and J. Vavra,"Electron Transitions on Deep Dirac Levels I," *Fusion Technology* **24**, 307 (1993).
54. A.O. Barut, "Prediction of New Tightly-Bound States of H_2^+ (D_2^+) and 'Cold Fusion' Experiments," *Int. J. Hydrogen Energy* **15**, 907 (1990).
55. Gryzinsky, M,"Theory of Electron Catalyzed Fusion in Pd Lattice," *AIP Conf. Proc.* (Provo, Utah) **228**, 717 (1990).
56. J-P Vigier,"New Hydrogen Energies in Specially Structured Dense Media: Capillary Chemistry and Capillary Fusion," *ICCF* (Nagoya,Japan) **3**,325 (1992).
57. L. Hoddeson, E. Braun, J. Teichmann, and S. Weart. *Out of the Crystal Maze* . England: Oxford Univ. Press, 1992, p.121.

MITH 94/8

COMMENTS ON THE CRITICISMS OF M. RABINOWITZ

Giuliano PREPARATA

Dipartimento di Fisica - Universita' di Milano
INFN - Sezione di Milano

ABSTRACT: This is a brief comment on the criticisms that M. Rabinowitz makes of my work on the theory of Cold Fusion in his presentation at the ICCF4 (Maui, Hawaii, December 1993).

The origin of the controversy

In his talk at the ICCF4 (International Conference on Cold Fusion 4) on the theories of Cold Fusion M. Rabinowitz blatantly neglected to mention the work that since May 1989 I have carried out on the theory of Cold Fusion, which has received a keen attention, in particular by the "founding fathers" Martin Fleischmann and Stanley Pons. To my polite reminder M. Rabinowitz reacted in a most unexpected and acrimonious way culminated in the statement that: "there are three types of mistakes that one can make in a scientific work: logical, factual and numerical: Preparata has made all of them!".

Being sincerely curious to learn about my mistakes (we are all fallible!) I demanded that in the written version of his talk M. Rabinowitz spell out his objections in detail. These objections have now been written down and, surprisingly, they fill out one page only, half of which concerned

with an alleged improper recognition on my part of the seminal work of R.H. Dicke. The following is my rebuttal of his criticisms.

Superradiance

M. Rabinowitz after an impressionistic description of the dynamics of a QED (Quantum Electro Dynamics) coherent plasma (that I formely called "superradiant"), notices that no mention is made in my papers on Cold Fusion of the inventor of Superradiance, R.H. Dicke.

Noting the gratuitousness of such remark, and its implication of dishonesty on my part, I wish to recall that

(i) Dicke's seminal work [1] has been mentioned in the many lectures that I have given on QED coherence [2,3];

(ii) as a matter of fact I have often been in the position to have to defend myself against an alleged improper use of the word "Superradiance", for many laser physicists could not recognize in what I have been doing the basic aim of Dicke's ideas: to produce a system that radiates strongly and coherently. Indeed the coherent systems that Q-E-D produces spontaneously in matter – the object of my interests – do not radiate in their environment;

(iii) it is for this reason that in my recent work I have abandoned the word Superradiance and used QED coherence instead.

Be that as it may, I believe that Dicke should be really credited to have been the first to comprehend the importance of electrodynamical coherence in macroscopic systems.

The Coulomb barrier

M. Rabinowitz states that by taking an unrealistically large value ($r_n \approx 20F$) for the nuclear radius in the tunneling probability D_T I have made a numerical error that is certainly $>10^2$. Thus instead of $D_T \approx 10^{-40}$, according to him one should have $D_T < 10^{-42}$. While noting that, due to the semiquantitative nature of the analysis performed in Ref. [4], two orders of magnitude are well within the alleged uncertainty of the calculation reported there, I would like to stress that had I chosen $r_n \approx 8F$, as M. Rabinowitz suggests, the reduction in D_T would be not two but one order of magnitude, and this is a real numerical mistake that my critic makes. As for the eq. (26) of Ref. [4], the qualitative nature of the approximation is clearly spelled out, together with order of magnitude estimates for the typical nuclear matrix elements.

As for the "excessive" screening that M. Rabinowitz accuses me of (see in particular Eq. (12) of Ref. [4]), the assumed large plasma oscillations of the $Z_d=10$ electrons of the d-shell of Palladium turn out to be perfectly possible in an electronic shell of thickness $\approx a_o$ (a_o is the Bohr radius), for the system of d-electrons is in equilibrium not only with the Coulomb field of the nucleus and of the remaining $Z-Z_d$ electrons of Pd, but also with the strong coherent electromagnetic field that oscillates in phase with the electron plasma. And are just these oscillations that, far from making the solid collapse, keep it in an ordered configuration, that is much more "airy" than it would be implied by the sheer close packing of Thomas-Fermi atoms.

The question then is: where are the three types of errors that I should have made?

REFERENCES

[1] R.H. Dicke, Phys. Rev. 93 (1954) 99;

[2] G. Preparata, Quantum Field Theory of Superradiance, in Problems of Fundamental Modern Physics, R. Cherubini, P. Dal Piaz and B. Minetti eds., World Scientific (1990);

[3] G. Preparata, Coherence in QCD and QED, in Common Problems and Ideas of Modern Physics; T. Bressani, B. Minetti and A. Zenoni eds., World Scientific (1992);

[4] G. Preparata, Some theories of "Cold" Nuclear Fusion: A Review, Fusion Tech. 20 (1991) 82.

Response to G. Preparata

Mario Rabinowitz
Electric Power Research Institute
P.O. Box 10412, Palo Alto
CA 94303, USA

Abstract

This is a brief response regarding G. Preparata's comments and his theory of Superradiance as related to his controversy at the Fourth International Conference on Cold Fusion (ICCF-4), Maui, Hawaii, December 1993. Even though the critique of Preparata's conceptual, algebraic (computational), and numeric errors was relatively short, in his response he has not really responded to the points raised.

1. Origin of the Controversy

Due to the great number of cold fusion theories and the limited time allowed for presentation, not all of them could be covered in my ICCF-4 talk. As seen by those in atttendance and as recorded on many tapes, at the end of my talk Preparata jumped up and viciously and repeatedly yelled out a charge of "intellectual dishonesty" simply because his theory had not been discussed. I assured him over and over that his work would be analyzed in our written paper. He would not accept this, and still violently insisted that I discuss his paper. Finally in response to his attacks, I replied that there are three kinds of mistakes that one can make in a theoretical paper, **conceptual, algebraic (computational)**, and **numeric**, and that I had found all three in his work.

Our written paper is not solely about Preparata's work and is subject to a page limitation so that only a small fraction of it concerns his work. Due to space restriction, a number of theories are not even covered. We have written a much longer paper [1] which covers most of the cold fusion theories accessible to us.

2. Proper Recognition

Failing to give credit to the work of other people which precedes Preparata's, may be considered a conceptual error.

2.1 Superradiance

Whether Preparata calls it **Superradiance (SR)** or **QED coherence**, by his own admission Preparata's work derives from Dicke's [2] seminal work and Preparata owes due recognition to Dicke. It is rather strange that Preparata claims to credit Dicke in his lectures, but does not bother to do so in his published papers on cold fusion [3-7]. Neither does Preparata give recognition to prior work on the shifted Coulomb potential, upon which he strongly relies in his calculations.

2.2 Shifted Coulomb Potential

The shifted Coulomb potential was developed by Rabinowitz [8-11] to facilitate an accurate approximate calculation of shielding effects on tunneling which could be done with ease analytically without the need for laborious computer calculations. A

screening model of a spherical shell of radius R of negative charge e surrounding each deuteron is the simplest conceptionally as well as computationally since it results in only a shifted Coulomb potential. In mks units this is

$$V = (e^2 / 4\pi\varepsilon)[(1/r) - (1/R)], \quad r_n \le r \le R, \tag{1}$$

where r_n is the nuclear well radius, and ε is the permittivity. Eq.(1) may be interpreted as the first order expansion of the exponentially shielded potential

$$V = (e^2 / 4\pi\varepsilon)\exp[-r/R]. \tag{2}$$

The way Preparata writes the shifted Coulomb potential masks the fact that it is identical to eq. (1). Preparata [6] in his eq. (15) writes

$$V(r) \cong \frac{\alpha}{r_o} - V_o \quad (V_o \cong 100 \text{ eV}), \tag{3}$$

where he is at the classical turning point r_0, and for any other point r_0 becomes r. In mks units, $V_0 = (e^2/4\pi\varepsilon R)$, and $\alpha = (e^2/4\pi\varepsilon)$. With these substitutions, one can see that Preparata's eq.(3) is identical to eq. (1).

3. Other Conceptual Errors

The use of superradiance (SR) may be considered a highly imaginative attempt at reformulating old established theoretical field concepts with possibly new twists. However, this work contradicts quantum mechanics in its overestimates of superscreening to achieve cold fusion (CF).

3.1 Fractoemission Error

Preparata [5] violates the laws of physics in trying to ensure a large enough time for the existence of a large charge density on the sides of a crack in terms of his superemissive (superradiance) model for the solid. This is an application of his SR conjecture to Fractoacceleration, since he has the cracks filled with coherent radiation generated in the solid by plasma oscillations of the nuclei. This is due to an exaggerated overestimate of the amplitude of the plasma oscillations as a free parameter [1]. In addition, according to his scheme highly energetic electrons ~ 100 keV should be emitted from such a process. These electrons have never been detected.

3.2 Screening Error

In the course of their screening estimate [6], an assertion is made that Z electrons orbiting in phase about a Pd nucleus look like a sphere of radius d defined by the dispersion of the plasma oscillations

$$\delta = \left[\frac{\hbar}{2m_e\omega_p}\right]^{1/2} \approx \frac{6.7\times10^{-9}}{Z^{1/4}}\text{cm}. \tag{4}$$

Due to electron oscillations, they assume a d may be covered by a cloud of Z electrons. According to these authors, the screening potential of these electrons takes the form

$$V_{screen} \equiv V_s \approx \frac{-Ze^2r^2}{2\delta^3} \quad \text{for } r \leq \delta. \tag{5}$$

$$\text{At } r = r_o = d(2/Z)^{1/2}, \; V_s + V_d = 0, \text{ since } V_d = e^2/d \text{ at } r = d. \tag{6}$$

With this abnormally large amount of screening the tunneling probability is exceedingly high especially for $E_d \sim 0$.

To understand this anomalous result, note that δ is close to the characteristic dimension of a Thomas-Fermi atom of atomic number Z,

$$R_{TF} = \frac{0.885\hbar^2}{me^2Z^{1/3}} = 4.5\text{x}10^{-9}\,\text{cm} / Z^{1/3} \tag{7}$$

Consequently, the arrangement of Z electrons inside the region $r \leq r_o \sim R_{TF}$ is possible only in the Coulomb potential Ze/r of a nucleus of charge Z, but not in the field of a singly charged d. One of the conceptual errors of this model is having Z electrons take part in steady state screening of the d's Coulomb field. Solids would collapse if such close equilibrium screening were possible.

4. Algebraic or Computational Errors

Preparata's eq.(26) is crucially important [6], but is not derived in detail in any of these papers. Its reliability is thus questionable. For the complex Feynman diagram (Fig. 5) it is not clear what approximations are made for the coupling constants and vertex functions. Preparata's eq. (26) appears overly simple, which suggests either algebraic errors or equivalently inappropriate computational approximations. This can be fully judged if and when he presents a thorough derivation. Preparata's reply in his preceding comments that, "the qualitative nature of the approximation is clearly spelled out" is no excuse for not showing his analysis.

5. Numeric Errors

Preparata [6] makes a number of numeric errors. His value of r_n= 20 fm is too large for the deuteron-deuteron (d-d) nuclear attraction radius. Blatt and Weisskopf (p. 506) list 1.1 fm as the d-d radius [12]. Kaplan (p. 520) lists 2 fm as the d-d radius [13]. Fermi et al (p.116) list 2.8 fm as the d-d radius [14]. Perhaps Preparata meant to use 2 fm rather than 20 fm. With r_n=2 fm, $D_T = 3.12 \times 10^{-43}$, which is smaller than his value of 10^{-40} by a factor of 320. However, using his value of r_n=20 fm, yields a tunneling probability of $D_T = 7.8 \times 10^{-42}$, significantly smaller than the value of 10^{-40} he gets from his eq. (16).

With $r_n < 8$ fm, $D_T < 1.39 \times 10^{-42}$, which differs from his value of 10^{-40} by a factor of >72. This is the factor of > 10^2 numeric error that I pointed out previously. Consequently, his claim of achieving the Jones level of CF is not supported. His disparity [6] with experiment increases considerably more than this factor of 10^2 since as shown above this model has too much shielding. Thus at the top of his p.88 [6] rather than "an enhancement of some 30 orders of magnitude over the tunneling amplitude for molecular deuterium", the resulting number is many orders of magnitude less.

For the convenience of those who would like to check these numbers , Preparata's eq. (16) is

$$D_T^{1/2} \equiv \exp\left\{-(2\mu\alpha r_o)^{1/2}\left[\frac{\pi}{2} - 2\left(\frac{r_n}{r_o}\right)^{1/2}\right]\right\}, \qquad (8)$$

where Preparata had set $\hbar = 1$. Squaring this equation and substituting for α,

$$D_T \equiv \exp\frac{-2r_o}{\hbar}\left\{(2\mu V_o)^{1/2}\left[\frac{\pi}{2} - 2\left(\frac{r_n}{r_o}\right)^{1/2}\right]\right\}, \qquad (9)$$

where in mks units $V_o = 100\text{eV} = 1.60 \times 10^{-17}$ J, $r_o = 1.44 \times 10^{-11}$ m, $\mu = 1.67 \times 10^{-27}$ kg, and $\hbar = 1.05 \times 10^{-34}$ J-sec.

6. Conclusion

Preparatta expresses dismay that the objections to his work took only one page, yet neglects to even address half of the objections. His answers to the other half are inadequate. His responses to the questions raised are about as valid as his recollection of what transpired at Maui.

REFERENCES

1. V.A.Chechin,T.A.Tsarev,M.Rabinowitz, and Y.E.Kim,"Critical Review of Theoretical Models for Anomalous Effects in Deuterated Metals,"*Intl.J.Theo.Phys.* **33**, 619 (1994).
2. R. H. Dicke,"Coherence in Spontaneous Radiation Processes," *Phys. Rev.* **93**, 99 (1954).
3. T. Bressani, E.D. Giudice, and G. Preparata, "First Steps Toward an Understanding of "Cold" Nuclear Fusion," *Nuovo Cimento* **101A**, 845 (1989).
4. G. Preparata et al, "Theoretical Ideas on Cold Fusion,"*Proc.Cold Fus.Conf.* (Salt Lake) 91 (1990).
5. G. Preparata, "Fracto Fusion Revisited," *AIP Conf. Proc.* (Provo, Utah) **228**, 840 (1990).
6. G. Preparata, "Some Theories of Cold Nuclear Fusion:A Review," *Fusion Tech.20*, 82 (1991).
7. G.Preparata,"Cold Fusion: What do the Laws of Nature Allow and Forbid," *Como Conf.Proc.* **33**,453 (1991).
8. M. Rabinowitz, "High Temperature Superconductivity and Cold Fusion," *Mod.Phys. Lett. B* **4**, 233 (1990).
9. M. Rabinowitz and D.H. Worledge, "Possible Mechanisms for Fusion in a Solid Lattice," *Proc. EPRI-NSF Workshop* (Wn.D.C.), 28-1.(1989).
10. M.Rabinowitz, "Cluster-Impact Fusion: New Physics or Experimental Error," *Mod.Phys. Lett. B* **4**, 665 (1990).
11. M. Rabinowitz and D.H. Worledge,"An Analysis of Cold and Lukewarm Fusion," *Fusion Technology 17*, 344 (1990).
12. J.M.Blatt and V.F.Weisskopf. *Theoretical Nuclear Physics*. New York: Wiley, 1952, p. 506.
13. I. Kaplan. *Nuclear Physics*. Mass.: Addison-Wesley, 2nd edition, 1963, p. 520.
14. E. Fermi, J. Orear, A.H. Rosenfeld, and R.A. Sshluter. *Nuclear Physics*. Univ.Chic:1950,p.116.

THE PHYSICAL AND METALLURGICAL ASPECTS OF HYDROGEN IN METALS

R.A. Oriani
Department of Chemical Engineering and Materials Science
The University of Minnesota
Minneapolis, MN 55455

Abstract

To attempt to optimize the anomalous phenomena that today go under the label "cold fusion" the experimentalist should be aware of the many aspects of the behavior of hydrogen in metals and of its entry into and egress from metals. This paper discusses the equilibrium characteristics of the isotopes of hydrogen in metals. The first section discusses the thermodynamics of the terminal solutions of metal-hydrogen systems including the enthalpies of solutions, H-H interactions, effect of third elements, distribution of isotopes between the phases, site occupation, and the molar volume of hydrogen in metallic solutions.

The mobility of hydrogen in a metal lattice is a very large subject. This discussion is restricted to the kinetics of hydrogen diffusion, at and above room temperature, with respect to the variation with temperature, hydrogen concentration, isotopic mass and concentration of third elements. A distinction is made between the effects on the mobility and the effects associated with the non-ideality of the solution. The decrease of the diffusivity due to attractive interactions with lattice defects such as those generated by cold work are discussed in terms of trapping theory. Brief consideration is given to diffusion of hydrogen along grain boundaries and along dislocation cores as well as to diffusion motivated by gradients of electrical potential, of temperature and of mechanical stress.

When hydrogen is absorbed from the molecular gas at fixed pressure and temperature, the overall driving force can be expressed in terms of thermodynamic parameters; the kinetic impediments to the ingress of hydrogen control the rate of entry and these are discussed. When hydrogen is presented to the metal by electrochemical means or by partially dissociated hydrogen gas the driving force for entry into the metal cannot be expressed thermodynamically, although the concept of input fugacity is often used. This concept is discussed and incorrect inferences sometimes made from it are pointed out. The entry and the egress of hydrogen produces mechanical stresses in the metal which modify the thermodynamics of metal-hydrogen systems. They necessitate a distinction to be made between coherent and incoherent phase diagrams, and change the driving force for the exchange of hydrogen between the metal and the environing gas phase. More importantly, the generated stresses can relax by producing

dislocations, grain rotation, cracks and microvoids. Examples of these phenomena are discussed. The generation of such lattice defects interacts in complicated ways with the intrinsic decohesioning effect of dissolved hydrogen to seriously affect the mechanical properties of metals. Some implications of these considerations for cold fusion research are pointed out.

Introduction

In a field like cold fusion in which experimental results are very difficult to reproduce it is beneficial to understand as well as possible the materials used in the experiments and the processes and reactions to which they are subjected. The phenomena accompanying the input of hydrogen into metals and the behavior of hydrogen therein have been investigated to a considerable extent for metals of construction. It appears useful to review that body of information and to show its relevance to metals of interest to cold fusion.

The paper first briefly discusses some equilibrium phenomena for hydrogen in metals that are useful for understanding the subsequent topics. In this section particular attention is given to the generation and the relaxation of mechanical stresses. The second section deals with the mobility of hydrogen within and upon the metal, as affected by lattice imperfections and as driven by various forces. The entry of hydrogen into the metal is considered in the third section with particular attention to the accompanying stress generation and its relaxation by dislocation generation and motion. The concomitant changes of shape and of surface topography are presented and discussed. The concept of input fugacity, which has led to some misconceptions in the past, is explained. The next short section very briefly touches on the manner in which hydrogen affects the mechanical properties of metals. The final section presents some of the implications of the foregoing material for cold fusion research.

For further information on some of the topics touched on in this review the reader is referred the books edited by Alefeld and Volkl (1), Kirchheim et al. (2).

Equilibrium Aspects of Hydrogen in Transition Metals

The Dissociated State of Dissolved Hydrogen

At moderate pressures, the concentration of hydrogen dissolved in solid metals is described to a good approximation by the empirical relation known as Sievert's law

$$c = sp^{1/2} \qquad (1)$$

where c is the concentration of dissolved hydrogen in equilibrium with gaseous hydrogen at pressure p, and s is the Sievert's parameter. If the equilibrium between gaseous hydrogen and dissolved hydrogen $\underline{H}$, is assumed to be

$$\frac{1}{2}H_2(g) = \underline{H} \qquad (2)$$

then one can write

$$a = Kf^{1/2} \qquad (3)$$

where a is the thermodynamic activity of the dissolved hydrogen, $\underline{H}$, f is the fugacity of the gaseous hydrogen, and K is the equilibrium constant for reaction (2). The activity

$$a = \gamma c \qquad (4)$$

at low concentrations where γ is an activity coefficient which at low concentrations is independent of c, and similarly, at low pressures $f = \beta p$, in which β is a fugacity coefficient which at low p is essentially unity. Hence, (1) can be written as

$$c = (K/\gamma\beta^{1/2})p^{1/2} \qquad (5)$$

so that $s = K/\gamma\beta^{1/2} \approx$ constant at a given temperature and over a small concentration range. The experimental verification of Sievert's law for a gas-metal system proves that the molecular gas dissociates upon dissolution in the metal. Furthermore, recalling that $\ln K = -\Delta\overline{G}^\circ/RT$, where ΔG° is the change of Gibbs free energy between standard states for reaction (2), one obtains

$$\ln s = -\Delta\overline{G}^\circ/RT - \ln(\gamma\beta^{1/2})$$

$$= -\frac{\Delta\overline{H}^\circ}{RT} + \frac{\Delta\overline{S}^\circ}{R} - \ln(\gamma\beta^{1/2}) \qquad (6)$$

In eq. (6), $\Delta\overline{H}^\circ$ and $\Delta\overline{S}^\circ$ are, respectively, the partial molal enthalpy and the entropy changes between standard states for reaction (2).

The partial molal enthalpy of solution, $\Delta\overline{H}^\circ$, maybe positive or negative, and metals are conventionally divided into endothermic and exothermic absorbers of hydrogen. There is no fundamental significance in this classification as to the qualitative aspects of the electronic interaction between $\underline{H}$ and the metal. It only categorizes metals into the group for which the energy of electronic interaction with dissolved hydrogen is a smaller, but negative quantity, than the energy of dissociation of molecular hydrogen, and into the class for which the opposite is the case. The important phenomenological distinction between the groups is that metals for which $\Delta\overline{H}^\circ < 0$ display a concentration (solubility) decreasing with increasing temperature, and those for which $\Delta\overline{H}^\circ > 0$ have the opposite behavior. As the concentration of dissolved hydrogen is increased, the activity coefficient of the dissolved hydrogen varies because of interactions between the hydrogens and because the electronic interaction between the hydrogen and the host

metal varies with concentration. This is reflected in the composition dependence of the quantities $\Delta\overline{H} = \overline{H} - \overline{H}°$ and $\Delta\overline{S} = \overline{S} - \overline{S}°$ for the dissolved hydrogen. As c increases a hydrogen-containing phase other than the terminal solid solution usually develops. This topic will be considered in a subsequent section.

The $\Delta\overline{G}°$ values, and hence the equilibrium constants, K, for reaction (2) are functions not only of temperature but also of the isotopic mass of hydrogen. For example, for the palladium-hydrogen* system

$$\ln K_H = \frac{1163}{T} - 6.45$$

and

$$\ln K_D = \frac{949}{T} - 6.40$$

in which the temperature T is in degrees Kelvin (3). Also, according to (4), for tritium, T,

$$\ln K_T = \frac{832}{T} - 6.25.$$

Consequently, for the same concentration and temperature, deuterium (D) and tritium (T) have higher equilibrium pressures in Pd than does protium (H). If one defines the equilibrium distribution of the isotopes H and D between the palladium (Pd) and the gas phase (g) as (n_i = number of i atoms):

$$\alpha^{g}_{Pd}(D,H) = \frac{(n_D / n_H)_g}{(n_D / n_H)_{Pd}} = \frac{(2p_{O_2} + p_{HD}) / (2p_{H_2} + p_{HD})}{(n_D / n_H)_{Pd}},$$

the measurements of Clewley et al. (5) yield, as the average of measurements on β-phase Pd(H),

$$\ln \alpha^{g}_{Pd}(D,H) = \frac{178}{T} + 0.175 = 2.16 \text{ at } 298 \text{ K}.$$

The equilibrium separation factor for tritium and protium in Pd was measured by Sicking (6) as

$$\ln \alpha^{g}_{Pd}(T,H) = \frac{320}{T} - 0.075 = 2.71 \text{ at } 298 \text{ K}.$$

---

* In this review, the term "hydrogen" is usually employed generically to signify all of the isotopes of hydrogen. However, in some portions where isotopic differences are discussed, "hydrogen" refers to protium, the lightest isotope.

The equilibrium separation factor for two isotopes between liquid water, L, and palladium can be defined as $\alpha^{L}_{Pd}(D,H) = (n_D/n_H)_L / (n_D/n_H)Pd$. Sicking (7) measured $\alpha^{L}_{Pd}(D,H) = 9.0$ at 298 K, and $\alpha^{L}_{Pd}(T,H)$ has been estimated (8) as 12.0 at 298 K. Note that the equilibrium distribution is different from the kinetically determined separation factors for cathodic deposition. For H and D on Pd-Pg alloy, the electrolytic separation factor, $\alpha = 9$ to 16 (9). See also ref. (10). Thus, in the case of palladium, the heavier isotope is favored in the gas phase.

At 298K and 1 bar of hydrogen pressure, $n_D/n_{Pd} = 0.65$ and $n_H/n_{Pd} = 0.7$. Similarly, deuterium adsorbed on Pd has a larger equilibrium pressure than does protium adsorbed on Pd at comparable coverage (11). However, Pd must be considered anomalous since other metals since other metals exhibit the opposite behavior; deuterium dissolved in Ta, Nb, or V exhibits smaller equilibrium pressures than does protium dissolved in these metals at the same concentrations and temperatures (8).

Interstitial Site Occupancy

Because the volume of a hydrogen atom, on a molar basis, is about 0.3 cm^3/mol, much smaller than the molar volume of a transition metal, the observed expansion of a metal lattice upon dissolution of hydrogen is evidence that the solution is not substitutional. That hydrogen occupies interstitial positions in metal lattices has been demonstrated by neutron diffraction in several cases and inferred from other evidence in other cases (1). The face-centered cubic lattice has one octahedral interstitial site per metal atom (at 1/2, 0, 0 and equivalent positions), and two tetrahedral interstitial sites per metal atom (at 1/4, 1/4, 1/4 and equivalent positions). The body-centered cubic lattice has three octahedral interstitial sites per metal atom (at the centers of the cube faces and of the cube edges) and six tetrahedral interstitial sites per metal atom (at 1/2, 1/4, 0) and equivalent positions). In the f.c.c. lattice the octahedral positions have the larger free volume, whereas in the b.c.c. lattice the tetrahedral sites are the larger.

Table 1 collects information on the location of dissolved hydrogen in various metals, and the magnitudes of the partial molal volumes, $\bar{V}$, of the dissolved hydrogen, where $\bar{V} = (\partial V/\partial m)$ at constant number of metal atoms, temperature, and pressure; V is the volume of the metallic solution and m is the number of moles of hydrogen introduced into the metallic system. Introduction of a hydrogen atom into an interstitial position increases the volume of the system by about 1/5 of the amount of the volume increase caused by the addition of one metal atom.

The displacement of the metal atoms by the introduction of a hydrogen atom can be represented (13) by virtual forces (the Kanzaki forces) applied to each lattice atom to reproduce the actual displacement of the metal atom. The Kanzaki force distribution is describable by a multipole expansion of which the dipole term, P_{ij} is usually sufficient, where

$$P_{ij} = \sum_m f_j^m x_i^m$$

with f_j^m being the Kanzaki force applied to the m'th atom situated at the distance x^m from the hydrogen atom. Because the octahedral sites of the f.c.c. lattice provide six metal atoms equidistant from the occupying hydrogen atom, P_{ij} is isotropic. However, around the octahedral site of the b.c.c. lattice two metal atoms are farther than the other four from the occupying solute atom so that the dipolar character of the force distribution, and the orientation of the dipole must in general be taken into account. In the case of interstitial carbon atoms in b.c.c. iron, the dipolar distortion is important and is responsible for the Snoek effect (13). In any case, for a random distribution of n_H hydrogen atoms in interstitial sites in a metal of atomic volume Ω, the volume change due to the hydrogens as measured by the change of lattice parameter, a, is

$$3\frac{\Delta a}{a} = \frac{\Delta V}{V} = (n_H/3\Omega)\kappa \text{Trace } P_{ij},$$

where κ is the compressibility.

To obtain an intuitive feel for the stress state produced by the occupation of an interstitial site by hydrogen (or other solute) it is useful to consider the "ball-in-hole" model in continuum elasticity (29). Consider an incompressible sphere (simulating the solute atom) fitted into a spherical cavity in a matrix (the cavity simulates the interstitial site), the cavity being smaller than the ball. If ΔV_1 is the volume change of the cavity occasioned by forcing in the incompressible ball, the outer free surface of the matrix will sweep over an additional volume (29)

$$\Delta V_2 = \frac{3(1-\nu)}{1+\nu}\Delta V_1$$

where ν is the Poisson ratio of the matrix. For a typical value of ν of 0.3, ΔV_2 is larger than ΔV_1 by 50%. This result is a consequence of the boundary condition that the outer surface of the matrix be stress free. Thus, the volume of the body increases by an amount larger than that required to accommodate the solute atom; this is the origin of the increase in lattice parameter produced in a metal lattice upon a absorption of hydrogen. It should be noted that whereas the misfitting ball is under compression by the expanded matrix, the matrix has zero hydrostatic component of stress and its external surface has zero stress. The argument is not changed when more than one center of dilatation is considered. A homogeneous distribution of interstitial solutes produces a matrix in which the interstitial sites are larger than in the solute-free matrix. It follows that the partial molal volume of an interstitial solute should decrease with increasing concentration (8). It is worth noting at this point that although equal concentrations of hydrogen may be injected into a metal by equilibrating with high-pressure molecular gas or by subjecting the metal to cathodic charging, the internal thermodynamic state of the dissolved hydrogen will be different in these two conditions. The large gas pressure upon the metal in the first case will decrease the expanding effect of the interstitial hydrogen by compressing the metal, whereas in the second case because of the absence of pressure on the external surface of the metal there will not be any decrease of the intrinsic expanding effect.

The occupation by hydrogen of interstitial sites, which necessarily constitute a finite population in any one specimen, leads to a thermodynamic description of the dissolved hydrogen in terms of Fermi-Dirac statistics. Thus, the activity of the dissolved hydrogen must be expressed more generally than by eq. (4) as

$$\mu = \mu^o + RT\ln a = \mu^o + RT \ln\left(\frac{\gamma\theta_1}{1-\theta_1}\right) \qquad (7)$$

Here, $\theta_1 = n_H/n_{s1}$, where n_H is the number of dissolved hydrogen atoms and n_{s1} is the number of interstitial positions of the class that produce the lowest Gibbs free energy state. In palladium s_1 would represent the octahedral positions. The important consequence of this is that as $\theta_1 \rightarrow 1$ the chemical potential, μ, of the interstitial hydrogen rises to very large values. Indeed, the source of the hydrogen cannot have a sufficiently high chemical potential to cause the filling of all of the lowest-energy class of sites. Therefore, a sufficiently large μ_{gas} would cause the next-higher energy class of interstitial sites to become partially populated at $\theta_1 < 1$. In the case of palladium one would predict some tetrahedral site occupancy at θ_1 (octahedral) < 1. Although data appear not to be available to verify this assertion about palladium, neutron diffraction (30) on V(D) at $n_D/n_v = 0.5$ showed that about 90% of the dissolved deuterium atoms occupy tetrahedral sites in the b.c.c. lattice, the rest being on octahedral positions. Similar results were found by Chervyakov et al. (31) with $n_D/n_v = 0.8$ in which 7% of the deuterium atoms are located on octahedral sites. It is also possible that interactions between the dissolved hydrogen atoms cause energetic distinctions between subclasses of interstitial sites of one symmetry type. Taking only one example, in the Ta (H) phase about the composition $n_H/n_{Ta} = 1/2$, the hydrogens occupy tetrahedral sites on only alternate $(\bar{1}10)$ planes (32,33), which of course means that the H atoms form an ordered sublattice. Hydrogen atoms in excess of $n_H/n_{Ta} = 1/2$ are accommodated in tetrahedral sites in the adjacent $(\bar{1}10)$ planes.

Hydrogen-Metal Interactions

The enthalpy of solution of hydrogen from the molecular gas into the metal is composed of two terms: the energy of dissociation of the molecule, which is, of course, independent of the nature of the metal, and the energy of interaction between the dissolved hydrogen atoms, and between the hydrogen and the metal. The latter term varies much from metal to metal and this variation is responsible for the phenomenological separation of metals into the two classes of endothermic and exothermic "occluders" of hydrogen. The latter term has been much investigated, especially for palladium, and presents challenging theoretical difficulties. The interests of the intended audience or this paper are served by a description of the broad picture for hydrogen in the transition metals.

Because measurements of physical properties such as the electronic specific heat, the magnetic susceptibility, the electrical resistance, the thermoelectric power, photoemission, etc., show much larger variation with hydrogen concentration than can

be attributed simply to the lattice expansion caused by hydrogen, it is clear that hydrogen strongly perturbs the electronic structure of the host metals. Although details differ from one metal to another, the broad picture is that the 1s- electron that accompanies the hydrogen nucleus enters the s- and d- bands of the host metal changing the density of states at the Fermi surface and causing shifts of the energy bands. The Fermi electrons then concentrate around the positive hydrogen nucleus to produce a closely screened entity that may loosely be thought of as a neutral atom, although the screening electrons are not in bound states.

Because the electron energy bands are affected there are long-range interactions between the dissolved hydrogens, and because of the localized heaping up of Fermi electrons about the hydrogen nuclei there are also short-range interactions among the hydrogens. Fritsche et al. (34) adduce repulsive interactions between the two hydrogens for the d-holes in the electronic structure of the Pd atom that is the common neighbor to both hydrogens. On the other hand, the hypothesis of attractive interactions between adjacent hydrogens produces a good description of the thermodynamic properties of Pd(H) solutions (8). The attractive interaction has been ascribed to the oscillatory decay of Fermi electron density about the hydrogen nucleus (35) (the so-called "Friedel wiggles"), and to elastic intereactions (36). Attractive interactions between nearest-neighbor hydrogens are consistent with internal friction experiments on Pd(H) (37) which are interpreted as reorientation of H-H pairs, and also with the evidence of hydrogen cluster formation in Pd(H) obtained by inelastic neutron scattering (38). Similarly, long-range interactions between hydrogens and also between hydrogen and other solutes in a metal lattice have been discussed in terms of electronic and elastic interactions. Concentrations of Ag, Sn, Au, B, and Pb increase the concentration of H in palladium for a given hydrogen gas pressure and temperature. This effect is attributed (8) to the expansion of the interstitial sites caused by these solutes (the lattice parameter is increased) so that it costs less energy to place hydrogens in the enlarged sites. However, the solubility enhancement by these solutes occurs only at low hydrogen contents. At larger hydrogen levels these solutes decrease the hydrogen solubility because the metal solutes fill up some of the empty 4d states of the palladium so that fewer electrons coming in with the hydrogen nuclei can be accommodated by the 4d-holes (8). Rh and Ni contract the Pd lattice so that they reduce hydrogen solubility at low hydrogen levels. Rh increases the number of empty 4d states available to hydrogen, so that the solubility of hydrogen is increased at high hydrogen levels.

Since hydrogen changes the local and the global electronic structure of the metal in which it resides, as well as increasing the mean separation between the atoms of the host metal, it is not surprising to find that the cohesive force (the force needed to increase the interatomic distance) between the metal atoms is affected by hydrogen. As yet, no experiment has been devised to measure this effect, but several different theoretical approaches agree that hydrogen reduces the cohesive forces in transition metals. A molecular-dynamics study (39) of Pd(H) has demonstrated that hydrogen reduces the bond strength between Pd atoms by filling antibonding states in the 4d band. Cluster calculations (40) and the embedded atom method (41) have verified that

hydrogen reduces cohesion in several transition metals. McMullen et al. (42) used an effective-medium model to calculate the force required to rigidly separate two halves of a 3d-metal crystal, and have shown that hydrogen decreases the necessary forces for Ti, V, Mn, Fe, Cu, and Ni among others. Fritsche and Muller (43) have demonstrated by cluster calculations that hydrogen weakens Pd-Pd bonds by decreasing the electron density between the metal atoms.

Interactions of Hydrogen with Lattice Imperfections

Metal lattices exhibit structural defects of various dimensionalities. "Zero-dimensional" defects are vacancies and self-interstitials of which the former can have concentrations consistent with thermodynamic equilibrium, increasing with increasing temperature. Both defects can be generated by plastic deformation and vacancies can be quenched in from high temperatures to produce populations in excess of the equilibrium value. Data for the interaction between these defects and dissolved hydrogen are scarce. Kirchheim (44) found that at concentrations of hydrogen in Pd below 40 ppm, the partial molal volume of hydrogen is a negative quantity; instead of the lattice expanding upon the absorption of hydrogen the lattice contracts. The only way to understand this is by the hydrogen atom occupying a vacancy where the H-Pd distance is large enough to be in the attractive portion of the H-Pd interaction curve. Kirchheim deduced that of all structural defects vacancies in Pd provide the strongest attractive interaction with hydrogen, although a quantitative evaluation was not attained. At concentrations above 40 ppm hydrogen expands the palladium lattice (44), as already discussed, because the expansion of the normal interstitial sites overcomes the negative effect of hydrogens in substitutional vacancies. Evidence exists that vacancies interact attractively with hydrogen dissolved in copper (45) and in gold (46).

One-dimensional, or linear defects are the dislocations produced in metals by plastic deformation and many other processes. The largest body of information on hydrogen-dislocation interaction in metals that exists is for iron and its alloys. Hydrogen dissolved in b.c.c. iron is strongly held at the cores of edge and of mixed-character dislocations, and less strongly at the cores of screw dislocations (see Table 2). Additionally, hydrogen is attracted elastically to the dilatant side of edge dislocations, the interaction energy varying inversely with distance. Because other larger interstitial solutes interact more strongly with dislocation cores, hydrogen in iron does not interact with dislocations upon which nitrogen is adsorbed (49).

Kirchheim (50) has evaluated the interaction energy of hydrogen dislocations in Pd. At the core of an edge dislocation the large interaction energy (see Table 2) includes a H-H attractive interaction energy of 18.5 kJ/mol H. At larger distances from the core, the interaction energy does not have a contribution from the H-H interaction, and the remainder decreases as the reciprocal of the distance. The additional population of hydrogens due to the attractive interaction with dislocations makes a significant contribution in Pd only at very small hydrogen concentrations.

Only sparse information is available concerning interaction of hydrogen with dislocations in other metals. Thomas (51) evaluated this interaction in nickel as 9.6 to 19.2 kJ/mol. Although a quantitative evaluation was not made, Ohma et al. (54) demonstrated attractive interaction between tritium and dislocations in f.c.c. stainless steel by autoradiography. Despite the absence of data for most metals, one can be sure that in any metal that exhibits a positive partial molal volume of hydrogen there is an attractive interaction between dissolved hydrogen and dislocations, leading to highly concentrated distribution of hydrogen along the dislocation line and to smaller excess concentrations in the tensile stress region about the dislocation.

Two-dimensional structural defects in a metal lattice include stacking faults, grain boundaries, interphase boundaries and the internal surfaces of microvoids and microcracks. That hydrogen dissolved f.c.c. iron interacts attractively with stacking faults was deduced (55) from the reduction of the energy needed to create a stacking fault in hydrogen-containing iron. Grain boundaries in iron (47), in Pd (52), in nickel and cobalt (53) have been shown to adsorb excess populations of hydrogen. Mutschelle and Kirchheim (52) have shown that there is a Gaussian distribution of interaction energies between dissolved hydrogen and grain boundaries in Pd, reflecting the variety of binding sites in grain boundaries. The mean interaction energy is 5.3 kJ/mol H, with the width of the Gaussian distribution being 15 kJ/mol so that at some grain boundary sites there are repulsive interactions. The heterogeneity of binding sites on grain boundaries for tritium was qualitatively demonstrated by Laurent et al. (56) for b.c.c. iron. It seems safe to assert that grain boundaries in any metal will exhibit attractive interactions for dissolved hydrogen.

Interfaces between second-phase particles and the crystalline iron in which they reside have been shown (see Table 2) to adsorb excess populations of hydrogen. Unfortunately, measurements in other metals seem not to be available. Dissolved hydrogen will also adsorb upon internal free surfaces in metals, meaning the surfaces bounding microvoids and microcracks. These defects in metals can develop in the processing and fabrication of the metals as well as during the charging of hydrogen into the metal (see below). These internal surfaces would adsorb hydrogen to the same extent as would external surfaces of the same metallic composition in contact with the molecular hydrogen gas producing the concentration of lattice-dissolved hydrogen. In addition, the volume of the internal cavity (a 3-dimensional defect) would at equilibrium acquire a molecular gaseous hydrogen concentration consistent with the input fugacity of the external hydrogen environment.

The interactions between dissolved hydrogen in a solid metal and structural imperfections in that metal can in general be divided into two categories, chemical and elastic. The latter refers to positions sufficiently far from the imperfection so that the atomic displacements from the positions in the perfect lattice are small, and linear elasticity may be applied to a sufficient degree of approximation. The former category refers to positions where the atomic displacements are large, e.g., at dislocation cores and internal interfaces. Calculations of the excess hydrogen concentrations in the elastic region about a structural imperfection are based upon the thermodynamic relation

between the chemical potential, μ_s, of an interstitial solute such as hydrogen at a position in a solid and the stress state at that position (57). The local stress may arise as a result of externally applied mechanical forces or because of structural imperfections. In either case, the chemical potential, of an interstitial solute in the stressed body is related to the chemical potential, $\mu_s(o)$, of the solute at the same concenration in the relaxed (zero stress) body as

$$\mu_s - \mu_s(o) = \sum_i \sum_j \int_o^{\sigma_i} [V_m s_{ij} + (1-x_s) V_m \partial s_{ij} / \partial x_s] \sigma_i d\sigma_j - V_m (1-x_s) \sum_i \sigma_i \partial \varepsilon_i / \partial x_s \quad (8)$$

in which V_m is the molal volume of the solid solution of solute mole fraction x_s having the isothermal compliances s_{ij} ($=\partial\varepsilon_i/\partial\sigma_j$). The σ_i ($\sigma_i > 0$ for tensile character)are the elements of the symmetric part of the stress tensor, and the ε_i are the corresponding elements of strain.

The first term of eq. 8 leads to terms of the form $\sigma^2 \overline{V}$ /2E where E is the Young modulus; these terms are unimportant except where the stress is a significant fraction of E. Dropping the first term and using x, y and z as the Cartesian coordinates, eq. (1) may be written as (57)

$$\mu_s - \mu_s(o) = -V_m(1-x_s)\{[\sigma_{xx} \frac{\partial \varepsilon_{xx}}{\partial x_s} + \sigma_{yy} \frac{\partial \varepsilon_{yy}}{\partial x_s} + \sigma_{zz} \frac{\partial \varepsilon_{zz}}{\partial x_s}]$$

$$+ [2\sigma_{xy} \frac{\partial \varepsilon_{xy}}{\partial x_s} + 2\,\sigma_{xz} \frac{\partial \varepsilon_{xz}}{\partial x_s}\; 2\sigma_{yz} \frac{\partial \varepsilon_{yz}}{\partial x_s}]\} \quad (9)$$

The diagonal ε terms represent the fractional increase in length of elements initially parallel to the coordinate axes. The off-diagonal elements represent half the decrease of the angle between the two elements initially along the axes indicated by the subscripts. If an interstitial solute dilates the lattice isotropically, e.g., hydrogen in palladium, the off-diagonal terms of eq. (9) may be omitted, and if in addition σ_{ii}/E is small, eq. (9) reduces to

$$\mu_s - \mu_s(o) = -\frac{\overline{V}_s}{3}(\sigma_{xx} + \sigma_{yy} + \sigma_{zz}) \equiv -\overline{V}_s \sigma_h \quad (10)$$

in which $\overline{V}_s$ is the partial molal volume of the interstitial solute. The thermodynamic theory was experimentally verified by Wriedt and Oriani (17) for the case of hydrogen in silver-palladium alloy under uniaxial stress ($\sigma_{xx} = \sigma_{zz} = 0$), for which $\overline{V}_H$ was an already known quantity.

It is emphasized that the above equations relate the chemical potential of the interstitial solute in the stressed body to that in the relaxed body at the same concentration. The equations can be converted to show the variation of concentration with stress for the same chemical potential of interstitial solute in the stressed as in the unstressed body. For example, eq. (10) yields, for uniaxial stress

$$\left(\frac{\partial \ln c_s}{\partial \sigma_{xx}}\right)_{\mu_s} = (\bar{V}_s / 3RT) / (\partial \ln a_s / \partial \ln c_s)_{\sigma_{xx}} \qquad (11)$$

where a_S and c_S are the activity and concentration of solute s, respectively. Thus in an inhomogeneously stressed body, such as the neighborhood of a dislocation, the equilibrium distribution (i.e., iso-activity) of hydrogen is non-uniform, being larger at positions of greater tensile stress. Similarly a spherical particle which expands the matrix produces stresses σ_1 and σ_2 which are decreasing functions of distance, r, from the center of the particle. In the matrix the stresses σ_1, σ_2 are orthogonal to each other and to σ_r which lies along the polar coordinate with origin at the particle center. Because $-\sigma_1 = -\sigma_2 = 1/2\sigma_r$, the hydrostatic component of stress (i.e., 1/3 the trace of the stress tensor) is zero, so that only the first term of eq. (8) persists. At the surface of the spherical particle, σ_r exerts a hydrostatic negative stress (i.e., a pressure) thereby raising the chemical potential of the solid solution of the particle. Suppose that the particle is a stoichiometric hydride $MH_{n+\delta}$, meaning that the compound MH_n tolerates only very small values of δ, the deviation from stoichiometry. In this case, the variation of concentration with distance, r, is given by (57).

$$\frac{c_H^\alpha(r)}{c_H^\alpha(\infty)} = \exp\left[-\frac{3\bar{V}_H^\alpha}{8G_\alpha RT}\left(\frac{12G_\alpha a^3(\Delta/a)}{r^3\left(3+4K_\beta G_\alpha\right)}\right)^2\right] \qquad (12)$$

In eq. (12) α refers to the matrix and β to the hydride, G is the shear modulus and K the compressibility, a is the relaxed radius of the hydride particle, and Δ is the difference between the relaxed radii of the hydride and of the hole in the matrix. $c_H^\alpha(\infty)$ is the hydrogen concentration far from the β particle, and is larger than c_H^α in equilibrium with unstressed β. Eq. (12) shows that the c_H^α is smaller near the particle than far from it. Very complicated expressions result (58) for the case where the particle can have a wide variation of composition.

Phase Diagrams and Phase Transitions

Metal-hydrogen systems exhibit phase diagrams of varying complexity, but the purpose of this section is not to present details of individual phase diagrams but only to describe some aspects of importance to understand behavior during charging in hydrogen or evolving hydrogen from a pre-charged metal.

Effect of Isotopic Mass. The isotopic mass affects not only the concentration of hydrogen in a metal at a given temperature and hydrogen pressure (see the section called The Dissociated State of Dissolved Hydrogen) but also the composition-temperature boundaries between solid phases. The physical reasons for the effect of isotopic mass on phase boundaries are related to differences in the zero-point energies of the dissolved hydrogen isotopes, the differences in the lattice expansions produced

by the isotopes, and the differences produced in the phonon spectrum. The reader is referred to ref. 18 for discussion of specific cases.

Effect of Lattice Stresses. The large mobility of hydrogen dissolved in a lattice, the metal atoms of which are virtually static by comparison, makes it very probable that the transition from one phase to another will initially be accomplished by the motion of only the hydrogen atoms. Consider the Pd-H system. Below the critical temperature of 292°C, this system is characterized by a miscibility gap within which two f.c.c. phases of different composition coexist. The one with the lower hydrogen content, usually called the α-phase has at 20°C $n_H / n_{Pd} = 0.008$ whereas the hydrogen-rich phase, usually termed the β-phase, has $n_H / n_{Pd} = 0.607$. The H_2 gas pressure in equilibrium with these co-existing solid phases is about 0.07 atm (59). The α and β phases have the same lattice symmetry (strictly speaking they represent portions of one phase field) but very different specific volumes; the change of volume for the transition $\alpha \rightarrow \beta$ is in fact 1.57 cm^3/mol H (8). Hence the transition involves a clustering together of hydrogen atoms such that 125 Pd atoms which in the α-configuration have only one H atom among them, in the β-configuration the 125 Pd atom cluster has nearly 76 H atoms for which the lattice parameter is 0.4025 nm instead of 0.3894 nm.

Because this cluster of Pd atoms has expanded within the α-phase, mechanical stresses must be generated analogously to the misfitting ball-in-hole model discussed in a previous section. The only way to mitigate the stresses is by removing Pd atoms of the surrounding α-phase to the external surface of the specimen. Hence, two extreme (or idealized) cases exist, one in which the stresses are not at all relieved and the other in which all stresses are relieved. This gives rise to two kinds of equilibrium, and hence to two kinds of phase diagrams the coherent and the incoherent equilibrium diagrams. It is emphasized that these are idealizations and that in practice a phase distribution of mixed character is achieved, the degree of stress relief being dependent on details of the experimental procedure.

In the idealized coherent equilibrium between two phases of a metal-hydrogen system one phase has grown within the parent phase without any diffusive motion of the metal atoms and without any plastic deformation. Hence, the lattice lines are continuous, although not straight, between one phase and the other, and the interface between the two is characterized by a change of composition and an inflection point in the lattice parameter-distance variation. The resulting coherency stresses change the chemical potential of the dissolved hydrogen in both phases along the principles described in a previous section, so that the compositions of the coexisting phases in equilibrium with a given hydrogen gas fugacity have values different from those that would exist in the absence of stresses at the same hydrogen gas fugacity. Furthermore, for a single crystal with free surfaces the compositions of coherent coexisting α and β phases would be functions of the shape of the crystal (60). This results from the coherency stresses being functions of the image forces at the free surfaces. For a long thin wire the effect of coherency stresses is negligible so that the compositions of coexisting coherent phases would be the same as for a fully incoherent equilibrium.

The coherent equilibrium is in general a metastable condition of higher free energy because of the elastic energy, than that of the corresponding incoherent equilibrium. The change from coherency to incoherency necessitates the nucleation of dislocations which can move the matrix atoms, by slip, away from the neighborhood of the coherent second-phase particle to free surfaces or to grain boundaries. The nucleation cannot occur until enough coherency elastic energy has accumulated by the growth of the coherent particles to "pay" for the self-energy of the dislocations. In general, coherency is lost by the formation of dislocations at the interface between the α and β phases and by the generation of dislocations which ideally should carry metal atoms to the free surface or to grain boundaries. However, this transport is never complete, so that the system usually ends up with large dislocation densities distributed throughout the metal grains. Although the excess free energy in the coherent equilibrium is considerably reduced by the transition to incoherence, it is not totally removed since the dislocations represent a free energy excess over the dislocation-free state. The coherence-incoherence transformation is the chief reason for the well-known hysteresis observed when trying to establish phase boundaries in metal-hydrogen systems. Coherency stresses and their reduction by dislocation generation occurs both in hydrogen charging into, and discharging from, a metal whenever more than one phase is produced by the ingress or egress of hydrogen (18, 61). The generated dislocations modify the mechanical properties, as is discussed in a subsequent section, and can affect microcracking of the metal.

Kinetic Aspects of Dissolved Hydrogen

Diffusion in the Volume of the "Perfect" Lattice

It is well known that hydrogen in metals diffuses more rapidly than any other solute. It may be less widely recognized that the mechanism of the rapid diffusion is not fully understood. Because hydrogen atoms have small masses quantum effects can be expected to play a role, and the fact that the activation energy for the diffusion of hydrogen in Nb, Ta, and V is a function of isotopic mass strengthens this expectation.

Kehr (62) points out that four different diffusion mechanisms should be considered for hydrogen in metals. At the lowest temperatures, hydrogen may be delocalized as a band state and its propagation in the band state would be limited by scattering by phonons and by lattice defects. At higher temperatures hydrogen is localized at specific interstitial positions and thermal energy is required to change location. One possibility is tunneling from one to another interstitial site, thermal energy being needed to bring the energy levels of both sites to the same value. The second possibility for hopping involves an activation energy to go over the energy barrier between sites. This is the classical mechanism of diffusion, and should be dominant at higher temperatures. At the highest temperatures the hydrogen would populate states above the energy barriers and its diffusion would resemble the diffusion in a dense gas or liquid. Many collisions would occur with the thermal fluctuations of the host lattice. The temperature regimes in which one or another mechanism operates are not sharply defined. This paper does

not discuss the degree to which experimental measurements support one or another mechanism. Readers interested in this aspect are directed to refs. (62) and (2).

Table 3 collects diffusivity data for the isotopes of hydrogen at low concentrations in various metals in terms of the pre-exponential term, D_o, and the activation energy, E_a, of the Arrhenius equation $D = D_o \exp(-E_a/RT)$. We note that the ratio of diffusivity of H and D in Pd does not follow the classical prediction that $D_H/D_D = (m_D/m_H)^{1/2}$, and furthermore the E_a depends on isotopic mass. This deviation is not fully understood, but it is affected by the difference in the anharmonic character of vibration of the hydrogen isotopes.

The diffusivity of H in Pd, in PdAg alloys, and in Nb and Ta is a weak function of hydrogen concentration, generally decreasing with increasing hydrogen. Most of the reason for this dependence is the non-ideality of the metal-hydrogen solid solution. The diffusivity as measured by the relaxation of a concentration gradient, is defined as

$$D = kTB(d \ln a / d \ln x) \qquad (13)$$

where x is the mole fraction of the mobile solute and a is its thermodynamic activity. B is the mobility of the solute. Because the relation between activity and concentration varies with concentration, D will vary. If a high hydrogen concentration is achieved by equilibrium with high pressure gaseous hydrogen one may ask if the compression of the lattice by the imposed pressure affects the mobility. Baranowski (68) asserts that this affect is small. The mobility can also be concentration dependent because with increasing hydrogen concentration the number of vacant interstitial positions into which the hydrogen can jump diminishes, and also the metal atom-hydrogen interaction changes as the lattice expands with increasing hydrogen concentration. A particularly interesting and large effect of hydrogen concentration on the diffusivity is observed in the vicinity of the critical concentration and temperature. In that region the diffusivity of hydrogen can decrease by several orders of magnitude because d ln a/d ln x approaches zero. The mobility is not anomalous in that region.

The Arrhenius relation is not obeyed over the investigated temperature range by H in Nb (63) but it is obeyed by D in Nb. Disobedience is found also for H and D in Ta. These deviations from the Arrhenius relation are thought to be related to changes in the mechanism of diffusion.

Two- and One-Dimensional Diffusion

Despite the importance of the diffusion of hydrogen, both in molecular and atomic forms, upon external surfaces of metals to the understanding of the absorption of hydrogen from the gas phase into the lattice, very little data exist on this topic. Gomer et al. (69) applied field emission microscopy to hydrogen on a tungsten surface, and found that hydrogen exhibits a mobility dependent on the degree of surface coverage. At coverages larger than one-half monolayer the activation energy for migration is 25

kJ/mol H, but as coverage decreases the activation energy rises to 40, and at very low coverages to 67 kJ/mol H. The reason for this variation is that at low coverages only sites characterized by large adsorption energy are occupied; the adsorbed hydrogen is tightly bound so that its mobility is restricted. Larger coverages put hydrogen on surface sites with smaller binding energies so that the mobility is greater. Nickel was also investigated by the same group (70) who found 30 kJ/mol H for the E_a of surface diffusion of hydrogen independent of coverage. This was interpreted as showing that there are very few tight-binding sites on the surface of the nickel. This is reasonable because the field-emitter tip of this f.c.c. metal consists of terraces and steps of only close-packed layers. From the data one can calculate that at 37°C, $D_H \approx 4 \times 10^{-8}$ $cm^2 s^{-1}$, which may be compared with $D_H = 4.5 \times 10^{-9}$ cm^2 s^{-1} for the diffusivity of hydrogen in the volume of Ni at the same temperature (71).

The same picture as for tungsten emerges in the investigation by Arantes et al. (72) of the diffusion of hydrogen along grain boundaries in palladium. By using nanocrystalline Pd they showed that at very low hydrogen concentrations. D_H in grain boundaries is about 1/10 of D_H in the volume, but the grain boundary diffusivity becomes larger than the volume diffusivity at larger coverages because grain boundary sites of smaller binding energy become occupied. At still higher coverages the D_H along grain boundaries decreases because of the attractive interactions between adjacent hydrogens. Overall, D_H along grain boundaries in Pd is 10 to 100 times larger than in the volume. A greater D_H along grain boundaries has been observed also in nickel (73).

Seebauer et al. (74) measured the diffusion of deuterium atoms on surfaces of platinum and rhodium. They found that on Pt the activation energy and the pre-exponential term decrease with increasing coverage, producing an increasing diffusivity with increasing coverage. On Rh, however, the activation energy increases somewhat with increasing coverage, while the pre-exponential term remains essentially constant. It may be that attractive D-D interactions produce the predominant effect in the case of rhodium.

The diffusivity of hydrogen along dislocation lines in palladium (the so-called "pipe diffusion") has been evaluated by Kirchheim (50) as about ten times the D_H in the volume.

Diffusion with Trapping

The concept of trapping (i.e., the short-or long-time detainment of a solute in diffusive motion) originated in the attempt to understand the tremendous decrease of the diffusivity of hydrogen in steels as a result of plastic deformation (75). Any structural imperfection (Table 2) or impurity atom (Table 4) with which dissolved hydrogen interacts attractively will cause the hydrogen atom to spend more time in its vicinity than at a normal lattice site, chiefly because the activation energy for escape from a tight-binding site will be increased approximately by the binding energy. Specific kinetic models for this effect have been constructed (81), as well as models which assume equilibrium between the trapped and untrapped populations (82). The reduction of diffusion of hydrogen by trapping has been measured in iron and steels by

dislocations (see refs. 82, 47) and by Ti and TiC interface (80); in palladium by dislocations (83), in vanadium by dissolved oxygen and titanium (78), and in niobium by dissolved oxygen and vanadium (77). Although direct experiments with other metals do not seem to exist it is safe to expect the trapping-reduced diffusivity to be a general phenomenon, which increases in importance as the normal lattice-dissolved concentration of hydrogen decreases.

Dislocation Drag

That moving dislocations can transport hydrogen faster than can motion by diffusive transport was first suggested by Bastien and Azou (84). The permeability of hydrogen during the plastic deformation of nickel was found (85) to increase the apparent diffusivity by five orders of magnitude; this was interpreted as transport of trapped hydrogen by moving dislocations. Louthan et al. (85, 85) observed that a stainless steel absorbed more tritium from the gas phase when the steel was deformed, and autoradiography showed that the tritium was enriched at slip lines. It was proven that the greater absorption was due to enhanced transport and not easier surface entry by investigating different surface finishes.

Although investigated in just a few metals, the mechanism of the drag of hydrogen by dislocations moving in response to stress can be confidently expected in other metals. It will be important in metals in which the product of lattice-dissolved hydrogen concentration and diffusivity is small.

Diffusion Driven by Gradients Other Than of Composition

Stress Gradients. Isothermal diffusion is a flux produced by the biasing of the random jumping of an atom (or a molecule) by a thermodynamic driving force, grad μ, where μ is the chemical potential of the mobile solute. The chemical potential is influenced by all the force fields that can affect the free energy of the solute. For the uncharged (neutral) dissolved hydrogen in a metal, under the conditions for which eq. (10) is valid, the diffusion flux can be written

$$J = -Bc\,grad\mu \qquad (14)$$

$$= -B\left[RT\left(1+\frac{d\ln\gamma}{d\ln c}\right)\right]gradc + Bc\overline{V}\,grad\sigma_h$$

$$= -D\left(gradc - \frac{c\overline{V}}{RT}grad\sigma_h\right) \qquad (15)$$

in which we have used eq. (13) as well as the Einstein relation D=BRT.

Thus, at zero grad c, stress-induced hydrogen diffusive flux will occur whether the inhomogeneous stress is caused by externally applied forces, by stress fields caused by second-phase particles, dislocations, or by the inhomogeneous distribution of dissolved hydrogen. In the latter case both grad c and grad σ_h will be operative. It should be emphasized that eq. (15) represents the simplest possible case; in the general case, gradients of the off-diagonal terms of the stress tensor must also be included (see eq. 9). The effect of stress gradients is not trivial. It can be shown (48) that the Δc that would just cancel a $\Delta\sigma_h$ is given by $\Delta\sigma_h/\Delta c = RT/c\bar{V}$ for the case where $d\ln\gamma/d\ln c = 0$. Letting $\Delta c = c - 0 = c$, $\Delta\sigma_h = RT/\bar{V} = 1.49 \times 10^{10}$ dyne/cm^2 at room temperature and for $\bar{V}$ = 1.68 cm^3/mol as in palladium. This is a smaller stress than that existing two Burgers vectors away from the core of an edge dislocation on its tensile side.

Electrical Potential Gradient. If one produces an electrical field gradient in a Pd(H) solid solution a flux of electrons results. Another consequence is that a flux of the dissolved hydrogen also occurs. This is an example of cross effects in diffusion as treated in the thermodynamics of irreversible processes (87). The production of a flux of metal-dissolved solute caused by the flux of charge carriers is called electromigration. It cannot be understood as a response to a thermodynamic driving force as it is in fact a kinetic phenomenon. In the absence of concentration and stress gradients, the flux of hydrogen in an electrical potential gradient, grad ϕ, is

$$J = cBF \equiv cB\, Z^* \text{ grad } \phi \qquad (16)$$

where Z^* is called the effective charge of the hydrogen in units of the electronic charge. Z^* is negative if the solute moves in the same direction as the electrons under the applied grad ϕ. Although full understanding of electromigration is not yet available (88), it can be said that Z^* is the sum of two effects: a "direct field effect" whereby the screened ion experiences a force from the grad ϕ, and a "wind effect" meaning that charge carriers (both electrons and electron holes) moving in response to the field transfer momentum to the solute atom. The view of this writer (89) is that the momentum transfer and the direct-field effect at the saddle point of the activated state are the relevant quantities to be considered. Irrespective of the details of the mechanisms embodied in the effective charge it is clear that the magnitude and sign of Z^* are not simply related to the "ionicity" of the dissolved hydrogen in its ground state. Table 5 collects some measured values of Z^* of hydrogen; where a range of values is given it is because Z^* was found to be temperature dependent. Attention is directed to the several negative values of Z* and to the temperature dependence in some cases, neither of which is understandable in the absence of a momentum-transfer contribution. The force F_ϕ upon dissolved hydrogen arising from an electrical potential gradient of 1 volt cm^{-1} is 6×10^{-13} dyne/atom, using $Z^* = 0.5$ for H in Pd. This may be compared with the force arising from a concentration gradient: $F_c = 4.1 \times 10^{-14}$ dyne/atom, calculated for (1/c) grade = 1 cm^{-1} at 295 K, so that the electromigration force is not insignificant.

Temperature Gradient. Another example of cross effects is the migration of solutes in metals caused by a temperature gradient, called thermomigration, or thermotransport. The force upon a solute due to a grad T is $F_T = (Q^*/T)$ grad T, where Q^* is called the

heat of transport. For Q^*=.065 eV for H in Pd, T = 700°K and grad T = 100°K/cm, $F_T=10^{-14}$ dyne/atom. The heat of transport is more complex than Z^* because the applied grad T produces fluxes of charge carriers and of phonons all of which interact with the solute in its activated state. In a metal, momentum transfer from collision with the charge carriers is probably the more important (90).

Phenomena Accompanying Input and Egress of Hydrogen

With Molecular Hydrogen Gas

The transition between the gaseous molecular state and the lattice-dissolved screened-ion state must involve the sequence: impingement of H_2 molecules of the gas upon the surface, adsorption of the H_2 molecule, dissociation into adsorbed H atoms, and transition between the adsorbed and the absorbed (dissolved) state. The details vary from metal to metal, and also from one type of crystallographic surface plane to another type for any one metal. Therefore, it is possible in this review only to indicate some generalities and to go into some detail for only one metal.

The rate of impingement of gaseous molecules is well described by the kinetic theory of gases. The fraction of the impinging molecules that stick (the sticking coefficient) is relatively small because the adsorption energy of the molecule is small. The molecule must diffuse along the surface to a position where the dissociative adsorption can proceed. The adsorption of the molecule and its dissociation are strongly impeded by pre-adsorbed species such as oxygen, nitrogen and atomically adsorbed hydrogen. The dissociation of the H_2 molecule upon a surface oxide is very difficult, so that virtually only metal atoms at the surface are effective. Finally, the adsorbed atoms must diffuse from the dissociation sites to locations on the surface providing low kinetic barriers for the passage from the surface to the interior of the lattice. Each of these steps is a strong function of the atomic topography of the metal surface, i.e., atomic steps, kinks on the steps, and surface vacancies. Further movement into the lattice proceeds by diffusion, the boundary condition for which is set by the concentration, c_o of dissolved hydrogen in the first lattice plane below the surface.

Some details can be given for hydrogen on palladium. Aldag and Schmidt (91) found very small sticking coefficients below 100 K, but at higher temperatures the coefficient rises to about 0.1. These investigators found four states for chemisorbed molecules on polycrystalline Pd with adsorption energies ranging from 54 to 146 kJ/mol H. Conrad et al. (92) found that the chemisorption of H_2 molecules increases the work function of Pd, so that the adsorbed species receives a net electron transfer from the metal. In this state the H atoms on Pt (111) planes are situated above triangles of Pt atoms forming an octahedral plane of their own with an interatomic separation of 0.0962 nm (93), compared with 0.0742 in the undistorted H_2 molecule. It is considered that dissociative chemisorption on Pd(111) proceeds in the same configuration. The absorption into the lattice does not proceed from the octahedral sites, however. The dissociated H atoms must diffuse (94) to the weak binding sites on the surface that correspond to tetrahedral sites in the bulk Pd lattice and to Aldag and Schmidt's weak binding sites. These sites

also correspond to the weak chemisorption investigated by Lynch and Flanagan (11). From these surface sites the adsorbed atoms make their entry into the lattice (94), and since these are also the sites of the initial adsorption of H_2 molecules, occupation of these sites by H_2 molecules interferes with the surface-to-volume transition of the adsorbed atoms. The rate-determining step for the whole process was found (94) to be the dissociation of the adsorbed H_2 molecule. Similarly, the rate of egress from the lattice dissolved state into the gaseous phase is kinetically limited by the rate of recombination. If adsorbed oxygen, or adsorbed C_2H_5, or other groups that can react with adsorbed hydrogen are present on the Pd surface, H-H recombination is not needed (94). It should be pointed out that in the absence of such reactive groups (which can have only a transient effect) whatever impedes the input of hydrogen should also impede the egress. This is an inference from the principle of microscopic reversibility, that the sequence of steps in the forward direction must be reversed for the backward direction. It should also be noted that whereas adsorbed species can affect the rates of ingress and egress of hydrogen, they do not affect the equilibrium concentration produced in the lattice at a given temperature and gas fugacity.

With Sources of Hydrogen Atoms

The dissociation of the H_2 molecule on the metal surface can be circumvented by depositing directly hydrogen atoms. This may be done by exposing the surface to a partially dissociated gas produced by a variety of techniques. The equilibrium ratio of H atoms to H_2 molecules in hydrogen gas at room temperature is 10^{-30}, but the concentration can be increased by many orders of magnitude in the immediate neighborhood of, for example, a hot tungsten wire. However, recombination occurs in the gas phase, on the walls of the containment chamber, and most importantly on the surface of the metal to be charged with hydrogen. For this reason, and also because there is not thermal equilibrium between the atoms and the molecules in the gas it is not possible to calculate a thermodynamic fugacity of the partially dissociated gas whereby to evaluate the driving force (i.e., the free energy change) for the process H(gas) $\rightarrow$ H(metal). In practice, it is possible to achieve much larger concentrations of hydrogen in metals by the use of partially dissociated hydrogen gas than with molecular gas at ordinary pressures. For example, nickel hydride (NiH) can be produced (95) by impinging H atoms on nickel at 25°C. Since a molecular gas pressure of 6 kbar is needed (68) at 25°C to produce NiH one may infer that the input fugacity of the dissociated gas in the experiment of ref. 80 was that corresponding to 6 kbar pressure. (The concept of input fugacity is discussed below). The concentration that may be reached in a metal by exposing it to a partially dissociated gas is very sensitive to surface contaminants and experimental conditions; this has not been studied systematically.

Electrolysis also deposits hydrogen atoms on the metal surface. In the case of aqueous electrolytes the deposition reaction can occur by the reduction of water or of hydronium ion. From fused salt electrolytes the hydrogen atom results from the oxidation (96) of the negative hydride ion. In either case the population of hydrogen atoms at the metal-

electrolyte interface is controlled by the kinetics of the recombination of the hydrogen atoms in competition with the kinetics of the transition between the surface state and the absorbed state. the recombination apparently occurs preferentially on specific surface sites having a distinctive atomic topography. For example, Stackelberg and Bischoff (97) found that on palladium bubbles of gaseous hydrogen form almost exclusively at grain boundaries on the surface, and Storms et al. (98) found that 7.6 wt % carbon in Pd significantly reduces the uptake of deuterium, although the mechanism of this effect was not elucidated. The rate of entry of hydrogen into iron can be increased over the rate of recombination to form gaseous hydrogen by various chemicals added to the electrolyte which apparently block the sites preferred for the recombination reaction. Such chemicals are certain compounds of elements of the V-A and VI-A groups of the periodic table. The precise way in which these compounds promote the entry of hydrogen into iron is still under investigation, although a well supported idea in that formation of the hydride is an essential step (99,100). Promoters of hydrogen entry into palladium have not been clearly identified. For example, Riley et al. (101) obtained contradictory results using various electrolytic solutions.

Promoters of hydrogen entry affect not only the rate of entry but can, in some circumstances discussed below, also control the steady-state hydrogen content attained within the metal. The rate of entry diminishes with increasing hydrogen content already in the metal. An extreme example of this is furnished by hydrogen charging from the gas phase (102) into titanium. If the gas fugacity is high enough to produce a hydride phase near the input surface, penetration of dissolved hydrogen deeper into the metal is seriously impeded by the low diffusivity of hydrogen in the hydride. Another impediment to the penetration of hydrogen beyond the immediate vicinity of the input surface is the generation of dislocations and other defects (see below) that can trap the incoming hydrogen.

Input Fugacity of Hydrogen

It has already been stated that with molecular gaseous hydrogen the thermodynamic driving force for the transition between the gaseous state and the lattice-dissolved state in a metal, and also the concentration of dissolved hydrogen at equilibrium, are fixed at any one temperature by specifying the fugacity of the gas (this neglects hysteretic phenomena) irrespective of surface conditions. Although this cannot be done in the cases of electrolytic charging or of partially dissociated or ionized hydrogen gas, it is sometimes useful to speak of the input fugacity, or effective fugacity, of the incoming hydrogen. Both methods of charging produce a population of adsorbed hydrogen atoms on the surface of the metal that is kinetically controlled as discussed previously. At steady state, such that the surface population everywhere on the metal surface and the concentration of hydrogen within the metal are uniform and independent of time, and furthermore the defect structure of the metal is independent of time, then one can say that there is thermodynamic equilibrium among all of the states of hydrogen within and upon the surface of the metal, but not between these states and the source of the hydrogen. In these circumstances, the lattice-dissolved hydrogen concentration, c^L everywhere in the metal can be related to the fugacity, f, of the molecular gas that at the

same temperature would produce at equilibrium the same value of c^L. That value of f is termed the input fugacity, f_i, produced by the charging system at its operating parameters, which include not only (for the electrolytic case as an example) the cathodic current density but also the composition of the electrolyte, its hydrodynamic state, the nature of the metal, and the chemical and structural state of the surface of the metal.

The identification of f_i from the c^L involves the thermodynamic relationship $c^L\left(f_{H_2(g)}\right)$ which at very large fugacities may not obey Sieverts' law because of H-H interactions in the dissolved state. Of course, f_{H_2} and the pressure, p_{H_2}, of the gas are thermodynamically related as shown by Table 6 (103). It should be clear that defining an f_i from the c^L by assuming that the f_i (c^L) relation is the same as the $f_{H_2}\left(c^L\right)$ relationship does not imply that the metal with the steady-state c^L under cathodic charging is itself under the hydrostatic pressure consistent with the thermodynamic function $f_{H_2}\left(p_{H_2}\right)$ for the gas. Under steady-state electrolytic charging or dissociated gas charging, the pressure upon the metal is the environing pressure. Furthermore, the H atoms within the metal experience only the mechanical reaction from the lattice associated with the expansion of the interstitial site that manifests itself as the partial molal volume. There is no external pressure, p_{H_2} coordinated with f_i, and in particular there is no force tending to push H atoms to smaller separations or to cause double occupancy of any one interstitial site. Because the metal under gaseous molecular hydrogen of fugacity f_{H_2} producing c_L is under a compression produced by the p_{H_2} that corresponds to f_{H_2} whereas the metal with steady-state dissolved concentration c^L produced by cathodic charging does not experience an external pressure p_{H_2}, the assumption that the functional relationship f_i (c^L) is identical with f_{H_2} (c^L) cannot be completely correct. However, at $f_{H_2} = 10^7$ atm, $p_{H_2} = 12 \times 10^3$ atm, and using a typical compressibility for metals of -5×10^{-7} atm^{-1}, the fractional volume change $\approx 6 \times 10^{-3}$, so that the volume compression caused by the molecular gas is small.

A technique that has been applied (49,104,105) to evaluate f_i in cathodic charging is to measure the steady-state permeation of hydrogen from which c_0^L, the sub-surface input concentration of hydrogen can be calculated if the diffusivity of hydrogen in the bulk of the metal is known. Again, the functional relationship $c^L(f_{H_2})$ is assumed to relate c_0^L to f_i. Note that this technique does not depend on equilibrium between the adsorbed population of hydrogen and the sub-surface concentration. Another way of putting this is that the technique for evaluating f_i does not depend on whether or not the permeation is under diffusion control. However, the technique depends on achieving steady state in all respects.

Development and Relief of Stresses

Coherency Stresses. That dislocations are produced in metals by diffusion of solutes, and by inference that stresses are produced by diffusion, has been realized for a long time. Schwuttke and Queisser (106) observed dislocations after the diffusion of Ga, B and P in silicon. Electron microscopy was used to study dislocations produced in silicon by the diffusion of B (107) and of P (108). Some calculations of diffusion-induced

stresses were made by Prussian (109) but Li (110) has made the most detailed calculations.

Consider a thin slab of thickness 2a in which an interstitial solute of partial molal volume, $\overline{V}$, is diffusing only in the thickness direction, x, towards the center, the boundary condition being a constant sub-surface solute concentration, c_o, for $t \geq 0$ and $c = 0$ at $t = 0$ everywhere except at the sub-surfaces. For constant Young's modulus, E, and Poisson ratio, ν, and in the absence of any plastic deformation, the stresses in the orthogonal directions normal to the thickness direction are given by (110)

$$\sigma_{yy} = \sigma_{zz} = \frac{2\overline{V}c_oE}{3(1-\nu)}\sum_{n=0}^{\infty}\frac{1}{\rho_n}\left[(-1)^n\cos\left(\frac{n\pi x}{a}\right)-\frac{1}{\rho_n}\right]\exp\left(\frac{-\rho_n^2Dt}{a^2}\right) \qquad (17)$$

in which c_o has units of moles cm^{-3}, $\rho_n \equiv (2n + 1)\pi/2$ and D is the diffusivity of the solute. This equation is plotted in Fig. _. The dashed lines represent the envelope of all the curves. It may be shown that the maximum stress developed by diffusion is

$$\sigma_{max} = -\frac{\overline{V}c_oE}{3(1-\nu)} \qquad (18)$$

Fig. 1 shows that it occurs at the input surfaces at the start of the diffusion ($\sigma > 0$ is tensile, $\sigma < 0$ is compressive).

Assume now a similar slab geometry with solute diffusing in from a constant subsurface concentration from only one surface, the other surface blocking the out-diffusion of the interstitial solute. The stress-time relationship is given by (111)

$$\sigma_{yy} = \sigma_{zz} = \frac{2\overline{V}Ec_o}{3(1-\nu)}\sum_{n=0}^{\infty}\frac{1}{\rho_n}\exp\left(\frac{-\rho_n^2Dt}{(2a)^2}\right)\left[\sin\left(\frac{\rho_n x}{2a}\right)-\frac{1}{2\rho_n}-\frac{3}{\rho_n^2}\sin\rho_n+\frac{3}{\rho_n^3}\right] \qquad (19)$$

and again the maximum stress is given by eq. (18) and occurs at the input surface at the start of diffusion. The expansion caused by the dissolution of hydrogen places the input region in compression because of the constraint by the underlying unexpanded hydrogen-free metal, and the plate develops concavity towards the blocked surface. As diffusion proceeds the stresses decrease. For the case of steady-state diffusion with solute going in at one surface and going out the other, as is the case in a typical hydrogen permeation experiment, if $\overline{V}$ and E are constant the resulting steady-state linear c(x) profile produces zero stresses.

Another geometry that is common in cathodic charging of hydrogen is that of a cylinder, at the cylindrical surface of which the solute concentration is held at c_o and at $t = 0$, $c = 0$ everywhere else. Fig. 2 shows the shear stress as a function of position (r is measured from the central axis of the cylinder and a is the cylinder radius) and time. The largest shear stress is at the input surface, which, calculated for palladium at a c_o corresponding to $D/Pd = 0.65$ at $Dt/a^2 = 0.01$, is about 4×10^9 Pa, which is much larger

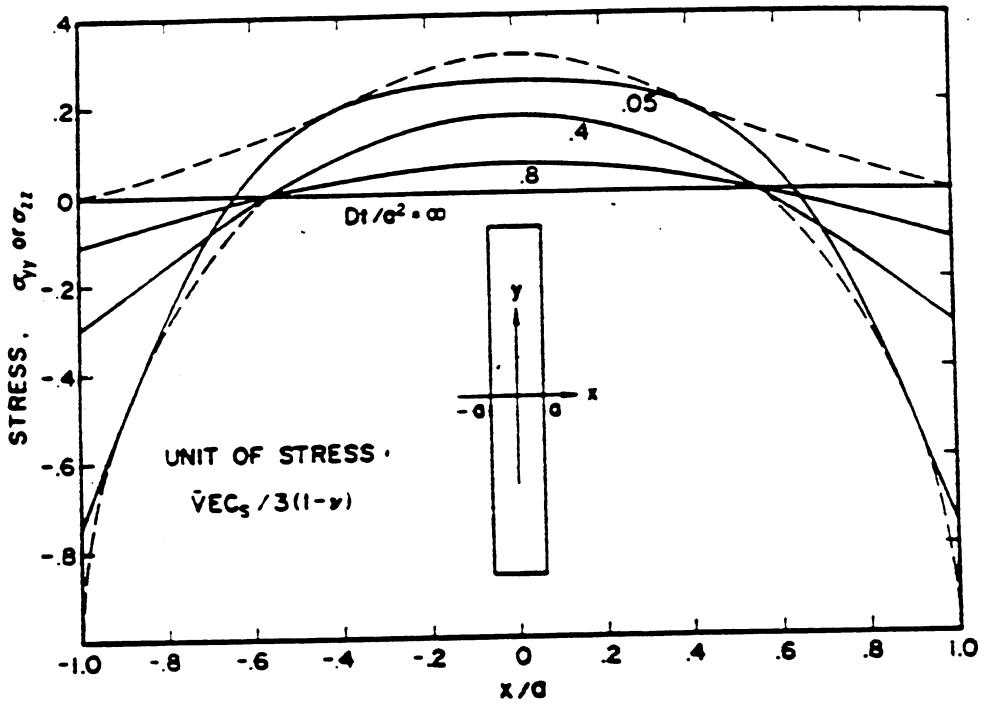

Figure 1. Stresses produced by the diffusion of hydrogen into both sides of a thin slab (Ref. 10).

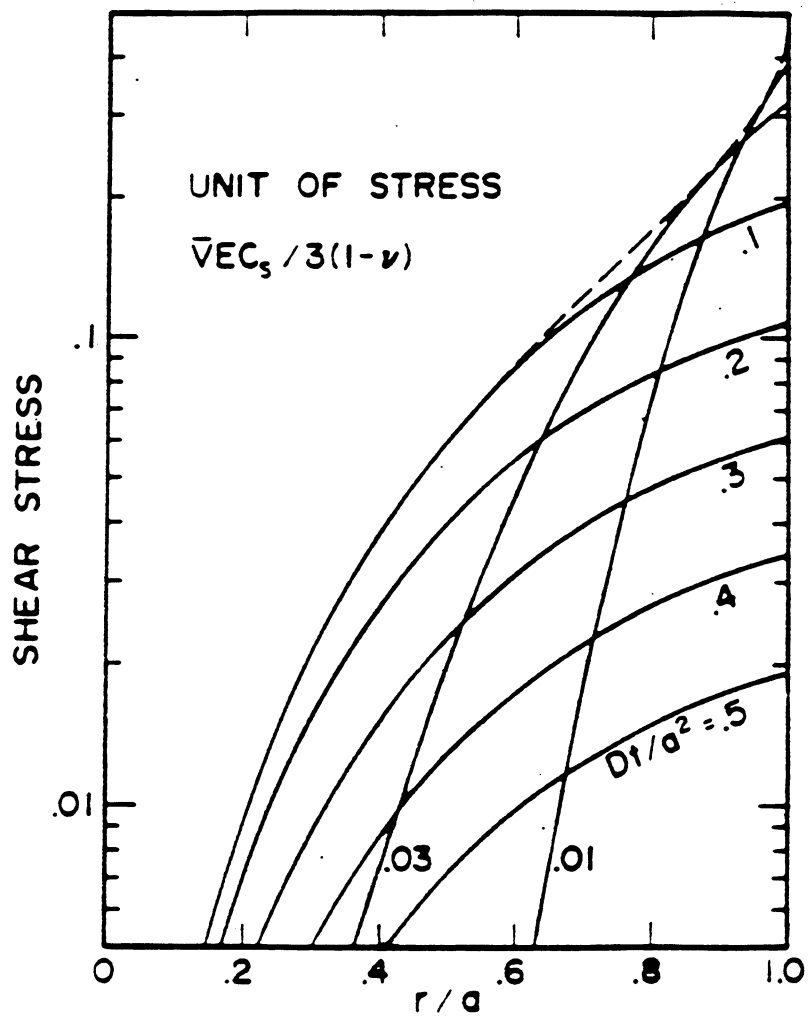

Figure 2. Shear stress produced by the diffusion of hydrogen into a thin cylindrical metal (Ref. 10).

than the yield stress of the metal. Hence, one must expect dislocations to be generated and to move in the stress gradient.

The above equations for stress are first-order calculations in the sense that diffusion is considered to be motivated only by a concentration gradient; no account is taken of the stress gradient itself affecting the driving force for diffusion. Improved calculations can be made by substituting for D in the stress equations an effective diffusivity given by

$$D = D_o\left[1+\left(\frac{\partial \ln x}{\partial \ln c}\right)+\frac{2c\bar{V}^2E}{9RT(1-\nu)}\right] \qquad (20)$$

derived by Li(110) for cases when stresses are caused only by diffusion. This equation includes the correction required for the concentration dependence of the activity coefficient, γ. Because in these geometries the gradient of the hydrostatic component of stress is proportional to the concentration gradient the stress-modified effective diffusivity is larger than the ordinary diffusivity.

Heterogeneous Generation of Dislocations. That the in-diffusion of hydrogen of hydrogen can generate stress larger than can be supported by the metal, even in the absence of phase changes, has been demonstrated experimentally (111) with a b.c.c. alloy, Ti-30 Mo which remains single phase with hydrogen contents up to about an atomic ratio of 0.6. In these experiments hydrogen was cathodically charged into only one side of a thin sheet of metal. Transmission electron microscopy showed very large density of dislocations distributed at random, in clusters and in networks (Fig. 1). The dislocation cluster in the left-hand side of Fig. 3 has a dislocation density about 1000 times that in an annealed sample, and resembles the clusters of dislocations found in nickel (112) after the diffusion of carbon. There are also pile-ups of dislocations at grain boundaries far from the input surface (Fig. 4); this is important because dislocation pile-ups can nucleate microcracks, and it shows that the diffusion-induced stresses cause the generated dislocations to glide into metal that is as yet free of hydrogen. Fig. 3 demonstrates that most of the dilocations are along slip planes in accord with similar findings in other systems after interstitial diffusion (113).

In addition to the generation and motion of dislocations that relax the stresses produced by the in-diffusion hydrogen into Ti-30 Mo alloy, other interesting phenomena were observed (111). The change of lattice parameter with diffusion time was measured for various grains of the polycrystalline alloy in the surface of the specimen that was not in contact with the electrolyte employed for the cathodic charging . It was found that the changes continued to occur over durations of hydrogen charging that were far longer than the time required for Fickian diffusion to have reached a steady state. This can be explained only by the trapping of hydrogen by the generated dislocations. Furthermore, the change of lattice parameter was different in different crystal grains (Fig. 5), and also the intensity of various Bragg peaks changed with time of charging. Indeed, to obtain maximum intensity for a given Bragg peak it was necessary to rotate the sample with respect to the x-ray detector and source. The necessary rotation was a

Figure 3. Clusters of dislocations produced in Ti-30 Mo alloy by cathodic charging of hydrogen (Ref. 111).

Figure 4. Dislocation networks and pile-ups at grain boundaries in Ti-30 Mo alloy after cathodic charging (Ref. 111).

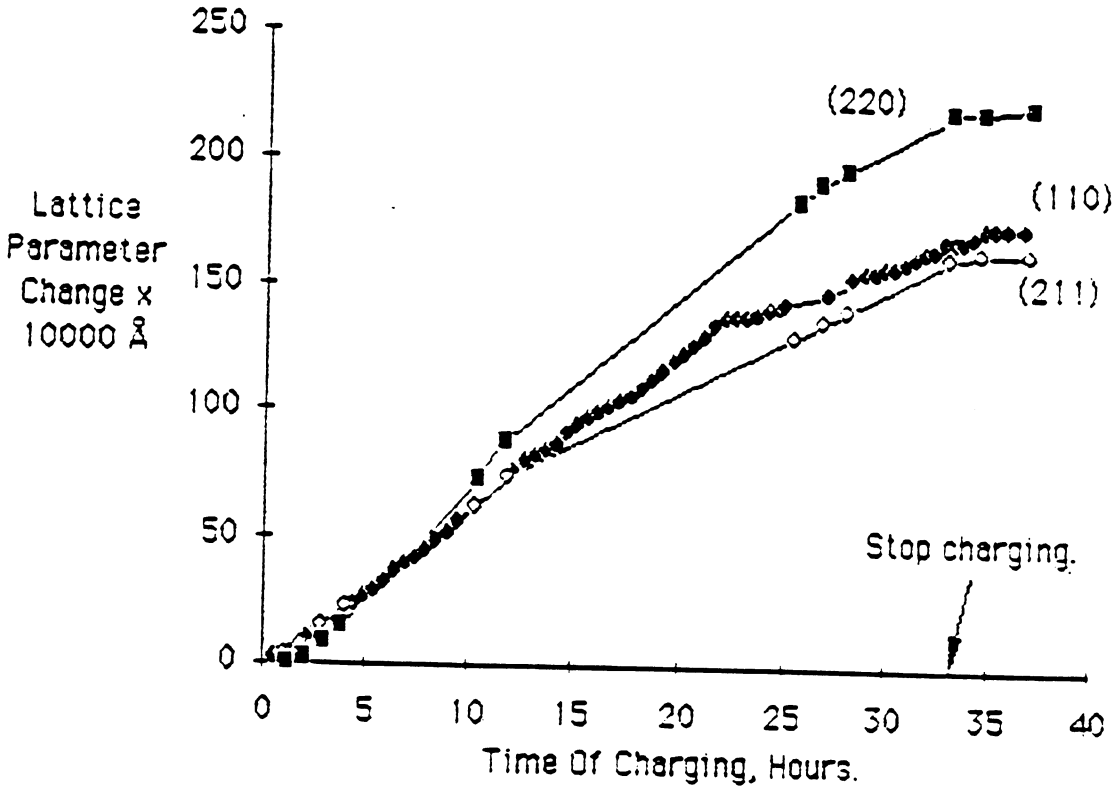

Figure 5. Change of lattice parameter with time of cathodic charging of hydrogen into one side of a Ti-30 Mo plate. The various Bragg reflections were taken from the side of the plate far from the input surface (Ref. 111).

function of time during charging and the dependence on time was different for different crystal grains (Fig. 6).

Recalling that the change of lattice parameter in any one grain reflects the change of dissolved hydrogen concentration in that grain, one concludes that at a given distance from the input surface, the lattice-dissolved hydrogen concentration was different in different grains. The rotation of the sample to obtain maximum intensity of any one Bragg peak means that the angular positions of the diffracting crystal planes were changing during charging. Other defects produced by hydrogen charging are deformation bands and microcracking at the far surface of the specimen. Deformation bands probably formed by accumulations of edge dislocations of the same sign on slip planes. Their formation in polycrystalline metals during deformation is known to be facilitated by the restraints imposed by grain boundaries. Circular protruberances were also found both on the input and the far surfaces. These were especially prominent in the tentalum and niobium specimens that were also studied (111).

These observations may be explained by the generation of dislocations, near the input surface initially, which trap the charged-in hydrogen; consequently the c_0, controlling Fickian diffusion beyond the dislocated region, is initially small. As the dislocation density increases in that region their mutual interactions grow so that the local flow stress increases, the rates of dislocation generation and of hydrogen trapping decreases. Consequently, c_0 increases so that the diffusion flux into the rest of the specimen thickness increases. This is responsible for the slow increase of hydrogen concentration, and hence of lattice parameter, at the far side of the specimen. At the same time, the shear stress at the input surface causes dislocations to glide towards the far side, carrying trapped hydrogen with them. This hydrogen is distributed to grain boundaries, to dislocation pile-ups at barriers and to grain interiors where they increase the lattice parameter, adding to the effect from diffused hydrogen. As the dislocations move away from the input side they interact with each other and with grain boundaries, annihilating each other, forming pile-ups some of these breaking through grain boundaries and others producing microcracks, and causing changes in grain boundary configuration. All these effects depend on the orientation and type of grain boundary, so that the distribution of the hydrogen, conveyed either by diffusion or by dislocation transport, between the volume of a grain and its boundary is a function of grain orientation in the specimen. This explains the heterogeneity of lattice parameters and their rates of change. The non-uniformity of lattice parameters among the grains means a non-uniformity of lattice expansions, which can be accommodated by sliding or rotation with respect to each other, causing a change in the angle of diffraction. The sliding of groups of grains can create protruberances at the surface.

A grain-dependent heterogeneity of response to interstitial solute input was also found in iron films (114) with hydrogen and in austenitic stainless steel (115). Cathodic charging of hydrogen into pure iron, low-carbon iron, and commercial steels causes dislocation tangles at grain boundaries and inclusion interfaces, as well as microvoids and microcracks (116-118). Raczynski (119) found that cathodic charging of extremely pure iron does not produce dislocations or internal voids. Beck et al. (120) found that

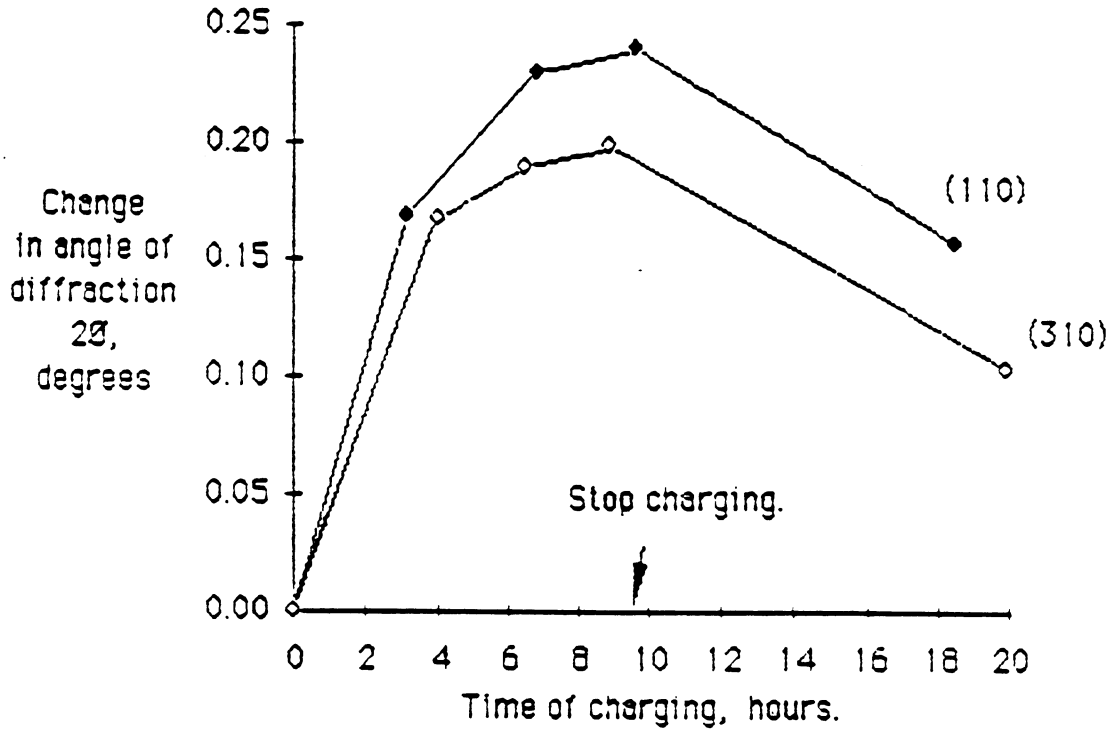

Figure 6. Rotation of crystal grains at the far side of a Ti-30 Mo plate caused by cathodic charging of hydrogen at the other side (Ref. 111).

nominally pure iron exhibits a threshold input fugacity for the production of internal defects, as observed by permeation transients. Charging in of hydrogen produced by low-pressure plasma was found (121) to produce dislocations in Monel and in 304 stainless steel even at depths beyond the penetration depth of the hydrogen ions.

The foregoing discussion deals with phenomena associated with coherency stresses produced by the lattice expansion stresses caused by the lattice expansion associated with lattice-dissolved hydrogen. If in addition second phases are formed as the hydrogen moves in, even greater motivation for dislocation generation results because of the large and abrupt volume change. For example, the precipitation of ε or β phase from Nb-H solid solution produces irregularly shaped particles which emit prismatic dislocation loops which persist even after the two-phase alloy is warmed into the one-phase field (122). Similar results were seen by Lecoq (123) with the formation of β phase in α-$TaH_{0.1}$; the β phase was found to be surrounded by dense dislocation tangles. For Pd, Wise et al. (124) found large dislocation densities in metal in which the β phase had formed and had subsequently decomposed. Jamieson et al. (61) observed that the disappearance of β phase, caused by allowing hydrogen to evolve from the Pd-H alloy, is accompanied by dislocation generation. Storms and Talcott-Storms (125) found a high dislocation density in a Pd sample that had been repeatedly cycled between low and high hydrogen content. Large dislocation density was seen by Guruswamy et al. (126) in a Pd electrode charged cathodically with deuterium. The plastic deformation was evidenced also by the increase of the electrical resistance by a factor of two and by Doppler line broadening of the electron-positron annihilation peak at 512 keV. Fewer dislocations are produced in palladium if hydrogen charging is carried out so that phase separation is avoided (127). Because the so-called α and β phases of the Pd-H system are really one phase into which a miscibility gap intrudes, abrupt volume changes can be avoided by adjusting hydrogen gas pressure and temperature to surmount the critical point of the miscibility gap.

Changes of Shape. That charging hydrogen into a metal can change the shape of the specimen is common knowledge. Smialowski (117) measured the expansion of the diameters of cylindrical specimens of low- and medium-carbon steels. He found that the dilation occurred only above an ill-defined threshold value of f_i, and that the relative expansion increased with decreasing specimen radius. Krause and Kahlenberg (115) found that cycling palladium between absorption and evolution of hydrogen increases the thickness and decreases the other dimensions of a specimen. Storms and Talcott-Storms (125) found that cycling Pd between a hydrogen concentration above the minimum concentration of the β phase and a low concentration thickens a disc-shaped specimen and decreases its diameter (as measured after extraction of hydrogen), and similar treatment of a rod of Pd increased the diameter and decreased the length. The change of the dimensions was accompanied by an increase of overall volume which was larger as the number of cycles was increased. In addition, large populations of microvoids were observed on polished cross-sections of the specimens after cycling. These authors inferred that the observed microvoids are the intersection of tubules, or channels, within the metal with the surface of observation. Matsumoto (128) observed, in Pd cathodically charged to an unspecified level of hydrogen or deuterium

concentration, "tiny spots" often arranged along grain boundaries. These features have all the characteristics of microvoids (Fig. 6); these, in other locations have linked together to form crevices. These crevices in some cases grow together to completely surround a metal grain; metallographic preparation apparently causes some of these "excavated" grains to fall out leaving a grain-shaped cavity. In addition, linear cracks are observed (Fig. 7) which in some cases appear to have formed by a linking up of the crevices at grain boundaries. Matsumoto (128) appears inclined to attribute these features to effects of cold fusion that are asserted to have been produced in all of the Pd specimens examined whether charged with deuterium or with hydrogen. Unfortunately, microstructural observations were not made on Pd electrodes that gave no reason to suspect the development of cold fusion. An extreme case of cracking and fissuring caused by deuterium charging is shown in Fig. 8. The 1/8-inch diameter Pd rod was the anode in a fused salt electrolyte in an attempt (129) to replicate Liaw et al.'s (96) high-temperature electrolysis.

It will be recognized that the microstructural phenomena observed in palladium after hydrogen charging have much in common with what happens in hydrogen-charged steels, a field which has been studied extensively (130). With steels, an increase of the diameter of a thin rod or of the thickness of a thin disk is usually associated with the formation and enlargement of microvoids and microcracks caused by the huge gas pressures developed in these internal spaces by recombination of the dissolved hydrogen which is at extremely high thermodynamic activity owing to the very large f_i of the cathodic charging process. The internal cavities expand in the direction of the smallest dimension of the specimen since that involves smallest resistance to plastic flow. The microvoids are preferentially nucleated at grain boundaries, and internal interfaces, especially at those having segregated impurities. It is also well known that the internally pressurized voids develop lenticular shapes and that they link together to produce cracks (131). The phenomena observed by Matsumoto have similar characteristics. The second-phase interfaces that help to nucleate microvoids may be at β-phase particles as well as at grain boundaries, the nucleation being produced by stress developed by dislocation pile-ups. However, this mechanism can operate in Pd only when f_i is so large that the corresponding pressure of the recombined gas within microcavities is large enough to overcome the flow stress in the metal. Extrapolation of the isotherms of Fig. 3.4 of ref. 6 shows that at H/Pd ≈0.9 at 20°C, $p_{H_2} \approx 10^3$ atm, so that the internal pressurization mechanism is not a probable one.

In steels voids form readily by interfacial decohesion around inclusions, by the cracking of second-phase particles, and by the operation of high stresses produced by plastic incompatibility in regions between particles. In hydrogen-charged palladium the second-phase particles are the β-phase nuclei growing in the α-matrix, and plastic flow is caused by the coherence stresses developed by the concentration gradient of the incoming hydrogen, as well as by the volume disparity between the β and the α-phases (calculated for an equal number of Pd atoms). Because the flow stress of the β-phase is larger than that of the surrounding α-phase (132), the disparity in plastic strain across the interface develops large stresses (133) tending to rupture the interface already weakened by impurities and by hydrogen (134). The microvoids thus nucleated grow

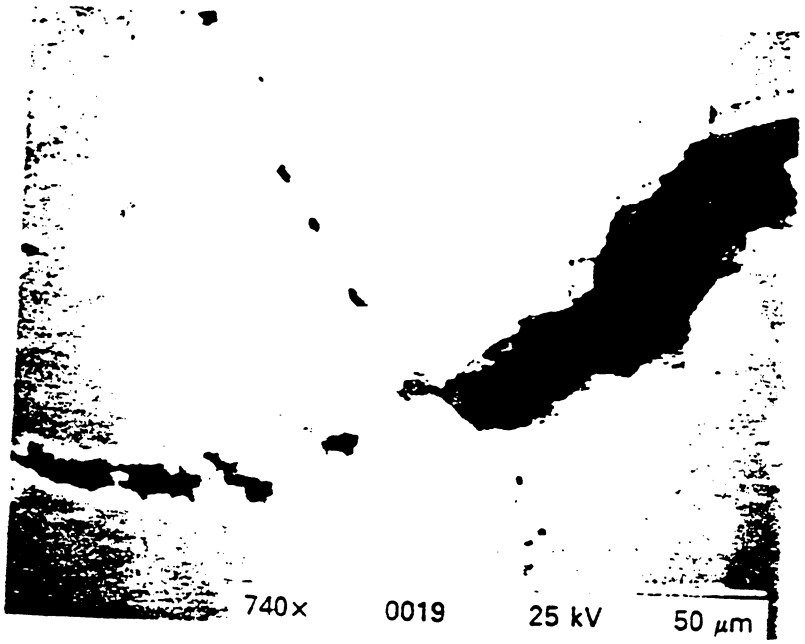

Figure 7. Cavities formed at grain boundaries in palladium by cathodic charging of hydrogen (Ref. 128).

Figure 8. Palladium rod after anodic charging with deuterium by high-temperature electrolysis in molten salt (Ref. 129).

in size by plastic mechanisms, and the growth causes the overall dimensions of the specimen to increase, the smaller dimension increasing more than the larger dimension. At the stage of charging when only β phase is present, compatibility stresses continue to exist because the amount of plastic deformation of any one β-grain depends on its orientation, as observed for Ti-30 Mo (111).

This mechanism does not explain the shrinkage of the length of a Pd rod and of the diameter of a disk (125). It is suggested that these effects result from the preferential direction of motion parallel to the diffusive flux of hydrogen of dislocations impelled by the coherency stresses generated by the hydrogen concentration gradient during charging. Effectively, mass is moved by the dislocations so as to shrink the diameter of the disk and increase its thickness. Cracks are formed in the palladium by the coalescence of closely spaced microvoids, the coalescence being caused by the development of plastic instability in the metal between the voids (135). Another probable mechanism is the localized slip that is known (136) to cause the advance of cracks in several metals. It the space opened up by decohesion at an interface has a lenticular shape with a sharp perimeter and if it is properly oriented with respect to the local stress, the microcrack can advance by hydrogen-aided emission (136) of edge dislocations or by decohesion (137).

Changes of Surface Structure. Rolison et al. (138) carefully studied the variety of surface morphologies produced on the input surfaces of palladium by cathodic charging with hydrogen and with deterium. The polycrystalline foil employed was first etched, producing a variety of micromorphologies; which morphology develops with etching presumably depends on the crystallography of the exposed surface. The long-duration of subsequent cathodic deposition made it impossible to obtain channeling patterns, good evidence for extensive plastic deformation. The micromorphology of the grain surfaces was changed, in different ways for different grain surfaces, by the cathodic charging. The changes are related to the plastic deformation of the grains, and the differences among the grains arise from the differences in the stresses developed, the rate of hydrogen absorption which depends on the crystallography of the surface, the disposition of slip planes with respect to the free surface, and the amount of plastic deformation produced in any one grain. That different modifications of the various etch-produced morphologies result from the cathodic charging is not surprising since the plastic response depends on many factors that very from grain to grain. Modification of the surface morphology by hydrogen charging into Ti-30 Mo alloy (111, 139) was discussed in a previous section; variations of surface morphology were observed but not specifically studied.

What is more surprising is the difference found (138) for the surface morphologies generated by hydrogen and by deuterium charging. Deuterium charging produced a morphology different from that produced by hydrogen, starting from the same type of etch-produced surface. In addition, deuterium charging caused some grains to protrude slightly beyond the plane of the surrounding grain surfaces. This effect was not seen with hydrogen charging. Several reasons for differences between hydrogen charging and deuterium charging may be cited: the difference in partial molal volume

producing a difference in the gradient-caused coherence stress, the presumed difference in the interaction with dislocation cores, and perhaps most important, the difference in f_i of cathodic charging despite the sameness of the imposed electrical charging current for both isotopes. This sameness does not insure identical f_i-time history because of the different ionic conductivities of the H_2O-Li_2SO_4 and D_2O-Li_2SO_4 electrolytes, and the presumed difference of atom recombination on the Pd surface. Very careful investigation will be needed to understand the difference between the two isotopes with respect to grain relief. However, that uplift can occur is not too surprising since protruberances were seen also in the cathodic charging of Ti-30 Mo (111).

Effects of Hydrogen on Mechanical Properties

Both the phenomenology of, and the attempts to understand, the effects of dissolved hydrogen on the mechanical responses of metals are very large subjects. This review can only briefly touch on the salient points.

The paramount and ubiquitous effect of hydrogen on mechanical properties is embrittlement. This means that with some hydrogen in the metal, less work is needed to cause mechanical failure for a given load-time history. This decrease may be manifested by a decrease in the tensile elongation (strain) to cause failure, by the decrease of static load that can be sustained by the metal, by a decrease of the number of load-no load cycles, or by an increase of the rate of crack propagation. It is important to recognize that the effects of hydrogen depend in complex and mutually interacting ways on purity level, impurity distribution, microstructure and phase distribution, prior mechanical history (e.g., extent and kind of deformation), surface chemistry and geometry (e.g., notches), etc., for a given alloy composition. For some metals a fraction of a part per million hydrogen content (e.g., in high -strength steels) is sufficient to develop catastrophic embrittlement (118). For others (e.g., Nb, Ta) sufficient hydrogen concentrations to sustain hydride formation is required for serious embrittlement.

This review can discuss the mechanism for the effects of hydrogen only very superficially. The most important factor is the ability of dissolved hydrogen to lessen the binding forces between metal atoms; this is discussed in a previous section of this review. This effect can manifest itself by a reduction of the force for the normal (i.e., co-linear) separation of two portions of a body, leading to the easier propagation of a cleavage crack (140), or by reduction of the force needed for the continuous emission of edge dislocations from the tip of a crack (141) leading to easier crack propagation by localized plasticity. Which of these occurs, or what mix of these modes takes place in any one instance depends on many factors. These problems have been intensively studied in materials of construction, but very little in palladium and its alloys.

Hydrogen at low concentrations in pure nickel, α-iron, α-titanium and niobium decreases the flow stress (142). At tips of cracks in bodies under externally applied tensile forces, the hydrogen concentrates and causes localized plasticity which produces an easier crack propagation. Impurities change the response drastically. Large concentrations of hydrogen in Ti, Ta, V and Nb produce brittleness because the

hydrides that are formed resist dislocation motion. In palladium (132) hydrogen increases the mechanical hardness. At low concentrations the flow stress is increased but, amazingly, the elongation at fracture is also, increased (132). This behavior may vary with impurity content, which was not explored by Hasegawa and Nakajima (132); it may explain the finding (125) that cycling the hydrogen content totally within the (α+β) field of palladium-hydrogen does not generate excess volume, that is, internal voids and fissures do not develop because plastic deformation of the α-phase remains easy. However, at high hydrogen concentrations such that only the β-phase is present, the elongation at fracture is much reduced because the mobility of dislocations is decreased. Thus, the cathodic charging of palladium, or of any metal, generates mechanical stresses through the kinetics of hydrogen input, and the hydrogen content modifies the responses of the metal to the mechanical stress. The dynamics of these processes deserve much more study than they have received.

Implications for Cold Fusion Research

A popular idea in the field of cold fusion research is that a large D/M ratio is a pre-requisite for the generation of the so-called excess power (143). To obtain a large loading ratio it is necessary to facilitate the entry of hydrogen from the ad-layer and to impede the recombination of hydrogen atoms that transit from the sub-surface layer to the ad-layer. Because the kinetics of transit into the metal and of recombination are each strong functions of the atomic arrangements of metal atoms on the surface one must expect that there will be differences in the rate of loading from one crystal grain to another depending on the nature of the surface that the grain presents to the environment. These differences can be large during charging. Under steady-state conditions small differences between grains in average hydrogen concentration should persist. It will be difficult to maintain a desirable surface configuration (i.e., one that facilitates input and impedes egress) because the surface topography is changed during charging by dislocation activity, as well as by the deposition of impurities.

Patches of surface characterized by low values of f_i will serve as leaks for high-concentration regions under adjoining patches of high-f_i surface. Thus, diffusion currents of dissolved hydrogen can be established between surface patches even at steady-state conditions. Other leaks for hydrogen would be, in some circumstances, grain boundaries and dislocations that terminate at the free surface. The role of microcracks as hydrogen leaks has been emphasized by Storms (125), if these communicate with the surface. If the microcracks or voids are totally within the volume of the metal, they will have only a transient effect on the local hydrogen concentration.

One of the views (144) as to the mechanism of cold fusion involves the periodic potential that would be provided by stoichiometric PdD. This mechanism must deal with the thermodynamic necessity that an interstitial solute cannot completely occupy one class of sites, as discussed in an earlier section. As D/Pd approaches one, some octahedral sites must remain empty with the additional D atoms going into tetrahedral sites of higher energy. What this does to the quantum mechanical picture (144) should

be considered. Incidentally, it can be expected that the deuterium atoms in tetrahedral sites will have a larger mobility than those in the lower-lying octahedral sites. Furthermore, if spatially large domains of near-perfect order are contemplated by this model (144), it would be highly desirable to avoid dislocation generation by slow charging in of hydrogen in such a way that the $\alpha+\beta$ phase field is avoided, or by the use of superlattice alloys that do not have a two-phase field of hydrogen solutions.

In considering various possibilities by which cold fusion may be thought to take place it will be helpful to realize that high input fugacity sources, used to produce large D/M ratios, do not generate pressure to push or squeeze dissolved deuterium atoms together, or into close proximity. In fact the lattice sites are expanded. Another idea that needs reconsideration is that of fractofusion (145), whereby the quickly separating crack surfaces become oppositely charged and the ensuing electric field accelerates deuterons the collision of which results in fusion. Leaving aside many questions that may be asked about this model, only the speed of separation of the crack surfaces will be mentioned here. If hydrogen-aided localized plasticity is the mechanism of cracking of palladium it is implausible that the created free surfaces will separate so rapidly that electrons will not have time to move to neutralize the putative charge on the crack surfaces.

The generation of dislocations by hydrogen charging makes another argument implausible. This is the argument that the excess heat that some investigators of cold fusion report is really the release of stored energy such a mechanical energy of the stresses in the metal. The problem with this idea is that the energy of the stress field, proportional to σ^2/E, is continually degraded into heat by the continuous generation and motion of dislocations and cracks. At the stress levels involved the multiplication of dislocations is easy, so that the mechanical energy cannot attain larger magnitudes. Furthermore, the conversion of the energy stored in the dislocations cannot be easily converted into heat, as shown by Shober (122) who found that raising the temperature was not effective in causing the disappearance of dislocations formed by the re-dissolution of ε-NbH_x.

References

1. "Hydrogen in Metals," G. Alefeld and J. Volkl, eds., Springer-Verlag, Berlin, Vols. 1 and 2, 1978.

2. "Metals-Hydrogen Systems," R. Kirchheim, E. Fromm, E. Wicke, R. Oldenbourg Verlag, Munchen, 1989.

3. E. Wicke and G.H. Nernst, Ber Bunsenges. Phys. Chem. 68, 224 (1964).

4. S. Schmidt, Diplomarbeti, Munster (1978).

5. J.D. Clewley, T. Curran, T.B. Flanagan and W.A. Oates, J. Chem. Soc. Faraday Trans. 169, 449 (1973).

6. G. Sicking, Z. Physik. Chem. (N.F.) 93, 53 (1974).

7. G. Sicking, Ber Bunsenges. Physik. Chem. 76, 790 (1972).

8. E. Wicke and H. Brodowsky, in Ref. 1, Vol. II, p. 73.

9. H. Brodowsky, H. Gibmeyer and E. Wicke, Z. Physik. Chem. (N.F.) 49, 222 (1966).

10. E. Storms and C.Talcott-Storms, Fusion Techn. 20, 246 (1991).

11. J.F. Lynch and T.B. Flanagan, J. Phys. Chem. 77, 2628 (1973).

12. U. Stolz, U. Nagorny and R. Kirchheim, Scripta Metall. 18, 347 (1984).

13. H. Peisl, in Ref. 1, Vol. I, p.53.

14. W.T. Lindsay Jr., Abstracts of ACS National Meeting, Pittsburgh, March 1966.

15. A.J. Maeland and T.B. Flanagan, J. Phys. Chem. 18, 1419 (1964).

16. R. Abbenseth and H. Wipf, J. Phys. E. Metal Phys. 10, 353 (1980); J.E. Shirber and B. Morosin, Phys. Rev. B 12, 117 (1975).

17. H.A. Wriedt and R.A. Oriani, Acta Metall. 18, 753 (1970), from data by W.T. Lindsay Jr.

18. T. Schober and H. Wenzel in Ref. 1, Vol II, p.11.

19. D.T. Peterson and H.M. Herro (Dept. Mater. Sci. Iowa State University, Ames), Abstracts of The Metallurgical Society.

20. R.A. Oriani, Trans. Metall. Soc. AIME, 236, 1368 (1966).

21. H. Wagenblast and H.A. Wriedt, Metall. Trans. 2, 1393 (1971).

22. R.A. Oriani, Proc. Conf. Fundamental Aspects of SCC, Columbus 1967, N.A.C.E., R.W. Staehle, A.J. Forty and D. Van Rooyen, eds., pp. 32-50 (1968).

23. A.D. McQuillan, C.E. Ellis, H. Pessal, A.P. Bennett, J. Basterfield and A.D. Wallbank: "The Solution of Hydrogen in B.C.C. Metals," Report from the University of Birmingham, 1964.

24. R.E. Rundle, C.G. Shull and E.O. Wollan, Acta Cryst. 5, 22 (1952).

25. J.L. Waisman, G. Sents and L.B. Robinson, Metall. Trans. 4, 291 (1973).

26. E.O. Wollan, J.W. Cable and W.C. Koehler, J. Phys. Chem. Solids 24, 1141 (1963).

27. B. Baranowski, S. Majehrzak and T.B. Flanagan, J. Phys. F: Metal Phys. 1, 258 (1971).

28. M. Krukowski and B. Baranowski, J. Less-Common Metals, 49, 385 (1976).

29. K. Heindlhofer, presented in "Physical Chemistry of Metals," L.S. Darken and R.W. Gurry, McGraw-Hill, 1953.

30. V.A. Somenkov, I.R. Entin, A.Y. Chervyakov, S. Sh. Shil'stein and A.A. Chertkov, Sov. Pys. Solid State 13, 2178 (1972).

31. A.Y. Chervyakov, I.R. Entin, V.A. Somenkov, S. Sh. Shil'stein and A.A. Chertkov, Sov. Phys. Solid State 13, 2172 (1972).

32. V.A. Semenkov, A.V. Gurskaya, M.G. Semlyanov, M.E. Kost, N.A. Chernoplekov, and A.A. Chertkov, Sov. Phys. Solid State 10, 2123 (1969).

33. V.F. Petrunin, V.A. Somenkov, S. Sh. Shil'stein, A.A. Chertkov, Sov. Phys. Cristallography 15, 137 (1970).

34. H.G. Fritsche, H. Muller and Ch. Optiz, in Rf. 2, p. 535.

35. J. Friedel, Ber. Bunsenges, Physik. Chem. 76, 828 (1972).

36. J.C. Fisher, Acta Metall. 6, 13 (1958).

37. G.J. Zimmerman, J. Less-Common Metals 49, 49 (1976).

38. W. Drexel, A. Murani, D. Tocchetti, W. Kley, I. Sosnowska, and D.K. Ross, J. Phys. Chem. Sol. 37 1135 (1976).

39. W. Zhong, Y. Cai, and D. Tomanek, Phys. Rev. B, 46, 8099 (1992).

40. R.P. Messmer and C.L. Briant, Acta Metall. 30, 457 (1982).

41. M.S. Daw and M.I. Baskes, Phys. Rev. B, 29, 6443 (1984).

42. T. McMullen, M.J. Stott and E. Zaremba, Phys. Rev. B, 35, 1076 (1987).

43. H.G. Fritsche and H.G. Muller, Z. Phys. Chem. (Leipzig), 266, 595 (1985).

44. R. Kirchheim, Acta Metall. 34, 37 (1986).

45. C. Budin, A. Lucasson, and P. Lucasson, J. Phys. (Paris) 25, 751 (1964).

46. G.R. Caskey Jr., R.G. Derrick, Scripta Metall. 10, 377 (1976).

47. J.P. Hirth, Metall. Trans. A, 11A, 861 (1980).

48. A.J. Kummick and H.H. Johnson, Acta Metall. 28, 33 (1980).

49. H.H. Podgurski and R.A. Oriani, Metall. Trans. 3, 2055 (1972).

50. R. Kirchheim, Acta Metall. 29, 835, 845 (1981).

51. G.J. Thomas, in "Hydrogen Effects in Metals," Met. Soc. AIME (1981), I.M. Bernstein and A.W. Thompson, eds., p. 77.

52. T. Mutschele and R. Kirchheim, Scripta Metall. 21, 135 (1987).

53. S.W. Stafford and R.B. McLellan, Acta Metall. 22, 1463 (1974).

54. H. Ohma, G.P. Tivari, Y. Iijima and K. Hirano, Proc. 2nd J.I.M. Intnl. Symp. "Hydrogen in Metals" (1979), Jap. Inst. Metals, p. 229.

55. M.B. Whiteman and A.R. Troiano, Phys. Status Solids, 7, K109 (1964).

56. J.P. Laurent, G. Lapasset, G. Aucouturier, and M. Lacombe, in "Hydrogen in Metals," Met. Soc. AIME (1974), I.M. Bernstein and A.W. Thompson, eds., p. 559.

57. J.C.M. Li, R.A. Oriani, and L.S. Darken, Z. Physik Chem. (N.F.) 49, 271 (1966).

58. R.A. Oriani, Acta Metall. 14, 84 (1966).

59. H. Frieske and E. Wicke, Ber. Bunsenges, Physik. Chem. 77, 50 (1973).

60. H. Wagner, in Ref. 1, Vol. 1, p. 5.

61. H.C. Jamieson, G.C. Weatherly, and F.D. Manchester, J. Less-Common Metals 50, 85 (1976).

62. K.W. Keher, in Ref. 1, Vol. I, p. 197.

63. J. Volkl and G. Alefeld, in Ref. 1, Vol. I, p. 321.

64. J. Volkl, G. Wollenweber, K.H. Klatt and G. Alefeld, Naturforsch 26A, 922 (1971).

65. H.G. Nelson and J.E. Stein, NASA Report TND-7265 (1973).

66. Ref. 22, calculated from O.D. Gonzalez, Trans. Metall. Soc. AIME 245, 607 (1969).

67. Y. Hayashi, H. Hagi and A. Tahara, in Ref. 2, p. 815.

68. B. Baranowski, in Ref. 1, Vol. II, p. 157.

69. R. Gomer, R. Wortman and R. Lundy, J. Chem. Phys. 26, 1147 (1957).

70. R. Wortman, R. Gomer, and R. Lundy, J. Chem. Phys. 27, 1099 (1957).

71. M.L. Hill and E.W. Johnson, Acta Metall. 3, 566 (1955).

72. D.R. Arantes, X.Y. Huang, C. Marte and R. Kirchheim, Acta Metall. 41, 3215 (1993).

73. T.M. Harris, and R.M. Latanision Metall. Trans A, 22A, 351 (1991).

74. E.G. Seebauer, A.C.F. Kong, and L.D. Schmidt, J. Chem. Phys. 88, 6597 (1988).

75. L.S. Darken and R.P. Smith, Corrosion 5, 1 (1949).

76. T. Matsumoto, J. Phys. Soc. Japan, 42, 1583 (1977).

77. C.A. Wert, in Ref. 1, Vol. II, p. 305.

78. O. Yoshinari, K. Suito, T. Miura, and K. Tanaka, in Ref. 2, p. 825.

79. C.G. Chen and H.K. Birnbaum, Phys. Status Solids 36a 687 (1976).

80. G.M. Pressouyre and I.M. Bernstein, Metall. Trans. A, 9A 571 (1978).

81. A.M. Nabb and P.K. Foster, Trans. Metall. Soc. AIME, 227, 618 (1963).

82. R.A. Oriani, Acta Metall. 18, 147 (1970).

83. R. Kirchheim, Scripta Metall. 14, 905 (1980).

84. P. Bastien and P. Azou, Compt. Rend. Acad. Sci. Paris, 232, 1845 (1951).

85. M.R. Louthan, G.R. Caskey, J.A. Donovan and D.W. Rawl, Mater. Sci. Eng. 10, 357 (1972).

86. M.R. Louthan, pp. 53-78 "Hydrogen in Metals," I.M. Bernstein and A.W. Thompson, eds. ASM, Metals Park, OH, 1974.

87. K.G. Denbigh, "The Thermodynamics of the Steady State," Methuen, London (1951).

88. H. Wipf, in Ref. 1, Vol. II, p. 273.

89. R.A. Oriani and O.D. Gonzalez, Trans. Met. Soc. AIME 239, 1041 (1967).

90. O.D. Gonzalez and R.A. Oriani, Trans. Met. Soc. AIME 233, 1878 (1965).

91. A.W. Aldag and L.D. Schmidt, J. Catalysis 22, 260 (1971).

92. H. Conrad, G. Ertl, and E.E. Latta, Surface Sci. 41, 435 (1974).

93. W.H. Weinberg and R.P. Merrill, Surface Sci. 33, 493 (1972).

94. W. Aver and H.J. Grabke, Ber. Bunsenges. Physik. Chem. 78, 58 (1974).

95. W. Palczewska, Bull. Acad. Polon. Sci., Ser. Sci. Chim. 12, 817 (1964).

96. B.Y. Liaw, P.-L. Tao, P. Turner, B.E. Liebert, J. Electronal, Chem. 319, 161 (1991).

97. Stackelberg and Bischoff, Z. Elektrochem. 58, 702 (1955).

98. E. Storms, C. Talcott and M.L. David, Proc. NSF-EPRI Workshop on Anomalous Effects in Deuterated Metlas, Washington 1989; p. 5-1.

99. J.F. Newman and L.L. Shreir, Corros. Sci. 9, 631 (1969).

100. T. Zakroczymski, Z. Szklarska-Smialowska and M. Smialowski, Werkst. Korros. 26, 624 (1975).

101. A.M. Riley, J.D. Seader, D.W. Pershing, A. Linton, and S. Shimizu, Report NCFI-3, National Cold Fusion Institute, Utah 1990.

102. A. Efron, Y. Lifshitz, I. Lewkowicz, in Ref. 2, p. 1255.

103. B.Baranowski, Ber. Bunsenges. Physik. 76, 714 (1972).

104. R.A. Oriani and P.H. Josephic, Proc. Symp. "Environment Sensitive Fracture of Engineering Materials," Met. So. AIME, Z.A. Foroulis, ed., (1979) pp. 440-450; R.A. Oriani, Proc. "Hydrogen Effects in Metals," I.M. Bernstein, A.W. Thompson, eds., Met. Soc. AIME 1981, pp. 235-54.

105. E. Riecke, Werkst. Korros. 29, 106 (1978).

106. G.H. Schwuttke and H.J. Queisser, J. Appl. Phys. 33 1540 (1962).

107. D.P. Miller, J.E. Moore, and C.R. Moore, J. Appl. Phys. 33, 2648 (1962).

108. J. Washburn, G. Thomas and H.J. Queisser, J. Appl. Phys. 35, 1909 (1964).

109. S. Prussin, J. Appl. Phys. 32, 1876 (1961).

110. J.C.M. Li, Metall. Trans. A, 9A, 1353 (1978).

111. M.E. Armacanqui and R.A. Oriani, Mater. Sci. Eng. 91, 143 (1987).

112. J.K. Boah and P.G. Winchell, Metall. Trans. A, 6A, 717 (1975).

113. T. Sakuma, S. Takada, M. Hasabe and T. Nishizawa Trans. Japan Inst. Met. 17, 637 (1976).

114. M.E. Armacanqui and R.A. Oriani, Mater. Sci. Eng. 92, 127 (1987).

115. W. Krause and L. Kahlenberg, Trans. Electrochem. Soc. 68, 449 (1935).

116. T. Takeyama and H. Takahashi, Proc. 2nd J.I.M. Intnl. Symp. "Hydrogen in Metals" (1979), Japan Inst. Metals p. 409.

117. M. Smialowski, Scripta Metall. 13, 393 (1979).

118. C.P. Ju, J. Don and J.M. Rigsbee, Mater. Sci. Eng. 77, 115 (1986).

119. W. Raczynski, personal communication from M. Smialowski, 1975.

120. W. Beck, J. O'M. Bockris, J. McBreen and L. Nanis, Proc. Roy. Soc. (London) A290, 220 (1966).

121. S. Veprek, F. Mattenberger, M. Heintze, M. Wiggins, M. Kitajima, K. Yamashita, and R. Gotthardt, J. Vac. Sci. Techn. A7, 69 (1989).

122. T. Schober, Scripta Metall. 7 1119 (1973).

123. P. Lecoq, Ph.D. thesis, University of Illinois 1974.

124. M. Wise, J. Farr, I. Harris and J. Hirst, in "L'Hydrogene dans les Metaux," Vol. 1, p. 1, Editions Schience et Industrie, Paris 1972.

125. E. Storms and C. Talcott-Storms, Fusion Techn. 20, 246 (1991).

126. S. Guruswamy, J.G. Byrne, J. Li and M.E. Wadsworth, Proc. EPRI-NSF Workshop on Anomalous Effects in Deuterated Metals, Washington, D.C., (1989) p. 16-1.

127. T.B. Flanagan, ibid., p. 4-1.

128. T. Matsumoto Fusion Techn. 19, 567 (1991).

129. R.A. Oriani, unpublished results.

130. "Hydrogen Degradation of Ferrous Alloys," R.A. Oriani, J.P. Hirth and M. Smialowshi, eds., Noyes Publications Park Ridge, NJ, 1985.

131. M. Iino, in Ref. 130, p. 737.

132. H. Hasegawa and K. Nakajima, Phys. F. Metal. Phys. 9, 1035 (1979).

133. L.M. Brown and J.D. Embury, Proc., The Institute of Metals, Vol. 1, p. 164 (1973); W. Roberts, B. Lehtinen and K.E. Easterling, Acta Metall. 24, 745 (1976).

134. K. Yoshiino and C.J. McMahon Jr., Metall. Trans. 5, 363 (1974).

135. O.A. Onyewuenyi, in Ref. 128, p. 414.

136. T. Tabata and h.K. Birnbaum, Scripta Metall. 17, 947 (1983); 18, 231 (1984).

137. R.A. Oriani, Corrosion 43, 390 (1987).

138. D.R. Rolison and P.P. Trzaskoma, J. Electroanal. Chem. 287, 375 (1990); P.P. Trzaskoma, D.R. Rolison and R.G. Vardiman, in Proc. "Application of Surface Analysis Methods to Environmental Materials Interactions," Electrochemical Society meeting Oct. 1990, Seattle.

139. M.E. Armacanqui and R.A. Oriani, Mater. Sci. Eng. 92, 127 (1987).

140. R.A. Oriani, Ann. Rev. Mater. Sci. 8, 327 (1978).

141. C.D. Beachem, Metall. Trans. 3, 437 (1972); S.P. Lynch, Scripta Metall. 13, 1051 (1979).

142. H.K. Birnbaum, Proc. 1st Intnl. Conf. "Environment-Induced Cracking of Metals," R.P. Gangloff, M.B. Iver, eds., NACE, 1990, pp. 21-30.

143. M.C.H. McKubre, S. Crouch-Baker, A.M. Riley, S.I. Smedley, and F.L. Tanzella, Proc. 3rd Intnl. Conf. Cold Fusion 1992.

144. T.A. Chubb and S.R. Chubb, Fusion Techn. 17, 710 (1990).

145. P.I. Golubnicki, V.A. Kurakin, A.D. Filonenko et. al., Dokl. Akad. Nauk. SSSR 307, 99 (1989). [Sov. Phys. Dokl. 34 (7) 628 (1989).

Table I. Partial Molal Volume of H and of D in Various Metals

Host Metal	$\bar{V}_H$ $cm^3\ mol^{-1}$	Reference	$\bar{V}_H/\bar{V}_D$	Reference	Site Occupied*	Reference
Pd	1.50	12	< 1	15	O	8
	1.57	8	> 1	16		
	1.68	13				
	1.73	14				
$Pd_{.9}Ag_{.1}$			0.97	13		
$Pd_{.75}Ag_{.25}$	1.90	17				
Ta	1.69	13	1.08	13	T	18
Nb	1.89	13	1.0	13	T	18
	1.57	19	0.88	19		
V	1.61	13	1.0	13	T	18
	1.78	19	0.94	19		
α-Ti	2	25				
β-Ti	1.6	23			T	24
β-ZrH_2	2.7	23			T	24
α-Fe	2.0	20,21			O	22
$NiH_{.6}$	1.85	13			O	26

* O: octahedral site; T: tetrahedral site

Table II. Interaction Enthalpies, kJ/mol H, Between Dissolved Hydrogen and Structural Defects

Metal	*Dislocation Cores*	*Reference*	*Grain Boundaries*	*Reference*	*Interphase Interfaces*	*Reference*
α-Fe	-20 to -30 (screw) -59 (mixed)	47 48	~-6.0	47	-65 (AlN) ~-85(Fe_3C) ~-95 (TiC)	49 47 47
Pd	-60 to -70 (edge)	50	-5.3 (σ=15)*	52		
Ni	-9.6 to -19.2	51	-4.3	53		
Co			-8.0	53		

* σ = width of Gaussian distribution

Table III. Diffusivity of Hydrogen at Low Concentrations and About Room Temperature

Host Metal	*Hydrogen Isotope*	*D_o cm^2s^{-1}*	*E_a $kJ\ mol^{-1}$*	*Temp Range, °C*	*Reference*
Pd	H	2.9×10^{-3}	22.2	-50 to 600	63
	H	5.3×10^{-3}	22.8		8
	D	2.7×10^{-3}	20.5		8
	D		19.8		64
	T	7.2×10^{-3}	30.1		8
Ni	H	4.8×10^{-3}	39.4	0 to 358	63
α-Fe	H	7.5×10^{-3}	10.1	0 to 770	65
	H	2.3×10^{-3}	6.66		65
	H	0.78×10^{-3}	7.9		66
	H	3.35×10^{-4}	3.4		67
	D	3.35×10^{-4}	5.0		67
Nb	H	5.0×10^{-4}	10.2	0 to 500	63
	D	5.2×10^{-4}	12.3	-125 to 300	63
	T	4.5×10^{-4}	13.0	-50 to 30	63
Ta	H	4.4×10^{-4}	13.5	-20 to 400	63
	D	4.6×10^{-4}	15.4		63
V	H	3.1×10^{-4}	4.3	-125 to 300	63
	D	3.8×10^{-4}	7.0		63
$Pd_{.8}Ag_{.2}$	H	3.4×10^{-3}	22.4		8
	D	1.6×10^{-3}	19.9		8
	T	5.6×10^{-3}	23.9		8
$Pd_{.8}Ni_{1.2}$	T	3.4×10^{-3}	23.9		8

Table IV. Interaction Enthalpies(kJ/molH) Between Dissolved Hydrogen and Dissolved Impurities

Host Metal	*Impurity*	*Interaction Energy*	*Reference*
Nb	V	-8.7	76
	O	-8.7	77
Ta	N	-5.8	77
V	O	-7.4	78
	Ti	-7.0	78
αFe	C	-3.3	79
	Ti	-26	80

Table V. Effective Charge, Z*, and Heat of Transport, Q*, of Hydrogen in Various Metals (From Ref. 88)

Host Metal	*Hydrogen Isotope*	*Z* (unites of electronic charge)*	*Q*, eV/atomH*
α-Ti	H		+0.23
β-Ti	H	Positive for H and D	+0.027
α-Zr	H	Negative	+0.26
β-Zr	H	Negative for H and D	+0.25 to +0.5
δ-Zr	H		+0.056
V	H	+1.6 to + 1.4	+.017 to 0.087
	D	+1.8 to + 1.5	
Nb	H	+2.6 to +2.4	+0.15 to +0.13
	D	+2.1 to +1.9	+0.13 to 0.11
αFe	H	+0.24 to +0.29	-0.35 to -0.24
	D	+0.42 to +0.43	-0.34 to -0.23
Ni	H	+0.67 to +0.57	-0.065 to -0.009
	D	+0.84 to +0.74	-0.056 to -0.035
Pd	H	+0.4 to +0.55	+0.065
	D	+0.51 to +0.59	
Ag	H	-6.8	
	D	-18	
Ta	H	+0.2 to +0.6	
	D	+0.2 to +0.5	

Note: The ranges of values for Z* and Q* pertain to temperature variations of those parameters.

Table VI. Fugacity - Pressure Relationship for Hydrogen Gas at 25°C (from Ref. 103).

Fugacity, atm	*Pressure, atm*
28.1	27.7
247	217
896	609
1860	987
3060	1315
6880	1955
1.25×10^4	2510
1.13×10^5	5045
1.67×10^6	8990
1.01×10^7	1.20×10^4
1.66×10^8	1.73×10^4
1.22×10^9	2.14×10^4

ALFRED COEHN AND AFTER: THE α, β, γ OF THE PALLADIUM-HYDROGEN SYSTEM

Claudia Bartolomeo
M. Fleischmann
G. Larramona
S. Pons
Jeanne Roulette
H. Sugiura
IMRA Europe, S.A.
Science Centre
220, Rue Albert Caquot
Sophia Antipolis, 06560
FRANCE

G. Preparata
University of Milan
Via Celoria, 16
20133 Milano
ITALY

Abstract

The Pd–H and Pd–alloy–H systems have been investigated for more than 100 years and, following the discovery of D, these studies have been extended to the Pd–D and Pd–alloy–D systems. The bulk of these investigations have dealt with:

(i) the behaviour of H and D in the dilute α–phase

(ii) the thermodynamics of the transition to and the structure of the β–phase.

It is frequently asserted that these studies give no support for the notion that D dissolved at high activities in Pd and Pd–alloys can take part in novel nuclear reactions; these assertions are made notwithstanding the fact that there is no satisfactory model which can explain the properties of these strange materials.

The major illustration of the unsatisfactory nature of the currently accepted models is provided by the investigations of Alfred Coehn; a series of experiments carried out in the late 1920's and early 1930's showed that hydrogen in palladium is present as protons and experiences the full changes of the Galvani potential within the metal. We will trace the fate of this generic observation and indicate its importance to the development of the investigation of anomalous nuclear processes in host lattices.

We will illustrate also that these anomalous nuclear processes take place under conditions which have not been covered by the conventional studies of the "hydride phases", (i) and (ii). Recent measurements of the loading of the host lattices with H and D as well as of

diffusion of H and D under the extreme conditions used in these studies indicate that a third, γ–phase is formed. The significance of this phase for the observation of anomalous nuclear processes will be discussed. It will be shown that the experiments of Alfred Coehn can be developed to give new insights into the behaviour of the "hydride phases".

Introduction

The bulk of the investigations of the Pd–H and Pd–D systems have been concerned with two themes:

(i) the behaviour of H and D in the dilute α –phase

(ii) the thermodynamics of the transition to and the structure of the β–phase

In discussing the background of the topic of "Cold Fusion" the interpretation of (i) and (ii) is usually presented as giving no credence to the notion that D electrochemically compressed in Pd and Pd–alloy host lattices (as well as related topics using other methodologies and host lattices) can undergo anomalous nuclear reactions. A representative example of this stance is given by the views expressed in the Report of the Energy Research Advisory Board of the United States Department of Energy[1]. In this report we find one additional item of information which can be summarised by:

(iii) the interaction between H–species in the lattice (or D–species in the lattice) is repulsive.

In considering the validity of this stance we must naturally start with a series of questions: These include:

(i) (a) is the behaviour of the α–phase understood?

(ii) (a) is the behaviour of the β–phase understood?

(iii) (a) is this conclusion correct?

One of the major objectives of the present paper is to bring into focus once again the work of Alfred Coehn[2] which we believe is central to developing an understanding of the Pd–H and Pd–D systems*. As we shall see this reconsideration of Coehn's work leads us to the conclusion

(i) (b) the behaviour of the α–phase cannot be explained by currently accepted models (see also [5])

and by implication to

*As we explain in a further paper presented at this meeting[3] it was our consideration of the consequences of Coehn's work (coupled to the quasi–thermodynamic analysis of the electrochemical potential developed by Lange[4]) which led us to pose the question: is it possible to induce nuclear reactions of D^+ in Pd host lattices by compressing these species by means of differences in the Galvani potential?

(iii) (b) while the conclusion (iii) is probably correct, the connotation in which this conclusion has been used is incorrect.

It is naturally possible that the behaviour of the β–phase is understood even though that of the α–phase is not (although this is an unlikely circumstance). However, the properties of the β–phase are not likely to be of principal concern in seeking an understanding of the strange behaviour of Pd and Pd–alloy cathodes polarised in D_2O solutions – at least as far as the generation of excess enthalpy is concerned. This phenomenon is observed under such extreme conditions (specifically high D:Pd ratios [6–8]) that it appears to be somewhat futile to consider the phenomena observed in the context of the supposedly known behaviour of the α and β Pd–D phases. We should address instead the questions (i)(a), (ii)(a) and (iii)(a) as well as:

(iv) what is the nature of the species present at high D/Pd (or H/Pd) ratios?

(v) what are the dynamics of D and H in Pd and Pd–alloy host lattices under these conditions?

(vi) how is the D/Pd (or H/Pd) ratio related to the experimental conditions at such high values of the ratio?

(vii) what is the structure of these systems under these conditions?

with the aim of seeing whether any of the information obtained can explain the behaviour of Pd and Pd–alloy cathodes polarised in D_2O solutions. There has been virtually no information available about this topic although this situation is now changing (eg see[9,10]). It is certainly possible that a further phase transformation takes place at high D:Pd ratios leading to the formation of a γ–phase[11] † and that it is the properties of this phase which will explain the nuclear processes induced in Pd and Pd–alloy host lattices.

In the next section we discuss the initial experiments of Alfred Coehn (and comment on the follow–up of this work) in the context of seeking an answer to question (i)(a) as well as the relevance of (iii) (see (iii)(b) above). In the following sections we indicate one particular way in which these experiments could be developed further to obtain an understanding of the Pd–H and Pd–D systems at high H:Pd and D:Pd ratios‡ The results obtained show very clearly the complexities of these systems at high charging ratios.

The significance of the experiments of Alfred Coehn

Coehn's original experiment is illustrated in Fig 1[2]. For quantitative experiments a 100μm diameter Pd wire was folded into a zig–zag shape. The bottom section was electrolytically charged with hydrogen and the assembly was then placed into xylene (a non–conducting liquid), a current of 1A being passed through the wire. The assembly was periodically removed from the organic insulating liquid and the positions reached by the hydrogen waves moving towards the negatively and positively polarised ends of the wire

†It is in part for this reason that we have chosen the second part of the title of this paper: "the α, β, γ of the Palladium–Hydrogen System." However, we also note that the Greek alphabet takes precedence over the Roman script.

‡It is possible to devise many new types of experiments based on generalisations of Coehn's original concept[12].

were determined (the arrival times at each zig–zag were determined by measuring the displacement of the potential towards the reversible hydrogen value by means of a calomel reference electrode having a capillary probe). Fig 2 indicates some of the results obtained: the hydrogen can be seen to move more rapidly towards the negatively polarised end of the wire than by diffusion alone and more slowly towards the positively polarised end. The implication is clear: the hydrogen must be in the form of a proton and this is confirmed by the reversal of the effects of the electric field (the gradient in the Galvani potential) on reversing the direction of the current, Fig 2 (see further below).

It would be difficult to overestimate the significance of these experiments in the modelling of the nature of the Pd–H and Pd–D systems[§]. For the conditions used, the lattice must have been in the α–phase domain and it is therefore plausible to apply "dilute solution" theory to the interpretation of the measurements. For such dilute solutions we can express the electrochemical potential as

$$\begin{aligned} \overline{\mu}_{H+} &= \mu + F\phi \\ &= \mu^{\circ}_{H+} + RT \ \ln C_{H+} + F\phi \end{aligned} \tag{1}$$

where we assume the limiting condition that the hydrogen has unit positive charge (see below). The flux in the direction of the z–axis due to the combined effects of diffusion and migration is then

$$f = -D_{H+}\frac{\partial C_{H+}}{\partial z} - U_{H+}C_{H+}\frac{\partial \phi}{\partial z} \tag{2}$$

where the diffusion coefficient, D_{H+}, and mobility, U_{H+}, are related by the Nernst–Einstein equation

$$U_{H+} \simeq \frac{F}{RT}D_{H+} \tag{3}$$

The measurements made by Coehn do in fact show that (3) applies so that we can conclude that the hydrogen is present as "bare protons" which experience the mean electrical field in the lattice.[¶] In view of the importance of these experiments, it is of some interest to reflect on their impact on the understanding of the Pd–H and Pd–D systems. The subject is not mentioned in the early "classical texts"[13–16] (although Kittel does refer

[§]Nernst (who had himself been interested in the correct description of hydrogen in the Pd–lattice) congratulated Coehn on the execution of this investigation.

[¶]We observe also that (2) gives the divergence

$$\frac{\partial C_{H+}}{\partial t} = D_{H+}\frac{\partial^2 C_{H+}}{\partial z^2} + U_{H+}C_{H+}\frac{\partial^2 \phi}{\partial z^2} + U_{H+}\frac{\partial C_{H+}}{\partial z}\frac{\partial \phi}{\partial z} \tag{4}$$

For a linear gradient in potential

$$\phi = \alpha + \beta z \tag{5}$$

we obtain

$$\frac{\partial C_{H+}}{\partial t} = D_H^+\frac{\partial^2 C_{H+}}{\partial z^2} + U_{H-}\beta\frac{\partial C_{H+}}{\partial z} \tag{6}$$

and, for the usual conditions

to early magnetic resonance experiments which were concerned with the state of hydrogen in the lattice[‖]). The topic reappears in the text by Lewis[17] spurred by the reinvestigation initiated by Wagner and Heller[18] using the experimental set–up illustrated in Fig 3. Lewis expressed reservations about this subject which we will discuss further below.

The investigation by Wagner and Heller have sparked a series of investigations (for references up to 1978 see[21]) and the topic is discussed in the text by Völkl and Alefeld[20,21]. In the interpretation of these later experiments it has been assumed that the proton (or deuteron) is partially screened so that (1) is modified to

$$\overline{\mu} = \mu + Z^* F \phi \tag{11}$$

Where Z^* is an effective charge number. Apart from the difficulty of assuming that we can ever have an independent species with a fractional charge[**] we note that the experiments based on that devised by Wagner and Heller[18], Fig 3, are ambiguous whereas that of Coehn[2], Fig 2, is not. Coehn measured the movement of the diffusion–migration wave towards both the negatively and positively polarised ends of the wire and characterised this using the arrival time of the wave front; on the other hand the experiments of Wagner and Heller (and of subsequent workers using experiment designs based on Fig 3[21]) are based on measurements of the flux through the wire. The interpretation requires that a leak free seal can be made for a wire having a defined length which is virtually impossible to achieve. Furthermore, the boundary condition at $z = \ell$ is ambiguous, see the next section. These difficulties no doubt explain the marked variability of the derived values of Z^* (which straddle $Z^* \simeq 0.5$) although some of the variability must be due to the marked changes of D with the charging ratio X = H/Pd[9], a topic which we discuss further in the final section of this paper.

In any event, the question of whether or not the proton or deuteron in the lattice carries a

---

$$D_{H+} \gg U_{H+}\beta \tag{7}$$

$$\frac{\partial C_{H+}}{\partial t} \simeq D_{H+}\frac{\partial^2 C_{H+}}{\partial z^2} \tag{8}$$

we obtain the "normal conditions" of Physics and Chemistry of processes controlled by diffusive motion. However, for the particular case of hydrogen or deuterium dissolved in host lattices it is possible to realise the condition

$$U_{H+}\beta \gg D_{H+} \tag{9}$$

especially for pulsed electrical potentials[12]) giving the first order wave equation

$$\frac{\partial C_{H+}}{\partial t} \simeq U_{H+}\beta\frac{\partial C_{H+}}{\partial z} \tag{10}$$

The conversion of (8) into (10) affords one of the simplest means of observing Physics and Chemistry in wave rather than in diffusive fields. As we have noted elsewhere at this meeting[3] it also affords a means of generating deuterons at extreme electrochemical potentials within the lattice.

[‖]The books by Smithells[13] and Barrer[14] contain a great deal of empirical information about the Pd–H system which is valuable to those wishing to set up experiments on excess enthalpy generation using the Pd–D system (it will explain some of the reasoning which underlies our own experimental protocols). Much of this information has disappeared from later texts[19,20,22].

[**]We can only have such a situation for a species which is part of a larger quantum system. a topic which we will discuss elsewhere[12]

partial charge is not critically important to the argument which we will develop based on the energetics of these species. We note here that the question of the state of this species was not discussed in the ERAB report[1]. The topic of migration is not covered in Volume I of a recent monograph[22]††.

We consider next the reservations which were expressed by Lewis and quote from pages 159 and 160 of [17]:

"at present in general, incomplete knowledge of the reason for the expansion of the lattice and of the form in which hydrogen is absorbed hinders application of an analysis of the energetics of lattice formation in terms of modified forms of Born–Haber cycles – such as has been attempted by Gibb(1962a)‡‡ in the case of hydrides for which the balance of evidence suggests that hydrogen is most likely to be in the form of a negative ion as a first approximation".

While it is certainly true that the application of Born–Haber type cycles can give convincing proofs that all energy terms have been fully taken into account, these cycles are not usually applied with that end in view. The objective rather is to use these cycles to evaluate energy terms which are not otherwise available. We have applied the Born–Haber cycle in this spirit[25] to the dissolution of protons in the lattice which brings us to the important conclusion that the "solvation energy" of these species must be at least 11.7 eV Fig 4. The reason why this is a lower limit is because we have neglected several terms which would increase the required "solvation energy term" still further (eg the change in the Fermi level and the work term required to expand the lattice).

The magnitude of this "solvation energy" is truly phenomenal and implies that the protons sit in extremely deep energy wells. It is this high interaction energy rather than the repulsion between the protons which determines the properties of the system. However, the latter undoubtedly contributes to the reversal in sign of the partial molar enthalpy of absorption with increasing charging ratio (see Fig 4 of [3]). As we have pointed out in this further paper presented at this meeting [3], the reversal in the partial molar heat of absorption has been of key importance in determining our choice of experimental protocols. It can be seen the observation (iii) (a) contained in the ERAB report has been entirely misconstrued, see (iii) (b).

We observe also that the energy wells would still be extremely deep even if the protons carried a fractional charge $z \simeq 0.5$. The conclusion that the protons sit in deep energy wells might be acceptable were it not for the fact that the protons (or deuterons) are highly mobile so much so that they behave as classical oscillators under the conditions which are required for the observation of excess enthalpy generation. We are therefore faced with the central conundrum which must be resolved by any model which seeks to account for the behaviour of these strange systems. This is embodied in the question:

"How can it be that the protons (or deuterons) are so tightly bound yet they are virtually unbound in their movement through the lattice?"

In our own view the answer must be:

"The protons (or deuterons) are in a collective state described by Macroscopic Quantum

††We do not know whether this topic has been discussed in Volume II[23]

‡‡our reference[24]

Mechanics so that they can experience intense anharmonic excitations"

We recall also the "bottom line" of an earlier study of the variation of the electrolytic H/D separation factor with potential [26]. The conclusion was:

"The variation of this separation factor with potential cannot be adequately explained in terms of simple models of localised oscillators"

A reading of this paper will show that this was equally true of the electrolytic discharge reaction.

Finally we note once again (compare[25,27]) that it is remarkable that the protons (or deuterons) are present at very high concentrations (~100M) in the presence of an even higher concentration of electrons (~1000M) yet hydrogen atoms (or deuterium atoms) are not formed. The high stability of the ensemble of protons (or deuterons) in the presence of the electron plasma requires a quite exceptional interaction energy of the collective proton (or deuteron) state and, in all probability, the intervention of a "third actor".

In the following Sections we outline one of our approaches to the extension of the experiments of Coehn although the results presented here deal mainly with the case of diffusion without significant migration (other experimental systems will be described elsewhere[12]). The results obtained demonstrate the hitherto unexpected complexities of the dynamics of the Pd–H system at high loading ratios.

A simple extension of the experiment of Coehn[2]

One of the simplest extensions of the experiment of Coehn is to measure the time dependent flux at a point $z = \ell$ of a thin wire where the concentration is maintained at zero throughout the experiment, the ingoing interface being maintained at a convenient point in the α–phase region. For the case where the surface of the wire $r = a,\ 0 < z < \ell$ is a perfect diffusion barrier: the solution is given in Appendix A by equation (A.7) and in dimensionless form by (A.15); for small T and/or large H the convergence is poor and we can then use the alternative expression (A.16). The corresponding equations for zero migration are (A.11) and (A.12). Fig 5 gives the plot for the case of diffusion alone and Fig 6 gives a number of plots with increasing effects of migration as expressed by the parameter H.

It should be noted that this particular experiment is quite different from those devised by both Coehn[2] and by Wagner and Heller[18] (and of succeeding investigations using essentially the same method eg see[21]). In the case discussed here the boundary condition (A.6) ensures simple and reproducible conditions at $z = \ell$; for the experiments of Coehn, the exact corresponding boundary condition is

$$D_{H+}\frac{\partial C_{H+}}{\partial z} + U_{H+}\beta C_{H+} = 0. \quad z = \ell \quad t > 0 \tag{11}$$

although, for the conditions of the actual measurements, it is probably sufficiently accurate to take

$$C_{H+} = 0. \quad z = \infty. \quad t > 0 \tag{12}$$

On the other hand the nature of the boundary conditions at $z = \ell$ for the experiments of Wagner and Heller[18] is by no means clear. As can be seen from Fig 3, the hydrogen pressure at the outgoing interface, $z = \ell$, is essentially the same as that at the ingoing interface, $z = 0$. We therefore have to consider the effects of the following reaction sequence at both interfaces:

$$\begin{aligned} (H^+)_{lattice} + e &\rightleftharpoons (H)_{ads} && (A) \\ (H)_{ads} + (H^+)_{lattice} + e &\rightleftharpoons (H_2)_{gas} && (B) \\ (H)_{ads} + (H)_{ads} &\rightleftharpoons (H_2)_{gas} && (C) \end{aligned}$$

where reactions (A) and (B) are the solid state analogues of the Butler–Volmer and Horiuti–Heyrovsky reaction steps of the electrochemical hydrogen evolution ((C) is the Tafel step). Furthermore if the dissociation

$$(H)_{lattice} \rightleftharpoons (H^+)_{lattice} + e \qquad (D)$$

in the lattice has to be taken into account**, then the kinetics of this reaction will appear as a source term in the differential equation (6). The reaction sequence (A)–(C) would also have to be augmented by the step

$$(H)_{lattice} \rightleftharpoons (H)_{ads} \qquad (E)$$

We observe also that the rates of the reaction steps (A) and (B) depend on the distribution of the surface potential, $\chi^{(3)}$, just as the rates of the equivalent electrochemical steps depend on the distribution of Galvani potential difference between the metal and solution.

The possibility that the kinetics of desorption of H_2 from Pd host lattices might be kinetically complicated was discussed some time ago[14] although, as we have noted above, the fact that hydrogen in the lattice exists as protons was not recognised. This topic does not appear to have been considered further. We observe that reaction sequence (A)–(C), (D) reduces to the boundary condition

$$-D_{H^+}\frac{\partial C_{H^+}}{\partial z} + U_{H^+}\beta C_{H^+} = k_1 C_{H^+} - k_2, \quad z = \ell, \quad t > 0 \qquad (13)$$

for restricted sets of conditions where the constants k_1 and k_2 depend in complex ways on the rates of the individual reaction steps[12]. Although it is possible to obtain an analytical solution of the differential equation (6) for this particular boundary condition, it is not clear whether this particular solution applies to the experiments of Wagner and Heller[18] and to later experiments based on the same principles[20].

The electrochemical variant of this experiment based on the simple boundary condition (A.6) is free from this ambiguity. In spite of this simplification it will be shown that the observed behaviour deviates markedly from the simple predictions made for this boundary condition together with (A.5); the reasons for these deviations are discussed and it is

**The apparent partial charge, z*, determined in electrodiffusion experiments could be explained in terms of such an equilibrium.

shown that these complexities must be taken into account in the interpretation of electrodiffusion experiments.

Experimental

A schematic diagram of the cell used in the particular experiments described here is shown in Fig 7. This cell was divided into two compartments separated by a short, insulated, electrodiffusion section. The epoxy adhesive Araldite was found to be satisfactory for insulating the two compartments*. The length of the seal was measured at the conclusion of each experiment by measuring the distances from the end of the tube to the tip and to the adhesive surface; this measurement is subject to appreciable errors.

For the experiments described here 25 or 50μ radius Pd wires were spot-welded to heavy gauge Pt lead wires maintained in the upper section. The Pd wires extended for a considerable distance into the electrolyte in the main compartment and this lower section was surrounded by a large helical Pt-counter electrode. When required, the relatively high electrolytic current in the lower section could serve to produce fields of intermediate value (up to $\beta \sim 0.5V$ cm^{-1}) in the electrodiffusion section, thereby avoiding the need to make a further connection to a heavy gauge lead wire. The Pd-wire extending into the lower section was polarised galvanostatically using a Hi-Tek DT2101 potentiostat connected as a galvanostat. When attempting to measure the behaviour due to diffusion alone, a cathodic current of 10 mA was applied (the field generated by this current in the electrodiffusion section can be neglected for currents of this magnitude). This cathodic current was increased to 0.1 - 0.5 A (giving $\beta = 0.18 - 0.27V$cm^{-}1) for experiments where the migrational component of electrodiffusion becomes significant.

The upper, internal, part of the cell contained a Saturated Calomel Electrode (SCE) and, for measurements at higher currents a further Pt-secondary electrode. Two different measurement strategies were used to measure the flux at $z = \ell$ (the end of the insulated section of the wire). In the first, suitable for low values of this flux, a potential of 0.5 or 0.75 V was applied directly with respect to the reference electrode by means of a battery driving a potential divider (as shown in Fig 7). In the second, suitable for higher currents, a potentiostat was used. In both cases the currents were measured using Keithley 617 programmable electrometers. In the second configuration the central wire was connected to ground of the potentiostat so as to by-pass the current follower of this instrument. The Keithley electrometer was then placed in series with the secondary electrode; the configuration of the galvanostat was adjusted so as to keep the Pd electrode connected to ground. The electrometers were controlled using a computer, the current-time data being written to disk. We note that at the high potentials applied to the Pd-wire in the upper electrode compartment ($\sim$0.75 - 1.0 V verses the Normal Hydrogen Electrode (NHE)), all the species reaching $z = \ell$ will be immediately oxidised so that the boundary condition (A.6) is maintained.

In the experiments reported here, both of the electrode compartments contained the same electrolyte, 1M H_2SO_4.

Results

Fig 8 illustrates the behaviour for a 50μ radius wire when diffusion is dominant while Fig 9 gives a comparable transient for a 25μ radius electrode; Fig 10 shows a transient where the

*Other methods for making such insulating sections (including the use of insulating layers of organic liquids, as in the original experiments of Coehn[2]) will be described elsewhere[12]. We note that although leak-tight seals can be achieved using fine Pd wires in glass, these fine wires then inevitably curl so that it becomes impossible to estimate the lengths of the insulated sections.

migration component is significant ($\beta = 0.27 V cm^{-1}, H = 3.3$).

It is immediately apparent that these $I - t$ transients do not fit the predictions made from the simple model, equations (A.7) and (A.8) Figs 5 and 6. Thus Fig 11 compares the experimental result of Fig 9 with predictions made from (A.8) ie for the case where diffusion is dominant (the basis of this prediction is discussed further below). We can make the following significant observations:

(i) the current at $z = \ell$ is initially far below the diffusion controlled value

(ii) the current then shows an extremely sharp rise which is not consistent with any simple model of diffusion

(iii) for 25μ radius wires the current–time curves display a maximum

(iv) the current–time curves are "noisy" after the maxima whereas they are free from "noise" in the region before the sharp rise, (ii); we observe that any simple model of stochastic processes would predict a bigger "noise" component before the sharp rise in the current.

Having noted these very significant deviations from the simple model, equations (A.7) and (A.8), we must also take note of the fact that in general terms the results show that we are indeed observing an electrodiffusion phenomenon. Thus the current levels for 50μ radius wires are about 4 times as high as those for the 25μ radius wires; the increase in the steady–state current due to the applied electric field is also of the correct magnitude giving a ratio of U_{H+}/D_{H+} of about 40 V^{-1} in accord with the Nernst–Einstein relation.

However, any detailed comparison of experiments with the theory, Appendix A , must inevitably fail. The form of the experimental current–time curves indicates a "redistribution" of the diffusional phenomena in the time and distance domains. The most plausible explanation of the facts that the flux is initially low and then shows a sharp rise ((i) and (ii) above) is that a phase formation process propagates down the length of the wire, this phase formation being driven by the electrochemical charging at $z = 0$. The most plausible explanation of the maxima in the flux with increasing time ((iii) above) is that a focussed wave front is being propagated while the fluctuations after the maxima ((iv) above) indicate fluctuations in the phase domains within the lattice.

Although a detailed comparison of the experiments with the simple model. Appendix A, must fail, we need also to take due note of the fact that such a detailed examination of the data gives a good indication of the way in which we can develop a more comprehensive interpretation. For example, we can examine the variation of the steady–state diffusion controlled current with the length, ℓ, of the diffusion path:

$$I_{steady-state} = \frac{\pi r^2 F D_{H+} C_0}{\ell} \tag{14}$$

A plot of the data according to equation(13), Fig 12, gives a slope of $\pi r^2 F D_{H+} C_0$ of $180.1/\mu$A with a standard error of $6.13/\mu$A. In turn this gives us the product $D_{H+} C_0$ of 9.5×10^{-8} M cm^{-1} s^{-1}. If we assume that C_0 is maximally 0.1 mole cm^{-3}, we obtain $D_{H+} \sim 10^{-6}$ cm^2 s^{-1}. This very high value of D_{H+} (about a factor of 10 higher than that for diffusion in the α–phase) is a reflection of the fact that there is a steep increase in the

diffusion coefficient as a phase is being driven down the wire by the electrochemical charging process at $z = 0$.

An alternative way of examining the anomalous diffusional behaviour is to apply the relation

$$t_{\frac{1}{2}} = \frac{0.14\ell^2}{D_{H+}} \tag{15}$$

to the region of the steep increase of the currents, Figs 8 and 9. Fig 13 shows a plot according to this relation; we obtain a slope of 6.27 x 10^5 s cm^{-2} with a standard error of 3.62 x 10^4 s cm^{-2} giving $D_{H+} \sim 2.2 \times 10^{-7}$ cm^2 s^{-1}. The fact that this is much closer to the known value of D_{H+} in the α–phase simply reflects that the diffusional anomaly has been spread out in space–time. However, the anomaly remains because we now obtain $C_0 \sim 0.4\ M$ cm^{-3} which is a factor of > 4 higher than the generally assumed maximum value corresponding to H/Pd = 1.

It should be noted that the comparison of the experimental current–time transients with that predicted from equations (A.8), Fig 11, has been based on the independent estimation of the parameters D_{H+} and C_0 using the Marquardt-Levenberg method‡. Fig 14 shows a comparison of an experimental transient with the predictions using equation (A.8) and the parameters D_{H+} and C_0 determined according to the three methods outlined here. The inadequacy of the simple model based on the "dilute solution theory approximation with D_{H+} independent of concentration" will be fully apparent.

Discussion

The starting point for our interpretations of electrodiffusion based on experiment designs of the type illustrated in Fig 7 was predicated on the assumption that the major part of the insulated section would be in the α–phase domain so that "dilute solution theory" could be applied, see Appendix A (other experiment designs will be discussed elsewhere[12]). It was our view that electrochemical loading in the lower section of the cell would convert the wire in the region near $z = 0$ into the β–phase but that this phase would not extend far into the insulated portion of the wire. However, as can be seen, this view has proved to be incorrect and "dilute solution theory" cannot account for the results, Figs 8–10. (results for experiments where the whole length of the wire is in the α–phase domain will be discussed elsewhere[12]). It is evident that the variation of the diffusion coefficient with the charging ratio must play a key rôle in the behaviour of the system as must the formation of higher phases of palladium hydride ie of phases beyond the α–phase. The first important question is therefore:

"can the behaviour be explained simply in terms of the formation of the β–phase or is there evidence for the formation of a further γ–phase[11]?"

The importance of this question to the topic of excess enthalpy generation in the lattice will be apparent as the achievement of high charging ratios [7,8] may be a necessary but not sufficient condition for the observation of this phenomenon (see also[3]).

It is fortunate that the results of an independent study of the variation of the diffusion

‡In our opinion this is the most unbiased method for making such estimates.

coefficient with the charging ratio have become available during our study, Fig 15[9]. These results are truly remarkable: the diffusion coefficient rises as the formation of the β–phase is completed (we will discuss elsewhere why such a variation would be expected to hold[12]) reaching a value of $10^{-6}cm^2s^{-1}$, a value 10–100 times higher that that for the α–phase. The diffusion coefficient then falls, symptomatic of a further phase transformation, to be followed by a further rise to values inthe region of $10^{-5}cm^2s^{-1}$ ie the diffusion coefficient approaches the value for H_3O^+ in aqueous solution (itself only explicable in terms of correlated motion) in a lattice where the loading ratio approaches unity! As diffusion is driven by the gradient of the chemical potential with distance, the variation shown in Fig 15 gives the evidence for the phase transformation referred to above.

We therefore examine the implications of the measurements of Mengoli et al[9] for the interpretation of both the steady state diffusion limited currents and the shapes of the current–time transients such as that shown in Fig 9. In view of the very marked rise of the diffusion coefficient with the charging ratio, the β–phase propagates towards $z = \ell$ to be followed by the higher phase. the putative γ–phase. As the diffusion coefficient of H^+ in the α–phase is low by comparison, we can neglect the effect of this phase which is confined to a narrow region close to $z = \ell$. In Appendix B we show how we can locate the position of the $\beta - \gamma$ phase boundary, characterised by z^*/ℓ, for a set of measurements made with wires of different lengths, see Table 1. It is evident that this boundary propagates to a position very close to $z = \ell$.

Table 1

Values of the Charging Ratio x_0 Achieved at $z = 0$ and of the Position of the Boundary between the β– and γ– Phases

ℓ/cm	I/A	x_0	z^*/ℓ
0.425	4.2×10^{-7}	1.135	0.947
0.30	6×10^{-7}	1.137	0.948
0.45	3.25×10^{-7}	1.106	0.936
0.50	4.0×10^{-7}	1.153	0.953
0.45	4.0×10^{-7}	1.137	0.948
0.75	2.5×10^{-7}	1.141	0.950
0.80	3.1×10^{-7}	1.188	0.962
0.525	3.5×10^{-7}	1.140	0.949
0.55	3.10×10^{-7}	1.129	0.945
0.55	3.25×10^{-7}	1.136	0.947

The calculation also gives an estimate of the charging ratio at $z = 0$. This value is determined by the electrochemical charging process in the vicinity of this region and the constancy of x_0 is highly significant. Bearing in mind the nature of the approximations made, it is also significant that x_0 has an entirely plausible value in the vicinity of unity.

As is shown in Appendix B, the non–steady state predicted by this model is also in good accord with the experimental observations, Fig 9. The current at $z = \ell$ is predicted to be

zero for a defined time, t_s, at which point there is a sharp rise, Fig 17. The quantitative estimate of the rise in current, equation (B.52), Table 2, is in good accord with the experimental measurements, Fig 9.

Table 2

Variation of the current with time due to the propagation of the phase boundary in the Pd wire

$10^{-5}t/s$	$10^{8}I/A$
0.7	6.4
0.8	21.3
0.9	29.3
1.0	35.7
1.1	41.1

The analysis outlined in Appendix B also explains the appearance of the maxima in the current–time curves, Fig 9.

We note finally three important topics which we will discuss further elsewhere[12] and which are dependent on the projection of the phase boundary towards $z = \ell$, see Table 1. In the first place, the marked fluctuations in the current at long times (at times longer than that of the maximum. Fig 9) must be due to fluctuations in the position of this boundary. Secondly, the elimination of the maximum for larger diameter wires, Fig 8, must be due to a defocussing of the wave–front. Finally, the projection of the phase boundary over appreciable distances shows that it should be feasible to charge relatively large volumes of the host lattices to high D/Pd ratios provided the insulated surfaces act as effective diffusion barriers. The conditions required to achieve this will be dicussed elsewhere [12].

General comments and conclusions

In presenting this paper. one of our major aims has been to draw attention to the fact that the understanding of the behaviour of hydrogen (or deuterium) in palladium and palladium alloy host lattices is at best incomplete and, at worst, erroneous. We have developed this supposition by drawing attention again to the all important work of Coehn[2]. A consideration of the implications of this work shows how the modelling of the palladium–hydrogen system (and of related systems) must be corrected.

We have developed our argument by posing the questions:

(i) (a) is the behaviour of the α–phase understood?

(ii) (b) is the behaviour of the β–phase understood?

(iii) (b) is the conclusion 'that the interaction between H–species in the lattice is repulsive' correct?

Our answers to these questions at this time are

(i) (b) no;

(iii) (b) probably yes, but the connotation in which this conclusion has been used is incorrect.

We do not know what the answer to (ii)(a) may be, although it is unlikely that the basic model of the β–phase can differ markedly from that of the α–phase. As we have pointed out, the properties of the β–phase are not of concern to the understanding of the phenomena of excess enthalpy generation because these phenomena take place at very high D/Pd ratios. Instead, we require answers to the questions (iv)–(vii).

(iv) what is the nature of the species present at high D/Pd (or H/Pd ratios?

(v) what are the dynamics of D and H in Pd and Pd–alloy host lattices under these conditions?

(vi) how is the D/Pd (or H/Pd) ratio related to the experimental conditions at such high values of the ratio?

(vii) what is the structure of these systems under these conditions?

In the second part of this paper, we have indicated one of the ways in which the studies initiated by Coehn could be developed further. Although the results presented here have been confined principally to the case of diffusion from regions at high charging ratios, these results show quite clearly that answers to questions (iv)–(vi) can be obtained in this way. The results obtained show that hitherto unsuspected phenomena must be taken into account in interpreting such measurements (in particular, the propagation of phase boundaries within the host lattices). We note finally that it should prove possible to extend the answers to question (vi) to cover the important case of the relationship of the charging ratios to Galvani potential differences established within lattices. Furthermore, it should prove posssible to develop electromigration systems for studies of the structure of the lattices at high loading ratios (question (vii)).

Glossary of Symbols Used

C	is the concentration.	[Mole (litre)$^{-1}$]
D	is the diffusion coefficient.	[cm^2 s^{-1}]
F	is the Faraday.	[coulomb (g Mole)$^{-1}$]
I	is a current.	[A]
k_1	is a rate constant.	[cm s^{-1}]
k_2	is a rate constant.	[Mole cm^{-2} s^{-1}]
ℓ	is a length.	[cm]
r	is a radius.	[cm]
t	is the time.	[s]
T	is the temperature.	[K]
U	is the mobility.	[cm^2 V^{-1} s^{-1}]
Z^*	is a fraction.	
z	is a coordinate.	[cm]
α	designation of the α–phase of Pd/H or Pd/D.	
α	is a constant.	[V]
β	designation of the β–phase of Pd/H or Pd/D.	
β	is the electric field.	[V cm^{-1}]
γ	designation of the γ–phase of Pd/H or Pd/D.	
μ	is the chemical potential.	[J]
$\overline{\mu}$	is the electrochemical potential.	[J]
ϕ	is the Galvani potential.	[V]

Appendix A

A simple model for electrodiffusion in wires

For a linear gradient of potential applied to a wire and for a diffusion coefficient and mobility which are independent of the concentration we need to consider the solution of

$$\frac{\partial C_{H+}}{\partial t} = D_{H+}\frac{\partial^2 C_{H+}}{\partial r^2} + \frac{D_{H+}}{r}\frac{\partial C_{H+}}{\partial r} + D_{H+}\frac{\partial^2 C_{H+}}{\partial z^2} + U_{H+}\beta\frac{\partial C_{H+}}{\partial z} \qquad (A.1)$$

The simplest situation will be the case of a perfect diffusion barrier at the surface $r = a,\ 0 < z < \ell$ of the wire

$$D_{H+}\frac{\partial C_{H+}}{\partial r} = 0, \quad r = a, \quad 0 < z < \ell, \quad t \leq 0 \qquad (A.2)$$

Furthermore, for sufficiently long and sufficently thin wires

$$a \ll \ell \qquad (A.3)$$

so that the diffusional relaxation time

$$(\tau)_r = \frac{a^2}{D_{H+}} \qquad (A.4)$$

will be short compared to the time-scales of the experiments. In that case we can assume that equilibrium will be maintained locally in the radial direction and equation (A.1) reduces to (6).

We next consider the boundary conditions at $z = 0$ and $z = \ell$. If equilibrium is maintained at $z = 0$, then we will have a constant concentration at this point:

$$C_{H+} = C_0 = \frac{k_1}{k_2},\ z = 0,\ t > 0 \qquad (A.5)$$

while for our update of Coehn's experiment

$$C_{H+} = 0, \quad z = \ell, \quad t \geq 0 \qquad (A.6)$$

The solution of the time-dependent problem is

$$I = \frac{\pi r^2 F U_{H+} \beta \exp\left(\frac{-U_{H+}\beta\ell}{2D_{H+}}\right)}{\exp\left(\frac{U_{H+}\beta\ell}{2D_{H+}}\right) - \exp\left(\frac{-U_{H+}\beta\ell}{2D_{H+}}\right)}$$

$$+\frac{2\pi r^2 F D_{H+} C_0}{\ell} \exp\left(\frac{-U_{H+}\beta\ell}{2D_{H+}}\right) \sum_{n=1}^{\infty} \frac{(-1)^n \left(\frac{n^2\pi^2 D_{H+}}{\ell^2}\right) \exp -\left(\frac{n^2\pi^2 D_{H+}}{\ell^2} + \frac{U_{H+}^2\beta^2}{4D_{H+}}\right)t}{\left(\frac{n^2\pi^2 D_{H+}}{\ell^2} + \frac{U_{H+}^2\beta^2}{4D_{H+}}\right)} \qquad (A.7)$$

In the absence of an electric field we obtain

$$I = \frac{\pi r^2 F D_{H+} C_0}{\ell} + \frac{2\pi r^2 F D_{H+} C_0}{\ell} \sum_{n=1}^{\infty} (-1)^n \exp -\left(\frac{n^2\pi^2 D_{H+} t}{\ell^2}\right) \qquad (A.8)$$

Defining a dimensionless time

$$T = \frac{D_{H+} t}{\ell^2} \qquad (A.9)$$

and a dimensionless current

$$J = \frac{I}{I_{steadystate.diffusion}} \qquad (A.10)$$

we can express (A.8) as

$$J = 1 + 2 \sum_{n=1}^{\infty} (-1)^n \exp(n^2\pi^2 T) \qquad (A.11)$$

As the terms of the series alternate in sign, the series converges, the error always being smaller than the term at which the series is truncated. At short times the series in (A.11) converges badly and we can use the alternative expression

$$J = \frac{2}{\pi^{\frac{1}{2}}} \left(\frac{1}{T}\right)^{\frac{1}{2}} \sum_{n=0}^{\infty} \exp -\left(\frac{(2n+1)^2}{4T}\right) \qquad (A.12)$$

developed from the Laplace Transform of the solution.

For the case of diffusion coupled to migration, we define the additional dimensionless parameter

$$H = \frac{U_{H+}\beta\ell}{2D_{H+}} \qquad (A.13)$$

and, by analogy to (A.10)

$$Y = \frac{I}{I_{diffusion+migration,steadystate}} \qquad (A.14)$$

We can then express (A.10) as

$$Y = 1 + \frac{2\sinh(H)}{H} \sum_{n=1}^{\infty} \frac{(-1)^n n^2\pi^2}{(n^2\pi^2 + H^2)} \exp -(n^2\pi^2 + H^2)T \qquad (A.15)$$

A solution which is useful at small values of T (and high values of H) is

$$Y = \frac{2\sinh(H)\exp -(H^2T)}{H(\pi T)^{\frac{1}{2}}} \Bigg\{ \sum_{m=0}^{\infty} \exp -\left[\frac{(2m+1)^2}{4T}\right]$$

$$+ \sum_{n=1}^{\infty} (4H^2T^2)^{(n+1)} i^{(2n+1)} \operatorname{erfc}\left(\frac{1}{2T^{\frac{1}{2}}}\right)$$

$$+ \sum_{n=1}^{\infty} (4H^2T^2)^{(n+1)} i^{(2n+1)} \operatorname{erfc}\left(\frac{3}{2T^{\frac{1}{2}}}\right)$$

$$+ \ldots\ldots \Bigg\} \qquad (A.16)$$

Under most conditions the repeated integrals of the complementary error functions are small compared to the first series in (A.16).

These solutions (and solutions for other boundary conditions and experiment designs) will be discussed more fully elsewhere[12].

Appendix B

Towards an improved model of diffusion in the presence of the higher phases of Pd-H.[†]

We examine the diffusional behaviour in the context of the variation of D_{H+} with x as revealed by the measurements of Mengoli et al[9].

A reasonable expression for this variation in the region of the β–phase is

$$D_\beta = D^*_\beta \exp -\alpha(x^* - x) \qquad (B.1)$$

where we take $x^* \simeq 0.7$ as the limit of the charging ratio in the β–phase and where $D_\beta = 10^{-6}$ cm^2 s^{-1} and $\alpha \simeq 20$(dimensionless).

We regard the sharp fall of D_{H+} at $0.7 < x < 0.75$ as a step function characteristic of a phase transformation and represent the variation in the region of the putative γ–phase by the parabolic form

$$D_\gamma = D^*_\gamma (x - x^*)^2 \qquad (B.2)$$

with $D^*_\gamma \simeq 3.3 \times 10^{-5}$cm^{2}s^{-1}.

As it is natural to represent the concentration dependence of D_{H+} in terms of the charging ratios, we will also express the concentrations in this way, namely:

$$C_{H+} = \frac{x}{V} \qquad (B.3)$$

where V [cm^3(Mole)$^{-1}$] is the molar volume of Pd. For the case where diffusion is dominant we replace (i) by

$$\frac{\partial x}{\partial t} = \frac{\partial}{\partial z}\left(D_{H+}\frac{\partial x}{\partial z}\right) \qquad (B.4)$$

(A.5) by

$$x = x_0, \quad z = 0, \quad t > 0 \qquad (B.5)$$

and (A.6) by

$$x = 0, \quad z = \ell, \quad t > 0 \qquad (B.6)$$

The initial condition becomes

$$x = 0, \quad 0 < z < \ell, \quad t = 0 \qquad (B.7)$$

[†]The interpretation of the behaviour where migration is significant will be given elsewhere[12]

and we regard the surface of the wire in the region $0 < z < \ell$ as being covered by a perfect diffusion barrier.

The steady state

In order to obtain the solution for the steady state we need to take note of the fact that a region of the wire $0 < z < z^*$ will be in the γ–phase whereas the region $z^* < z < \ell$ will be in the β–phase. In view of the high values of D_{H+} in these phases in comparison to that in the α–phase, we will neglect the short region close to $z = \ell$ which must be converted into this α–phase.

The fluxes in the two phases are

$$f(z) = -\frac{D^*_\gamma}{V}(\mathrm{x} - \mathrm{x}^*)^2 \frac{\mathrm{dx}}{\mathrm{dz}}, \quad 0 < \mathrm{z} < \mathrm{z}^* \tag{B.8}$$

and

$$f(z) = -\frac{D^*_\beta}{V} \exp -\alpha(\mathrm{x} - \mathrm{x}^*)^2 \frac{\mathrm{dx}}{\mathrm{dz}}, \quad \mathrm{z}^* < \mathrm{z} < \ell \tag{B.9}$$

The integral of (B.8) is

$$\mathrm{x}_\gamma(\mathrm{z}) = \mathrm{x}^* + \left[\frac{3\mathrm{fV}}{\mathrm{D}^*_\gamma}(\mathrm{z}^* - \mathrm{z})\right]^{\frac{1}{3}} \tag{B.10}$$

where the integration constant has been determined using

$$\mathrm{x}_\gamma(\mathrm{z}^*) = \mathrm{x}^* \tag{B.11}$$

The condition

$$\mathrm{x}_\gamma(0) = \mathrm{x}_0 = \mathrm{x}^* + \left[\frac{3\mathrm{fVz}^*}{\mathrm{D}^*_\gamma}\right]^{\frac{1}{3}} \tag{B.12}$$

establishes the relation between f, x_0 and z^*.

For the region of the β–phase we obtain

$$\mathrm{x}(\mathrm{z}) = \mathrm{x}^* + \frac{1}{\alpha}\ln\left[\frac{\alpha\mathrm{fV}}{\mathrm{D}^*_\beta}(\ell - \mathrm{z}) + \exp(-\alpha \mathrm{x}^*)\right] \tag{B.13}$$

where the boundary condition (B.6) has been used to determine the integration constant. The condition (B.11) at the boundary between the γ and β phases implies that to a good

level of approximation

$$\frac{\alpha f V}{D^*_\beta}(\ell - z) = 1 \qquad (B.14)$$

so that (B.8) with (B.12) gives

$$f = \frac{1}{3\ell V}\left[\frac{3D^*_\beta}{\alpha} + D^*_\gamma(\mathrm{x_0} - \mathrm{x^*})^3\right] \qquad (B.15)$$

the current measured at $z = \ell$ being

$$I = \pi r^2 F f = \frac{\pi r^2 F}{3\ell V}\left[\frac{3D^*_\beta}{\alpha} + D^*_\gamma(\mathrm{x_0} - \mathrm{x^*})^3\right] \qquad (B.16)$$

The location of the boundary between the two phases is determined from

$$\frac{z^*}{\ell} = 1 - \frac{D^*_\beta}{\alpha \ell f V} \qquad (B.17)$$

The non-steady state

We have drawn attention to the deviations (i)-(iv) between the experimentally observed current-time transients, Fig 9, and those predicted by a simple model of diffusion with a concentration independent value of the diffusion coefficient, equation (A.8). It is important to establish first of all a physical picture for these phenomena. The region close to $z = 0$ will be charged by the electrochemical reaction into the region of the γ–domain. As the diffusion coefficient falls markedly with decreasing x, Fig 15[‡], a steep wave–front must develop at the head of the γ–phase which in turn drives a narrow domain of the β–phase towards $z = \ell$ (we again neglect the effects of the α–phase). At the first level of interpretation we can consider this phenomenon to be due to a discontinuity in the diffusion coefficient. Since diffusion is simply an expression of the gradient of the chemical potential with distance, this discontinuity in turn implies a focussing of energy at the head of the wave–front. The final part of the picture is that the wave–front moves in one dimension down the narrow wire: the situation resembles the conditions for the development of a soliton and we have therefore sought for the presence of a "solitonic type" solution in the mathematical description of the processes.

In developing this interpretation we note first of all that the values of x_0 and of z^*/ℓ which are derived from the steady–state behaviour are not greatly affected by the variation of D_β with x. For the purposes of the non–steady–state, we have found it more convenient to

[‡]The fall by ~ 2 orders of magnitude must be a lower bound because the experimental measurements inevitably lead to some averaging over the z–domain.

replace (B.15) by

$$D_\beta = \frac{D^*_\beta}{\left[\frac{(\mathrm{x}^* - \mathrm{x})}{\mu} + 1\right]^4} \tag{B.18}$$

where we again take $D^*_\beta = 10^{-6}\mathrm{cm}^2\mathrm{s}^{-1}$, $\mathrm{x}^* = 0.7$ and where $\mu = 0.1$ gives a good representation of the experimental data. We note next that we can formally integrate the equation for the flux

$$f = \frac{-D_\beta}{V}\frac{\partial \mathrm{x}}{\partial \mathrm{z}} \tag{B.19}$$

over the region of space of the β–phase to give

$$Q = \int_z^\ell \mathrm{Vf}(\mathrm{z}', \mathrm{t})\mathrm{dz}' \tag{B.20}$$

With (B.18) we obtain

$$\mathrm{x}_\beta = \mathrm{x}^* + \mu\left[1 - \frac{1}{(\varepsilon + \mathrm{q})^{\frac{1}{3}}}\right] \tag{B.21}$$

where

$$q = \frac{Q}{Q^*} \tag{B.22}$$

$$Q^* = Q(z^*) \simeq \frac{\mu D^*_\beta}{3} = 3.3 \times 10^{-8}\mathrm{cm}^2\mathrm{s}^{-1} \tag{B.23}$$

and where ε is a relatively small quantity

$$\varepsilon = \left(\frac{\mathrm{x}^*}{\mu} + 1\right)^{-3} \simeq 1.95 \times 10^{-3} \tag{B.24}$$

With these transformations, the flux is given by

$$f = -\frac{Q^*}{V}\frac{dq}{dz} \tag{B.25}$$

and the diffusion equation becomes

$$\frac{\partial \mathrm{x}}{\partial \mathrm{t}} = -V\frac{\partial f}{\partial z} \qquad (B.26)$$

For the region of the β–phase we obtain the non–linear differential equation

$$\frac{\partial q}{\partial t} = D^*_\beta(\varepsilon + q)^{\frac{4}{3}}\frac{\partial^2 q}{\partial z^2} \qquad (B.27)$$

For the region of the γ–phase we have as before (B.2) and we obtain

$$\mathrm{x}_\gamma = \mathrm{x}^* + \left(\frac{3\mathrm{Q}^*}{\mathrm{D}^*_\gamma}\right)^{\frac{1}{3}}(\mathrm{q}-1)^{\frac{1}{3}} \qquad (B.28)$$

where

$$\left(\frac{3Q^*}{D^*_\gamma}\right)^{\frac{1}{3}} \simeq 0.144 \qquad (B.29)$$

The diffusion equation for this region becomes

$$\frac{\partial q}{\partial t} = (D^*_\gamma)^{\frac{1}{3}}[3Q^*(q-1)]^{\frac{2}{3}}\frac{\partial^2 q}{\partial z^2} \qquad (B.30)$$

or

$$\frac{\partial q}{\partial t} = [d(q-1)]^{\frac{2}{3}}\ \frac{\partial^2 q}{\partial z^2} \qquad (B.31)$$

where

$$d = (qD^*_\gamma Q^{*2})^{\frac{1}{3}} = 6.86 \times 10^{-7}\mathrm{cm}^2\mathrm{s}^{-1} \qquad (B.32)$$

According to the general considerations outlined above, we search for a solution for the propagation of a wave–front in this phase. Setting

$$\kappa = (q-1) \qquad (B.33)$$

we obtain

$$\frac{\partial \kappa}{\partial t} = d\kappa^{\frac{2}{3}}\ \frac{\partial^2 \kappa}{\partial z^2} \qquad (B.34)$$

and we seek for a solution in the form g(z(t) - z) We obtain

$$g(z(t)-z) = \lambda(z(t)-z)^{\frac{3}{2}} \tag{B.35}$$

provided

$$\frac{dz(t)}{dt} = \frac{d\lambda^{\frac{2}{3}}}{2} \tag{B.36}$$

The evolution of κ with time along the length of the wire is illustrated by the schematic diagram. Fig 16. The motion of the zero $z = z(t)$ is linear, the velocity depending on the amplitude λ. The boundary will reach $z = \ell$ at a time

$$t_s = \frac{2\ell}{d\lambda^{\frac{2}{3}}} \tag{B.37}$$

at which stage the flux must show a sharp increase.

Since the flux is given by

$$f = -\frac{Q^*}{V}\frac{\partial\kappa}{\partial z} = \frac{3Q^*\lambda}{2V}[z(t)-z]^{\frac{1}{2}} \tag{B.38}$$

the flux at $z = \ell$ will be given by

$$(f)_{z=\ell} = \frac{3Q^*\lambda\ell^{\frac{1}{2}}}{2V}\left[\frac{z(t)}{\ell}-1\right]^{\frac{1}{2}} \tag{B.39}$$

The expected variation of the current with time due to the this wave propagation is shown in the schematic diagram. Fig 17. However, we note that the increase in current must become limited at the point when $\kappa(0,t)$ reaches the value κ_0 at the boundary $z = 0$. If x_0=1.2 (as is indicated by the interpretation of the steady state), then

$$\kappa_0 = \left(\frac{x_0 - x^*}{0.144}\right)^3 \simeq 41 \tag{B.40}$$

At this stage there is no power source to drive the wave and we must revert to the normal diffusional process. The profile of κ will then be quite flat so that we can examine the behaviour of

$$\frac{\partial\kappa}{\partial t} = \bar{d}\ \frac{\partial^2\kappa}{\partial z^2} \tag{B.41}$$

where

$$\bar{d} = d\ \overline{\kappa^{\frac{2}{3}}} \tag{B.42}$$

The solution can be expressed in the form of a Green's function

$$\kappa(t,z) = \int_0^{\ell} G(t-t_s,z,z')\kappa(t_s,z')dz' \qquad (B.43)$$

where

$$G(t,z,z') = \frac{1}{\ell}\sum_{n=-\infty}^{+\infty} \exp\frac{i2\pi n(t-t')}{\ell}\exp\left(\frac{-4\pi^{-2}n^2\overline{d}t}{\ell^2}\right) \qquad (B.44)$$

We obtain

$$f(t) = \frac{2}{\pi^{\frac{1}{2}}}\int_0^{\ell}\exp\left(\frac{-z^2}{dt}\right)\frac{f(\ell-z)}{(dt)^{\frac{1}{2}}}dz$$

$$= \frac{2}{\pi^{\frac{1}{2}}}\int_0^{\ell/(\overline{d}t)^{\frac{1}{2}}}\exp(-u^2)f[\ell-(\overline{d}t)^{\frac{1}{2}}u]du \qquad (B.45)$$

for the time domain t> t_0. Equation (B.45) has a negative derivative

$$\frac{df}{dt} \simeq \frac{-2}{\pi^{\frac{1}{2}}}\frac{\ell}{2\overline{d}^{\frac{1}{2}}t^{\frac{3}{2}}}\exp\left(\frac{-\ell^2}{dt}\right) \qquad (B.46)$$

so that we predict the behaviour as illustrated in the schematic diagram Fig 18. In order to obtain more quantitative estimates we need to determine λ. One such estimate follows by noting that the propagation of the γ–phase wavefront is due to a redistribution of the diffusion coefficient in space and time. We can therefore equate the arrival time of the wave–front at $z = \ell$ given by equation (B.37) with the arrival time by a purely diffusive wave moving with the average diffusion coefficient $\overline{D}$ ie

$$t_{\overline{D}} = \frac{\ell^2}{\overline{D}} \qquad (B.47)$$

where $\overline{D} \simeq= 3\times10^{-6}\mathrm{cm}^2\mathrm{s}^{-1}$. We obtain

$$\lambda = \left(\frac{2\overline{D}}{d\ell}\right)^{\frac{3}{2}} \simeq 85\mathrm{cm}^{-3/2}\text{for}\ \ \ell = 0.45\mathrm{cm} \qquad (B.48)$$

This gives

$$t_s = 0.69\times10^5 s \qquad (B.49)$$

which appears to be a reasonable value. We also obtain

$$\kappa(0, t_s) = \lambda(\ell)^{\frac{3}{2}} = 25.6 \tag{B.50}$$

which we can compare to

$$\kappa_{max} = 42 \tag{B.51}$$

corresponding to $x_0 = 1.2$. For a 25μ radius wire the current–time transient is

$$I = \frac{3\lambda Q^*}{2}(z(t) - \ell)^{\frac{1}{2}}$$

$$= \frac{3\lambda Q^* \ell^{\frac{1}{2}}}{2}\left(\frac{t}{t_s} - 1\right)^{\frac{1}{2}} \tag{B.52}$$

which gives a very sharp rise of the current with time (see Table 2 of the main text)

We note also that this regime ends when κ at the origin reaches κ_{max} in the reflected wave ie for

$$\kappa(0, t_0) = \kappa_{max} = 42 \tag{B.53}$$

because there is no further energy available to drive the wave–front at this stage. Using

$$\kappa(0, t) = \lambda \ell^{\frac{3}{2}}\left(\frac{t_0}{t_s} - 1\right)^{\frac{3}{2}} \tag{B.54}$$

we obtain the estimate $t_0 = 0.96 \times 10^5$s which demonstrates further the extremely sharp rise in the current induced by the propagation of the wave–front.

Glossary of Symbols Used in the Appendices

a	is a radius.	[cm]
erfc	is the complementary error function.	
f	is a flux.	[Moles cm^{-2} s^{-1}]
H	is a dimensionless parameter characterising the effect of the electric field.	
i^nerfc	is the nth integral of the complementary error function.	
J	is a dimensionless parameter characterising the flux.	
ℓ	is a length.	[cm]
Q	is a variable characterising the flux.	[cm^2 s^{-1}]
q	is a dimensionless variable.	
T	is a dimensionless parameter characterising time.	
V	is the molar volume.	[cm^3 $(Mole)^{-1}$]
x	is the charging ratio H/Pd.	
Y	is a dimensionless parameter characterising the flux in the presence of an electric field.	
α	is a constant.	
ϵ	is a constant.	
λ	is a parameter defining a characteristic length reciprocal distance.	[$(cm)^{-\frac{3}{2}}$]
μ	is a constant.	
τ	is a time.	[s]

References

1. J.R. Huizenga, "Cold Fusion Research", Report of the Energy Research Advisory Board to the United States Department of Energy, November 1989.

2. A. Coehn, Z. Elektrochem., 35 (1929) 676.

3. M. Fleischmann, S. Pons, Jeanne Roulette, T. Roulette and Monique Le Roux, "Calorimetry of the Pd–D_2O System: the Search for Simplicity and Accuracy". Paper C1.1 presented at the 4th International Conference on Cold Fusion, Maui, Hawaii USA, (December 6–9, 1993).

4. E. Lange and K.P. Miscenko, Z. Phys. Chem., 149 (1930) 1.
   E. Lange, Z. Elektrochem., 55 (1951) 76.

5. G. Preparata "Cold Fusion '93: Some Theoretical Ideas," paper No. T1.2 presented at the 4th International Conference on Cold Fusion, Maui, Hawaii (December 6-9 1993).

6. M. Fleischmann, "An Overview of Cold Fusion Phenomena" Paper presented at the 1st Annual conference on Cold Fusion, Salt Lake City, Utah, March 1990.

7. M.C.H. McKubre, S. Crouch–Baker, A.M. Riley, S.I. Smedley and F.L. Tanzella, "Excess Power Observations in Electrochemical Studies of the D/Pd System; the Influence of Loading" in "*Frontiers of Cold Fusion*" Ed. H. Ikegami, Proceedings of the 3rd International Conference on Cold Fusion, Nagoya October 21–25, 1993, Universal Academy Press Inc., Tokyo, 1993 page 5; ISSN 0915-8502.

8. K.Kunimatsu, H.Hasegawa, A. Kubota, N.Imai, M. Ishikawa, H.Akita and Y. Tsuchida, "Deuterium Loading Ratio and Excess Heat Generation during Electroloysis of Heavy Water by a Palladium Cathode in a Closed Cell Using a Partially Immersed Fuel Cell Anode." in "*Frontiers of Cold Fusion*" Ed. H. Ikegami, Proceedings of 3rd International Conference on Cold Fusion, Nagoya October 21–25, 1993, Universal Academy Press Inc., Tokyo, 1993 page 31; ISSN 0915-8502.

9. G. Mengoli, M. Fabrizio, C. Manochuchi and G. Zannoni, J. Electroanal. Chem., 350 (1993) 57.

10. Y.Fukai and N. Okuma, Japanese J. Appl. Phys., 32 (1993) L 1256.

11. G. Preparata, "Towards a Theory of Cold Fusion Phenomena," Proceedings of the Rome Workshop on Cold Fusion, February 1993, B. Stella, (ed).

12. To be published.

13. C.J. Smithells, "Gases and Metals", Chapman and Hall, London 1937.

14. R.M. Barrer, "Diffusion in and through Solids" Cambridge University Press, 1941.

15. J. Crank, "The Mathematics of Diffusion" Clarendon Press, Oxford, 1956.

16. C. Kittel, "Introduction to Solid State Physics" John Wiley, New York, Chapman and Hall, London, 1956. Library of Congress Card Number 56-9822.

17. F.A. Lewis, "The Palladium Hydrogen System" Academic Press, London, 1967.

18. C. Wagner and G. Heller, Z. Physik. Chem., B46 (1940) 242.

19. G. Alefeld and J. Völkl, "Hydrogen in Metals I" Springer Verlag, Berlin, Heidelberg, New York, 1978 ISBN 3-540-08705-2; 0-387-08705-2.

20. G. Alefeld and J. Völkl "Hydrogen in Metals II" Springer Verlag, Berlin, Heidelberg, New York, 1978. ISBN 3-540-08883-0; 0-387-08883-0.

21. H.Wipf in chapter 7 reference[20].

22. L. Schlapbach "Hydrogen in Intermetallic Compounds I", Springer Verlag, Berlin, Heidelberg, New York, London, Paris, Tokyo, 1988. ISBN 3-540-18333-7; 0-387-18333-7.

23. L. Schlapbach "Hydrogen in Intermetallic Compounds II".

24. T.P.P. Gibb, J. Inorg. Nucl. Chem., 24 (1962) 349.

25. M. Fleischmann, S. Pons and G. Preparata, Nuovo Cimento, 107A (1994) TBA.

26. B. Dandapani and M. Fleischmann, J. Electroanal. Chem., 39 (1972) 323.

27. M. Fleischmann, S. Pons and M. Hawkins, J. Electroanal. Chem., 261 (1989) 301; for corrections see J. Electroanal. Chem., 263 (1989) 187.

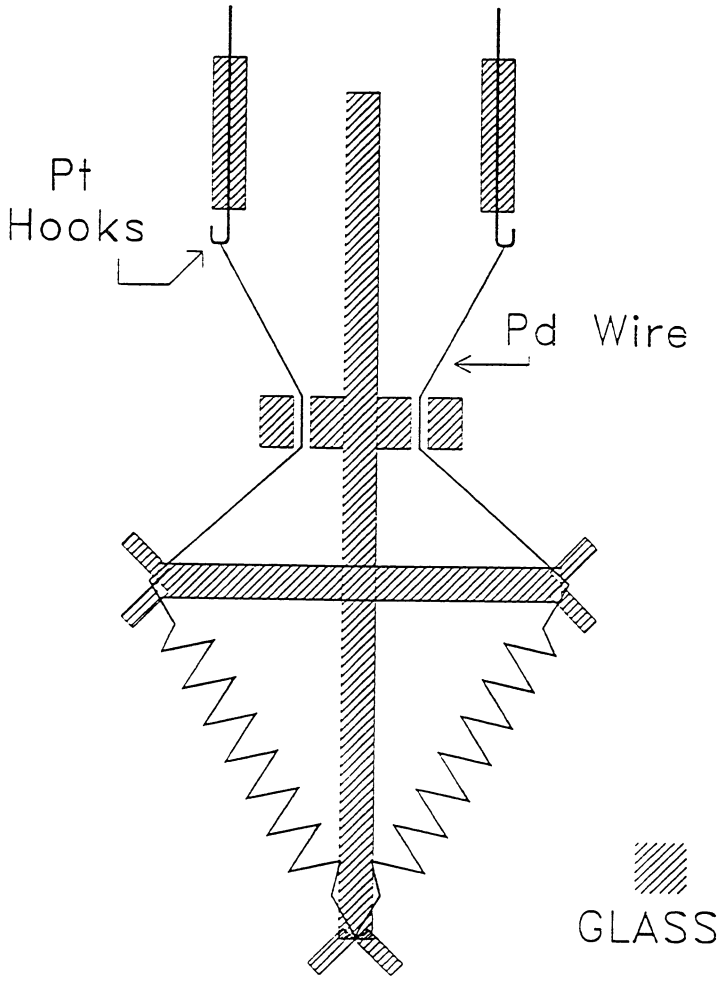

Fig 1. Schematic of Coehn's original experiment[2] for measuring the electrodiffusion of hydrogen along a palladium wire.

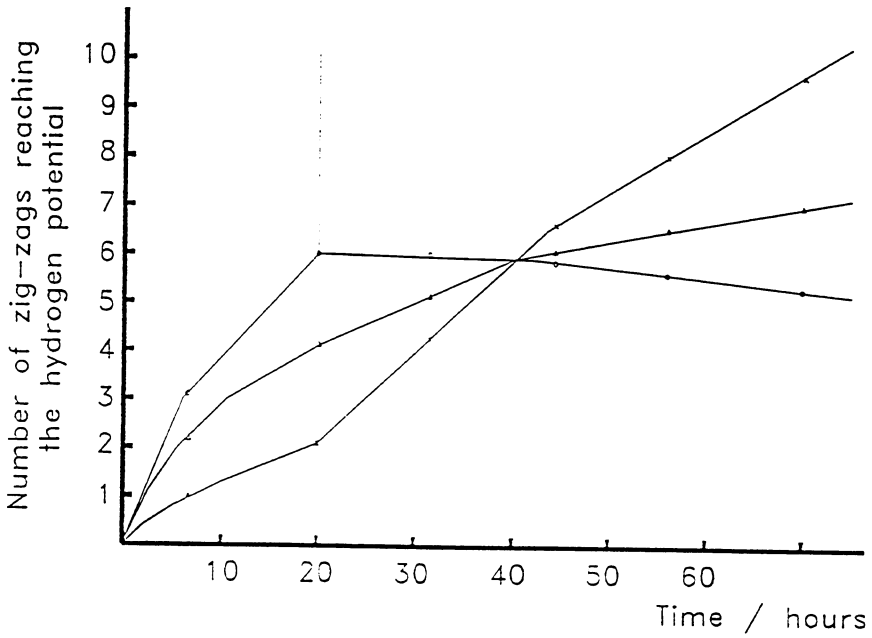

Fig 2. An example of Coehn's measurements[2] (distance between zig-zags = 1.85 mm).

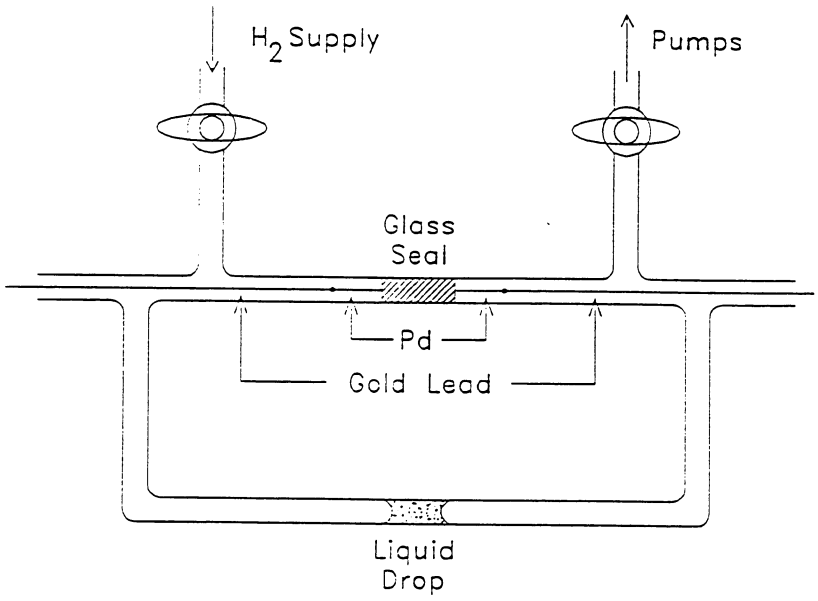

Fig 3. Schematic of the apparatus of Wagner and Heller[18] for measuring the electrodiffusion of hydrogen through palladium.

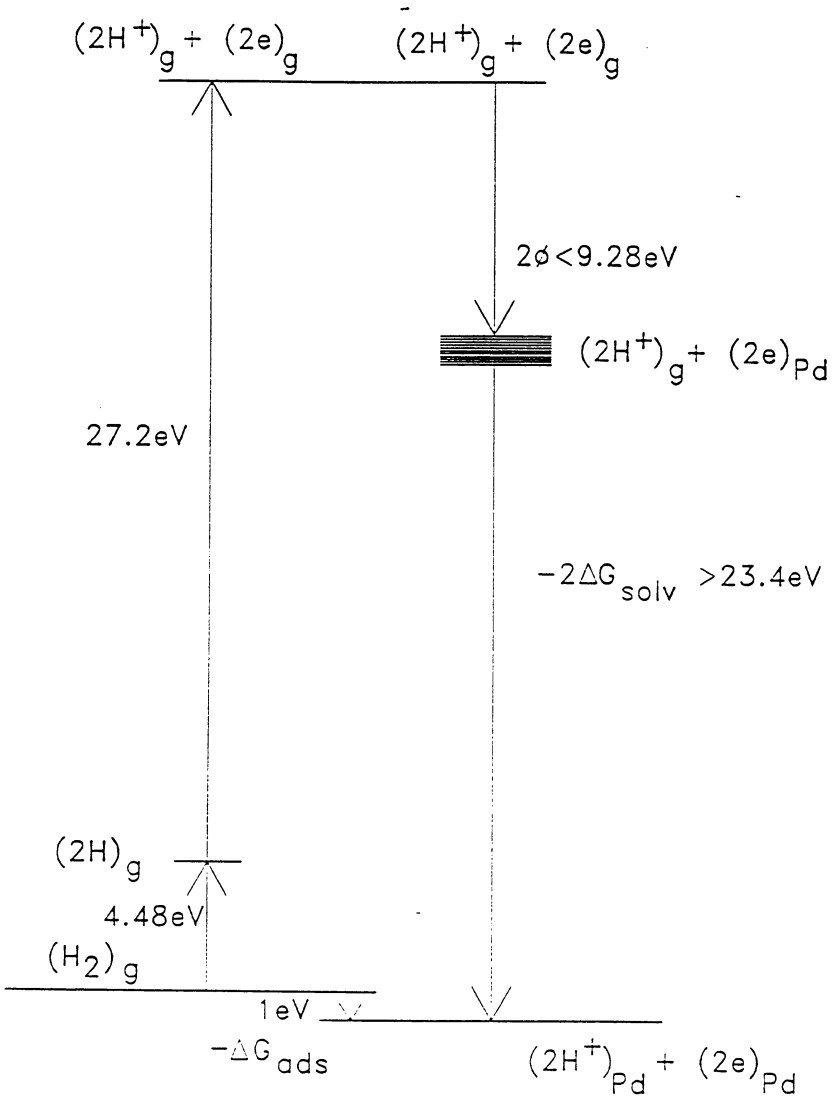

Fig 4. Born-Haber cycle for calculating the solvation energy of H^+ in the Pd host lattice.

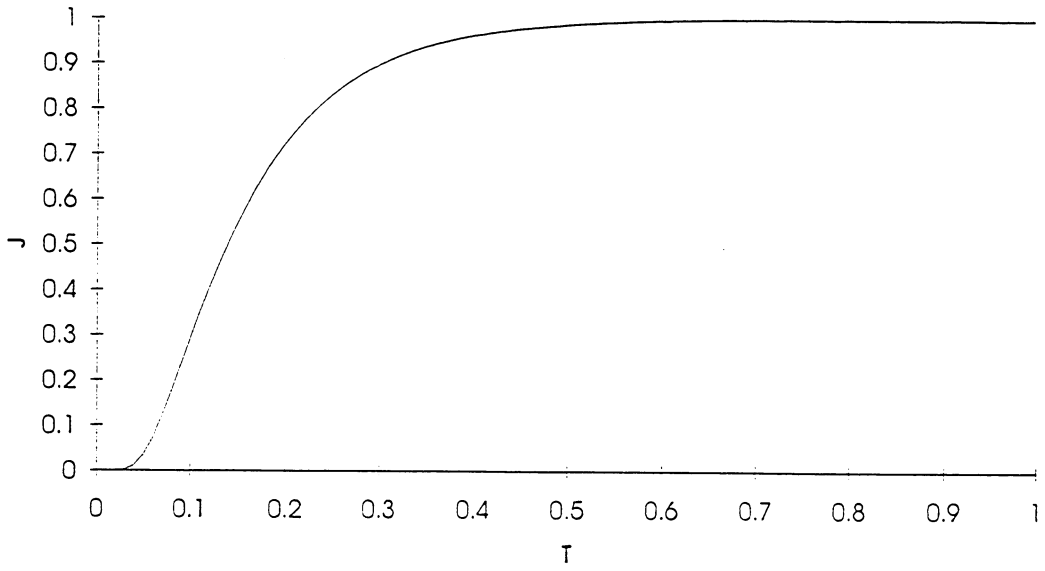

Fig 5. Plot of the dimensionless flux J due to diffusion alone observed at $z = \ell$ versus the dimensionless time $\overline{T}$ (equations (A.11) and (A.12)).

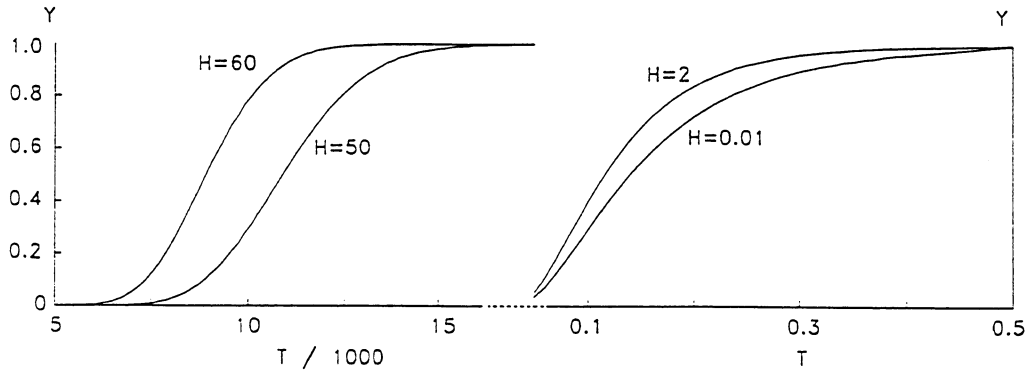

Fig 6. Plots of the dimensionless flux Y due to diffusion and migration observed at $z = \ell$ versus the dimensionless time T for different values of the parameter H (equations (A.15) and (A.16)).

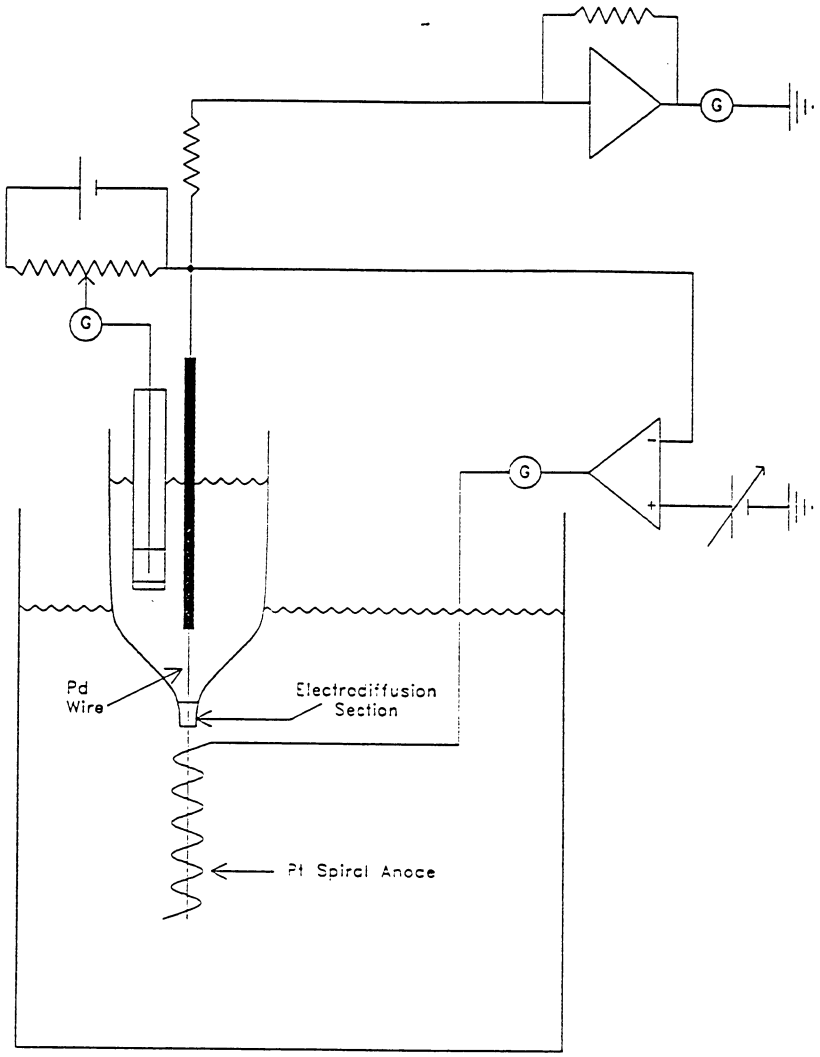

Fig 7. The cell used in the measurements reported in this paper.

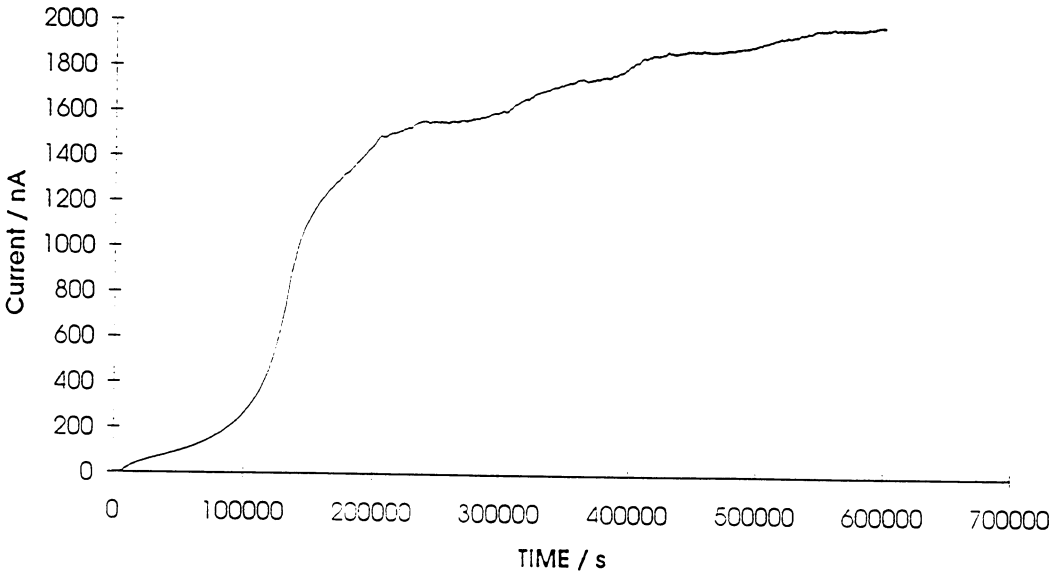

Fig 8. Current–time transient due to electrodiffusion of H^+ to $z = \ell$ (with diffusion dominant). Diameter of wire = 100μ: length of insulated section = 0.5 cm. The wire was charged electrolytically in the region $z < 0$ (cell illustrated in Fig 7).

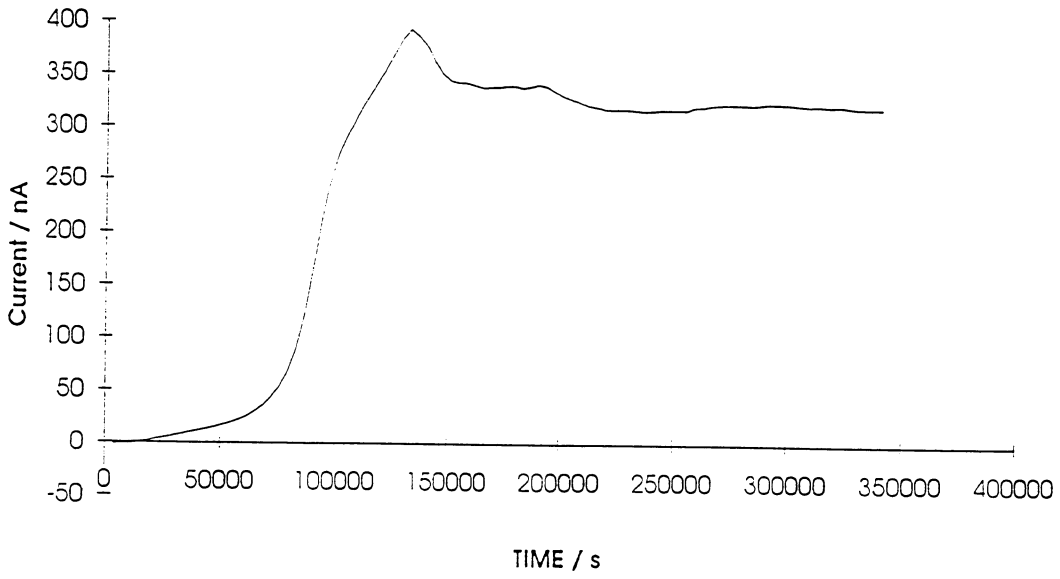

Fig 9. Current–time transient measured as in Fig 8 but using a 50μ diameter wire of length 0.45 cm.

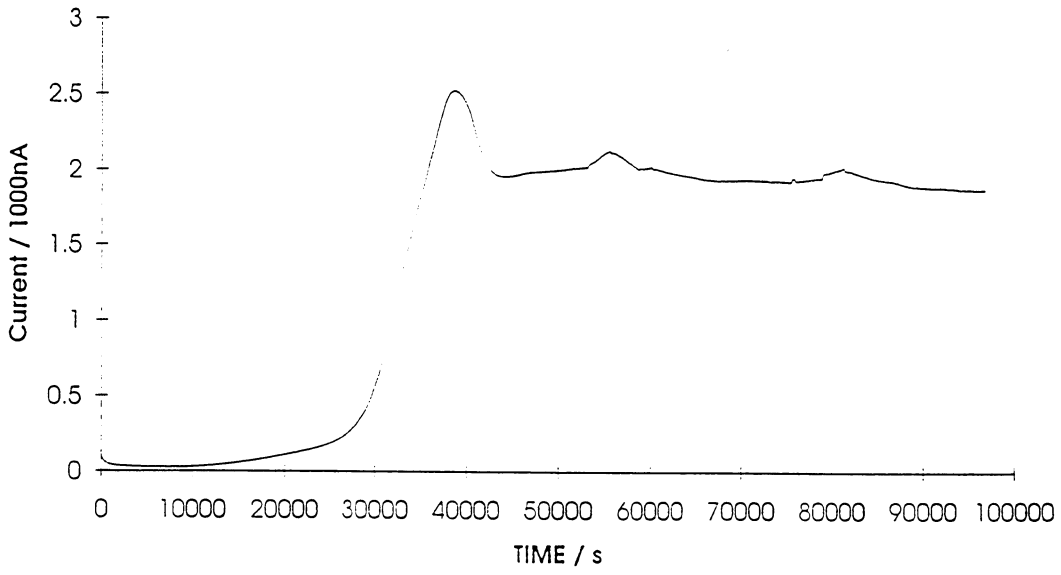

Fig 10. Current–time transient due to electrodiffusion of H^+ to $z = \ell$ (when migration is significant: electric field = 0.27 V cm^{-1}; diameter of wire = 50μ; length of insulated section = 0.6 cm.

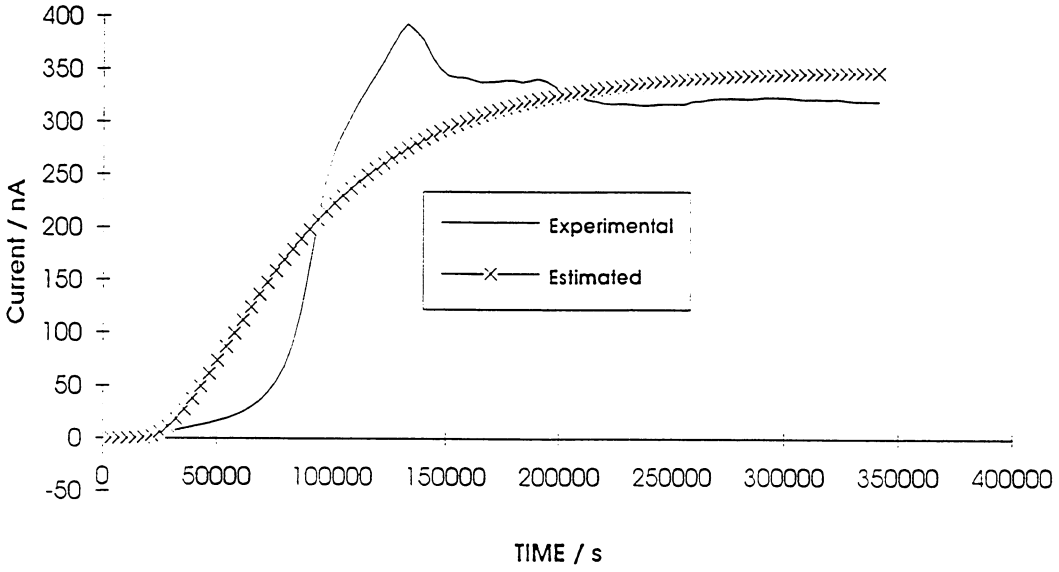

Fig 11. Comparison of the experimentally observed current–time transient (Fig 9) with that predicted from equation (A.8); D_{H+} and C_0 estimated by using the Marquardt-Levenberg algorithm (see text).

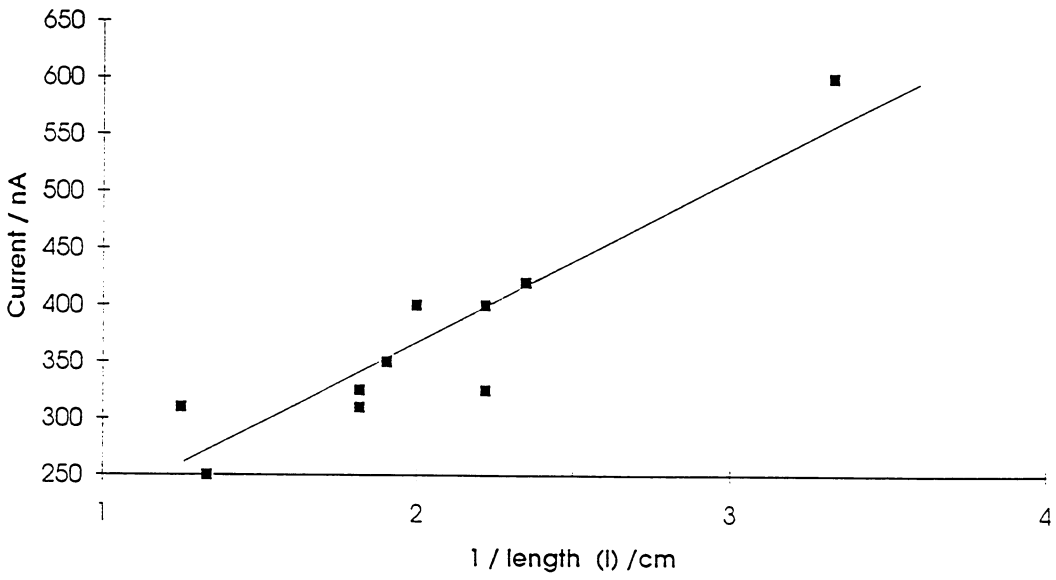

Fig 12. Plot of the experimentally measured diffusion limited currents (diffusion dominant) versus $1/\ell$ (see equation (14)).

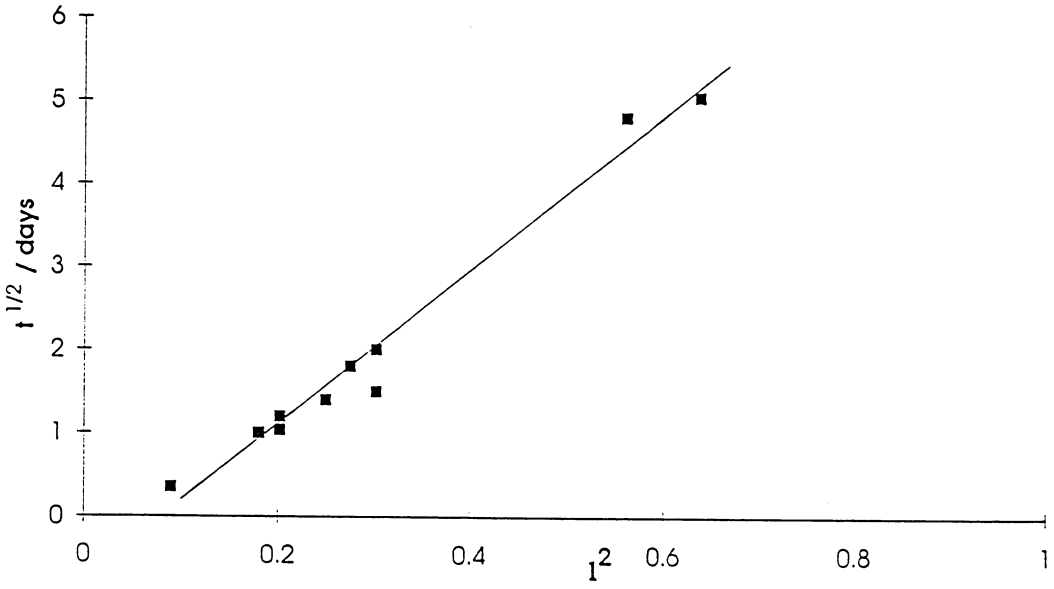

Fig 13. Plot of the measured values of $t_{\frac{1}{2}}$ versus ℓ^2 for a series of experiments (see equation (15)).

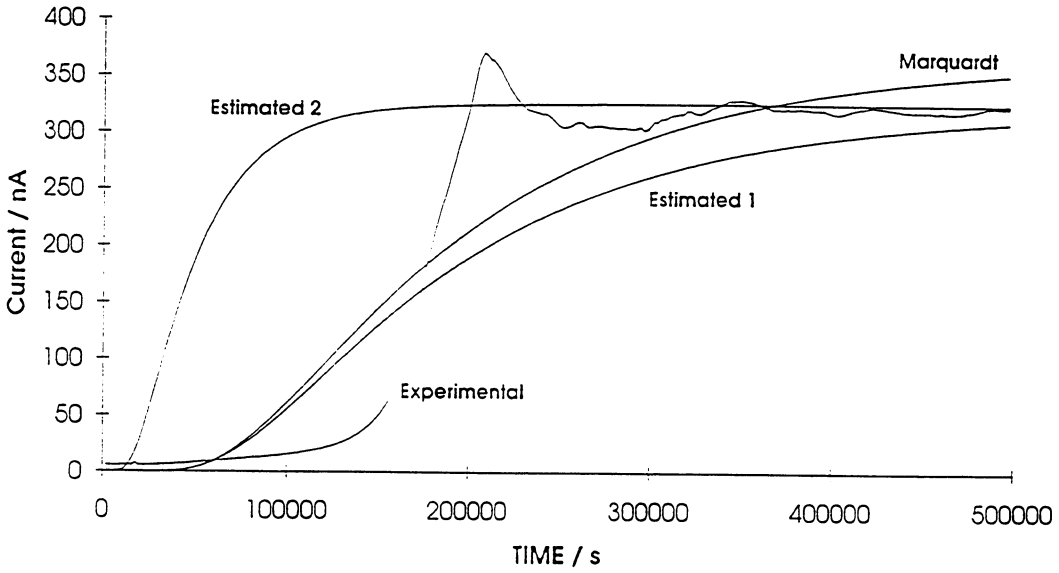

Fig 14. Comparison of the experimentally measured current–time transient (Fig 9) with that predicted from equation (A.8) using D_{H+} and C_0 estimated in three different ways (see text).

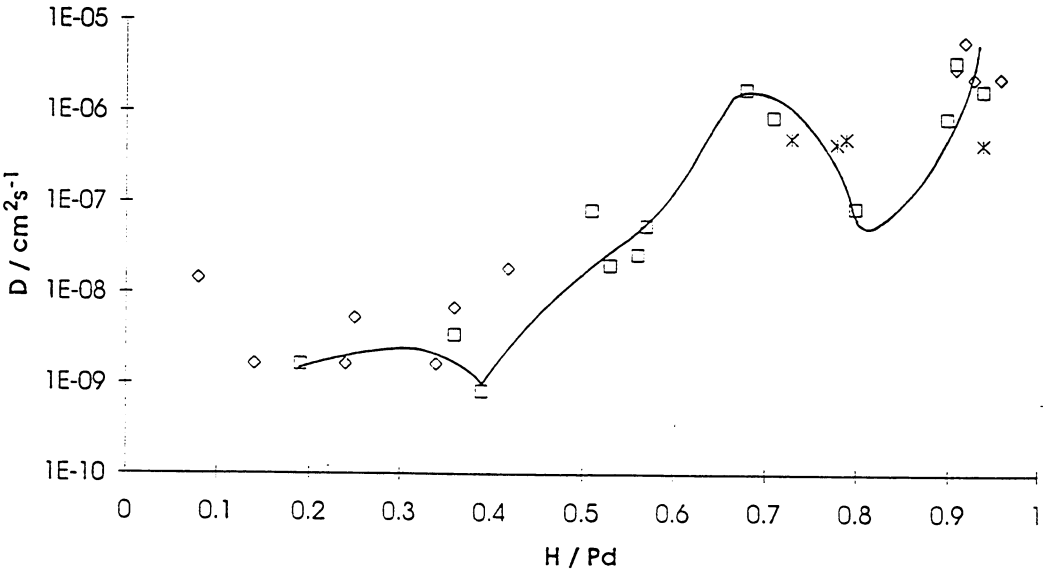

Fig 15. Diffusion coefficient of hydrogen in Pd plotted versus the H/Pd ratio.

◇ 0.1 M LiOH
□ 0.5 M Li_2SO_4
* 1.0 M LiOH
Data from reference[8].

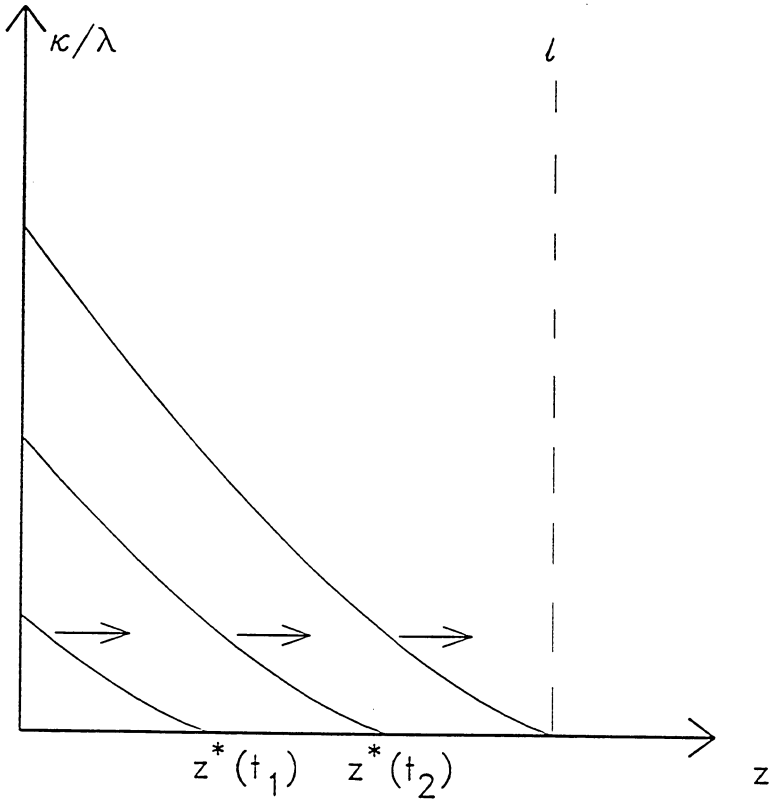

Fig 16. Variation of κ/λ with z; the values of $z^*(t)$ denote the distances reached by the propagated wave at different times.

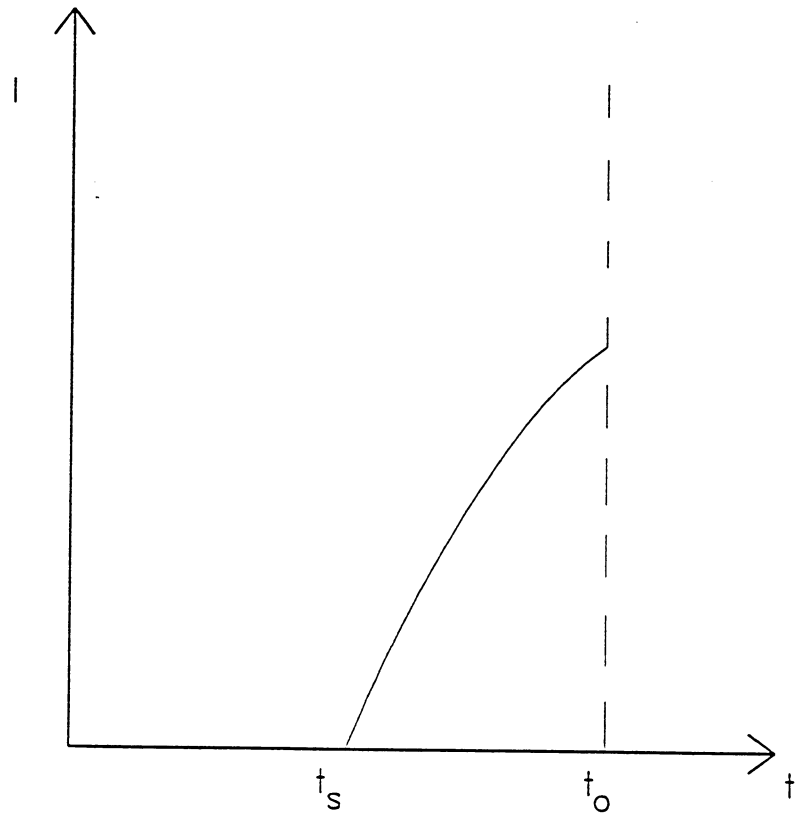

Fig 17. Current–time transient measured at $z = \ell$ due to the arrival of the propagated wave; the process terminates at t_0.

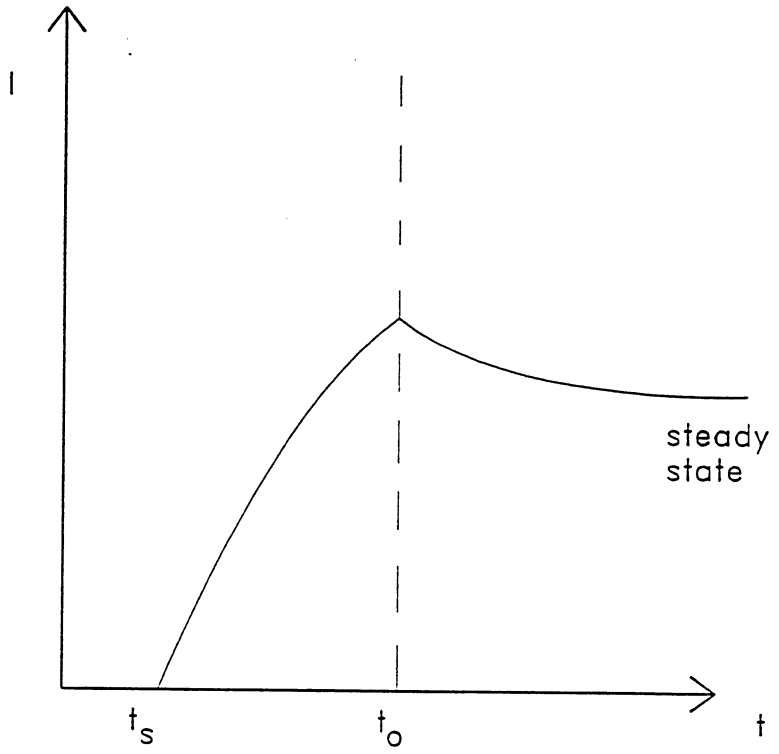

Fig 18. Current–time transient measured at $z = \ell$. At $t > t_0$ the propagation wave is replaced by normal diffusion.

THE MEASUREMENTS AND THE CONTROL OF THE LOADING RATIO OF DEUTERIUM IN PALLADIUM

G. S. Huang, D. W. Mo, W. Z. Yu, M. Y. Yao, and X. Z. Li
Department of Physics, Tsinghua University
Beijing 100084, CHINA

B. Y. Liaw
Hawaii Natural Energy Institute,
School of Ocean and Earth Science and Technology
University of Hawaii at Manoa
Honolulu, HI 96822, USA

Abstract

It is important to find the condition under which the loading ratio may be greater than a threshold, namely D/Pd≈0.84, for anomalous effects to be seen in the Pd-D system. We found that loading deuterium is more difficult than hydrogen in gas phase, similar to the case of electrolysis. We have tried different procedures such as heating, vacuum degassing, annealing, surface cleaning, glow discharge and cryogenic treatment. The loading ratio was monitored by electrical resistance method and verified by weighting method as well. The preliminary results showed that the glow discharge was not effective to enhance either the loading ratio or the loading speed.

Introduction

The research on the anomalous phenomena in the deuterium/solid system have been going on at Tsinghua University in two major efforts. The first one was trying to set up a Chinese-based reproducible experiment, and the second one was trying to study the key parameters that control the reproducibility. The glow discharge experiment with flowing deuterium gas[1] was supposed to be an active effort among the first. The detection of energetic charged-particles[2] using CR-39 plastic track detectors in previous gas-loading experiments and the recent pressurized heavy water electrolysis were other examples. The focus of these experiments has been the anomalous effects not the mechanism. Recently, the second effort of studying key parameters were increasingly emphasized. Thus, the deuterium-to-palladium loading ratio (D/Pd) was carefully studied[3]. Since the SRI experiments[4] have shown that the loading ratio was a key parameter for the anomalous effects, we decided to measure the loading ratio accordingly to find methods of controlling this parameter.

In this set of experiments, we are interested in finding the conditions under which the loading ratio can be enhanced; particularly, the condition under which the loading ratio

can be greater than the threshold value revealed by the work at SRI, namely D/Pd≈0.84. We did not try to detect any nuclear signals in these experiments.

In our earlier experiments[3] hydrogen gas was used instead of deuterium, and gas-loading method was used instead of electrolysis. We found that multiple-step cycles of alternating loading and unloading might enhance the loading ratio up to H/Pd≈0.89. The present experiments used deuterium gas. We found that the deuterium gas loading was more difficult than the hydrogen. However, D/Pd≈0.89 can be achieved eventually.

The loading ratio was monitored in real time by resistance ratio measurements of the palladium wire, and the value was verified by weighting method at the end of the experiments.

We have identified some factors that affect the loading ratio or the loading speed. It is interesting that we found the glow discharge with flowing deuterium had little effect on either the loading ratio or the loading speed, contradict to what one might expect.

Motivation

The SRI experiments[4] have shown the critical loading ratio of 0.84 for producing the excess heat anomalous phenomenon in the Pd-D_2O electrolysis. We, however, do not know if a similar threshold loading ratio for gas-loading experiment exists. Particularly, there have been some observations of anomaly in Chinese early experiments in the Pd-D_2 system. The researchers in the Southwestern Institute of Nuclear Physics and Chemistry observed some abnormal neutron emissions in the discharge tube[5] in April, 1989. Later, a group in the Sichuan Institute of Material Technology observed some abnormal nuclear radiation[1] as well. A group in the Southwestern Institute of Physics observed some neutron bursts in a magnetic mirror machine[6], where palladium and titanium samples immersed in a deuterium plasma were implanted with deuterons by a biased voltage. At the same time the Russian scientists published their observation in a discharge tube with a much lower voltage and a higher discharge current[7]. The Indian scientists observed anomalous phenomena in plasma focus device[8] as well. All those reports imply that the surface treatment by electrical discharge might play an important role in enhancing the loading ratio or the loading speed. We are particularly interested in whether this treatment may push the loading ratio over the threshold at a lower pressure (say, < 30 atm).

Experimental Setup

During the past three years, the Tsinghua University team has tried several approaches to investigate what surface treatments might enhance the loading ratio and the loading speed in the gas-loading process. Fig. 1 shows one of the approaches. The advantage of this approach is that it can test not only the effect of electrical discharge but also the effect due to cooling by liquid nitrogen or by in-situ resistive heating of the sample using an external current. The bottom of the vessel was made of a stainless steel base plate with high voltage feedthroughs, which can withstand a high gas pressure up to 30 atm, with good insulation among three electrodes. The top of the vessel was sealed with an indium ring and a mechanical structure similar to that of the closed container used in the SRI's electrolytic cell[4]. A Pd wire (ø 0.125 mm x 100 cm) was wound on a ceramic

support. This Pd wire served for several purposes: it acts as an absorber of hydrogen, as a resistance probe to monitor the loading ratio, as a resistive heater to raise the sample temperature, and as a discharge cathode for experiment. A Pt resistive probe (not shown in Fig. 1) was used for temperature measurements. A mechanical pump was used to evacuate the system (to ~1 Pa), and a silicon film pressure gauge was used to measure the pressure (in the range of 1 to 30 atm). A thermocouple gauge was used for monitoring the pressure in vacuum. The whole vessel can be submerged in a liquid nitrogen Dewar to 77 K, and the Pd wire can be heated to 200~300°C by the electrical heating up to 35 W. When the vessel ran in the electrical discharge mode, the vessel wall was used as the anode.

Electrical Discharge Mode

Fig. 2 shows the results of one discharge experiment that was set to test the change of loading rate after the discharge. The voltage between the Pd wire and the vessel wall was 400 V, and the discharge current was 3 mA. The discharge lasted for about 70 min. After the discharge the deuterium gas was filled up to 7 atm. The resistance (R) of the Pd wire changed only a little and very slowly. The rate of change in $\Delta R/R$ was about 0.2% per hour. The dip in the pressure (P) curve corresponds to the start of discharge. The hump in the resistance curve was due to the rise in temperature (T) caused by the discharge current. It was somehow unexpected that the glow discharge caused little effect on gas-loading. Later, we began to test whether the degassing may be affected by discharge, since literature suggested that anomalous phenomena preferably occurred in the degassing state. Fig. 3 shows the results corresponding to degassing after electrical discharge. The Pd wire was loaded under a high pressure first. The electrical discharge then began with a low pressure (~0.01 Torr). The pressure was maintained low after the discharge. The resistance of the Pd wire was almost constant for about ten hours. The hump in the resistance curve was again due to the ohmic heating effect. We found that the Pd did not outgas even though the external pressure was low, and the surface was under a short period (~40 min.) of discharge cleaning, which is usually considered an effective method of cleaning surface in controlled nuclear fusion devices.

Cryogenic Treatment

Some early experiments reporting anomalous neutron emission were conducted using gas-loading method and freeze-and-thaw temperature-cycling from room temperature to liquid-nitrogen temperature. Thus it is interesting to investigate the cryogenic effect on loading ratio and loading speed by cooling the vessel inside a liquid nitrogen Dewar. Fig. 4 shows the results of such a cryogenic experiment. In this figure the rising of the temperature curve, however, represents a cooling effect of the vessel. We found that the cooling process might increase the loading speed, but it did not change the terminal loading ratio. Once the resistance ratio reached $R/R_0 \sim 1.6$, loading remained relatively constant for about one day. This resistance ratio corresponded to a loading ratio < 0.84. It seems difficult to obtain a high loading using this method. The early experiments that ran at different pressure ranges (4 to 90 atm)[2,9,10,11] did not report if the loading ratio was higher than the threshold ($D/Pd \approx 0.84$) or not.

Pulse Heating Effect

The pulse heating method induced a clear effect on the loading speed. Fig. 5 shows a comparison between a sample with pulse heating and another without pulse heating. The heating power was about 35 W, and the heating current was about 1 A with a pulse

length of 5 sec. and a 50 sec. intermission. After 20~30 cycles the resistance of the heated wire (R) increased rapidly with a rate of $\Delta R/R \sim 4.5\%$ per hour. In contrast, the resistance of the sample without pulse heating (R*) increased at a much slower rate ($\Delta R^*/R^* \sim 0.3\%$ per hour). These two samples were cut from the same Pd wire, and they were loaded in the same vessel with almost the same deuterium environment. The only difference was the pulse heating. However, the pulse heating did not enhance the loading ratio. At 7.8 atm the terminal loading ratio was still less than 0.74.

Summary of Hydrogen and Deuterium Loading Experiments

Tables 1 and 2 show the results of loading experiments from 1991-1993. In general, the multiple-step loading method worked quite well for hydrogen loading in Pd wires. We loaded and unloaded the Pd wires through pressurized-hydrogen and vacuum cycles. The loading ratio was enhanced gradually as measured by the resistance method. We found that the resistance rose to the maximum resistance ratio and then decreased. Hence we were sure that the loading ratio was higher than 0.74. This was verified by the weighting method at the end of the experiment. The highest loading ratio at $R/R_0 \sim 0.89$ was obtained at 21 atm using a newly annealed sample.

The deuterium loading was much more difficult than the hydrogen loading. Only in one experiment using 30 atm of deuterium and an annealed sample the loading ratio has passed the maximum of the resistance curve. Pulse heating had a significant effect on loading speed but not on the terminal loading ratio. The electrical discharge had no significant effect on deuterium loading. Cooling down to 77 K showed no enhancement on loading either.

Discussion

The loading ratio and resistance ratio are considered volumetric parameters. We found from both resistance ratio and weighting measurements that the loading ratio can be enhanced by annealing (e.g., annealing at ~500°C for 2 hours at 10^{-5} Torr and then furnace cooling in vacuum to room temperature in ~5 hours) and by multiple-step gas-loading (such as by repeated cycles of gas-loading under a high hydrogen pressure and then degassing in vacuum; or sometimes, in the degassing period, by resistive heating of the Pd wire to accelerate the degassing). The mechanisms of how the loading ratio was enhanced by these two methods are not clear at this time. It is possible that the multiple-step gas-loading produced a large amount of defects such as dislocations and traps that facilitate hydrogen absorption and increase the concentration. On the other hand, the annealing is an effective method to reduce stress in the lattice and promote the hydrogen absorption. Further experiments are underway to investigate any microstructure changes from each method to elucidate the cause of these behaviors.

The loading speed is often determined by surface processes, since the bulk diffusion of hydrogen in metals proceed very fast. Some Thermal Deposition Spectrum (TDS) study has shown that the shape of TDS heavily depends on surface condition. The Pd wire, powder, and foil should have different shapes of TDS[12]. The pulse heating in deuterium gas is considered a surface activation process. One possibility for such an activation is a surface quenching process. Because the deuterium is a relatively good cooling agent, when the Pd wire was heated to 200°C by pulse heating, the presence of deuterium gas should provide a cooling effect. This effect may induce a surface reconstruction that creates active sites for deuterium absorption. Another possibility is the high pressure of

deuterium removes surface absorbed impurities that block the active sites. By making these sites available to deuterium, this process may activate the Pd surface, allowing deuterium to permeate fast and promoting the loading speed.

The electrical discharge method did not show any significant effect of promoting the loading speed. Although the electrical discharge was widely used in hot fusion experiments to remove sticking gases on the surface of metals, it does not help in increasing the loading ratio. It may be due to the low deuterium pressure making the cooling effect negligible. The heating effect (at ~1.2 W and ~200°C) by the discharge current is too weak to produce any surface quenching effect. The low pressure of deuterium may also not effective in removing the absorbed surface impurities for activation.

Acknowledgments
This work was supported by the State Commission of Science and Technology and the Natural Science Foundation in China. One of the authors (X. Z. Li) would like to thank the Hawaii Natural Energy Institute in the University of Hawaii at Manoa for partial support of his sabbatical.

References

1. H. Q. Long, et al. "The Anomalous Nuclear Effects Inducing by the Dynamic Pressure Gas Discharge in a Deuterium/Palladium System." in *Frontiers of Cold Fusion*, Edited by H. Ikegami, Universal Academy Press, Tokyo, 1993, pp. 455-459.

2. X. Z. Li, et al. "The Precursor of 'Cold Fusion' Phenomenon in Deuterium/Solid Systems." in *Anomalous Nuclear Effects in Deuterium/Solid Systems*. AIP Conference Proceedings 228, Edited by S. E. Jones, 1991, pp. 419-429.

3. D. W. Mo, et al. "Real Time Measurements of the Energetic Charged Particles and the Loading Ratio (D/Pd)" in *Frontiers of Cold Fusion*, Edited by H. Ikegami, Universal Academy Press, Tokyo, 1993, pp. 535-538.

4. M. C. H. McKubre, et al. "Calorimetry and Electrochemistry in the D/Pd System." in Proceedings of the First Annual Conference on Cold Fusion, Salt Lake City, March 28-31, 1991, Edited by the National Cold Fusion Institute, 1990, pp. 20-31; and "Excess Power Observations in Electrochemical Studies of the D/Pd System; the Influence of Loading." in *Frontiers of Cold Fusion*, Edited by H. Ikegami, Universal Academy Press, Tokyo, 1993, pp. 5-19.

5. R. H. Xiong, et al. "Anomalous Neutron Emission from the Discharge Tube with Palladium Electrode and Deuterium Gas," Presented at the Symposium on Cold Fusion in China, Beijing, CHINA, (May, 1990).

6. S. Y. Duan, et al. "Fusion Neutron Emission Induced by Injection of Deuterium into Titanium Target in a Mirror Plasma." in *The Science of Cold Fusion*, Edited by T. Bressani, et al., Italian Physical Society, Bologna, pp. 139-143 (1991).

7. A. B. Karabut, Ya. R. Kucherov, and I. B. Savvatimova. "Nuclear Product Ratio for Glow Discharge in Deuterium." Physics Letters. A. Vol. 170, p. 265 (1992).

8. M. Srinivasan, et al. "Observation of Tritium in Gas/Plasma Loaded Titanium Samples." in *Anomalous Nuclear Effects in Deuterium/Solid Systems.* AIP Conference Proceedings 228, Edited by S. E. Jones, 1991, pp. 514-534.

9. F. D. Amato, A. De Ninno, and F. Scaramuzzi, et al. "Search for Nuclear Phenomena by the Interaction between Titanium and Deuterium." in Proceedings of the First Annual Conference on Cold Fusion, Salt Lake City, March 28-31, 1990, the National Cold Fusion Institute, 1991, pp. 170-174.

10. H. O. Menlove, et al. "Reproducible Neutron Emission Measurements from Ti Metal in Pressurized D_2 Gas." in *Anomalous Nuclear Effects in Deuterium/Solid Systems.* AIP Conference Proceedings 228, Edited by S. E. Jones, 1991, pp. 287-301.

11. J. Y. He, et al. "Experimental Study on Anomalous Neutron Production in Deuterium/Solid System." in *Anomalous Nuclear Effects in Deuterium/Solid Systems.* AIP Conference Proceedings 228, Edited by S. E. Jones, 1991, pp. 193-205.

12. M. H. Mintz, et al. in *Hydrogen in Intermetallic Compounds II, Surface and Dynamic Properties, Applications,* Edited by L. Schlapbach, Springer-Verlag, Berlin, 1992, pp. 283-317.

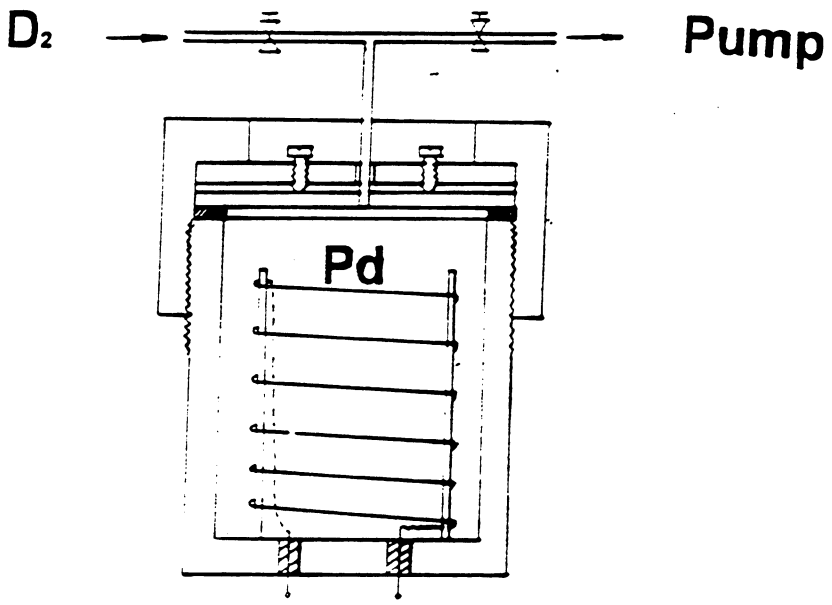

Fig.1. Schematics of Gas Loading Device

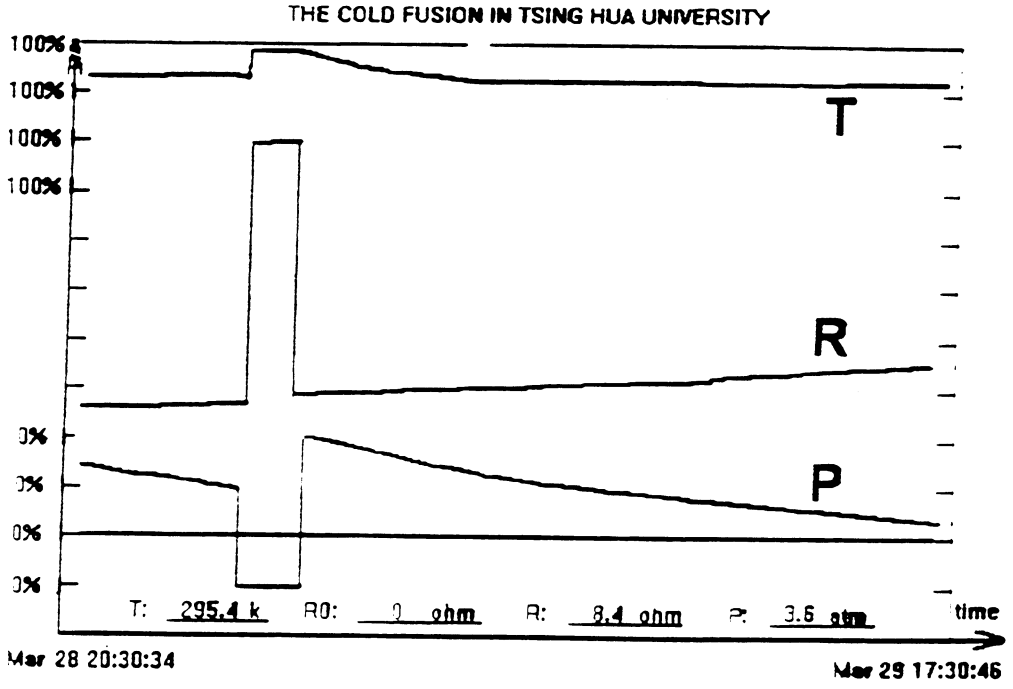

Fig.2. Effect of Electrical Discharge on Deuterium Loading under Pressure (7 atm.)

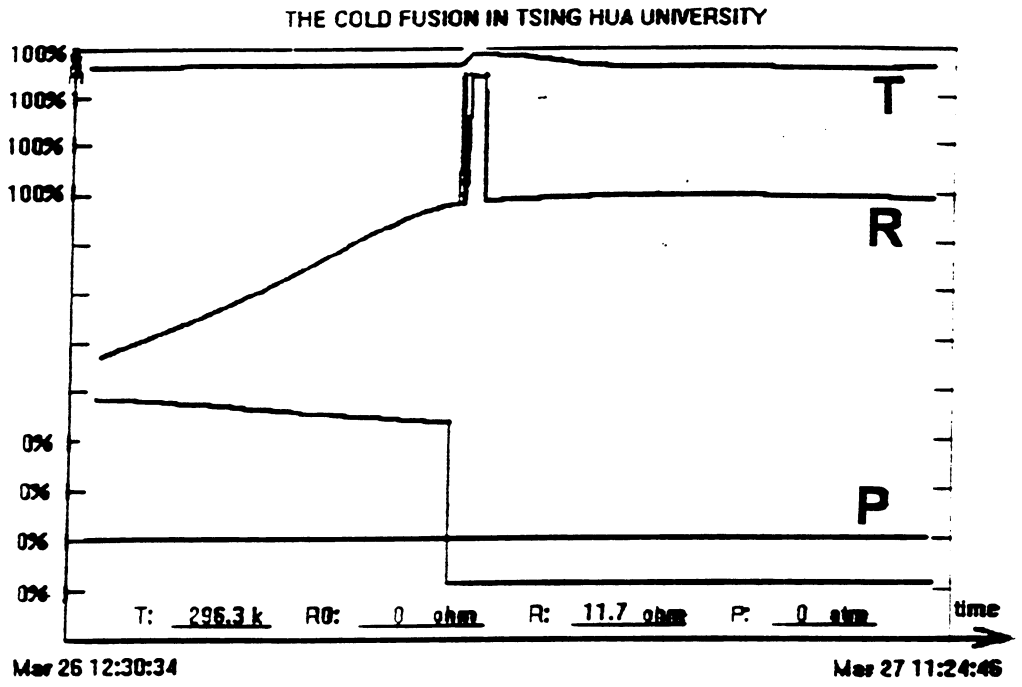

Fig.3. Effect of Electrical Discharge on Degassing in Vacuum (0.01 Torr.)

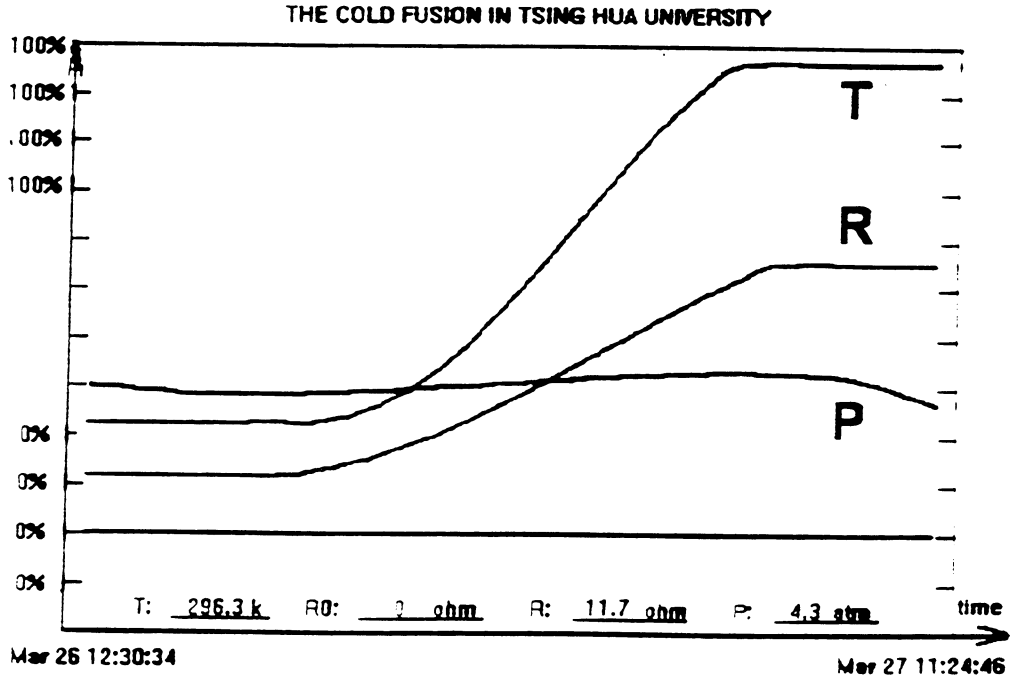

Fig.4. Effect of Cryogenics on Deuterium Loading

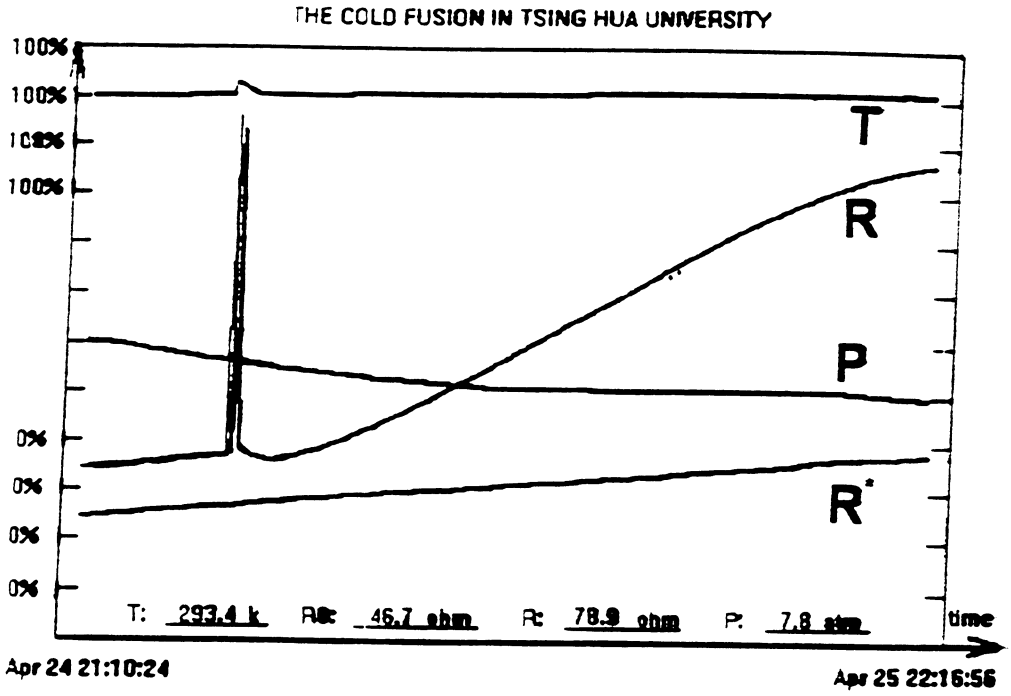

Fig.5. Effect of Pulse Heating on Deuterium Loading

Table 1 Loading with Hydrogen Gas for Different Treatments of Samples

TREATMENT	TIME (hrs.) FOR REACHING $(H/Pd)_{max}$	$(H/Pd)_{max}$	CROSS PEAK	REMARKS
HALF YEAR AFTER ANNEALING	16	0.74	YES	9-14 atm.
AS IT IS	75	0.85	YES	6-23 atm.
2 days AFTER ANNEALING	< 4.5	0.89*	YES	20-21atm.
5 days AFTER ANNEALING	6	0.88	YES	16 atm.
15 days AFTER ANNEALING	7.5	0.74	YES	19-12 atm.

* Checked by weighting method

Table 2 Loading with Deuterium Gas for Different Treatments of Samples

TREATMENT	LOADING RATE (% PER HOUR)	$(R/R_o)_{max}$	CROSS PEAK	REMARKS
AS IT IS	0.29	1.33	NO	8-11 atm. 1 week
PULSE HEATING	4.5	1.95	NO	8-11 atm. 1 week
DISCHARGE	0.27	1.13	NO	6-8 atm. 2 days
COOLING	~ 0	1.95	NO	start cooling after (R/R_o) ~ 1.95
ANNEALING	4.7	1.90	YES	30 atm. 2 days
ANNEALING & ACID CLEANING	2.0	1.87	NO	30 atm. 2 days

Electrolytic Hydrogen/Deuterium absorption into Pd, Pd-Rh and Pd-Ag alloys in fuel cell type closed cell

H.Akita, Y.Tsuchida, T.Nakata, A.Kubota, A.Kubota, M.Kobayashi,
Y.Yamamoto, N.Hasegawa, N.Hayakawa and K.Kunimatsu
IMRA JAPAN CO., LTD.
3-6 Techno Park 2 Cho-me Simonopporo Atsubetsu-ku, Sapporo 004, JAPAN

ABSTRACT

The many parameters controlling electrolytic hydrogen and deuterium loading into Pd and Pd based alloy cathodes were investigated.

The result is summarized as follows;

1. Modifying the palladium surface by chemisorbed molecules as well as by a thin metallic film, is an effective way to achieve D/Pd greater than 0.9.
2. Pd-Rh (5, 10atm%)alloy cathodes give D/M >0.9.

INTRODUCTION

Recently, it has been recognized that the excess heat generation during heavy water electrolysis with a Pd cathode depends on deuterium loading ratio, D/Pd. Excess heat is generated at deuterium loading ratio higher than around 0.84 and becomes larger with increasing D/Pd.[1,2] However, it is difficult to attain D/Pd higher than 0.88 in ordinary electrolysis because the loading can be influenced by many experimental parameters.

Therefore, we investigated influence of many important parameters on hydrogen and deuterium loading into the palladium cathode for the purpose of attaining D/Pd higher than 0.9.

EXPERIMENTALS

The electrolysis was conducted in a closed cell with fuel cell anode shown in Fig.1 under galvanostatic conditions between 0 and 1A/cm^2. A platinized platinum electrode in the same solution acted as a reference electrode RHE to measure hydrogen or deuterium overvoltage at the Pd cathode. The initial pressure of H_2 or D_2 before electrolysis was 5～8kg/cm^2. The principle of the D/Pd measurement in a closed cell with a fuel cell anode has been described elsewhere.[2]

The loading ratio was determined mostly from the pressure decrease during the electrolysis. In some cases the loading ratio was determined also from cathode resistance measurements in order to check consistency between the loading data obtained by the two methods. However, after the ICCF4 we found an small error in the determination of the internal volume, which is typically ca 200cc. The correct value has turned out to be ca 7cc smaller and this has reduced the D/Pd value by a few percent according to the above equation.

The effect of electrolyte on hydrogen or deuterium loading into Pd was studied focusing on the alkaline solutions which gave higher cathode overvoltage than acidic solutions for a given current density. Especially the role of alkali metal cations, Li^+, Na^+, K^+, were investigated by comparing H/Pd and D/Pd in LiOH/LiOD, NaOH/NaOD, KOH/KOD and tetramethyl ammonium hydroxide, $(CH_3)_4NOH$.

The effect of temperature was studied by observing change of cathode loading by hydrogen/deuterium when temperature was changed from 10 ℃ to 60 ℃ . The temperature change was executed in two ways: firstly cathode loading was determined at each temperature in different cells, and secondly the temperature change was given after the cathode loading of hydrogen in 1M LiOH and of deuterium in 1M LiOD has reached 0.92 and 0.85 respectively at 10℃. The temperature dependence at the high loading conditions both for hydrogen and deuterium were studied in this way.

Effect of surface modification was studied in two ways; firstly by adding a catalytic poison such as thiourea to the electrolyte, which is adsorbed on the cathode surface and inhibits the hydrogen desorption process, 2H(adsorbed) → H_2. The organic substance like thiourea can be used only in the fuel cell type cell in which potential of the fuel cell anode during electrolysis is not high enough to evolve oxygen and consequently thiourea is not oxidized at the anode.

Secondly the Pd surface was modified geometrically by a sputtered gold film leaving a minor portion of the Pd surface exposed to the electrolyte. The electrolysis current is focused to the exposed Pd surface at which the actual current density could be much higher than the average current density over the cathode surface. The loading of hydrogen into such a Pd cathode would be higher because of the higher cathode overvoltage.

The effect of cathode materials on the loading was studied by comparing the loading on Pd, Pd–Rh alloys and Pd–Ag alloys. A composite of palladium and silver made by diffusion joint of those plates using a plasma sintering method was also studied and its loading characteristics was compared with Pd and Pd–Ag alloy.

Results and Discussion

1. Determination of H/Pd by resistance measurements and pressure measurements

First of all, we checked accuracy of our D/Pd determination in a closed cell with fuel cell anode by conducting simultaneous measurements of cathode resistance as well as the hydrogen pressure in the electrolysis cell.

Figure 2 shows dependence of H/Pd determined by various methods on R/R_0 for Pd in 1M LiOH at 20℃ where R_0 and R are the cathode resistances measured by the four terminal method before and after hydrogen loading, respectively.[3,4,5,6,7] The cathode loading determined by resistance measurement is consistent with the present data obtained by pressure measurement in a fuel cell type closed cell.

Therefore the H/Pd data determined by pressure measurement in a closed cell with fuel cell anode is in good agreement with those determined by resistance measurement.

2. The effect of electrolyte on loading ratio

(1)Alkali metal cations, Li^+, Na^+, K^+

Figures 3, 4 show dependence of H/Pd and D/Pd respectively on current density for Pd in various alkaline solutions at 10℃. The absorption of hydrogen and deuterium into Pd are strongly influenced by the kind of alkali metal cations in the electrolyte. Then the D(H)/Pd for a given current density decreases in the order, LiOD(H)>NaOD(H)>KOD(H). Therefore, the D(H)/Pd is reduced strongly by potassium ions at high current densities.

We further investigated the reason why H(D)/Pd is highest in LiOH(D). Figure 5 shows the relation between cathode overvoltage and current density in 1M LiOH, NaOH and KOH. The overvoltage in 1M LiOH is lowest in the three alkaline solutions, which suggests that the cathode overvoltage is not an important factor contributing to the highest H/Pd in 1M LiOH. The data in Figs. 3 and 4 suggest as if Li^+ ions were "promoting" cathode loading while K^+ ions were acting in the opposite way.

The effect of alkali metal cations can be interpreted in terms of their underpotential deposition and its effect on the electronic nature of the Pd cathode. In fact incorporation of Li into Pd cathode was detected by SIMS analysis of the cathode after electrolysis, and the presence of Li was interpreted in favor of its role in promoting the cathode loading.[8]

We investigated if really Li incorporated into Pd cathode promotes electrolytic hydrogen loading into the cathode by conducting H/Pd measurements in a typical alkali metal free alkaline solution, i.e. tetramethyl ammonium hydroxide, $(CH_3)_4NOH$.

(2)Tetramethyl ammonium hydroxide, $(CH_3)_4NOH$

Figure 6 shows comparison of H/Pd in 1M $(CH_3)_4NOH$ (TMAOH) and 1M LiOH for Pd at 10℃. The H/Pd in TMAOH is higher than that in LiOH by 2 to 7%, the maximum value of H/Pd being 0.96.

Figure 7 shows dependence of overvoltage on current density for Pd in various alkaline solutions at 10℃. Overvoltage in 1M TMAOH is lower than the other alkaline solutions, 1M LiOH, NaOH and KOH.

Figure 8 shows hydrogen desorption from Pd cathode after current interruption from $3mA/cm^2$ at 10℃. The desorption process in 1M LiOH containing thiourea which is a typical catalytic poison is much slower than that in 1M LiOH. However the desorption rate in TMAOH is similar to that in LiOH. So the TMA^+ cation is not working as a catalytic poison.

To summarize these results, the higher H/Pd is attained in 1M TMAOH than 1M LiOH, and the TMA^+ is not working as catalytic poison. Therefore the cathode loading is in fact reduced by Li incorporated into Pd cathode by underpotential deposition.

It is not clear at the moment, however, if the highest and the lowest H/Pd in 1M LiOH and 1M KOH, respectively, can be related to their actual quantity incorporated into the Pd cathode or to their specific effect on the nature of the cathode.

Comparative SIMS analysis of the Pd cathode after electrolysis in 1M LiOH and KOH would greatly contribute to the further understanding of the role of alkali metals in the cathode loading.

3. The temperature effect on H/Pd and D/Pd at 10℃, 30℃ and 60℃

Figures 9 and 10 show temperature dependence of H/Pd and D/Pd between 10℃ and 60℃ for Pd in 1M LiOH and 1M LiOD. The H/Pd and D/Pd at 60℃ is lower than at 10℃. On the other hand, it has been said that loading process may change from exothermic to endothermic when H(D)/Pd value is higher than 0.85 based on the dependence of enthalpy of hydrogen absorption into Pd on the loading ratio.[9]

However when the temperature change was given after the cathode loading of hydrogen in 1M LiOH and of deuterium in 1M LiOD has reached 0.92 and 0.85 respectively at 10℃, the H/Pd and D/Pd decreased and finally coincided with the value at 60℃.

Figure11 shows dependence of D/Pd on current density at 10℃, 30℃ and 60℃. The D/Pd decreases in the order, 10℃>30℃>60℃.

To summarize these results, the D/Pd decreases with increasing temperature, which is consistent with the P-C-T curves.[10] Therefore the data presented above strongly suggests that the electrolytic loading process does not change from exothermic to endothermic even when H/Pd or D/Pd is higher than 0.85.

4. The effect of surface modification

(1)Surface modification by Thiourea, $(NH_2)_2C=S$

Thiourea, THU, is chemisorbed on the cathode surface and inhibits the hydrogen desorption process as demonstrated in Figure 8. Figures 12 and 13 show effect of THU on H/Pd and D/Pd for Pd in 1M LiOH and 1M LiOD respectively at 10℃.

Addition of 600 μM THU increased H/Pd and D/Pd by ca 2～10% to give rise to the maximum values of H/Pd and D/Pd 1.00 and 0.91 respectively.

Therefore, the surface modification of the Pd cathode by chemisorbed molecules such as THU is effective to have D/Pd≧0.9.

(2)Surface modification by a sputtered Au film (7000Å)

Gold is electrochemically less active than Pd. So when most of the Pd surface is covered by a gold film, current density on the exposed Pd surface could be raised substantially and this could lead to higher deuterium loading. Three types of Pd cathodes with 7000 Å gold film have been prepared by RF magnetron sputtering controlling the surface coverage by Au film to 80%, 97%, 100%, respectively (Fig.14).

Figure 15 shows change of D/Pd with time on Pd with a sputtered Au film in 1M LiOD at 10℃ and i=30mA/cm^2. Loading rate of Pd with Au film becomes lower with increased coverage of the surface by the gold film. The Pd cathode totally covered by the gold film has been loaded by deuterium as well. Therefore it seems that deuterium atoms permeate through the gold film and are absorbed into Pd.

Figure 16 shows dependence of D/Pd on current density for the Pd cathodes with the sputtered gold films in 1M LiOD at 10℃. Cathode loading is greatly improved by the sputtered Au film. The Pd cathode 97% covered by the Au film gave max. D/Pd=0.91, while Pd cathode 80% covered by the Au film gave 0.87.

Figure 17 shows dependence of overvoltage on current density for the Pd cathode with the sputtered Au films in 1M LiOD at 10℃. Overvoltage on gold cathode is a little bit higher than that on Pd above 0.1A/cm^2, while overvoltage of the Pd cathodes with a Au film is significantly higher than that of gold.

Figure 18 shows dependence of D/Pd on overvoltage for Pd with and without sputtered Au film in 1M LiOD at 10℃. The D/Pd on Pd with the sputtered Au film becomes much higher than that on Pd without the gold film, which is apparently due to much higher cathode overvoltage on Pd with a Au film.

To summarize these results, deuterium atoms adsorbed on the gold film which were generated by Volmer step of hydrogen electrode reaction permeated through the gold film and are absorbed into Pd.

We do not know, however, why presence of the gold film on the Pd cathode gives rise to much higher cathode overvoltage than Pd and Au. Further studies are needed in order to understand the role of the Au film on the cathode loading.

5.The effect of cathode materials

(1)Pd-Rh alloys

Pd-Rh alloys are known to be a better hydrogen absorber than Pd in gas phase under high hydrogen pressures.[11] The lattice parameter of the Pd-Rh alloys decreases

while their hydrogen absorption characteristics is improved with the increase of rhodium content up to 30～40%. This makes Pd–Rh alloys very attractive in raising the deuterium density in the alloy lattice. We investigated electrolytic deuterium loading into the Pd–Rh alloys in 1M LiOD.

Figure 19 shows dependence of D/M on overvoltage for Pd–Rh alloys in 1M LiOD at 10℃. The D/M=0.97 is achieved for Pd–10at% Rh alloy cathode. Therefore there is possibility that Pd–Rh alloys can be used as cathodes in excess heat measurements for D/Pd≧0.9 region.

(2)Pd–Ag alloy

Pd–Ag alloys are the well known materials for hydrogen diffusion tubes to purify hydrogen gas, and their P–C–T curves for hydrogen absorption show that H/Pd for a given hydrogen pressure decreases with increasing Ag content in the alloy.[12] We investigated the electrolytic deuterium loading into 10atom.% Pd–Ag alloy cathode.

Figure 20 shows comparison of H and D loading on Pd and Pd–10at%Ag alloy cathodes at 10℃. Hydrogen and deuterium loading of the Pd–Ag alloy cathode is more than 15% lower than Pd. Therefore, Pd–Ag alloy is not a better cathode material in attaining higher D/Pd than 0.9 as inferred from the P–C–T curves determined in gas phase.

(3)Pd–Ag composite

A composite of palladium and silver made by diffusion joint of those plates using a spark plasma sintering method was studied and its loading characteristics was compared with Pd and Pd–Ag alloy.

Figure 21 shows dependence of H/Pd or H/M on overvoltage for Pd, Pd–Ag alloy and Pd–Ag composite cathodes in 2.8M H_2SO_4. The H/Pd of the Pd–Ag composite cathode is much higher than Pd–Ag alloy, but almost equals to that on Pd for a given overvoltage. The data on the Pd–Ag composite is extended to the higher overvoltage region, however, to achieve the higher H/Pd than Pd, which is due to the higher cathode overvoltage for a given current density as shown in Fig.22.

Figure 22 shows dependence of overvoltage on current density for Pd, Pd–Ag alloy and Pd–Ag composite cathodes in 2.8M H_2SO_4. Overvoltage of the Pd–Ag composite cathode is more than 200mV higher than Pd and Pd–Ag alloy cathodes for a given current density.

One more peculiar nature of the Pd-Ag composite cathode is demonstrated in its loading process.

Figure 23 shows change of H/Pd with time on Pd and the Pd-Ag composite cathodes. Loading rate of the Pd-Ag composite is much lower than that of Pd despite of its much smaller hydrogen diffusion distance, i.e. the thickness of the Pd, which is 0.5mm, compared to 2mm for the Pd rod cathode of 4mm diameter.

These results strongly suggest that the mechanism of loading process is different on the Pd-Ag composite cathode.

Conclusion

The loading ratio depends on many experimental parameters. In particular, the followings are summarized in conclusion as effective ways for the improved cathode loading by deuterium;

1. Modifying the Pd surface by chemisorbed molecules as well as by thin metallic films, which are electrochemically less active than Pd.
2. Employing cathode materials such as Pd-Rh alloys, which give D/M = 0.97.

References

1) M.C.H.Mckubre, S.Crouch-Baker, A.M.Riley, S.I.Smedley and F.L.Tanzella :Frontirs of Cold Fusion, Proceedings of ICCF3 (1992),p5
2) K.Kunimatsu, N.Hasegawa, A.Kubota, N.Imai, M.Ishikawa, H.Akita and Y.Tsuchida: Frontiers of Cold Fusion, Proceedings of ICCF3, (1993) 31.
3) T.B.Flanagan and F.A.Lewis, Z.physik.chem.,27,104(1961)
4) J.C.Barton, F.A.Lewis, and I.Woodwaard, Trans.Faraday Soc., 59, 1201(1963)
5) B.Baranowski, F.A.Lewis, W.D.Mcfall, S.Filipek and T.C.Witherspoon, Proc.R.Soc.Lond.A 386, 309(1983)
6) A.W.Szafranski and B.Baranowski, phis.stat.sol.(a) 9, 435(1972)
7) M.C.H.Mckubre, R.C.Rocha-Filho, J.Chao, B.Chexal, T.Passel, and J.Santucci, The First Annual Conference on Cold Fusion Conference Proceedings, p20(1991)
8) M.NAKADA, T.KUSUNOKI, M.OKAMOTO and O.ODAWARA, Frontiers of Cold Fusion, proceedings of ICCF3(1992), p581.
9) P.S.Rudman:"ENTHALPY OF METAL-HYDROGEN SYSTEMS:A PAIR BOND MODEL", p49-54, vol.6. ELECTRONIC STRUCTURE AND PROPERTIES OF HYDROGEN IN METALS, NATO. CONFERENCE SERIES. SERIES VI:Materials

Science
10) T.R.P.Gibb:"Primary Solid Hydrides", p315–509, in Progress in Inorganic Chemistry, vol.3, ed. by F.A.Cotton(Interscience, New York, London 1962)
11) B.Baranowski, S.Majchrzak, and Ted B.Flanagan:"A High–Pressure Investigation of the Rhodium/Palladium/Hydrogen System", The Journal of Physical Chemistry, vol.77, No.1, 1973
12) H.Brodwsky, E.Poeschel:Z.Physik. Chem. NF 144, 143(1965) E.Poeschel : Dissertation, Münster(1964)

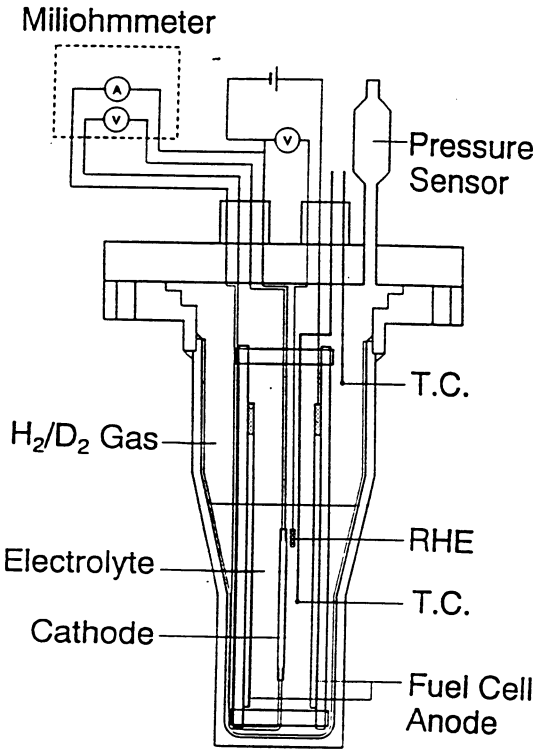

Fig. 1 Closed cell for simultaneous determination of R/R_0 and H/Pd.

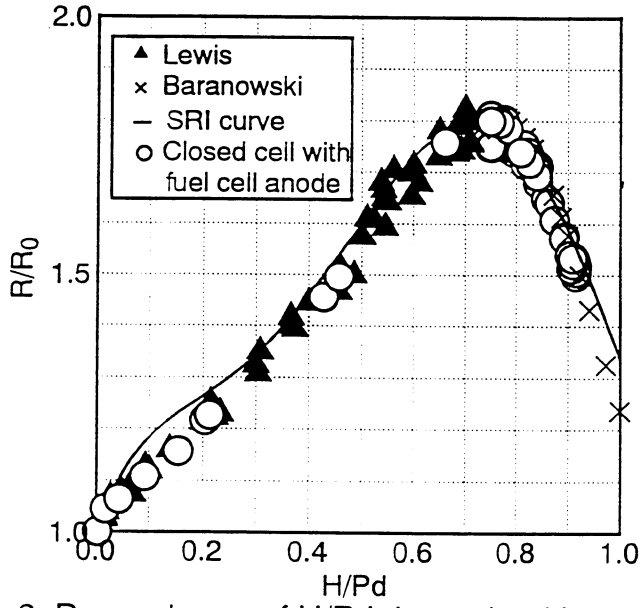

Fig. 2 Dependence of H/Pd determined by various methods on R/R_0 for Pd in 1M LiOH at 20°C.

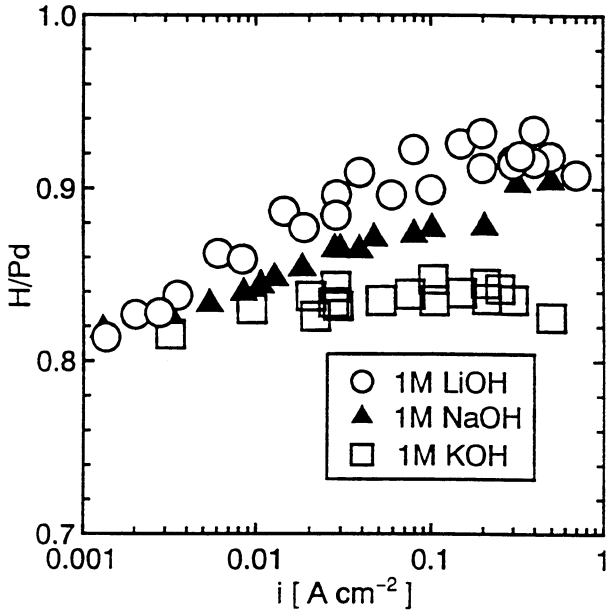

Fig. 3 Dependence of H/Pd on current density for ϕ4 Pd in various alkaline solutions at 10℃.

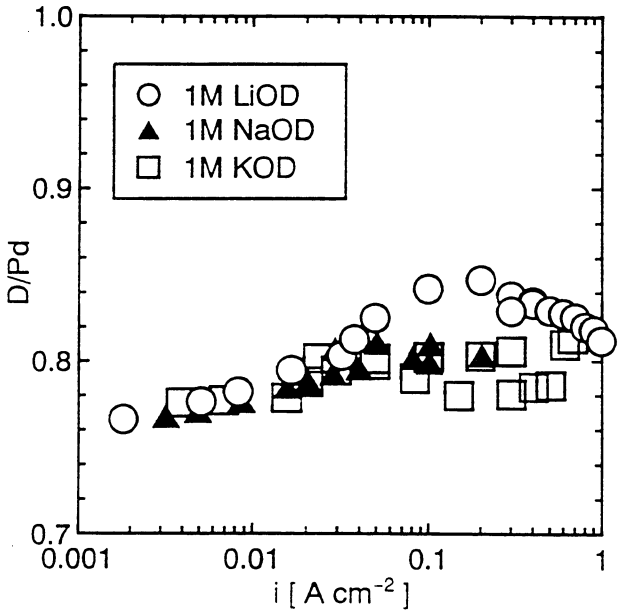

Fig. 4 Dependence of D/Pd on current density for ϕ4 Pd in various alkaline solutions at 10℃.

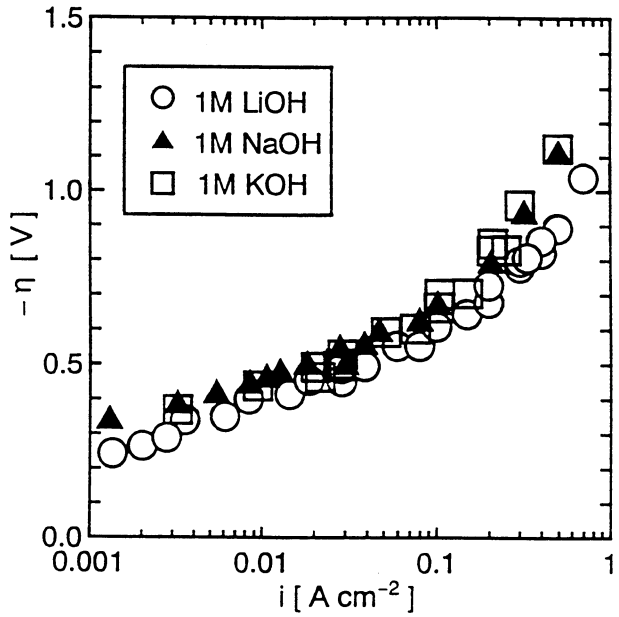

Fig. 5 Dependence of overvoltage on current density for φ4 Pd in various alkaline solutions at 10℃.

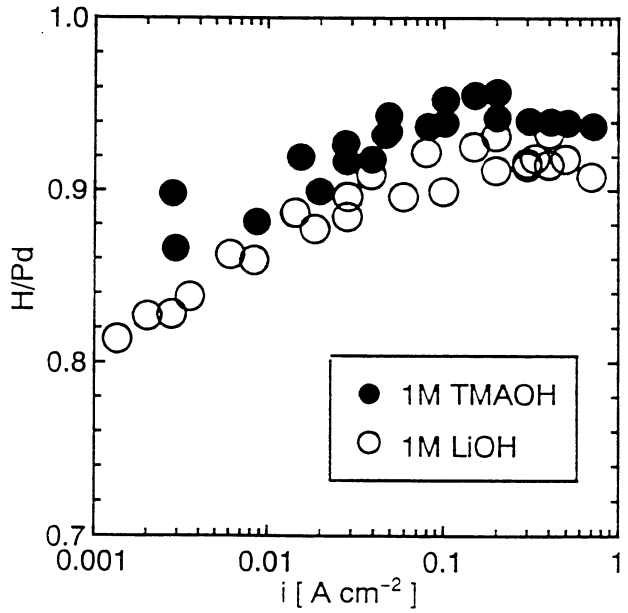

Fig. 6 Comparison of H/Pd in 1M TMAOH and 1M LiOH for φ4 Pd at 10℃.

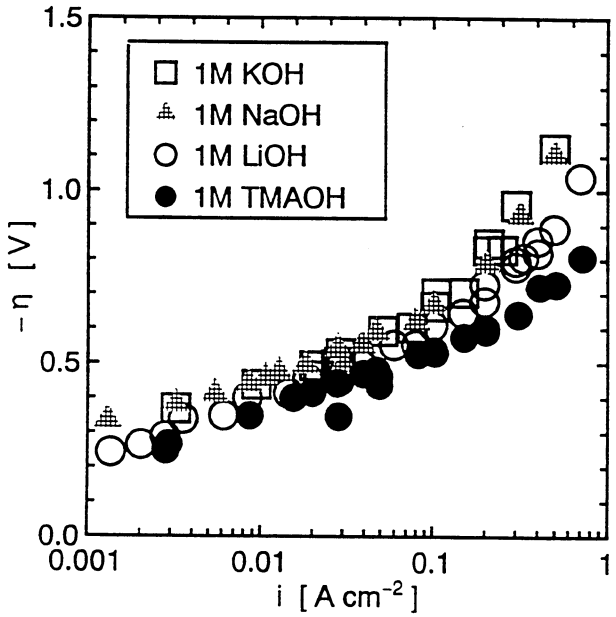

Fig. 7 Dependence of overvoltage on current density for Pd in various electrolyte at 10℃.

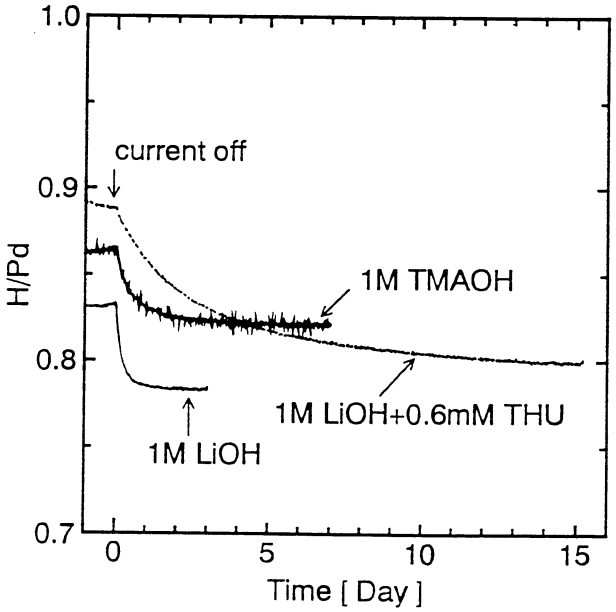

Fig. 8 Hydrogen desorption from Pd cathode after current interruption from 3mA/cm^2 at 10℃.

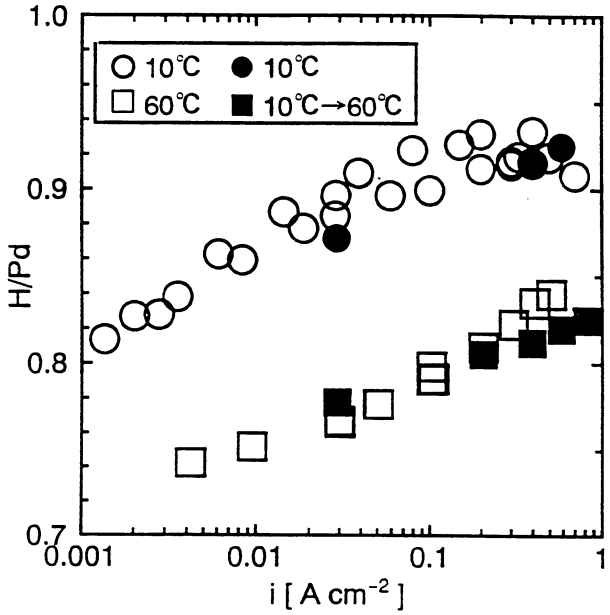

Fig. 9 Temperature dependence of H/Pd between 10℃ and 60℃ for ϕ4 Pd in 1M LiOH.

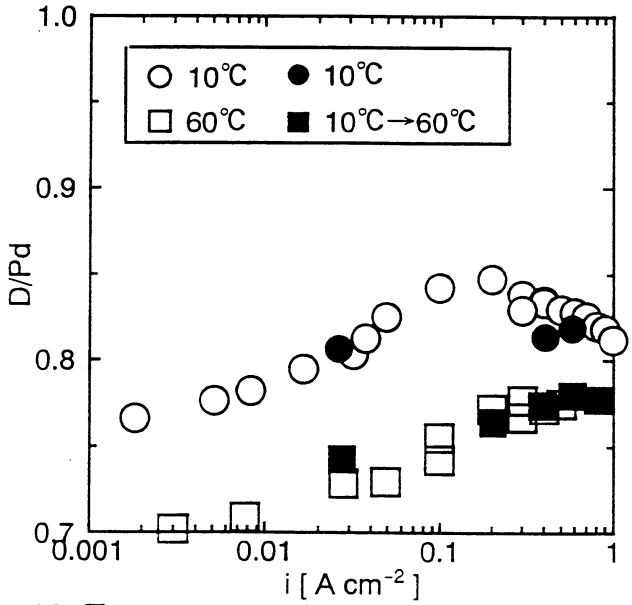

Fig. 10 Temperature dependence of D/Pd between 10℃ and 60℃ for ϕ4 Pd in 1M LiOD.

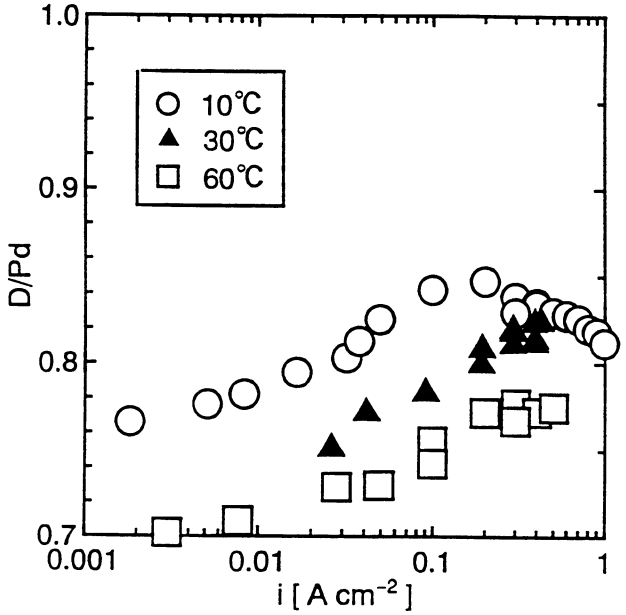

Fig. 11 Dependence of D/Pd on current density for φ4 Pd in 1M LiOD at 10℃, 30℃ and 60℃.

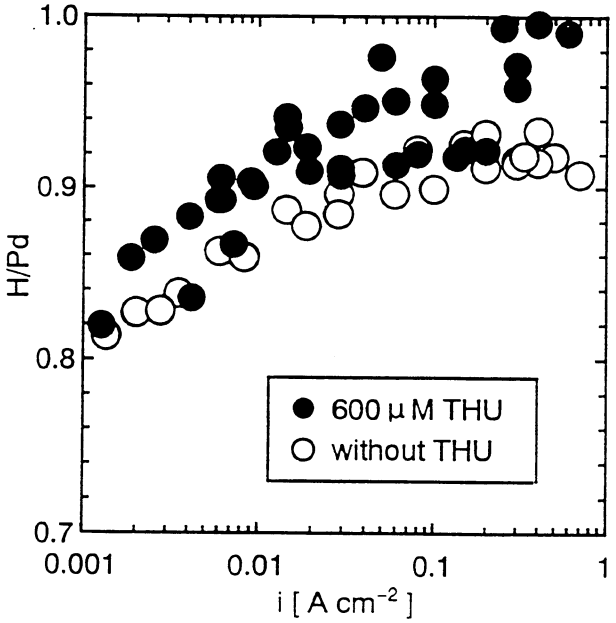

Fig. 12 Effect of Thiourea on H/Pd in 1M LiOH, φ5 Pd at 10℃.

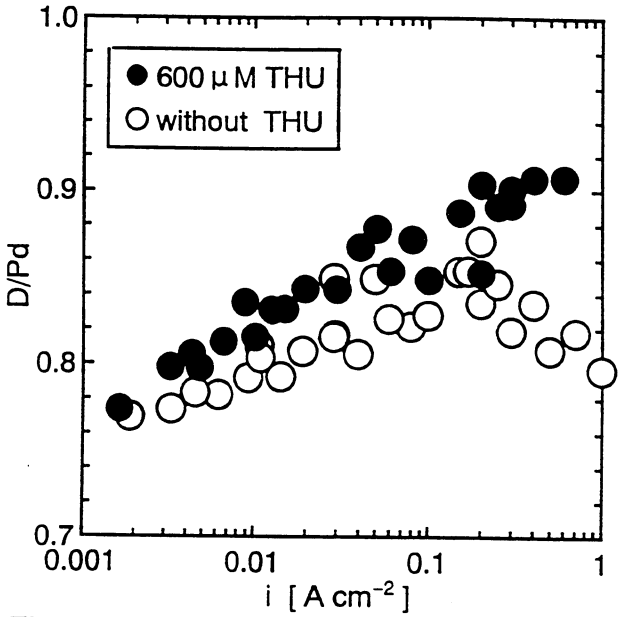

Fig. 13 Effect of Thiourea on D/Pd for φ4 Pd in 1M LiOD at 10℃.

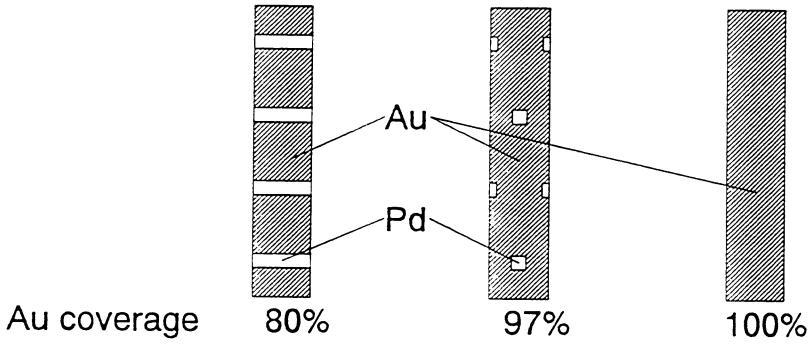

Fig.14 The Pd cathodes(φ4x20mm) with 7000 Å Au film by RF magnetron sputtering.

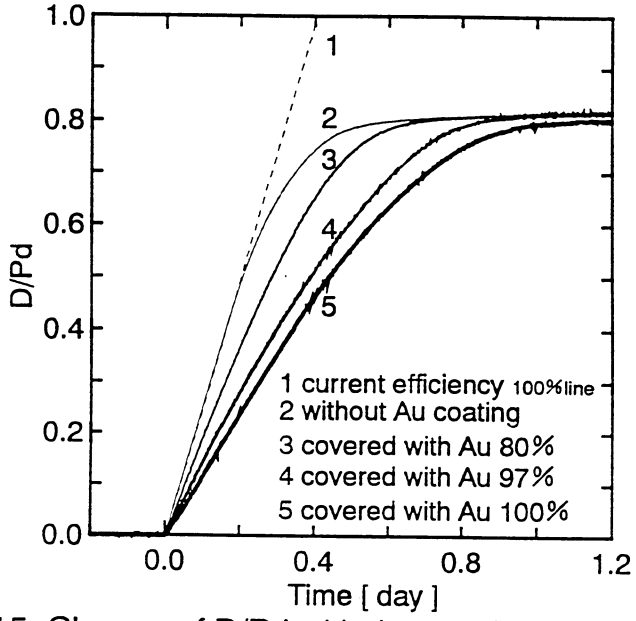

Fig. 15 Change of D/Pd with time on Pd with sputtered Au film in 1M LiOD at 10℃, i=30mA/cm^2.

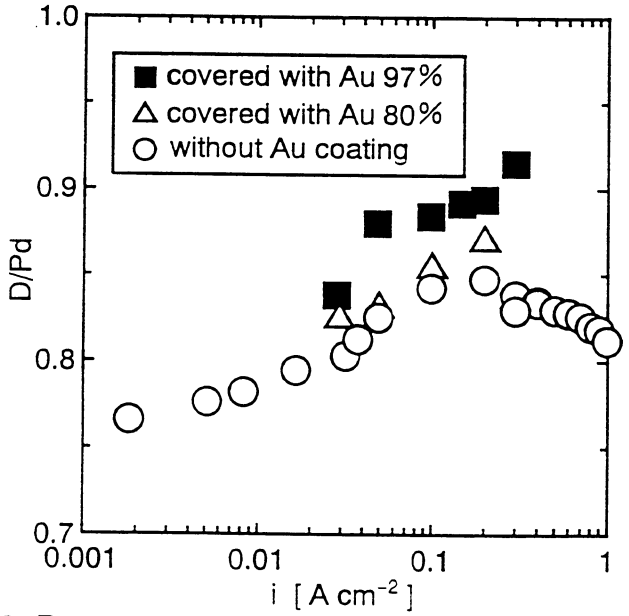

Fig. 16 Dependence of D/Pd on current density for φ4 Pd with sputtered Au film (7000Å) in 1M LiOD at 10℃.

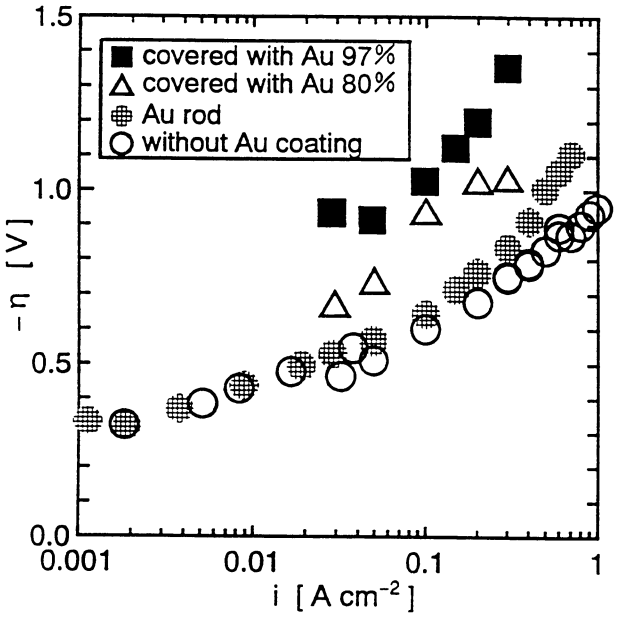

Fig. 17 Dependence of overvoltage on current density for φ4 Pd with sputtered Au film in 1M LiOD at 10℃.

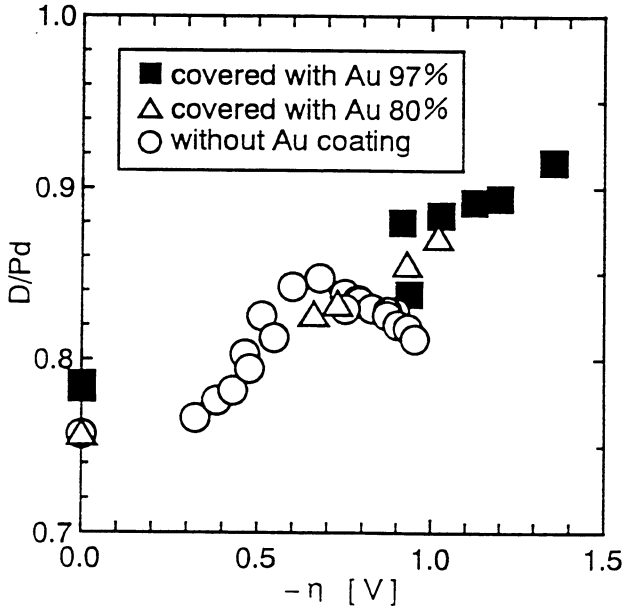

Fig. 18 Dependence of D/Pd on overvoltage for φ4 Pd with and without sputtered Au film in 1M LiOD at 10℃.

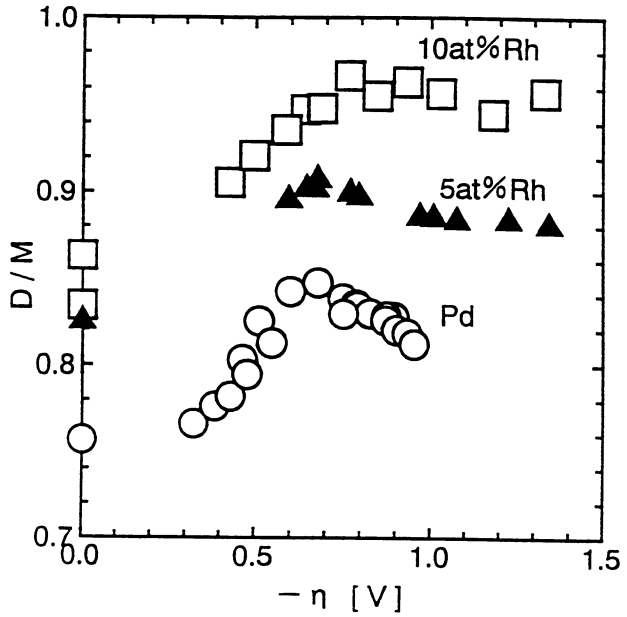

Fig. 19 Dependence of D/M on overvoltage for φ4 Pd–Rh alloys in 1M LiOD at 10℃.

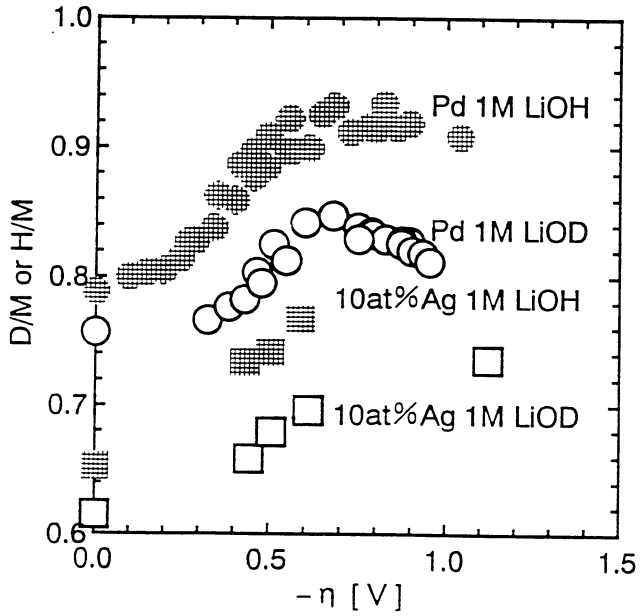

Fig. 20 Dependence of D/M and H/M on overvoltage for Pd and Pd–Ag alloy at 10℃.

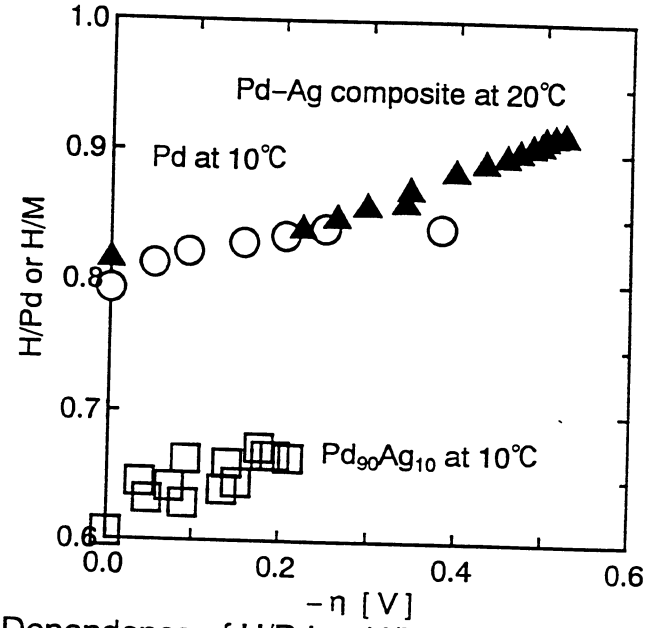

Fig. 21 Dependence of H/Pd or H/M on overvoltage for Pd, Pd–Ag alloy and Pd–Ag composite cathodes in 2.8M H_2SO_4.

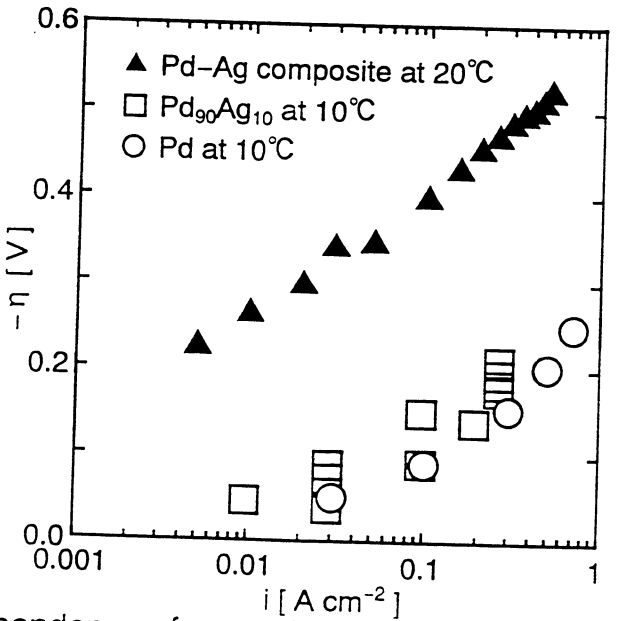

Fig. 22 Dependence of overvoltage on current density for Pd, Pd–Ag alloy and Pd–Ag composite cathodes in 2.8M H_2SO_4.

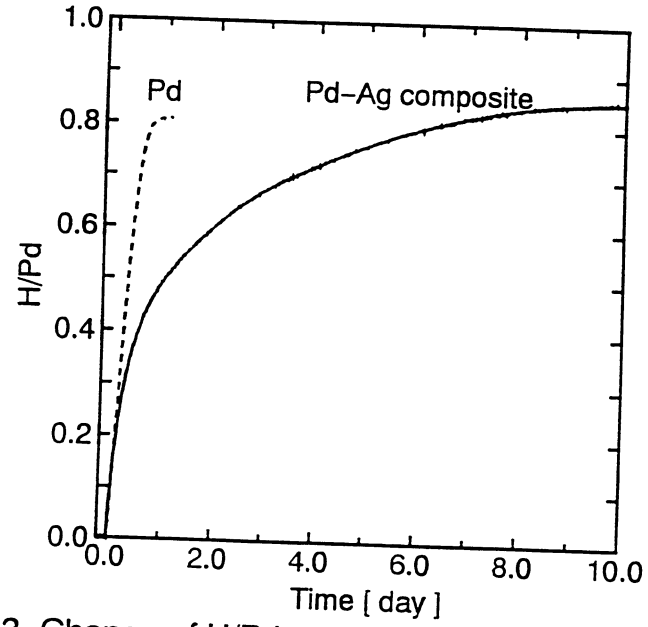

Fig. 23 Change of H/Pd with time on Pd(ϕ 4mm) and Pd–Ag composite(t0.5mm) cathodes in 2.8M H_2SO_4 at 10℃ and 20℃ respectively, i=20mA/cm^2.

HIGH POWER μs PULSED ELECTROLYSIS FOR LARGE DEUTERIUM LOADING ON Pd PLATES.

F.Celani
A.Spallone
P.Tripodi
A.Nuvoli
A.Petrocchi
D.Di Gioacchino
M.Boutet
INFN, Laboratori Nazionali di Frascati,
via E.Fermi, 00044 Frascati (Italy).

P.Marini
V.Di Stefano
SKITEK, IRI, Pomezia (Italy)

(*)

Abstract

An high peak current (up to 100 A) and a very short pulse (1 μs) generator was used to perform electrolysis in D_2O-LiOD solution using a Pd sheet as a cathode and a Pt net as an anode. This high power pulse (up to 50 KW) can be rated up to 20 KHz.

Very high D/Pd values (up to about 1:1) has been reached with any cold-worked Pd sheets used. A very hard sheet (about 300 Hv) has generated an excess heat of the order of 15% for a long time (some weeks).

Some considerations about the metallurgy of electrodes are performed and an effort is made to correlate the excess heat with metallurgical parameters, over-voltage and surface resistance.

1. The Experimental Set-Up

The adopted electrolytical system was already described in the previous ICCF3 Conference at Nagoya (Japan)[1] and consists of a flow calorimeter composed by a cylindric polyethylene vessel containing a double

---

(*) Work supported by: INFN-LNF, INFM (Italy); ORIM S.r.l. Macerata (Italy)
Pd plates provided by: TANAKA K.K. and IMRA-Research (Japan)

turned copper coil used as a cooler. The ordinary water, passing through the coil, cools the solution. Seven temperature sensors are properly located in order to measure the produced heat and to cross-check the calorimeter operation.

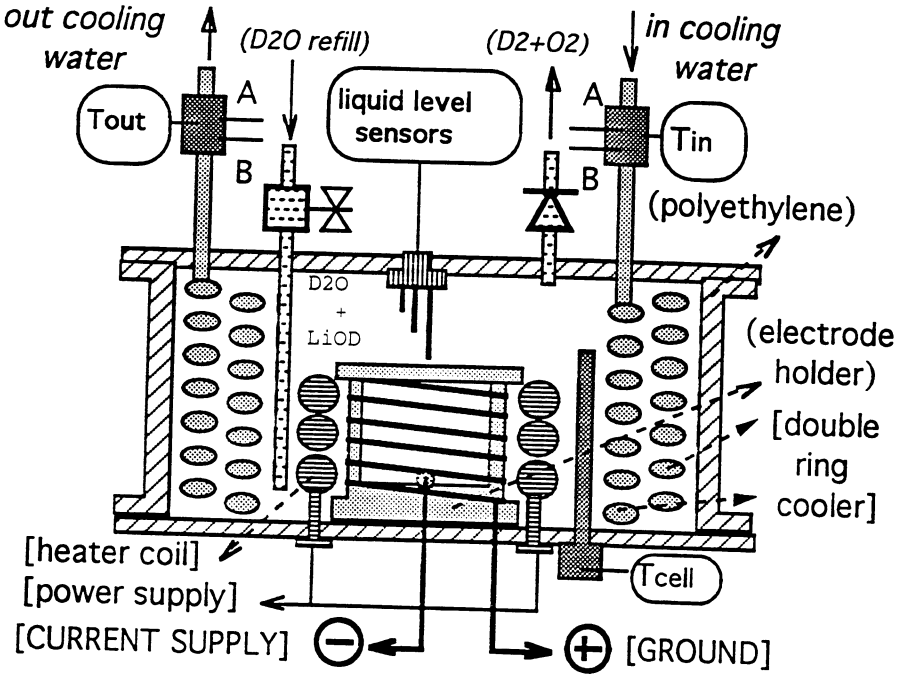

a) Inner cell

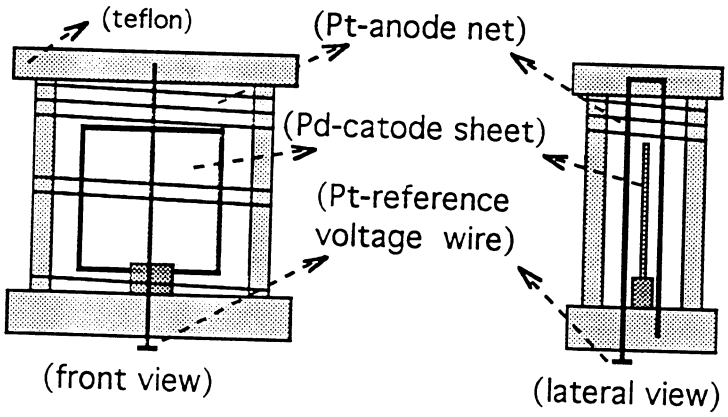

b) electrode holder

Fig. 1 - Inner cell design and electrode holder

In respect to the Conference at Nagoya, we improved the system modifying the Pt sample-holder net at the anode (fig. 1). The Pt wire was turned around in an opportune way in order to smooth the not-uniform electric field at the edges of the sheet. In this way we reduced the effect of the Deuterium discharge at the edges due to the strong electric field gradients. In this figure it is shown the reference electrode, consisting in a Pt wire, located in front of the Pd plate (2mm distant); the wired Pt anode net is 1 cm far from the cathode and the electrolytic solution is LiOD 0.3 M/l D_2O.

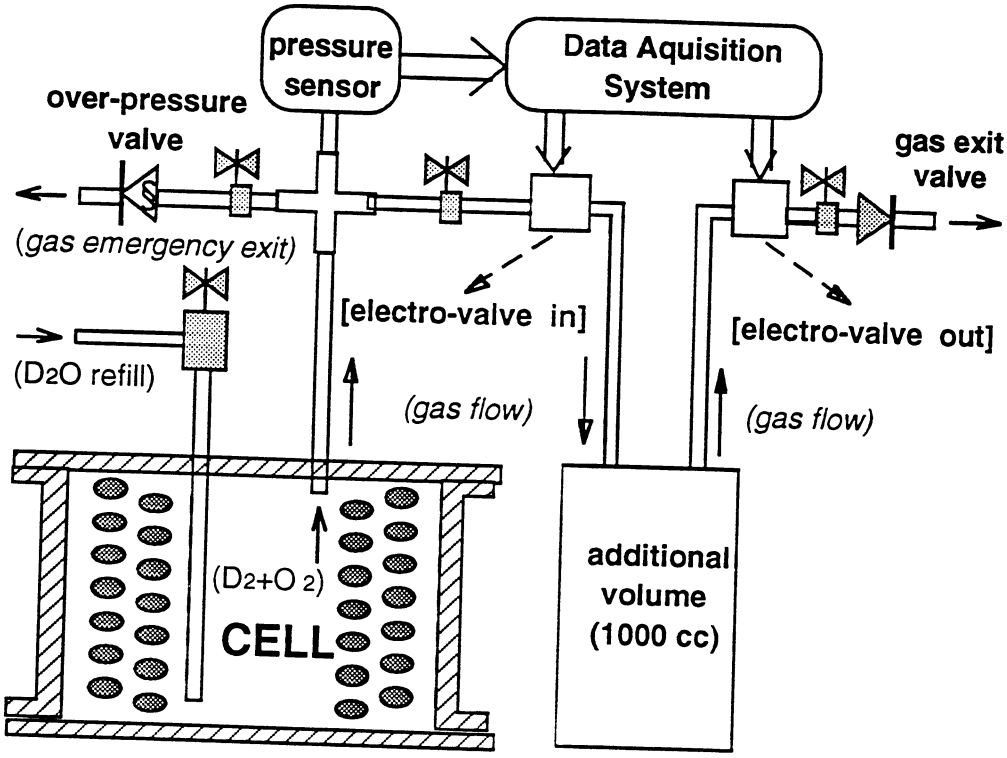

Fig. 2 - Outgoing cell gas system

A significative improvement was performed to the gas system. Two electrovalves were inserted (fig. 2): the first one on the top of the cell and the second one after an additional volume. Depending on which electrovalve is closed or opened, it is possible to have two well-defined volumes (a smaller volume of about 100 cc and a larger one of about 1000 cc). We determine these volumes measuring the gas pressure developed during the electrolysis and knowing the electric charge flowed through the electrodes (using the gas law and the Faraday equation). In this way we calculate the quantity of moles of D_2 absorbed by the Pd, measuring the missing pressure. We usually

operate leaving close the input electrovalve until the gas pressure reaches a definite value (50 mbar), further on we open this valve allowing to the gas to flow away. A proper circuitry was made to control this cyclic operation. The two volumes are chosen according to the value "low"(<200 mA) or "high" of the mean electrolytic current, in order to reduce the relative error in the measurement of the absorbed D_2 moles.

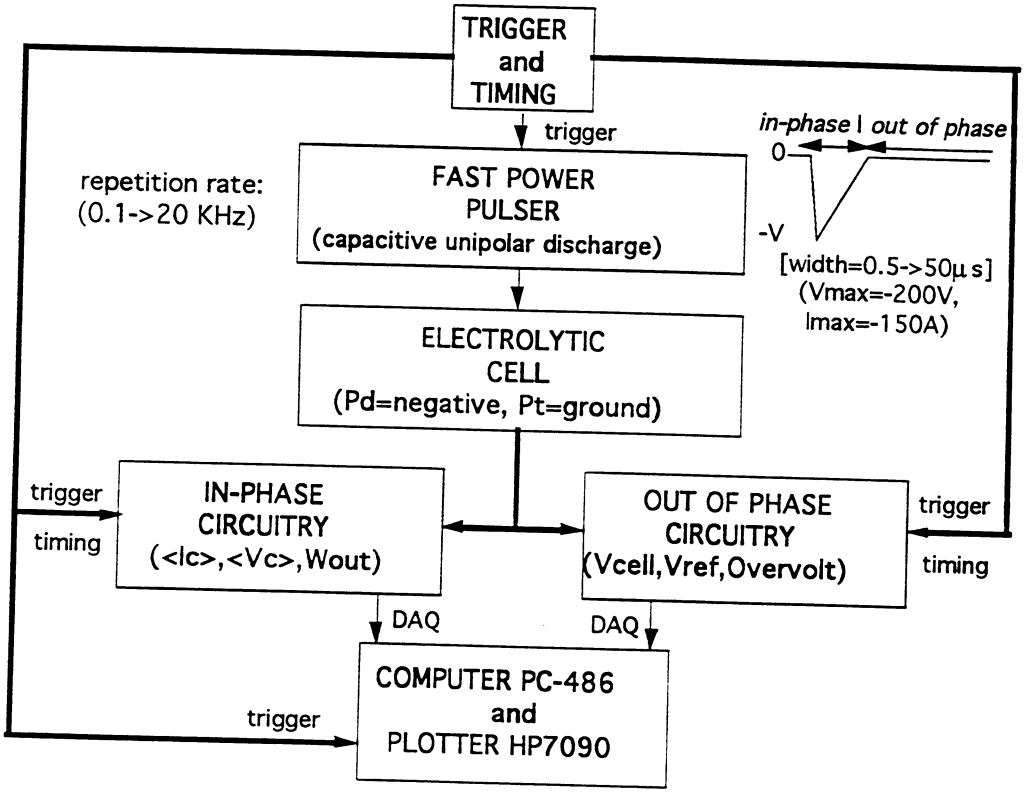

Fig. 3 - High power pulse circuitry: block scheme

A specific circuitry was made to generate a very sharp high current pulse as shown in figure 3. The in-phase circuit measures the flowing electric charge and the energy absorbed from the cell in a single pulse. The out-of-phase circuit measures the voltage of the cathode and the voltage of the Pt floating electrode, which is put in the solution close to the cathode (2 mm). These voltages are properly used to determine the over-voltage parameter too. The out-of-phase voltage measurement is performed after a delay (30 μs) from the end of the pulse. This enough long delay allows to avoid electric noise, during the measurement of low level signals (about 2 V), generated by the high level pulse (up to 150 V).

2. The Deuterium Absorption Measurements

We performed same blank runs using an Au plate to test the functionality of the circuitry and to calibrate the input power reading module. We tested the gas collecting system and we measured the D_2 absorbed by the stuff present into the cell (solution, polyethylene, heater, teflon etc.). This D_2 absorption, occurring only during the first charging-up, slowly decreases in time (it disappears, in our case, after about 600 C of electrolytic charge) and the D/Au reaches a maximum value of 0.01. In the following calculations we took into account this small effect performing the opportune corrections to the data.

We tested three cold-worked Pd sheets (25x25x1 mm) named: T05, T18 (TANAKA K.K.) and I85 (IMRA-Japan). The TANAKA plates (very high hardness value: 300 Hv) were prepared with proper impurities (2780 ppm) enclosed during the melting preparation: the high hardness reached is due to the doping (under patent).

The following operating conditions have been used for the T05 plate: pulse peak current 16 A, pulse width 0.5 μs, pulse repetition rate 5 KHz. These conditions are equivalent to an electrolytical mean current of about 64 mA.

In figure 4.a it is shown the absorption rate (in Mole/s·cm^2). It provides informations about the quantity of Deuterium flowing through the Pd-surface per time unit and surface unit. The absorption efficiency (defined as the ratio of the quantity of absorbed Deuterium to the Deuterium developed during the electrolysis) reaches its maximum value in the α phase (about 71% as reported in tab. 1). The α+β phase is identified by the shoulder of the curve. The absorption rate decreases during the β phase, zeroing when the D/Pd concentration reaches its maximum value equal to 1:1 (fig. 4.b). The D/Pd concentration has been evaluated cumulating the absorbed Deuterium moles in the time.

In figure 4.c it is shown the over-voltage as a function of the charge. We define the over-voltage as the difference between the cathodic potential and the reference electrode previously described. All electric potentials are measured in respect to the Pt net electrode which is connected to the electric circuit ground. During the electrolysis the Deuterium gas, developed at the cathode, surrounds the reference electrode and we can assume it as equivalent to a R.H.E. (Reversible Hydrogen Electrode). In the over-voltage calculation we take into account the fact that the peak-up electrode surrounded by the D_2 gas is not a platinized Pt, but just a pure Pt: this difference is reported by the literature to be 0.09 V for H_2 gas; we consider this value for our calculations. The over-voltage can be related to the Deuterium concentration into the Pd electrode (fig.s 4.b ,4.c); sudden drops of the over-voltage (fig. 4.c) seem to indicate partial degassing effects occurred on the surface zone for the Pd sheet.

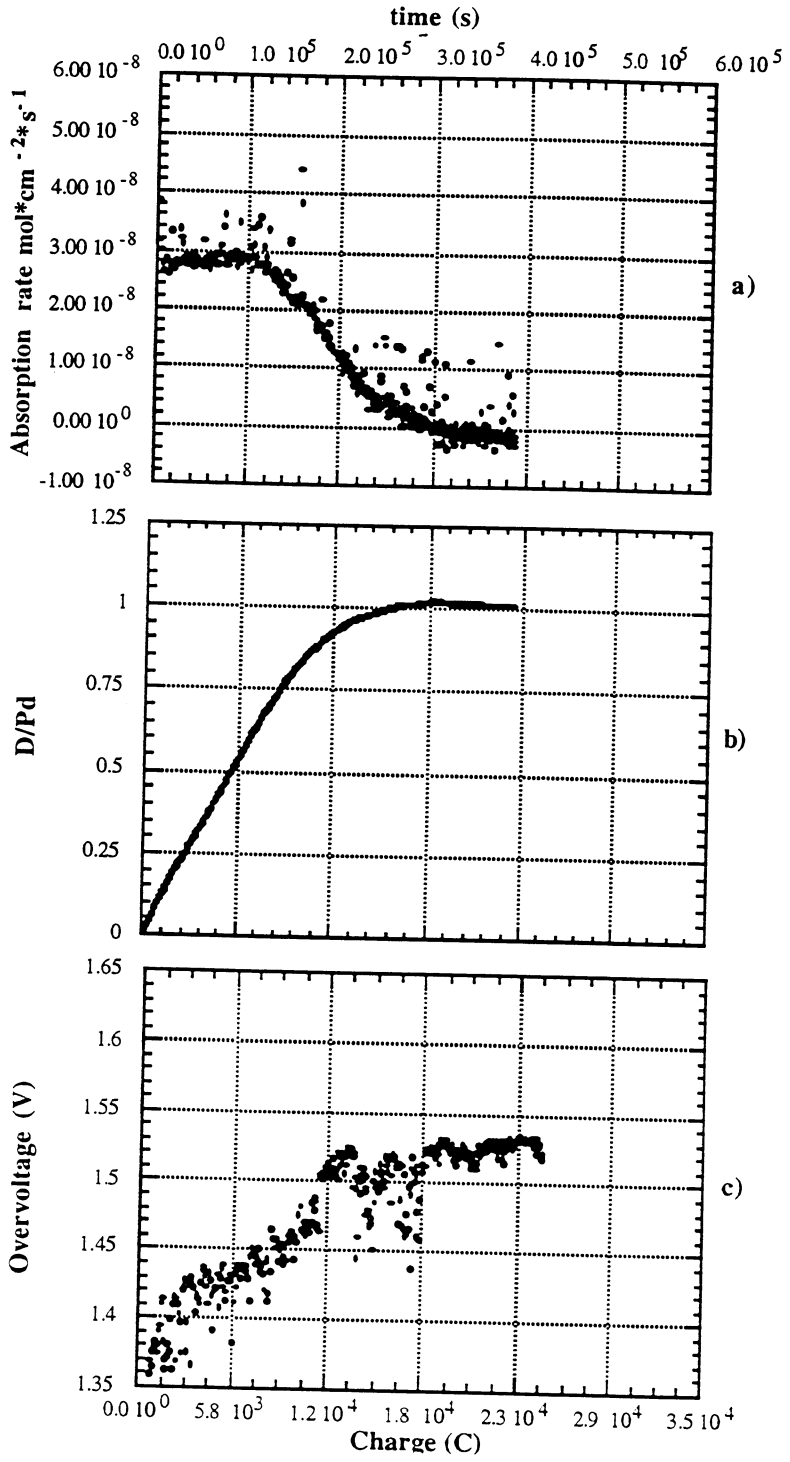

Fig. 4 - T05 Pd plate: first charging up.

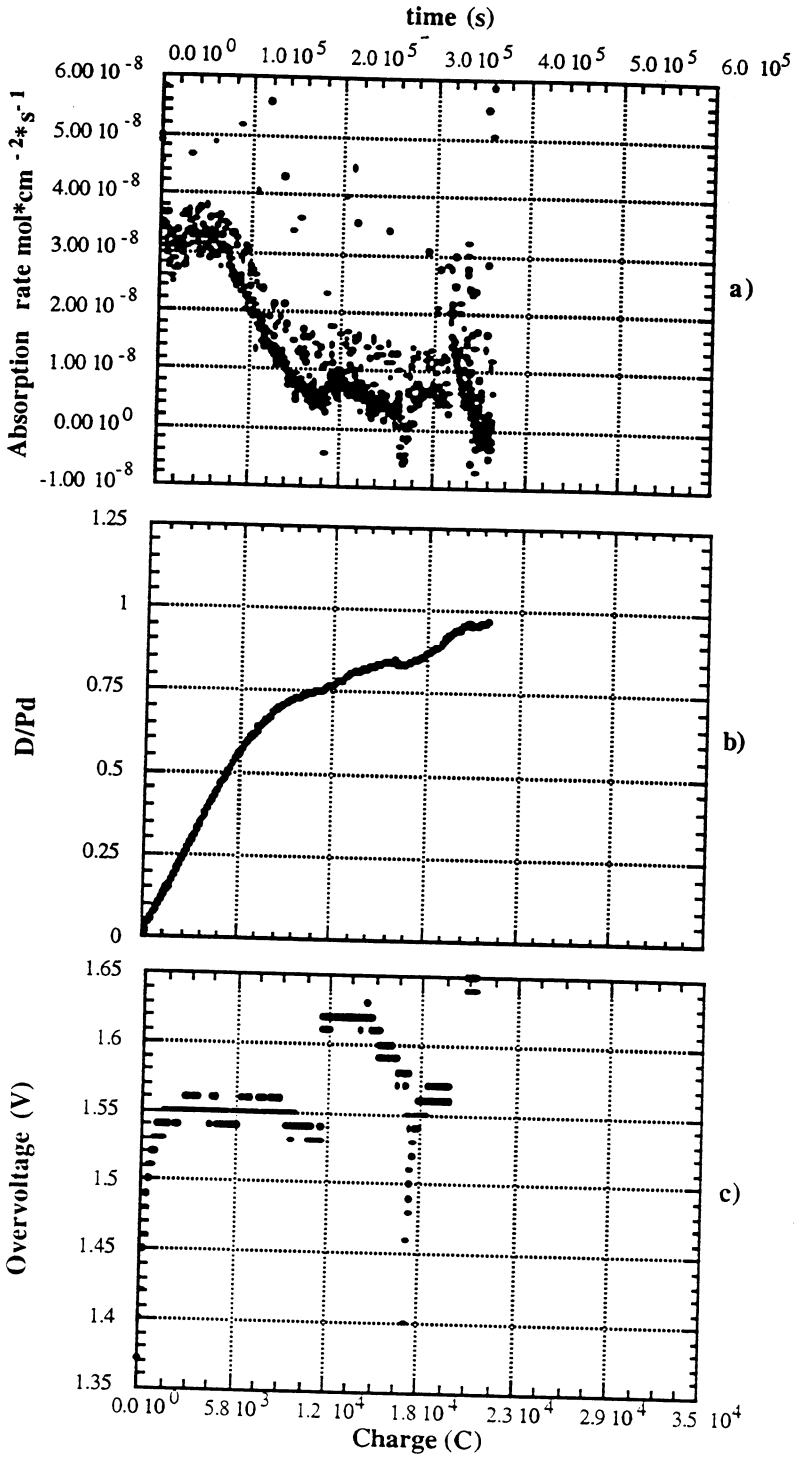

Fig. 5 - T18 Pd plate: first charging up.

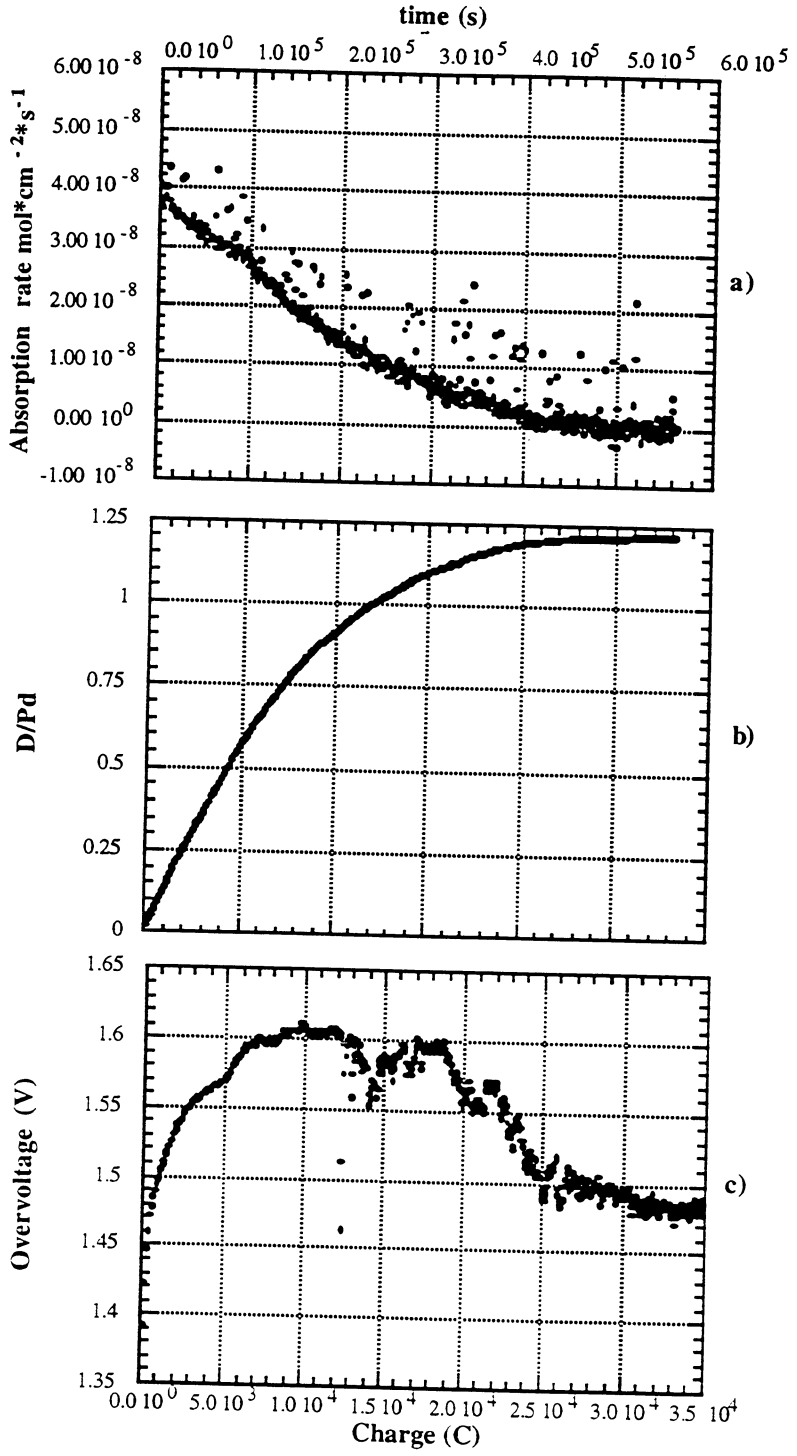

Fig. 6 - 185 Pd plate: first charging up.

The following operating conditions have been used for the T18 plate: peak current pulse 16 A, pulse width 1.8 μs, pulse repetition rate 2 KHz (mean current equivalent to 64 mA).

In figure 5.a we observe, regarding the α and the α+β phase, a curve shape similar to one of the plate previously described. As shown in figure 5.b, the D/Pd value was going to reach a plateau at 0.75, then we increased the peak current to 32 A and we reduced the pulse repetition rate down to 1 KHz as such as to maintain the same mean current at 64 mA: the absorption rate increased and the D/Pd too. To increase further this value we operated at 45 A and 750 Hz and after that at 60 A and 500 Hz, in both cases the mean current was kept costant at 64 mA. The final D/Pd value reached was 0.95. In figure 5.a negative values of absorption rate correspond to a short discharge occurred during the performed operation. In figure 5.c the over-voltage apparently increased in respect to the previous case described, because of the increase of peak current density (this value should be corrected by the Tafel contribute). In this way we want to stress that is possible to increase the D/Pd value operating on the peak current and the frequency of the pulses.

The operating conditions of the I85 plate (182 Hv) are the same of the T05 plate.

Observing the figure 6.a, the curve shape of the absorption rate is quite different from the T05: the shoulder occurring at the α+β phase is nearly completely disappeared. This plate reaches, as shown in figure 6.b, the highest D/Pd value (1.2:1) ever reached in our experiments. The over-voltage increases up to a very high value (1.61 V) as reported in figure 6.c, but it sharply decreases when the D/Pd value is about 0.9. After this value the over-voltage is no more steady and slowly decreases in time. Perhaps it means that something of disrupting is occurred on the plate surface.

In this last experiment a direct Deuterium absorption control was performed by the weight of the Pd plate: we stopped the electrolysis and we weighted it, after that we warmed the plate for many hours at the temperature of 250 °C and we weighted again the plate (the mass difference corresponds to the whole Deuterium flown out from the Pd). This measurement confirmed the high D/Pd value (> 0.95) found during the charging-up.

3. Excess Heat Results

Blank tests, using Au plate instead of Pd, were performed. This tests were used as a reference to calculate the input/output energy involved in the pulsed electrolysis process, as well as the absorption rate and the over-voltage parameters. Several operanting conditions, about the pulses, were tested and changed: peak amplitude, repetition rate, width.

The T18 plate was tested along about 2 months: it presented a detectable excess heat already a few days after the first charging up. During this time, many operations were performed to discover if there were a

correlation between the type of the pulse and the excess heat. No relevant dependence was found in the frequency range (from 5 to 20 KHz) that we explored. In figure 7 we report the comparition between the Au and Pd plate operating in the same conditions: the pulse peak current was about 60 A and the width 0.5 μs. The effective input power was calculated as the product of single pulse electric energy times pulses repetition rate (the heavy water dissociation contribute was subtracted). The output power is the thermal energy per time unit measured by the flow calorimeter (the thermal dissipation contribute is not included). As shown in figure 7, the output power measured using the Pd plate is always larger then the Au blank reference plate and if we try to fit the curves, the relative excess power corrisponds to a +12%. Operating at 15 KHz, this effect was meanly steady (about +15%) along some weeks.

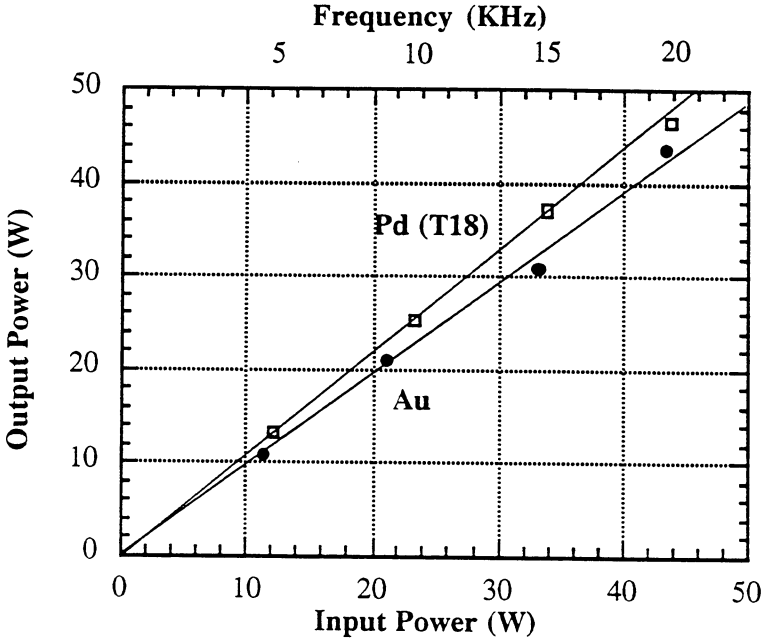

Fig. 7 - Excess power: T18 Pd respect to Au

The T05 and I85 were tested for about 2 weeks in stationary conditions: peak current about 16 A, width 500 ns and repetition rate of 5 KHz. No relevant excess heat (< 5%) was found and tests have been stopped.

In Table 1 are reported the main parameters and properties of the three Pd plates.

Plate	Au	T05	T18	I85
Hardness (HV)	60Rk⁻	300	300	182
Density	19.31	11.90	11.90	11.99
Process made	Fus	C-W	C-W	C-W
Load efficency (%) α		71	71	73
β		56	64	64
Max D/M	0.01	1.00	0.95	1.20
Var.Overvolt (mV)		340	400	240
Max Overvolt (mV)		1530	1650	1620
Rmax-Rmin (Ohm)	0.06	0.17	0.10	0.32
<DW/W> (%)	0	<5	15	<5
Peak current (A)	16	16	16	16
Mean current (mA)	64	64	164	64
Rep.tion-rate (KHz)	5	5	5	5
Pulse width (ns)	500	500	1800	500
Impurity (ppm)	<100	2700	2700	<300

Tab. 1 - Values of Pd plates and Au reference plate.

4. Metallurgical Aspects

All the Pd plates tested had cold worked treatments operated with different procedures. The hardness parameter is the value that we use to indicate the quality of the cold working procedure. This parameter is increased by the cold working from a value of 50 Hv (ordinary Pd) to about 180 Hv. In the case of Tanaka plates some impurities were intentionally added to the Pd in order to increase this value up to 300 Hv.

There are clear indications that the absorption rate is a function of the plates hardness. In particular, the plates with higher value of hardness (300 Hv) show a high and constant absorption rate in the α and $\alpha+\beta$ phase up to D/Pd equal to 0.67. Further on the absorption rate starts to exponentially decrease until that the equilibrium condition has been reached: no Deuterium is adsorbed and the D/Pd curve reaches a plateau. As regards the plates with lower value of hardness (180 Hv), we only observed an absorption rate with a decreasing exponential behaviour. Furthermore, higher hardness seems to negatively affect D/Pd charging ratio (taking into account this parameter only, IMRA samples appeared to be remarkably better).

Regarding the electric resistance, very large differences has been detected. In figures 8 are reported the electric resistances (as the ratio between the mean voltage and mean current of the cell) of T05 and I85 versus the D/Pd ratio. The I85 low hardness plate shows (fig. 8.b) a shape very similar to the ordinary curve (as reported by [2] 'Bockris et al') having a maximum at 1.1:1 D/Pd (in [2] it is at 0.85: beginning of phase γ). The T05 (fig. 8.a) high hardness plate has a different shape: the maximum value is at 0.1 D/Pd (end of phase α) and it is evident a drop at 0.8. Such anomalous behavior could be explained considering that a skin effect could occour because of the fast rise time (hundred nano-seconds) of the pulse; probably in such thin skin a strong and fast Deuterium charging occurs.

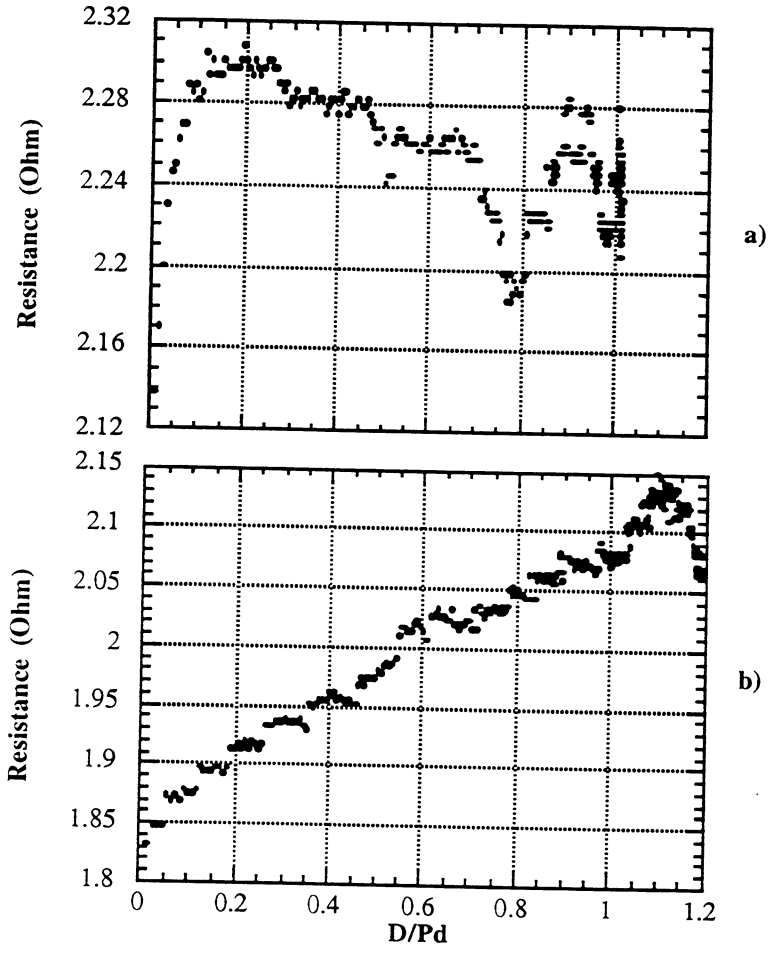

Fig. 8 - Resistance vs D/Pd: a) T05; b) I85.

We would like to anticipate that the ionic Li, present in the solution, can play an important role, depending by the metallurgycal proprieties of the surfaces. In such a way, the over-voltage and plate surface resistance parameters could give strong indications about surface modifications during the charging up. In order to better understand these effects, some Au plates were used instead of Pd plates. In this way the Deuterium absortion effect on the surface was minimized and it is possible to better identify the role played by the Li or Li compounds (like LiD) on the surface itself.
We like to note that exist a parameter, closely related to the D/Pd value, achieved after long-time electrolysis. It is represented by the η_2 component of the over-voltage, namely the total over-voltage without the η_1 (3,4) contribute due to the "Tafel" current density. We observed, keeping unchanged the pulse shape (t_{width}=500ns , I_{peak}=16 A and ν=5KHz), that the η_2 parameter has different behaviours, related to the D/Pd ratio, depending by different plate hardness.
Specific studies about these latter parameters and the role of Li are in progress.

Conclusion

Indipendently by the metallurgy of the Pd electrodes, we developed an high pulse tecnique to highly charge Pd plates (D/Pd around 1:1). However, the metallurgy of the plates affects the absorption rate "shape" parameter. The over-voltage and electric resistance parameters give useful indications about the Pd plate surface status during the Deuterium absorption. An important role can play the ionic Li on the surface, in particular way when the Pd plate reaches high D/Pd values.
The excess heat occurring for some Pd plates seems dependent by the metallurgy of the electrode: a high hardness plates (doped by proper impurities) can give excess heat (around 15% in our case) for very long time (some weeks). This condition seems to be necessary but not still sufficient, because the first charging-up procedure seems to play an important role depending on the samples hardness. Moreover, observing the plates at the end of the tests, we can point-out that the excess heat occurs when there were no cracks on the plate surfaces. In other words the peak pulse current should be limited to avoid disrupting effects to the plates.

Acknowledgements

We are indebted to both Dr. K.Mori and Drs. M.Nakamura (TANAKA K.K.) because their time spent to developed the new Pd-CTC material (patented) just starting from an our original idea and Dr. S.Nezu (IMRA-Research) because provided us not only with pure Pd plates of very different metallurgical properties but even of very usefull suggestions.

We would like to thank Prof. G.Preparata (Milan Univ., Italy), Prof. H.Ikegami (NIFS, Nagoya, Japan), Prof. J.P.Vigier (Paris Univ., France), Dr.

K.Kunimatsu (IMRA-Japan), Prof. M.Enyo (Okkaido Univ., Japan) and Dr. A.Mancini (ORIM S.r.l., Italy) for their stimulating discussions, criticism and suggestions.

We are grate to Drs F.Ferrarotto, M.Corradi and Prof. B.Stella (Rome Univ., Italy) for their suggestions.

The palladium plates were kindly provided from Tanaka K.K. and IMRA-Research, both from Japan.

References

1. F.Celani, A.Spallone, P. Tripodi, A. Nuvoli.
FRONTIERS OF COLD FUSION, Edited by H.Ikegami, p.93 (1992)
Frontier Science Series n.4, Univ. Acad. Press, Tokyo (Japan).
2. M.C.H. McKubre et al,
FRONTIERS OF COLD FUSION, Edited by H.Ikegami, p.5 (1992)
Frontier Science Series n.4, Univ. Acad. Press, Tokyo (Japan).
3. M. Enyo.
FRONTIERS OF COLD FUSION, Edited by H.Ikegami, p.255 (1992)
Frontier Science Series n.4, Univ. Acad. Press, Tokyo (Japan).
4. K. Kunimatsu et al,
FRONTIERS OF COLD FUSION, Edited by H.Ikegami, p.31 (1992)
Frontier Science Series n.4, Univ. Acad. Press, Tokyo (Japan).

4TH INTERNATIONAL CONFERENCE ON COLD FUSION
12/06/93 - 12/09/93

Hyatt Regency Maui
200 Nohea Kai Drive
Lahaina,Maui, HI 96761-1990

LIST OF ATTENDEES

Tadashi Akimoto
Rsch. Assoc. Dept. of Nuclear Engrg
Hokkaido University
Faculty of Engineering
North 13, West 8, Kitaku
Sapparo 060, JAPAN
011-716-2111 x6684
011-736-2856 (Fax)

Takayoshi Aoki
Associate Professor of Physics
University of Tsukuba
Isotope Center
Tsukuba, 305
JAPAN
0298-53-2513
0298-53-2511 (Fax)

A. Baraboshkin
ENECO
University of Utah Research Center
391-B Chipeta Way
Salt Lake City, UT 74108
(801) 583-2000
(801) 583-6245 (Fax)

Steven Barrowes
Physics Department
University of Utah
201 JFB
Salt Lake City, UT 84112
(801) 585-5832
(801) 581-4801 (Fax)

Robert W. Bass
Member, Scientific Advisory Board
ENECO
391-B Chipeta Way
Salt Lake City, UT 84108
(805) 373-6256
(805) 373-6256 (Fax)

Gregory Basting
University of Scranton
15 Emerson Dr.
Moosic, PA 18507
(717) 344-3788

Charles Becker
ENECO
University of Utah Research Park,
391-B Chipeta Way
Salt Lake City, UT 84108
(801) 583-2000
(801) 583-6245 (Fax)

Leroy Becker
ENECO
University of Utah Research Park
391-B Chipeta Way
Salt Lake City, UT 84108
(801) 583-2000
(801) 583-6245 (Fax)

Thomas B. Benson
President
Scott Laboratories
304 Grand Ave.
Suite 208
South San Francisco, CA 94080
(415) 952-6617
(415) 952-6618 (Fax)

Haven Bergeson
Professor, Physics Department
University of Utah
Salt Lake City, UT 84112
(801) 581-7115
(801) 581-4801 (Fax)

Luciano Bertalot
ENEA
CRE Frascati - Via E. Fermi, 27
00044 Frascati
(Roma), ITALY
39-6-94005300
39-6-94005400 (Fax)

Jean-Paul Biberian
Departement de Physique
Faculte Des Sciences
70 Route Leon Lachamp
13288 Marseille, Cedex
FRANCE
(33) 9141-5209
(33) 9106-7501 (Fax)

Jerry Bishop
Science Reporter
Wall Street Journal
200 Liberty Street
New York, NY 10281
(212) 416-3323
(212) 416-2653 (Fax)

John Bockris
Distinguished Professor, Chemistry
ENECO
391-B Chipeta Way
Salt Lake City, UT 84108
(409) 845-5335
(409) 845-4205 (Fax)

Elena Botta
Doctor
Istituto Nazionale di Fisica Nucliare
via Sette Comuni 56
Torino 10127
ITALY
39-11-6198347
39-11-6190665 (Fax)

Tullio Bressani
Prof., Dept. di Fisica Sperimentale
Universita Degli Studi di Torino
via P. Guiria 1
I 10125 Torino
ITALY
39-11-6707-322
39-11-6707-323 (Fax)

Ben Bush
SRI International
988 Rose Ave
Redwood City, CA 94063
(415) 859-3521
(415) 859-4286 (Fax)

Robert T. Bush
ENECO
391-B Chipeta Way
Salt Lake City, UT 84108
(801) 583-2000

Daniela Calvo
Engineer
Instituto Nazionale Fisica Nucliare
via Sette Comuni 5
Torino 10127
ITALY
39-11-6198347
39-11-6190665 (Fax)

Francesco Celani
Ph.D.
Instituto Nazionale Di Fisica Nucleare
Via Enrico Fermi 13
Frascati -(RM)- 00044
ITALY
33-6-9403201
39-6-9403548 (Fax)

George P. Chambers
Research Physicist/Condensed Matter
Naval Research Laboratory
4555 Overlook Avenue
Washington, DC 20375-5345
(202) 767-4800
(202) 767-5301 (Fax)

Scott R. Chubb
Research Physicist
Naval Research Laboratory
Research Systems Inc.,
5023N 38th Street
Arlington, VA 22007
(202) 767-2003
(202) 767-5599 (Fax)

Talbot A. Chubb
Research Systems, Inc.
5023 N. 38th Street
Arlington, VA 22207
(703) 536-4427

Angelina Chukanov
Engineer
Space Energy LLC
3520 West Old Bingham Hwy.
Suite B
West Jordan, UT T84088
(801) 569-3133
(801) 569-3192 (Fax)

Kiril B. Chukanov
President, Owner
Space Energy LLC
3520 W. Old Bingham Hwy.
Unit B
West Jordon, UT 84088
(801) 569-3133
(801) 569-3192 (Fax)

Thomas N. Claytor
Physicist, Unit Leader, Systems Dev
Los Alamos National Laboratory
WX Devision
M/S C914
Los Alamos, NM 87545
(505) 667-6218
(505) 665-7176 (Fax)

Andre Clerc-Renaud
Executive President
C.R. Consultants
116, Avenue des Champs-Elysees
75008 Paris
FRANCE
33-1-3962-1776
33-1-3912-1336 (Fax)

James W. Cobble
Professor, Chemistry
San Diego State University
5300 Campanile Drive
San Diego, CA 92182-0328
(619) 594-5139
(619) 594-3561 (Fax)

Bill Collis
Strada Sottopizaao 18
14056 Boglietto di Costigliole (AT)
ITALY
39-141-968602

Robert Cornog
Consultant
2242-20th Street
Apt. 4
Santa Monica, CA 90405
(310) 452-3335

Dennis Cravens
ENECO
2222 Wheeler St.
Vernon, TX 76384
(817) 553-1209
(817) 553-1209 (Fax)

Ernest E. Criddle
Research Associate
ESTCO Univeristy of Ottawa
33 Mann Ave.
Ottawa
Ontario KIN 6N5, CANADA
(613) 564-6818
(613) 564-9842 (Fax)

Mark Crookston
Engineering Consultant
(MRI) Manufacturing Research Inst.
7332 South 1700 East
Ogden, UT 84405
(801) 626-6917
(801) 626-7531 (Fax)

Steven Crouch-Baker
SRI International
333 Ravenswood Avenue
Menlo Park, CA 94025
(415) 859-2964
(415) 859-4286 (Fax)

John Dash
Professor, Physics Dept.
Portland State University
P.O. Box 751
Portland, OR 97207
(503) 725-4222
(503) 725-3813 (Fax)

Emilio Del Giudice
INFN
Via Celoria 16
20133 Milano
ITALY
392-2392250
392-2392480 (Fax)

Kenneth C. Dewhirst
Consultant
410 Bayou Cove
Houston, TX
(713) 780-0590
(713) 780-0761 (Fax)

Dawn Dominguez
Research Chemist
Naval Research Laboratory
Code 6170
Washington, DC 20375-5000
(202) 767-2998
(202) 767-3321 (Fax)

Jerome Drexler
Drexler Technology
25440 Becky Lane
Los Altos Hills, CA 94022
(415) 969-7277
(415) 969-6121 (Fax)

Jeff Driscoll
21 Genetti St.
Bedford, MA 01703
(617) 275-1800 x3717

Thomas F. Droege
President
Environmental Optics Corp.
2 S. 942 Thornecrest Lane
Batavia, IL 60510
(708) 879-2949
(708) 840-2876 (Fax)

Jacques Dufour
Relations Scientifiques
Shell Recherche SA
76530 Grand Couronne
FRANCE
33-140278463
33140272842 (Fax)

Robert D. Eagleton
Physics Professor
ENECO
391-B Chipeta Way
Salt Lake City, UT 84108
(909) 869-4019
(909) 869-4396 (Fax)

Rolf R. Engel
Associate Professor
University of Minnesota
701 Park Ave. South
Minneapolis, MN 55415
(612) 347-2958

Michio Enyo
Professor
Hokkaido University
Catalysis Research Center
Kita-ku, N-11, W-10
Sapporo, 010, JAPAN
81-11-757-8130
81-11-709-4748 (Fax)

Roberto Felici
Doctor, Researcher
1st Struttura Della Materia, CNR
via E. Fermi 38
ITALY
39-6-942-6335
39-6-941-7003 (Fax)

Fabio Ferrarotto
INFN-Rome University
Rome, ITALY
0039-6-4331434 x4

Oleg Finodeyev
ENECO
University of Utah Research Park
391-B Chipeta Way
Salt Lake City, UT 84108
(801) 583-2000
(801) 583-6245 (Fax)

John C. Fisher
600 Arbol Verde
Carpinteria, CA 93013
(805) 684-1465

Martin Fleischmann
Professor, Director of Research
IMRA Europe, S.A.
Science Center, 220 Rue Albert Caquot
Sophia, Autipolis, 0640, Valbonne
FRANCE
33-92-95-73-37
33-93-95-73-51 (Fax)

Ronald N. Flores
15 ch des Colombettes
1202 Geneva
SWITZERLAND
41-22-733-1182

Jacques Foos
Professor
CNAM
Laborataire des Ciences Nucliares
292 Rue Saint Martin
75003 Paris, FRANCE
33140272400

Hal Fox
President
Fusion Info Center
P.O. Box 58639
Salt Lake City, UT 84158
(801) 583-6232
(801) 583-6245 (Fax)

Tomonari Fujita
Central Research Inst. of Electric Power
Industry, (CRIEPI)
11-1 Iwato Kita, 2-Chome,
Komai-Shi, Tokyo 201, JAPAN
81-3-34802111
3480-7956 (Fax)

Guido Gigli
Professor
University of Rome "La Sapienza"
Ple Aldo Moro 5
Rome 00185, ITALY
39-649913373
39-649913951 (Fax)

Russ George, Consultant
E-Quest Sciences
3309 Alma Street
Palo Alto, CA 94306
415-856-4217
Fax 415-952-6618

David M. Golden
V.P., Physical Sciences Division
SRI International
333 Ravenswood Ave.
Menlo Park, CA 94025
(415) 859-3811
(415) 859-4321 (Fax)

Igor Goryachev
ENECO
University of Utah Research Park
391-B Chipeta Way
Salt Lake City, UT 84108
(801) 583-2000
(801) 583-6245 (Fax)

Daniele Gozzi
Professor, Dept. of Chemistry
University of Rome "La Sapienza"
P.L.E. Aldo Moro 5
Rome 00185, ITALY
39-649913849
39-649913951 (Fax)

Wayne Green
Editor
Science Frontiers
70 R202 N
Peterborough, NH 03458-1107
(603) 924-0058
(603) 924-8613 (Fax)

Stephen E. Gregory
Power Systems Industries
2255 North University Parkway
15-3
Provo, UT 84604
(801) 371-0897
(801) 371-0898 (Fax)

James L. Griggs
V.P., Research
Hydro Dynamics Inc.
611 Grassdale Rd.
Cartersville, GA 30120
(404) 386-2649
(404) 386-8139 (Fax)

Linda Grow
9767 Little Cottonwood Pl.
Sandy, UT 84092
(801) 943-4648
(801) 944-1942 (Fax)

Richard W. Grow
Professor & Director, MDPEL
University of Utah
Electrical Engineering Department
Salt Lake City, UT 84112
(801) 581-7634
(801) 581-5281 (Fax)

Robert J. Grow
9767 Little Cottonwood Pl.
Sandy, UT 84092
(801) 943-4648
(801) 944-1942 (Fax)

Raymond Guenther
Professor & Chairman
University of Nebraska at Omaha
Dept. of Physics
Omaha, NE 68182
(402) 554-3726

Joseph P. Guokas
Vice President
J & J Manufacturing
2820 Honolulu Ave
Suite 325
Verdugo City, CA 91046-4601
(818) 242-6296

B. Guzhouskii
ENECO
University of Utah Research Park
391-B Chipeta Way
Salt Lake City, UT 84108
(801) 583-2000
(801) 583-6245 (Fax)

Peter Hagelstein
Associate Professor, EE&CS
Massachusetts Institute of Technology
77 Massachusetts Ave.
Cambridge, MA 02139
(617) 253-0899
(617) 258-7864 (Fax)

Gerald M. Hale
Staff Member
Los Alamos National Laboratory
Nuclear Theory & Applications Group
Mail Stop B243
Los Alamos, NM 87545
(505) 667-7738
(505) 667-9671 (Fax)

Michio Hamano
Dir., International Joint Reseach
New Energy & Industrial Tech. Dev. Org.
Sunshine 60, 2IF, 1-1, 3-chome
Higashi-Ikebukuro, Toshima-ku
Tokyo, 170, JAPAN
81-33-987-9357
81-33-981-1536 (Fax)

Teru Hanawa
Professor, General Education
Osaka Institute of Technology
Ohmiya, Asahiku, Osaka 535
JAPAN
6-952-3131
6-957-2137 (Fax)

Peter H. Handel
Professor
University of Missouri
Physics Dept of Missouri
8001 Natural Bridge Rd.
St. Louis, MO 63121
(314) 553-5021
(314) 553-6152 (Fax)

Wilford N. Hansen
Professor of Physics and Chemistry
Utah State University
Physics Dept.
Logan, UT 84322-4415
(801) 750-2852
(801) 750-2492 (Fax)

Hiroyuki Harada
Sr. Adviser, Regd. Consulting Engr.
Plant Technology Corporation
Bungei Shunju Shinkan 4F
3-23, Kioi-Cho, Chiyoda-Ku
Tokyo 102, JAPAN
03-3221-5779
03-3221-0705 (Fax)

Norifumi Hasegawa
IMRA Japan Co. Ltd.
3-6 Techno Park 2 Cho-Me
Shimonopporo, Atsubetsu-Ku
Sapporo, 004, JAPAN
011-898-7999
011-898-7990 (Fax)

Jing-Tang He
Professor
Inst. of High Energy Physics
19 Yuquan Lu
Beijing, 100039, CHINA
861-8213344 x374
861-8213374 (Fax)

John Hilborn
Scientific Advisor to Gen. Mgr.
AECL Research
Chalk River Laboratories
Chalk River, Ontario K0J 1J0
CANADA
(613) 584-3311
(613) 584-4010 (Fax)

Sotoji Hiragi
Research Associate
JAIST
15 Asahidai, Tatsunokuchimachi
Nomi-Gun, Jshikawa
923-12, JAPAN
81-761-51-1650
81-761-51-1655 (Fax)

Mark Hittinger
Software Development Mgr.
Renlar Systems, Inc.
2640 Palumbo Drive
Lexington, KY 40509
(800) 264-5414
(606) 266-5414 (Fax)

Nathan Hoffman
Chief Scientist
Rockwell Mill
P.O. Box 7930
Canoga Park, CA 91309

Graham Hubler
Physicist
Naval Research Lab.
Code 6671
Washington, DC 20375

Kelly Hudson
President
Hydro Dynamics Inc.
611 Grassdale Rd.
Cartersville, GA 30120
(404) 386-2649
(404) 386-8139 (Fax)

Robert A. Huggins
Stanford University/ENECO
c/o ZSW Helmholtzstrasse 8
89081 Ulm
GERMANY
(493)731-95300
493-7319530666 (Fax)

Mark Hugo
Northern States Power Co.
414 Nicollet Mall
Minneapolis, MN 55336
(612) 347-7201
(612) 347-7369 (Fax)

John R. Huizenga
Tracy H. Harris Professor Emeritus
University of Rochester
Department of Chemistry
Rochester, NY 14627-0216
(716) 275-4217
(716) 473-6889 (Fax)

Felice Iazzi
Professor
Insituto Nazionale di Fisica Nucliare
via Sette Comuni 56
Torino 10127
ITALY
39-11-6198347
39-11-6190662 (Fax)

Setsuo Ichimaru
The University of Tokyo
Faculty of Science, Dept. of Physics
7-3-1 Hongo, Bunkyo-Ku
Tokyo 113, JAPAN
81-3-5802-2988 (Fax)

Joseph N. Ignat
Proteus Processes & Technology, Inc.
1570 Emerson Street
Suite 100
Denver, CO 80218-1450
(303) 863-0200
(303) 863-0921 (Fax)

Toshiyuki Iida
Associate Professor
Osaka University
Dept. of Nuclear Engineering
Yamada-oka, Suita
Osaka, 565, JAPAN
6-877-5111
6-877-3264 (Fax)

Hideo Ikegami
Professor
National Institute for Fusion Science
Nagoya 464-01
JAPAN
(052) 781-5134
(052) 781-9564 (Fax)

M.Ashraf Imam
Scientist
Naval Research Laboratory
Code 6320
Washington, DC 20375-5320
(202) 767-2185
(202) 767-2623 (Fax)

Hideo Isono
Imidas Division
Shueisha Inc.
2-5-10 Hitotsubashi
Chiyoda, Tokyo 101-50
JAPAN
81-3-3230-6054
91-3-3239-4080 (Fax)

Yasuhiro Iwamura
Mitsubishi Heavy Industries, Ltd.
Advanced Technology Research Center
1-8-1 Sachiura
Kanazawa-ku, Yokohama,236, JAPAN
81-45771-1316
81-45771-3879 (Fax)

Frederick G. Jaeger
President
ENECO
391-B Chipeta Way
Salt Lake City, UT 84108
(801) 583-2000
(801) 583-6245 (Fax)

Joe Johnson
Vice President
Space Energy LLC
3520 West Old Bingham Hwy.
Suite B
West Jordon, UT 84088
(801) 569-3133
(801) 569-3192 (Fax)

Keith H. Johnson
Professor/Materials Science
Massachusetts Institute of Technology
Room 13-5013
77 Mass Ave.
Cambridge, MA 02138
(617) 253-6935
(617) 491-0786 (Fax)

Melinda Johnson
Space Energy LLC
3520 West Old Bingham Hwy.
Suite B
West Jordan, UT 84088
(801) 569-3133
(801) 569-3192 (Fax)

S. Jones
Professor of Physics
Brigham Young University
Provo, UT 84602
(801) 378-2749
(801) 378-2265 (Fax)

Kabir Kaliev
Doctor of Chemistry
Inst. of High Temp. Electochem, URAL Div - Academy of Science of Russia
S. Kovalevskaya 20 Ekaterinburg, 620219
RUSSIA
44-27-29
3432-557002 (Fax)

Atsushi Kamei
Mgr. Research Planning Dept.
Technova Inc.
13th Fl., Fukoku Seimei Bldg.
2-2 Uchisaiwai-cho 2-chome
Chiyoda-ku, Tokyo 100, JAPAN
03-3508-2280
03-3508-7578 (Fax)

Hiroshi Kanbe
NTT Basic Research Labs
3-1, Morinosato Wakamiya
Atsugi-shi, Kanagawa-ken 243-01
JAPAN
81-462-40-3415
81-462-40-4713 (Fax)

A. Karabut
ENECO
University of Utah Research Park
391-B Chipeta Way
Salt Lake City, UT 84108
(801) 583-2000
(801) 583-6245 (Fax)

Jirohta Kasagi
Professor
Tohoku University
Laboratory of Nuclear Science
Mikamine 1-2-1, Taihakuku, Sendai 981
JAPAN
81-22-245-2151
81-22-243-0965 (Fax)

Kikuo Kato
Executive Vice President
Aisin Seiki Co., Ltd.
1 Asahi-Machi, 2-Chome
Kariya City, Aichi Pref
448, JAPAN
81-566-248143
81-566248890 (Fax)

Takahiko Kato
Dir. & General Mgr., Planning Dept.
IMRA Material R&D Co., Ltd.
5-50 Hachiken-cho
Kariya, Aichi, 448
JAPAN
81-566-24-8316
81-566-24-9370 (Fax)

Kiyoshi Kawamoto
Patent Attorney
Equos Research Co., Ltd.
No. 2-19-12 Sotokanda
Chiyoda-Ku, Tokyo
JAPAN
(03) 3255-9766
(03) 3255-9760 (Fax)

Elliot B. Kennel
Nuclear Engineer
Space Exploration Assoc.
P.O. Box 579
Cedarville, OH 45387
(513) 766-2050
(513) 766-5886 (Fax)

Yeong E. Kim
Professor, Dept. of Physics
Purdue University
Physics Building
West Lafayette, IN 47907
(317) 494-3042
(317) 494-0706 (Fax)

Gustave K. Kohn
Industrial Chemist
198 Pine Lane
Los Altos, CA 94022
(415) 949-1833

Hisatoki Komaki
Professor, President
Biological & Agricultural Research Inst.
2-6-18 Akamoto, Otsu
Shiga-Ken 520-01
JAPAN
(0775) 79-0194

Kenji Konashi
Institute for Material Research
Tohoku University
Oarai, Ibaraki-ken, 311-13
JAPAN
81-292-67-3181
1-292-67-4947 (Fax)

Valery Koretsky
Erzion Center
P.O. Box 134
119633 Moscow
RUSSIA
095-292-6511 (Fax)

Hideo Kozima
Ph.D., Professor
Shizuoka University
836 Oya
Shuzuoka, 422
JAPAN
54-237-111 x5505
54-238-0993 (Fax)

Mike Kreager
ENECO
University of Utah Research Park
391-B Chipeta Way
Salt Lake City, UT 84108
(801) 583-2000
(801) 583-6245 (Fax)

Alexander Krivoshein
Scientific Research Center
Physical Technical Center
Erzion Center
126083 Moscow, RUSSIA

Akiko Kubota
IMRA Japan Co. Ltd.
3-6 Techno Park 2 Cho-Me
Shimonopporo, Atsubetsu-Ku
Sapporo, 004, JAPAN
011-898-7999
011-898-7990 (Fax)

Yan Kucherov
ENECO
391-B Chipeta Way
Salt Lake City, UT 84018
(801) 583-2000
(801) 583-6245 (Fax)

Keiji Kunimatsu
Imra Japan Co. Ltd.
c/o Aisin Aw, 3-6 Techno Park
2 Cho-me Simonopporo
Atsubetsu-ku, Sapporo, JAPAN
898-7999
898-7990 (Fax)

J.J. Lagowski
Professor
University of Texas
Dept. of Chemistry & Biochemistry
Austin, TX 78712
(512) 471-3288
(512) 471-8696 (Fax)

Kerry Lane
M.D.
North American Palladium
621 Andrews Avenue
Delray Beach, FL 33483
(407) 278-3060
(407) 278-8084 (Fax)

Myung W. Lee
Advisory Scientist
Savannah River Technology Center
Westinghouse
Aiken, SC 24802
(803) 725-5866
(803) 725-4704 (Fax)

Sang-Moo Lee
Assoc. Professor, Inst. of Physics
University of Tsukuba
Ibaraki 305
JAPAN
81-298-53-2492
81-298-53-2565 (Fax)

Dennis Letts
ENECO
University of Utah Research Park
391-B Chipeta Way
Salt Lake City, UT 84108
(801) 583-2000
(801) 583-6245 (Fax)

Bruce Lewenstein
Dept. of Communcation
Cornell University
321 Kennedy Hall
Ithaca, NY 14853
(607) 255-8310
(607) 255-7905 (Fax)

Xing Z. Li
Prof., Head of Fusion Power Program
Tsinghua University
Dept. of Physics
Beijing, 100084
CHINA
86-1-259-4343
86-1-256-2768 (Fax)

Bor Y. Liaw
Assistant Researcher
University of Hawaii at Manoa
Hawaii Natural Energy Institute
2540 Dole Street, Holmes Hall 246
Honolulu, HI 96822
(808) 956-2339
(808) 956-2336 (Fax)

A.G. Lipson
Institute of Physical Chemistry
Russian Academy of Sciences
31 Leninsky Prospect
117915 GSP, Moscow, RUSSIA
095-952-7514 (Fax)

Robert F. Machacek
Product Manager-Heavy Water
Ontario Hydro International
700 University Avenue - A14
Toronto,
Ontario M5G 1X6, CANADA
(416) 506-4945
(416) 506-4684 (Fax)

Sandi Magaoay
Writer for Ka Leo O Hawaii
University of Hawaii
1755 Pope Road
Honolulu, HI 96822
(808) 521-9707

Eugene F. Mallove
President
Starbound Engineering
171 Woodhill-Hooksett Rd.
Bow, NH 03304
(603) 228-4516
(603) 224-5975 (Fax)

Ignazio Massa
Professor, Dept. of Physics
University of Bologna
via Irnerio 46-40126
Bologna
ITALY
39-5135-1030
39-5124-9847 (Fax)

Kazuaki Matsui
Director, R&D Division
Institute of Applied Energy
14-2 Nishishinbashi 1-chome
Minato-ku, Tokyo, 105
JAPAN
81-33-508-8894
81-33-501-1785 (Fax)

Takaaki Matsumoto
Dept. of Nuclear Engineering
Hokkaido University
North 13, West 8
Sapporo 060
JAPAN
81-11-716-2111
81-11-736-2856 (Fax)

Fred Mayer
President
Mayer Applied Research Inc.
1417 Dicken Drive
Ann Arbor, MI 48103
(313) 662-3841
(313) 662-3920 (Fax)

Mary Mayer
Mayer Applied Research Inc.
1417 Dicken Drive
Ann Arbor, MI 48103
(313) 662-3841
(313) 662-3920 (Fax)

Joan McDavid
J & J Manufacturing
2820 Honolulu Ave,
Suite 325
Verdugo City, CA 91046-4601
(818) 242-6296

Robert C. McDonald
Bose Corp.
The Mountain
Framingham, MA 01701
(508) 879-7330

Mike McKubre
SRI International
333 Ravenswood Avenue
Menlo Park, CA 94025
(415) 859-3868
(415) 859-4286 (Fax)

Michael E. Melich
Naval Postgraduate School
Physics Department
Code PH/MM
Monterey, CA 93943-5000
(904) 729-1873
(904) 729-1873 (Fax)

Howard Menlove
Los Alamos National Laboratory
P.O. Box 1663
Los Alamos, NM 87545
(505) 667-2182
(505) 665-4433 (Fax)

Nobuaki Miki
Director, Technology Center
IMRA Japan Co. Ltd.
c/o Aisin Aw-306 Techno Park 2 Cho-me
Shimonopporo, Atsubetsu-ku
Sapporo, 004, JAPAN
11-898-7999
77-898-7990 (Fax)

Melvin H. Miles
Research Chemist
NAWC
Weapons Division
Code CO 2353
China Lake, CA 93555
(619) 939-1562
(610) 939-1617 (Fax)

George H. Miley
Professor, Nuclear & Electrical Eng
University of Illinois at Urbana
100 Nel, 1093 S. Goodwin Ave.
Urbana, IL 61801-2984
(217) 333-3772
(217) 333-2906 (Fax)

Alan Miller
President
Pedro Point Technology, Inc.
175 Essex Way
Pacifica, CA 94044
(415) 355-8264
(415) 359-8264 (Fax)

Jean-Paul Millot
Framatome
Dept. of Nuclear Engineering
Tour Fiat, Cedex 16-92084
Paris, La Defense, FRANCE
33-167953731
33-1-47965224 (Fax)

Hiroyuku Miyamaru
Master of Science
Osaka University
Dept. of Nuclear Engineering
Yamadaoka 2-1, Suita
Osaka, 565, JAPAN
6-877-5111
6-877-3264 (Fax)

Shinya Miyamoto
Student of Chemistry
Tokyo Metropolitan University
Minami-ohsawa 1-1, Hachioji-shi
Tokyo, 192-03
JAPAN
81-426-77-2548
81-426-77-2525 (Fax)

Nobuji Miyasaka
Deputy General Mgr.
Fundamental Research Laboratories
Osaka Gas Co. Ltd.,
6-19-9 Torishima Konohana-Ku
Osaka 554, JAPAN
06-462-3231
06-464-1805 (Fax)

Takeshi Mizota
Research Assoc., Inst. of Physics
University of Tsukuba
Ibaraki 305
JAPAN
81-298-53-2492
81-298-53-2565 (Fax)

Tadahiko Mizuno
Research Associate
Hokkaido University
Faculty of Engineering
Kitaku North 13 West 8
Sapporo 060, JAPAN
81-11-716-2111 x6689
81-11-757-6143 (Fax)

Cesare Moroni
Professor, Dept. of Physics
University of Bologna
via Irnerio 46
Bologna 40126
ITALY
39-5135-1035
39-5124-9847 (Fax)

Douglas R. Morrison
CERN
Geneva 23
SWITZERLAND
4122-767-3532
4122-783-0600 (Fax)

Dean Musgrave
Aerospace Engineer
400 S. Claremont
Dearborn, MI 48124
(313) 565-3869

Roberto Monti
National Research Council
Instituto Tesre-Cnr
Via Castagnoli No. 1
Bologna, 40126, Italy
0039-5128-7040
51-229702 Fax

David J. Nagel
Supt. Condensed Matter & Radiation
Naval Research Laboratory
(Code 6600)
4555 Overlook Avenue SW
Washington, DC 20375-5345
(202) 767-2931
(202) 767-3709 (Fax)

Kikujiro Namba
President
Technova Inc.
13th Fl. Fukoku Seimei Bldg. 2-2
Uchisaiwai-cho 2-chome
Chiyoda-ku, Tokyo 100, JAPAN
03-3508-2280
03-3508-7578 (Fax)

Linda Nelson
Conference Coordinator
EPRI
3412 Hillview Avenue
Palo Alto, CA 94303
(415) 855-2127
(415) 855-2041 (Fax)

Shinji Nezu
Chief Research Scientist, R&D
IMRA Material R&D Co., Ltd.
5-5- Hachiken-cho
Kariya, Aichi, 448
JAPAN
81-566-24-8316
81-566-24-9370 (Fax)

Reiko Notoya
Doctor of Science, Research Assoc.
Hokkaido University
Catalysis Research Center
Kita-11, Nishi-10, Kita-ku
Sapporo, 060, JAPAN
81-11-716-2111
81-11-709-4748 (Fax)

Robert Nowak
Dr/Chemistry Division
Office of Naval Research
ONR 33
800 N. Quincy St.
Arlington, VA 22217-5660
703-696-4409

Kenichi Ohkubo
Senior Engineer, R&D Division
Institute of Applied Energy
14-2 Nishishinbashi 1-Chome
Minatoku, Tokyo, 105
JAPAN
81-33-508-8894
81-33-501-1735 (Fax)

Tadayoshi Ohmori
Research Associates
Hokkaido University
Catalysis Research Center
Kita-ku, N-11, W-10
Sapporo, 060, JAPAN
81-11-716-2111 x2620
81-11-709-4748 (Fax)

TsuTomu Ohtsuki
Lab. of Nuclear Sci.
Tohoku University
1-2-1 Mikamine, Taihaku
Sendai
JAPAN

Hikaru Okamoto
Research Scientst, R&D Dept.
IMRA Material R&D Co., Ltd.
5-50 Hachiken-cho
Kariya, Aichi, 448
JAPAN
81-566-27-8316
81-566-24-9370 (Fax)

Makoto Okamoto
Professor, Res Lab Nuclear Reactors
Tokyo Institute of Technology
2-12-1, Ookayama, Meguro-city
Tokyo, 152
JAPAN
81-3-3726-1111
81-3-3729-1875 (Fax)

Albert Okazaki
P.O. Box 829
Deep River, Ontario KOJ 1P0
CANADA
(613) 584-2715

R.A. Oriani
Professor Emeritus
University of Minnesota
121 Amundson Hall
Minneapolis, MN 55455
(612) 625-5862

Michael Orillion
Technical Staff
FMC Corporation
1205 Coleman Ave.
Santa Clara, CA 95052

Ken-Ichiro Ota
Associate Prof., Energy Engineering
Yokohama National University
156 Tokiwadai
Hodogaya-ku
Yokohama, JAPAN
45-335-1451 x2970
45-333-7643 (Fax)

Noboru Oyama
Tokyo University of Agriculture & Tech.
Dept. of Applied Chemistry
2-24-16 Nakamachi
Koganei, Tokyo 184, JAPAN
81-423-834719
81-423-843804 (Fax)

William S. Page
Freelance Consulting
Daneliuk & Page
640 Jig Street, R.R. # 1
Oxford Mills
Ontario, KOG 1S0, CANADA
(613) 258-4040
(613) 258-4719 (Fax)

Tom Passell
Mgr. Chem. Ctl.Tech.
EPRI
3412 Hillview Avenue
Palo Alto, CA 94303
(415) 855-2070
(415) 855-2774 (Fax)

James A. Patterson
President and Chairman
Patterson Ventures
2074 20th Street
Sarasota, FL 34236
(813) 957-3109
(813) 921-1915 (Fax)

Stan Pons
Associate Director, Professor
IMRA Europe, S.A.
Science Center, 220 Rue Albert Caquot
0650 Valbonne
FRANCE
33-93-95-73-37
33-93-95-73-53 (Fax)

Guiliano Preparata
University of Milano
Department of Physics
Via Celoria 16,
20133 Milano, ITALY

Thomas V. Prevenslik
Consultant
3-6-7 Rroseheim #613 Azusawa
Itabashi-Ku, Tokyo 174
JAPAN

John G. Pronko
Lockheed
R&D, D96-50 B255
3251 Hanover St.
Palo Alto, CA 94304-1191
(415) 424-2073
(415) 424-3306 (Fax)

Mario Rabinowitz
EPRI
3412 Hillview Avenue
Palo Alto, CA 94303

Evan Ragland
6640 Ahekolo Circle
Diamondhead, MS 39525
(601) 255-9480
(601) 255-3008 (Fax)

Michel Rambaut
57H Rue De La Hacquiniere
91440, Bures-sur-Yvette
FRANCE
33-1-6907-5839
33-1-6829-9188 (Fax)

H.E. Ransford
Vice President, Engineering
Nova Resources Group, Inc.
1553 Platte Street
Suite 301
Denver, CO 80202
(303) 433-5582
(303) 433-6702 (Fax)

William L. Reber
Dir. of Technology, New Enterprises
Motorola, Inc.
1303 East Algonquin Road
Schaumburg, IL 60196-1065
(708) 538-3459
(708) 576-7185 (Fax)

Debra R. Rolison
Research Chemist
Naval Research Laboratory
4555 Overlook Avenue, SW
Washington, DC 20375-5542
(202) 767-3617
(202) 767-3321 (Fax)

Charles E. Rosenberry
President
Global Resources
729 Rising Star Dr.
Henderson, NJ 89014
(702) 456-7345
(702) 456-7345 (Fax)

Dana R. Rotegard
Chief Research & Dev. Officer
Irish Holdings Ltd
Minnesota Cold Fusions Alliance
#2 223 Ridgewood
Minneapolis, MN 55403
(612) 455-7777

Jed Rothwell
Cold Fusion Research Advocates
2060 Peachtree Ind. Ct.
Suite 313
Chamblee, GA 30341
(404) 451-9890
(404) 458-2404 (Fax)

W.M. Sackinger
Director, I.P.&L.
University of Alaska
Geophysical Institute
Fairbanks, AK 99775-7320
(901) 474-7865
(901) 474-5679 (Fax)

Alexander L. Samgin
Applied Technology, Inc.
ENECO
391-B Chipeta Way
Salt Lake City, UT 84108
(801) 583-2000
(801) 583-6245 (Fax)

Carlos Sanchez
Prof. Fisica de Materiales Dept.C-4
Universidad Autonoma
Cantoblanco
Madrid - 28049
SPAIN
34-1-3974766
34-1-3978579 (Fax)

I. Savvatimova
ENECO
University of Utah Research Park
391-B Chipeta Way
Salt Lake City, UT 84108
(801) 583-2000
(801) 583-6245 (Fax)

Franco Scaramuzzi
Professor
ENEA
CRE Frascati - Via E. Fermi, 27
00044 Frascati
(Roma), ITALY
39-6-94005300
39-6-94005400 (Fax)

Michael J. Schaffer
Sr. Staff Scientist/Fusion
10586 Rookwood Dr.
San Diego, CA 92131-1618
(619) 455-2841
(619) 455-4156 (Fax)

Sakamoto Shigeyasu
Professor, Nuclear Engineering
Tokai University
1117 Kitakanami,Hiratsuka-Shi
Kanagawa
JAPAN
463-58-1211 x4140

Toshiaki Shirakawa
Professor
Otuma Women's University
Dept. of Social Information Processing
9-1 Kamioyamadacho
Tama, Tokyo 206, JAPAN
81-423-39-0051
81-423-39-0044 (Fax)

Bart Simon
University of California at San Diego
Science Studies Program
9500 Gilman Dr.
La Jolla, CA 92093-0102
(619) 534-0491
(619) 534-3388 (Fax)

Stuart Smedley
Program Mgr. Electrochemistry
SRI International
333 Ravenswood Avenue
Palo Alto, CA 94025
(415) 859-6173
(415) 859-3678 (Fax)

Donald R. Smith
Dir., Mechanical & Aerospace Eng.
University of Missouri
Coorindated Engineering Programs
UMKC Truman Champos, 600 W. Mechanic
Indepndence, MO 64050-1799
(816) 235-1252
(816) 235-1260 (Fax)

Antonio Spallone
Professor
Instituto Nazionale Di Fisica Nucleare
via Enrico Fermi
Frascati -(RM)- 00044
ITALY
33-6-9703201
39-6-9403548 (Fax)

Mahadevi Srinivasan
Int'l Fellow, Energy Rsch. Center
SRI International
333 Ravenswood Avenue
Menlo Park, CA 94025
(415) 859-2814
(415) 859-4286 (Fax)

Bruno Stella
Professor
University of Roma
P.A. Moro 2
00185 Roma, ITALY
00396/49914344

Edmund K. Storms
ENECO
270 Hyde Park Estates
Santa Fe, NM 87501
(505) 988-3673

Roger Stringham
E-Quest Sciences
P.O. Box 60642
Palo Alto, CA 94306

Udo Strohbusch
University of Hamburg and DESY
Physics Institute
Luruper Chausse 149
22761 Hamburg, GERMANY
49-40-89982142
494089982143 (Fax)

Masao Sumi
Mitsubishi Heavy Industries, Ltd.
2-1-1 Shinhama Arai-Cho
Takasago, Hyogo Pref
676, JAPAN
794-45-6734
794-45-6924 (Fax)

Raghavan Sundaresan
Research Associate, Chemistry Dept.
Texas A&M University
Department of Chemistry
College Station, TX 77843-3255
(409) 845-8409
(409) 845-4205 (Fax)

Yoshikazu Suzumua
Researcher
Technova Inc.
13th Fl., Fukoku Seimei Bldg.
2-2 Uchisaiwai-cho, 2-chome
Chiyoda-ku, Tokyo 100, JAPAN
03-3508-2280
03-3508-7578 (Fax)

Mitchell Swartz
Editor
Cold Fusion Times
16 Pembroke Road
Weston, MA 02193
(617) 239-8383

Akito Takahashi
Professor, Nuclear Engineering
Osaka University
Yamadaoka 2-1,
Suita
Osaka, 565, JAPAN
81-6-877-5111
81-6-877-3264 (Fax)

Masanori Takahashi
Mgr., R&D Ctr.-New Hydrogen Energy
Institute of Applied Energy
22-5, Nishishinbashi 1-chome
Minato -ku, Tokyo, 105
JAPAN
81-33-508-8901
81-33-508-8902 (Fax)

Ryoji Takahashi
Emeritus Professor
University of Tokyo
Setagaya-Ku
Seta 2-26-21, Tokyo
JAPAN
3 700-5265

Yasuhito Takeuchi
Manager, R & D
Yokogawa Medical Systems, Ltd.
47127 Asahigaoka
Hino 191
JAPAN
81 425 855 117
81 425 855 725 (Fax)

Carol Talcott
LANL
270 Hyde Park Estates
Santa Fe, NM 87501

Ryoichi Taniguchi
Researcher, Radiation Physics Div.
University of Osaka Prefecture
Gakuen-Cho, Sakai
Osaka 593
JAPAN
722-36-2221
722-36-3876 (Fax)

Francis Tanzella
Energy Research Center
SRI International
333 Ravenswood Avenue
Menlo Park, CA 94025
(415) 859-4701
(415) 859-4286 (Fax)

Stuart F. Taylor
Los Alamos National Laboratory
MS 0914
Los Alamos, NM 87545
(505) 667-1211
(505) 665-7176 (Fax)

Makoto Teshigawara
Graduate Student
Tohoku University
Institute for Materials Research
Oarai, Ibarakiken, 311-13
JAPAN
81-292-67-3181
81-292-67-4947 (Fax)

David Thompson
Consultant
Tech Specialist & Univ/Industry Relation
Newlands, Whitchurch Hill, Reading
England RG8 7PN
UK
44-734-842551
44-734-845717 (Fax)

Gale Thorne
ENECO
University of Utah Research Park
391-B Chipeta Way
Salt Lake City, UT 84108
(801) 583-2000
(801) 583-6245 (Fax)

Ron Tolman
ENECO
University of Utah Research Park
391-B Chipeta Way
Salk Lake City, UT 84108
(801) 583-2000
(801) 583-6245 (Fax)

Kenichi Tsuchiya
Associate Professor
Tokyo National College of Technology
1220-2 Kunugida
Hachioji, Tokyo 193, JAPAN
0426-68-5191
0426-68-5097 (Fax)

Dale Tuggle
Los Alamos National Laboratory
33 Grand Canyon
Los Alamos, NM 87544
(505) 672-4606

Joe Veranth
Vice President, R&D
Bose Corp.
The Mountain
Framingham, MA 01701
(508) 879-7330
(508) 820-4865 (Fax)

Jean-Pierre Vigier
D' of Theoretical Physics
University of Paris VI
Pierre et M. Curie
4 Place Jussieu, Paris VI
FRANCE
31-14-427-4214
31-14-051-0661 (Fax)

James T. Waber
Research Professor
Michigan Technological University
Houghton, MI 49931
(505) 986-6134
(505) 986-6134 (Fax)

Joseph L. Waisman
Consultant
Waisman & Associates
25 Redwood Tree Lane
Irvine, CA 92715-2226
(714) 786-9311

Xiaozhong Wang
Assoc. Professor, Radiochemistry
China Institute of Atomic Energy
P.O. Box 275-48
Bijing, 102413
CHINA
935 7390
935 7008 (Fax)

Jack Ward
ENECO
University of Utah Research Park
391-B Chipeta Way
Salt Lake City, UT 84108
(801) 583-2000
(810) 583-6245 (Fax)

Dwayne Watson
Vice President
Space Energy LLC
3520 West Old Bingham Hwy.
Suite B
West Jordon, UT 84088
(801) 569-3133
(801) 569-3192 (Fax)

Pati Watson
Space Energy LLC
3520 West Old Bingham Hwy.
Suite B
West Jordan, UT 84088
(801) 569-3133
(801) 569-3192 (Fax)

Carol White
21st Century Science & Technology
P.O. Box 16285
Washington, DC 20041-0285
(703) 777-7473
(703) 777-8853 (Fax)

Fritz G. Will
Visiting Scientist
EPRI
P.O. Box 10412
Palo Alto, CA 94304
(415) 855-2772
(415) 855-2287 (Fax)

Tony Wilson
Chief Scientist
Feenix Laboratories
611 S. Pennsylvania
Denver, CO 80209
(303) 674-9384

Charles Wyndham
Investment Advisor/Private
P.O. Box 2518
Las Cruces, NM 88004
(505) 527-8564

Norio Yabuuchi
President of Laboratory
High Scientific Research Laboratory
204 Marusen Bldg.
Marunouchi Tsu Mie
514, JAPAN
05926-2-0877
0592-28-2006 (Fax)

Eiichi Yamaguchi
Sr. Rsch. Scientist, Supvr.
IMRA Europe, S.A.
220 Rue Albert Caquot, Sophia Antipolis
06560 Valbonne
FRANCE
33-93957337
33-93957330 (Fax)

Hisashi Yamamoto
Sr. Chief Engineer, Nuclear Power
Hitachi, Ltd.
4-6, Kanda-Surugadai
Chiyoda-Ku
Tokyo, 101, JAPAN
3-3258-111
3-3258-2348 (Fax)

Harumi Yamato
Research & Development Center
Toshiba
4-1, Ukishima-cho, Kawasaki-ku
Kawasaki, 210
JAPAN
44-288-8003
44-288-8204 (Fax)

Yuri Yoshinaga
Student, Res. Lab Nuclear Reactors
Tokyo Institute of Technology
c/o Prof. Okamoto
Meguro-city, Tokyo 152
JAPAN
81-3-3726-1111
81-3-3729-1875 (Fax)

Daniel G. Zavela
Business Planner
Patterson Ventures
431 Pheasant Ridge Road
Del Rey Oaks, CA 93940
(415) 513-1621

Yue-Chang Zhang
Prof., Shanghai Jao Univ.
Osaka University
II-1 Mihogaoka Ibaraki
Osaka 567
JAPAN
06-877-5111 x3669
06-878-3110 (Fax)

Zhang Zhongliang
Prof., Chemical Thermodynamic Lab
Institute of Chemistry
Academia Sinica
Beijing, Zhongguanchun, 100080
CHINA
254-4601
256-9504 (Fax)

4TH INTERNATIONAL CONFERENCE ON COLD FUSION
12/06/93 - 12/09/93

ATTENDEE LIST BY COMPANY

Company	Attendee Name
	Bill Collis
	Robert Cornog
	Kenneth C. Dewhirst
	Jeff Driscoll
	Roberto Felici
	John C. Fisher
	Ronald N. Flores
	Linda Grow
	Robert J. Grow
	Gustave K. Kohn
	Dean Musgrave
	Albert Okazaki
	Thomas V. Prevenslik
	Evan Ragland
	Michel Rambaut
	Michael J. Schaffer
	Charles Wyndham
(MRI) Manufacturing Research Inst.	Mark Crookston
Aisin Seiki Co., Ltd.	Kikuo Kato
Applied Technology, Inc.	Alexander L. Samgin
AECL Research	John Hilborn
Biological & Agricultural Research Inst.	Hisatoki Komaki
Bose Corp.	Robert C. McDonald
	Joe Veranth
Brigham Young University	S. Jones
C.R. Consultants	Andre Clerc-Renaud
Central Research Inst. of Electric Power	Tomonari Fujita
China Institute of Atomic Energy	Xiaozhong Wang
Cold Fusion Research Advocates	Jed Rothwell
Cold Fusion Times	Mitchell Swartz
Cornell University	Bruce Lewenstein
CERN	Douglas R. Morrison
CNAM	Jacques Foos

4TH INTERNATIONAL CONFERENCE ON COLD FUSION
12/06/93 - 12/09/93

ATTENDEE LIST BY COMPANY

Company	Attendee Name
Daneliuk & Page	William S. Page
Drexler Technology	Jerome Drexler
E-Quest Sciences	Russ George
	Roger Stringham
Environmental Optics Corp.	Thomas F. Droege
Equos Research Co., Ltd.	Kiyoshi Kawamoto
Erzion Center	Valery Koretsky
ENEA	Luciano Bertalot
	Franco Scaramuzzi
ENECO	A. Baraboshkin
	Robert W. Bass
	Charles Becker
	Leroy Becker
	John Bockris
	Robert T. Bush
	Dennis Cravens
	Robert D. Eagleton
	Oleg Finodeyev
	Igor Goryachev
	B. Guzhouskii
	Frederick G. Jaeger
	A. Karabut
	Mike Kreager
	Yan Kucherov
	Dennis Letts
	I. Savvatimova
	Edmund K. Storms
	Gale Thorne
	Ron Tolman
	Jack Ward
EPRI	Linda Nelson
	Tom Passell
	Mario Rabinowitz
	Fritz G. Will
ESTCO Univeristy of Ottawa	Ernest E. Criddle
Faculte Des Sciences	Jean-Paul Biberian
Feenix Laboratories	Tony Wilson

4TH INTERNATIONAL CONFERENCE ON COLD FUSION
12/06/93 - 12/09/93

ATTENDEE LIST BY COMPANY

Company	Attendee Name
Framatome	Jean-Paul Millot
Fundamental Research Laboratories	Nobuji Miyasaka
Fusion Info Center	Hal Fox
FMC Corporation	Michael Orillion
Global Resources	Charles E. Rosenberry
High Scientific Research Laboratory	Norio Yabuuchi
Hitachi, Ltd.	Hisashi Yamamoto
Hokkaido University	Tadashi Akimoto Michio Enyo Takaaki Matsumoto Tadahiko Mizuno Reiko Notoya Tadayoshi Ohmori
Hydro Dynamics Inc.	James L. Griggs Kelly Hudson
Imra Japan Co. Ltd.	Keiji Kunimatsu
Insituto Nazionale di Fisica Nucliare	Felice Iazzi
Inst. of High Energy Physics	Jing-Tang He
Inst. of High Temp. Electochem. URAL Div	Kabir Kaliev
Institute of Applied Energy	Kazuaki Matsui Kenichi Ohkubo Masanori Takahashi
Institute of Chemistry	Zhang Zhongliang
Institute of Physical Chemistry	A.G. Lipson
Instituto Nazionale Di Fisica Nucleare	Francesco Celani Antonio Spallone
Instituto Nazionale Fisica Nucliare	Daniela Calvo
Irish Holdings Ltd	Dana R. Rotegard
Istituto Nazionale di Fisica Nucliare	Elena Botta

4TH INTERNATIONAL CONFERENCE ON COLD FUSION
12/06/93 - 12/09/93

ATTENDEE LIST BY COMPANY

Company	Attendee Name
IMRA Europe, S.A.	Martin Fleischmann Stan Pons Eiichi Yamaguchi
IMRA Japan Co. Ltd.	Norifumi Hasegawa Akiko Kubota Nobuaki Miki
IMRA Material R&D Co., Ltd.	Takahiko Kato Shinji Nezu Hikaru Okamoto
INFN	Emilio Del Giudice
INFN-Rome University	Fabio Ferrarotto
J & J Manufacturing	Joseph P. Guokas Joan McDavid
JAIST	Sotoji Hiragi
Lockheed	John G. Pronko
Los Alamos National Laboratory	Thomas N. Claytor Gerald M. Hale Howard Menlove Stuart F. Taylor Dale Tuggle
LANL	Carol Talcott
Massachusetts Institute of Technology	Peter Hagelstein Keith H. Johnson
Mayer Applied Research Inc.	Fred Mayer Mary Mayer
Michigan Technological University	James T. Waber
Mitsubishi Heavy Industries, Ltd.	Yasuhiro Iwamura Masao Sumi
Motorola, Inc.	William L. Reber
National Institute for Fusion Science	Hideo Ikegami
Naval Postgraduate School	Michael E. Melich

4TH INTERNATIONAL CONFERENCE ON COLD FUSION
12/06/93 - 12/09/93

ATTENDEE LIST BY COMPANY

Company	Attendee Name
Naval Research Lab.	Graham Hubler
Naval Research Laboratory	George P. Chambers Scott R. Chubb Dawn Dominguez M.Ashraf Imam David J. Nagel Debra R. Rolison
New Energy & Industrial Tech. Dev. Org.	Michio Hamano
North American Palladium	Kerry Lane
Northern States Power Co.	Mark Hugo
Nova Resources Group, Inc.	H.E. Ransford
NAWC	Melvin H. Miles
NTT Basic Research Labs	Hiroshi Kanbe
Office of Naval Research	Robert Nowak
Ontario Hydro International	Robert F. Machacek
Osaka Institute of Technology	Teru Hanawa
Osaka University	Toshiyuki Iida Hiroyuku Miyamaru Akito Takahashi Yue-Chang Zhang
Otuma Women's University	Toshiaki Shirakawa
Patterson Ventures	James A. Patterson Daniel G. Zavela
Pedro Point Technology, Inc.	Alan Miller
Plant Technology Corporation	Hiroyuki Harada
Portland State University	John Dash
Power Systems Industries	Stephen E. Gregory
Proteus Processes & Technology, Inc.	Joseph N. Ignat
Purdue University	Yeong E. Kim

4TH INTERNATIONAL CONFERENCE ON COLD FUSION
12/06/93 - 12/09/93

ATTENDEE LIST BY COMPANY

Company	Attendee Name
Renlar Systems, Inc.	Mark Hittinger
Research Systems, Inc.	Talbot A. Chubb
Rockwell Mill	Nathan Hoffman
San Diego State University	James W. Cobble
Savannah River Technology Center	Myung W. Lee
Science Frontiers	Wayne Green
Scientific Research Center	Alexander Krivoshein
Scott Laboratories	Thomas B. Benson
Shell Recherche SA	Jacques Dufour
Shizuoka University	Hideo Kozima
Shueisha Inc.	Hideo Isono
Space Energy LLC	Angelina Chukanov Kiril B. Chukanov Joe Johnson Melinda Johnson Dwayne Watson Pati Watson
Space Exploration Assoc.	Elliot B. Kennel
Stanford University/ENECO	Robert A. Huggins
Starbound Engineering	Eugene F. Mallove
SRI International	Ben Bush Steven Crouch-Baker David M. Golden Mike McKubre Stuart Smedley Mahadevi Srinivasan Francis Tanzella
Tech Specialist & Univ/Industry Relation	David Thompson
Technova Inc.	Atsushi Kamei Kikujiro Namba Yoshikazu Suzumua

4TH INTERNATIONAL CONFERENCE ON COLD FUSION
12/06/93 - 12/09/93

ATTENDEE LIST BY COMPANY

Company	Attendee Name
Texas A&M University	Raghavan Sundaresan
The University of Tokyo	Setsuo Ichimaru
Tohoku University	Jirohta Kasagi Kenji Konashi TsuTomu Ohtsuki Makoto Teshigawara
Tokai University	Sakamoto Shigeyasu
Tokyo Institute of Technology	Makoto Okamoto Yuri Yoshinaga
Tokyo Metropolitan University	Shinya Miyamoto
Tokyo National College of Technology	Kenichi Tsuchiya
Tokyo University of Agriculture & Tech.	Noboru Oyama
Toshiba	Harumi Yamato
Tsinghua University	Xing Z. Li
Universidad Autonoma	Carlos Sanchez
Universita Degli Studi di Torino	Tullio Bressani
University of Alaska	W.M. Sackinger
University of Bologna	Ignazio Massa Cesare Moroni
University of California at San Diego	Bart Simon
University of Hamburg and DESY	Udo Strohbusch
University of Hawaii	Sandi Magaoay
University of Hawaii at Manoa	Bor Y. Liaw
University of Illinois at Urbana	George H. Miley
University of Milano	Guiliano Preperata
University of Minnesota	Rolf R. Engel R.A. Oriani

4TH INTERNATIONAL CONFERENCE ON COLD FUSION
12/06/93 - 12/09/93

ATTENDEE LIST BY COMPANY

Company	Attendee Name
University of Missouri	Peter H. Handel Donald R. Smith
University of Nebraska at Omaha	Raymond Guenther
University of Osaka Prefecture	Ryoichi Taniguchi
University of Paris VI	Jean-Pierre Vigier
University of Rochester	John R. Huizenga
University of Roma	Bruno Stella
University of Rome "La Sapienza"	Guido Gigli Daniele Gozzi
University of Scranton	Gregory Basting
University of Texas	J.J. Lagowski
University of Tokyo	Ryoji Takahashi
University of Tsukuba	Takayoshi Aoki Sang-Moo Lee Takeshi Mizota
University of Utah	Steven Barrowes Haven Bergeson Richard W. Grow
Utah State University	Wilford N. Hansen
Waisman & Associates	Joseph L. Waisman
Wall Street Journal	Jerry Bishop
Yokogawa Medical Systems, Ltd.	Yasuhito Takeuchi
Yokohama National University	Ken-Ichiro Ota
21st Century Science & Technology	Carol White

Fourth International Conference on Cold Fusion
(ICCF-4)

December 6-9, 1993
Hyatt Regency Maui
Lahaina
Maui

Sunday:	Welcome Reception and Registration, 6:00 p.m. - 7:30 p.m
Monday:	Continental Breakfast & Registration 7:00 a.m. - 8:00 a.m. Plenary Session 8:00 a.m. - 12:00 Noon Lunch 12:00 noon to 1:30 p.m. Parallel Sessions 1:30 - 6:00 p.m.
Tuesday:	Continental Breakfast 7:30 a.m. - 8:00 a.m. Plenary Session 8:00 a.m. - 12:00 Noon Lunch 12:00 noon - 1:30 p.m. Parallel Sessions 1:30 - 6:00 p.m. Grand Luau Reception 7:00 p.m. - 10.00 p.m.
Wednesday:	Continental Breakfast 7:30 a.m. - 8:00 a.m. Plenary Session 8:00 a.m. - 12:00 Noon Lunch 12:00 noon - 1:30 p.m. Parallel Sessions 1:30 - 6:00 p.m. Poster Session & Reception 6:00 p.m. - 8:30 p.m.
Thursday:	Continental Breakfast 7:30 a.m. - 8:00 a.m. Plenary Session 8:00 a.m. - 12:00 Noon Lunch 12:00 noon - 1:30 p.m. Panel Discussion 1:30 - 5:00 p.m.

Plenary	**Monday AM**		
C 1.1	8:00 AM	Fleischmann, Pons, Le Roux, Roulette	Calorimetry of the Pd-D2O System: the Search for Simplicity and Accuracy
C 1.2	8:40 AM	Gozzi, Balducci, Caputo, Cignini, Gigli, Tomellini Frullani, Cisbani, Garibaldi, Jodice, Urciuoli	Excess Heat and Nuclear Product Measurements in Cold Fusion Electrochemical Cells
C 1.3	9:20 AM	Hasegawa, Hayakawa, Yamamoto, Kunimatsu	Observation of Excess Heat During Electrolysis of 1M LiOD in a Fuel Cell Type Closed Cell
	10:00 AM	**Break**	
C 2.1	10:40 AM	Bertalot, DeMarco, DeNinno, LaBarbera, Scaramuzzi Violante	Deuterium Charging in Palladium by the Electrolysis of Heavy Water: Production of Heat Excess
C 1.5	11:20 AM	McKubre, Bush, Crouch-Baker, Hauser, Jevtic, Passel, Smedley, Tanzella, Williams, Wing	Calorimetric Studies of the D / Pd System
Parallel I	**Monday PM**		
C 1.4	1:30 PM	Bockris, Sundaresan, Letts, Minevski	Triggering and Structural Changes in Cold Fusion Electrodes
C 2.2	2:10 PM	Miyamaru, Chimi, Inokuchi, Takahashi	Search for Nuclear Products of Cold Fusion
C 2.3	2:30 PM	Arata, Zhang	A Remarkable Excess Heat Generated Using a New Type Pd Cathode
C 2.4	2:50 PM	Okamoto, Yoshinaga, Kusunoki	Excess Heat Generation, the Over Voltage Deviation and the Neutron Emission in D2O-LiOD-Pd Systems
C 2.6	3:10 PM	Storms	Some Characteristics of Heat Production Using the "Cold Fusion" Effect
	3:30 PM	**Break**	
C 2.7	3:50 PM	Ota, Yoshitake, Yamazaki, Kuratsuka, Yamaki, Ando Iida, Kamiya	Heat Measurement of Water Electrolysis Using Pd Cathode and the Electrochemistry
C 2.8	4:10 PM	Lipson, Lyakhov, Derjaguin	Reproducible Anomalous Heat Production and "Cold Fusion" in (Au)/Pd/PdO Heterostructure Electrochemically Saturated by Hydrogen (or Deuterium)
C 2.9	4:30 PM	Miles, Bush	Heat and Helium Measurements in Deuterated Palladium
C 2.10	4:50 PM	Oyama, Hirasawa, Tatsuma, Yamamoto	Calorimetry of D2O Electrolysis Using a Palladium Cathode in a Closed Cell System: AC Current Electrolysis Method
C 2.11	5:10 PM	Handel	Subtraction of a New Thermoelectrochemical Effect from the Excess Heat, and the Emerging Avenues to Cold Fusion
C 2.12	5:30 PM	Pons, Fleischmann	Heat After Death
Parallel II	**Tuesday PM**		

Plenary	**Tuesday AM**		
N 1.1	8:00 AM	Wolf	**Title to be announced**
N 1.2	8:40 AM	Kucherov, Karabut, Savvatimova	**Calorimetric and Nuclear Products Measurements at Glow Discharge in Deuterium**
N 1.3	9:20 AM	Gozzi, Balducci, Caputo, Cignini, Gigli, Tomellini, Frullani, Cisbani, Garibaldi, Jodice, Urciuoli	**Helium-4 Quantitative Measurements in the Gas Phase of Cold Fusion Electrochemical Cells**
	10:00 AM	**Break**	
N 1.4	10:40 AM	Tuggle, Claytor, Taylor	**Tritium Evolution from Various Morphologies of Palladium**
N 1.5	11:20 AM	Will, Cedzynska, Linton	**Tritium Generation in Palladium Cathodes with High Deuterium Loading During Heavy Water Electrolysis**
N 1.6	11:40 AM	Dufour, Foos, Millot	**Cold Fusion by Sparking in Hydrogen Isotopes Energy Balances and Search for Fusion By-Products**
Parallel I	**Monday PM**		
N 2.1	1:30 PM	Notoya	**Alkali-Hydrogen Cold Fusion Accompanied with Tritium Production on Nickel**
N 2.2	1:50 PM	Bush, Eagleton	**Strontium Production in Two Electrolytic Cells with Light Water Based Rubidium Carbonate Electrolytes and Nickel Mesh Cathodes**
N 2.3	2:10 PM	Ohmori, Enyo	**Detection of Iron Atoms on Gold Electrodes Used in Electrolysis of H2O and D2O in Neutral and Alkaline Media**
N 2.4	2:30 PM	Sankaranarayanan, Srinivasan, Bajpai, Gupta	**Investigation of Low Level Tritium Generation in Ni-H2O Electrolytic Cells**
N 2.5	2:50 PM	Lipson, Sakov, Derjaguin	**Generation of Cold Fusion Products in Deuterated High Tc Superconductors Upon the Phase Transition to Superconducting State**
N 2.6	3:10 PM	Jin, Zhan, Liu	**Deuterium Absorbability and Anomalous Nuclear Effect of YBCO High Temperature Superconductor**
	3:30 PM	**Break**	
N 2.7	3:50 PM	Samgin, Baraboshkin, Andreev, Murigin, Gorelov, Vakarin, Tsvetkov, Shalyapin, Golikov, Fomina	**Neutron Generation in the Solid Protonic Conductors with Perovskite-Type Structure**
N 2.8	4:10 PM	Shirakawa, Fujii, Chiba, Sueki, Ikebe, Yamaoka, Miura, Watanabe, Hirose, Nakahara, Utsumi	**Particle Acceleration and Neutron Emission in a Fracture Process of a Piezoelectric Material**
N 2.9	4:30 PM	Qi, Ma, Chen, Huang, Yu, Mo, Li	**The Analysis of the Neutron Emission from the Glow Discharge in Deuterium Gas Tube**
N 2.10	4:50 PM	Bazhutov, Koretskiy, Kuznetsov, Baranov, Skuratnic, Khokhlov, Sukovatkin	**Experimental Testing of the Erzion Model by Reacting of Electron Flux on the Target**
N 2.11	5:10 PM	He	**A Study on Anomalous Nuclear Fusion Reaction by Using HV Pulse Discharge**
N 2.12	5:30 PM	Matsumoto	**Cold Fusion Experiments by Using Electrical Discharge in Water**

		Ferroelectric Phase Transition
N 4.8	Romodanov, Savin, Skuratnik, Korneev	Concept of Target Material Choice for Nuclear Reactions in Condensed Media
N 4.9	Xiaozhong, Rongbao, Peijia, Wenliang, Hengjun, Feng Guoan, Jagun, Zhonglin	A New Device for Measuring Neutron Burst in Cold Fusion Experiment
N 4.10	Chindarkar, Paithankar, Bhagwat, Naik, Iyyengar Srinivasan	Observation of High Energy (~1 MeV) Charged Particles During Implantation of 5 KeV Protons on Pd and Ti Foils Using CR-39 SSNTD's
N 4.11	Qin, Yin-Wen, Xin-Wei, Jun, Wu-Shou, Hong-Qing Ze, Quan-Ren, Zu-Ying, Bu-Jia, Yong-Hui, Xiao-Zhong, Yi	New Experiment Results of Anomalous Nuclear Effect in Deuterium/Metal Systems
N 4.12	Kucherov, Karabut, Savvatimova	Heat Release and Product Yield of Nuclear Reactions in Pd-D System
N 4.13	Alguero, Fernandez, Cuevas, Sanchez	On the Subsistence of Anomalous Nuclear Effects after Interrupting the Electrolysis in F-P type Experiments with Deuterated Ti Cathodes

Parallel II **Tuesday PM**

T 3.1	1:30 PM Chubb, Chubb	The Role of Hydrogen Ion Band States in Cold Fusion
T 3.2	1:50 PM Waber, Llano	Boson Condensation in the Solid State Within a Sea of Fermions as a Model for Cold Fusion
T 3.3	2:10 PM Takahashi	Some Considerations on Multibody-Fusion in Metal-Deuterides
T 3.4	2:30 PM Chaudhary, Kaushik, Johnson, Hagelstein	Embedded Atom Models for PdD and Applications
T 3.5	2:50 PM Yang, Chen, Tang	Cold Fusion and New Physics (I)
T 3.6	3:10 PM Andermann	The Nature and Consequences of the Electron Capture Model for Rationalizing Excess Energy Production in Cold Fusion
	3:30 PM **Break**	
T 3.7	3:50 PM Prevenslik	Sonoluminescence, Cold Fusion, and Blue Water Lasers
T 3.8	4:10 PM Fisher	The Role of Polyneutrons in Cold Fusion Reactions
T 3.9	4:30 PM Bush	A Unifying Model for Cold Fusion
T 3.10	4:50 PM Yabuuchi	Wave of Deuterons and Cold Fusion
T 3.11	5:10 PM Sapogin	Deuteron Interaction in Unitary Quantum Theory
T 3.12	5:30 PM Tsuchiya	Mechanism of Cold Nuclear Fusion II

Posters

T 4.1	Sioda	A Mechanistic Model of Cold Fusion Based on Hot Spot Hypothesis
T 4.2	Vysotskii	Conditions and Mechanism of Nonbarrier Double-Particle Fusion in Potential Pit in Crystal
T 4.3	Vaidya	Coherent Nuclear Reactions in Crystalline Solids
T 4.4	Swartz	Catastrophic Active Medium (CAM) Theory of Cold Fusion
T 4.5	Valdya	On Bose-Einstein Condensation of Deuterons in PdD
T 4.6	Ragland	An Alternate Model of the Atomic Nucleus
T 4.7	Rambaut	One Can Account for Cold Fusion by Two Concepts: Screening by Electrons and Harmonic Oscillator Resonance
T 4.8	Bazhutov	Possible Exhibition of the Erzion-Nuclear Transmutation in Astrophysics

Plenary	**Thursday AM**		
M 1.1	8:00 AM	Orlani	**Physical and Metallurgical Aspects of the Entry of Hydrogen into Metals**
M 1.2	8:40 AM	Fleischmann, Larramona, Pons, Preparata, Sugiura	**Alfred Cohen and After; the alpha, beta, gamma of the Pd-H System**
M 1.3	9:20 AM	LI	**Helium / Hydrogen Behavior in Palladium**
	10:00 AM	**Break**	
M 1.4	10:40 AM	Akita, Tsuchida, Nakata, Kubota, Kobayashi, Yamamoto Hasegawa, Hayakawa, Kunimatsu	**Electrolytic Hydrogen/Deuterium Absorption into Pd, Pd-Rh and Pd-Ag Alloys in Fuel Cell Type Closed Cell**
M 1.5	11:20 AM	Celani, Spallone, Tripodi, Nuvoli, Petrocchi, Di Gioacchino, Boutet	**High Power μs Pulsed Electrolysis for Large Deuterium Loading on Pd Plates**
Parallel I	**Wednesday PM**		
M 2.1	1:30 PM	Dash, Noble	**Surface Morphology and Microcomposition of Palladium Cathodes after Electrolysis in Acidified Light and Heavy Water**
M 2.2	1:50 PM	Huggins	**Some Materials Aspects of the Electrochemical Insertion of Hydrogen and Deuterium into Metals**
M 2.3	2:10 PM	Okamoto, Nezu	**Measurements of Hydrogen Loading Ratio of Pd Anodes Polarized in LIH-LICI-KCI Molten Salt Systems**
M 2.4	2:30 PM	Miyamoto, Sueki, Fujii, Shirakawa, Chiba, Kobayashi Yanokura, Aratani, Nakahara	**Movement of LI during Electrolysis of 0.1M-LIOD/D2O Solution**
M 2.5	2:50 PM	Cilloco, Felici, Bertalot, DeMarco, DeNinno, LaBarbera, Scaramuzzi, Violante	**Deuterium Charging in Palladium by the Electrolysis of Heavy Water: Measurement of the Cell Parameter**
M 2.6	3:10 PM	Fukushima, Yamamoto	**Sonofusion: Maximum Temperature of Hot Spots**
	3:30 PM	**Break**	
M 2.7	3:50 PM	Llaw, Liebert, Ding	**Charging Hydrogen into NI in Hydride-Containing Molten Salts**
M 2.8	4:10 PM	Sano, Nezu	**Measurements of Hydrogen Loading Ratio of Pd Electrodes Cathodically Polarized in Aqueous Solutions**
M 2.9	4:30 PM	Criddle	**Evidence of Agglomeration and Syneresis in Regular and Excess Heat Cells in H2O**
M 2.10	4:50 PM	Tsuchida, Akita, Nakata, Kunimatsu	**Absorption of Hydrogen into Palladium Hydrogen Electrode-Effect of Thiourea**
M 2.11	5:10 PM	Shao, Huang, Mo, Yu, Yao, LI	**The Measurements and the Control of the Loading Ratio of Deuterium in Palladium**
M 2.12	5:30 PM	Waber, Perger, Schleitzer	**Relativistic Band Structure Calculation of Palladium Hydride**

Parallel I	Wednesday PM	
D 1.1	1:30 PM Fox	Cold Nuclear Fusion & Enhanced Energy Devices: A Progress Report
D 1.2	1:50 PM Morrison	Review of Progress in Cold Fusion
D 1.3	2:10 PM Mallove	Cold Fusion: The High Frontier Implications for Space Technology
D 1.4	2:30 PM Chukanov	New Pulse Gas Loading Cold Fusion Technology
D 1.5	2:50 PM Cornog	Cheap Electric Power From Nuclear Fusion?
D 1.6	3:10 PM Bass	Proposed Nuclear Physics Experiment to Conclusively Demonstrate and Explain Cold Fusion
	3:30 PM **Break**	
D 1.7	3:50 PM Guokas	Cold Fusion and Nuclear Proliferation
D 1.8	4:10 PM Romodanov, Savin, Skuratnik, Korneev, Glagolev	Ecological Aspects of Thermal Systems Using Hydrogen Isotopes